

DESIGN, SYNTHESIS AND APPLICATIONS OF BIOMIMETIC FLAVIN-BASED
ORGANOCATALYSTS

by

MOHAMMAD SHAWKAT HOSSAIN

Presented to the Faculty of the Graduate School of
The University of Texas at Arlington in Partial Fulfillment
of the Requirements
for the Degree of

DOCTOR OF PHILOSOPHY

THE UNIVERSITY OF TEXAS AT ARLINGTON

December 2015

Copyright © by Mohammad Shawkat Hossain 2015

All Rights Reserved



Acknowledgements

I would like to express my sincere gratitude to my mentor Professor Frank W. Foss Jr. for letting me do research in an interesting topic to explore and learn the different fields of organic chemistry. Professor Foss guides each student to understand the chemistry and goal of the project which helps student to think deeply about the project. His broad knowledge of chemistry and experience always helped us to overcome difficulties in synthesis, purification and characterization. He always appreciates and advances new ideas, which helps us to think independently about the future prospects of the current research. Professor Foss' ability to collaborate with diverse field of researchers helps me to interact with them and broaden my knowledge about different sciences. Professor Frank W. Foss and Dr. Ann Foss are very cordial to arrange get together parties to interact with students and their families.

I would like to thank my other committee members Professor Carl J. Lovely, Dr. Junha Jeon to guide me to understand my research and improve its quality.

Dr. Shuai Chen was the pioneer of my research project. The way of his work encouraged me to produce high quality work. I was lucky to have Diego, Andra, Pawan, Akop, Shakar, Sumit, John, as my colleagues. We shared chemistry knowledge on daily basis.

I would like to thank my dad, mom, wife and other family members to encourage me to study science and accomplish doctoral degree. I am very glad to have Sheheli as my spouse who continuously encouraged me about research.

Finally, I would like to thank ALLAH for giving me the opportunity to start and complete my doctoral degree at The University of Texas at Arlington.

November 17, 2015

Abstract

DESIGN, SYNTHESIS AND APPLICATIONS OF BIO-INSPIRED FLAVIN-BASED ORGANOCATALYSTS

Mohammad Shawkat Hossain, PhD

The University of Texas at Arlington, 2015

Supervising Professor: Frank W. Foss Jr.

Oxidation reactions are one of the most important transformations in synthetic chemistry. Most commonly used oxidants are metal oxides, which are neither green nor selective towards multi-functional molecules. The efficiency of the reactions can be improved by the introduction of a catalyst by lowering the activation energy. In nature, oxidation reactions are highly specific and are controlled by enzymes, co-enzymes, and availability of a renewable terminal oxidant, molecular oxygen. Among the various enzymatic oxidative transformations, our research was inspired by the oxidations controlled by co-enzymes FMN or FAD in the presence of flavoproteins and molecular oxygen. Flavin mimics were often studied/used to oxidize heteroatoms; however, the goal of this research was initially focused on mimicking other chemoselective oxidations of flavins, primarily at carbon centers.

In chapter one, the function of natural flavins in nature and different approaches to perform nucleophilic and electrophilic oxidation using artificial flavin is described.

In chapter two, flavin reactivity was extended to the Dakin oxidation of electron-rich benzaldehydes. This conversion of aryl aldehyde to phenol worked efficiently under mild conditions with either hydrogen peroxide or molecular oxygen as terminal oxidant. The mechanism was understood by various reaction rates studies. Substituent effects of

catalysts and substrates aided in the identification of the rate determining step. The order of reagents and extensive pH studies reveal the various way flavin catalysts enable oxo-transfer under mild, more neutral conditions, by altering both the pKa of the active nucleophilic oxygen source, and by lowering the energy of the oxide leaving group, as previously hypothesized by Briuce and coworkers.

In chapter three, pre-heteroaromatic compounds (initially investigated as possible reducing agents for flavin mimics) were transformed to their aromatic form aerobically using flavin catalyst in arguably the most mild methods described to date.

Chapters four through six describe the preparation and function of various classes of flavins. Chapter four discussed the bioactivity of new flavin species against cancerous and normal breast cells. Chapter five details the preparation of water-soluble classes of flavins and their photochemical properties (O_2 activation and Methyl Orange degradation). And Chapter six discusses the preparation of redox active flavins that were prepared for tethering to metal oxide photocatalyst and various electrode surfaces.

Chapter seven describes a new preparation of 5-deazaflavin cofactors - deazariboflavin, 8-hydroxydeazariboflavin (an F_{420} -precursor), and 10-methyl deazaflavin. An improved route to these species is described, and their redox activity were investigated in F_{420} -dependent enzymes.

Finally, chapter eight shows a new, concise and high yielding synthetic route explored for the synthesis of flavin catalysts, which includes the synthesis of different *o*-phenylenediamine derivatives and alloxan derivatives.

Table of Contents

Acknowledgements	iii
Abstract	iv
List of Illustrations	ix
List of Tables	xv
Chapter 1 Introduction of flavin chemistry.....	1
1.1 Structure, function and mechanism of flavoproteins	1
1.1.1 Discovery and structures of flavins	1
1.1.2 Flavoenzymes – Classification and Reactions.....	2
1.1.3 Catalytic cycle of flavin	4
1.1.4 Flavoprotein monooxygenase	5
1.1.5 Flavin dehydrogenases	8
1.2 Biomimetic Flavin organocatalysts	10
1.2.1 Flavin catalyzed electrophilic oxidation (Heteroatom (S, N) oxidation)	10
1.2.2 Flavin Catalyzed Nucleophilic Oxidation	18
1.3 Role of Flavin as Photocatalyst	21
1.3.1 Molecular oxygen activation	22
1.3.2 Flavin-sensitized organic molecule degradation	24
1.4 Medicinal importance of flavin	26
1.4.1 Flavin dependent enzymes in cancer progression.....	26
1.4.2 DNA modification using flavin.....	29
1.4.3 Flavin as biomarker	31
1.4.4 Flavin drug carrier	31
1.5 Deazaflavin	32

1.5.1	Biological importance of deazaflavin	32
Chapter 2	Flavin-catalyzed Dakin Oxidation	35
2.1	Dakin oxidation	35
2.1.1	General reaction mechanism	35
2.1.2	Detailed reaction mechanism	36
2.2	Current methods for Dakin oxidation	40
2.3	Flavin catalyzed organocatalytic Dakin oxidation	42
2.3.1	Synthesis of Flavinium catalysts	42
2.3.2	Optimization of reaction condition	43
2.3.3	Effect of different catalysts on overall reaction rate	53
2.3.4	Effect of reagent concentrations on overall reaction rate	56
2.3.5	Effect of temperature on reaction rate	62
2.3.6	Effect of substituents on Salicylaldehyde on reaction rate	65
2.4	Plausible mechanism for catalyzed reaction	67
2.5	Summary of the reaction kinetics	68
2.6	Application of catalysts on Dakin oxidation	70
Chapter 3	Flavin catalyzed Heterocycle Aromatization	73
3.1	Heterocyclic aromatization reactions	73
3.1.1	Dihydropyridine	73
3.1.2	Benzothiazoline	77
3.2	Flavin-catalyzed aromatization of dihydropyridine and benzothiazoline	80
Chapter 4	Flavin as cancer cell inhibitor	88
4.1	Introduction	88
4.2	Synthesis of artificial flavin analogs	89

4.3	MCF7 and MCF10 cell inhibition	91
Chapter 5 Water-soluble Flavin catalysts		97
5.1	Introduction	97
5.2	Synthesis of water-soluble flavin molecule.....	98
5.3	Application of water-soluble water molecule	101
5.3.1	Electrochemical activation of molecular oxygen	101
5.3.2	Methyl orange degradation.....	104
Chapter 6 Metal-flavin hybrid systems.....		108
6.1	Introduction	108
6.2	Synthesis of flavins with metal-binding groups.....	110
6.3	Application of tethered flavin molecules	114
Chapter 7 Deazaflavins.....		116
7.1	Introduction	116
7.2	Synthesis of FO	117
7.3	Application of FO	121
Chapter 8 Synthesis of new flavin derivatives		123
8.1	Objective.....	123
8.2	Synthesis of lumichrome derivatives	123
8.3	Synthesis of alloxazine catalysts with different 7,8d-disubstitution patterns.....	125
Appendix A List of abbreviations.....		130
Appendix B General experimental procedure.....		132
Appendix C NMR spectra of compounds.....		197
References.....		428
Biographical Information		439

List of Illustrations

Figure 1.1 Riboflavin, isoalloxazine and alloxazine	1
Figure 1.2 Flavin mononucleotide (FMN) and flavin adenosine dinucleotide (FAD)	2
Figure 1.3 Reactions catalyzed by flavoenzymes	3
Figure 1.4 Substrate scopes for BVMOs ⁸	4
Figure 1.5 Catalytic cycle of flavin with single electron transfer process	5
Figure 1.6 Mechanism of flavin monooxygenase	6
Figure 1.7 Role of R337 in stabilization of the intermediate ¹⁸	7
Figure 1.8 Role of flavin containing dehydrogenase and reductase	8
Figure 1.9 Acyl-CoA dehydrogenase	9
Figure 1.10 H ₂ O ₂ oxidation of sulfides and amines with isoalloxazine catalyst	11
Figure 1.11 Aerobic oxidation using isoalloxazine	12
Figure 1.12 Oxidation of sulfides using alloxazinium catalysts	14
Figure 1.13 Alloxazinium and isoalloxazinium catalysts with different substituents	15
Figure 1.14 Sulfide oxidation with immobilized flavin	15
Figure 1.15 Amphiphilic flavin catalysts	16
Figure 1.16 L-valinol derived bridged flavinium catalysts	16
Figure 1.17 Chiral sulfide oxidation using flavin catalyst	17
Figure 1.18 Isoalloxazinium catalyzed BVO of cyclobutanones with H ₂ O ₂	18
Figure 1.19 Electron deficient flavin catalysts	19
Figure 1.20 Asymmetric BVO of cyclobutanones	19
Figure 1.21 Aerobic Baeyer-Villiger oxidation	20
Figure 1.22 Different redox and protonation states of flavins ³⁸	21
Figure 1.23 One of the first reported chemical reactions with flavins ⁴⁰	22
Figure 1.24 Catalytic cycle of flavin redox reactions	23

Figure 1.25 Examples of photocatalysis using flavin	24
Figure 1.26 Flavin derivatives used for photo degradation of organic compounds	25
Figure 1.27 Possible reaction mechanisms for organic molecule degradation	26
Figure 1.28 Common pathways of epigenetics and inhibition ⁶⁴	27
Figure 1.29 A possible pathway for demethylation of diMeK4H3 by LSD1	28
Figure 1.30 Damaging and repairing of DNA using flavin dependent photolyase	30
Figure 1.31 Riboflavin derived biomarker for detecting tumor cell.....	31
Figure 1.32 Blue light induced dissociation of flavin from dodecin	32
Figure 1.33 Structures of FO and F ₄₂₀	33
Figure 1.34 Oxidative chemistry of deazaflavins	34
Figure 2.1 General reaction mechanism for BVO and Dakin oxidation	36
Figure 2.2 Plausible Dakin oxidation mechanism with strong and weak bases	40
Figure 2.3 Methyltrioxorhenium (MTO), and oxidized derivatives	41
Figure 2.4 MTO catalyzed Dakin oxidation in ionic liquid	41
Figure 2.5 Dakin oxidation with different oxidants	42
Figure 2.6 Synthesis of flavinium catalysts	43
Figure 2.7 Flavin catalytic cycle with the shunt process	43
Figure 2.8 General reaction condition for Dakin condition.....	44
Figure 2.9 Effect of methanol:water (95:5) on bases	45
Figure 2.10 Effect of aqueous ethanol on bases	46
Figure 2.11 Effect of isopropanol on bases	46
Figure 2.12 Effect of t-Butanol on bases.....	47
Figure 2.13 Effect of DMSO on bases	47
Figure 2.14 Effect of DMF on bases	48
Figure 2.15 Effect of dioxane on bases	48

Figure 2.16 Effect of THF on bases	49
Figure 2.17 Effect of trifluoroethanol on bases	49
Figure 2.18 Effect of solvents on NaOH	50
Figure 2.19 Effect of solvents on KOH.....	50
Figure 2.20 Effect of solvents on NaHCO ₃	51
Figure 2.21 Effect of solvents on KHCO ₃	51
Figure 2.22 Effect of aqueous solvents on Na ₂ CO ₃	52
Figure 2.23 Effect of solvents on K ₂ CO ₃	52
Figure 2.24 Possible flavin degradation under strong base.....	53
Figure 2.25 Reaction conditions for the catalyst optimization.....	54
Figure 2.26 Dakin reaction rate with different alloxazinium catalysts	54
Figure 2.27 Comparison of catalyst loading with hydrogen peroxide concentration	55
Figure 2.28 Effect of reagent concentrations on the reaction rate.....	58
Figure 2.29 Relative pKa of flavin hydrogen peroxide and hydrogen peroxide	59
Figure 2.30 Effect of catalyst concentration on the reaction rate	61
Figure 2.31 Hammett plot to relate initial rates with substituent effect	62
Figure 2.32 Relative reaction rates with temperature	63
Figure 2.33 Arrhenius plot for activation energy	64
Figure 2.34 Eyring plot for kinetic parameters	64
Figure 2.35 Reaction condition for substrate study	65
Figure 2.36 Relative reaction rates with different substrates.....	67
Figure 2.37 Plausible reaction mechanism for catalyzed reaction	68
Figure 2.38 Dakin oxidation of aldehydes and ketones with hydrogen peroxide	71
Figure 2.39 Formation of benzoic acid from electron poor benzaldehydes by Carbery and coworkers. ⁹⁴	72

Figure 3.1 Hypertension treating drugs with dihydropyridine core	73
Figure 3.2 Cerivastatin to treat atherosclerosis	74
Figure 3.3 Aerobic DHP oxidation using RuCl ₃ and molecular oxygen	75
Figure 3.4 DHP oxidation using Heteropolyacid (HPA)	75
Figure 3.5 Use of different oxidants for the DHP oxidation.....	76
Figure 3.6 Photo-induced oxidation of 1,4-dihydropyridine	77
Figure 3.7 Chiral phosphoric acid catalyzed asymmetric ketamine reduction.....	77
Figure 3.8 Biologically active benzothiazole derivatives.....	78
Figure 3.9 Pd catalyzed one pot synthesis of benzothiazole.....	78
Figure 3.10 Aerobic benzothiazole synthesis catalyzed by I ₂	79
Figure 3.11 Cu-catalyzed benzothiazole synthesis in ethanol.....	79
Figure 3.12 Aerobic benzothiazole synthesis in DMSO at higher temperature	79
Figure 3.13 Biomimetic cycle to oxidize pre-aromatic compounds.....	80
Figure 3.14 Synthesis of 1,4-dihydropyridines.....	81
Figure 3.15 Alloxazine catalyzed aromatization of dihydropyridines	82
Figure 3.16 Multi-component synthesis of pyridines.....	83
Figure 3.17 Isoalloxazine catalyzed oxidation of 4a-substituted dihydropyridines	84
Figure 3.18 The plausible mechanism for acid catalyzed aromatization	85
Figure 3.19 Alloxazine catalyzed benzothiazoline aromatization	86
Figure 3.20 Two components one pot aromatization of benzothiazolines.....	87
Figure 4.1 Alloxazine derivatives synthesis	89
Figure 4.2 Synthesis of 10-Ph isoalloxazine derivatives.....	90
Figure 4.3 Synthesis of 3,10-dimethyl isoalloxazine 4.14.....	90
Figure 4.4 Comparison of binding affinities with the natural substrate	94
Figure 4.5 Overlapping of six flavin mimics in the binding site	95

Figure 4.6 Comparison of binding orientation with natural cofactor (FAD)	95
Figure 5.1 Structures of natural flavins and water soluble flavin analogs.....	98
Figure 5.2 Initial approach to install quaternary group.....	99
Figure 5.3 Synthesis of quaternary ammonium derivative of alloxazine	100
Figure 5.4 Synthesis of sulfonic acid derivatives of alloxazine	100
Figure 5.5 Synthesis of water soluble 3- substituted 10-Ph isoalloxazine derivatives ...	101
Figure 5.6 Cyclic voltammetry of 5.3 with 0.1M Na ₂ SO ₄ and scan rate 0.02 V/sec	102
Figure 5.7 Cyclic voltammetry data comparing alloxazine and isoalloxazines	103
Figure 5.8 Catalytic electrochemical activation of O ₂ using isoalloxazines	103
Figure 5.9 Comparing conditions of MO degradation with F1 = 5.3 and F4 = 5.7	105
Figure 5.10 Degradation of alloxazine 5.3 under UV-vis light.....	105
Figure 5.11 Degradation of alloxazine 5.3 under visible light	106
Figure 5.12 Degradation of MO in presence of alloxazine and UV-vis light	106
Figure 6.1 Organic pollutant degradation using TiO ₂ as photocatalyst.....	109
Figure 6.2 Different binding modes between phosphonic acids SAMs and TiO ₂	110
Figure 6.3 Flavin derivatives for SAMs study	111
Figure 6.4 Synthesis of carboxylic acid derivatives	112
Figure 6.5 Synthesis of phosphonic acids	112
Figure 6.6 Synthesis of phosphonic acid 6.8 and 6.9.	113
Figure 6.7 The kinetics for photodegradation of ethanol	114
Figure 6.8 The kinetics of SA degradation.....	115
Figure 7.1 Structures and Properties of FO and F ₄₂₀	117
Figure 7.2 Prior syntheses of 7.1 and 7.2	118
Figure 7.3 Synthesis of stable hydrophobic intermediates.	120
Figure 7.4 Synthesis of uracil and condensation to 7.1, FO	121

Figure 8.1 Synthesized Lumichrome and its derivatives	124
Figure 8.2 General synthesis of lumichrome derivatives	124
Figure 8.3 Synthesis of 8.10-8.12	125
Figure 8.4 Alloxazine structure with one (left) and two (right) head groups	126
Figure 8.5 Synthesis of alloxazines with two linkers	126
Figure 8.6 Synthesis of alloxazine with single linker.....	127
Figure 8.7 Synthesis of 10-Ph isoalloxazine amine	128
Figure 8.8 Synthesis of alloxazine derivatives with mono amine and diamine.....	128

List of Tables

Table 1.1 Examples of flavoenzymes with functions ⁵	3
Table 1.2 Summary of flavin catalyzed oxidations	20
Table 1.3 Inhibition of ubiquitination of p53 by HDM268	29
Table 2.1 List of solvents and bases	45
Table 2.2 Initial rate for the control reactions	56
Table 2.3 Relative reaction rate with variable reagent concentrations	57
Table 2.4 Activation energy and kinetic parameters	65
Table 2.5 Relative reaction rates with different substrates	66
Table 4.1 Data for MCF7 cell inhibition	92
Table 4.2 MCF10 growth assay with artificial flavins	93

Chapter 1

Introduction of flavin chemistry

1.1 Structure, function and mechanism of flavoproteins

1.1.1 Discovery and structures of flavins

More than 130 years ago, riboflavin was first isolated from cow milk as a bright yellow pigment by Wynter Blyth. On the basis of the source, he termed the pigment as lactochrome.^{1,2} Later the yellow pigment was synthesized and the structure was confirmed by Richard Kuhn and Paul Karrer almost concurrently in 1934 and 1935.^{3,4} The compound was recognized as a component of vitamin B complex and named as riboflavin. The name was derived from the *N*-10 ribityl group and its characteristics yellow color (*flavous* in Latin). In general, flavin is used as a generic term for the compounds with the tricyclic core structure of riboflavin (isoalloxazine) and its isomer (alloxazine).

(Figure 1.1)

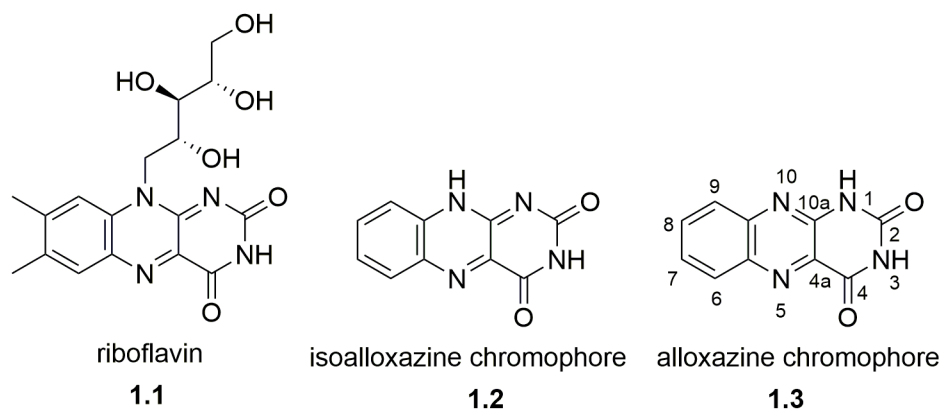


Figure 1.1 Riboflavin, isoalloxazine and alloxazine

Riboflavin derivatives function as cofactors in two forms – flavin mononucleotide (FMN) and flavin adenosine dinucleotide (FAD) (Figure 1.2). Structurally, they are different in *N*-10 side chain, which differentiates their biological function as cofactors.⁵

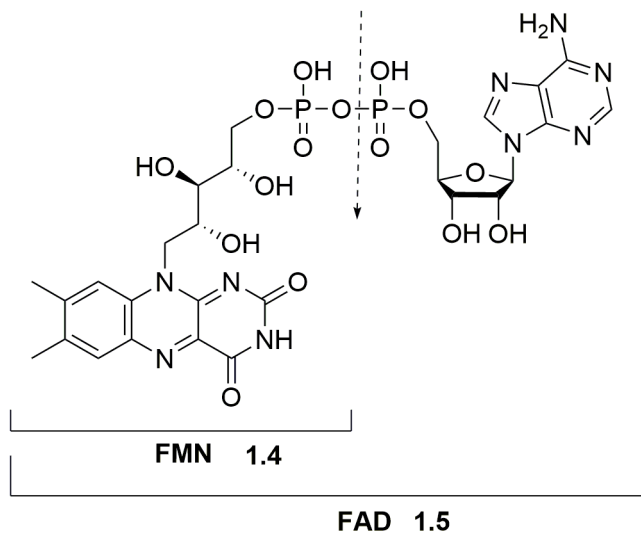


Figure 1.2 Flavin mononucleotide (FMN) and flavin adenosine dinucleotide (FAD)

1.1.2 Flavoenzymes – Classification and Reactions

A number of flavin-dependent enzymes were reported and a large class of reactions is performed by flavoenzymes. Depending on the reactivity, flavoenzymes are classified as monooxygenases, hydroxylases, and dehydrogenases (**Table 1.1**).^{2,5-8} Monooxygenases catalyze a single oxygen atom transfer to substrate, whereas hydroxylase catalyze hydroxylations and dehydrogenase catalyzes hydrogen molecule abstraction from various substrates. A variety of substrate specific reactions, performed by flavoenzymes are shown in **Figure 1.3**. Baeyer-Villiger monooxygenases (BVMOs) are a class of enzymes that catalyzes the oxidation of ketones to lactones or esters and oxidation of some sulfides.⁸ The cyclohexanone monooxygenase (CHMO),⁹ cyclopentanone monooxygenase (CPMO),¹⁰ and 4-hydroxyacetophenone monooxygenase (HAPMO)¹¹ are three examples of BVMOs that catalyze oxidation of corresponding ketone as well as oxidation of thioanisole to the corresponding sulfoxide with higher enantioselectivity⁸ (**Figure 1.4**).

Table 1.1 Examples of flavoenzymes with functions⁵

Prototype	Reactions	Co-factor	Co-enzyme
<i>p</i> -hydroxybenzoate hydroxylase	Hydroxylation, epoxidation	FAD	NAD(P)H
Cyclohexanone monooxygenase	Baeyer-Villiger, N-oxidation	FAD	NADPH
Luciferase	Light emission, Baeyer-Villiger		FMN/NAD(P)H
<i>p</i> -hydroxyphenylacetate hydroxylase	Hydroxylation		FAD/NAD(P)H
Styrene monooxygenase	Epoxidation		FAD/NAD(P)H
Tryptophan 7-halogenase	Halogenation		FAD/NAD(P)H

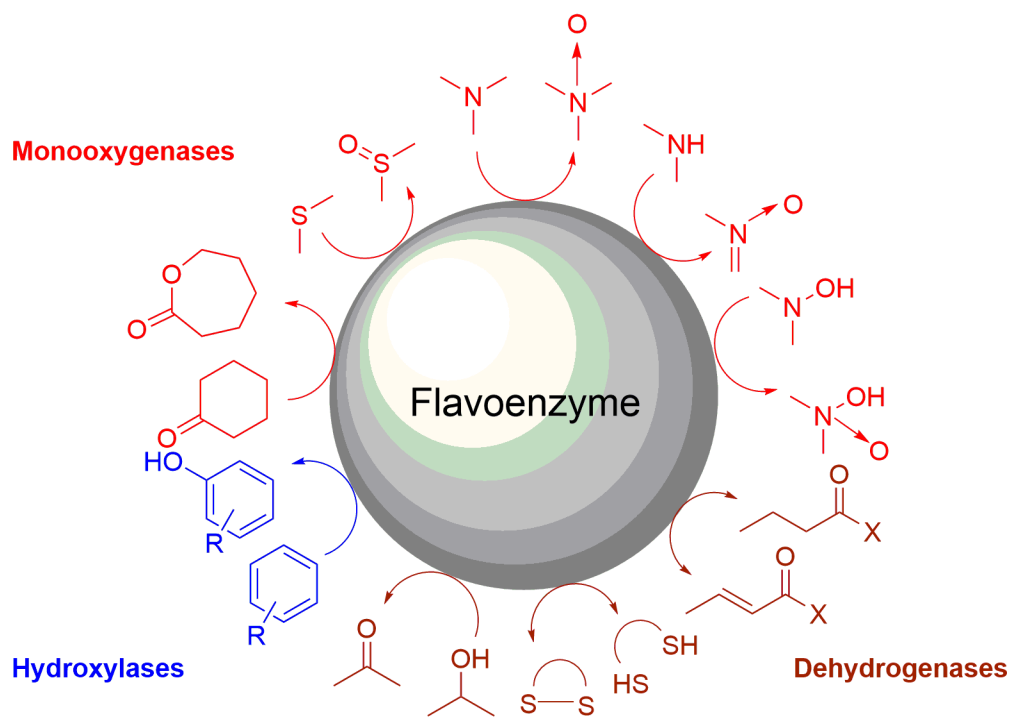


Figure 1.3 Reactions catalyzed by flavoenzymes

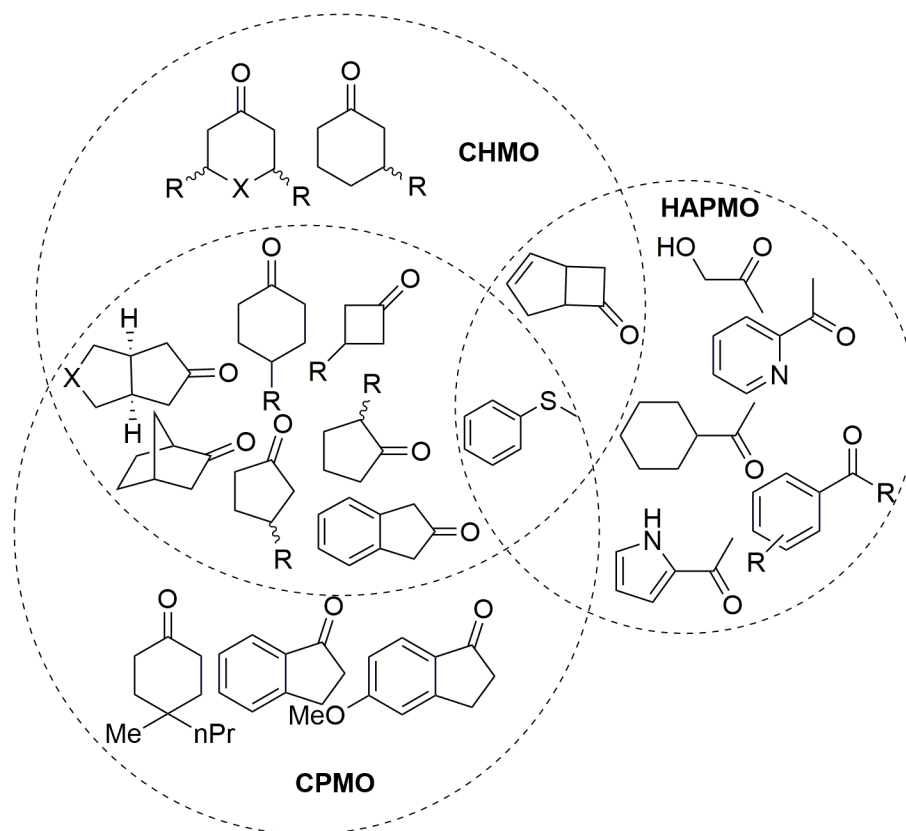


Figure 1.4 Substrate scopes for BVMOs⁸

1.1.3 Catalytic cycle of flavin

Both the Bruce and Massey groups have intensively studied the role of flavins in oxidation. The 4a-hydroperoxide was first proposed by Massey and coworkers in 1969.¹² During the catalytic cycle of flavin (**Figure 1.5**), the oxidized flavin **1.6** can be fully reduced to **1.7** either by a two-electron reduction process or by two one-electron reduction processes. The single electron reduced flavin radical is defined as flavin semiquinone **1.10**. The reduced flavin activates molecular oxygen by donating one electron to form the 4a-hydroperoxy flavin (FIOOH **1.8**). FIOOH **1.8** oxidizes substrates to products and converts itself to 4a-hydroxyflavin **1.9**, which finally transforms to the

oxidized form of the flavin **1.6** by eliminating one water molecule. The oxidized flavin **1.6** can also be treated with H_2O_2 to form the FIOOH **1.8**, which is known as the peroxide shunt process. This process is clearly reversible, FIOOH **1.8** can eliminate H_2O_2 to form the oxidized flavin $\text{FI}(\text{ox})$ **1.6**.

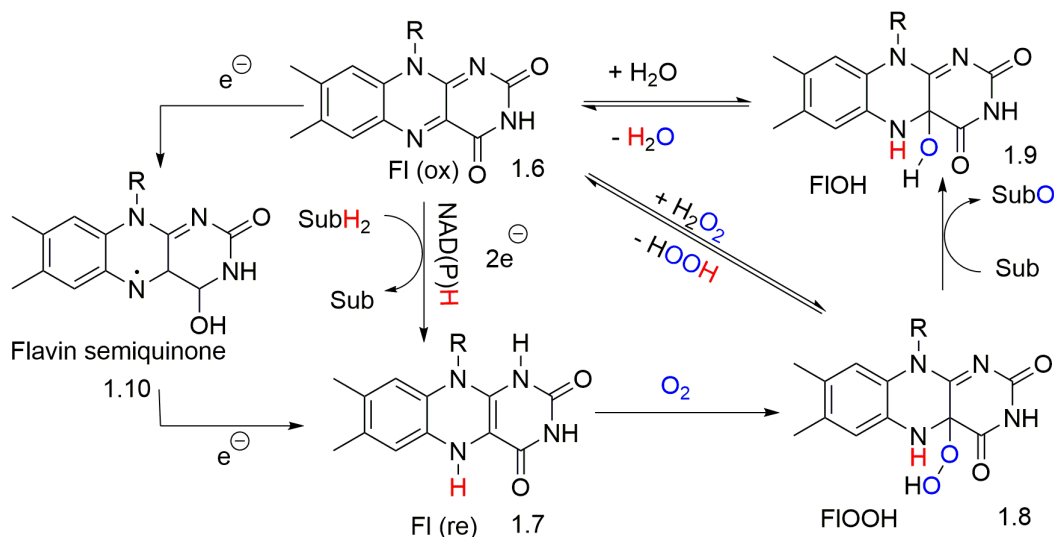


Figure 1.5 Catalytic cycle of flavin with single electron transfer process

1.1.4 Flavoprotein monooxygenase

Flavoprotein monooxygenases incorporate a single oxygen atom from molecular oxygen to the substrate molecule. In this process, the oxidized flavin **1.6** undergoes reduction by NAD(P)H **1.11**. The reduced flavin **1.7**, containing a polarized and electron rich alkene, reacts with triplet molecular oxygen to yield hydroperoxyflavin **1.8**. The reaction between triplet and singlet molecules is a spin forbidden process because the rate of chemical combination is faster than the rate of spin inversion. However, easily oxidizable singlet organic molecules, such as reduced flavin **1.7**, are able to couple with triplet oxygen to form a resonance-stabilized radical, which subsequently interact with the

superoxide to form the triplet complex **1.10**. The singlet 4*a*-hydroperoxyflavin **1.8** is generated by spin inversion sequentially (**Figure 1.6**).¹³⁻¹⁴

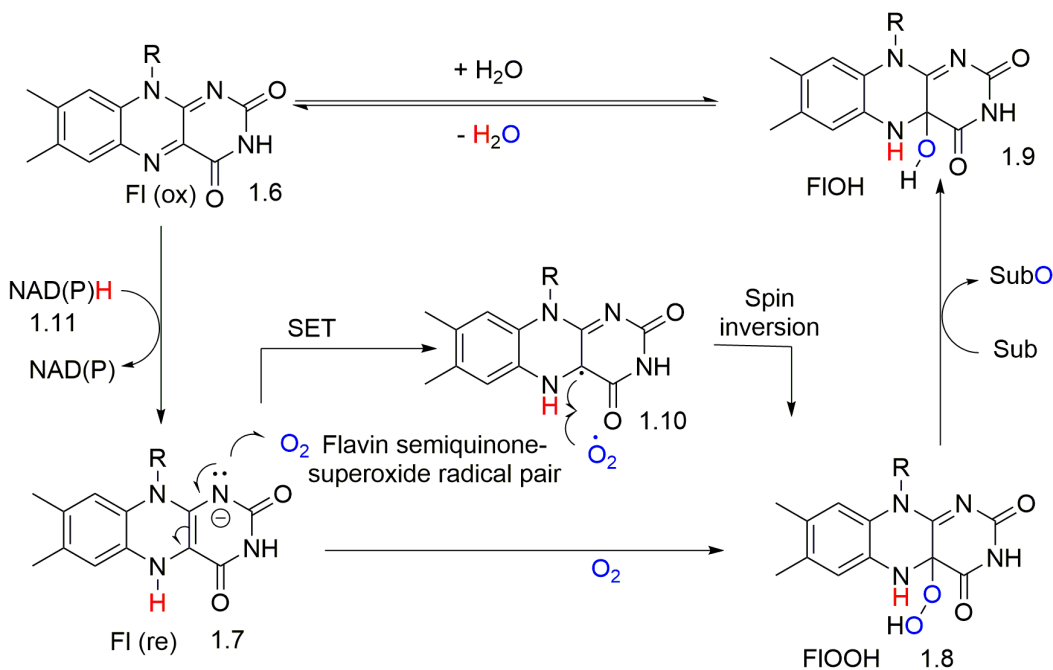


Figure 1.6 Mechanism of flavin monooxygenase

The O-O bond of 4*a*-hydroperoxyflavin **1.8** is inductively polarized by the electronegativity of the *N*-1, *N*-5, *N*-10 and C=O of the ring. This decreases the p*K*_a of the terminal proton of the FIOOH and increases the electrophilicity of the peroxide's terminal oxygen. FIOOH is a powerful reagent for the electrophilic N-oxidation of tertiary, secondary and hydroxyl amines as well as S-oxidation of sulfides. These oxidations are first order in both FIOOH and the substrate to generate N-oxide or S-oxide and the FIOH pseudo base **1.9**. The second order rate constant was determined to be higher than the rate obtained with H₂O₂ and t-BuOOH by 10⁴ to 10⁵ times.¹⁵

In addition to electrophilic oxidations, the nucleophilic Baeyer-Villiger oxidation of ketones to lactones or esters are known to be achieved by flavoproteins.¹⁶ Different types of flavoenzymes and their reactivity were discussed in section 1.1.2.

The crystal structure study of these enzymes revealed that the monooxygenases has a FAD-binding and NADPH-binding domains and the active site can be found at the interface between these two domains. The active site has a conserved arginine (R 337 in PAMO) (**Figure 1.7**), which plays an important role in the activation and stabilization of the 4a-hydroperoxyflavin and the high-energy Criegee intermediate. However, recent studies showed that the replacement of Arg 337 with aniline did not alter the reactivity of these enzymes, questioning the need for the cationic activation and stabilization of this transformation.¹⁷

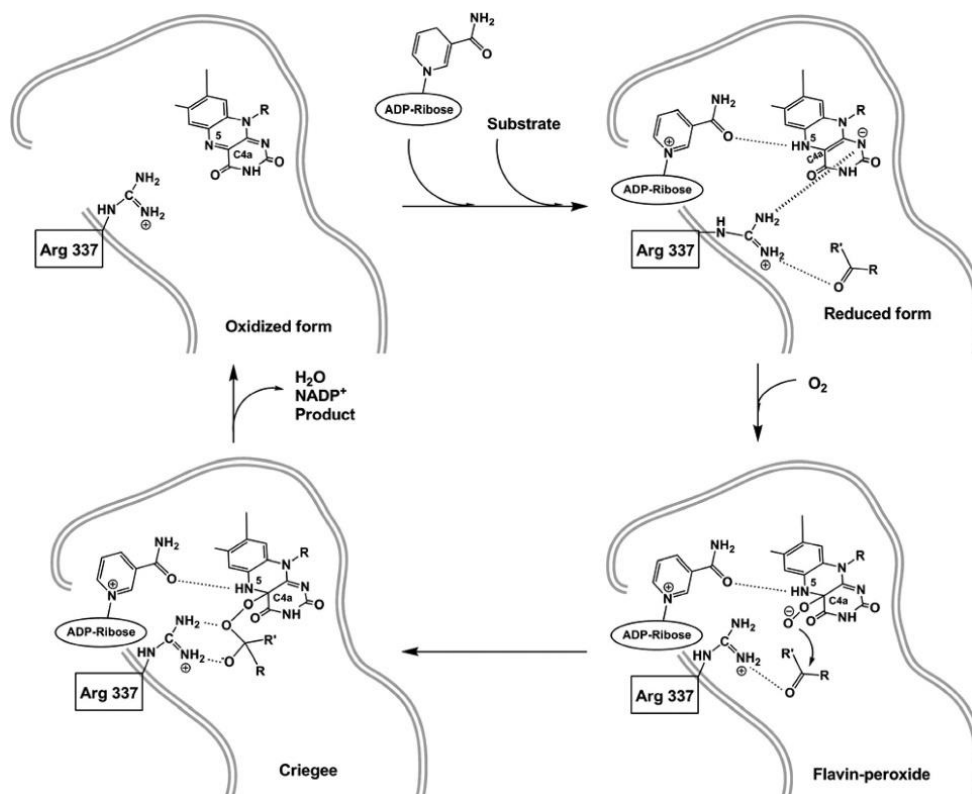


Figure 1.7 Role of R337 in stabilization of the intermediate¹⁸

1.1.5 Flavin dehydrogenases

Dehydrogenase and reductase enzymes transfer electrons from one substrate to another. Dehydrogenases oxidize a substrate with the use of a specific acceptor such as NAD(P)⁺ **1.12** while reductases transfer electrons from a specific electron donor such as NAD(P)H **1.11** to the substrate. (**Figure 1.8**)

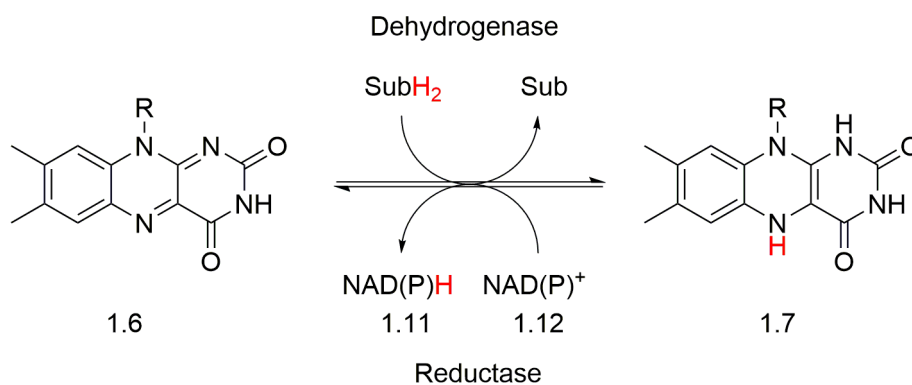


Figure 1.8 Role of flavin containing dehydrogenase and reductase

The introduction of α,β -unsaturation to carbonyl group is performed by an important group of flavoenzymes. Acyl-CoA dehydrogenases involved the flavin molecule.¹⁹ The mechanism designates the concerted removal of pro-R- α -hydrogen as a proton and transfer of the corresponding pro-R- β hydrogen as a hydride to the N-5 position of the flavin **1.6** (**Figure 1.9**).

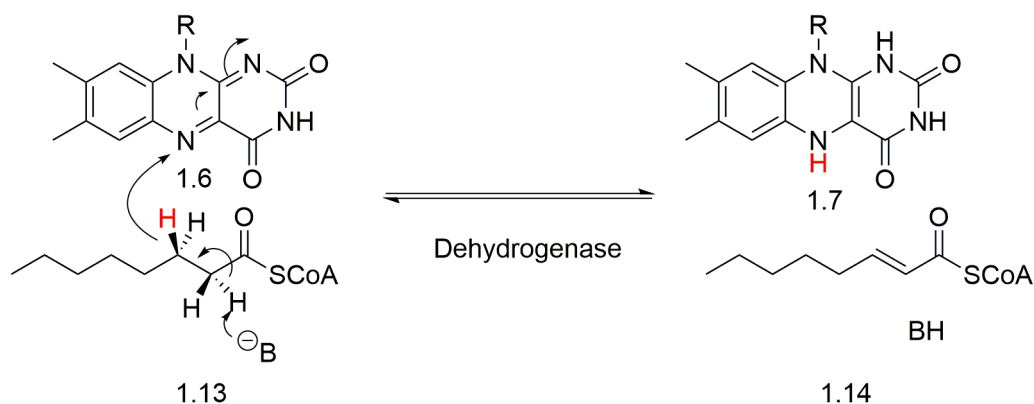


Figure 1.9 Acyl-CoA dehydrogenase

Organocatalysis may be argued to have superior advantages over biocatalysis and metal catalysis.²⁰ Biocatalysis requires sensitive and specific enzymatic systems and stoichiometric bio-reagents such as NAD(P)H, on the other hand organocatalysts have broader substrate scope, more tolerance of concentration, heat, air and moisture as well as relatively cheaper. Compared to metal catalysis, organocatalysts have the advantages of lower toxicity and cost. Therefore, organocatalysts are very attractive in the development of selective, mild, sustainable, and cost effective reaction processes.²⁰

Currently, flavin organocatalyzed oxidations are limited to monooxygenase and dehydrogenase chemistry. In addition to expanding the organocatalytic ability of flavin mimics, atom economical reducing agents and flavin mimics with stability under higher acid and base concentrations are also desirable. During the course of our work, it was noted that improved synthetic routes for cost effective catalysts were also needed.

Because of higher reactivity towards electrophilic and nucleophilic oxidation reactions, flavin organocatalysts were studied extensively for the last few decades. Both alloxazine **1.3** and isoalloxazine **1.2** derivatives were synthesized and their specific applications were studied in the literature. Both electrophilic and nucleophilic oxidations

with flavin molecules will be discussed in the following sections. Also, the importance of flavin as photocatalyst, cancer cell growth inhibitor, dye degrader, drug delivery carrier and tools for bio-image will also be discussed. Finally, an improved synthesis of related 7,8-didemethyl-8-hydroxy-5-deazaflavin (Fo) will be discussed.

1.2 Biomimetic Flavin organocatalysts

1.2.1. *Flavin catalyzed electrophilic oxidation (Heteroatom (S, N) oxidation)*

Murahashi and coworkers reported the oxidation of aliphatic and aromatic sulfides, secondary amines, tertiary amines, and hydroxyl amines using lumiflavin derived catalyst **1.15 (Figure 1.10)**, which is a milestone in flavin chemistry.²¹ The mechanistic investigation indicates the peroxide shunt process of flavin catalytic cycle. The work was as significant as the previous work reported by Bruice and coworkers.²²⁻²³ Sulfoxides can be further oxidized to sulfones with one additional equivalent of H₂O₂.

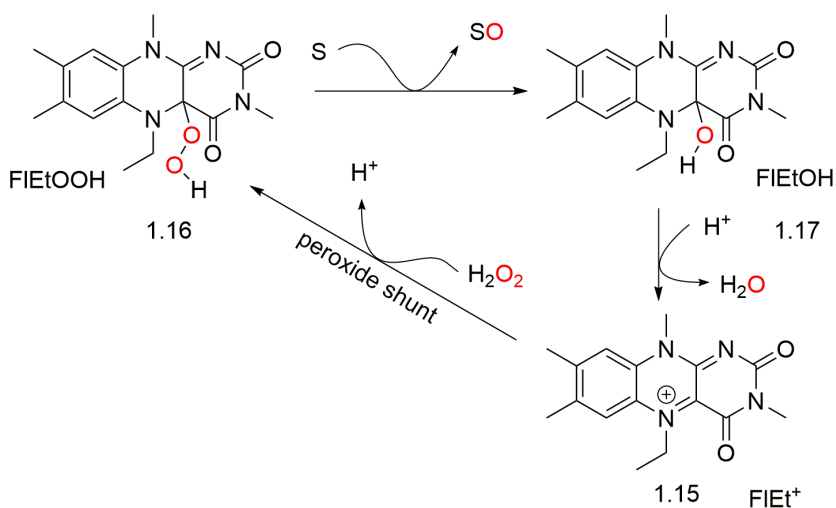
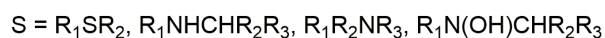
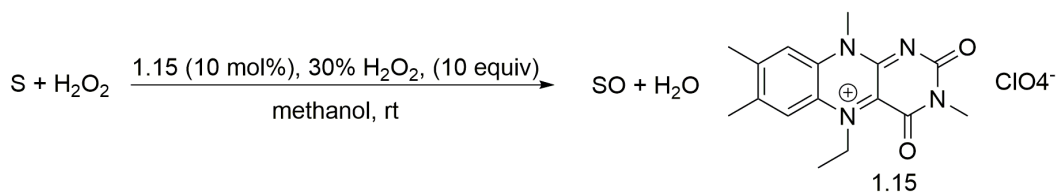


Figure 1.10 H₂O₂ oxidation of sulfides and amines with isoalloxazine catalyst

Murahashi and coworkers also reported the aerobic oxidation of sulfides to sulfoxide with the same catalyst.²⁴ To turn over the catalyst, the authors used hydrazine as the reducing agent and they used molecular oxygen as the terminal oxidant instead of hydrogen peroxide (**Figure 1.11**). The aerobic condition found to be effective under fluorinated (more acidic) solvents like trifluoroethanol (TFE) and 1,1,1,3,3,3-hexafluoro-2-propanol because of the higher solubility of the oxygen in these solvents. The aerobic oxidation was achieved with greater atom economy and greener way where the byproducts are only nitrogen and water.

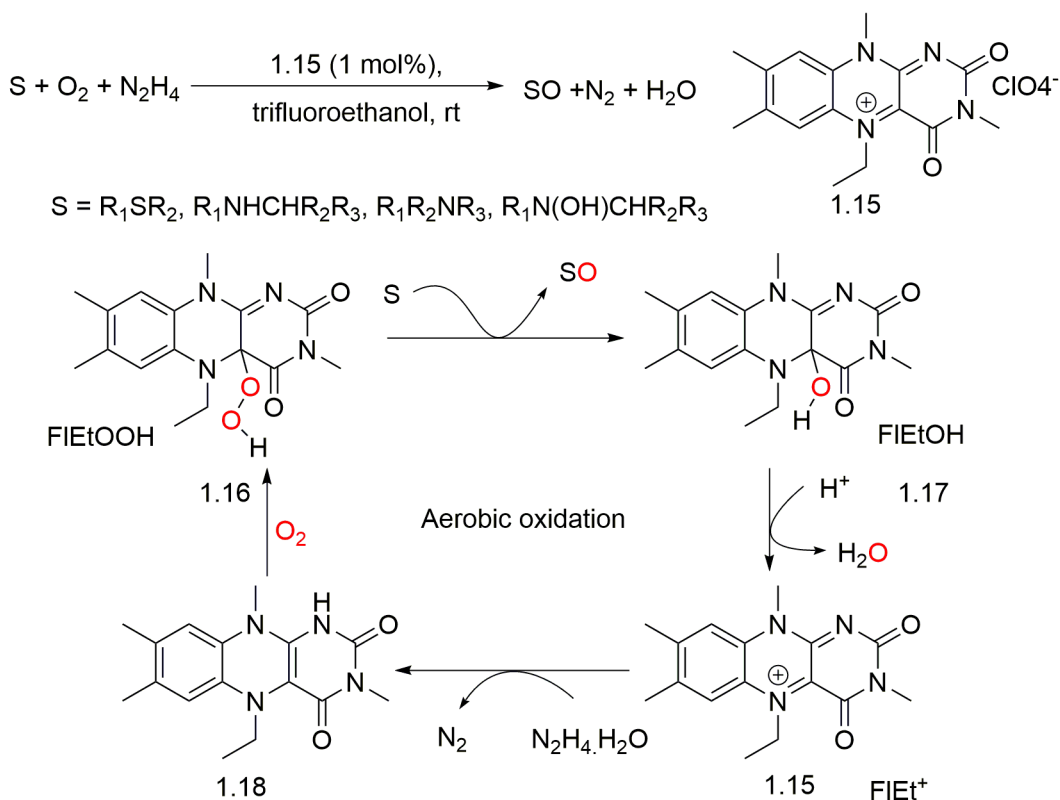


Figure 1.11 Aerobic oxidation using isoalloxazine

Bäckvall and coworkers used an *N,N,N*-1,3,5-trialkylated alloxazinium catalyst to accelerate the oxidation of a series of vinyl sulfides by hydrogen peroxide with great chemoselectivity (**Figure 1.12**).²⁵ No sulfones were isolated and the reactions were performed in methanol. The use of alloxazinium catalyst over isoalloxazinium catalyst, which was used by Murahashi and coworkers concluded that the elimination of water molecule from the 4a-hydroxy flavin to form the oxidized flavin is enhanced due to aromatization. Bäckvall and coworkers synthesized a series of alloxazinium catalysts with different substituents at C-7 and C-8 positions of the catalyst. After studying the reaction rate of different catalysts (**Figure 1.13**) on both S-oxidation and N-oxidation under the

given condition, they suggested that the presence of electronegative groups on the alloxazinium increases the rate of substrate oxidation.²⁶ The proposed reason was the increasing electrophilicity of 4a-hydroperoxyflavin through inductive effects. Also alloxazinium catalysts were better than isoalloxazinium due to faster elimination of water molecule from the 4a-hydroxyflavin, under the reaction conditions, to form the oxidized flavin.

Carboxylated flavin **1.31** immobilized in an ionic liquid ([BMIm]PF₆) **1.32** was used by Bäckvall and coworkers to perform highly selective oxidation of sulfides to sulfoxides with hydrogen peroxide.²⁷ (**Figure 1.14**) without any detectable over oxidation to sulfone. The catalyst immobilized in ionic liquid was recycled seven times without the loss of activity or selectivity.

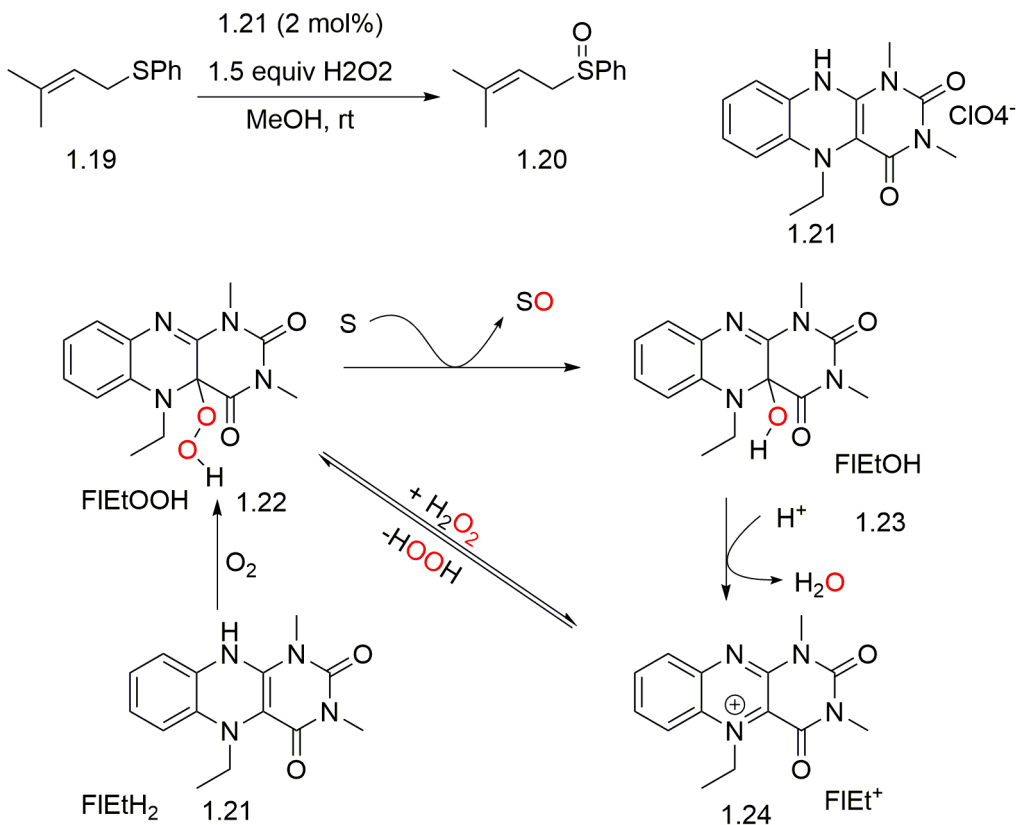


Figure 1.12 Oxidation of sulfides using alloxazinium catalysts

Cibulka and coworkers also studied the effect of alloxazinium and isoalloxazinium catalysts on both the sulfide and amine oxidation.²⁸ They reported that both catalysts enhanced the rate of sulfide oxidation but in case of tertiary amine oxidation alloxazinium derivatives work better than isoalloxazinium catalysts under basic condition due to a change in the rate determining step. Cibulka and coworkers also reported the synthesis of a series of amphiphilic alloxazinium and isoalloxazinium derivatives and their effect on sulfide oxidation in different micellar media like sodium dodecylsulfate (SDS), hexadecyltrimethylammonium nitrate (CTANO₃) and Brij 35 (Polyethylene glycol dodecyl ether). Amphiphilic alloxazinium catalysts **1.33** functioned

more effectively than the isoalloxaziniums **1.34** But the most effective catalyst was found to be the non-amphiphilic 5-ethyl-1,3-dimethylalloxazinium perchlorate **1.34a** in CTANO₃ micelles.²⁹

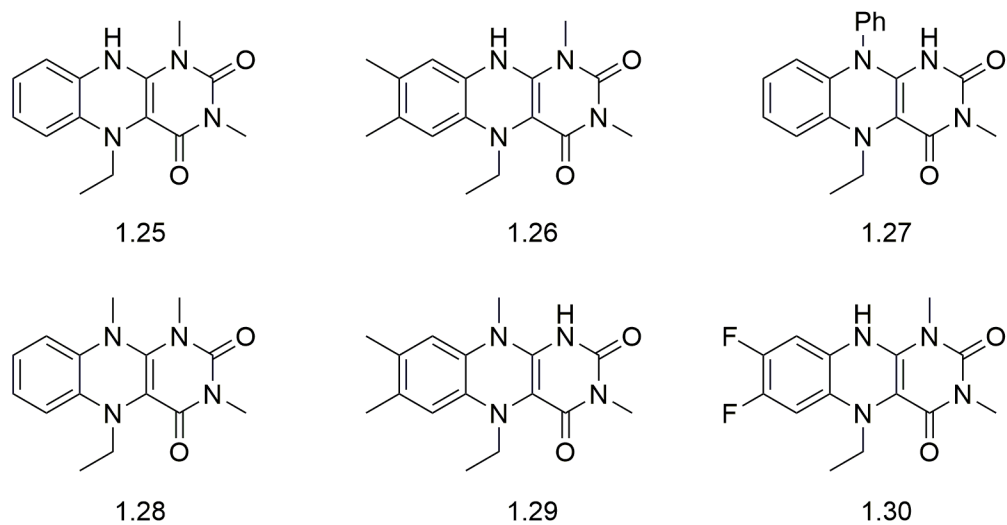


Figure 1.13 Alloxazinium and isoalloxazinium catalysts with different substituents

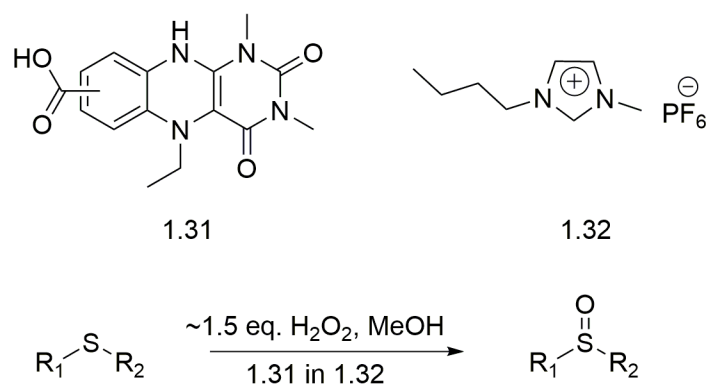


Figure 1.14 Sulfide oxidation with immobilized flavin

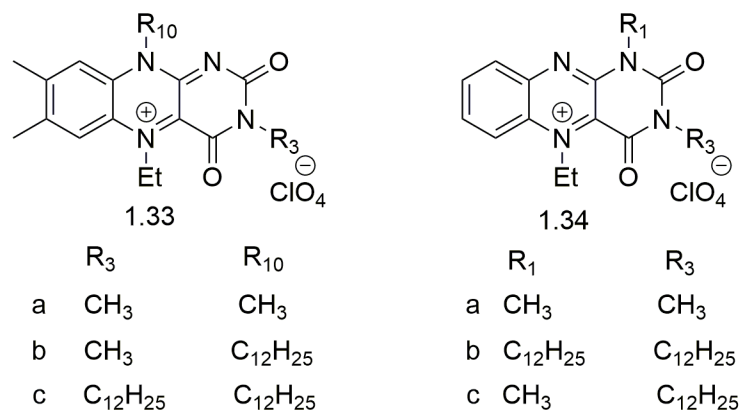


Figure 1.15 Amphiphilic flavin catalysts

Cibulka and coworkers synthesized chiral, non-racemic *N*-1,*N*-10-ethylene-bridged flavinium salts with a stereogenic center derived from L-valinol to catalyze the oxidation of sulfides to sulfoxides and the oxidation of 3-phenylcyclobutanone to the corresponding lactone at room temperature.³⁰ The catalyst reacts with the hydrogen peroxide to form flavin hydroperoxides **1.35**, **1.36**, which is the active catalyst. Due to the 3:1 asymmetric ratio **1.35** and **1.36** are unsuccessful for the asymmetric oxidation of sulfides (**Figure 1.16**).

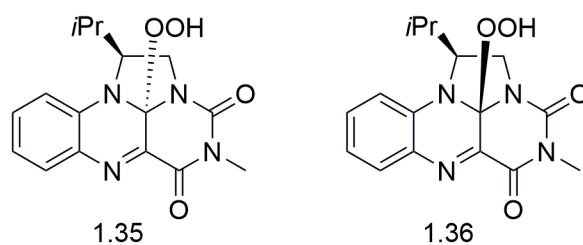


Figure 1.16 L-valinol derived bridged flavinium catalysts

Cibulka and coworkers designed a novel planar chiral flavinium salt **1.37**, which bears a phenyl cap that covers one side of the isoalloxazinium skeleton plane (**Figure 1.17**). Chiral HPLC was used to separate the racemic precatalyst followed by *N*-5

reductive alkylation to activate the catalyst. The catalyst performs oxidation of sulfides with 34-54% e.e. at 20 °C.³¹ The same research group also synthesized the flavin conjugated beta-cyclodextrin **1.38** for the oxidation of electron rich methyl phenyl sulfides to sulfoxides efficiently by hydrogen peroxide.³² The reaction provided near quantitative conversions with high enantioselectivity, reaching up to 80% e.e. The reaction was also performed in aqueous media with only 0.2 mol% catalyst loading.

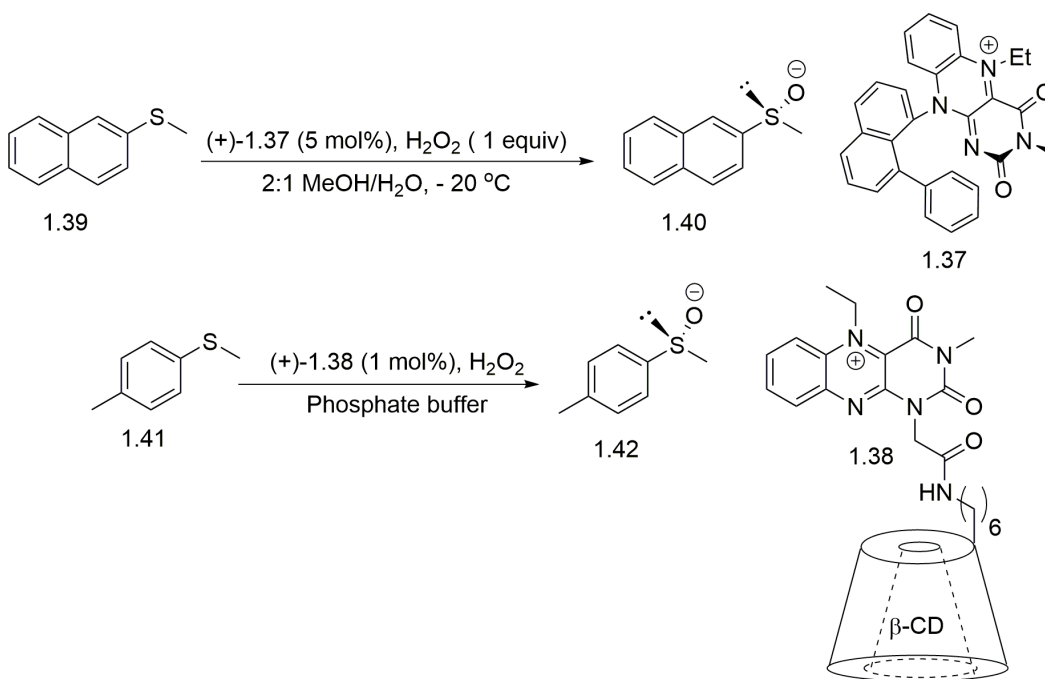


Figure 1.17 Chiral sulfide oxidation using flavin catalyst

Overall the sulfide and amine oxidation depend on the structures of the flavin catalysts, solvent effect, pH of the system, chirality within the catalyst. One of these criteria can affect the overall reaction mechanism and the rate of the reaction.

1.2.2 Flavin Catalyzed Nucleophilic Oxidation

During the flavin catalyzed nucleophilic oxidations, 4*a*-hydroperoxyflavin or 4*a*-hydroperoxy flavin anion attack the electrophilic center of the substrate and transfer oxygen to the substrate by forming the hydroxyl flavin. Hydroxy flavin eliminates one water molecule to form the oxidized flavin.

Furstoss and coworkers used isoalloxazinium catalyst **1.41** in the Baeyer-Villiger oxidation of cyclobutanones **1.39** to γ -lactone **1.40** in *t*-BuOH with two equivalents of H₂O₂. The reported reaction condition was limited to the four membered rings.³³

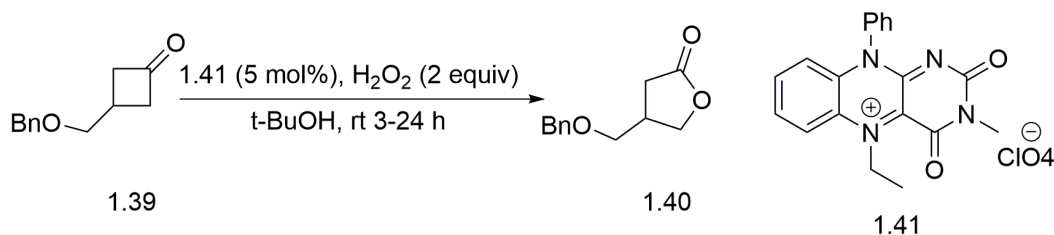


Figure 1.18 Isoalloxazinium catalyzed BVO of cyclobutanones with H₂O₂

Since the oxidizing power of the flavin catalyst correlated to the acidity of C(4*a*), electron deficient flavins were shown to be better oxidizing agents than the normal flavins. On the basis of previous statement, Furstoss and coworkers synthesized two flavin analogs **1.42** and **1.43** with nitrogen atom in the aromatic ring. This type of derivatives were electron deficient and suggesting increased acidity of C(4*a*) and higher catalytic activity. Under the same reaction condition **1.42** was found to be three times active than **1.41**. Unfortunately, **1.43** did not show any catalytic activity.³⁴

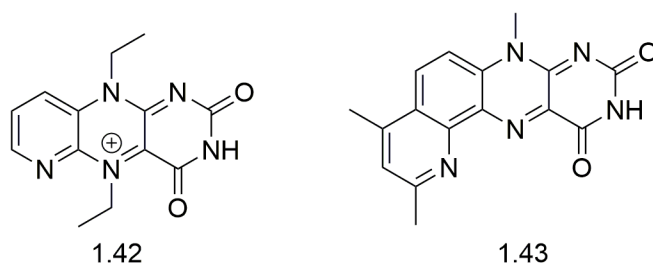


Figure 1.19 Electron deficient flavin catalysts

Murahashi and coworkers reported asymmetric Baeyer-Villiger oxidation of cyclobutanones by using a C₂-symmetric *bis*-alloxazinium perchlorate salt **1.44**.³⁵ Substrates with aromatic rings have pi-pi interaction with the catalyst to provide higher e.e. The report showed a maximum of 74% e.e. at -50 °C in a solvent mixture of CF₃CH₂OH/MeOH/H₂O. Like the previous report, the reaction condition was limited to cyclobutanones.

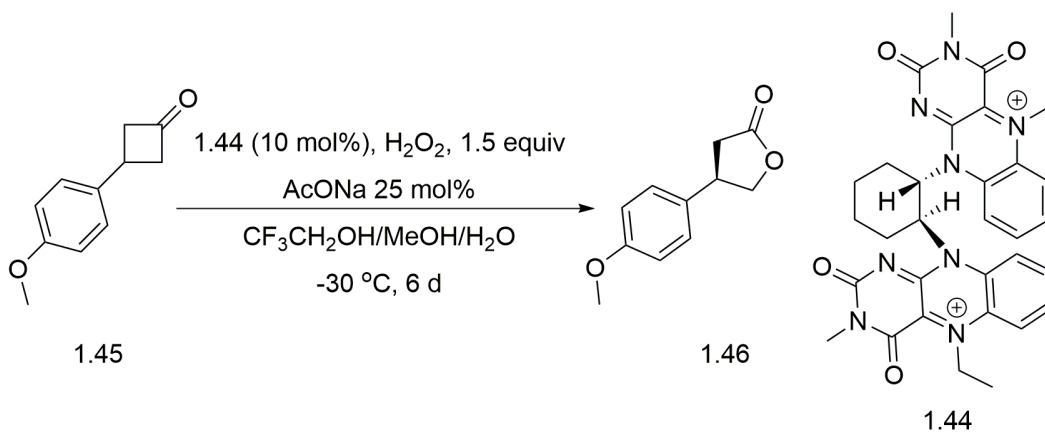


Figure 1.20 Asymmetric BVO of cyclobutanones

Murahashi and coworkers also revealed the use of riboflavin derived isoalloxazinium catalysts **1.47** to perform Baeyer-Villiger oxidation of cyclobutanones

aerobically using Zn as the reducing agent to turn over the catalytic cycle of the catalyst.³⁶ The process used molecular oxygen as the terminal oxidant. Unfortunately, no cyclopentanone or cyclohexanone oxidation was reported with the catalyst.

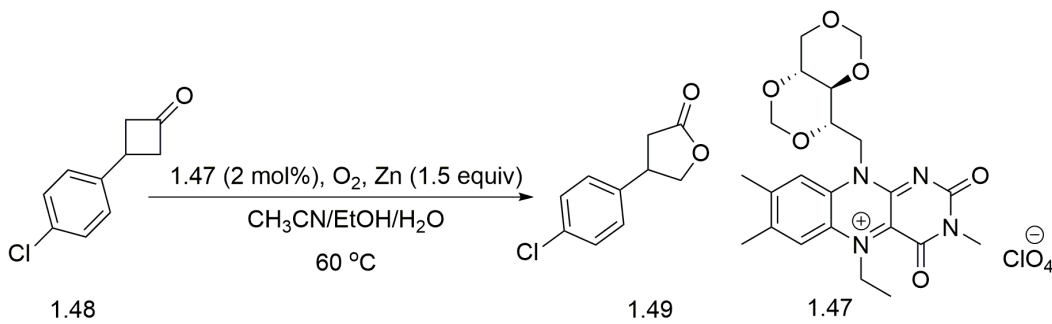


Figure 1.21 Aerobic Baeyer-Villiger oxidation

In summary the oxidation with flavin catalysts depend on a number factors - catalyst type - alloxazine or isoalloxazine, solvent, temperature, pH, additives, etc. The following **Table 1.2** showed a summary of the reactions.

Table 1.2 Summary of flavin catalyzed oxidations

Oxidation	S-oxidation		N-oxidation		BV oxidation	
	H ₂ O ₂	O ₂	H ₂ O ₂	O ₂	H ₂ O ₂	O ₂
Terminal oxidant	H ₂ O ₂	O ₂	H ₂ O ₂	O ₂	H ₂ O ₂	O ₂
Catalyst	I & II	I & II	I	I	I	I
Solvent	MeOH	CF ₃ CH ₂ OH	CF ₃ CH ₂ OH	MeOH	t-BuOH	Mixed
Reductant		NH ₂ NH ₂		NH ₂ NH ₂		Zn

Type I = alloxazinium

Type II = isoalloxazinium

1.3 Role of Flavin as Photocatalyst

Riboflavin and its derivatives are yellow in color and able to absorb visible light with a maximum absorption of blue light 440 nm. Upon exciting flavin with 440 nm, the redox power increases by up to 2.48 eV.³⁷ This represents the maximal (theoretical) energy of light, which can be used in photocatalysis by flavins. The use of artificial flavin in photochemical reaction has not been well investigated.

Flavin can exist in three redox states: oxidized, one-electron reduced (semiquinone) and two electron reduced state (fully reduced). Depending on the pH of the system each of these redox state can have three protonation states. All the states are described in the following **Figure 1.22**.³⁸

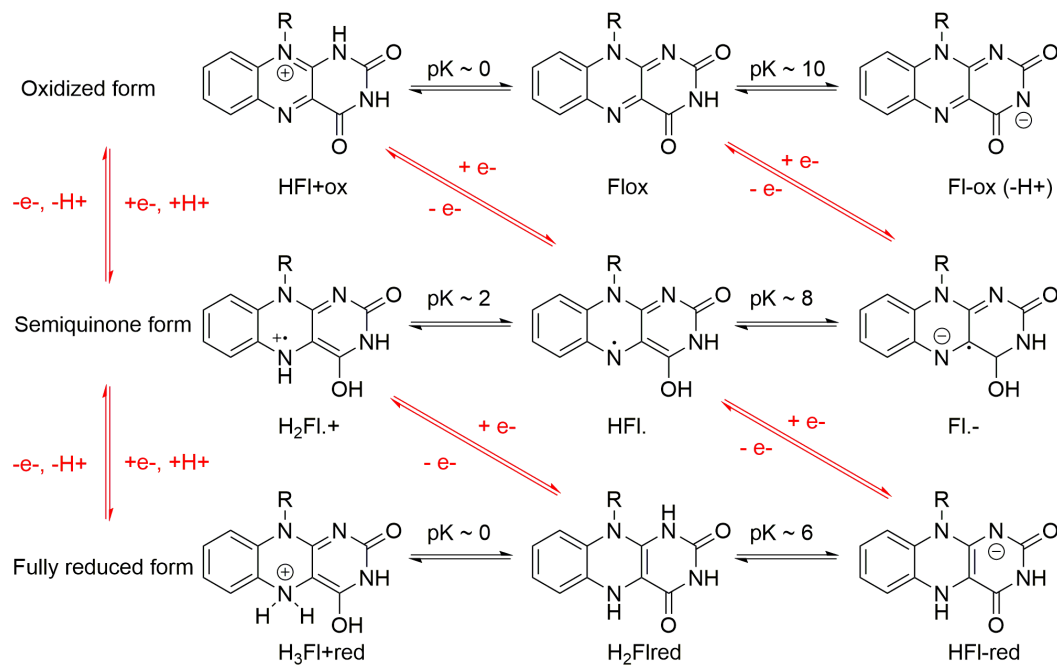


Figure 1.22 Different redox and protonation states of flavins³⁸

In principle, the flavin catalytic cycle can be used for reductions and as well as for oxidations. To reduce substrates a sacrificial electron donor like EDTA, trimethylamine, or triethanol amine is needed while for oxidation, the air is sufficient to reoxidize flavin.³⁸⁻³⁹

1.3.1 Molecular oxygen activation

The use of riboflavin as photosensitizer for the oxidation of ascorbic acid was reported in 1948 and the proposed mechanism considered the formation of water instead of hydrogen peroxide as the product for interaction of riboflavin with O₂.⁴⁰

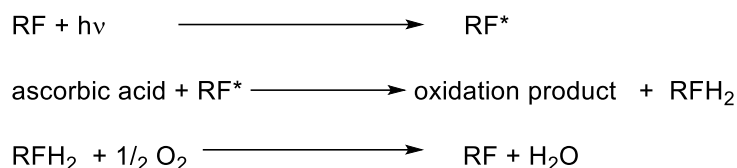


Figure 1.23 One of the first reported chemical reactions with flavins⁴⁰

Massey and coworkers summarized the chemical and biological versatility of riboflavin and described the possible reactions of the reduced flavin with oxygen. When oxidized flavin is irradiated with blue light the redox energy of the excited flavin is sufficient to activate substrates with lower reactivity. But when the reduced flavin converts back to the oxidized state, it can activate the molecular oxygen for subsequent reaction. The photocatalytic effect of flavin is shown in **Figure 1.24** with an example showing the oxidation of benzyl alcohol aerobically.⁴¹

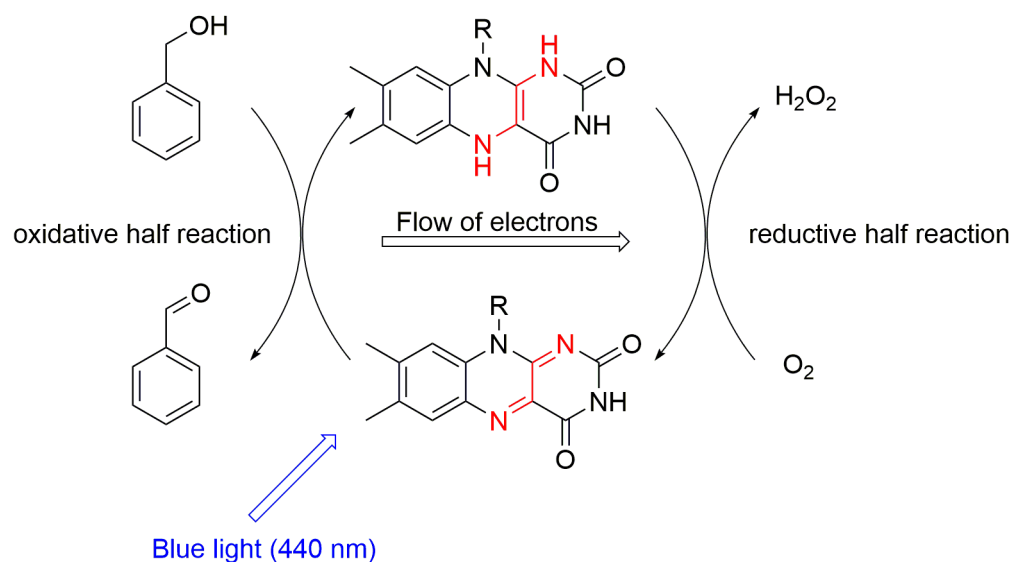


Figure 1.24 Catalytic cycle of flavin redox reactions

Fukuzumi and coworkers reported the effect of metal ions on the oxidation power of the photoexcited flavins. The effect of rare earth metals (Sc^{3+} , Lu^{3+} , and La^{3+}) is more pronounced than the effect of Mg^{2+} or Zn^{2+} ions. The metal interacts with one or both carbonyl groups of the flavin to shift the reduction potential of the singlet excited state ($^1\text{Fl}^*$) positively by 390 mV for Mg^{2+} and even higher by 780 mV for Sc^{3+} .⁴²

König and coworkers described that thiourea enhanced flavin photooxidation of benzyl alcohol in acetonitrile solution. The turn over number (TON) for the system was reported to be about 580. A possible reason for this observation was suggested to be the coordination of the thiourea with the flavin to make the flavin more electron deficient.⁴³

Among the different photochemistry of flavin, König and coworkers also reported the oxidation and deprotection of primary benzyl amines, oxidative cleavage of styrene and stilbenes, oxidation of benzyl ethers to esters or benzyl amides to the amides.⁴⁴

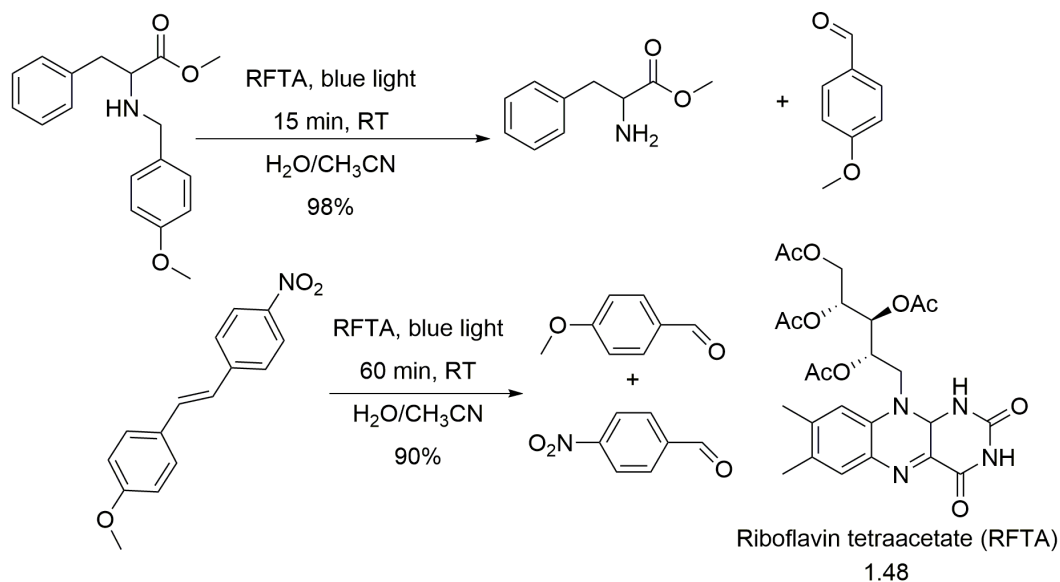


Figure 1.25 Examples of photocatalysis using flavin

1.3.2 Flavin-sensitized organic molecule degradation

Riboflavin and derivatives of riboflavin were used as a photosensitizer for the photocatalytic degradation of dyes and organic pollutants. Bio-cofactors FMN and FAD were also studied as photosensitizers in dye degradation. Previous studies confirm the degradation of amino acids,⁴⁵⁻⁴⁷ pesticides,⁴⁸ fungicides,⁴⁹⁻⁵⁰ herbicides,⁵¹⁻⁵² aromatic amines,⁵³ phenols,⁵⁴ glucose,⁵⁵ trinitrotoluene,⁵⁶ and triazines⁵⁷ using riboflavin, FMN and FAD. Due to the lower solubility and instability of the riboflavin and natural cofactors riboflavin tetraacetate (RTA) **1.48** and 3-methyl riboflavin tetraacetate **1.51** were also used for the degradation of organic compounds.⁵⁸⁻⁵⁹ The riboflavin was reported to be unstable and degrades to lumiflavin **1.49** and lumichrome **1.50** by losing its ribityl chain at higher and lower pH respectively. At neutral pH, riboflavin converts to lumichrome, which was considered to be the active photosensitizer for the degradation of organic compounds.⁶⁰

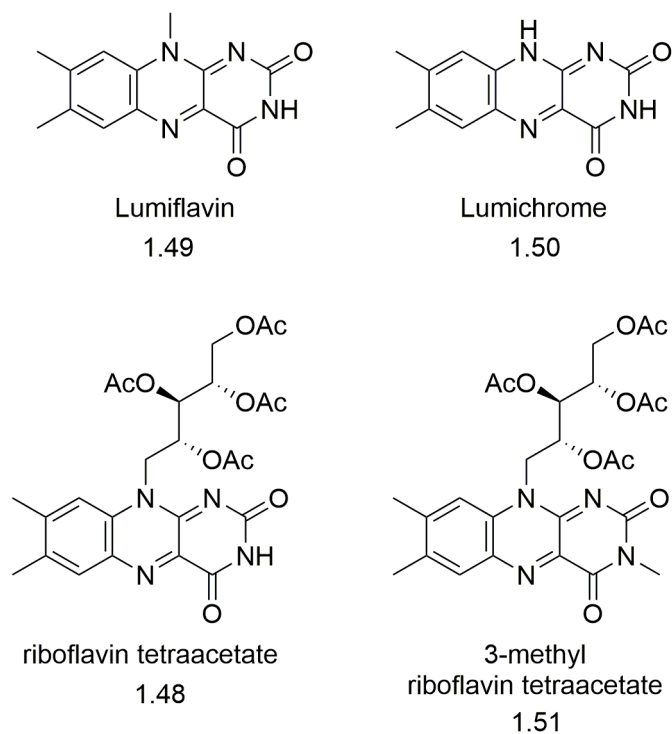


Figure 1.26 Flavin derivatives used for photo degradation of organic compounds

Two possible mechanisms were proposed for the degradation of organic molecules. The first mechanism proposed the excitation of the singlet flavin molecule to the triplet flavin using light. The triplet flavin can directly interact with the organic molecule to form the product. The other mechanism involved the formation of singlet oxygen by the interaction of triplet flavin with molecular oxygen. The singlet oxygen can interact with organic compounds to form the degraded products (**Figure 1.27**).⁶¹⁻⁶²

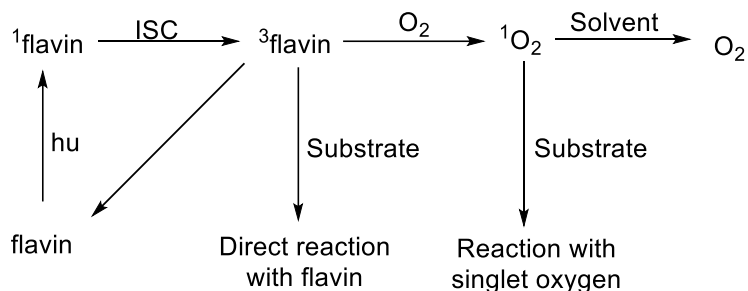


Figure 1.27 Possible reaction mechanisms for organic molecule degradation

In summary, riboflavin and its derivatives are able to oxidize different classes of organic compounds. An improvement in the flavin catalyst is required to increase the stability and the solubility of the photosensitizer in water to study the degradation of dyes and other organic environmental pollutants.

1.4 Medicinal importance of flavin

1.4.1 *Flavin dependent enzymes in cancer progression*

Epigenetic deregulation events are associated with every step of tumor development and progression. Epigenetics involve DNA methylation, histone modifications and expression of noncoding RNAs. All these modifications are interconnected and may work to establish and maintain specific gene activity states in normal cells (**Figure 1.28**).⁶³ Treatments for cancer involve the alterations of these modifications. Four epigenetic drugs were previously approved by US Food and Drug Administration (FDA). Two of those are DNA demethylating agents, 5-azacytidine and decitabine and two histone deacetylase (HDAC) inhibitors, vorinostat and valproic acid.

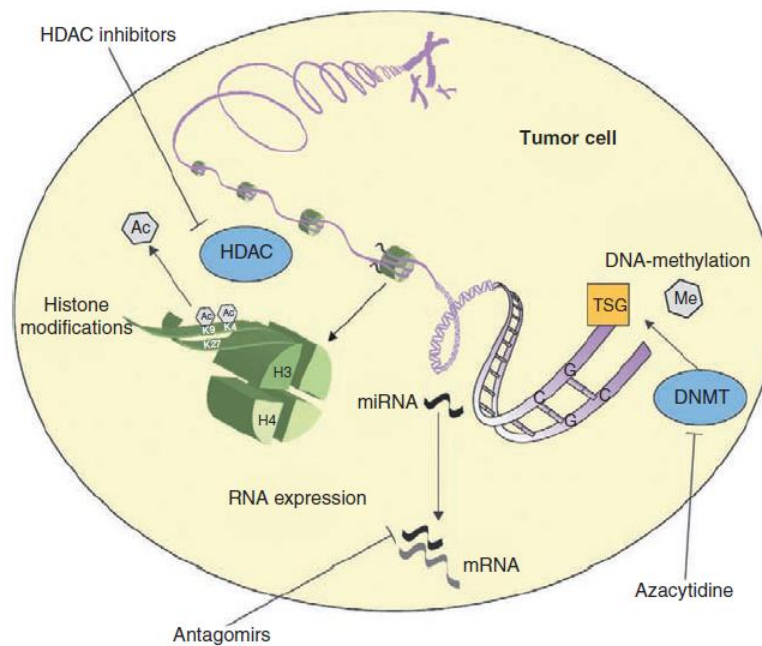


Figure 1.28 Common pathways of epigenetics and inhibition⁶⁴

Histone modification therapy of cancer is based on the generation of drugs that are able to interfere with the activity of enzymes involved in histone modifications.

Histone methylation is a heritable modification, which influences the state of the chromatin. Among the different histone modifications, methylation and especially demethylation are poorly understood. Histone methylation can be either an activating or repressing mark depending on the site and degree of methylation. Histone methylation occurs on lysine and arginine residues and is mediated by lysine methyltransferase and protein arginine methyltransferase respectively, which transfer a methyl group to the substrate from the cofactor S-adenosyl-L-methionine. These abnormalities can cause human diseases like cancer.⁶⁵

Shi and coworkers reported that histone methylation could be reversely modified by histone demethylases. Lysine specific demethylase I (LSD-1) is an amine oxidase that functions in concert with methyltransferase to maintain histone methylation patterns.⁶⁶

LSD-1 protein is a flavin dependent enzyme, which uses FAD to convert the methylated product to the corresponding demethylated one. A possible mechanism is shown in **Figure 1.29** explaining the demethylation process by forming formaldehyde and H_2O_2 as byproducts. Berger and coworkers also showed that p53, the tumor suppressor and transcriptional activator, is also regulated by LSD1. In human cells, LSD1 interacts with p53 to repress p53-mediated transcriptional activation and to inhibit the role of p53 in promoting apoptosis.⁶⁷

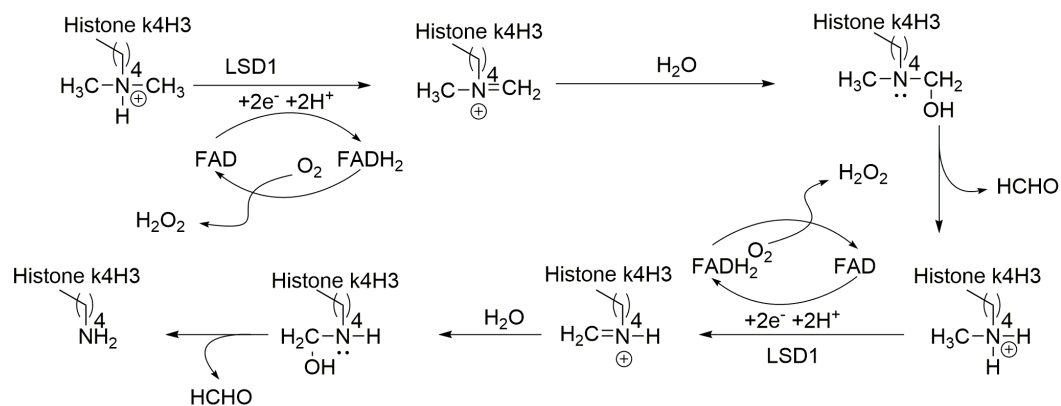


Figure 1.29 A possible pathway for demethylation of diMeK4H3 by LSD1

Fischer and coworkers reported the use of deazaflavin derivatives as the inhibitor of p53 ubiquitination, which is known as tumor suppressor. p53 is central to the protection of mammalian cells against genetic damage and p53 becomes dysfunctional in a large proportion of the cancer cells.⁶⁸ The HDM2 and p53 genes are linked in a negative feedback loop, in which p53 activates HDM2 and the latter promoted degradation of p53 protein as an ubiquitin E3 ligase. To reactivate the p53 activities two strategies can be applied – blocking the protein-protein interaction between p53 and N-terminal domain of HDM2, or by inhibiting the E3 ligase activity of HDM2.

A series of deazaflavins were synthesized by the same group to study the structure activity relationships (SARs) to HDM2 E3 ligase inhibition and 10-aryl

substituted deazaflavins were found to be inhibit the E3 ligase. Most active structures were given in the following **table 1.3**.

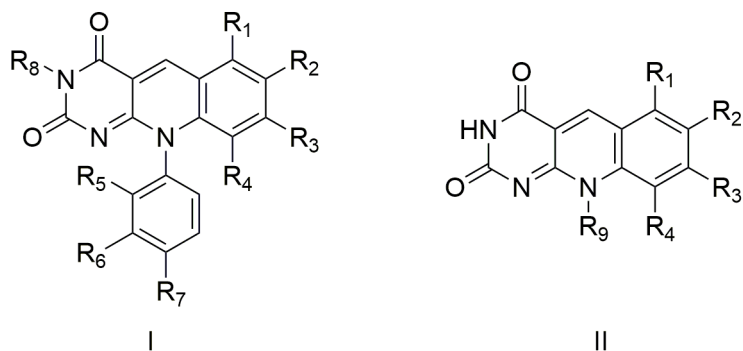


Table 1.3 Inhibition of ubiquitination of p53 by HDM268

Type	R1	R2	R3	R4	R5	R6	R7	R8	R9	IC ₅₀ (μM)
I	H	H	H	CF ₃	H	H	H	H	-	17.5
I	H	H	H	CF ₃	H	H	Cl	H	-	11.9
I	H	H	H	CF ₃	H	Cl	H	H	-	1.5
I	H	H	H	CF ₃	H	Cl	Cl	H	-	10.7
I	H	H	H	CF ₃	H	F	H	H	-	12.3
I	H	H	H	CF ₃	H	H	F	H	-	13.1
I	H	H	H	CF ₃	H	CH ₃	H	H	-	8.4
II	H	H	H	CF ₃	-	-	-	H	Bn	>100

1.4.2 DNA modification using flavin

UV-radiation of the biosphere causes DNA damage by the formation of cyclobutane pyrimidine dimers (CPDs), which can cause skin cancer. Photolyase, a photoenzyme, responsible for repairing UV-damaged DNA.⁶⁹ A number of biomimetic

systems have been synthesized to mimic the repair by photolyase. Although the DNA repair by photolyase is very efficient with quantum yield 0.80-0.95⁶⁹ but the model systems were low efficient, for example, 0.016-0.06 for flavin-thymine dimer systems⁷⁰ and 0.06-0.40 for indole-thymine systems.⁷¹ Zhong and coworkers reported the repair model of CPDs using a biomimetic lumiflavin-thymine dimer adduct. The general mechanism involves the donation of single electron from flavin to the CPD upon exciting isoalloxazine ring with blue light. The cyclobutane ring then splits to the monomeric form and returns the electron to the flavin. (**Figure 1.30**)

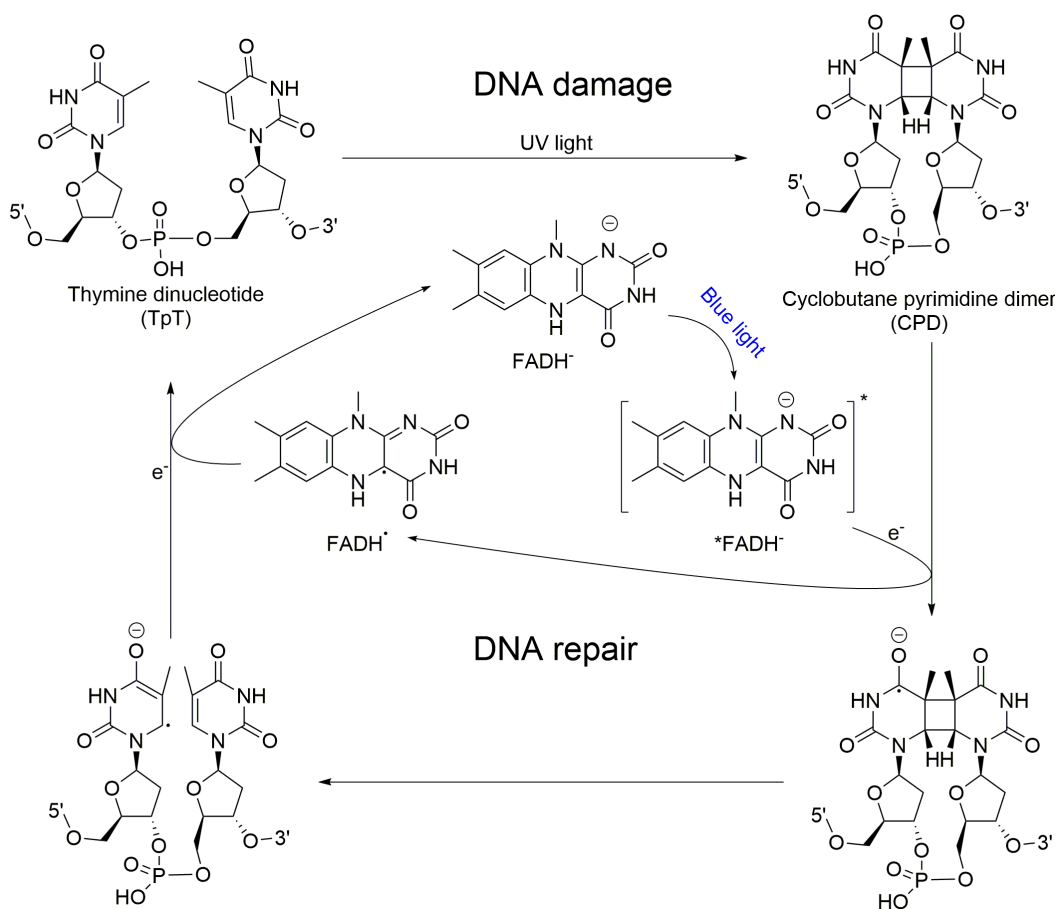


Figure 1.30 Damaging and repairing of DNA using flavin dependent photolyase

1.4.3 Flavin as biomarker

Riboflavin is an essential cofactor for cellular metabolism and highly regulated in metabolically active cells. Tumor cells are highly energy demanding and required relatively higher amount of flavin cofactors for the catabolic enzymes, Fabian and coworkers designed FMN coated Ultra Small Super Paramagnetic Iron Oxide nanoparticles (USPIO) (**Figure 1.31**) for the detection of riboflavin carrier proteins. High efficiency of labeling of cancer cells like PC-3, DU-145, LnCap and other endothelial cells were detected with this novel biomarker.⁷²

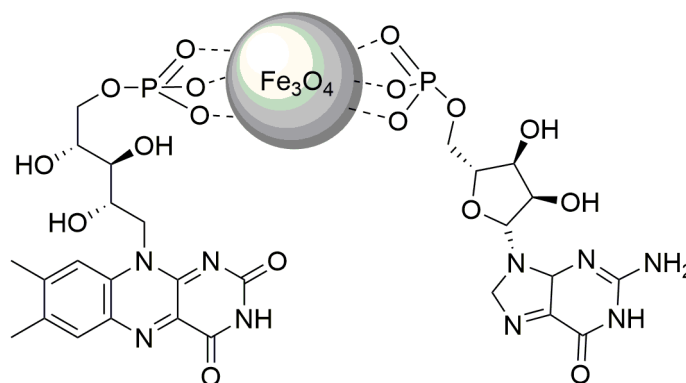


Figure 1.31 Riboflavin derived biomarker for detecting tumor cell

1.4.4 Flavin drug carrier

Dodecin protein from *Halobacterium salinarum* has higher affinity towards riboflavin. Nolls group developed a drug-riboflavin molecule bound to dodecin to deliver the drug to the target position. Dodecin binds to the oxidized flavin with higher affinity and the flavin is reduced with blue light, the drug can be delivered to the desired location at higher accuracy. (**Figure 1.32**)⁷³

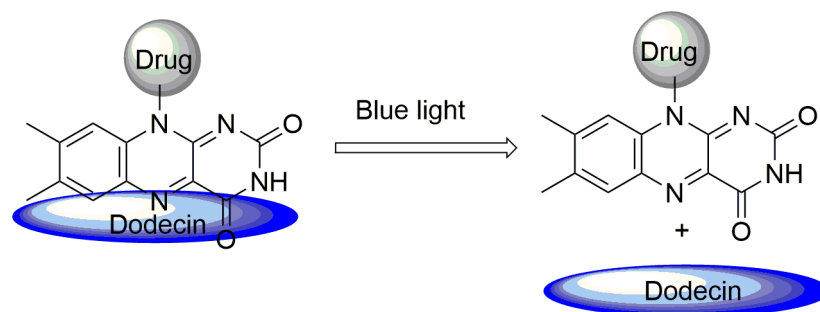


Figure 1.32 Blue light induced dissociation of flavin from dodecin

1.5 Deazaflavin

Generally 5-deazaflavins were known as deazaflavins. Due to the similar structural features, both flavin and deazaflavin have similar chemistry like activation of molecular oxygen. But in nature the role of deazaflavins has some characteristic functions due to different redox potential compared to the flavins.⁷⁴

1.5.1 Biological importance of deazaflavin

Deazaflavins are widely studied for their selective hydride transfer catalysis. 7,8-Didemethyl-8-hydroxy-5-deazariboflavin is one of the members of deazariboflavin family, known as F₄₂₀, (**Figure 1.33**) is able to transfer hydride with NAD(P)H in equilibrium. To study the biological importance of natural cofactors, a mimetic structure FO is used widely that lacks the phosphate and the glutamate chain. Anionic FO was studied for the repair of DNA as photolyase and recently it was found to be a light harvesting molecule in *Drosophila*. F₄₂₀ also plays an important role in the conversion of carbon dioxide to methane enzymatically.⁷⁵

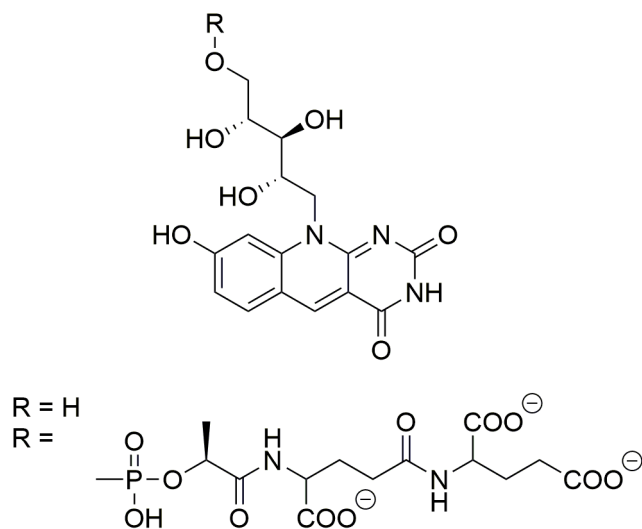


Figure 1.33 Structures of FO and F₄₂₀

Yoneda and coworkers reported the total synthesis of F₄₂₀ and also a series of applications of deazaflavin derivatives. They reported the aerobic oxidation of the benzaldehyde and benzylamine also the chiral reduction of ethyl benzoylformate in the presence of chiral ligand (**Figure 1.34**).⁷⁶⁻⁷⁸ A class of deazaflavins were reported as cancer cell inhibitor (section 1.4.1).

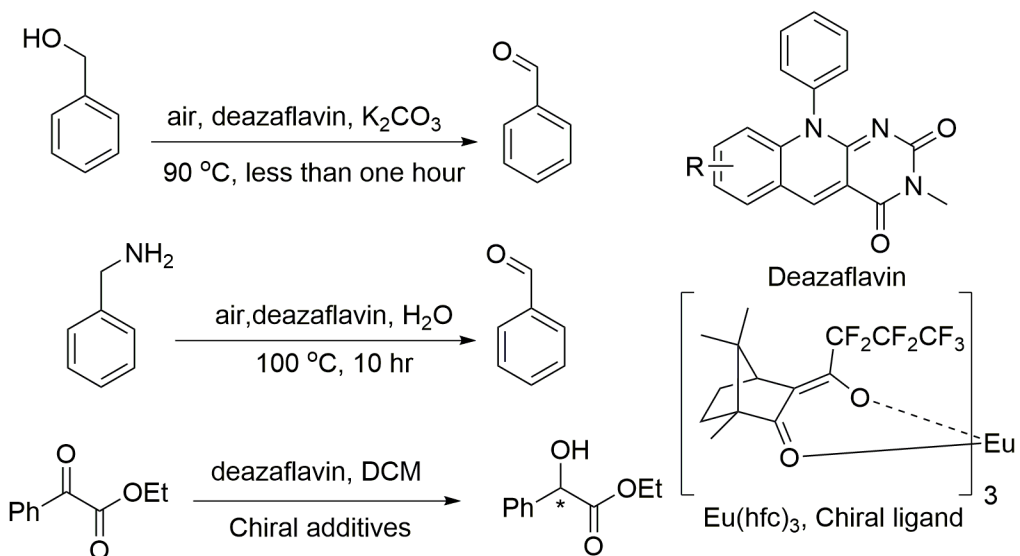


Figure 1.34 Oxidative chemistry of deazaflavins

A convenient method of synthesizing FO and report its binding capacity towards the Fno enzyme is discussed later in chapter seven.

Outline of the dissertation

In this dissertation, we will discuss the reaction kinetics of the organocatalytic Dakin oxidation with possible reaction mechanism. Aerobic oxidation of pre-aromatic heterocyclic compounds will also be discussed. A major part of the dissertation will focus on the development of new biomimetic organocatalysts depending on the applications like dye degradation and molecular oxygen activation in homogeneous and heterogeneous systems. The function of artificial flavins as MCF7 cell inhibitor will be discussed with the synthesis of artificial flavins. We will also focus on the convenient synthesis of FO and flavin catalysts.

Chapter 2

Flavin-catalyzed Dakin Oxidation

2.1 Dakin oxidation

Dakin reported the oxidation of hydroxy benzaldehydes and acetophenones and related compounds in 1909.⁷⁹ The reaction was found to be mechanistically similar to the Baeyer-Villiger reaction, which was reported in 1899, but not fully understood until almost 60 years.⁸⁰ The Dakin oxidation has been considered as a variant of the Baeyer-Villiger oxidation since the mid-to late 70's.

2.1.1 *General reaction mechanism*

Generally, both the Baeyer-Villiger oxidation and the Dakin oxidation involve the nucleophilic attack of a peroxide or peroxy acid to the carbonyl group to form a high-energy and tetrahedral Criegee intermediate, which degrades by 1,2-aryl(or alkyl) migration. The Dakin oxidation involves an extra hydrolysis step of the Baeyer-Villiger oxidized product (phenyl formate to phenol). Both mechanisms were compared in **Figure 2.1**. Usually in the Dakin oxidation, the substrates are electron rich aromatic aldehydes and ketones and the reaction is base catalyzed. A variant of the Dakin oxidation includes the acid-catalyzed reaction of electron-deficient aromatic aldehydes, however, this leads to a different product due to migratory aptitude of substituents at the respective Criegee intermediates.⁸¹ In many ways, the Dakin oxidation is simply a subset of a larger class of Baeyer-Villiger oxidations, followed by in situ hydrolysis of the intermediate ester..

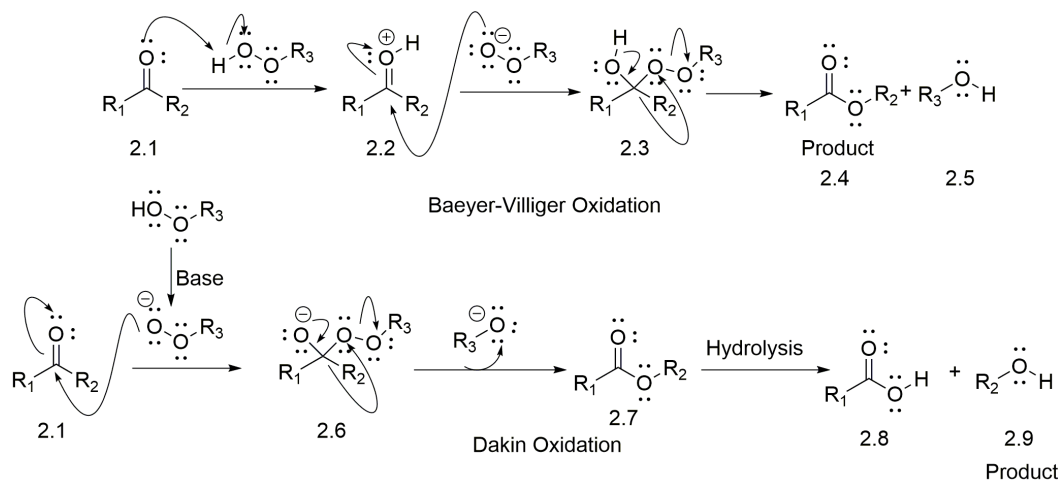


Figure 2.1 General reaction mechanism for BVO and Dakin oxidation

2.1.2 Detailed reaction mechanism

The mechanism of Dakin oxidation consists of three major steps

1. Nucleophilic attack on the substrate

This step depends on the nucleophilic nature of the hydroperoxide anion and electrophilicity of the substrate. The hydroperoxide with lower pKa will form a stronger nucleophile in presence of base and also a substrate containing an electron withdrawing group will form a better electrophilic carbonyl center.

2. 1,2-Aryl migration

This step depends on the ability of migration and stability of the leaving group. The electron rich substrates will enhance the rate of migration and also a better leaving group will enhance the rate of reaction.

3. Hydrolysis of the intermediate

The hydrolysis of the ester will be dependent on the pH of the reaction. A higher pH of the reaction will increase the rate of hydrolysis. Also the presence of hydroxyl group in the aromatic group enhances the rate of hydrolysis. Hansen and coworkers

reported the hydrolysis of catechol monoacetate is more than 700 times faster than the hydrolysis of phenyl acetate.⁸² Since the hydroxyl group is not a good leaving group, the aromatic hydroxyl substituents may be able to provide strong anchimeric assistance for the heterolytic cleavage of the O-O bond (*o*-hydroxyphenyl ~ *p*-hydroxyphenyl >> phenyl).⁸³

The role of reagents on the reaction mechanism

1. Role of base

The primary roles of the base are to deprotonate the salicylaldehyde (pKa ~ 8.17), and the hydrogen peroxide (pKa ~11.75). Because of the large difference in pKa's of the substrate and nucleophile, it is important in the uncatalyzed Dakin oxidation to have excess base, which will deprotonate the hydrogen peroxide to form a better nucleophile (hydrogen peroxide anion). Additionally, the hydrolysis of the ester depends on the basicity of the solution. With excess strong base, like NaOH, the reaction rate is independent of the base concentration and the rate-determining step is considered to be the 1,2-aryl migration of the intermediate. Hocking and his group studied the reaction rate with variable amounts of NaOH and reported that the rate is dependent on the concentration of NaOH. When the pH of the solution dropped to less than 10, the reaction yield was low and this indicated the lower concentration of the hydroperoxide anion (active nucleophile).⁸⁴ Also, at higher pH (excess base) the phenol will exist as ionized form, which undergoes 1,2-aryl migration faster than the protonated phenol.

2. Role of peroxide

In the Dakin oxidation, although hydrogen peroxide was used as an oxidant, the active nucleophile is the hydroperoxide anion, which will form after deprotonation with

base. The amount of nucleophile is dependent on the pH of the reaction. Due to the high pH of systems with excess NaOH solution, the dissociation of the hydrogen peroxide did not impact the reaction rate; however, in limited or weak base conditions the deprotonation of the hydrogen peroxide could be rate determining. Peroxide structures having more acidic protons will increase the capability to form the active peroxide anion and thus enhance the rate of the reaction with limited amount of base. The structure of the peroxide will also play an important role in the 1,2-phenyl migration step, if the leaving group (RO^-) is stable after the migration, then the rate of reaction will be increased in the presence of stabilized RO^- .

3. Role of substrate

The structure of the substrate plays an important role in forming the product and also in determining the rate-determining step. Due to lower pK_a of the phenolic group compared to the H_2O_2 , the deprotonated phenol will predominate in presence of base.⁸⁴ Deprotonated salicylaldehyde will affect the initial attack of the nucleophile on the carbonyl carbon, which will decrease its electrophilicity by donation of electron density from the phenolic oxygen through resonance. On the other hand, the deprotonated phenol will increase the electron density on the migrating carbon to facilitate the 1,2-phenyl migration to form the intermediate. Dakin, in his original report, showed the successful oxidation of benzaldehyde derivatives with hydroxyl group at ortho or para positions of the aldehyde group and some unsuccessful oxidations of benzaldehydes with a hydroxyl group meta to the aldehyde group.⁷⁹ This supports the claim that 1,2-phenyl migration is slower than the deprotonation of salicylaldehyde, hydrogen peroxide, and the nucleophilic attack of the peroxide anion on the carbonyl carbon in presence of excess strong base.

Several research groups studied the Dakin oxidation mechanism and the overall reaction mechanism is shown in detail in **Figure 2.2**, using salicylaldehyde as substrate and considering both higher and lower concentration of base. The introduction of weak base limited the formation of hydroperoxide anion, which will lower the effective concentration of nucleophile and hence lower the overall rate of formation of the product. The use of limited base (or weaker base) may change the usual rate-determining step (1,2-aryl migration) to the formation of the nucleophile.

Two alternate options can be utilized to change the rate-determining step and enhance the reaction rate in presence of limited or weaker base. The first alternative is the use of peroxide with lower pKa, which can be deprotonated at lower base concentration (low pH) to restore the available concentration of the nucleophile. Also the use of peroxide with stabilized "R" group will stabilize the leaving group "RO-" formed after 1,2-phenyl migration to enhance the rate of the reaction. An alkyl peroxide with lower pKa and more stable leaving group will be useful to successfully perform the Dakin oxidation with weak bases.

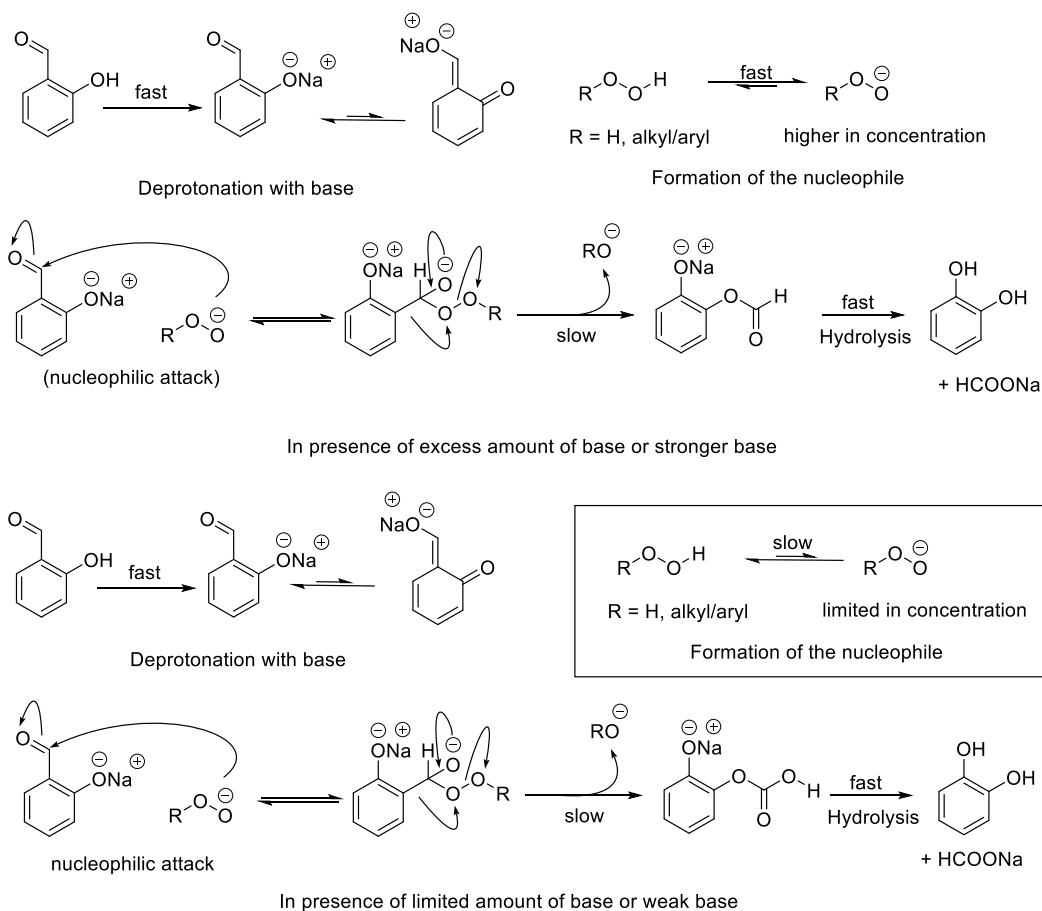


Figure 2.2 Plausible Dakin oxidation mechanism with strong and weak bases

2.2 Current methods for Dakin oxidation

Methyltrioxorhenium (MTO) **2.1** was used as a catalyst to accomplish Dakin oxidation of *meta*- or *para*-methoxy or -hydroxyl substituted benzaldehydes to form the corresponding phenols. The terminal oxidant used was H_2O_2 and the active oxidant was the product formed with H_2O_2 and MTO, a bis-peroxo metal complex $[CH_3Re(O_2)_2]$, dpRe **2.3**. The reaction was performed with excess H_2O_2 , 2 mol% of MTO, at 50 °C and usually

for 24 hours. In some cases noticeable amount of benzoic acid and unhydrolyzed ester were also isolated.⁸⁵

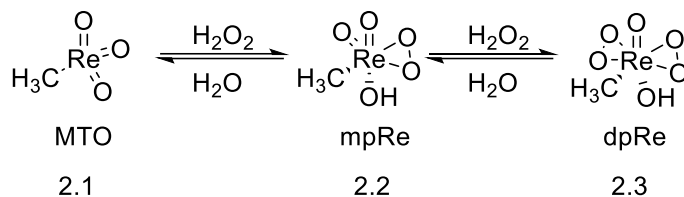


Figure 2.3 Methyltrioxorhenium (MTO), and oxidized derivatives

The same catalyst was also used in combination with ionic liquid [bmim]PF₆ **2.1** as solvent.⁸⁶ The reaction was found to be faster in ionic liquid than in the previously reported organic solvent.

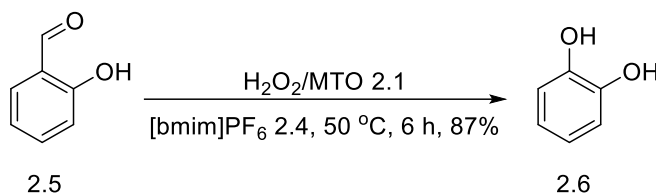


Figure 2.4 MTO catalyzed Dakin oxidation in ionic liquid

Solvent free Dakin oxidation was accomplished by mixing benzaldehyde and solid *m*-CPBA in a mortar-pestle. A range of non-hydroxylated benzaldehydes were converted to the corresponding phenols in the absence of base.⁸⁷

Sodium percarbonate (Na₂CO₃ · 1.5 H₂O₂) **2.7** was also reported as stoichiometric oxidant for the oxidation of a range of hydroxyl benzaldehyde and acetophenones.⁸⁸ Urea-hydrogen peroxide **2.8** was also used as stoichiometric oxidant for the oxidation of benzaldehydes and acetophenones. The reaction was operated at 85 °C.⁹⁰

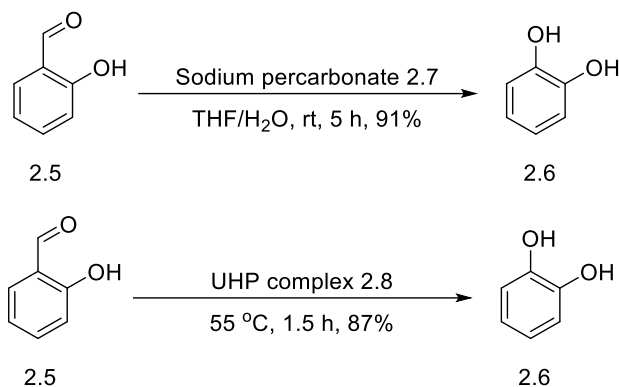


Figure 2.5 Dakin oxidation with different oxidants

Dakin oxidation was also reported to occur under acidic conditions. The reported reaction conditions incorporate 5 equivalents of H_3BO_3 , 2 equivalent of H_2O_2 and excess H_2SO_4 ; Benzoic acid was also formed as a byproduct.⁸⁹

2.3 Flavin catalyzed organocatalytic Dakin oxidation

Nature performs Baeyer-Villiger oxidation, sulfur and amine oxidation using flavin dependent monooxygenases, which has been described in detail in section 1.1. Although different reaction conditions were reported for Dakin oxidation, some of the conditions required heat, metal catalysts, harsh pH, stoichiometric powerful oxidant and extended reaction times. Due to the similarity in the mechanism of the Dakin oxidation and the Baeyer-Villiger oxidation, we have designed an approach to study the Dakin oxidation with biomimetic flavin catalysts and study the reaction kinetics in details.

2.3.1 Synthesis of Flavinium catalysts

To study the Dakin oxidation with artificial flavin analogs, five flavinium catalysts were used initially which were synthesized and characterized by Dr. Chen in our lab according to the **Figure 2.5**.⁹¹

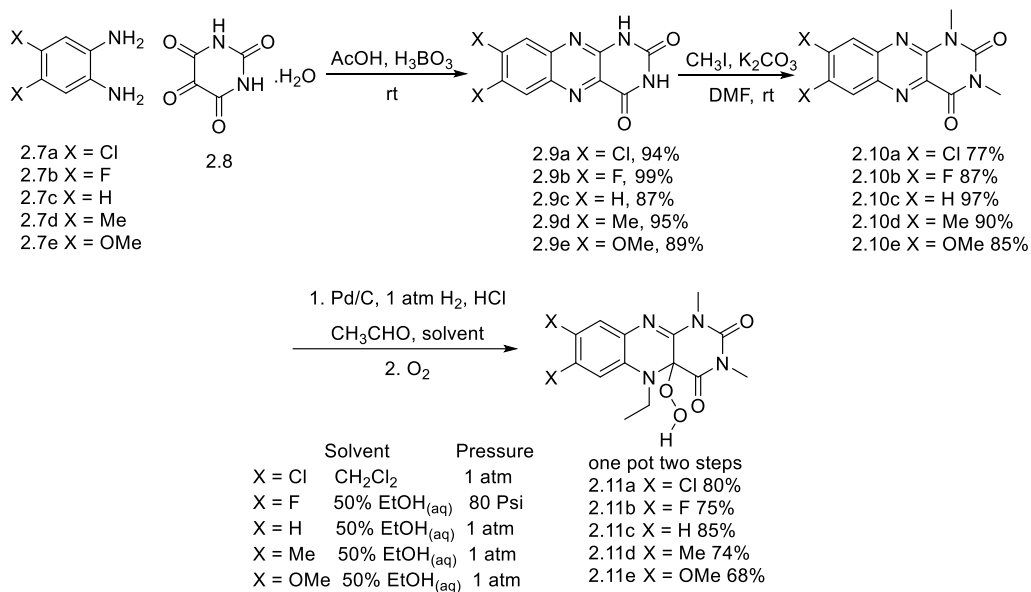


Figure 2.6 Synthesis of flavinium catalysts

2.3.2 Optimization of reaction condition

Dakin oxidation was studied using flavinium catalysts with H₂O₂ as the terminal oxidant to mimic the H₂O₂ mediated shunt process of the catalytic cycle.

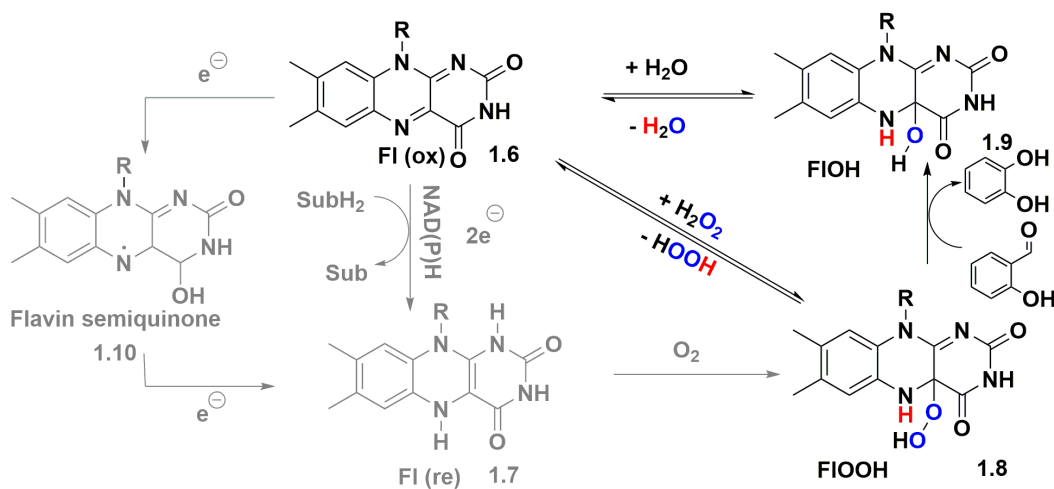


Figure 2.7 Flavin catalytic cycle with the shunt process

The reaction conditions were optimized by studying the Dakin reaction of salicylaldehyde in presence of different solvents ranging from polar protic to non-polar solvents in combination with a series of bases (**Table 2.1**). All possible combinations of solvents and bases (1 equiv.) were studied with H₂O₂ (1 equiv). Each reaction was monitored by analyzing a reaction aliquot using high performance liquid chromatography (HPLC) with a Phenomenex PFP column. Each reaction was performed with a known amount of an internal standard. A 10 ul reaction aliquot was withdrawn just before adding the terminal oxidant (H₂O₂). After the addition of H₂O₂, two reaction aliquots (10 ul) were collected after 30 min and 60 min of the reaction and quenched with 2 mL of Na₂S₂O₄ solution to monitor the consumption of the starting material (salicylaldehyde) and each experiment was duplicated to confirm the reproducibility of the results. 85% Water and 15% acetonitrile with 0.1% formic acid was used as the mobile phase. Both control and catalyzed reactions for each solvent-base pair were run in parallel at constant temperature 25 °C. For the initial study, 7,8-diH alloxazinium catalyst **2.11C** was used. The reaction was studied with 1 equiv of base 1 mol% catalyst and 1 equiv H₂O₂. **Figure 2.9- 2.22** indicates the effect of solvents and bases on the reaction rate.

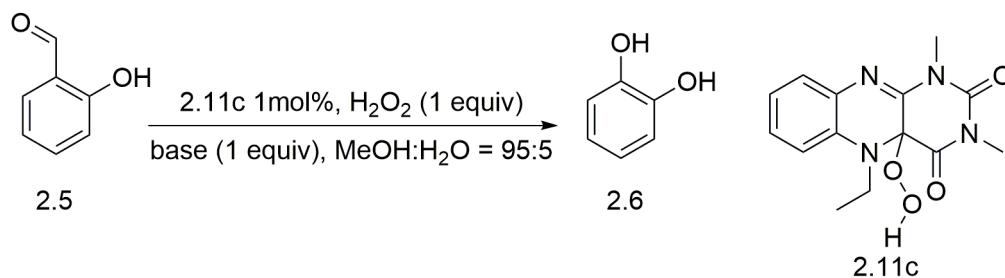


Figure 2.8 General reaction condition for Dakin condition

Table 2.1 List of solvents and bases

Solvents	Base
Methanol	NaOH
Ethanol	KOH
<i>iso</i> -Propanol	NaHCO ₃
<i>tert</i> -Butanol	KHCO ₃
DMSO	Na ₂ CO ₃
DMF	K ₂ CO ₃
THF	
1,4-Dioxane	
Trifluoroethanol	

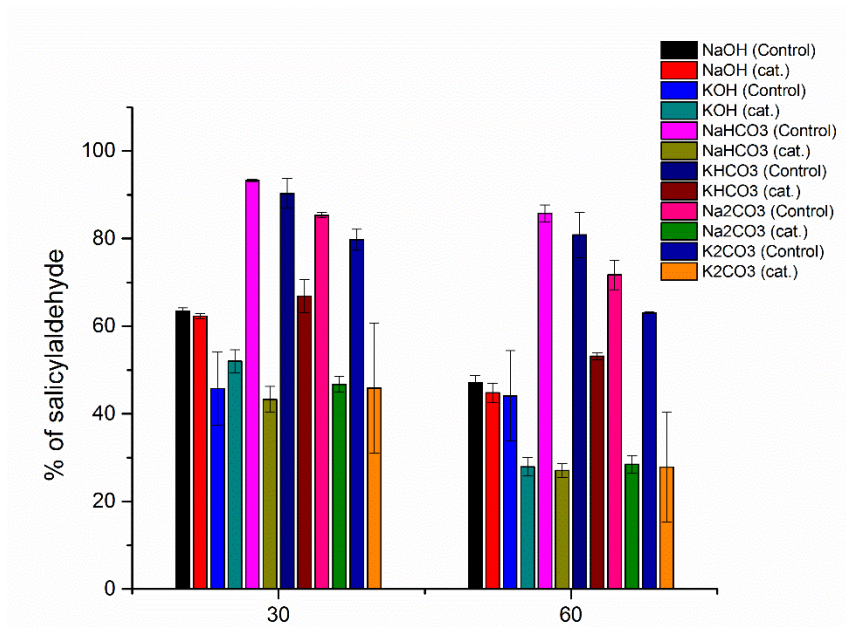


Figure 2.9 Effect of methanol:water (95:5) on bases

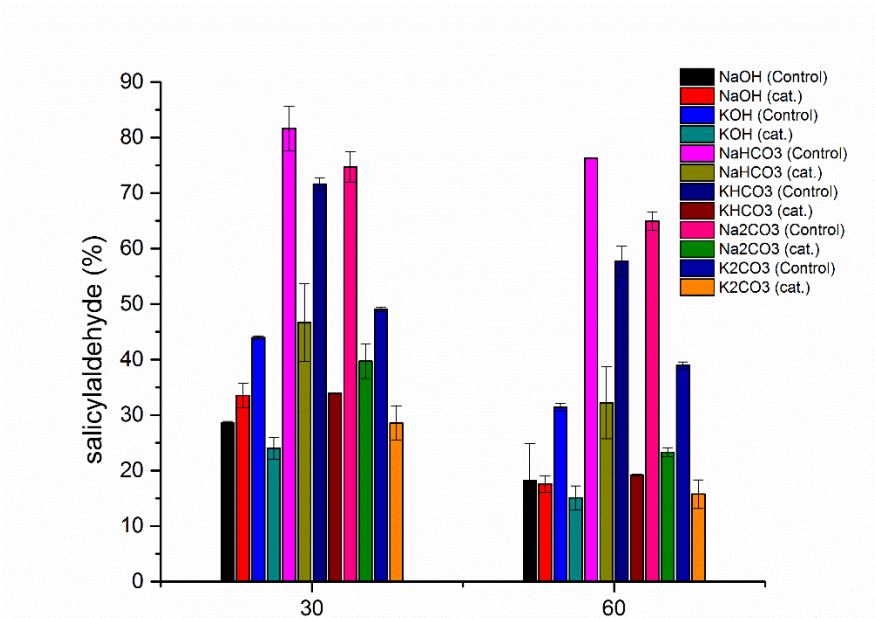


Figure 2.10 Effect of aqueous ethanol on bases

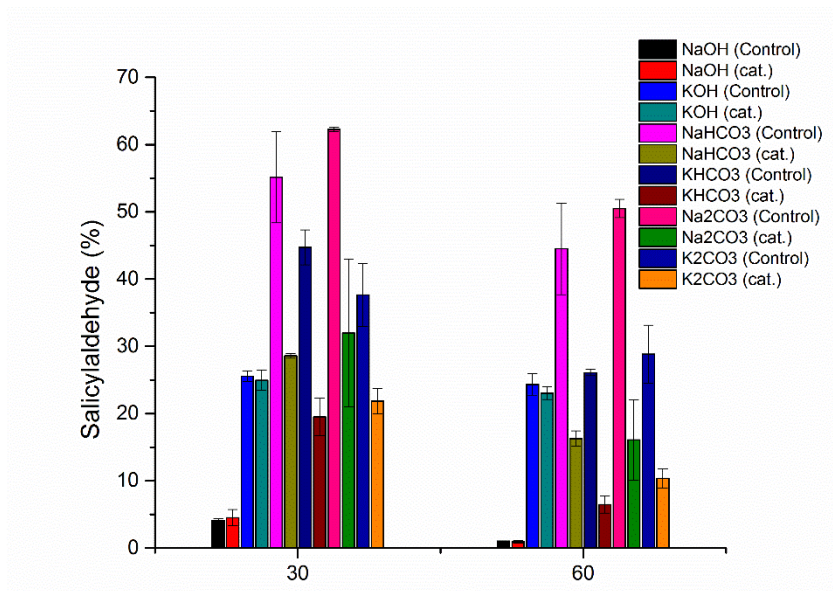


Figure 2.11 Effect of isopropanol on bases

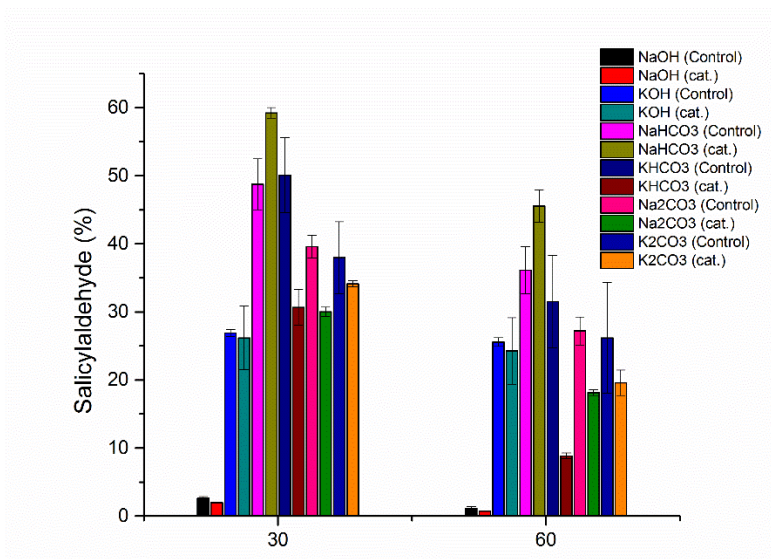


Figure 2.12 Effect of t-Butanol on bases

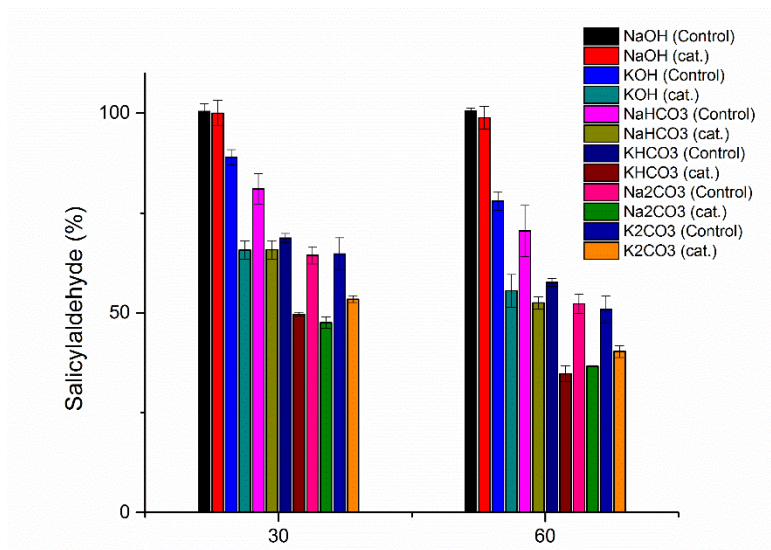


Figure 2.13 Effect of DMSO on bases

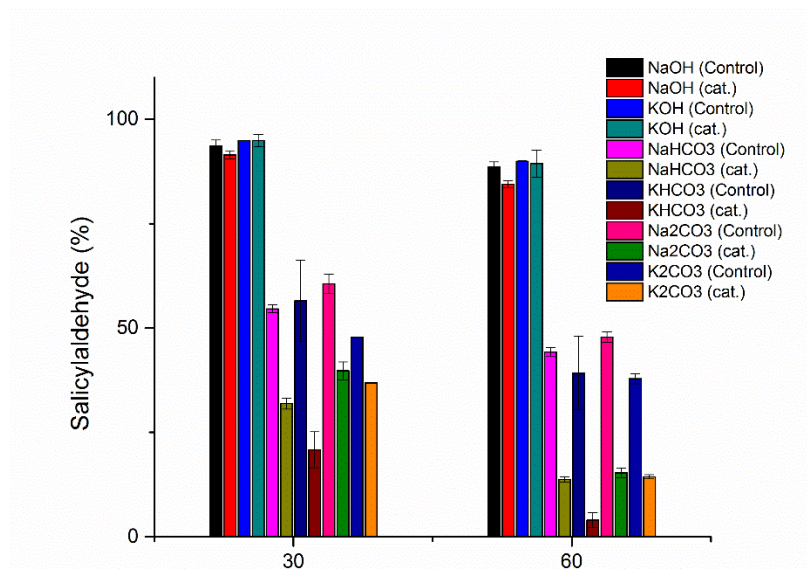


Figure 2.14 Effect of DMF on bases

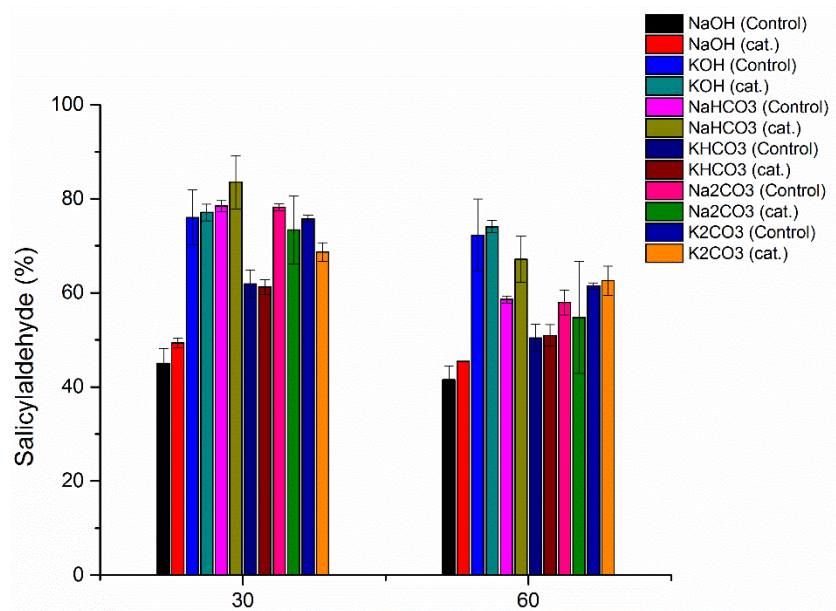


Figure 2.15 Effect of dioxane on bases

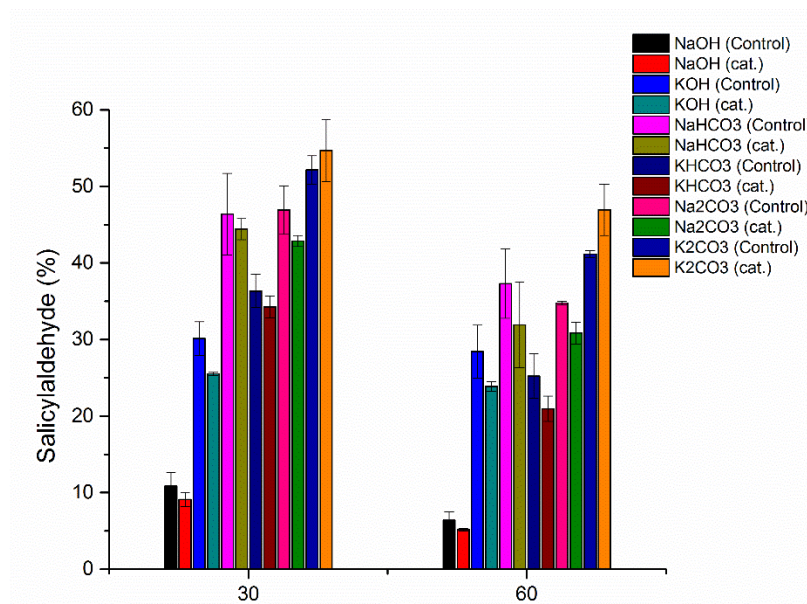


Figure 2.16 Effect of THF on bases

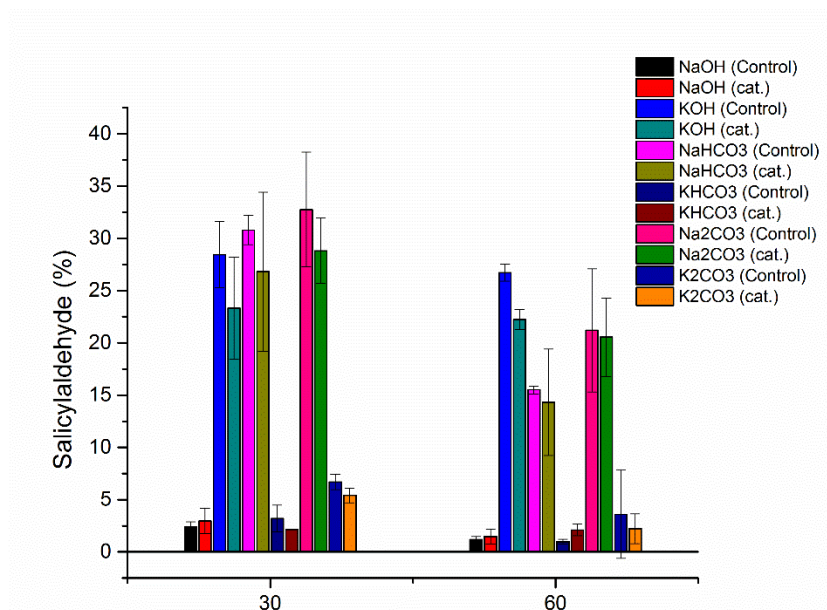


Figure 2.17 Effect of trifluoroethanol on bases

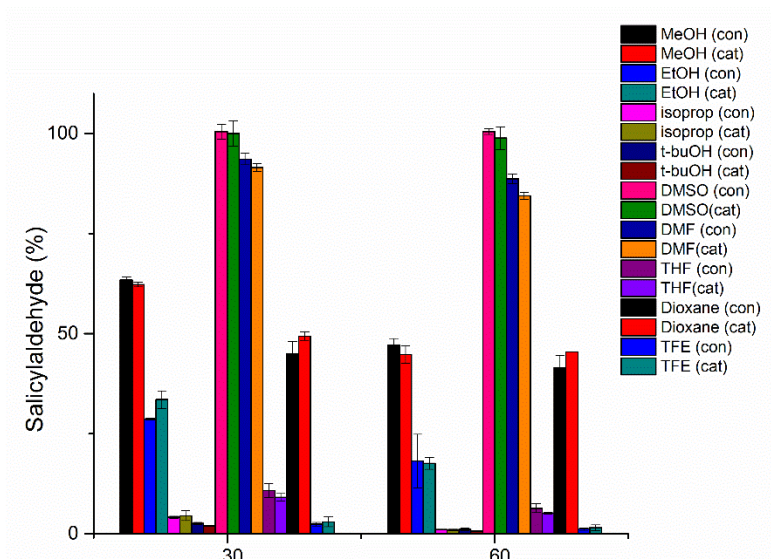


Figure 2.18 Effect of solvents on NaOH

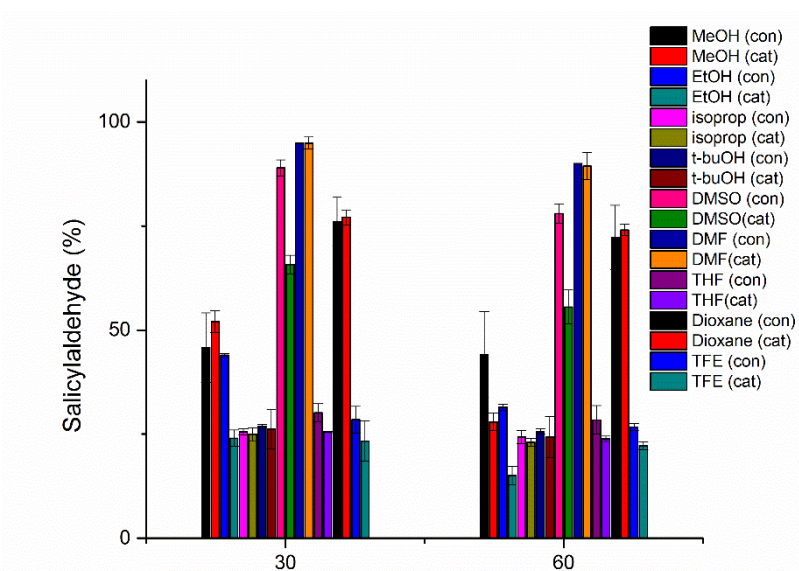


Figure 2.19 Effect of solvents on KOH

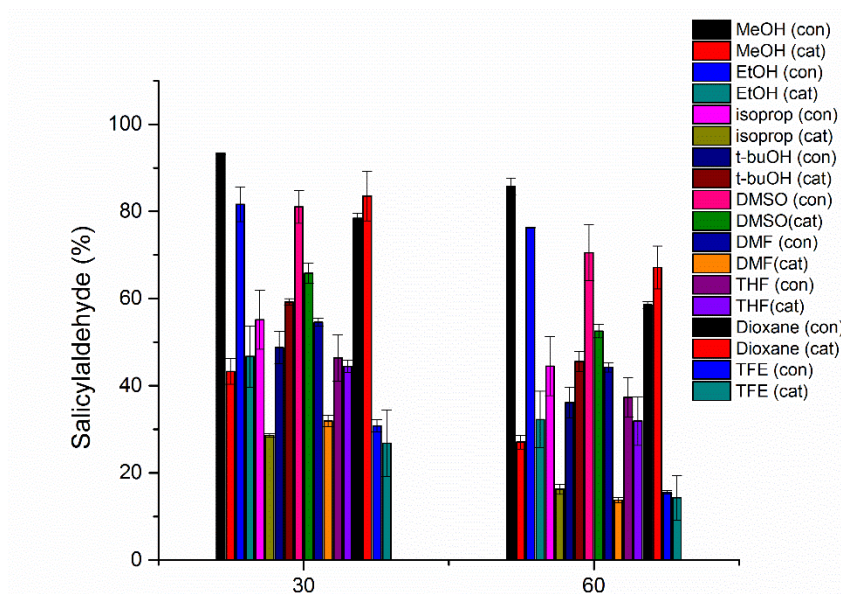


Figure 2.20 Effect of solvents on NaHCO_3

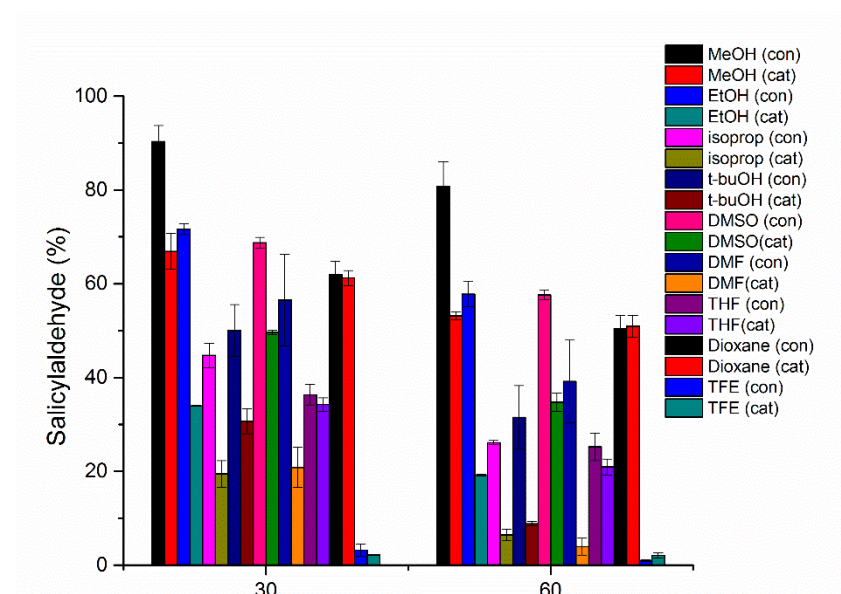


Figure 2.21 Effect of solvents on KHCO_3

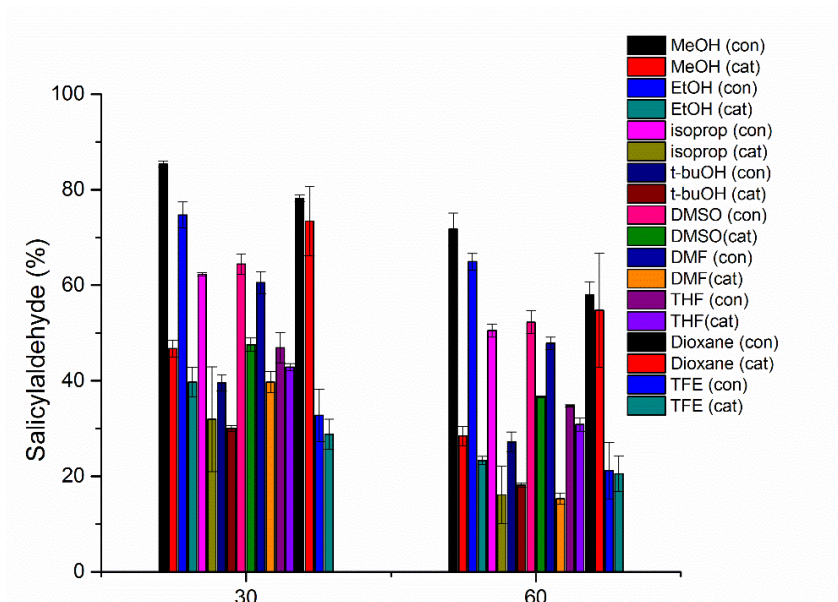


Figure 2.22 Effect of aqueous solvents on Na_2CO_3

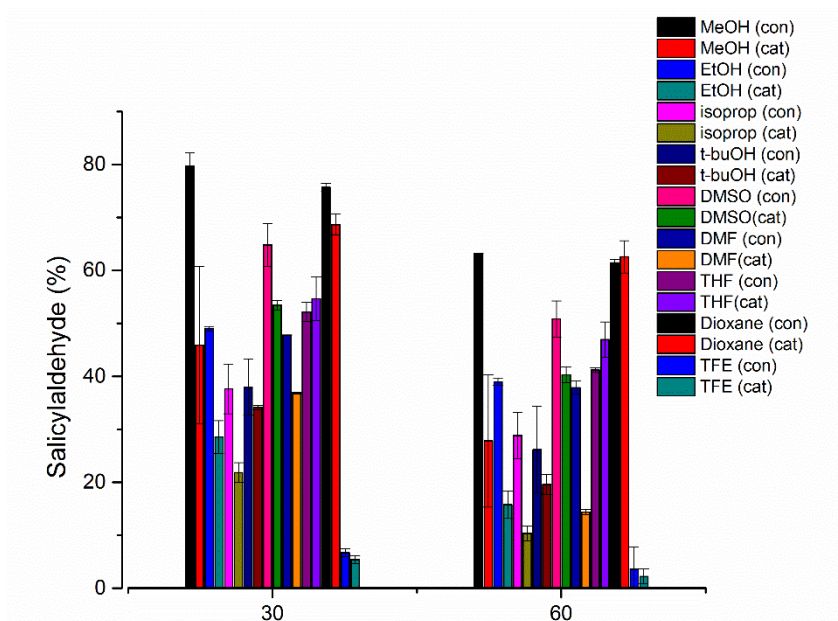


Figure 2.23 Effect of solvents on K_2CO_3

Among the solvents, protic polar solvents like methanol and ethanol increased the reaction rate more than other solvents. No catalytic activity was observed when the alcoholic solvents were used with nucleophilic bases like NaOH or KOH but with the weaker bases like NaHCO₃, KHCO₃ and Na₂CO₃ the rate of the catalytic reaction was enhanced compared to the control reaction. In the presence of stronger bases, it is possible that catalysts may undergo some degradation. The degradation of alloxazines in presence of stronger base was followed by NMR (Figure 2.24).

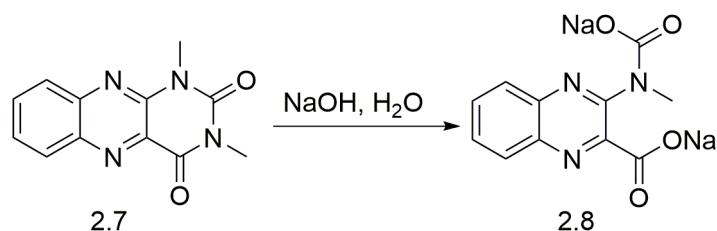


Figure 2.24 Possible flavin degradation under strong base

The kinetic data indicate about 60% conversion of the starting material after 30 min with methanol as solvent and NaHCO₃ as base. Due to the enhanced reactivity of the flavinium catalysts with weaker bases and alcoholic solvents, we selected NaHCO₃ as the base and aqueous methanol as solvent for further study of the reaction kinetics.

2.3.3 Effect of different catalysts on overall reaction rate

To study the substituent effect on the catalyst, **2.11a-2.11e** were used for the Dakin oxidation of salicylaldehyde. Among the five catalysts the 7,8-dichloroalloxazinium catalyst **2.11a** was found to be the best and the reaction was complete within 10 minutes with NaHCO₃ as base and aqueous methanol as solvent. Under the same reaction condition, only 60% of the starting material converted to product with 7,8-dimethoxyalloxazinium **2.11e** catalyst. The result clearly demonstrated (**Figure 2.26**) that the presence of electron withdrawing group (Cl, F) at 7- and 8-positions of the flavinium

increases the rate of reaction but the electron donating groups (CH₃, OCH₃) in those positions decreases the reaction rate.

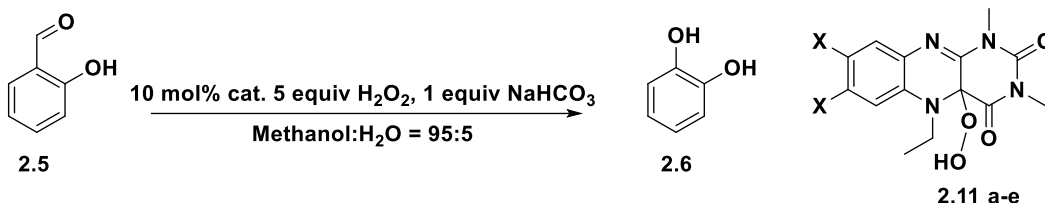


Figure 2.25 Reaction conditions for the catalyst optimization

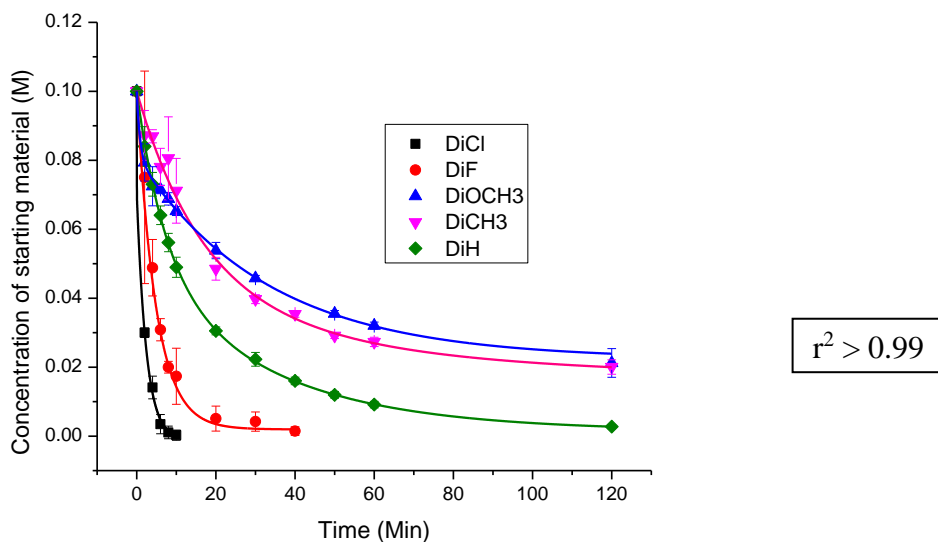


Figure 2.26 Dakin reaction rate with different alloxazinium catalysts

To compare the reaction rates of catalyzed and control reaction with different concentration of oxidants and catalyst loading, a set of experiments were performed with 7,8-difluoroalloxzinium catalyst **2.11b** with the same solvent (95% aq. MeOH) and base (NaHCO₃).

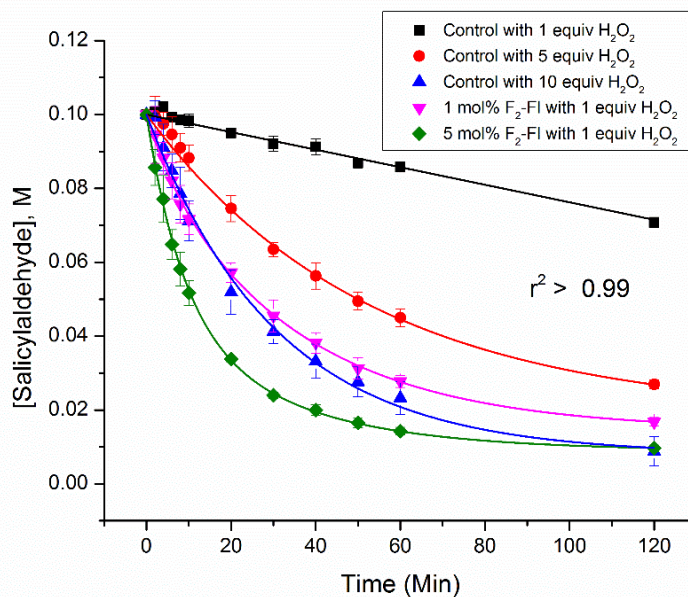
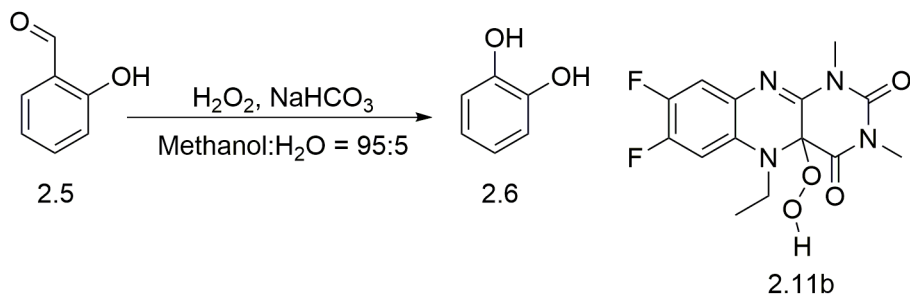


Figure 2.27 Comparison of catalyst loading with hydrogen peroxide concentration

The relative reaction rate study showed that the use of catalyst will lower the use of excess hydrogen peroxide (**Figure 2.27**). A catalytic reaction with 1 mol % catalyst and 1 equiv of hydrogen peroxide (purple) has the initial rate comparable to a control reaction with 10 equiv of H₂O₂ (blue). With 5 mol % of the catalyst with one equivalent of H₂O₂ increases the rate of reaction (green) compared to the control reaction with 1 equiv. of hydrogen peroxide.

2.3.4 Effect of reagent concentrations on overall reaction rate

To study the effect of substrate, base, hydrogen peroxide and catalyst on the rate of reaction a series of experiments with varying relative concentrations of each component was performed. The relative reaction rates are reported in the following **Table 2.2** and **2.3**. A combined plot for the effect of reagents on the reaction rate is shown in **Figure 2.28** and **2.30**.

Table 2.2 Initial rate for the control reactions

Experiment	[SM]/M	[NaHCO ₃]/M	[H ₂ O ₂]/M	Initial rate	SD
1	0.1	0.5	0.5	1.90× 10 ⁻²	5.56× 10 ⁻⁴
2	0.2	0.5	0.5	1.95× 10 ⁻²	3.52× 10 ⁻⁴
3	0.3	0.5	0.5	1.92× 10 ⁻²	5.66× 10 ⁻⁵
4	0.4	0.5	0.5	1.71× 10 ⁻²	1.51× 10 ⁻³
5	0.5	0.5	0.5	1.83× 10 ⁻²	6.44× 10 ⁻³
6	0.1	0.1	0.1	2.19× 10 ⁻⁴	1.55× 10 ⁻⁵
7	0.1	0.2	0.1	4.88× 10 ⁻⁴	3.55× 10 ⁻⁵
8	0.1	0.3	0.1	7.72× 10 ⁻⁴	1.02× 10 ⁻⁴
9	0.1	0.4	0.1	1.65× 10 ⁻³	3.55× 10 ⁻⁴
10	0.1	0.5	0.1	4.39× 10 ⁻³	1.24× 10 ⁻³
11	0.1	0.5	0.2	4.90× 10 ⁻³	1.62× 10 ⁻⁴
12	0.1	0.5	0.3	8.78× 10 ⁻³	4.04× 10 ⁻⁵
13	0.1	0.5	0.4	1.25× 10 ⁻²	5.25× 10 ⁻⁴

Table 2.3 Relative reaction rate with variable reagent concentrations

Experiment	[SM]/ M	[NaHCO ₃]/ M	[H ₂ O ₂]/ M	[catalyst] /M	Initial rate	SD
1	0.1	0.5	0.5	0.001	1.87× 10 ⁻²	1.31× 10 ⁻³
2	0.2	0.5	0.5	0.001	2.46× 10 ⁻²	1.21× 10 ⁻³
3	0.3	0.5	0.5	0.001	3.08× 10 ⁻²	2.79× 10 ⁻³
4	0.4	0.5	0.5	0.001	3.12× 10 ⁻²	2.89× 10 ⁻⁵
5	0.5	0.5	0.5	0.001	3.16× 10 ⁻²	3.07× 10 ⁻³
6	0.1	0.1	0.1	0.001	2.25× 10 ⁻³	3.39× 10 ⁻⁴
7	0.1	0.2	0.1	0.001	2.81× 10 ⁻³	1.66× 10 ⁻⁴
8	0.1	0.3	0.1	0.001	3.21× 10 ⁻³	3.35× 10 ⁻⁴
9	0.1	0.4	0.1	0.001	4.40× 10 ⁻³	5.55× 10 ⁻⁴
10	0.1	0.5	0.1	0.001	5.61× 10 ⁻³	5.00× 10 ⁻⁵
11	0.1	0.1	0.2	0.001	1.48× 10 ⁻²	5.77× 10 ⁻⁶
12	0.1	0.1	0.3	0.001	2.05× 10 ⁻²	7.38× 10 ⁻⁴
13	0.1	0.1	0.4	0.001	2.11× 10 ⁻²	1.52× 10 ⁻³
14	0.1	0.1	0.5	0.001	2.82× 10 ⁻²	3.49× 10 ⁻³
15	0.1	0.1	0.1	0.002	3.96× 10 ⁻³	2.54× 10 ⁻⁴
16	0.1	0.1	0.1	0.003	4.93× 10 ⁻³	9.29× 10 ⁻⁵
17	0.1	0.1	0.1	0.004	5.83× 10 ⁻³	1.10× 10 ⁻⁴
18	0.1	0.1	0.1	0.005	6.82× 10 ⁻³	3.50× 10 ⁻⁴

The rate of the Dakin reaction depends on the relative concentration of the reagents.

With one equivalent of base and one equivalent of starting material, the amount of base

was increased from one equivalent to five equivalents (blue line) as shown in **Figure 2.28** indicates a slow increase in the rate of reaction for the control reaction. In presence of weak base in excess (0.5 M) compared to the Salicylaldehyde (0.1M) and hydrogen peroxide (0.1M), the rate of the control reaction is comparable to the catalytic reaction

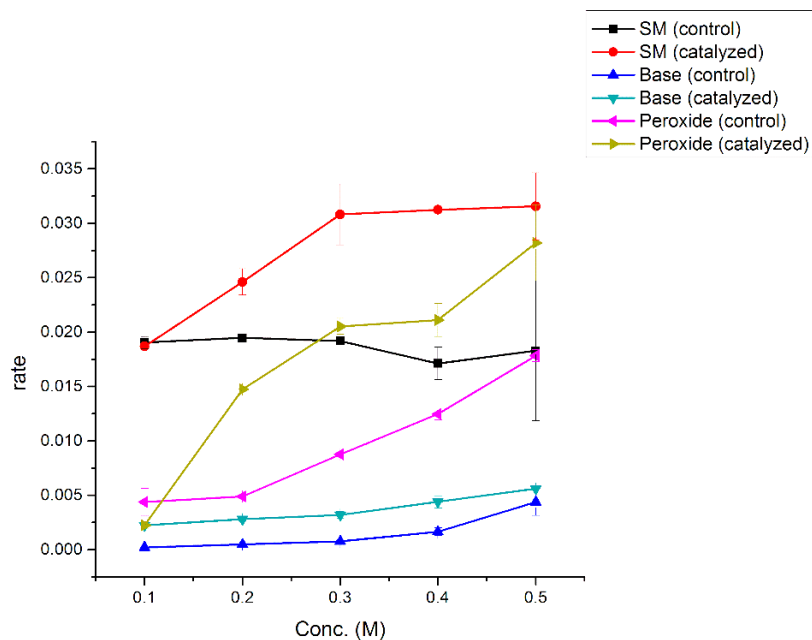


Figure 2.28 Effect of reagent concentrations on the reaction rate.

Red line $[\text{H}_2\text{O}_2] = 0.5 \text{ M}$, $[\text{NaHCO}_3] = 0.5 \text{ M}$, Catalyst = $[0.001 \text{ M}]$; Black line $[\text{H}_2\text{O}_2] = 0.5 \text{ M}$, $[\text{NaHCO}_3] = 0.5 \text{ M}$; Yellow line $[\text{SM}] = 0.1 \text{ M}$, $[\text{Base}] = 0.1 \text{ M}$, $[\text{catalyst}] = 0.001 \text{ M}$; Purple line $[\text{SM}] = 0.1 \text{ M}$, $[\text{Base}] = 0.5 \text{ M}$; Turquoise line $[\text{SM}] = 0.1 \text{ M}$, $[\text{H}_2\text{O}_2] = 0.1 \text{ M}$, $[\text{catalyst}] = 0.001 \text{ M}$; Blue line $[\text{SM}] = 0.1 \text{ M}$, $[\text{H}_2\text{O}_2] = 0.1 \text{ M}$.

rate with 1 mol% catalyst **2.11b** (turquoise line). In the peroxide shunt process (**Figure 2.7**), the flavin catalyst will form the flavin hydrogen peroxide, which has lower pKa compared to the hydrogen peroxide. Bruce and coworkers reported a lower pKa (~ 9.4)⁹²

for a similar flavin catalyst **2.9** compared hydrogen peroxide (pKa ~11.75). Limited concentration of base could be sufficient to deprotonate the flavin hydroperoxide in the catalyzed reaction and a slow increase in reaction rate indicates the lower effect of base on the formation of nucleophile. The lower pKa of flavin hydroperoxide can also be supported by comparing the reaction rate of the catalyzed reaction with limiting amount of the base. The yellow line in **Figure 2.28**, represents the reaction rate with increasing amount (0.1 M to 0.5 M) of hydrogen peroxide in presence of limited base (0.1 M NaHCO₃) and 0.1 M salicylaldehyde in presence of the catalyst. The rate of reaction increases rapidly with the increase of peroxide in presence of limited amount of base. On the other hand, with 0.1 M salicylaldehyde and excess amount of base (0.5 M) the reaction rate of the control reaction also increases almost linearly with the concentration of hydrogen peroxide. The excess base concentration helps the rate of deprotonation of the hydrogen peroxide to form a nucleophile for the enhancement of the reaction rate (magenta line).

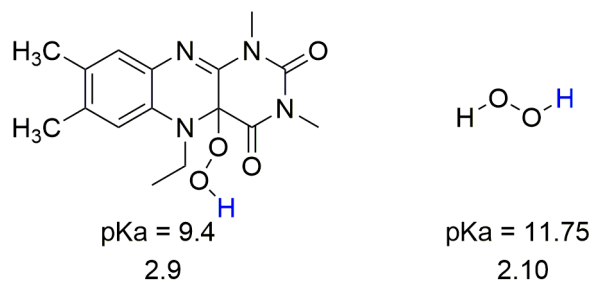


Figure 2.29 Relative pKa of flavin hydroperoxide and hydrogen peroxide

The change in rate of reaction with the concentration of salicylaldehyde in limiting base concentration also helps us to understand the role of base in rate determining step. Both control (black line) and catalyzed reaction (red line) have the similar rate of reaction in presence of excess 0.5 M base and 0.5 M hydrogen peroxide. As the concentration of salicylaldehyde (containing a phenolic group) increases, the concentration of base

decreases and lowers the extent of deprotonation of the peroxide. For the control reactions, the reaction rate remained almost constant with the increasing amounts of salicylaldehyde, which indicates that the reaction rate is independent of salicylaldehyde and the deprotonation of the hydrogen peroxide is the slowest step to control the reaction rate. The reaction rate of the catalyzed reaction initially increases with the concentration of salicylaldehyde and then it slows down as the concentration of salicylaldehyde approaches close to concentration of base. As the concentration of the salicylaldehyde increases close to the base concentration, the base concentration decreases because of the higher acidity of salicylaldehyde. The lower base concentration limited the deprotonation of the flavin hydroperoxide to generate the reactive nucleophile.

The rate of reaction linearly increases with the concentration of the catalyst at lower concentration of base (0.1 M) and peroxide (0.1 M) with 0.1 M salicylaldehyde (**Figure 2.30**). As the catalyst amount increases, the rate of formation of flavin hydroperoxide will increase via the peroxide shunt route. Due to the lower pK_a of the flavin hydroperoxide and the stability of the flavin oxide (leaving group) compared to the hydrogen peroxide the flavinium salt is functioning as a catalyst in the Dakin oxidation. The presence of electron withdrawing groups on the flavinium catalyst increase the rate of reaction, which supports the rate enhancement with the stabilized leaving group.

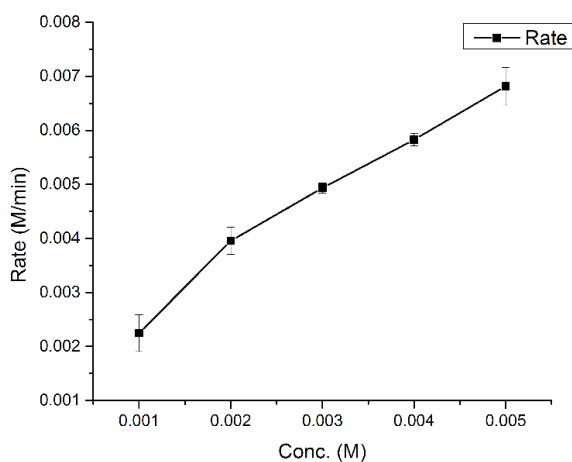


Figure 2.30 Effect of catalyst concentration on the reaction rate

A linear free energy relationship (Hammett plot) was plotted with the initial rate of the Dakin oxidation with salicylaldehyde using five different catalysts (**2.11a-e**) to determine the substituent effect and the reaction constant (from **Figure 2.26**). Three different plots were generated by considering inductive substituent constant for meta (7-substituent, blue line), para (8-substituent, red line) and meta+para (7 and 8 positions, green line). All these plots generates a positive slope, which indicates the increment of negative charge on flavin in the rate-determining step (**Figure 2.31**). The presence of electron withdrawing groups on the flavinium catalysts stabilizes the negative charge on the flavinium oxide (FIO⁻) to form a better leaving group to enhance the rate of reaction.

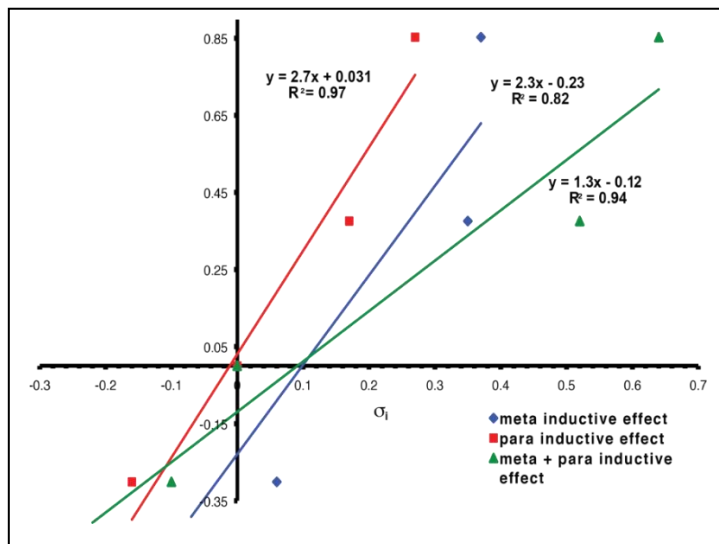


Figure 2.31 Hammett plot to relate initial rates with substituent effect meta (7-substituent, blue line), para (8-substituent, red line) and meta+para (7 and 8 positions, green line).

2.3.5 Effect of temperature on reaction rate

For a general reaction,



$$\text{Reaction rate} = k [A]^a [B]^b [C]^c [D]^d \quad k = \text{rate constant}$$

$$\ln(\text{rate}) = \ln k + a \ln[A] + b \ln[B] + c \ln[C] + d \ln[D]$$

For reactions at different temperatures with constant reactant concentration,

$$\ln(\text{rate}) \propto \ln k$$

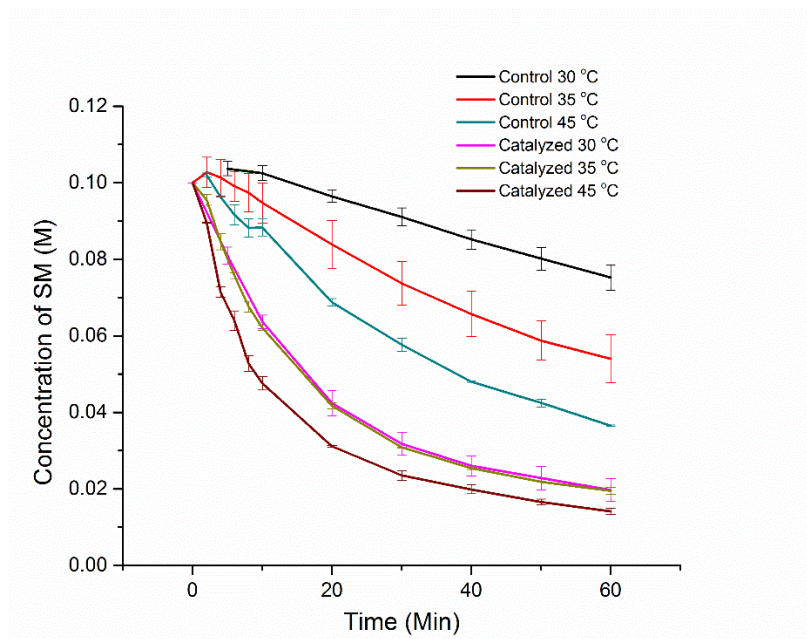


Figure 2.32 Relative reaction rates with temperature

The dependence of reaction rate on temperature was studied at three different temperatures (30 °C, 35 °C and 45 °C) with salicylaldehyde (0.1 M), NaHCO_3 (0.1 M), H_2O_2 (0.1 M) and 1mol% of **2.11 b**. Reaction rates for both control and catalyzed reaction increase but the temperature affects the control reaction more than the catalyzed reaction, which indicates a lower activation energy for the catalyzed reaction (**Figure 2.32**). The relative lower slope of the Arrhenius and Eyring plot were also indicative of the lower activation energy for the catalyzed Dakin reaction (**Figure 2.33** and **2.34**). Since $\ln(\text{rate})$ is proportional to the $\ln(\text{rate constant})$, we are going to use $\ln(\text{rate})$ instead of $\ln k$ to calculate the kinetic parameters.

The Arrhenius equation can be used to calculate the activation energy of a reaction by calculating the reaction rate at different temperature.

$$k = A e^{-E_a/RT}$$

$$\ln k = \ln A - E_a/RT$$

$$\ln k = \ln A - (E_a/R) \cdot 1/T$$

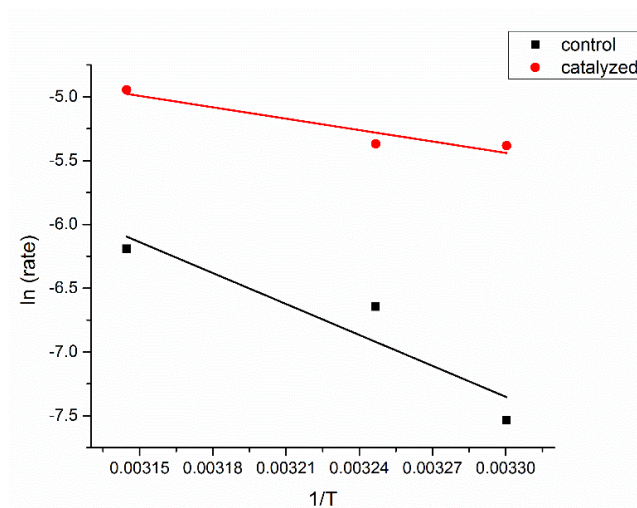


Figure 2.33 Arrhenius plot for activation energy

The Eyring equation relates enthalpy of activation and entropy of activation to the rate constant by

$$\ln(k/T) = - \Delta H^\ddagger/R \cdot 1/T + \ln(k_B/h) + \Delta S^\ddagger/R$$

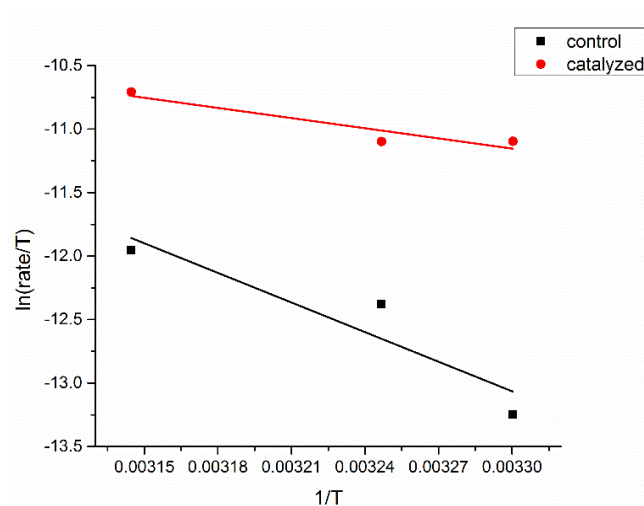


Figure 2.34 Eyring plot for kinetic parameters

Table 2.4 Activation energy and kinetic parameters

Reaction	E_a (KJ mol ⁻¹)	ΔH^\ddagger (KJ mol ⁻¹)	ΔS^\ddagger (Jmol ⁻¹ K ⁻¹)
Control	67.2	64.6	-92.9
Catalyzed	24.8	22.2	-217.1

According to the Arrhenius and Eyring plots, both the activation energy and enthalpy of activation decreases about 42 KJ mol⁻¹ and the activation of entropy also decreases by 124 Jmol⁻¹K⁻¹. Hocking and coworkers also reported the enthalpy of activation and entropy for the control reaction as 65.7 KJ/mol and -16.3 eu.⁹³ The lower activation of enthalpy and entropy for catalyzed reaction indicates that the catalyzed reaction follows a reaction with lower activation energy and it also undergoes through a highly organized transition state.

2.3.6 Effect of substituents on Salicylaldehyde on reaction rate

The effect of substituents on the substrate was studied by using a range of benzaldehydes with different substituents ranging from electron withdrawing to electron donating groups.

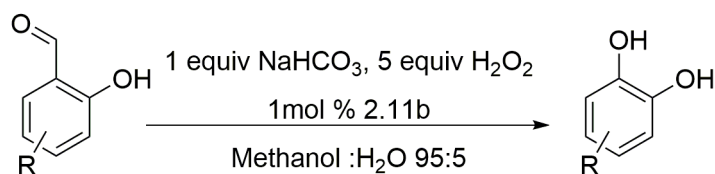


Figure 2.35 Reaction condition for substrate study

All the reactions were studied with a limiting amount of base (1 equivalent) and an excess amount of hydrogen peroxide (5 equivalent). For catalyzed reaction 1 mol% catalyst was used. Both the control and catalyzed reactions were monitored for 20 min. to

determine the initial rates. For all the substrates the initial rates for catalyzed reaction were greater than the control reaction. 5-Hydroxysalicylaldehyde showed a slower reaction rate and no effect in presence of the catalyst. Due to the presence of two acidic phenolic groups, under limited base concentration (1 equiv) the concentration of base may not be enough to deprotonate the peroxide to form the peroxide anion. The maximum reaction rate was observed in presence of electron donating groups like methoxy and methyl. On the other hand, the presence of electron withdrawing groups like NO₂ lowers the reaction rate. There was almost no reaction for the control reaction with 5-nitrosalicylaldehyde (**Figure 2.36**). The results directly correlates with the 1,2-aryl migration as the rate determining step, which favors electron rich aromatic compounds.

Table 2.5 Relative reaction rates with different substrates

Substrate	Catalyzed (M sec ⁻¹)	SD	Control (M sec ⁻¹)	SD
4-Methoxysalicylaldehyde	4.1×10 ⁻²	9.5×10 ⁻⁴	7.6×10 ⁻³	1.9×10 ⁻³
5-Methylsalicylaldehyde	3.7×10 ⁻²	6.4×10 ⁻⁴	1.7×10 ⁻³	2.9×10 ⁻⁴
5- <i>t</i> -butylsalicylaldehyde	3.2×10 ⁻²	9.3×10 ⁻⁴	2.4×10 ⁻³	7.1×10 ⁻⁵
Salicylaldehyde	3.1×10 ⁻²	2.5×10 ⁻³	3.6×10 ⁻³	1.5×10 ⁻³
5-Methoxysalicylaldehyde	2.9×10 ⁻²	1.7×10 ⁻³	1.7×10 ⁻²	8.3×10 ⁻⁴
4-Methylsalicylaldehyde	2.2×10 ⁻²	9.2×10 ⁻³	2.1×10 ⁻³	1.0×10 ⁻⁴
5-Chlorosalicylaldehyde	2.0×10 ⁻²	9.4×10 ⁻⁴	3.1×10 ⁻³	2.7×10 ⁻⁴
4-Bromosalicylaldehyde	1.6×10 ⁻²	0	1.2×10 ⁻³	1.2×10 ⁻⁴
5-Bromosalicylaldehyde	1.5×10 ⁻²	8.7×10 ⁻⁴	2.5×10 ⁻³	6.4×10 ⁻⁵
5-Iodosalicylaldehyde	1.0×10 ⁻²	1.7×10 ⁻³	1.9×10 ⁻³	2.5×10 ⁻⁴
5-Nitrosalicylaldehyde	2.8×10 ⁻³	2.7×10 ⁻⁴	6.5×10 ⁻⁴	5.4×10 ⁻⁴
5-Hydroxysalicylaldehyde	1.8×10 ⁻²	9.9×10 ⁻⁵	1.7×10 ⁻³	9.9×10 ⁻⁵

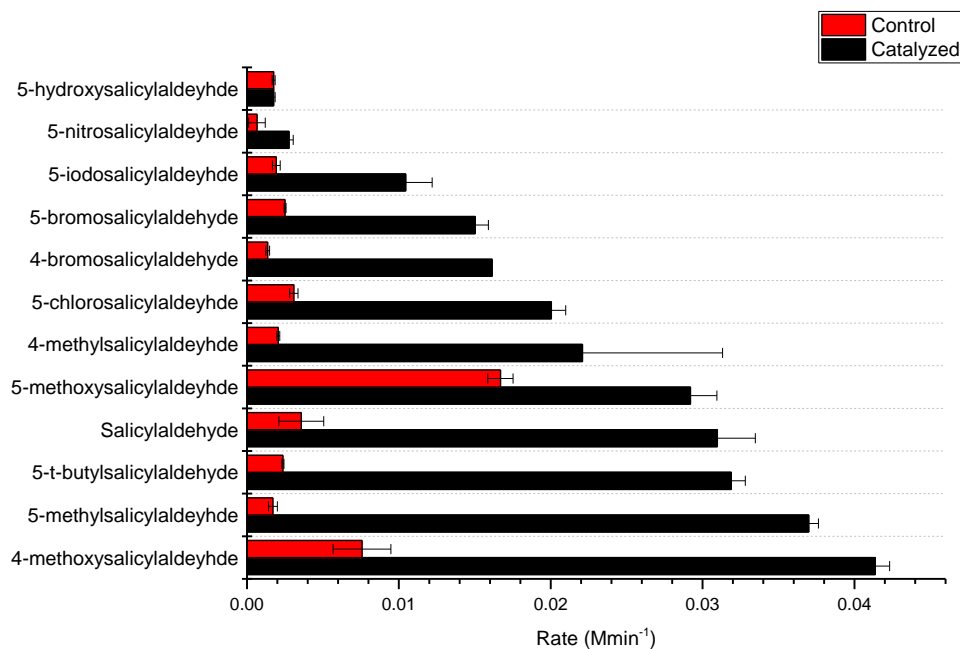


Figure 2.36 Relative reaction rates with different substrates

2.4 Plausible mechanism for catalyzed reaction

The plausible reaction mechanism involves the formation of flavinium hydrogen peroxide **2.11**, which undergoes deprotonation to form flavin hydroperoxide anion (nucleophile) **2.9** at relatively lower pK_a which will attack the deprotonated salicylaldehyde to form a Criegee intermediate **2.12**. The 1,2-aryl migration of the intermediate will form an ester and FIO^- (leaving group) **2.13**, which will be stabilized by the electron withdrawing groups and also participates in the catalytic cycle. The rapid hydrolysis of the ester will lead to the catechol and a salt of formic acid.

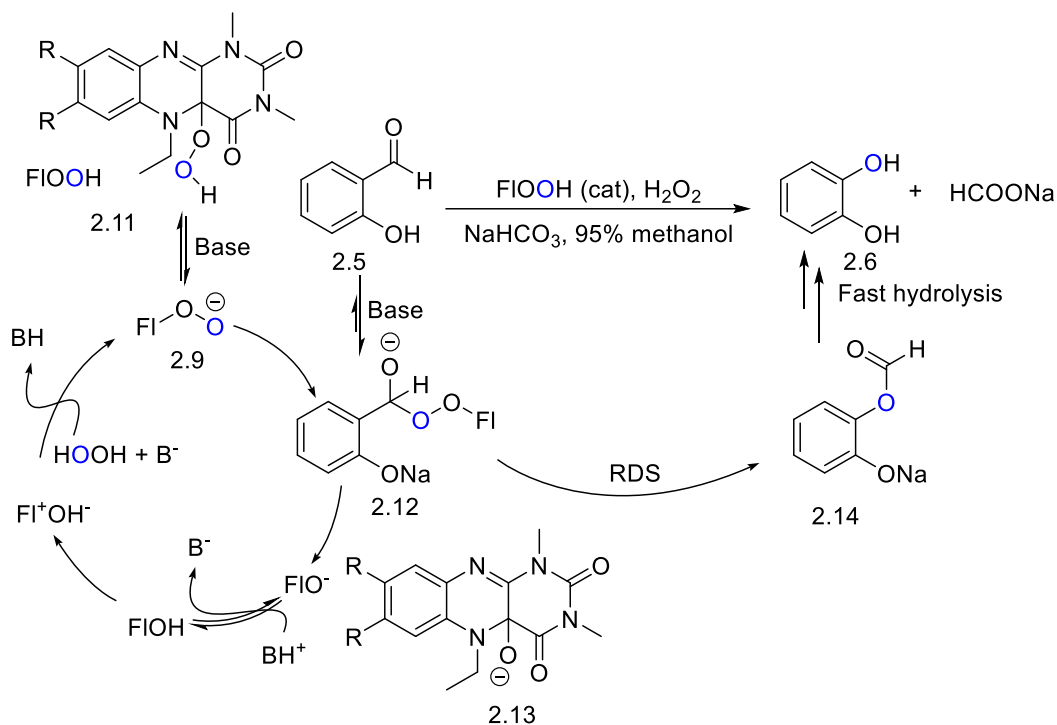


Figure 2.37 Plausible reaction mechanism for catalyzed reaction

2.5 Summary of the reaction kinetics

All the experiments with variable reagent concentrations, variable temperatures, different catalysts and substrates indicate that the reaction rate is dependent on the relative concentration of the base and peroxide anion. The lack of formation of peroxide anion at lower base concentration will limit the consecutive steps to complete the reaction.

Flavin hydroperoxide, having a lower pK_a than H_2O_2 , will form the flavin peroxide anion at lower base concentration and the following nucleophilic attack on the substrate will lead to the formation of product. Due to the higher rate of ester hydrolysis, the hydrolysis step has no effect on the rate determining step.

The temperature dependent experiments indicate the lowering of activation energy, enthalpy of activation and entropy of activation. The probable reason would be the formation of highly organized transition state and the relatively facile formation of the peroxide anion.

Both the catalyst and substrate react alternatively in presence of the electron withdrawing and electron donating substituents. Electron withdrawing groups on flavin increases the rate of reaction and on the other hand electron withdrawing groups on substrate decrease the rate of reaction. This suggests 1,2-aryl migration as the rate determining step, which favors electron rich substrate and also enhance stability of the anionic leaving group (FIO^-).

All the observations support the plausible reaction mechanism as shown in **Figure 2.37**.

2.6 Application of catalysts on Dakin oxidation

The synthetic application of flavinium catalysts was investigated by using the optimized reaction conditions and **2.11a** as the catalyst. A number of benzaldehyde and acetophenone derivatives were studied in the Dakin oxidation. Under optimized conditions, only *ortho*- and *para*-hydroxyl containing benzaldehydes form the corresponding phenolic product. The reaction condition and the yield for the different substrates were shown in **Figure 2.38**. This work was done in collaboration with Dr. Shuai Chen, who did most of the initial screening and isolation of the products. The compounds highlighted in blue are reported in this dissertation.

The inactivity of acetophenones was also observed by Dakin in his original research.⁷⁹ In this research, only 2-hydroxyacetophenone **2.9k** was converted to the catechol. It should be pointed out that this occurs in the presence of DMSO, a serendipitous discovery, which we do not have a complete answer for at this point in time. No product was observed with acetophenones without 2-hydroxyl group.

The outcome of this research indicates the importance of *ortho* and *para* hydroxyl group on the benzaldehyde. Under basic conditions the deprotonated phenolic group increases the electron density on the aromatic ring which facilitates the 1,2-aryl migration of the Criegee intermediate to form the ester.

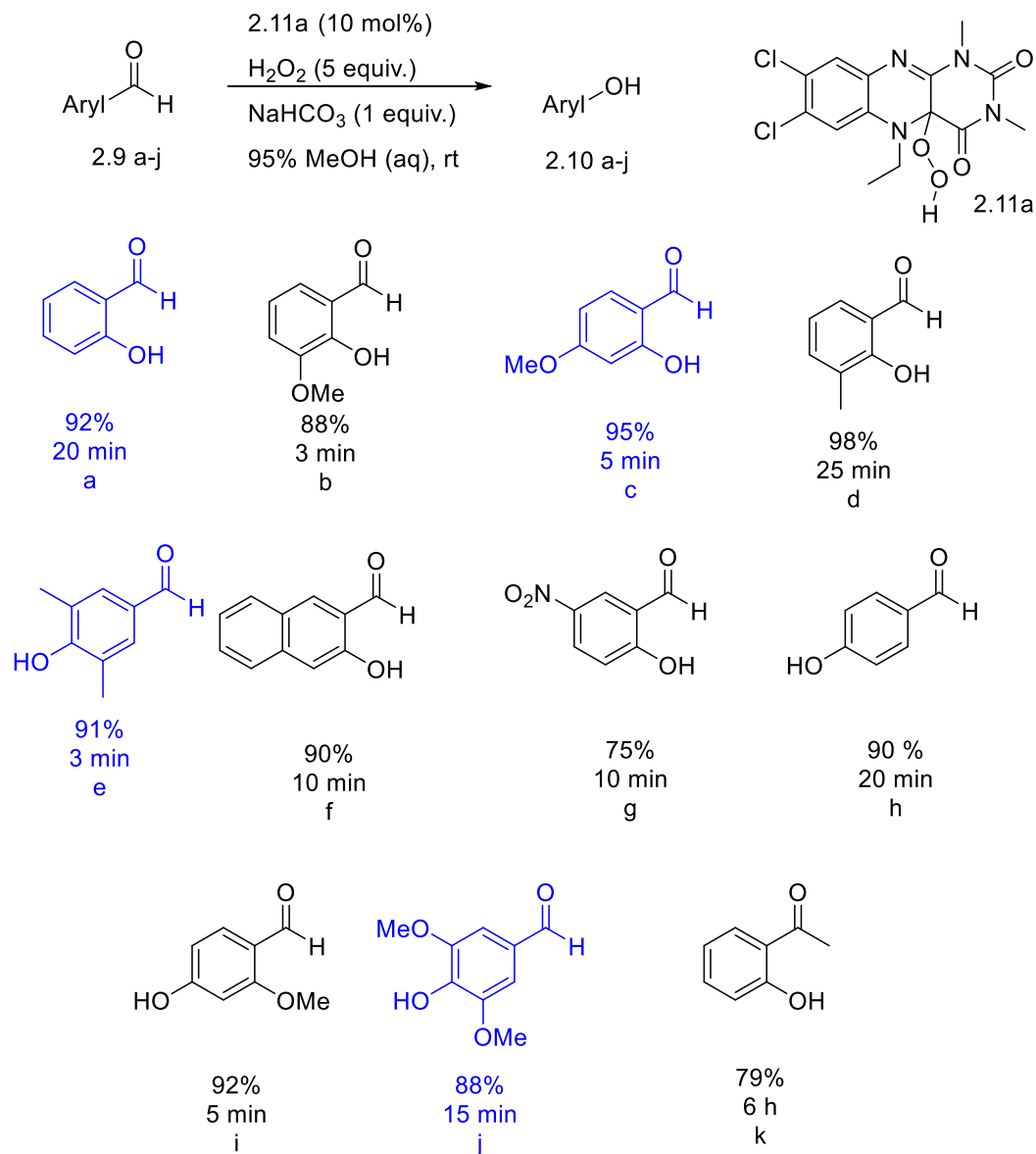


Figure 2.38 Dakin oxidation of aldehydes and ketones with hydrogen peroxide

Carbery and co-workers reported the presence of electron withdrawing group on benzaldehyde forms benzoic acid in presence of bridged flavinium catalysts.⁹⁴ The mechanism involved the 1,2-hydride transfer instead of aryl migration, which is unfavorable due to the lack of electron density.

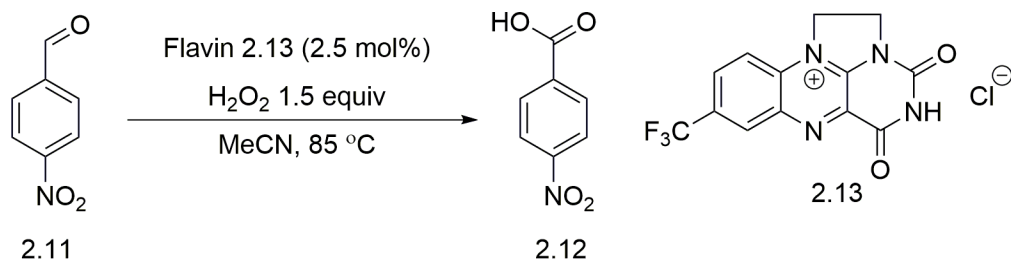


Figure 2.39 Formation of benzoic acid from electron poor benzaldehydes by Carbery and coworkers.⁹⁴

In summary, a plausible reaction mechanism of the flavin-catalyzed Dakin oxidation was proposed after studying the initial rate using a range of substrates and catalysts, varying the reaction temperatures, and varying concentration of reagents and catalysts. The mechanism of the catalyzed process showcases the ability of flavinium catalysts to lower the pKa of the effective peroxide, as well as the enhanced leaving group ability of the flavin hydroxide as compared to the hydroxide ion. A wide variety of electron rich salicylaldehyde derivatives were converted to the corresponding catechol within 30 mins.

Chapter 3

Flavin catalyzed Heterocycle Aromatization

3.1 Heterocyclic aromatization reactions

Dihydropyridine, benzothiazole, benzimidazole and benzoxazole units are important building blocks for numerous natural products and biologically active reagents. Some of them are used as drugs and synthesized in pharmaceutical industry. A part of the synthetic community focused on the convenient synthesis of these hetero-aromatic compounds.

3.1.1 Dihydropyridine

Dihydropyridine was first synthesized by Arthur Hantzsch about a century ago.⁹⁵ The reaction synthesized 1,4-dihydropyridine (1,4-DHP) as an isolable intermediate, which can be oxidized to pyridines. The synthesis attracted attention in 1980s when 1,4-DHP was reported to treat hypertension. Amlodipine **3.1**, felodipine **3.2**, isradipine **3.3** and nifedipine **3.4** are among the bestselling 1,4-dihydropyridine drugs.⁹⁶ (**Figure 3.1**)

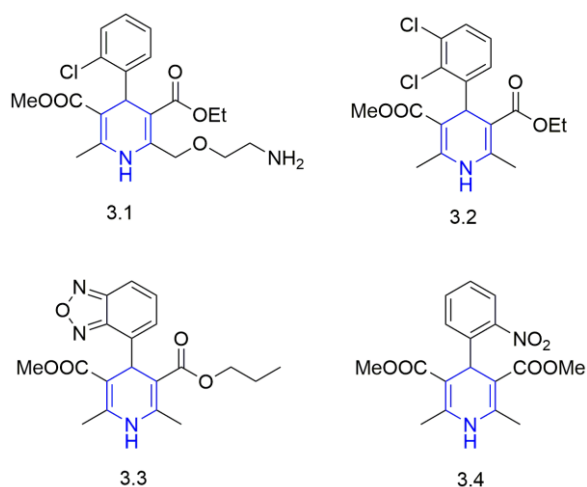


Figure 3.1 Hypertension treating drugs with dihydropyridine core

These drugs bind to the calcium channel and consequently decrease the passage of the transmembrane calcium current. These relax the cardiac muscle by reducing the contractility throughout the heart.⁹⁷⁻⁹⁸

Metabolically, these drugs were converted to the corresponding pyridine by the action of P450 in the human liver.⁹⁹ The result shows the enzyme P450 IIIA4 is probably the major human catalyst involved in the dehydrogenase of many, but not all types, of 1,4-dihydropyridine. 1,4-DHP's have similar structural features as NAD(P)H and natural NAD(P)H undergoes oxidation in presence of flavin cofactors, but no report has provided evidence of metabolic degradation of these drugs in presence of flavin containing proteins in human body.

The oxidized products of 1,4-dihydropyridines were reported to exhibit anti-hypoxic and anti-ischemic activity. One of the representative drug is Cerivastatin **3.5**, which is active in the treatment of atherosclerosis and other coronary diseases.¹⁰⁰ Therefore, the oxidative aromatization of 1,4-dihydropyrimidine attracts both organic and medicinal chemists.

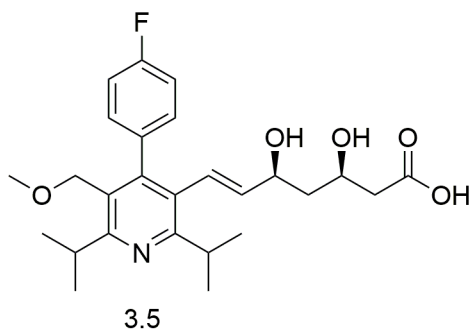


Figure 3.2 Cerivastatin to treat atherosclerosis

Several methods have been developed for the oxidative aromatization of 1,4-dihydropyridines to pyridines.

Ru(III)Cl and molecular oxygen was developed to oxidize 1,4-DHP catalytically.¹⁰¹ The proposed mechanism involved single electron oxidation of DHP via Ru(III). The DHP went through radical intermediate and another single electron oxidation forms the final oxidized pyridine. The reduced metal Ru(II) will be reoxidized to Ru(III) by molecular oxygen to turn over the catalytic cycle. **(Figure 3.3)**

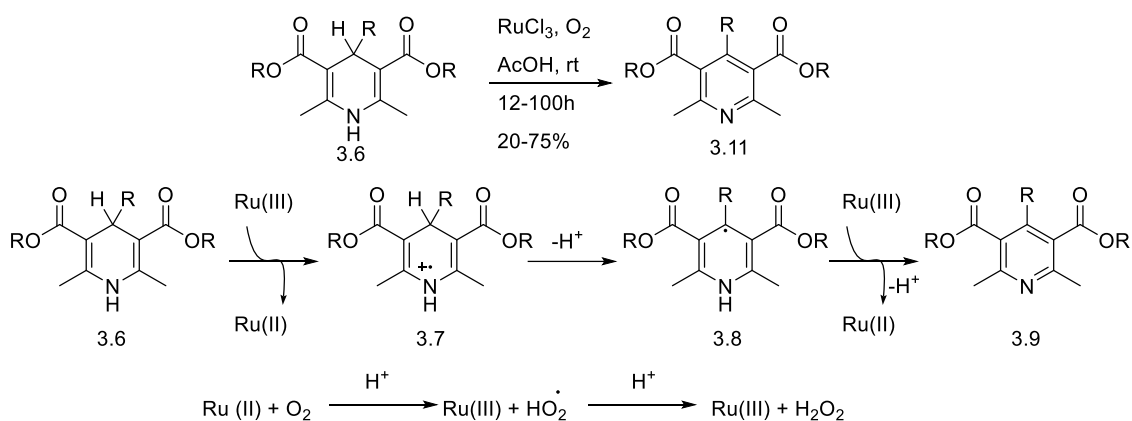


Figure 3.3 Aerobic DHP oxidation using RuCl₃ and molecular oxygen

A Keggin type heteropolyacid, H₆PMo₉V₃O₄₀, **3.10** was used to oxidize a variety of 1,4-dihydropyridine in high yield by refluxing with acetic acid and molecular oxygen was used to regenerate the acid.¹⁰²

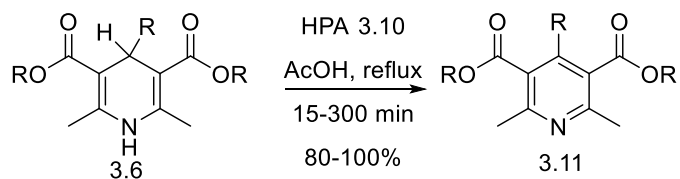


Figure 3.4 DHP oxidation using Heteropolyacid (HPA)

The oxidation of 1,4-dihydropyridine was also achieved by using I₂O₅ in water.¹⁰³ The mechanism is believed to be a radical process with hypervalent iodine as the

terminal oxidant. Another report converted DHP to pyridine effectively by using catalytic amount of Pd/C in acetic acid at 80 °C.¹⁰⁴ Potassium permanganate was also used to oxidize the 1,4-dihydropyridine. The author observed the formation of a dealkylation product when the 4-position of the substrate contains benzyl or alkyl group like ethyl. Single product **3.11** was isolated for C-4 aryl substituted dihydropyridines.¹⁰⁵

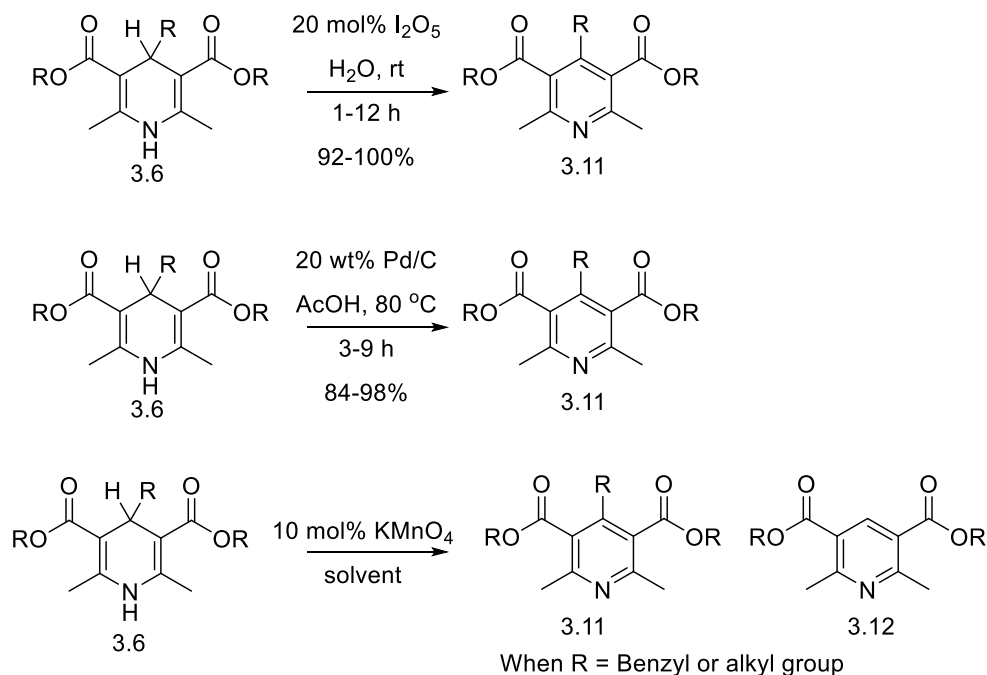


Figure 3.5 Use of different oxidants for the DHP oxidation

1,4-Dihydropyridine was also converted to the pyridine by photoirradiation ($\lambda > 300$) under an oxygen atmosphere.¹⁰⁶ Mechanistically photoinduced single electron transfer from the dihydropyridine to molecular oxygen occurs. The generated superoxide radical anion ($O_2^{\cdot-}$) is proposed to be responsible for the photochemical oxidation (**Figure 3.6**)

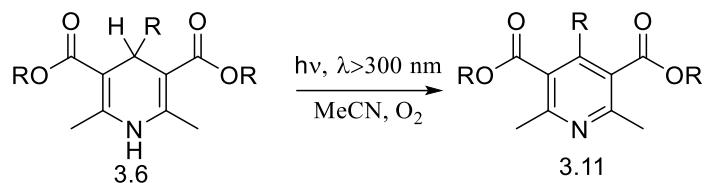


Figure 3.6 Photo-induced oxidation of 1,4-dihydropyridine

3.1.2 Benzothiazoline

Benzothiazoles occur naturally,¹⁰⁷ but a number of synthetic benzothiazoles are biologically active. The acquisition of aromaticity in the benzothiazole is the driving force for the oxidation of benzothiazoline. This property renders benzothiazoline as a useful reducing agent and hydride transfer reagent.¹⁰⁸

The use of benzothiazoline as hydrogen source was first reported by Aklyama and coworkers for asymmetric reduction of ketimines **3.13** with catalytic amount of chiral phosphoric acid **3.17**. Benzothiazole **3.16** was formed as a byproduct. This is a simple approach that gives higher enantioselectivity in the imine reduction. (**Figure 3.7**)¹⁰⁹

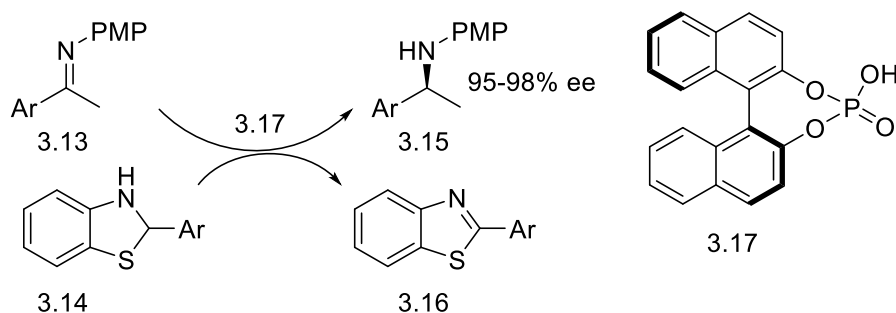


Figure 3.7 Chiral phosphoric acid catalyzed asymmetric ketamine reduction

Benzothiazoles are an important class of heterocyclic compounds that have strong biological and pharmaceutical importance. Benzothiazole-containing compounds possess biological activities, such as antimicrobial, anticancer, antifungal, anthelmintic and anti-diabetic.¹¹⁰ (**Figure 3.8**)

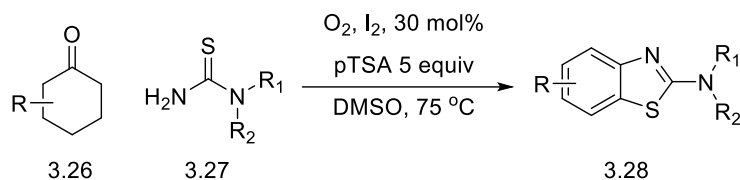


Figure 3.10 Aerobic benzothiazole synthesis catalyzed by I₂

A recently developed method to synthesize 2-benzothiazoles has been described via a copper catalyzed condensation of 2-aminothiophenol **3.29** with nitriles **3.30**.¹¹³ This method used ethanol as solvent and an inexpensive Cu catalyst.

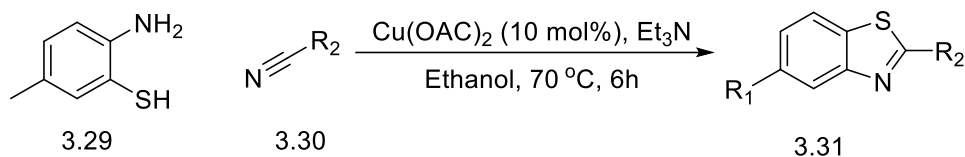


Figure 3.11 Cu-catalyzed benzothiazole synthesis in ethanol

The synthesis of 2-aryl benzothiazole from aryl ketone **3.33** and 2-aminobenzenethiols **3.32** without metal and I₂ free condition was described. This method includes DMSO as solvent and higher temperature to obtain a good yield.¹¹⁴ (**Figure 3.12**)

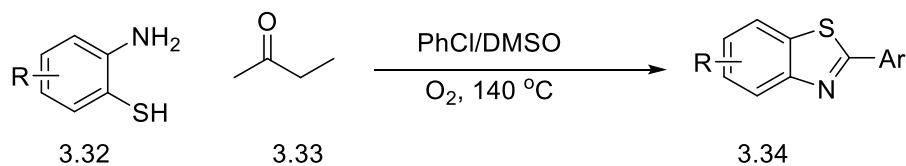


Figure 3.12 Aerobic benzothiazole synthesis in DMSO at higher temperature

3.2 Flavin-catalyzed aromatization of dihydropyridine and benzothiazoline

The use of organocatalysts has not been investigated for the oxidation of benzothiazolines. After successful aerobic Dakin oxidation with Hantzsch ester as the reducing agent and molecular oxygen as terminal oxygen, the research was focused on the oxidation of pre-heteroaromatic compounds. The oxidation of the substrates will reduce flavin and turn over the flavin catalytic cycle as shown in **Figure 3.13**.

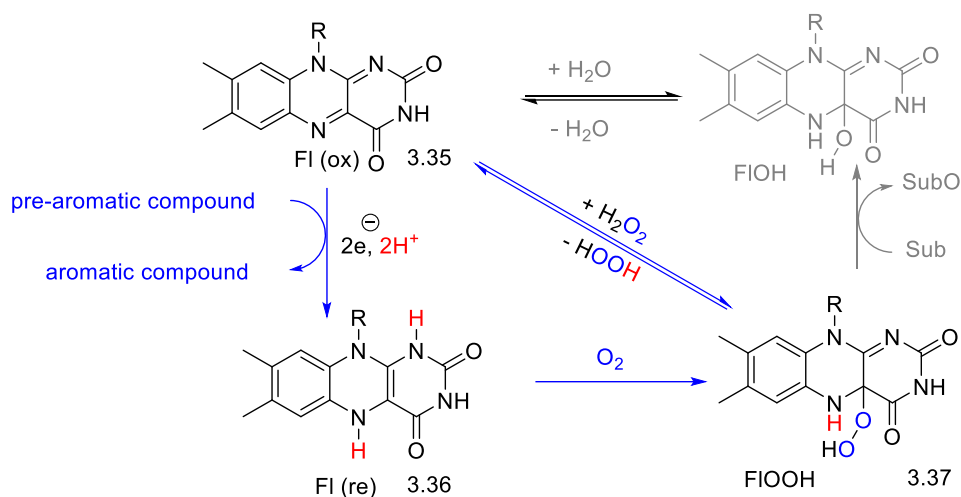


Figure 3.13 Biomimetic cycle to oxidize pre-aromatic compounds

The optimization of the reaction condition for the dehydrogenation was done by Dr. Chen in our group. To study the dehydrogenation, a series of 1,4-dihydropyridines **3.41-3.54** (**Figure 3.14**) were synthesized by following the report from Beifuss and coworkers.¹¹⁵

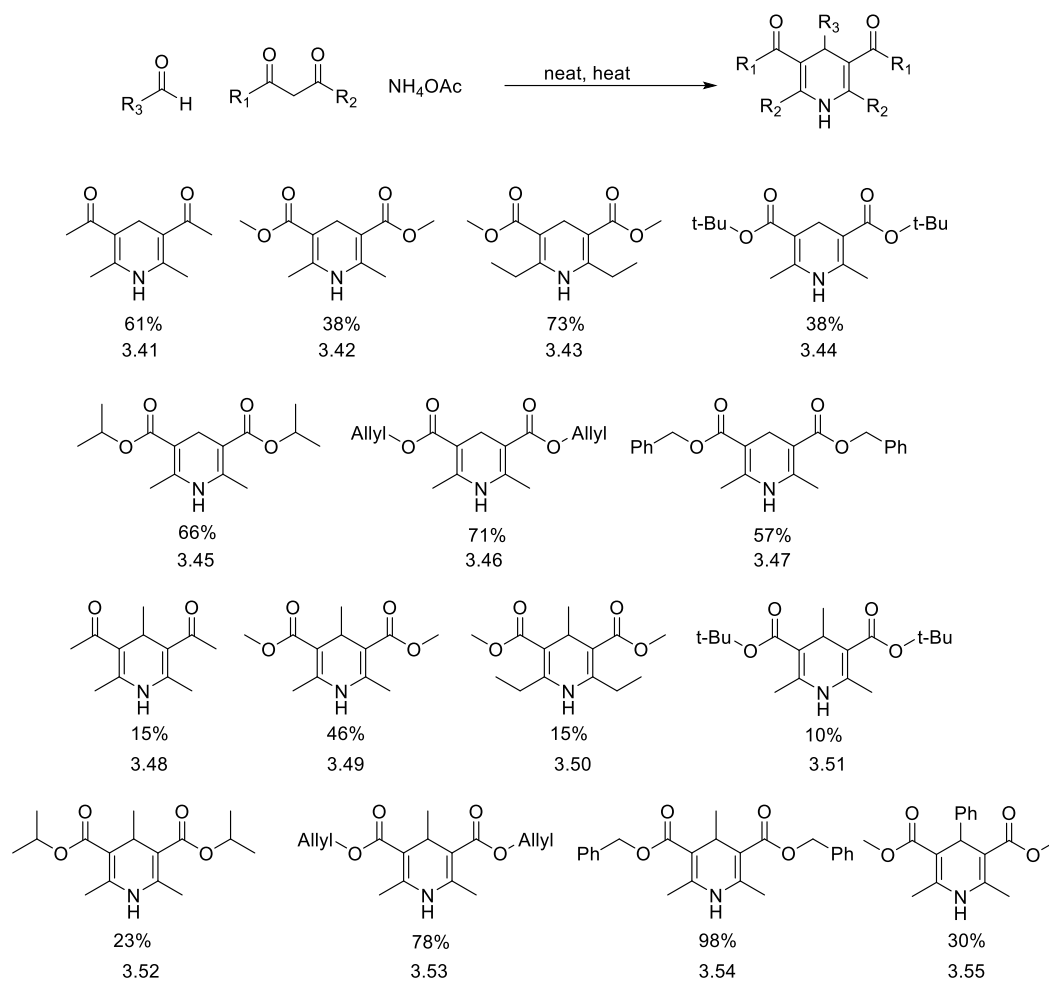


Figure 3.14 Synthesis of 1,4-dihydropyridines

The oxidized products were synthesized and characterized by Dr. Chen. The optimized reaction condition includes methanol as solvent, 5 mol% of the flavin catalyst **3.40** and room temperature. Quantitative yield was obtained by simply evaporating off the solvent, and the purity of the product greater than 95% (**Figure 3.15**).

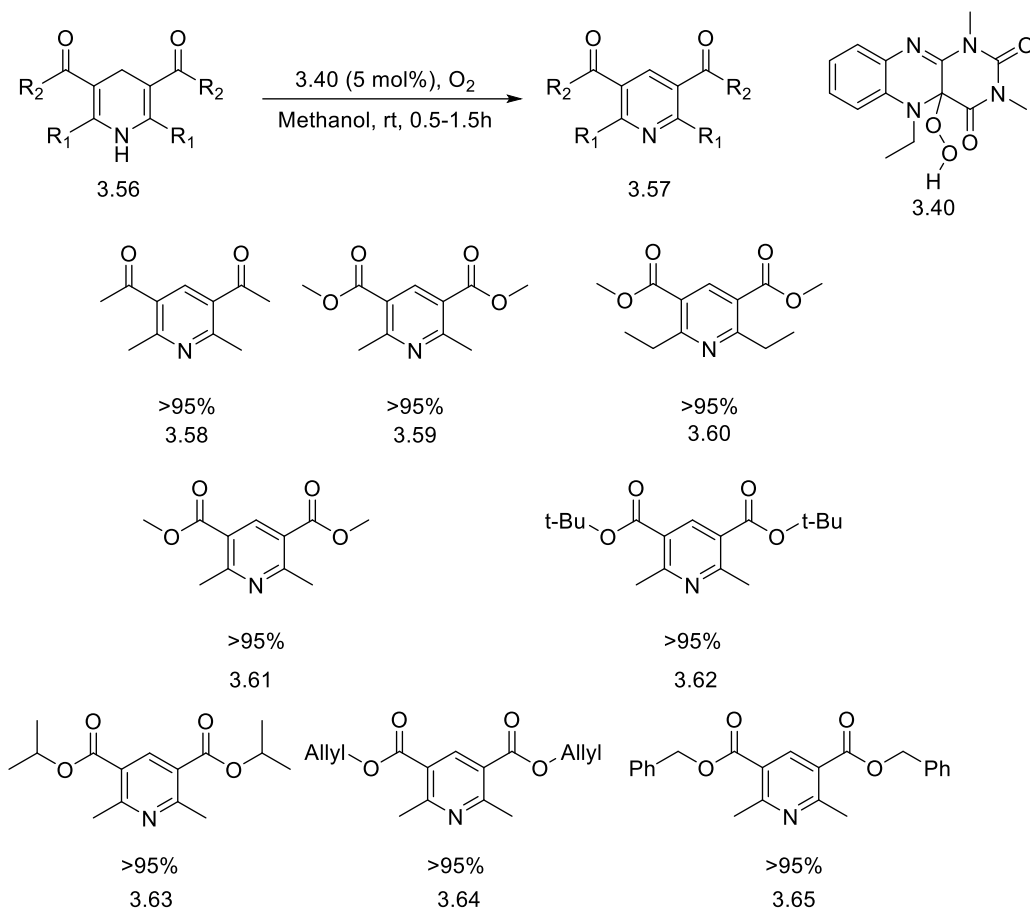


Figure 3.15 Alloxazine catalyzed aromatization of dihydropyridines

After successful oxidation of dihydropyridines using flavin as catalyst and molecular oxygen as terminal oxidant, the tandem synthesis of pyridines was completed using formaldehyde (37% in water) **3.66**, ammonium acetate **3.68** and the corresponding acetonacetates **3.67** (Figure 3-16). The synthesis was catalyzed by 2 mol% flavin catalyst and air as the source of oxygen. Dr. Chen reported this one pot synthesis of pyridine derivatives.¹¹⁶

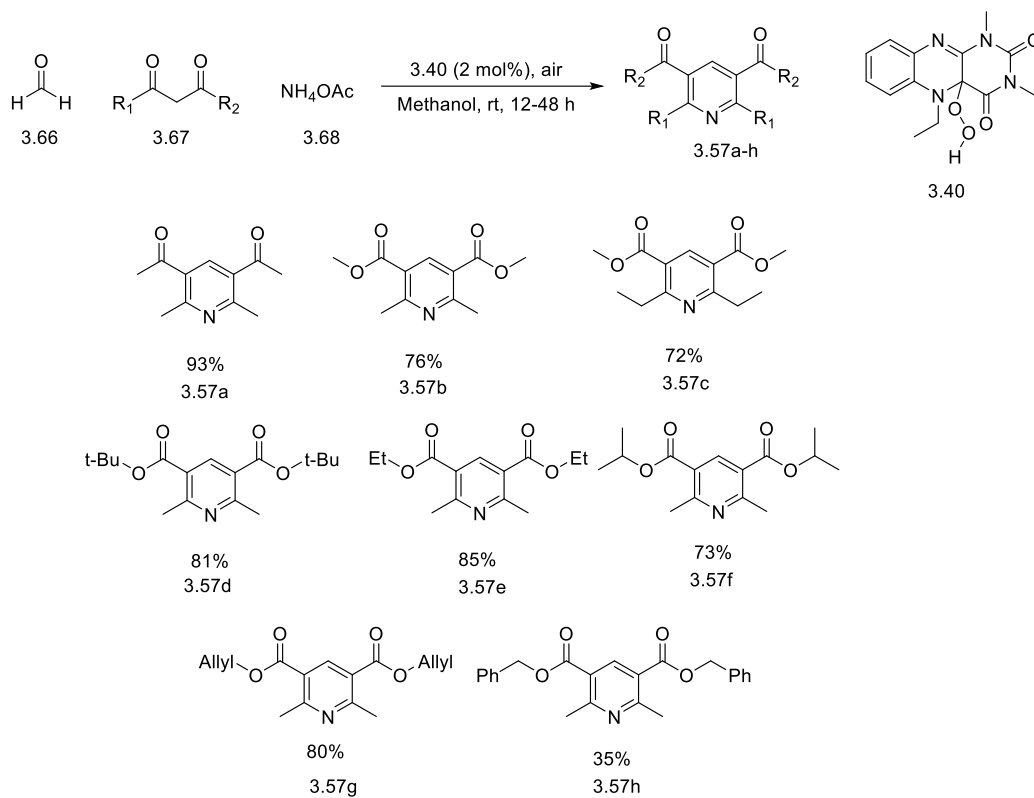


Figure 3.16 Multi-component synthesis of pyridines

C-4 Substituted dihydropyridines were not oxidized by using an alloxazine catalyst over longer reaction time and at elevated temperature. Cibulka and coworkers reported the greater electrophilicity of isoalloxazines than the alloxazines and also reported that the use of acid increases the formation of oxidized flavin from the flavin pseudo base.¹¹⁷ After screening a set of acids, Dr. Chen used HClO_4 successfully as an acid for the oxidation of C-4 substituted dihydropyridines with isoalloxazinum catalyst **3.71** in good to excellent yields (**Figure 3.17**).¹¹⁸

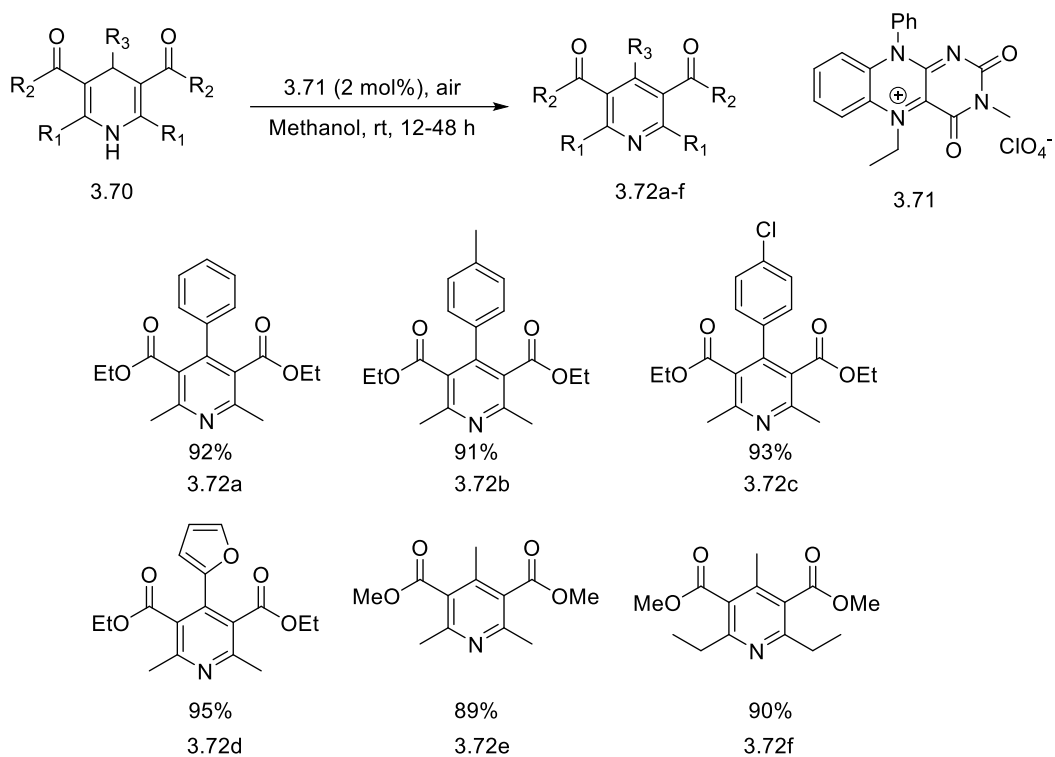


Figure 3.17 Isoalloxazine catalyzed oxidation of 4a-substituted dihydropyridines

A plausible mechanism involves the reduction of the isoalloxazinium **3.71** to the reduced flavin with dihydropyridine. The reduced flavin **3.71a** will interact with the molecular oxygen to form the flavin hydroperoxide **3.71b**, which will eliminate H_2O_2 to form the oxidized flavin **3.71**. The elimination of H_2O_2 is enhanced by the presence of an acid (**Figure 3-18**)

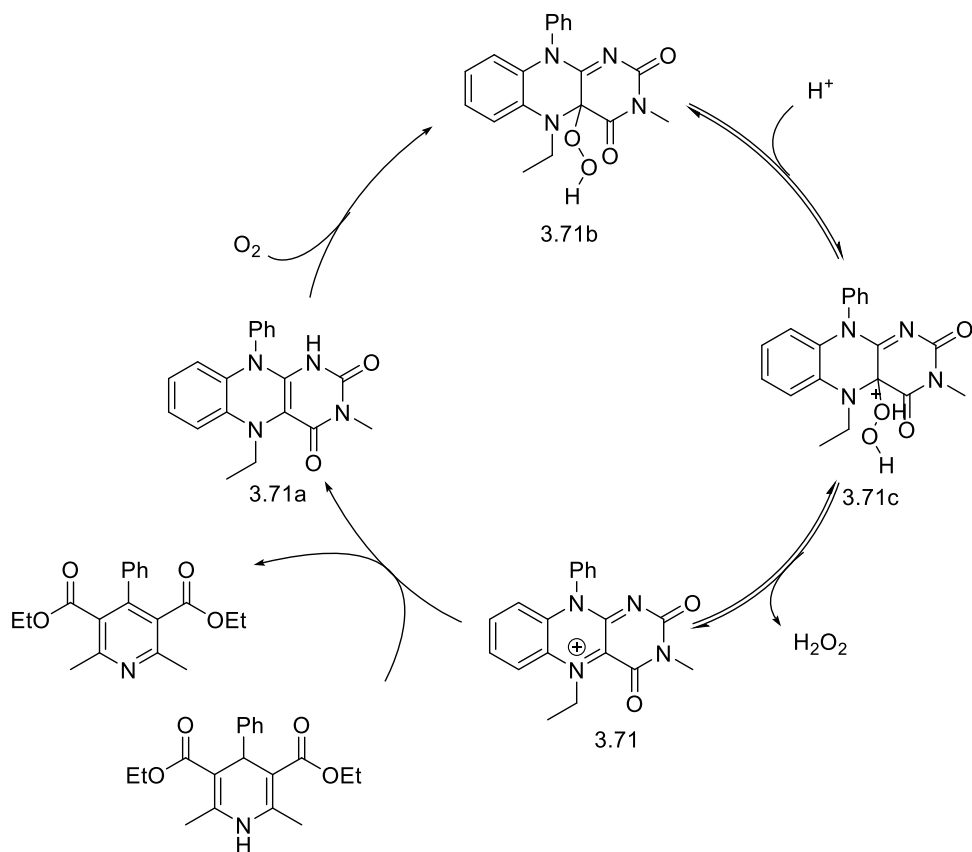


Figure 3.18 The plausible mechanism for acid catalyzed aromatization

The benzothiazoline compounds were oxidized to the respective benzothiazole using the alloxazinium catalyst **3.40**. Although it was reported that the benzothiazoline undergoes autooxidation in presence of chloroform but distilled chloroform shows no conversion of the product. In our acid and metal free catalyzed reaction, the reaction is complete within 90 minutes. Some electron rich benzothiazoline **3.74d**, **3.74g** formed 20% and 25% benzothiazole under the control reaction condition (**Figure 3.19**). Most of the substrates were used by Dr. Chen except the substrates **3.74c**, **3.74e** and **3.74f**.

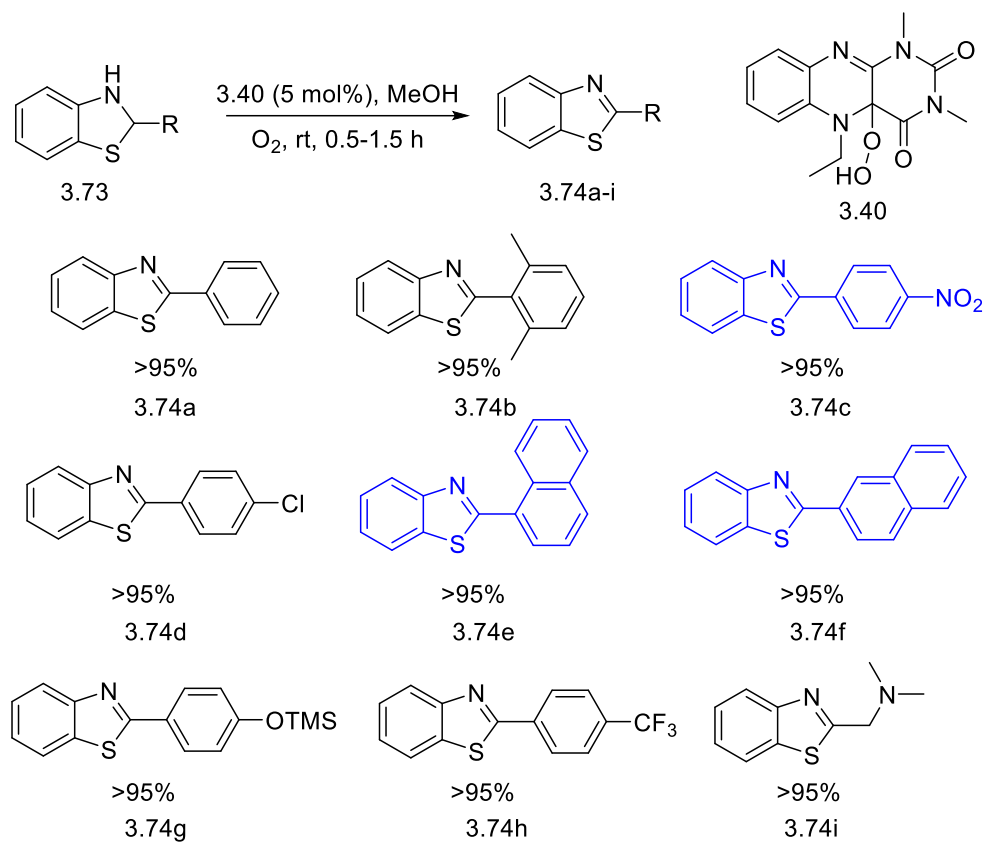


Figure 3.19 Alloxazine catalyzed benzothiazoline aromatization

After successful conversion of benzothiazoline to benzothiazole, Dr. Chen also reported the synthesis of a series of benzothiazole in a one-pot method using aminothiophenol and an aldehyde with 5 mol% catalyst and in presence of air. (**Figure 3.20**)

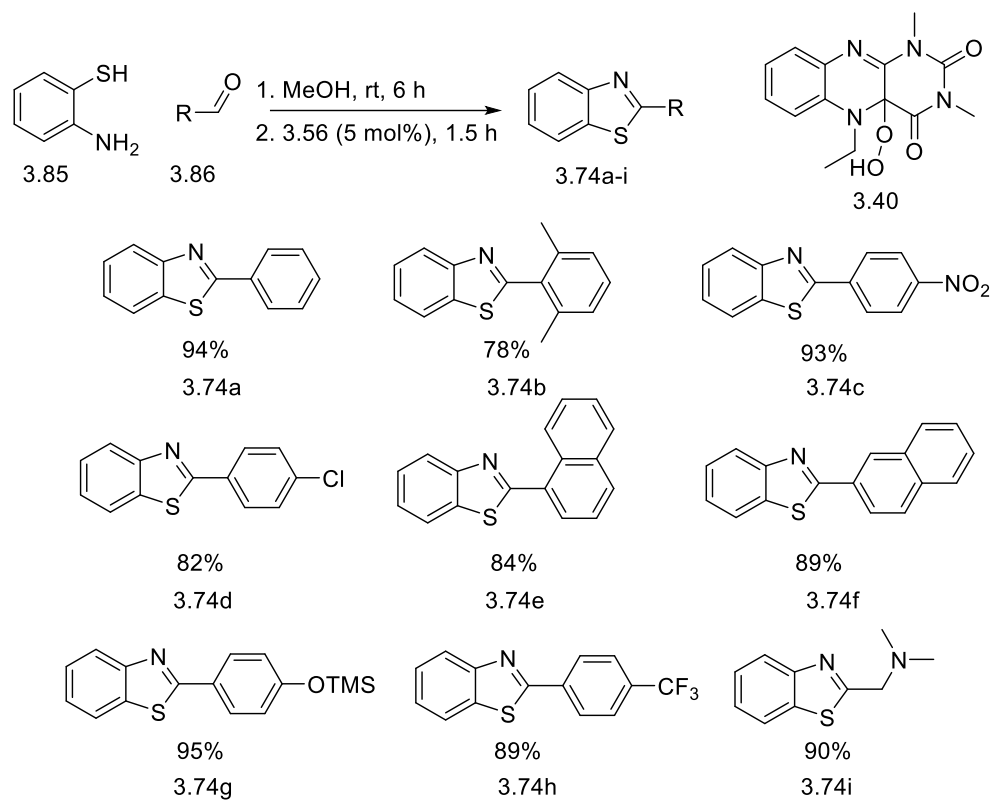


Figure 3.20 Two components one pot aromatization of benzothiazolines

In summary, a green and biomimetic oxidative aromatization was developed using flavinium catalysts. A series of dihydropyridines and benzothiazolines were oxidized to pyridine and benzothiazole using oxygen as terminal oxidant. One-pot syntheses of benzothiazole and pyridine was also developed using 2-5 mol% of flavinium catalyst at room temperature and shorter reaction time. The improvement in catalyst design to incorporate on solid support will be very useful to increase the reusability of the catalyst. This milder method of oxidation will open a new horizon for the selective, efficient and sustainable oxidation of other prearomatic compounds including benzimidazolines, benzoxazolines.

Chapter 4

Flavin as cancer cell inhibitor

4.1 Introduction

A number of approaches have been developed to inhibit the growth of the cancer cells. Among several classes of epigenetics drugs, DNA demethylating agents inhibits DNA methyltransferase to reduce overall levels of DNA methylation. There are two types of DNA demethylating agents, nucleoside DNMT (DNA methyl transferase) inhibitors and nonnucleoside DNMT. First nucleoside DNMT was developed in 1960s¹¹⁹ and the activity of drug involves the incorporation with DNA. But the nonnucleoside DNMT does not incorporate with DNA therefore less toxic and better tolerated in clinical settings.

Another class of drug known as histone deacetylase inhibitors (HDACis), which alters the acetylation condition of the several membrane proteins. Due to the crosstalk between different epigenetic mechanisms, a combination of drugs was used to treat the cancer cell growth.

Histone methylation occurs on lysine and arginine residues and mediated by histone methyl transferases (HMTs) and protein arginine methyltransferases (PRMTs) respectively. This modification correlated with a variety of human diseases including cancer. Recently it has been reported that Lysine-specific-demethylase (LSD1) is an amine oxidase that works with methyl transferases to maintain the global methylation pattern of histone. LSD1 is a FAD dependent protein, which forms formaldehyde and Hydrogen peroxide after demethylation of the N-terminal methyl groups. Several reports supports the role of LSD1 in tumorigenesis.⁶⁶

Fischer and coworkers screened a number of 5-deazaflavins as potent activators of p53 to inhibit cancer cells.⁶⁸

4.2 Synthesis of artificial flavin analogs

A number of artificial alloxazine and isoalloxazine analogs with different types of polar and nonpolar substituents were synthesized using a novel procedure via potassium salt of the alloxaziunium and isoalloxazinium.

The general procedure includes the synthesis of the core structure of the alloxazine and isoalloxazine by condensing *o*-phenylenediamine **4.1** and *N*-Ph-*o*-phenylenediamine **4.6** with alloxan monohydrate **4.2** in presence of boric acid and acetic acid. The salt of the alloxazine **4.4** and isoalloxazine **4.8** were formed by heating with K_2CO_3 in DMF. The isolated salt was used further without any extra purification step. Depending on the final structure of the artificial flavin **4.5a-f** and **4.10a-c**, the alkylation of the salt was performed in DMF. (Figure 4.1)

Previous synthetic protocol involved the one pot synthesis of flavin with K_2CO_3 and alkylating agent. The deportation of flavin required heating prior to alkylation and some of the alkylating agents undergo elimination reaction in presence of base and heat to lower the overall reaction rate. The two pot synthesis improves the overall yield of the reaction by forming the potassium salt in absence of the alkylating agents.

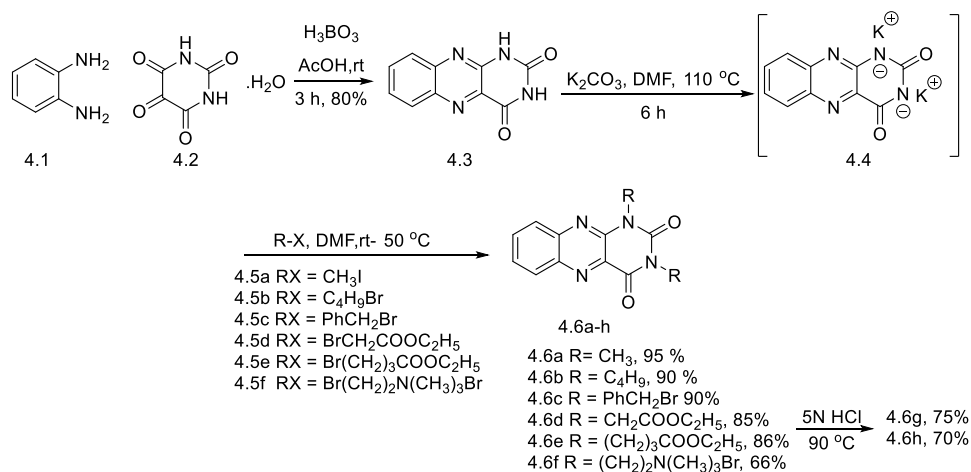


Figure 4.1 Alloxazine derivatives synthesis

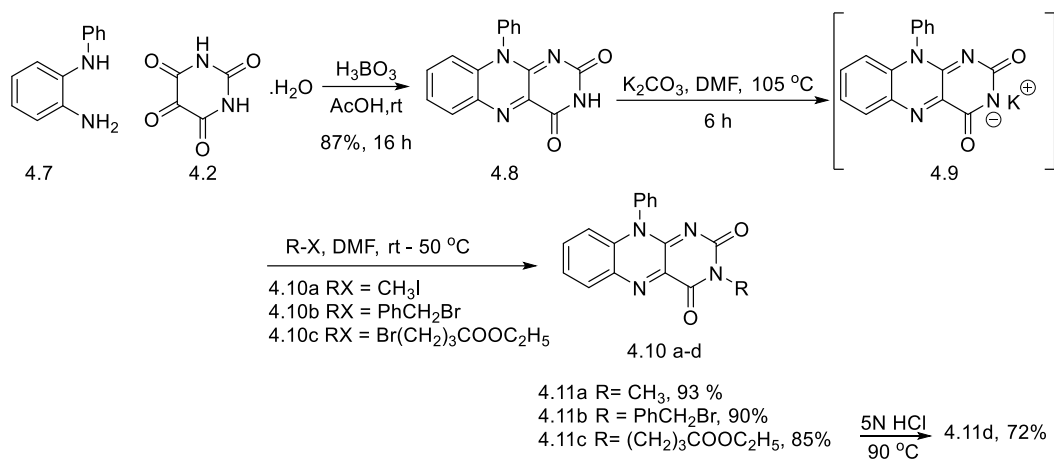


Figure 4.2 Synthesis of 10-Ph isoalloxazine derivatives

Compound **4.6g**, **4.6h** and **4.11d** were synthesized by acid hydrolysis of the corresponding esters with 5N HCl at 90 °C.

The synthesis of compound **4.13** will be discussed in chapter 7 and the compound **4.12** was synthesized according to the published report¹²⁰ 3,10-dimethylalloxazine **4.14** was synthesized by condensing *N*-methyl-*o*-phenylenediamine **4.15** with alloxane monohydrate and followed by alkylation with methyl iodide in presence of potassium carbonate.

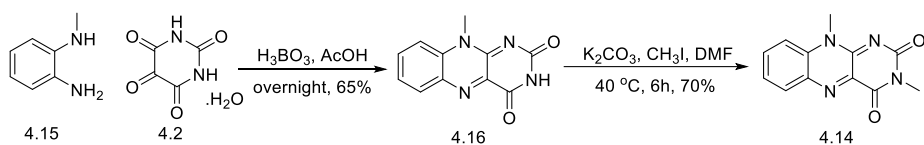


Figure 4.3 Synthesis of 3,10-dimethyl isoalloxazine 4.14

4.3 MCF7 and MCF10 cell inhibition

The artificial flavin compounds were screened for the growth inhibition of human breast cancer cells MCF7 using MTT growth assay with *cis*-platin ($IC_{50} = 19.4 \mu\text{M}$) as the positive control.¹²¹⁻¹²⁵ These results were produced in collaboration with Professor Subhrangshu Mandal and coworkers. The inhibition results were tabulated in Table 4.1. The 5-deazariboflavins **4.12** and **4.13** were found to be inactive ($IC_{50} = >100 \mu\text{M}$) as growth inhibitors. Among the alloxazine and isoalloxazine derivatives, **4.6a-h** and **4.11a-c**, compounds containing acidic, ammonium and ester groups at *N*-1 and *N*-3 positions showed lower inhibition. In between the two classes, isoalloxazines with nonpolar groups in *N*-3 and *N*-5 positions exhibited more inhibition than the alloxazines. Among the compounds, 10-Ph isoalloxazine derivatives **4.11a** ($IC_{50} = 14.8 \mu\text{M}$) and **4.11b** ($IC_{50} = 19.4 \mu\text{M}$) inhibited the growth of MCF7 cells comparable to the *cis*-platin.

To study the selectivity of inhibition for cancer cells vs. healthy cells with artificial flavins, two analogs **4.11a** and **4.11b** were screened against the non-malignant breast epithelial cells (MCF10) using MTT growth assay. Surprisingly, compounds **4.11a** and **4.11b** showed significant selectivity towards breast cancer cells (MCF7) over non-malignant breast epithelial cells (MCF10). In between these two artificial flavins, **4.11b** showed less inhibition of MCF10 cell growth compared to *cis*-platin. The result is shown in **Table 4.2**.

Table 4.1 Data for MCF7 cell inhibition

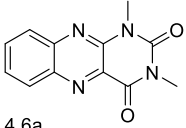
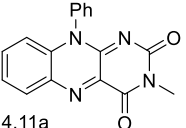
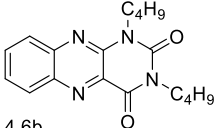
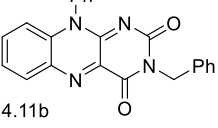
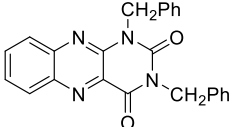
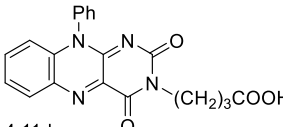
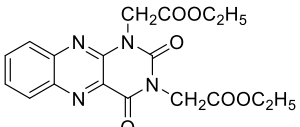
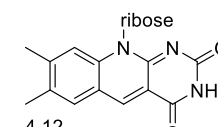
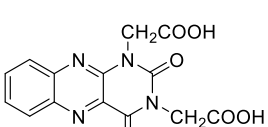
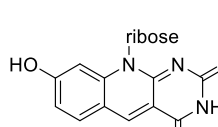
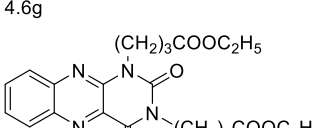
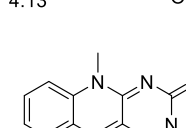
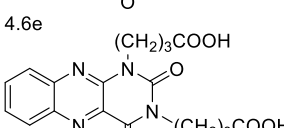
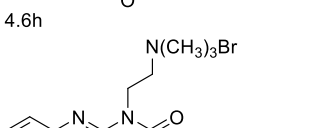
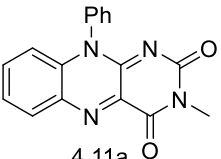
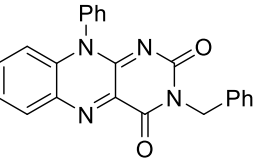
Substrate	IC ₅₀ (μM)	SEM	Substrate	IC ₅₀ (μM)	SEM
 4.6a	45.1	0.85	 4.11a	14.8	3.56
 4.6b	59.4	1.55	 4.11b	19.4	2.15
 4.6c	67.7	1.05	 4.11d	>100	NA
 4.6d	>100	NA	 4.12	> 100	NA
 4.6g	>100	NA	 4.13	> 100	NA
 4.6e	>100	NA	 4.14	23.3	2.05
 4.6h	>100	NA			
 4.6f	>100	NA			

Table 4.2 MCF10 growth assay with artificial flavins

Substrate	IC ₅₀ (μM)	SEM
 <p>4.11a</p>	72.4	1.28
 <p>4.11b</p>	>100	NA
cis-platin	90.5	1.48

In summary, among the different classes of artificial flavins, isoalloxazines were found to be better cancer cell (MCF7) growth inhibitors than alloxazines. Among the alloxazines, compounds with smaller substituents at *N*-1 and *N*-3 positions inhibited the growth of MCF cancer cells effectively.

4.4 Docking experiment

Among the different proteins involved in cancer cells, LSD1 is a FAD (flavin adenine dinucleotide) dependent protein, which controls the demethylation of lysine in histone. The synthesized artificial flavins have the similar isoalloxazine core structures as FAD. A docking experiment was studied to compare the possible binding capability of the artificial flavins in the binding site of the FAD using Autodock.¹²⁶ This computational study was done in collaboration with Diego Lopez. To our delight, both active flavin analogs **4.11a** and **4.11b** have the ability to bind in the same binding site as FAD with similar orientation and energy.

The relative binding energy of the substrates compared to the FAD is shown in **Figure 4.4**, also the relative orientation and overlapping of substrates with FAD in the active site are shown in **Figure 4.5-4.6**.

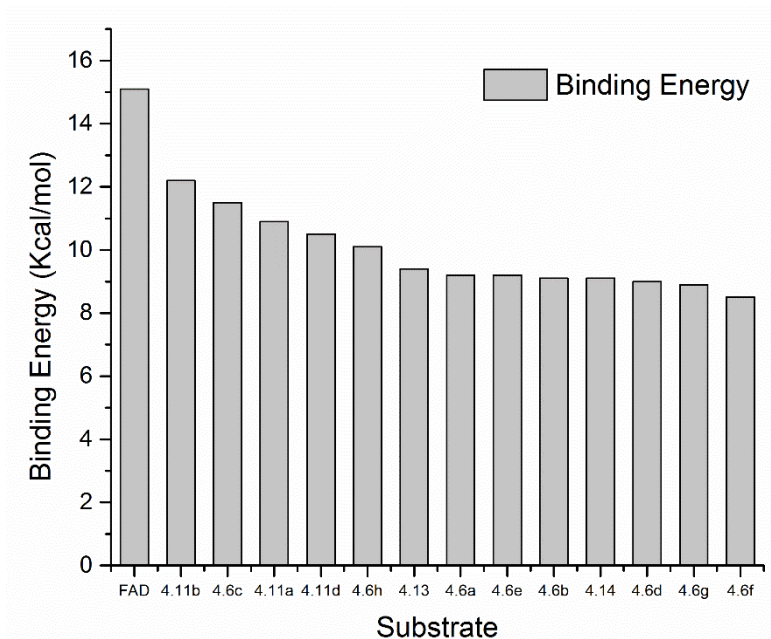


Figure 4.4 Comparison of binding affinities with the natural substrate
(Binding energy is in negative scale)

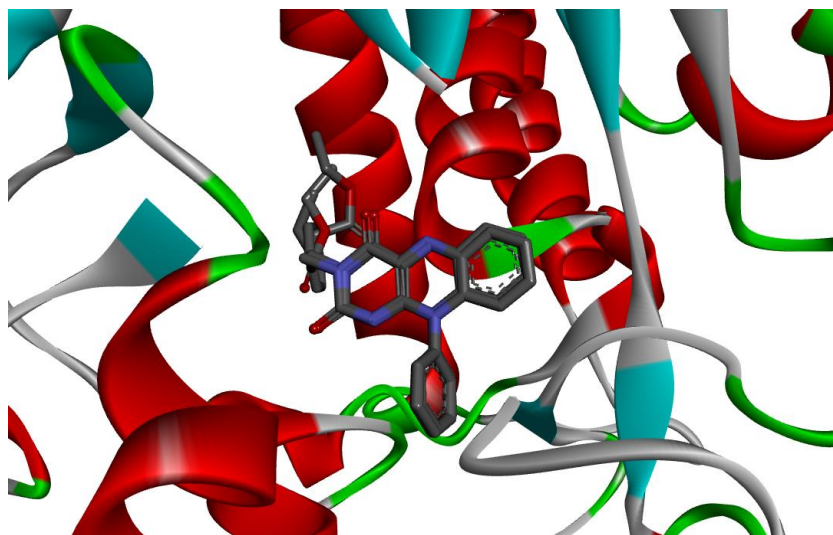


Figure 4.5 Overlapping of six flavin mimics in the binding site

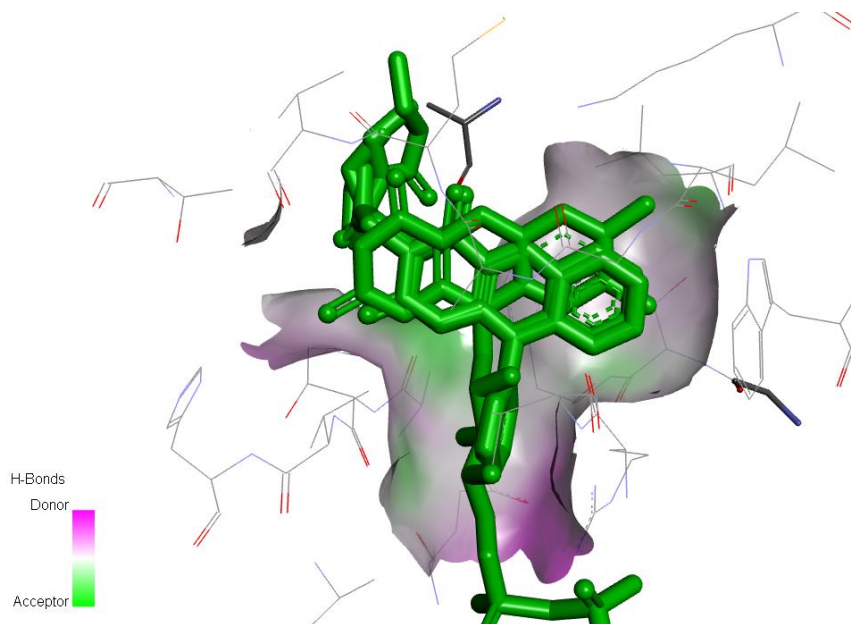


Figure 4.6 Comparison of binding orientation with natural cofactor (FAD)

Figure 4.5 represents the overlapping of six of the artificial flavins in the active site and **figure 4.6** represents the relative orientation of artificial flavins with FAD in the active site.

In summary, this is the first report to use the artificial flavin as the inhibitor for the MCF7 type breast cancer cell. Initial screening of the flavin mimics showed the inhibition for MCF7 but they are not active inhibitor for non-malignant MCF10 cells. The activity of the artificial flavins may be related to the demethylation of histone in presence of LSD1 or it may act as the 5-deazaflavins.⁶⁸ This initial screening opened a research ground to investigate the role of flavin in cancer cell inhibition specially to design new flavin molecules with polar and non-polar substituents on the benzene ring of the *N*-3 and *N*-10 positions of **4.11b**.

Chapter 5

Water-soluble Flavin catalysts

5.1 Introduction

Natural flavins, flavin adenosine dinucleotide (FAD) **5.1** and flavin mononucleotide (FMN) **5.2** exhibits important role as redox cofactors in enzymatic processes. The stability and solubility of these natural flavins in different solvents limited the investigation of the properties of flavin molecules. Robust flavin mimic structures are required to study the functions of flavins in solvents comparable to natural system. Synthetic alloxazine (I) and isoalloxazine (II) are used for decades to investigate the flavin properties as well as to mimic the redox chemistry of natural flavins.^{13,127} To improve the solubility as well as the reactivity of these artificial flavins, *N*-5 alkylation is an essential step, which modifies the electronics of the tricyclic core structure but this modification encumbers the natural substrate mimicking. The ribose moiety in FMN and FAD decreases the stability of the natural flavins. Current research involves designing new water soluble robust flavin analogs without *N*-5 alkylation and their application in biomimetic research.

Chemical space modification of *N*-1 and *N*-3 positions of the alloxazine and *N*-3 *position* of the isoalloxazine lead us to design new highly water soluble flavin analogs. We have introduced both positively and negatively charged side chains, which facilitates the water solubility in a new synthetic approach.

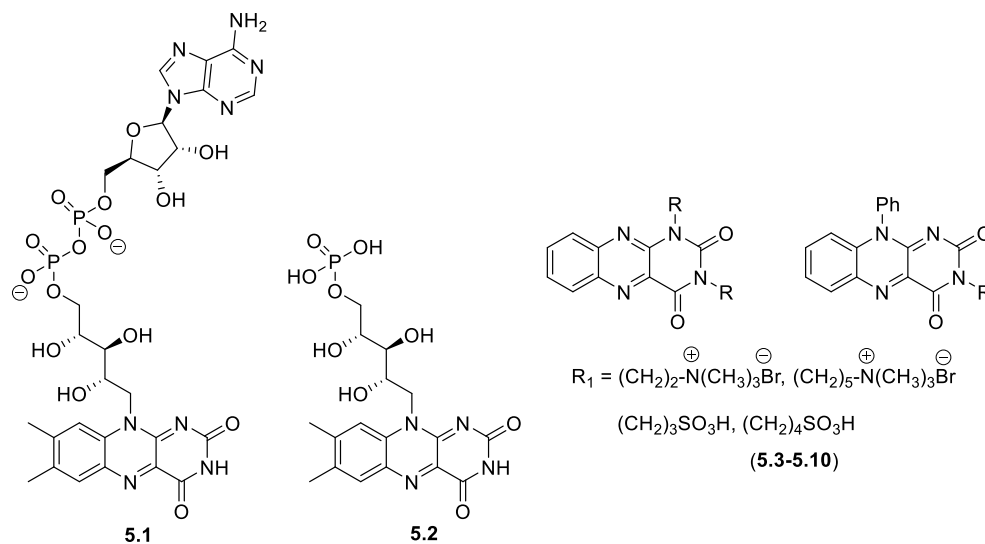


Figure 5.1 Structures of natural flavins and water soluble flavin analogs

5.2 Synthesis of water-soluble flavin molecule

The synthesis of alloxazine moiety (**5.13**) was accomplished by condensing *o*-phenylenediamine (**5.11**) with alloxan monohydrate (**5.12**) in acetic acid in presence of boric acid. The isolated product was used for alkylation with **5.14** and **5.15** at *N*-1 and *N*-3 position by using the regular methods used for in situ methylation.⁹¹ Due to different reactivity and thermal stabilities of these alkylating agents compared to regular alkyl halides, no desired product was isolated with **5.14** at room temperature and also at higher temperature we isolated the *N*-1 and *N*-3 di methylated alloxazine product, which is the indication of Hoffman elimination product (**5.16**) of the alkylating agent.

For an alternate route to introduce quaternary ammonium group at *N*1 and *N*3 positions we tried to use *N,N*-dimethylated reagent (**5.17**) instead of *N,N,N*-trimethylated (**5.14** or **5.15**) reagent to introduce the tertiary amine followed by methylation to synthesize the quaternary product.

But the reaction between the alloxazine and the tertiary amine lead us to intermolecular product (**5.18**) instead of alkylation.

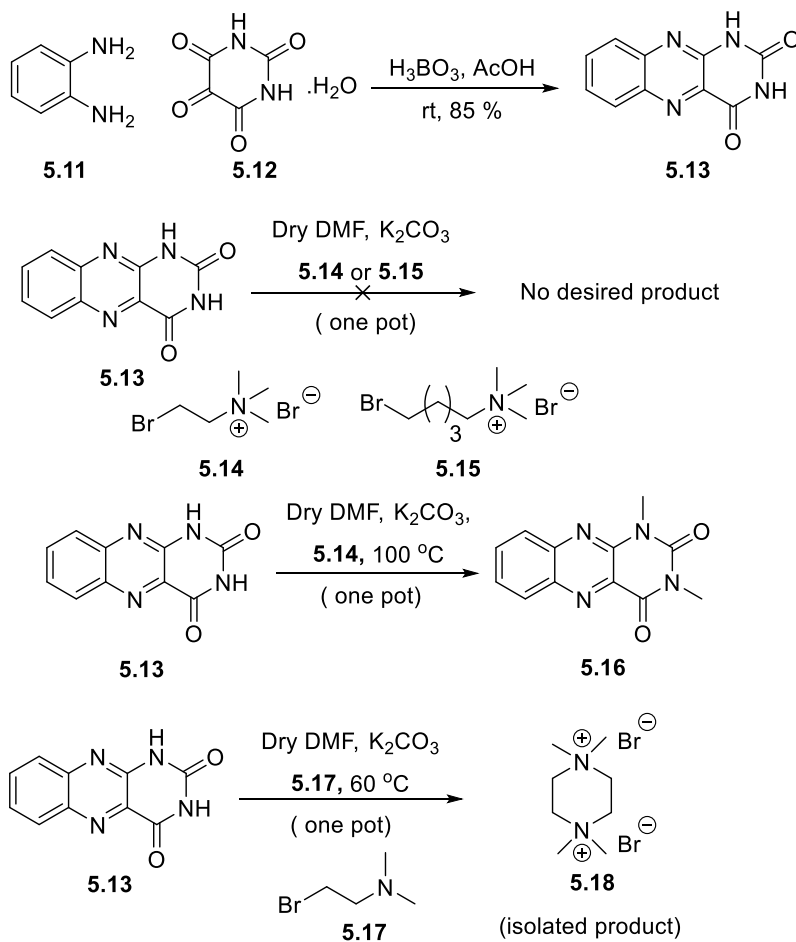


Figure 5.2 Initial approach to install quaternary group

We have designed another approach to accomplish the synthesis of quaternary amine containing flavin molecule, which comprises two steps – first the synthesis of dipotassium alloxazine (**5.19**) species by heating alloxazine with potassium carbonate in DMF and second treatment of the isolated salt with the desired bromo alkyl ammonium species (**5.14 or 5.15**) in DMF to synthesize the desired product with higher yields.

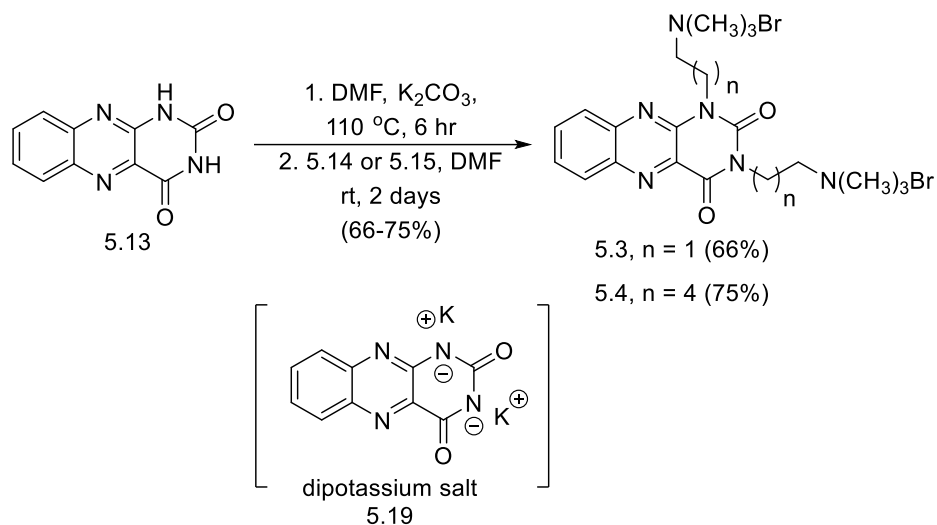


Figure 5.3 Synthesis of quaternary ammonium derivative of alloxazine

The isolated dipotassium salt of alloxazine was also used to synthesize the water soluble sulfonic acid derivatives of alloxazines. Both propane sultone (**5.20**) and butane sultone (**5.21**) were reacted with the dipotassium salt of alloxazine to yield the corresponding sulfonic acid (**5.5** and **5.6**) in higher yields.

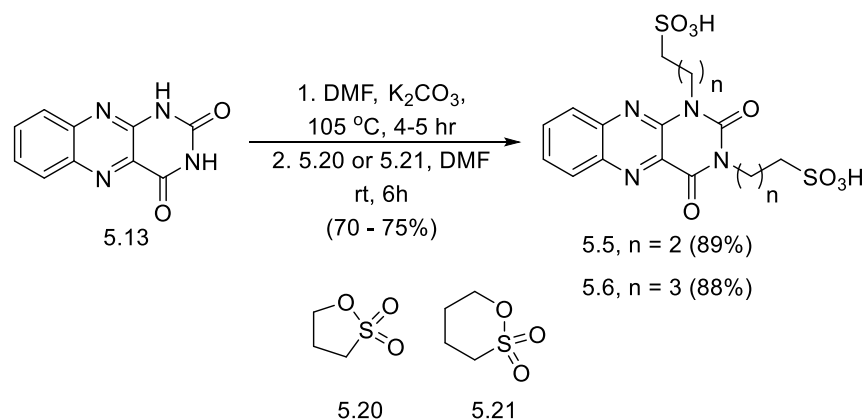


Figure 5.4 Synthesis of sulfonic acid derivatives of alloxazine

The tricyclic 10-Ph isoalloxazine (**5.23**) structure was synthesized by using *N*-phenyl-*o*-phenylenediamine (**5.22**) and alloxan monohydrate (**5.12**) in acetic acid in the presence of boric acid. Similar to the alloxazine, monopotassium salt (**5.24**) of the 10-Ph isoalloxazine was synthesized by heating **5.23** with potassium carbonate in DMF and the salt was used with corresponding alkylating agents **5.14**, **5.15**, **5.20** and **5.21** to synthesize the compounds **5.7**, **5.8**, **5.9** and **5.10** respectively with good yields.

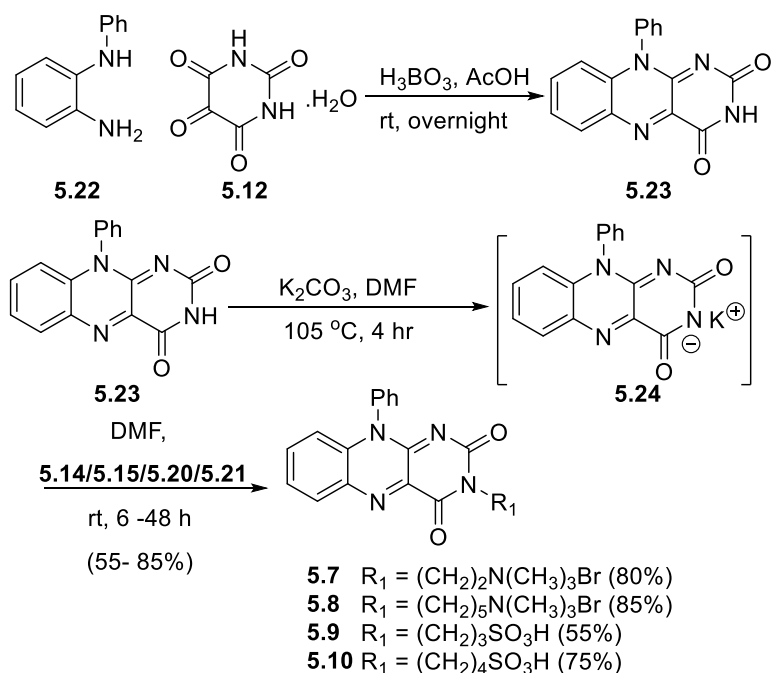


Figure 5.5 Synthesis of water soluble 3- substituted 10-Ph isoalloxazine derivatives

5.3 Application of water-soluble water molecule

5.3.1 Electrochemical activation of molecular oxygen

The Flavin catalytic cycle involves the reduction of oxidized flavin, the reduced flavin is capable to activate oxygen to form reactive oxygen species like H_2O_2 . It was already reported from our group the use of Hantzsch ester, benzothiazoline as the

reducing agent. Since electrons are the cheapest reductant, we have studied the electrochemical properties of water soluble flavins in N₂ and O₂ atmosphere. The research was conducted in collaboration with Dr. Rajeshwar using cyclic voltammetry. In presence of oxygen, flavin (5.3) catalytically activates oxygen, which was indicated by the large amount of current generation compared to the system with N₂ atmosphere. (Figure 5.6)

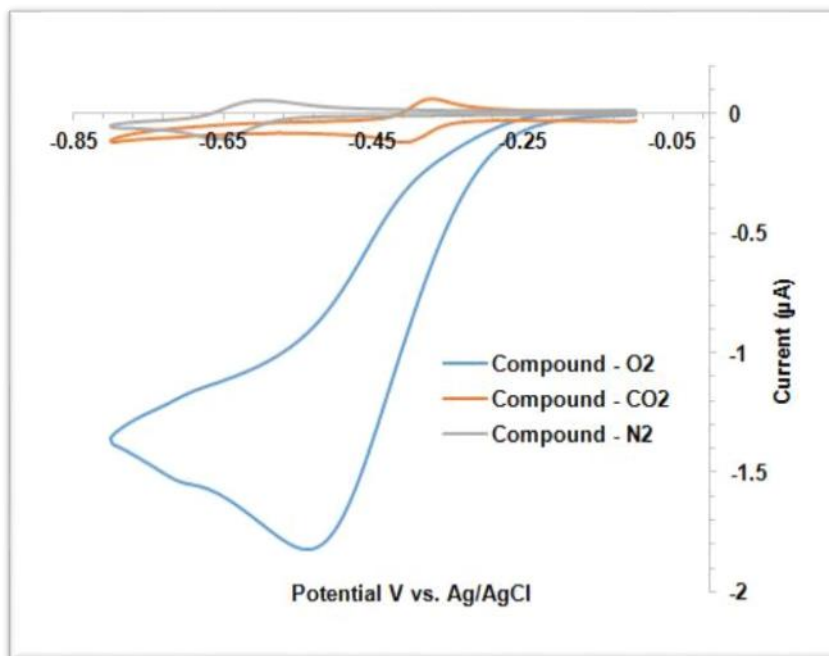


Figure 5.6 Cyclic voltammetry of 5.3 with 0.1M Na₂SO₄ and scan rate 0.02 V/sec

A comparison of cyclic voltammetry data of alloxazine (5.3) and isoalloxazines (5.7, 5.8 and 5.10) indicates higher half potential for isoalloxazine than the alloxazines (Figure 5.7). All the isoalloxazines have the similar half potential and all of the compounds electrochemically activate the molecular oxygen (Figure 5.8).

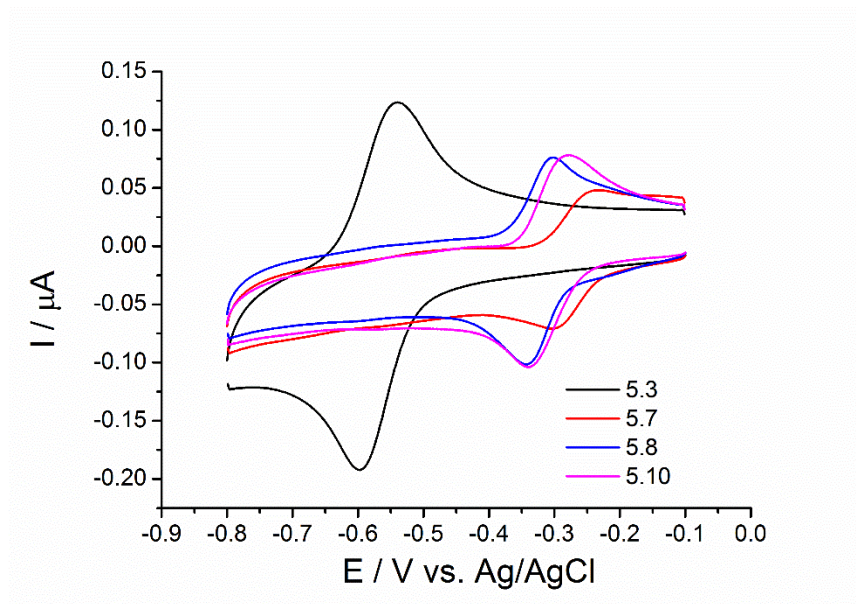


Figure 5.7 Cyclic voltammetry data comparing alloxazine and isoalloxazines

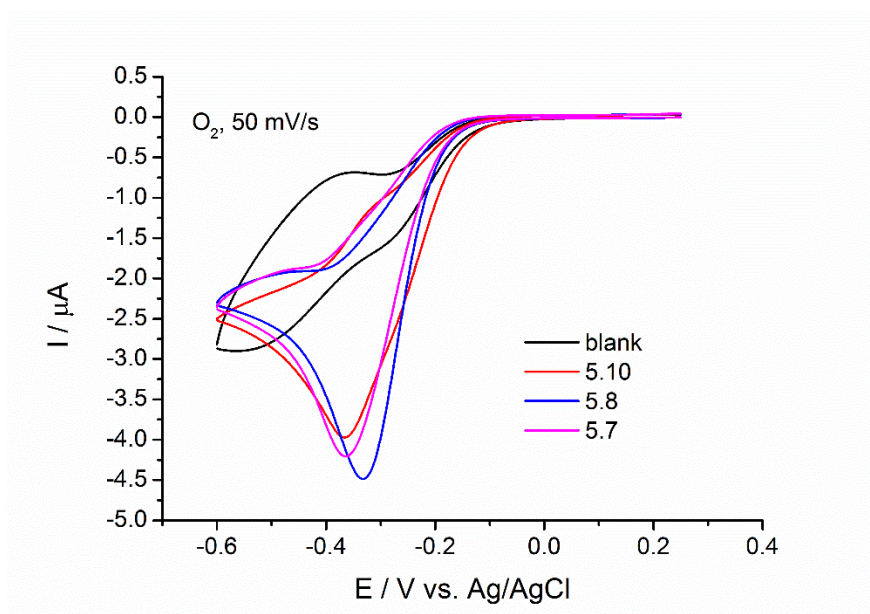


Figure 5.8 Catalytic electrochemical activation of O_2 using isoalloxazines

5.3.2 Methyl orange degradation

The degradation of organic molecules with riboflavin as photosensitizer using light is being studied extensively. The proposed mechanism involved the photo-excitation of singlet riboflavin to the triplet state and relaxation of singlet riboflavin to triplet through inter system crossing (ISC) and final relaxation to the singlet ground state. The emitted energy can be transformed to the triplet oxygen to form reactive singlet oxygen. Reactive oxygen can further degrade the organic products.

The instability of the riboflavin under UV-vis light indicates the formation of lumichrome via the formation of lumiflavin and lumichrome is reported to be the active photosensitizer for the degradation of flavin. Another drawback of the riboflavin is the extremely lower solubility of the lumichrome and riboflavin.

To study the function of artificial alloxazine and isoalloxazines as photosensitizer, this research was conducted in collaboration with Dr. Rajeshwar.

Alloxazine compound having the similar core structure as lumichrome is being used to study the degradation of methyl orange. The synthesized water soluble alloxazinium **5.3** was found to be an active photosensitizer under visible light (400W medium pressure mercury light) in presence of O₂. The rate of degradation of methyl orange (100 μM) is higher for alloxazine **5.3** (100 μM) than isoalloxazine **5.7** (100 μM) in presence of oxygen and TiO₂. No significant photodegradation of methyl orange was observed in the absence of light. The incorporation of TiO₂ with alloxazine improved the rate of degradation of dye slightly (**Figure 5.9**). In a different experiment, it was found that TiO₂ enhanced the degradation of flavin in presence of UV light. Also UV light itself degrades alloxazine (**5.3**) slowly (**Figure 5.10**), but under visible light the flavin (**5.3**) is highly robust (**Figure 5. 11**).

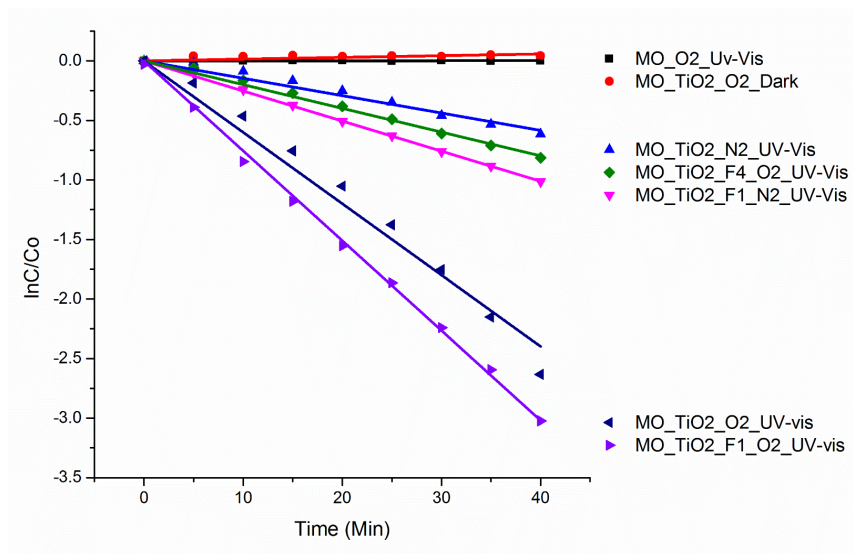


Figure 5.9 Comparing conditions of MO degradation with F1 = 5.3 and F4 = 5.7

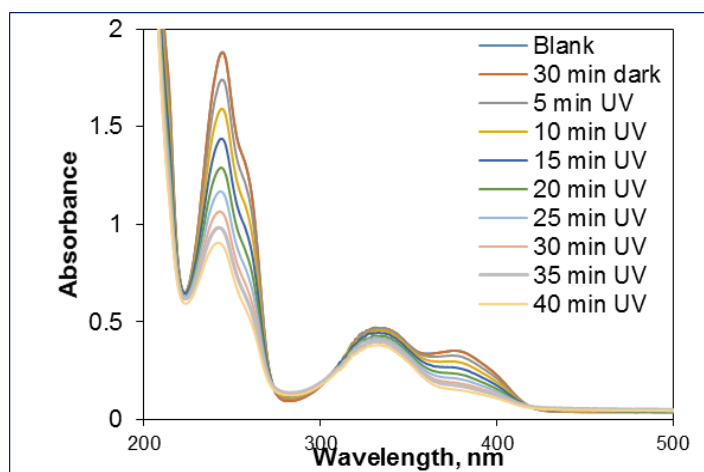


Figure 5.10 Degradation of alloxazine 5.3 under UV-vis light

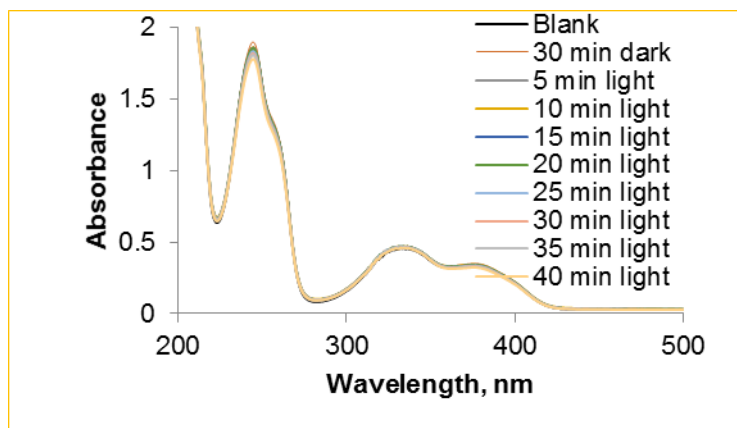


Figure 5.11 Degradation of alloxazine 5.3 under visible light

Due to instability of alloxazine (**5.3**) in presence of TiO_2 and UV light, the degradation of methyl orange (MO) was studied in presence of visible light (using 0.72M NaNO_2 solution filter) and the result showed a rapid degradation of methyl orange (**Figure 5.12**). The peak at about 550 nm represents the methyl orange where the peak at about 450 nm represents alloxazine (**5.3**).

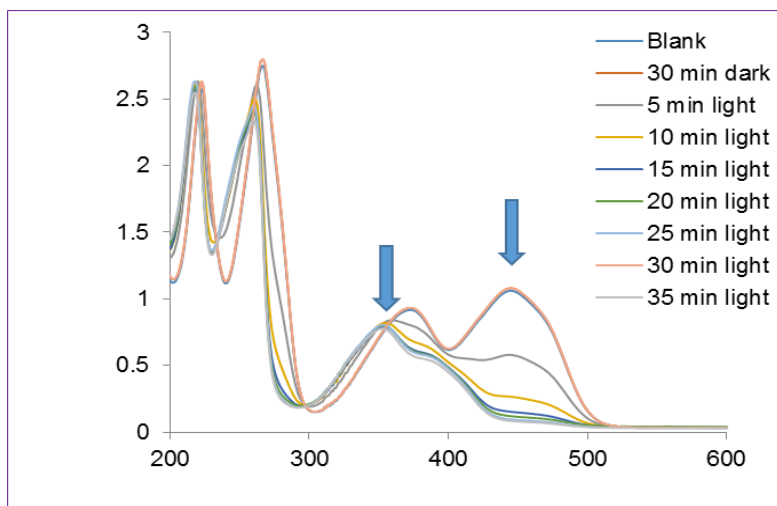


Figure 5.12 Degradation of MO in presence of alloxazine and UV-vis light

In summary, this research is the first report to use artificial flavins as the photosensitizer. It also proved the higher stability and higher activity of alloxazine as a photosensitizer than isoalloxazines. The outcome of the research will not limited to the degradation of dyes, it can be extend to the removal of organic pollutant photocatalytically. This preliminary data will encourage us to design new artificial flavins with different substituents to tune both the stability and solubility. A heterogeneous catalytic system could also be designed to increase the turn over number of the flavins.

Chapter 6

Metal-flavin hybrid systems

6.1 Introduction

Among the metal oxides, TiO₂ is the most promising photocatalyst, which has been studied for the degradation of organic pollutants, water dissociation, solar energy conversion and disinfection.¹²⁸ But due to the energy band gap of 3.2 eV, TiO₂ can only be excited by a small fraction of UV light of sunlight. The higher rate of electron-hole recombination also results lower quantum yield and poor efficiency of TiO₂.

Various attempts were made to sensitize TiO₂ for much larger visible light regions including doping of TiO₂ with transition metal ions.¹²⁹ Chemical doping of transition metals can introduce donor and /acceptor energy level in the forbidden band of TiO₂ to exhibit visible light response. Novel metals like Au, Ag, Pt doped TiO₂ was also reported as promoting organics degradation using TiO₂ under UV irradiation.¹³⁰⁻¹³² Self-assembled monolayers (SAMs) grown on the solid metal oxide using linker group containing organic compounds was studied for the degradation of organic pollutants. Due to the lower cost, nontoxicity and relatively higher efficiency of anatase form of TiO₂ was used not only for water and air decontamination¹³³ but also for self-cleaning applications.¹³⁴ The photocatalytic degradation of organic pollutants involves the excitation of electrons from the valance band to the conduction band creating electron-hole pairs. The holes are trapped by H₂O or OH⁻ to form hydroxyl radicals and on the other hand, the electrons reduce adsorbed oxygen to superoxide radicals. The generated reactive oxygen species (ROS) attacks the organic pollutants to form the stable molecules such as CO₂ and H₂O. **(Figure 6.1)**¹³⁵ The surface properties of the metal (Au, Ag) , metal oxides (SiO₂, TiO₂, Al₂O₃, BiOCl), and semiconductors (Si, GaN, InP) can be altered by the SAMs. This modification can led to the phenomenon like wetting properties (hydrophobicity,

hydrophilicity, and oleophobicity), electronic properties (affecting the band to form charge conduction) and also to form a tailored three-dimensional supramolecular arrays by attaching a specific molecule to an external functional group.

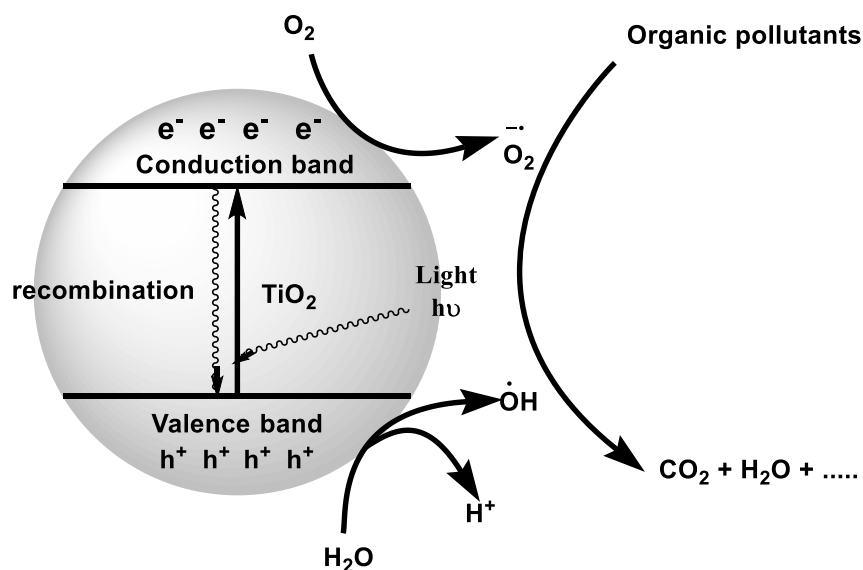


Figure 6.1 Organic pollutant degradation using TiO_2 as photocatalyst

Since both SiO_2 and TiO_2 are capable of forming surface hydroxyls, the SAMs on titania may resemble the SAMs on the silica. This similarity varies on the type of the linker that connects the surface and the organic tails. Because of the different electronegativity of Ti (1.50) compared to Si (1.90) the polarity of M-O bond of the oxide, the zero charge of the oxide and the number of OH sites on the surface will be different.

SAMs of TiO_2 with phosphonic acids were not clearly understood. The presence of P-O-Ti, P=O, and P-OH indicated that mono-, bi- and tridentate surface phosphonate units can be present in these monolayers (**Figure 6.2**). The composition of these bonds is dependent on the tail group too.

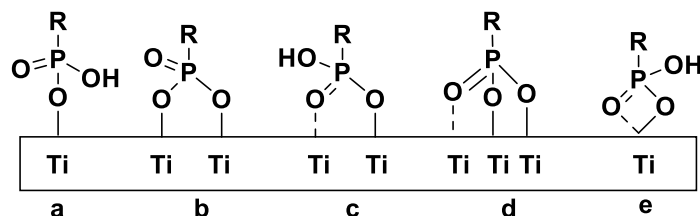


Figure 6.2 Different binding modes between phosphonic acids SAMs and TiO_2

(a) monodentate, (b) and (c) bridging bidentate, (d) bridging tridentate, (e) chelating bidentate¹³⁶

Because of the almost irreversible adsorption of SAMs on the TiO_2 surface, transforms TiO_2 -SAM as a tool to study fundamental phenomenon in photocatalysis as they provide a way to decouple and reaction. SAMs are also utilized to study the so called “remote degradation effect”, namely the effect of degradation of molecules, which are far from the TiO_2 surface.

6.2 Synthesis of flavins with metal-binding groups

To study the SAMs of metal oxide (TiO_2 and BiOCl) and flavins, a number of flavin derivatives were synthesized with different head groups. Among the head groups we have synthesized carboxylic acid, phosphonic acids, sulfonic acid and 1° amine containing compounds (**Figure 6.3**). The synthesis, characterization and application of metal-flavin SAMs have been studied in Dr. Paz lab at Technion, Haifa, Israel.

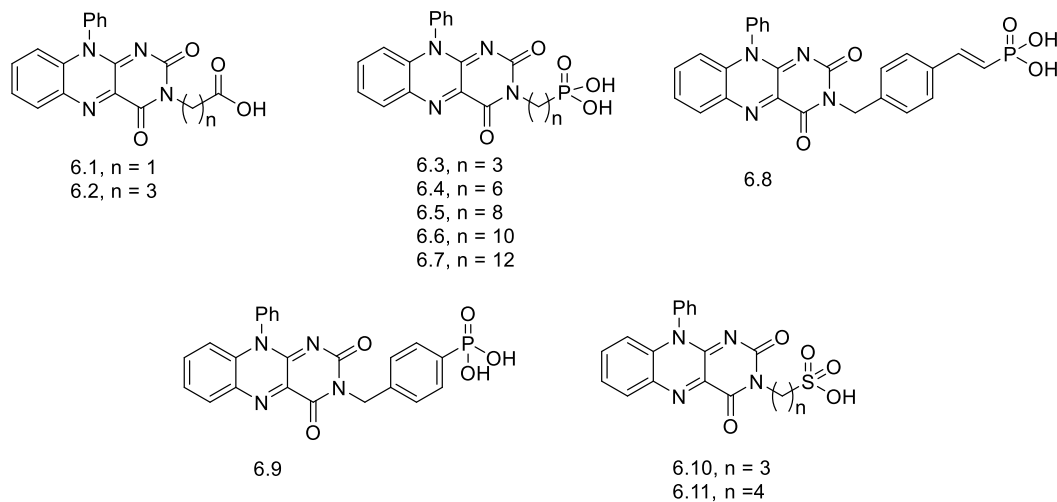


Figure 6.3 Flavin derivatives for SAMs study

Synthetically all the 10-Ph isoalloxazine derivatives were synthesized by using potassium salt of the 10-Ph isoalloxazine (**6.15**), which has been synthesized by condensation of *N*-phenyl *o*-phenylenediamine (**6.12**) with alloxan monohydrate (**6.13**). The substituents at *N*-3 position of the isoalloxazine was introduced by either synthesizing or commercially available reagents.

Carboxylic acids (**6.1** and **6.2**) were synthesized by acid hydrolysis of the corresponding esters (**6.18** and **6.19**), which were synthesized using commercially available ethyl bromocarboxylates (**6.16**, **6.17**) respectively (**Figure 6.4**).

Phosphonic acids (**6.3–6.7**) were synthesized from the corresponding diethylphosphonates (**6.25–6.29**). Different bromo diethylphosphonates (**6.20–6.24**) were reacted with the potassium salt of the 10-Ph isoalloxazine to form the *N*-3 substituted phosphonates. A general Arbuzov reaction was used to synthesize the phosphonates using a dibromoalkane and triethyl phosphite (**Figure 6.5**).

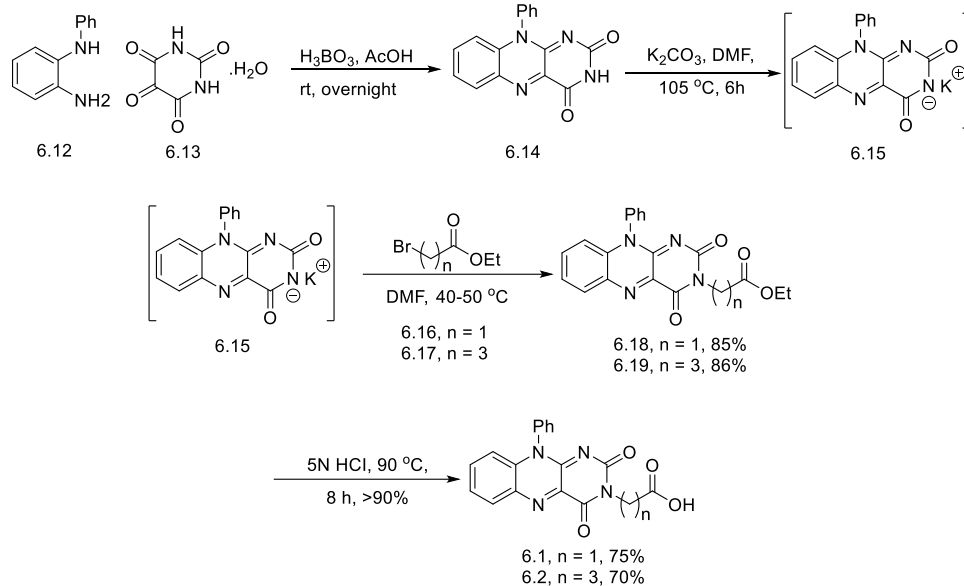


Figure 6.4 Synthesis of carboxylic acid derivatives

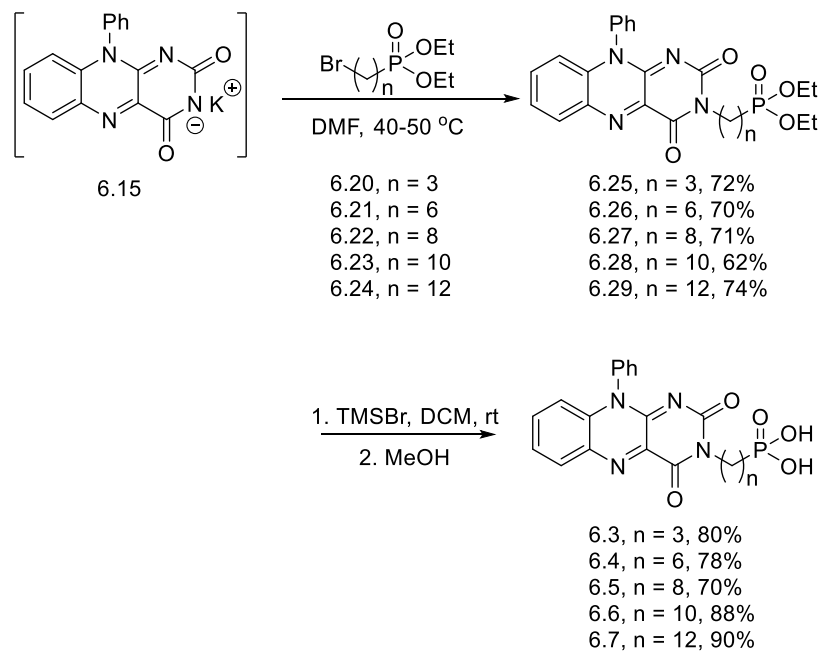


Figure 6.5 Synthesis of phosphonic acids

Compound **6.8** and **6.9** were synthesized as mentioned in **Figure 6.6** with good yields.

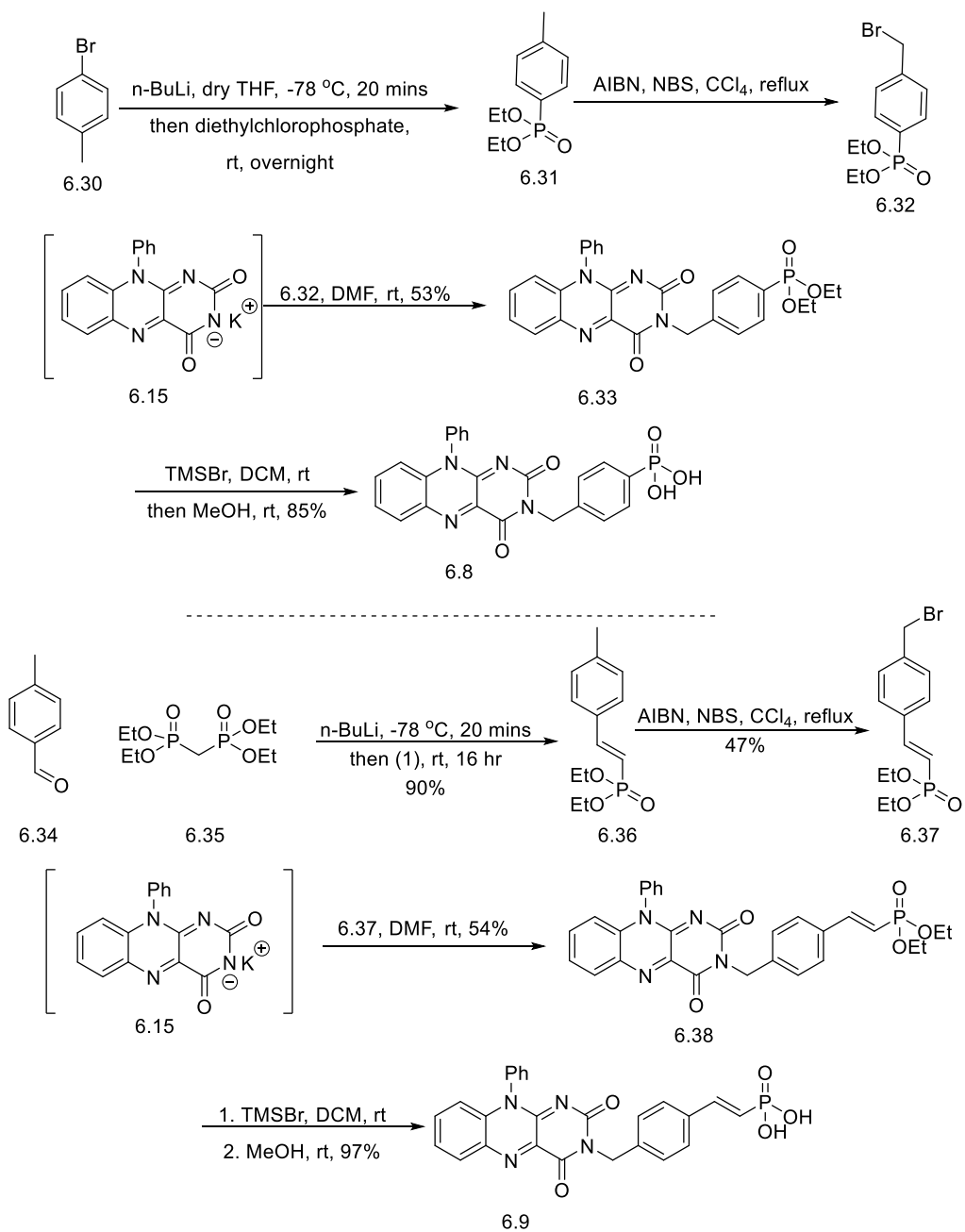


Figure 6.6 Synthesis of phosphonic acid **6.8** and **6.9**.

Propane sultone and butane sultone were used to react with the potassium salt of the 10-Ph isoalloxazine to form the sulfonic acids (**6.10-6.11**) as mentioned in Chapter 5 as **5.9** and **5.10**.

6.3 Application of tethered flavin molecules

The synthesized flavins were used to for SAMs with TiO_2 and BiOCl to investigate the use of redox properties of flavins. Among these phosphonic acids C8-phosphonic acid **6.5** was found to form SAM with TiO_2 effectively and C-4 carboxylic acid **6.2** was effective with BiOCl . To study the photodegradation of organic molecules, ethanol was chosen as experimental standard and surprisingly the TiO_2 -flavin SAM is found to be effective compared to the control. **Figure 6.7** was shared from Dr. Paz lab.

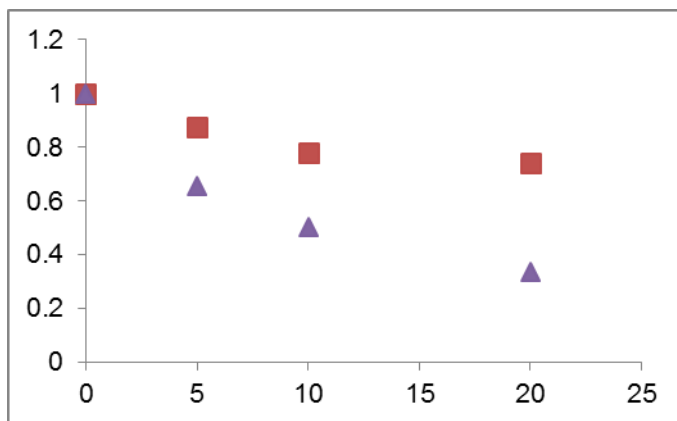


Figure 6.7 The kinetics for photodegradation of ethanol
 TiO_2 -Flavin (purple triangle) and TiO_2 only (red square)

The degradation of salicylic acid was studied with BiOCl-Flavin SAM and the initial screening shows the higher degradation rate of salicylic acid under visible light. A comparison was shared from Dr. Paz lab (**Figure 6.8**).

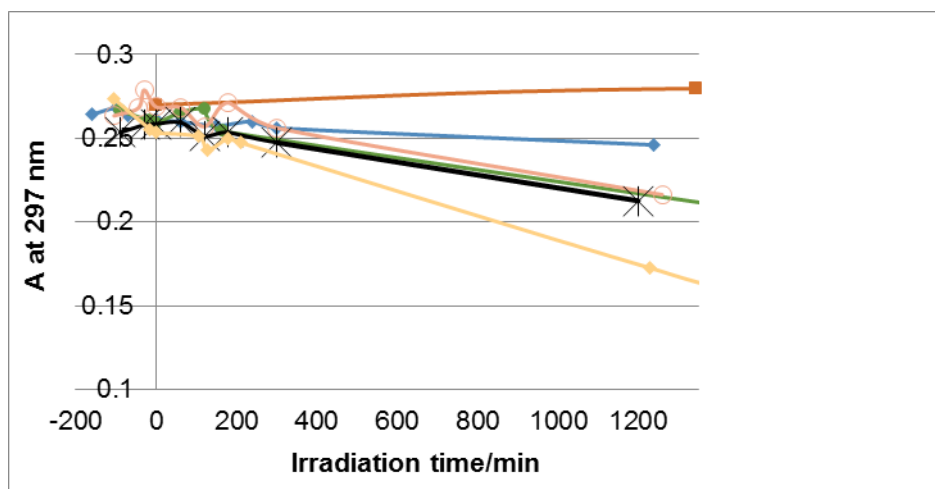


Figure 6.8 The kinetics of SA degradation

6.2/BiOCl (orange circles), 6.3/BiOCl (pink empty circles), 6.5/BiOCl (black asterisk) and by 6.9/BiOCl (purple diamonds) (prepared in the dark) and in the absence of flavins (blue diamond), absence of photocatalyst (red)

In summary, metal-flavin SAMs were showing effective degradation of small organic molecules. A complete kinetic study will open the mechanism for “remote degradation” effect. Synthetic alloxazine type derivatives can also be utilized to investigate the chemistry of isoalloxazine and isoalloxazines. Future research can also introduce photovoltaic cell using metal-Flavin SAM as the mediator between the photosensitizer and metal oxide as acceptor.

Chapter 7

Deazaflavins

7.1 Introduction

5-deazaflavins are structurally similar to flavin with carbon instead of nitrogen at the 5-position. Due to this difference, the redox properties of deazaflavins resembles pyridine nucleotides (nicotinamides) more than the flavin. The deazaflavoproteins undergoes reduction at least 100 times slower than the flavoproteins, flavoproteins usually do not show catalytic turn over, and also among the three main functions of flavoproteins – (de)hydrogenation, O₂-activation and electron transfer, deazaflavoproteins retained the reversible dehydrogenase of the specific substrate enzymes.

Cofactor F₄₂₀ (**7.2, Figure 7.1**), a 7,8-didemethyl-8-hydroxy-5-deazariboflavin derivative, was discovered in the 1970's^{137,138} and is functionally similar to nicotinamide cofactors, NAD(P)⁺, while structurally reminiscent of the isoalloxazine tricyclic system found in flavin cofactors, FAD and FMN. Found primarily in prokaryotes,¹³⁸⁻¹⁴⁴ F₄₂₀ and its precursor 5-deaza-7,8-didemethyl-8-hydroxy-5-deazariboflavin (FO, **7.1**), are important metabolites and unique organic redox-active coenzymes ($E_{1/2} = -340$ to -350 mV) capable of reducing both NAD(P) (ca. -320 mV) and FAD/FMN (ca. -210 mV) in a thermodynamically favourable manner.¹⁴⁵ Due to the relatively acidic phenolic residue at C8, the activity of these species is pH dependent. In the neutral state, reduced FO (FOH₂) performs hydride transfer reactions with relatively enhanced reducing power as compared to NADH. Deprotonated FO was discovered to be a light-harvesting molecule for DNA photolyase in *Drosophila*. We set out to prepare FO synthetically as part of our studies of F₄₂₀ dependant NADP⁺ reductase (Fno), an important enzyme for methanogens, which convert CO₂ to CH₄.¹⁴⁶

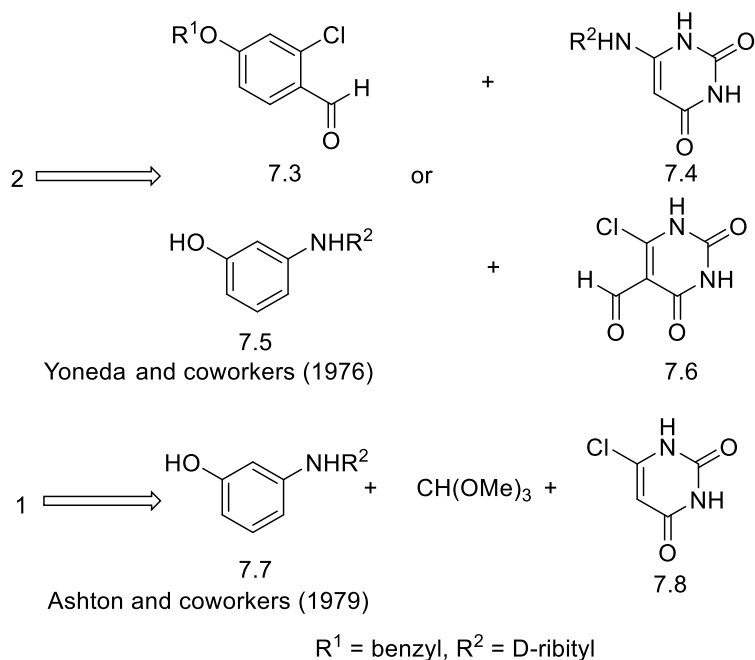


Figure 7.2 Prior syntheses of 7.1 and 7.2

These chemical preparations contain significantly unstable intermediates, making these synthetic achievements quite impressive, but leave the field without convenient preparations of FO or F₄₂₀.^{150,155} This work displays a preparation of FO in the context of prior methods, which were instructional to the overall synthesis. Stability of intermediates was gained by a protection strategy for 3-aminophenol that added a single step to the synthesis and allowed for normal phase chromatography. The reported procedure does not require anaerobic ion exchange chromatography.

The photo-degradation of riboflavin and related metabolites to lumichrome or lumiflavin is indicative of the intermediate instability challenging syntheses of FO.¹⁵⁶ Purification challenges for natural and non-natural deazariboflavins and riboflavins pre-date FO and F₄₂₀ syntheses, but the electron-rich and acidic 7-hydroxyl substituent of FO and F₄₂₀ increase the challenges to these preparations.¹⁵⁷ Prior work (**Figure 7.2**) required anaerobic and dark conditions for early-stage intermediates, specifically

involving compound **7.5**, in addition to separations of polar, acidic intermediates by ion-exchange chromatography.^{151,152,158}

We wondered if a combination of prior approaches and steric *O*-protection of 3-aminophenol could address the instability and related purification challenges of early-stage polar intermediates. Redox shuttle additives in batteries (e.g. di-*tert*-butyl-1,4-dimethoxybenzene) are kinetically stabilized by steric hindrance, rather than thermodynamically stabilized by alteration of their electron density.¹⁵⁹ Satisfyingly, the introduction of a *tert*-butyldimethylsilyl (TBDMS) protecting group to 3-aminophenol addressed numerous issues, including: chemoselective *O*- vs. *N*-protection, enhanced redox stability, and simplified purification. Furthermore, the protecting group imparted no apparent affect on later transformations and, as described below, concomitant TBDMS-*O*-deprotection was achieved during the final HCl-generating transformation. Related silyl-protecting group, TBDPS-, was investigated, but negatively impacted the final condensation cyclization and required an additional reaction for *O*-deprotection under more harsh conditions. Conversely, benzyl-protection, used in Yoneda's synthesis of **F₄₂₀**, yielded only 75% of the *O*-protected product, with the *N*-protected byproduct. Unfortunately, the *O*-benzyl protected analogue of **7.12** did not cyclize with **7.6**, leading us to believe that the facile deprotection of TBDMS reveals the more electron-rich phenolate, aiding in final cyclization.

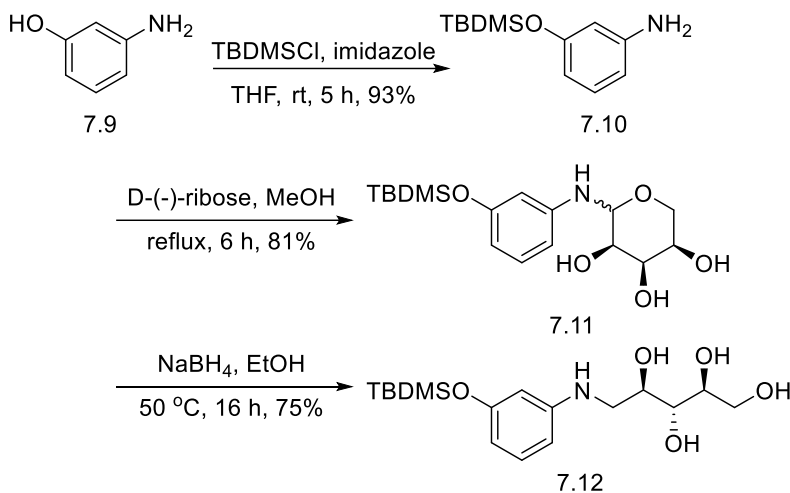


Figure 7.3 Synthesis of stable hydrophobic intermediates.

Selective *O*-protection of commercial 3-aminophenol **7.9** was achieved in 93% isolated yield (**Figure 7.3**).¹⁶⁰ Protected **7.10** and *D*-ribose were refluxed in dry methanol to yield *N*-ribosylaniline **7.11** as a white powder, which was purified by flash chromatography (silica). The resultant *N*-ribosyl compound was reduced to the corresponding *N*-ribitylaminophenol **7.12**,¹⁵⁸ as an amorphous white solid after purification, again by normal phase flash chromatography. In our experience with the prior literature, handling the unprotected ribityl species **7.5** was a major source of anguish, especially during purification. This was presumably due to (photo)oxidation products, i.e. careful anaerobic and dark techniques did improve yields by limiting, but not eliminating, the formation of a brown multicomponent impurity, which could not be carried through subsequent reactions. Purified **7.12** was stable at room temperature for a few hours and could be stored at $-20\text{ }^\circ\text{C}$ for over a month with no noticeable degradation.

We found Yoneda's uracil derivative **7.6** to be the best condensation partner for fragment **7.12**. To prepare this species, barbituric acid **7.13** was converted to 2,4,6-trichloro-5-formyluracil **7.14** by Vilsmaier–Haack conditions.¹⁶¹ The resulting

trichloroformylpyrimidine **7.14** was converted to 6-chloro-5-formyluracil **7.6** in good yields by Yoneda's method.¹⁶² The convergent synthesis of **7.1** was completed by condensation of **7.6** and **7.12** at 130 °C in DMF for ca. 90 minutes. TBDMS-O was fully deprotected during the cyclization, which generates HCl.

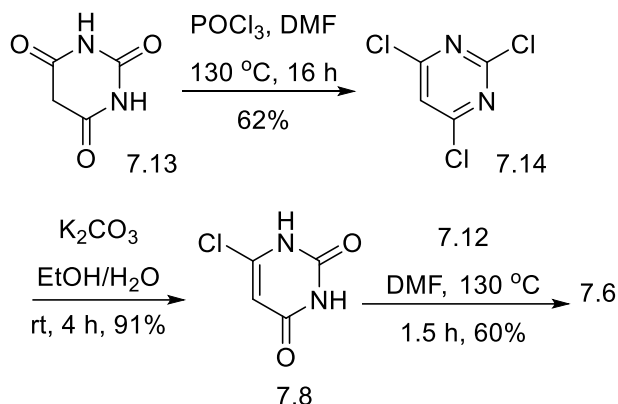


Figure 7.4 Synthesis of uracil and condensation to 7.1, FO

7.3 Application of FO

The application of FO in enzyme kinetics was investigated by Dr. Kayunta Johnson-Winters and the following data has been shared. The reduction of FO by NADPH in place of F₄₂₀ in wild-type Fno (**Figure 7.5**) from *Archaeoglobus fulgidus*, which was expressed and purified in C 41 DE3 *E. coli* cells. FO's activity in Fno (200 nM) was examined aerobically by steady-state kinetics with a saturating concentration of NADPH, 600 μM, and varying concentrations of FO from 2 μM to 30 μM. Standard Michaelis-Menten kinetics were observed at pH 6.5 and 23 °C (**Figure 2**). The k_{cat} for *wt*-Fno was $5.27 \pm 0.14 \text{ s}^{-1}$.

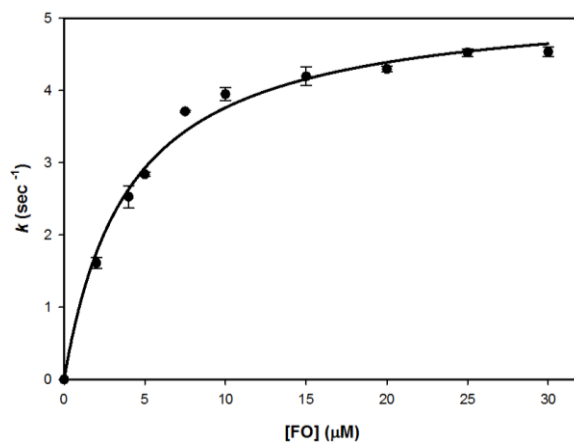


Figure 7.5. The steady state experiment of *wt*-Fno with constant [NADPH] and varying F_o concentration. The data points were fit with the Henri-Michaelis-Menten equation

$$(k = \frac{k_{cat} [S]}{K_m + [S]}).$$

The observed K_m for oxidized FO at 23 °C and pH = 6.5 was found to be $4.00 \pm 0.39 \mu\text{M}$. Previously reported K_m values of *wt*-Fno were: $20 \mu\text{M}$ at 65 °C for the natural substrate, reduced $F_{420}H_2$; and $10 \mu\text{M}$ at 65 °C for oxidized F_{420} .¹⁶³⁻¹⁶⁴ FO lacks the charged poly-glutamate tail of F_{420} cofactor, eliminating putative points of contact between the coenzyme and Fno's binding site. However, oxidized FO still binds relatively tightly to Fno, in comparison to F_{420} .

Chapter 8

Synthesis of new flavin derivatives

8.1 Objective

Initial screening of the flavin catalyst in different applications encourage us to design and synthesize structurally different flavin molecules. The photodegradation of methyl orange using artificial flavin indicates the lumichrome as the most active photosensitizer and also isoalloxazine derivatives are comparatively less reactive than alloxazine. Molecular oxygen activation using flavin in aqueous solution helps us to design catalyst to build a flavin coated electrode to generate reactive oxygen species in aqueous solution. Self-assembled monolayer study indicates the importance of linker group on alloxazine.

Mechanism of Dakin oxidation and aromatization reaction indicates the importance of electron withdrawing groups other than halogens on N-5 alkylated flavinium salts. Since groups like nitro (NO_2) and nitrile (CN) are unstable towards strong reductive environment, it is a great challenge to synthesize N-5 alkylated flavinium salts with these groups.

In this part of the research we will discuss the synthesis of new flavin catalysts.

8.2 Synthesis of lumichrome derivatives

All the compounds except 8.11, 8.12 and 8.13 were synthesized by the condensation of alloxan monohydrate with the corresponding commercially available o-phenylenediamine (**Figure 8.1**). The synthesis of 8.11, 8.12 and 8.13 started with the protection of o-phenylenediamine using either p-toluenesulfonyl chloride or thionyl chloride, followed by nitration or bromination and finally the deprotection led to the o-

phenyleneamine derivative and which can be condensed with alloxan monohydrate to yield the desired product (**Figure 8.2**) .

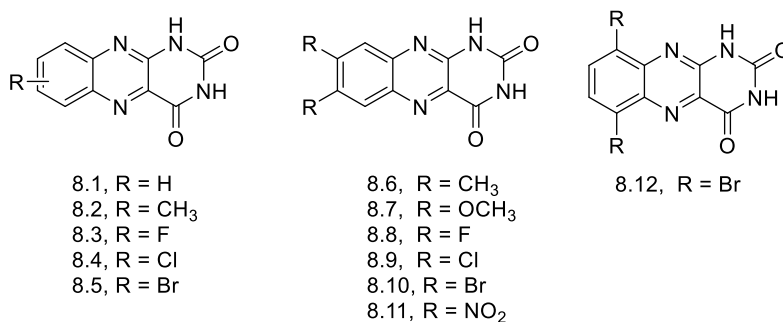


Figure 8.1 Synthesized Lumichrome and its derivatives

All the lumichrome derivatives will be a series of compounds to study the effect of substituents on the photosensitizer and also to study the date of degradation of methyl orange.

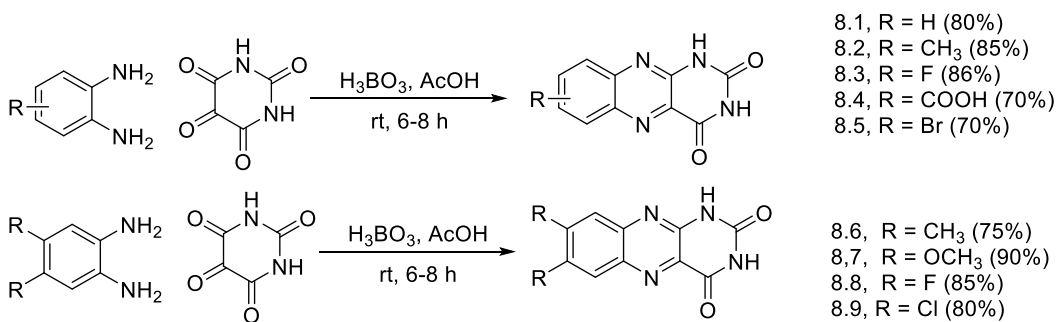


Figure 8.2 General synthesis of lumichrome derivatives

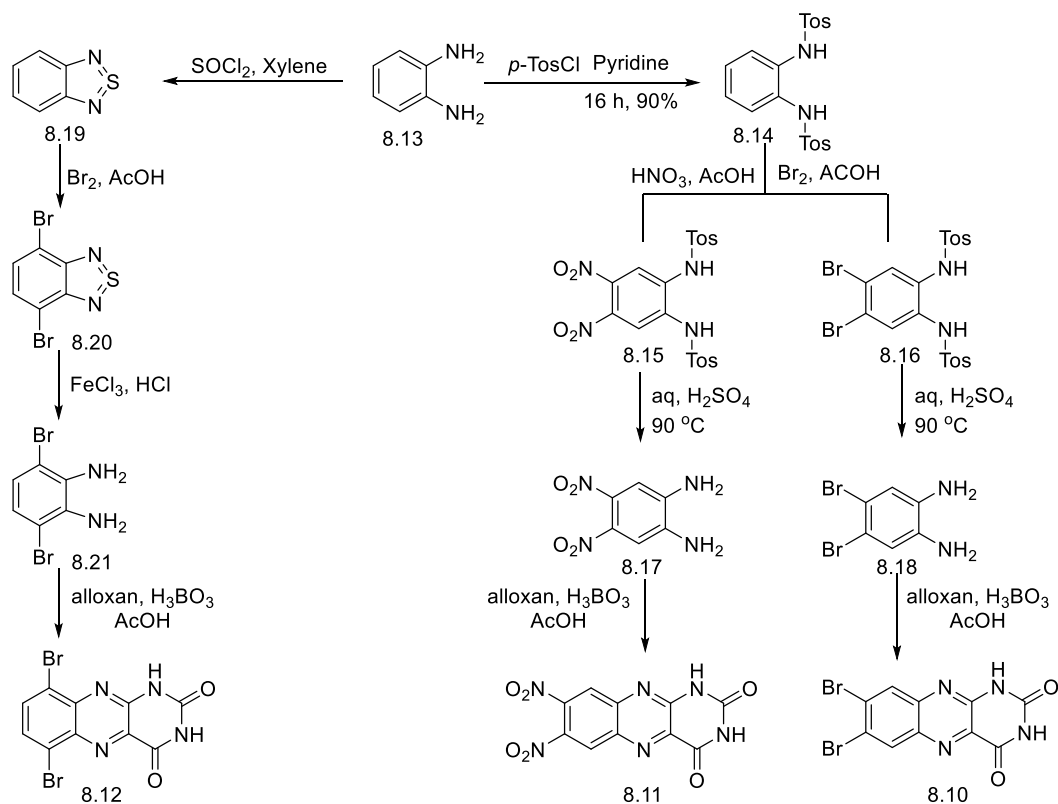
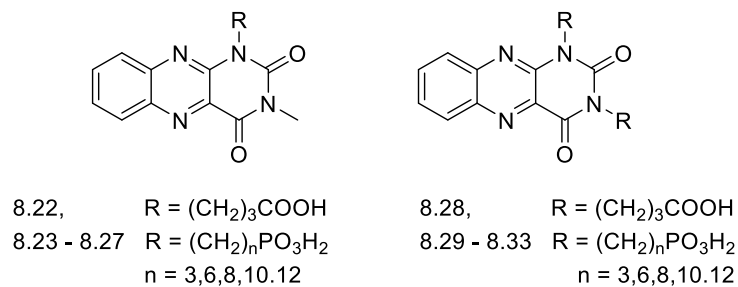


Figure 8.3 Synthesis of 8.10-8.12

8.3 Synthesis of alloxazine catalysts with different 7,8d-disubstitution patterns.

The use of isoalloxazine derivatives for SAM on TiO_2 and BiOCl indicates the effectiveness of flavin structures on degradation of small organic molecule. Due to the higher stability of the alloxazine over isoalloxazines, we have designed a number of alloxazine structures with one or two head groups.



R = linker with head groups

Figure 8.4 Alloxazine structure with one (left) and two (right) head groups

A general scheme to synthesize alloxazine with two linkers and one linker are shown in **Figure 8.5** and **8.6**.

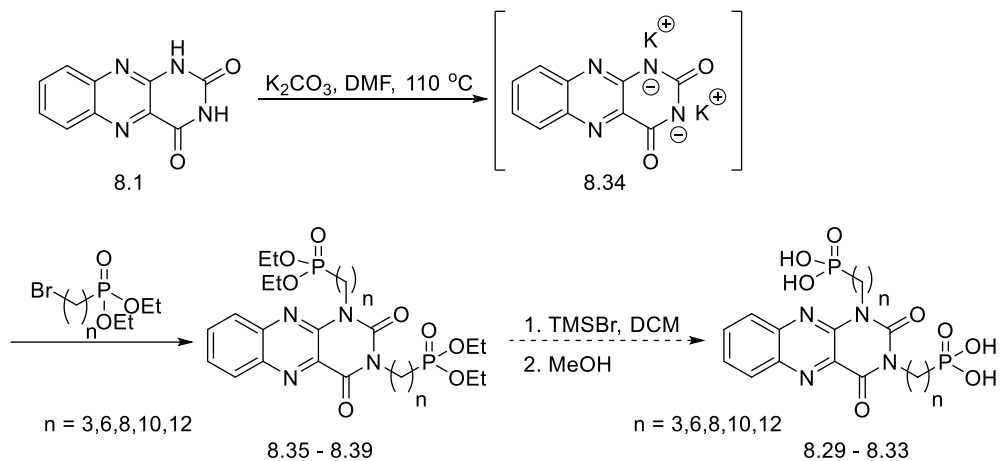


Figure 8.5 Synthesis of alloxazines with two linkers

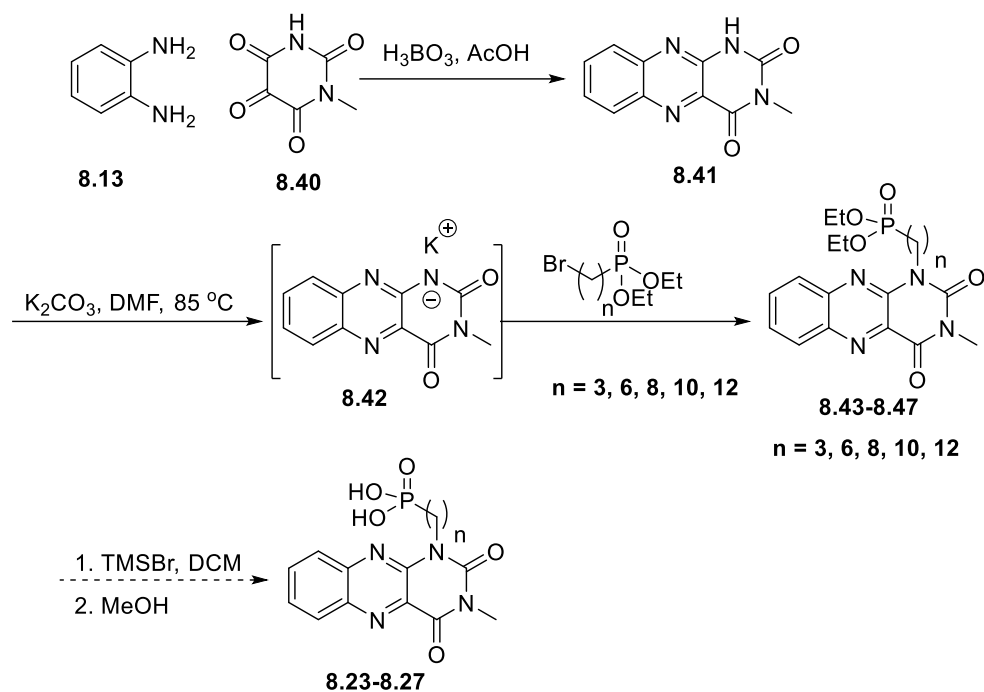


Figure 8.6 Synthesis of alloxazine with single linker

To study the molecular oxygen activation in water, flavin coated electrode will be a good tool for investigation. An amine containing derivative of both isoalloxazine and alloxazines were synthesized as shown in **Figure 8.7** and **8.8**. These flavins can be successfully coated on the oxidized glassy carbon electrode using peptide coupling reaction.

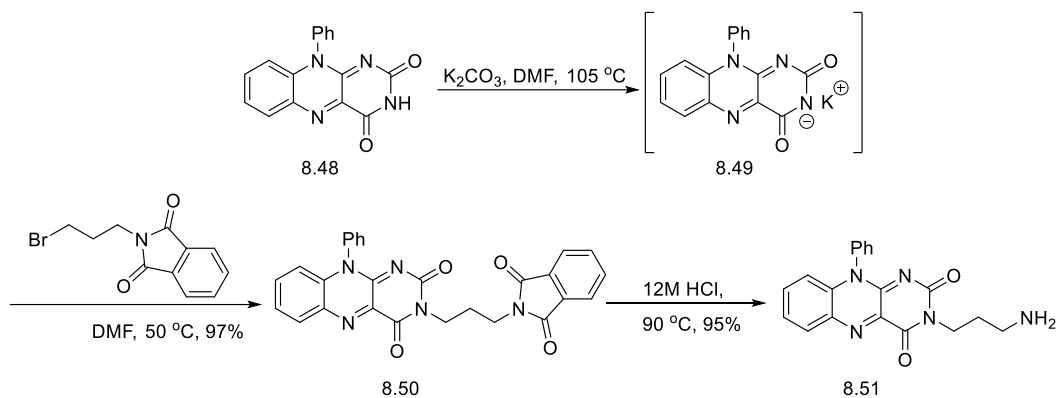


Figure 8.7 Synthesis of 10-Ph isoalloxazine amine

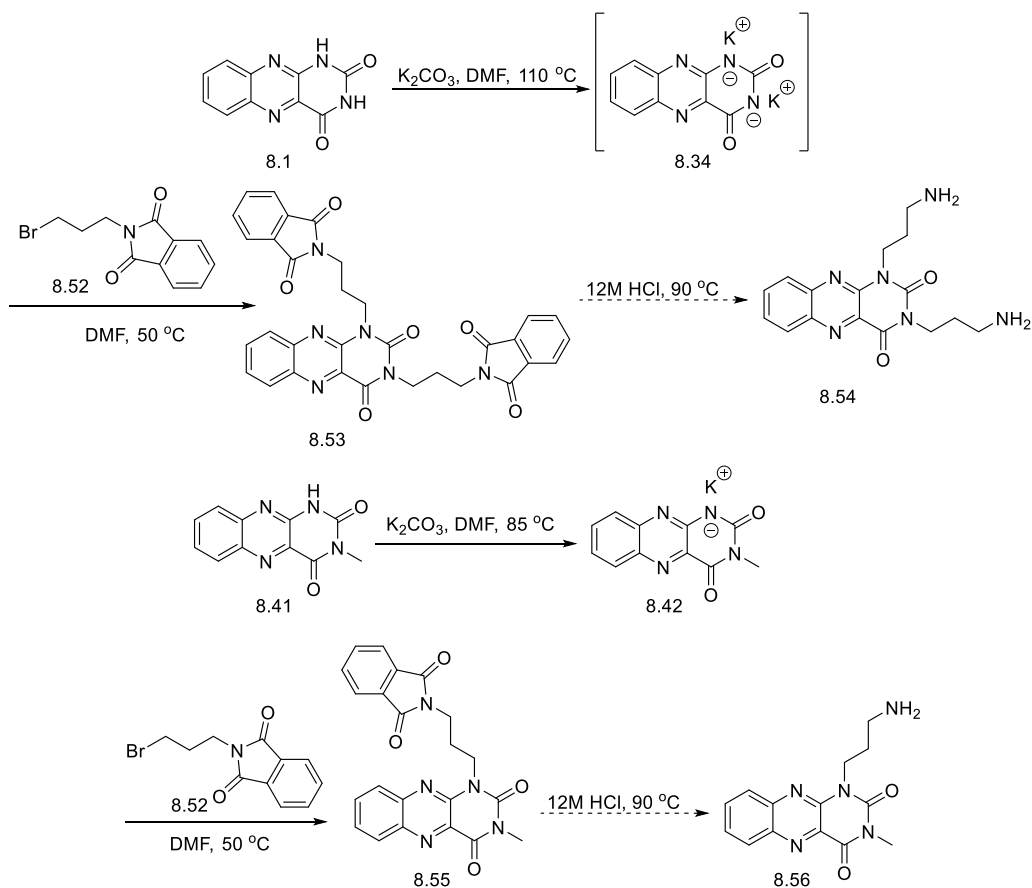


Figure 8.8 Synthesis of alloxazine derivatives with mono amine and diamine

In summary, the proposed and synthesized flavin molecules have a great future impact to study flavin catalyzed oxidase chemistry, photochemistry, electrochemistry and electrochemistry. The synthesis of flavin compounds from the potassium salt of the flavin improved the way of installation of linker groups efficiently. Flavin attached to solid surface could be useful in making a heterogeneous catalysis system, which could be useful for higher catalytic turnover number. The initial electrochemical and photocatalytic results will encourage to design robust and active flavin molecules.

Appendix A
List of abbreviations

Cat	Catalyst
CPD	Cyclobutane pyrimidine dimers
CTANO ₃	Hexadecyltrimethylammonium nitrate
DCM	dDichloromethane
DMF	<i>N,N</i> -dimethyl formamide
DMSO	Dimethyl sulfoxide
DNA	Deoxy nucleic acid
equiv	Equivalent
ESI	Electron spray ionization
FDA	Food and Drug Administration
HDAC	Histone deacetylase
HEH	Hantzsch ester
HPLC	High performance liquid chromatography
HRMS	High resolution mass spectrometry
Hz	Hertz
IR	Infra-red
LSD	Lysine specific demethylase
MO	Methyl Orange
mp	Melting point
MS	Mass spectroscopy
NMR	Nuclear magnetic resonance
PTSA	<i>p</i> -toluene sulfonic acid
rt	Room temperature
SDS	Sodium dodecylsulfate
TFE	2,2,2-trifluoroethanol
TLC	Thin layer chromatography
TON	Turn over number

Appendix B

General experimental procedure

General procedure for reaction kinetics

0.1 mmol of the salicylaldehyde derivative, and 10 μl anisole (internal standard) were dissolved in 1 ml of the 95% $\text{MeOH}_{(\text{aq})}$ in a one dram glass vial, 0.1 ml of 1M NaHCO_3 was added, followed by the addition of 1-10 equiv (0.01-0.1 mmol) of flavinium catalyst and finally the addition of 1-10 equiv of 35% H_2O_2 . The control reactions were run without the addition of catalyst. The initial ($t = 0$) aliquot was withdrawn just before the addition of the hydrogen peroxide and the reaction aliquots were withdrawn at a certain time to quench in 2 ml of 0.01M $\text{Na}_2\text{S}_4\text{O}_6$ solution and the solution was used as sample for HPLC to analyze the consumption of the starting material. Phenomenex PFP column was used for separation and for mobile phase 85% water with acetonitrile with 0.1% formic was used. The flow rate was in between 0.3-0.5 ml/min and retention time was varied on the substrate structure.

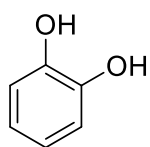
The peak area of the starting material was normalized with the peak area of the internal standard. The peak area was converted to the concentration considering the $t=0$ min as 0.1 M of the substrate.

Each experiment was either duplicated or triplicated for reproducibility and also to minimize the error in the calculation.

The concentration vs time plot was processed with Origin 9.0 and the best fitted curve was selected to determine the initial change in concentration for each experiment. The initial rates at different temperatures were used to calculate kinetic parameter using Arrhenius and Eyring equation.

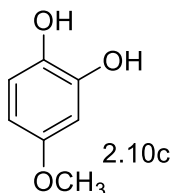
General Synthesis of **2.10a,c,e,j**

A one dram glass vial was equipped with Salicylaldehyde derivative **2.9** (0.2 mmol), flavin **2.11a** (0.02 mmol, 7.5 mg). 200 μ L of 1M NaHCO₃ (1 equiv), 35% H₂O₂ solution (5 equiv) and 2 ml of solvent (MeOH/H₂O = 95/5) were added. The reaction was stirred at room temperature and monitored by TLC. When completed, the reaction mixture was transferred to a round bottom flask and 50 mg silica gel was added to adsorb the compound and the solvent was removed using rotary evaporator. The product was purified using flash chromatography with 1:3 ethyl acetate/hexane as eluent.



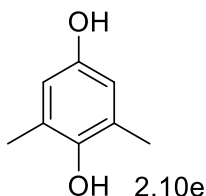
2.10a

Catechol **2.10a**, (20.3 mg, 92%) white solid, mp. 103 – 104 °C (lit. mp. 102 - 103 °C).¹⁷³ ¹H NMR (500 MHz, CDCl₃) δ : 6.90 - 6.84 (m, 2 H), 6.84 - 6.74 (m, 2 H), 5.19 - 5.06 (m, 2 H); ¹³C NMR (125 MHz, CDCl₃) δ : 143.53, 121.41, 115.61.



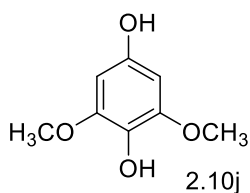
2.10c

4-methoxycatechol **2.10c**, (26.6 mg, 95%), white solid, mp. 56 – 57 °C. (lit. mp. 49 – 51 °C).¹⁷⁴ ¹H NMR (500 MHz, CDCl₃) δ : 6.76 (d, *J* = 8.6 Hz, 1 H), 6.50 (d, *J*=2.9 Hz, 1 H), 6.34 (dd, *J* = 2.9, 8.6 Hz, 1 H), 5.52 (br. s., 2 H), 3.72 (s, 3 H); ¹³C NMR (125 MHz, CDCl₃) δ : 154.31, 144.73, 137.37, 116.01, 105.50, 102.57, 55.92.



2.10e

2,6-dimethylhydroquinone **2.10e**, (25.1 mg, 91%), white solid, mp. 148 - 149 °C (lit. mp. 145 - 148 °C).¹⁷⁵ ¹H NMR (300MHz, DMSO-d₆) δ : 8.43 (s, 1 H), 7.38 (s, 1 H), 6.27 (s, 2H), 2.03 (s, 6 H); ¹³C NMR (75 MHz, DMSO-d₆) δ : 150.26, 145.94, 125.99, 115.09, 17.32.



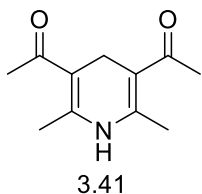
2,6-dimethoxycatechol **2.10j**, (30.0 mg, 88%) white solid, mp. 158 - 160 °C (lit. mp. 162 °C).¹⁷⁶ ¹H NMR (500 MHz, CDCl₃) δ: 5.84 (s, 2 H), 3.81 (s, 6 H); ¹³C NMR (125 MHz, CDCl₃) δ: 186.95, 176.78, 157.41, 107.51, 56.58.

General synthesis of 1,4-dihydropyridines (**3.41-3.47**)

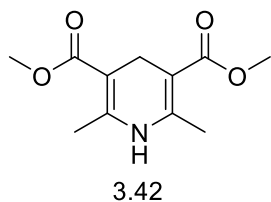
The synthesis of 1,4-dihydropyridines was followed by the report from Beifuss and coworkers¹¹⁵ Both ¹H and ¹³C NMR spectra matched the reported spectra.

Generally paraformaldehyde (50 mg, 1.67 mmol), corresponding 1,3-dicarbonyl compound (2 mmol) and ammonium acetate (193 mg, 1.5 mmol) were heated in a high pressure round bottom flask at 80 °C for 10-20 mins and quenching with ice cold water.

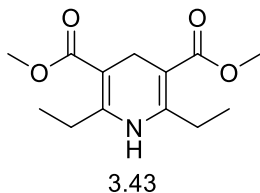
Filtration followed by recrystallization from methanol yields **3.41-3.47**.



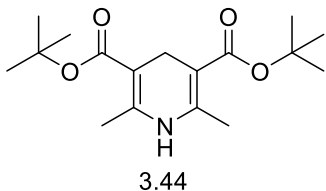
3,5-Diacetyl-1,4-dihydro-2,6-dimethylpyridine **3.41**, (3.9 g, 61 %), yellow powder; mp. 215 - 217 °C, (lit. mp. 213 - 215 °C).¹¹⁵ ¹H NMR (500 MHz, DMSO-*d*₆) δ: 8.26 (s, 1H), 3.24 (s, 2H), 2.11 (s, 6H), 2.08 (s, 6H). ¹³C NMR (126 MHz, DMSO-*D*₆) δ: 196.66, 145.27, 107.64, 30.13, 26.43, 18.71.



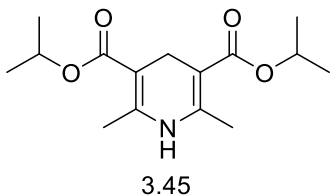
3,5-Bis(carbomethoxy)-1,4-dihydro-2,6-dimethylpyridine **3.42**, (2.8 g, 38%), yellow powder, mp. 211 - 213 °C. (lit. mp. 210 - 212 °C).¹¹⁵ ¹H NMR (500 MHz, DMSO-*d*₆) δ: 8.32 (s, 1H), 3.58 (s, 6H), 3.13 (s, 2H), 2.11 (s, 6H). ¹³C NMR (126 MHz, DMSO-*d*₆) δ: 167.48, 146.80, 96.91, 50.64, 24.81, 17.84.



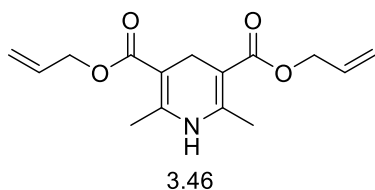
3,5-Bis(carbomethoxy)-1,4-dihydro-2,6-diethylpyridine, **3.43**, (6.2 g, 73%), yellow powder, mp. 130 - 131 °C, (lit. mp. 129 - 131 °C).¹¹⁵ ¹H NMR (500 MHz, CDCl₃) δ: 5.36 (s, 1H), 3.69 (s, 6H), 3.26 (s, 2H), 2.60 (q, *J* = 7.5 Hz, 4H), 1.14 (t, *J* = 7.5 Hz, 6H). ¹³C NMR (126 MHz, CDCl₃) δ: 168.05, 151.30, 98.22, 51.11, 25.71, 24.98, 12.71.



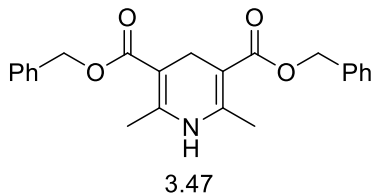
3,5-di-tert-Butoxycarbonyl-1,4-dihydro-2,6-dimethylpyridine **3.44**, (3.9 g, 38%), white crystals, mp. 152 - 155 °C (lit. mp. 151 - 153 °C).¹¹⁵ ¹H NMR (500 MHz, CDCl₃) δ: 5.13 (s, 1H), 3.16 (s, 2H), 2.13 (s, 6H), 1.46 (s, 18H). ¹³C NMR (126 MHz, CDCl₃) δ: 167.70, 143.90, 100.90, 79.51, 28.45, 25.50, 19.27.



3,5-diisopropoxycarbonyl-1,4-dihydro-2,6-dimethylpyridine **3.45**, (6.3 g, 67%), white solid, mp. 120 - 123 °C, (lit. mp. 119 - 121 °C).¹¹⁵ ¹H NMR (500 MHz, CDCl₃) δ 5.21 (s, 1H), 5.03 (hept, *J* = 6.2 Hz, 2H), 3.22 (s, 2H), 2.16 (s, 6H), 1.24 (d, *J* = 6.2 Hz, 12H). ¹³C NMR (126 MHz, CDCl₃) δ 167.75, 144.53, 99.89, 66.89, 24.93, 22.18, 19.31.



3,5-Diallyloxycarbonyl-1,4-dihydro-2,6-dimethylpyridine **3.46**, (6.6 g, 71%), yellow powder, mp. 165 - 167 °C (lit. mp. 164 - 166 °C).¹¹⁵ ¹H NMR (500 MHz, CDCl₃) δ 5.95 (ddt, *J* = 15.9, 10.6, 5.4 Hz, 2H), 5.31 (dd, *J* = 17.1, 1.4 Hz, 2H), 5.20 (dd, *J* = 10.5, 1.1 Hz, 2H), 4.62 (d, *J* = 5.4 Hz, 4H), 3.33 (s, 2H), 2.20 (s, 6H). ¹³C NMR (126 MHz, CDCl₃) δ 167.63, 145.42, 133.02, 117.29, 99.40, 64.48, 24.83, 19.30.

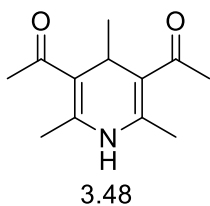


3,5-Dibenzoyloxycarbonyl-1,4-dihydro-2,6-dimethylpyridine **3.47**, (7.2 g, 57%), yellow solid, mp. 112 - 117 °C (lit. mp. 113 - 115 °C).¹⁷⁷ ¹H NMR (500 MHz, CDCl₃) δ: 7.41 – 7.27 (m, 10H), 5.17 (s, 4H), 3.39 (s, 2H), 2.20 (s, 6H). ¹³C NMR (126 MHz, CDCl₃) δ: 167.80, 145.67, 136.89, 128.55, 127.86, 127.75, 99.33, 65.53, 24.93, 19.28.

General synthesis of 3.48-3.54

The synthesis of 1,4-dihydropyridines followed by the report from Beifuss and coworkers¹¹⁵

Generally acetaldehyde (500 mg, 11.4 mmol), corresponding 1,3-dicarbonyl compound (22.7 mmol) and ammonium acetate (1.31 g, 17.0 mmol) were heated in a high pressure round bottom flask at 80 °C for 10-45 mins and quenching with ice cold water. Filtration followed by recrystallization from suitable solvent to yield **3.48-3.54**.



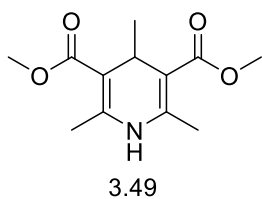
1,1'-(2,4,6-trimethyl-1,4-dihydropyridine-3,5-diyl)bis(ethan-1-one)

3.48, recrystallized from ethyl acetate (0.7 g, 15%), light yellow solid, mp. 152 - 154 °C (lit. mp. 155 - 156 °C).¹⁷⁸ ¹H NMR (500

MHz, CDCl₃) δ: 5.74 (s, 1H), 3.81 (q, *J* = 6.6 Hz, 1H), 2.31 (s,

6H), 2.28 (s, 6H), 0.96 (d, *J* = 6.6 Hz, 3H). ¹³C NMR (126 MHz,

CDCl₃) δ: 198.04, 143.34, 114.37, 30.01, 29.42, 22.23, 20.45.



Dimethyl 2,4,6-trimethyl-1,4-dihydropyridine-3,5-

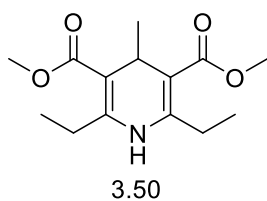
dicarboxylate **3.49**, recrystallized from methanol (2.5 g, 46%),

light yellow crystal, mp. 150 - 152 °C, (lit mp. 153 - 155 °C).¹¹⁵

¹H NMR (500 MHz, CDCl₃) δ: 5.67 (s, 1H), 3.80 (q, *J* = 6.4

Hz, 1H), 3.71 (s, 6H), 2.27 (s, 6H), 0.95 (d, *J* = 6.5 Hz, 3H). ¹³C NMR (126 MHz, CDCl₃)

δ: 168.35, 144.76, 104.50, 51.07, 28.51, 22.37, 19.51.



Dimethyl 2,6-diethyl-4-methyl-1,4-dihydropyridine-3,5-

dicarboxylate **3.50**, recrystallized from methanol, (0.9 g,

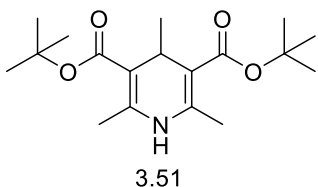
15%), yellow solid, mp. 135 - 138 °C. ¹H NMR (500 MHz,

CDCl₃) δ: 5.67 (s, 1H), 3.80 (q, *J* = 6.5 Hz, 1H), 3.71 (s, 6H),

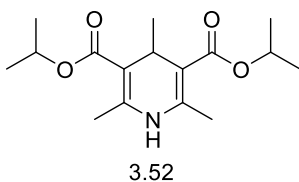
2.87 (dq, *J* = 14.8, 7.5 Hz, 2H), 2.49 (dq, *J* = 14.9, 7.5 Hz, 2H), 1.16 (t, *J* = 7.5 Hz, 6H),

0.94 (d, *J* = 6.5 Hz, 3H). ¹³C NMR (126 MHz, CDCl₃) δ: 167.84, 150.54, 103.64, 51.06,

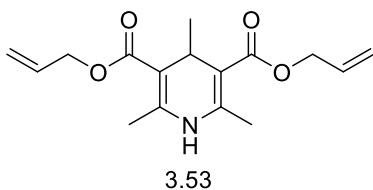
28.45, 25.95, 22.03, 12.88.



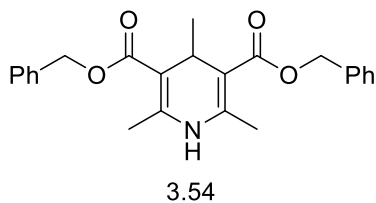
Di-tert-butyl 2,4,6-trimethyl-1,4-dihydropyridine-3,5-dicarboxylate **3.51**, recrystallized from hexane, (0.7 g, 10%), yellow solid, mp. 128-130 °C (lit mp. 126 – 130 °C).¹⁷⁹ ¹H NMR (500 MHz, CDCl₃) δ: 5.35 (s, 1H), 3.75 (q, *J* = 6.4 Hz, 1H), 2.21 (s, 6H), 1.49 (s, 18H), 0.95 (d, *J* = 6.5 Hz, 3H). ¹³C NMR (126 MHz, CDCl₃) δ: 167.40, 143.21, 106.13, 79.38, 29.26, 28.45, 22.24, 19.57.



Diisopropyl 2,4,6-trimethyl-1,4-dihydropyridine-3,5-dicarboxylate **3.52**, recrystallized from methanol, (1.6 g, 23%), yellow solid, mp. 129 - 121 °C. ¹H NMR (500 MHz, CDCl₃) δ: 5.46 (s, 1H), 5.06 (hept, *J* = 6.2 Hz, 2H), 3.82 (q, *J* = 6.4 Hz, 1H), 2.25 (s, 6H), 1.26 (d, *J* = 6.2 Hz, 12H), 0.96 (d, *J* = 6.5 Hz, 3H). ¹³C NMR (126 MHz, CDCl₃) δ: 167.49, 143.91, 105.12, 66.78, 28.71, 22.32, 22.17, 22.08, 19.62.



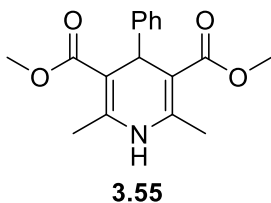
Diallyl 2,4,6-trimethyl-1,4-dihydropyridine-3,5-dicarboxylate **3.53**, recrystallized from methanol, (2.6 g, 78%), yellow solid, mp. 96 - 97 °C. ¹H NMR (500 MHz, CDCl₃) δ: 5.97 (ddt, *J* = 15.8, 10.5, 5.2 Hz, 2H), 5.59 (d, *J* = 34.7 Hz, 1H), 5.33 (d, *J* = 17.2 Hz, 2H), 5.21 (d, *J* = 10.4 Hz, 2H), 4.64 (qd, *J* = 13.6, 4.8 Hz, 4H), 3.90 (q, *J* = 6.2 Hz, 1H), 2.28 (s, 6H), 1.00 (d, *J* = 6.4 Hz, 3H). ¹³C NMR (126 MHz, CDCl₃) δ: 167.44, 144.80, 133.05, 117.25, 104.63, 64.45, 28.54, 22.45, 19.66.



Dibenzyl 2,4,6-trimethyl-1,4-dihydropyridine-3,5-dicarboxylate **3.54**, crystallized from methanol, (5.2 g, quant.), yellow solid, mp. 118 -120 °C. ¹H NMR (500 MHz, CDCl₃) δ: 7.41 – 7.25 (m, 10H), 5.66 (s, 1H), 5.19 (q, *J* = 12.7 Hz, 4H), 3.98 (q, *J* = 6.4 Hz,

1H), 2.27 (s, 6H), 1.01 (d, *J* = 6.5 Hz, 3H). ¹³C NMR (126 MHz, CDCl₃) δ: 167.56, 145.01, 136.95, 128.56, 127.84, 127.75, 104.58, 65.54, 28.59, 22.62, 19.67.

Synthesis of dimethyl 2,6-dimethyl-4-phenyl-1,4-dihydropyridine-3,5-dicarboxylate **3.55**

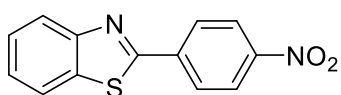


Benzaldehyde (4.72 mmol), methyl acetoacetate (1.02 ml, 9.43 mmol) and ammonium acetate (546 mg, 7.08 mmol) were heated in a sealed round bottom flask at 80 °C for 10-45 mins and quenching with ice cold water. Filtration

followed by recrystallization from methanol to yield **3.55** (427 mg, 30%). mp. 195-198 °C (lit mp. 199 - 200 °C).¹⁸⁰ ¹H NMR (500 MHz, CDCl₃) δ: 7.27 – 7.25 (m, 2H), 7.21 (t, *J* = 7.5 Hz, 2H), 7.13 (t, *J* = 7.2 Hz, 1H), 5.64 (s, 1H), 5.00 (s, 1H), 3.64 (s, 6H), 2.34 (s, 6H). ¹³C NMR (126 MHz, CDCl₃) δ: 168.10, 147.46, 144.23, 128.12, 127.72, 126.29, 104.03, 51.09, 39.35, 19.72.

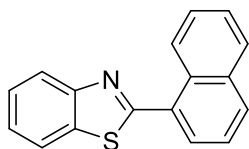
General synthesis of benzothiazole 3.78, 3.80 and 3.81

Benzothiazoline derivative (0.2 mmol) flavin catalyst (0.01 mmol) and 2 mL of methanol were added to a one dram vial and the vial was filled with oxygen with a balloon. The reaction was monitored by TLC, after completion the solvent was removed by evaporation to give the product. The product purity was more than 95% by NMR.



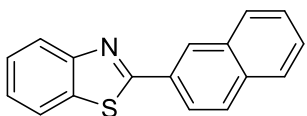
3.78

2-(4-nitrophenyl)benzo[d]thiazole **3.78** (49 mg, 96%), yellow solid. mp. 225 - 226 °C (lit. mp. 226 - 228 °C).¹⁸¹ ¹H NMR (500 MHz, CDCl₃) δ: 8.35 (d, *J* = 8.6 Hz, 2 H), 8.27 (d, *J* = 8.6 Hz, 2 H), 8.13 (d, *J* = 8.0 Hz, 1 H), 7.96 (d, *J* = 8.0 Hz, 1 H), 7.55 (t, *J* = 7.7 Hz, 1 H), 7.46 (t, *J* = 7.5 Hz, 1H); ¹³C NMR (125 MHz, CDCl₃) δ: 164.93, 154.19, 149.12, 139.28, 135.58, 128.33, 127.0, 126.3, 124.42, 124.03, 121.94.



3.80

2-(naphthalen-1-yl)benzo[d]thiazole **3.80** (50.7 mg, 97%), white solid. mp. 126 - 127 °C (lit. mp. 126 °C).¹⁸² ¹H NMR (500 MHz, CDCl₃) δ: 8.57 (br. s., 1 H), 8.21 (d, *J* = 8.0 Hz, 1 H), 8.12 (d, *J* = 7.4 Hz, 1 H), 8.02 - 7.82 (m, 4H), 7.61 - 7.47 (m, 3 H), 7.40 (t, *J* = 7.2 Hz, 1 H); ¹³C NMR (125 MHz, CDCl₃) δ: 168.22, 154.36, 135.24, 134.72, 133.29, 131.09, 128.94, 127.99, 127.69, 127.57, 127.00, 126.50, 125.36, 124.55, 123.35, 121.76.



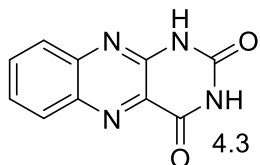
3.81

2-(naphthalen-2-yl)benzo[d]thiazole **3.81** (50.2 mg, 96%), white solid. mp. 126 - 128 °C (lit. mp. 129.5 °C).¹⁸³ ¹H NMR (500 MHz, CDCl₃) δ: 9.09 (s, 1 H), 8.13(d, 7.4 Hz, 1 H), 8.01 (d, *J* = 8.6 Hz, 1 H), 7.93 (d, *J* = 8.0 Hz, 1H), 7.75

(d, $J = 8.0$ Hz, 1 H), 7.67 (t, $J = 7.4$ Hz, 1 H), 7.58 (m, 2H), 7.28 - 7.23 (m, 2 H), 7.22 - 7.13 (m, 2 H); ^{13}C NMR (125 MHz, CDCl_3) δ : 160.49, 149.62, 134.08, 132.58, 132.30, 131.57, 131.33, 128.81, 128.01, 127.14, 127.05, 126.47, 126.23, 125.34, 125.02, 117.22.

Synthesis of benzo[g]pteridine-2,4(1H,3H)-dione **4.3**

o-phenylenediamine **4.1** (324 mg, 3.0 mmol), alloxan monohydrate **4.2** (481 mg, 3.0 mmol), boric acid (186 mg, 3 mmol) and acetic acid (20



ml) was added to a 50 ml round bottom flask and the reaction was stirred at room temperature for 3 hours and a yellow solid started to form which was filtered and washed with acetic acid (15 ml) and diethyl ether (30

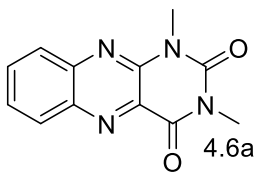
ml) to remove excess acetic acid. The product was dried further with high vacuum pump to yield a yellow solid **4.3** (514 mg, 80%). mp. 345 °C (dec), IR (cm^{-1}): 3173, 3085, 1735, 1690, ^1H NMR (500 MHz, $\text{DMSO}-d_6$) δ : 11.91 (s, 1H), 11.73 (s, 1H), 8.13 (d, $J = 8.2$ Hz, 1H), 7.89 (s, 2H), 7.74 (s, 1H). ^{13}C NMR (126 MHz, $\text{DMSO}-d_6$) δ : 161.00, 150.67, 147.39, 143.14, 139.71, 133.86, 132.22, 130.66, 128.93, 127.49.

General procedure for the synthesis of alloxazine **4.6 a-e**

Benzo[g]pteridine-2,4(1H,3H)-dione **4.3** (1 mmol) and K_2CO_3 (4 mmol) and DMF (50 mL) were mixed in a 100 mL round bottom flask. The reaction was heated at 110 °C for 6 hours and a bright yellow solid formed. The solid was filtered and washed with DMF (20 mL). The resultant solid was used for the next step without any further purification. The solid was suspended in DMF (50 mL) and alkylating agent (**4.5a-e**, 4 mmol) was added and stirred at room temperature to 50 °C under argon. The reaction mixture was filtered and the filtrate was dried by blowing air. The resultant solid was dissolved in DCM-water

(1:1, 50 mL) and the product was extracted with DCM (3x50 ml). The organic layer was dried over MgSO₄ and solvent was removed and flash chromatography was used with 1-2% MeOH in DCM to purify the products as yellow solids.

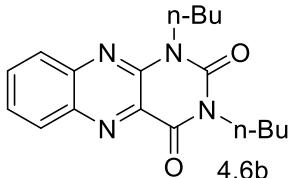
1,3-dimethylbenzo[g]pteridine-2,4(1H,3H)-dione **4.6a**, light yellow solid, (230 mg, 95%),



mp. 253 °C (dec), IR (cm⁻¹): 1718, 1668, 1555, 774, 744. ¹H NMR (500 MHz, CDCl₃) δ: 8.35 (d, *J* = 8.5 Hz, 1H), 8.04 (d, *J* = 8.3 Hz, 1H), 7.91 (ddd, *J* = 8.4, 7.0, 1.2 Hz, 1H), 7.77 (ddd, *J* = 8.2, 6.8, 1.1 Hz, 1H), 3.84 (s, 3H), 3.61 (s, 3H).

¹³C NMR (126 MHz, CDCl₃) δ: 159.91, 150.81, 145.43, 143.45, 140.10, 133.97, 130.91, 129.73, 129.25, 127.93, 29.70, 29.31. HRMS (ESI) *m/z* [M+Na]⁺ calculated for C₁₂H₁₀N₄O₂ 265.0696, found 265.0681 .

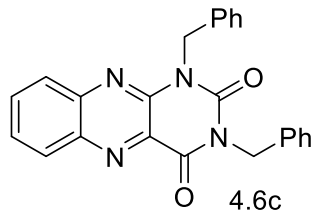
1,3-dibutylbenzo[g]pteridine-2,4(1H,3H)-dione **4.6b**, light yellow solid (294 mg, 90%), mp.



144-145 °C, IR (cm⁻¹): 1722, 1664, 1558. ¹H NMR (500 MHz, CDCl₃) δ: 8.33 (d, *J* = 8.5 Hz, 1H), 8.02 (d, *J* = 8.5 Hz, 1H), 7.89 (ddd, *J* = 8.3, 6.8, 1.1 Hz, 1H), 7.78 – 7.71 (m, 1H), 4.49 – 4.42 (m, 2H), 4.22 – 4.15 (m, 2H), 1.79 (p, *J* = 6.8, 6.2 Hz, 2H), 1.73 (p, *J* = 7.7, 6.8 Hz, 2H), 1.46

(ddd, *J* = 18.7, 15.1, 7.5 Hz, 4H), 1.02 (t, *J* = 7.4 Hz, 3H), 0.98 (t, *J* = 7.4 Hz, 3H). ¹³C NMR (126 MHz, CDCl₃) δ: 159.70, 150.28, 145.17, 143.53, 140.07, 133.74, 130.87, 129.91, 129.07, 127.99, 42.64, 42.49, 29.96, 29.74, 20.27, 20.21, 13.91, 13.88. HRMS (ESI) *m/z* [M+H]⁺ calculated for C₁₈H₂₂N₄O₂ 327.1816, found 327.1807.

1,3-dibenzylbenzo[g]pteridine-2,4(1H,3H)-dione **4.6c**, Light yellow solid (355 mg, 90%),



mp. 188-192 °C, IR (cm⁻¹): 1723, 1669, 1560, 694. ¹H

NMR (500 MHz, CDCl₃) δ: 8.32 (d, *J* = 8.5 Hz, 1H),

8.05 (d, *J* = 8.5 Hz, 1H), 7.90 (ddd, *J* = 8.3, 6.8, 1.1 Hz,

1H), 7.75 (ddd, *J* = 8.2, 6.9, 1.1 Hz, 1H), 7.59 (t, *J* =

7.9 Hz, 4H), 7.34 – 7.26 (m, 6H), 5.65 (s, 2H), 5.38 (s,

2H). ¹³C NMR (126 MHz, CDCl₃) δ: 159.65, 150.56, 145.02, 143.32, 140.30, 136.43,

136.33, 134.04, 130.90, 129.87, 129.61, 129.37, 129.13, 128.64, 128.62, 128.09, 127.98,

45.76, 45.72. HRMS (ESI) *m/z* [M+H]⁺ calculated for C₂₄H₁₈N₄O₂ 395.1503, found

395.1500.

Diethyl-2,2'-(2,4-dioxobenzo[g]pteridine-1,3(2H,4H)-diyl)diacetate **4.6d**, light yellow solid

(328 mg, 85%), mp. 265-266 °C, IR (cm⁻¹):

1731,1684,1561,1202. ¹H NMR (500 MHz, CDCl₃) δ:

8.35 (d, *J* = 8.4 Hz, 1H), 8.00 (d, *J* = 8.4 Hz, 1H), 7.91

(ddd, *J* = 8.3, 6.8, 1.1 Hz, 1H), 7.78 (ddd, *J* = 8.1, 6.8,

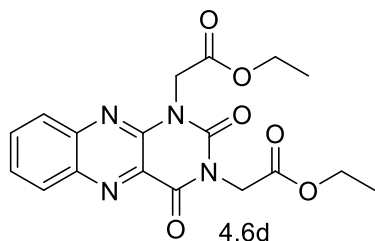
1.0 Hz, 1H), 5.20 (s, 2H), 4.93 (s, 2H), 4.26 (q, *J* = 7.1

Hz, 4H), 1.32 – 1.28 (m, 6H). ¹³C NMR (126 MHz, CDCl₃) δ: 167.74, 167.33, 159.15,

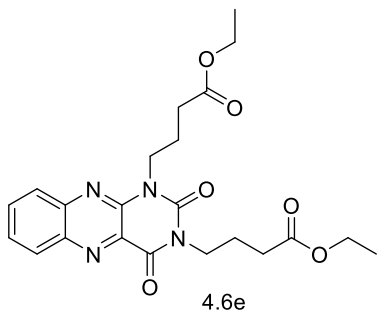
150.10, 144.62, 143.14, 140.54, 134.34, 130.96, 129.68, 129.51, 128.97, 62.01, 61.98,

43.55, 43.28, 14.23, 14.20. HRMS (ESI) *m/z* [M+H]⁺ calculated for C₁₈H₁₈N₄O₆ 387.1299,

found 387.1290.



Diethyl-4,4'-(2,4-dioxobenzo[g]pteridine-1,3(2H,4H)-diyl)dibutyrate **4.6e**, light yellow solid



(380 mg, 86%), mp. 136-138 °C , IR (cm⁻¹): 1716, 1660, 1558. ¹H NMR (500 MHz, Acetone-*d*₆) δ: 8.17 (d, *J* = 8.4 Hz, 1H), 8.00 (d, *J* = 8.4 Hz, 1H), 7.95 (ddd, *J* = 8.4, 6.8, 1.2 Hz, 1H), 7.80 (ddd, *J* = 8.2, 6.9, 1.3 Hz, 1H), 4.49 (t, *J* = 6.7 Hz, 2H), 4.16 (t, *J* = 6.9 Hz, 2H), 4.08 – 3.97 (m, 4H), 2.50 – 2.37 (m, 4H), 2.12 (p, *J* = 7.0 Hz, 2H), 2.07 – 1.97 (m, 4H),

1.17 (t, *J* = 7.1 Hz, 3H), 1.12 (t, *J* = 7.1 Hz, 3H). ¹³C NMR (126 MHz, Acetone-*d*₆) δ: 172.49, 172.41, 159.34, 150.75, 146.00, 142.75, 139.62, 133.41, 131.54, 130.28, 128.74, 128.73, 127.74, 59.77, 41.59, 41.27, 31.24, 31.13, 23.08, 22.89, 13.71, 13.67. HRMS (ESI) *m/z* [M+H]⁺ calculated for C₂₂H₂₆N₄O₆ 443.1925, found 443.1928.

Synthesis of 2,2'-(2,4-dioxobenzo[g]pteridine-1,3(2H,4H)-diyl)diacetic acid **4.6g** and 4,4'-(2,4-dioxobenzo[g]pteridine-1,3(2H,4H)-diyl)dibutyric acid **4.6h**

Diethyl-2,2'-(2,4-dioxobenzo[g]pteridine-1,3(2H,4H)-diyl)diacetate **4.6d** (1.15 g, 3 mmol) or diethyl-4,4'-(2,4-dioxobenzo[g]pteridine-1,3(2H,4H)-diyl)dibutyrate **4.6e** (1.3 g, 3 mmol) was mixed with 5M HCl (100 mL) and the mixture was heated at 90 °C for 6 hours. The reaction turned transparent and the solvent was removed by using rotary evaporator. The dried reaction mixture was diluted with distilled water and a yellow solid formed. The mixture was stirred for 3 hours and filtered to get the product. The product was washed with diethyl ether to isolate the product **4.6g** (743 mg, 75%) and **4.6h** (811 mg, 70%) respectively as yellow solid.

2,2'-(2,4-dioxobenzo[g]pteridine-1,3(2H,4H)-diyl)diacetic acid **4.6g**, light yellow solid; (743

mg, 75%), mp. 206 °C (dec), IR (cm⁻¹): 1719, 1673,

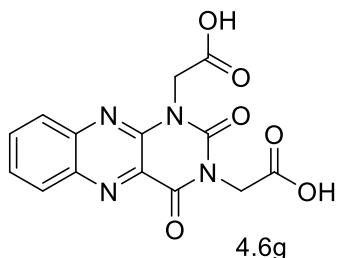
1557. ¹H NMR (500 MHz, DMSO-*d*₆) δ: 8.30 (d, *J* = 8.4

Hz, 1H), 8.09 – 8.00 (m, 2H), 7.94 – 7.86 (m, 1H), 5.01

(s, 2H), 4.71 (s, 2H). ¹³C NMR (126 MHz, CD₃OD) δ:

171.21, 170.80, 160.89, 151.50, 146.23, 144.36,

141.06, 135.43, 131.10, 131.00, 130.78, 128.97, 44.26,



43.95. HRMS (ESI) *m/z* [M-H]⁻ calculated for C₁₄H₁₀N₄O₆ 329.0533, found 329.0528.

4,4'-(2,4-dioxobenzo[g]pteridine-1,3(2H,4H)-diyl)dibutyric acid **4.6h**, light yellow solid,

(811 mg, 70%), mp. 200-202 °C. IR (cm⁻¹): 2953,

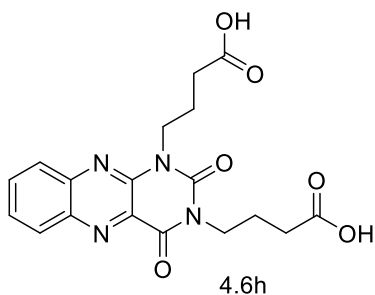
1721, 1691, 1666. ¹H NMR (500 MHz, DMSO-*d*₆) δ:

12.00 (s, 2H), 8.20 (d, *J* = 8.3 Hz, 1H), 8.08 – 7.90

(m, 2H), 7.88 – 7.62 (m, 1H), 4.33 (t, *J* = 6.5 Hz,

2H), 4.01 (t, *J* = 6.8 Hz, 2H), 2.40 – 2.20 (m, 4H),

1.95 (p, *J* = 7.0 Hz, 2H), 1.86 (p, *J* = 7.1 Hz, 2H).



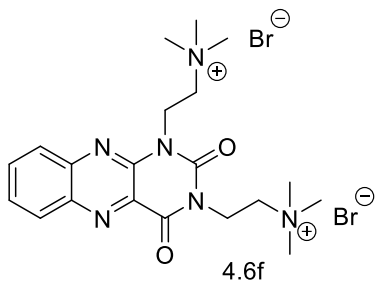
¹³C NMR (126 MHz, DMSO-*d*₆) δ: 174.71, 174.66, 159.88, 150.89, 146.11, 142.54,

139.28, 133.95, 132.02, 130.44, 129.31, 128.00, 41.87, 41.58, 31.62, 31.49, 23.22,

23.10. HRMS (ESI) *m/z* [M+Na]⁺ calculated for C₁₈H₁₈N₄O₆ 409.1119, found 409.1113.

Synthesis of 2,2'-(2,4-dioxobenzo[g]pteridine-1,3(2H,4H)-diyl)bis(N,N,N-trimethylethan-1-aminium) bromide **4.6f**

A mixture of Benzo[g]pteridine-2,4(1H,3H)-dione **4.3** (2.02 g, 4.7 mmol) and K₂CO₃ (1.98 g, 14.3 mmol) was dissolved in DMF (100 mL) and



the mixture was heated at 110 °C for three hours.

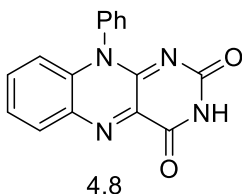
The resulted insoluble dark yellow solid was filtered and washed with DMF (30 ml) and dried. The resultant dark yellow solid was the dipotassium salt of the alloxazine which was used in the next step

without further purification. The proton NMR indicated the absence of N-H proton signals.

The resultant solid was suspended in DMF (200 mL) and (2-Bromoethyl)trimethylammonium bromide (2.50 g, 10.1 mmol) was added and stirred for 48 hours at room temperature and the product **4.6f** was formed as light yellow solid. The product was filtered and a hot ethanol wash was used to purify the product as light yellow solid (1.71 g, 66%), mp. 305 °C (dec.), IR(cm⁻¹): 1648, 1632, 1598. ¹H NMR (500 MHz, D₂O) δ: 8.21 (d, *J* = 8.5 Hz, 1H), 8.14 (d, *J* = 8.6 Hz, 1H), 8.07 (ddd, *J* = 8.4, 6.9, 1.2 Hz, 1H), 7.93 (ddd, *J* = 8.3, 6.9, 1.3 Hz, 1H), 4.95 (t, *J* = 7.5 Hz, 2H), 4.64 (t, *J* = 7.5 Hz, 2H), 3.83 (t, *J* = 7.5 Hz, 2H), 3.75 (t, *J* = 7.5 Hz, 2H), 3.39 (s, 9H), 3.34 (s, 9H). ¹³C NMR (126 MHz, D₂O) δ: 160.82, 150.65, 144.28, 143.34, 139.56, 135.18, 130.71, 129.50, 129.43, 127.94, 61.94, 53.61, 53.52, 36.66, 36.25. MS (ESI) *m/z* [M+H]⁺ calculated for C₂₀H₃₀N₆O₂²⁺ 193.1209, found 193.1210.

Synthesis of 10-phenylbenzo[g]pteridine-2,4(3H,10H)-dione **4.8**

Alloxan monohydrate (10.0 g, 62.5 mmol), *N*-phenyl-*o*-phenylenediamine (11.5 g, 62.5 mmol) and boric acid (3.9 g, 62.5 mmol) were added to glacial



acetic acid (250 mL) and the solution was stirred overnight at room temperature (~15 h). The product precipitated as a dark yellow solid. The resultant solid was filtered and washed with acetic acid (20 mL) followed by deionized water. Finally, the

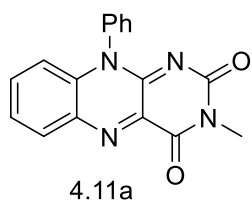
solid was washed with diethyl ether and dried in a desiccator to yield the product **4.8** as a yellow solid (15.8 g, 87%), mp. >400 °C. IR (cm⁻¹): 3025, 2833, 1659, 1537. ¹H NMR (500 MHz, DMSO-*d*₆) δ: 11.43 (s, 1H), 8.40 – 8.04 (m, 1H), 7.95 – 7.57 (m, 5H), 7.45 (s, 2H), 6.96 – 6.57 (m, 1H). ¹³C NMR (126 MHz, DMSO-*d*₆) δ: 159.56, 155.56, 151.75, 139.52, 136.10, 134.78 (2 peaks), 134.06, 131.39, 130.34, 129.83, 127.84, 126.02, 116.78.

Synthesis of **4.11a-4.11c**

10-phenylbenzo[g]pteridine-2,4(3H,10H)-dione **4.8** (290 mg, 1 mmol) and K₂CO₃ (276 mg, 2 mmol) and DMF (50 mL) were mixed in a 100 ml round bottom flask. The reaction was heated at 105 °C for 6 hours and a dark yellow solid formed. The solid was filtered and washed with DMF (20 mL). The resultant solid was used for the next step without any further purification. The solid was suspended in DMF (50 mL) and alkylating agent (**4.10a-c**, 3 mmol) was added and stirred at room temperature to 50 °C. The reaction mixture was filtered and the filtrate was dried by blowing air. The resultant solid was dissolved in DCM-water (1:1, 50 mL) and the product was extracted with DCM (3×50 ml). The organic layer was dried over MgSO₄ and solvent was removed using rotary

evaporator and flash chromatography was used with 1-2% MeOH in DCM to purify the products as yellow solids.

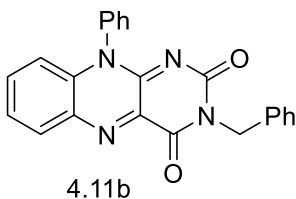
3-methyl-10-phenylbenzo[g]pteridine-2,4 (3H,10H)-dione **4.11a**, yellow solid (283 mg, 93%), mp. 307 °C (dec) IR (cm⁻¹):1661, 1551, 1271. ¹H



NMR (500 MHz, CDCl₃) δ: 8.38 – 8.33 (m, 1H), 7.71 – 7.56 (m, 5H), 7.29 (d, *J* = 7.1 Hz, 2H), 6.89 (d, *J* = 8.5 Hz, 1H), 3.50 (s, 3H). ¹³C NMR (126 MHz, CDCl₃) δ: 159.66, 155.62, 150.03, 137.79, 135.72, 135.42, 135.10, 134.25, 132.74,

130.92, 130.58, 127.59, 126.65, 117.15, 28.95. HRMS (ESI) *m/z* [M+Na]⁺ calculated for C₁₇H₁₂N₄O₂ 327.0852, found 327.0842.

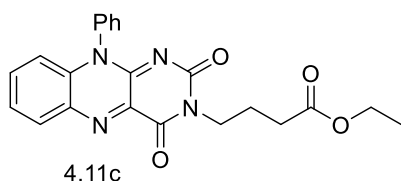
3-benzyl-10-phenylbenzo[g]pteridine-2,4(3H,10H)-dione **4.11b**, yellow solid (342 mg, 90%), mp. 338-340 °C (dec), IR (cm⁻¹): 1645, 1548, 1485.



¹H NMR (500 MHz, CDCl₃) δ: 8.34 – 8.28 (m, 1H), 7.69 – 7.60 (m, 4H), 7.60 – 7.53 (m, 3H), 7.31 – 7.20 (m, 5H), 6.88 (dd, *J* = 8.5, 0.9 Hz, 1H), 5.27 (s, 2H). ¹³C NMR (126 MHz, DMSO-*D*₆) δ: 159.25, 154.68, 150.53, 138.75,

137.24, 135.86, 135.07, 135.02, 134.00, 131.44, 130.36, 129.94, 128.21, 127.82, 127.65, 127.05, 126.18, 116.83, 44.03. HRMS (ESI) *m/z* [M+H]⁺ calculated for C₂₃H₁₆N₄O₂ 381.1346, found 381.1334.

Ethyl-4-(2,4-dioxo-10-phenyl-4,10-dihydrobenzo[g]pteridin-3(2H)-yl)butanoate **4.11c**,

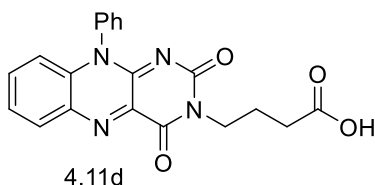


yellow solid (344 mg, 85%), mp. 250 °C (dec), IR (cm⁻¹): 1723, 1699, 1644, 1549. ¹H NMR (500 MHz, CDCl₃) δ: 8.33 (dd, *J* = 8.2, 1.3 Hz, 1H), 7.71 – 7.54 (m, 5H), 7.33 – 7.27 (m, 2H), 6.89 (d, *J* = 8.5 Hz, 1H), 4.18 – 4.05 (m, 4H), 2.40 (t, *J* =

7.7 Hz, 2H), 2.06 (p, *J* = 7.4 Hz, 2H), 1.24 (t, *J* = 7.1 Hz, 3H). ¹³C NMR (126 MHz, CDCl₃) δ: 173.05, 159.52, 155.24, 150.15, 137.92, 135.78, 135.47, 135.14, 134.30, 132.79, 130.96, 130.61, 127.66, 126.69, 117.18, 60.55, 41.43, 32.03, 23.33, 14.36. HRMS (ESI) *m/z* [M+Na]⁺ calculated for C₂₂H₂₀N₄O₄ 427.1377, found 427.1380.

Synthesis of 4-(2,4-dioxo-10-phenyl-4,10-dihydrobenzo[g]pteridin-3(2H)-yl)butanoic acid **4.11d**

Ethyl-4-(2,4-dioxo-10-phenyl-4,10-dihydrobenzo[g]pteridin-3(2H)-yl)butanoate **4.11c** (810



mg, 2 mmol) was mixed with 5M HCl (50 mL) and the mixture was heated at 90 °C for 6 hours. The reaction turned transparent and the solvent was removed by using rotary evaporator. The dried reaction mixture was diluted with distilled water and

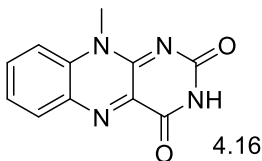
a yellow solid formed. The mixture was stirred for 3 hours and filtered to get the product.

The product was washed with diethyl ether to isolate product **4.11d** (582 mg, 72%) as yellow solid. mp. 250 °C (dec). IR (cm⁻¹): 1645, 1546, 1521. ¹H NMR (500 MHz, DMSO-*d*₆) δ: 8.23 (d, *J* = 8.1 Hz, 1H), 7.80 – 7.61 (m, 5H), 7.44 (d, *J* = 7.3 Hz, 2H), 6.79 (d, *J* = 8.5 Hz, 1H), 3.91 (t, *J* = 6.8 Hz, 2H), 2.26 (t, *J* = 7.5 Hz, 2H), 1.81 (p, *J* = 7.3 Hz, 2H). ¹³C NMR (126 MHz, DMSO-*D*₆) δ: 174.00, 159.23, 154.79, 150.40, 138.72, 135.83, 134.94,

133.92, 131.42, 130.38, 129.93, 127.84, 126.10, 116.8, 40.22, 39.5, 31.09, 22.89. HRMS (ESI) m/z $[M+Na]^+$ calculated for $C_{20}H_{16}N_4O_4$ 399.1064, found 399.1074.

Synthesis of 10-methylbenzo[*g*]pteridine-2,4(3*H*,10*H*)-dione **4.16**

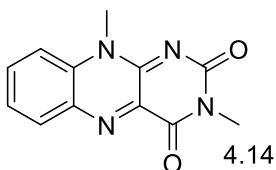
Alloxan monohydrate **4.2** (1.0 g, 6.25 mmol), *N*-methyl-*o*-phenylenediamine **4.15** (764 mg, 6.25 mmol) and boric acid (390 mg, 6.25 mmol) were



added to glacial acetic acid (50 mL) and the solution was stirred overnight (~15 h). The product precipitated as a light brown-yellow solid. The resultant solid was filtered and washed with acetic acid (20 mL) followed by deionized water. Finally, the solid was washed with diethyl ether and dried in a desiccator to yield product **4.16** as a brownish-yellow solid **4.16** (925 mg, 65%). mp. 350 °C (dec). IR (cm^{-1}): 1681, 1547, 1271. 1H NMR (500 MHz, $DMSO-d_6$) δ : 11.40 (s, 1H), 8.19 – 8.07 (m, 1H), 7.95 (d, $J = 4.9$ Hz, 2H), 7.66 (t, $J = 5.8$ Hz, 1H), 3.98 (s, 3H). ^{13}C NMR (126 MHz, $DMSO-D_6$) δ : 159.74, 155.57, 150.90, 138.64, 134.95, 134.63, 133.30, 131.61, 126.06, 116.57, 31.88. HRMS (ESI) m/z $[M+H]^+$ calculated for $C_{11}H_8N_4O_2$ 229.0720, found 229.0648.

Synthesis of 3,10-dimethylbenzo[g]pteridine-2,4(3H,10H)-dione **4.14**

10-methylbenzo[g]pteridine-2,4(3H,10H)-dione **4.16** (500 mg, 2.2 mmol) was stirred with



K_2CO_3 (912 mg, 6.6 mmol) and iodomethane (1.34 ml, 22 mmol) in DMF (50 mL) at 40 °C for 6 hours. The reaction mixture was filtered and the filtrate was dried by blowing air.

The resultant solid was dissolved in DCM-water (1:1, 50 mL)

and the product was extracted with DCM (3x50 ml). The organic layer was dried over

$MgSO_4$ and solvent was removed using rotary evaporator and flash chromatography was

used with 1-3% MeOH in DCM to purify the product as yellow solid (373 mg, 70%) mp.

253 °C (dec). IR (cm^{-1}): 1703, 1646, 1548. 1H NMR (500 MHz, $CDCl_3$) δ : 8.34 (d, $J = 8.1$

Hz, 1H), 7.92 (t, $J = 7.9$ Hz, 1H), 7.71 – 7.58 (m, 2H), 4.14 (s, 3H), 3.53 (s, 3H). ^{13}C NMR

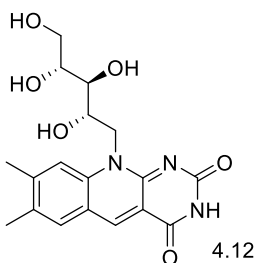
(126 MHz, $CDCl_3$) δ : 159.83, 155.92, 149.41, 137.13, 135.98, 135.83, 133.51, 133.48,

126.76, 115.28, 32.20, 28.99. HRMS (ESI) m/z $[M+H]^+$ calculated for $C_{12}H_{10}N_4O_2$

243.0877, found 243.0876.

Synthesis of 7,8-dimethyl-10-((2S,3S,4R)-2,3,4,5-tetrahydroxypentyl)pyrimido[4,5-b]quinoline-2,4(3H,10H)-dione **4.12**

The product was synthesized by following the known procedure¹²⁰



mp. 280 - 282 °C, (lit. mp. 278 - 282 °C).¹⁸⁴ 1H NMR (500

MHz, $DMSO-d_6$) δ : 11.05 (s, 1H), 8.89 (s, 1H), 7.97 (s, 1H),

7.90 (s, 1H), 5.15 (d, $J = 4.9$ Hz, 1H), 4.91 (d, $J = 4.7$ Hz, 1H),

4.82 (d, $J = 5.8$ Hz, 1H), 4.66 (d, $J = 13.5$ Hz, 1H), 4.51 (d, $J =$

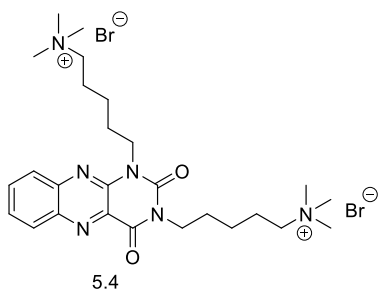
5.4 Hz, 1H), 4.24 (s, 1H), 3.70 – 3.58 (m, 3H), 3.50 – 3.42 (m,

2H), 2.47 (s, 3H), 2.35 (s, 3H). ^{13}C NMR (126 MHz, $DMSO-$

D_6) δ : 162.24, 157.59, 156.41, 146.02, 141.08, 139.97, 133.64, 130.62, 119.70, 117.95, 113.78, 73.70, 73.70, 69.59, 63.48, 47.26, 20.97, 18.69.

5,5'-(2,4-dioxobenzo[g]pteridine-1,3(2H,4H)-diyl)bis(N,N,N-trimethylpentan-1-aminium) bromide **5.4**

The synthesis of **5.4** was synthesized by following the procedure of **4.6f**.

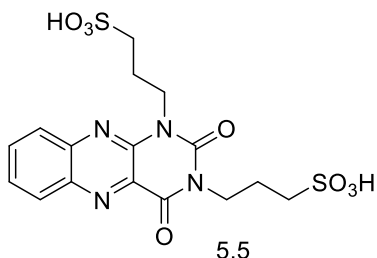


Yellow solid, (2.2 g, 75%) mp.180-182 °C, IR (cm⁻¹): 1722, 1678, 1559. ¹H NMR (301 MHz, D₂O) δ : 8.08 – 7.68 (m, 4H), 4.19 (t, $J = 7.2$ Hz, 2H), 4.01 (t, $J = 6.9$ Hz, 2H), 3.44 – 3.28 (m, 4H), 3.13 (s, 18H), 2.03 – 1.84 (m, 4H), 1.84 – 1.65 (m, 4H), 1.62 – 1.32 (m, 4H). ¹³C NMR (76 MHz, D₂O) δ : 160.47, 150.77,

144.24, 142.83, 138.54, 134.61, 130.05, 129.20, 128.81, 127.45, 66.46, 52.94, 42.34, 26.40, 26.28, 22.99, 22.87, 22.13, 22.03. HRMS (ESI) m/z [M+2H]²⁺ calculated for C₂₆H₄₂N₆O₂ 235.1679, found 235.1662.

Benzo[g]pteridine-2,4(1H,3H)-dione **5.13** was converted to the corresponding potassium salt using potassium carbonate as previously described. The salt was stirred with propane sultone **5.20** (3 equiv) or butane sultone **5.21** (3 equiv) in DMF to synthesize the corresponding alloxazine sulfonic acid **5.5** and **5.6**. After overnight reaction at room temperature, the reaction was filtered and filtrate was dried using air blow. The resultant solid was dissolved in minimum amount of water and acetone was added to the solution to separate the product as precipitate. The precipitate was filtered and washed with diethyl ether and dried under vacuum.

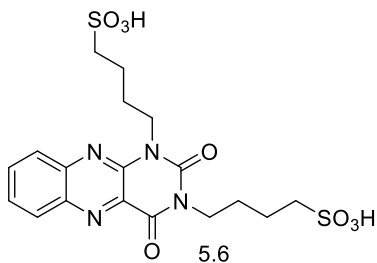
3,3'-(2,4-dioxobenzo[g]pteridine-1,3(2H,4H)-diyl)bis(propane-1-sulfonic acid) **5.5**



Yellow solid (89%), mp. 280 °C (dec), IR (cm⁻¹): 1717, 1668, 1557, 1171, 1038. ¹H NMR (500 MHz, D₂O) δ: 7.92 (d, *J* = 8.4 Hz, 1H), 7.89 – 7.79 (m, 2H), 7.70 (t, *J* = 7.4 Hz, 1H), 4.30 (t, *J* = 7.0 Hz, 2H), 4.07 (t, *J* = 7.2 Hz, 2H), 3.01 – 2.87 (m, 4H), 2.06 (m, *J* = 4H). ¹³C NMR (126 MHz, D₂O) δ:

160.26, 150.58, 144.06, 142.66, 138.40, 134.59, 130.14, 129.15, 128.50, 127.55, 48.72, 48.61, 41.63, 22.75, 22.62. HRMS (ESI) *m/z* [M-H]⁻ calculated for C₁₆H₁₈N₄O₈S₂ 457.0493, found 457.0498.

4,4'-(2,4-dioxobenzo[g]pteridine-1,3(2H,4H)-diyl)bis(butane-1-sulfonic acid) **5.6**

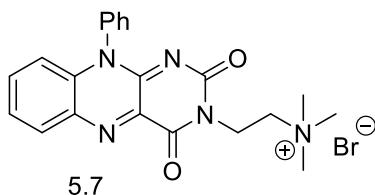


Yellow solid (88%), mp. 278 °C (dec), IR (cm⁻¹): 1666, 1557, 1177, 1042. ¹H NMR (500 MHz, D₂O) δ: 7.85 (d, *J* = 8.3 Hz, 1H), 7.83 – 7.73 (m, 2H), 7.71 – 7.62 (m, 1H), 4.13 (t, *J* = 5.8 Hz, 2H), 3.94 (t, *J* = 5.7 Hz, 2H), 2.92 (s, 4H), 1.74 (s, 8H). ¹³C NMR (126 MHz, D₂O) δ: 160.59, 150.78, 144.29, 142.89,

138.58, 134.54, 130.05, 129.17, 128.78, 127.53, 50.65, 42.24, 42.05, 26.98, 25.78, 21.76, 21.43. HRMS (ESI) *m/z* [M+H]⁺ calculated for C₁₈H₂₂N₄O₈S₂ 487.0952, found 487.0943.

Synthesis of 2-(2,4-dioxo-10-phenyl-4,10-dihydrobenzo[g]pteridin-3(2H)-yl)-N,N,N-trimethylethan-1-aminium bromide **5.7**

A mixture of 10-phenylbenzo[g]pteridine-2,4(3H,10H)-dione **5.23** (1.01 g, 3.4 mmol) and K_2CO_3 (0.56 g, 4.08 mmol) was suspended in DMF

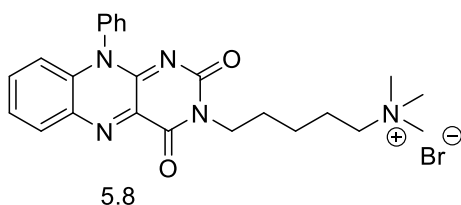


(100 mL) and the mixture was heated at 90 °C for four hours. The resulted insoluble dark yellow solid was filtered and washed with DMF (20 ml) and dried. The resultant dark yellow solid, salt of the

5.23, was used in the next step without further purification. The resultant solid was suspended in DMF (100 mL) and (2-Bromoethyl)trimethylammonium bromide (1.01g, 4.08 mmol) was added and stirred for overnight at room temperature and the product **5.7** was formed as light yellow solid. The solid was washed with hot ethanol to purify the product (1.21 g, 80%). Yellow solid, mp. 260 °C (dec). IR (cm^{-1}): 1716, 1670, 1554. 1H NMR (500 MHz, D_2O) δ : 8.28 (d, $J = 8.0$ Hz, 1H), 7.89 (t, $J = 7.6$ Hz, 1H), 7.84 – 7.72 (m, 4H), 7.44 (d, $J = 3.6$ Hz, 2H), 7.16 (d, $J = 8.5$ Hz, 1H), 4.51 (t, $J = 7.5$ Hz, 2H), 3.67 (t, $J = 7.5$ Hz, 2H), 3.29 (s, 9H). ^{13}C NMR (126 MHz, D_2O) δ : 160.98 (K_2CO_3), 160.57, 156.05, 150.40, 136.99, 136.67, 136.24, 134.81, 134.42, 131.31, 131.09, 130.91, 128.21, 127.26, 118.18, 62.14, 53.35, 35.73. HRMS (ESI) m/z $[M+H]^+$ calculated for $C_{21}H_{22}N_5O_2$ 376.1768, found 376.1743.

5-(2,4-dioxo-10-phenyl-4,10-dihydrobenzo[g]pteridin-3(2H)-yl)-N,N,N-trimethylpentan-1-aminium bromide **5.8**

A mixture of 10-phenylbenzo[g]pteridine-2,4(3H,10H)-dione **5.13** (1.01 g, 3.4 mmol) and



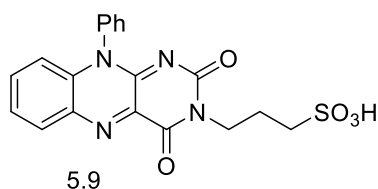
K_2CO_3 (0.56 g, 4.08 mmol) was suspended in DMF (100 mL) and the mixture was heated at 90 °C for four hours. The resulted insoluble dark yellow solid was filtered and washed with DMF (20 ml) and dried. The

resultant dark yellow solid salt of the **5.23** was used in the next step without further purification. The resultant solid was suspended in DMF (100 mL) and (5-Bromopentyl)trimethylammonium bromide (1.20 g, 4.15 mmol) was added and stirred for overnight at room temperature and the product **5.8** was formed as yellow solid. The solid was washed with ethanol to purify the product (1.42 g, 85%). Yellow solid, mp. 220 °C (dec). IR (cm^{-1}): 3053, 1680, 1652, 1543. 1H NMR (500 MHz, D_2O) δ : 8.19 (d, J = 7.9 Hz, 1H), 7.87 – 7.70 (m, 5H), 7.46 (dd, J = 7.4, 1.9 Hz, 2H), 7.12 (d, J = 8.6 Hz, 1H), 3.94 (t, J = 7.3 Hz, 2H), 3.31 (t, J = 7.5 Hz, 2H), 3.10 (s, 9H), 1.89 – 1.79 (m, 2H), 1.71 (dt, J = 14.8, 7.5 Hz, 2H), 1.41 (dt, J = 14.9, 7.5 Hz, 2H). ^{13}C NMR (126 MHz, D_2O) δ : 160.64, 156.04, 149.35, 136.97, 136.44, 136.13, 134.50, 134.05, 131.25, 130.98, 128.26, 127.27, 118.14, 66.43, 52.86, 41.67, 26.27, 22.83, 21.93. HRMS (ESI) m/z $[M+H]^+$ calculated for $C_{24}H_{28}N_5O_2$ 418.2238, found 418.2239 .

Synthesis of 3-(2,4-dioxo-10-phenyl-4,10-dihydrobenzo[g]pteridin-3(2H)-yl)propane-1-sulfonic acid **5.9** and 4-(2,4-dioxo-10-phenyl-4,10-dihydrobenzo[g]pteridin-3(2H)-yl)butane-1-sulfonic acid **5.10**

Both sulfonic acid derivatives of 10-phenylbenzo[g]pteridine-2,4(3H,10H)-dione were synthesized from the potassium salt of the isoalloxazine. 10-phenylbenzo[g]pteridine-2,4(3H,10H)-dione **5.23** was converted to the corresponding potassium salt using potassium carbonate as described early. The salt was stirred with propane sultone **5.20** (2 equiv) and butane sultone **5.21** (2 equiv) in DMF to synthesize the corresponding 10-Ph isoalloxazine sulfonic acid **5.9** and **5.10**. After overnight, reaction was filtered and filtrate was dried using air flow. The resultant solid was dissolved in minimum amount of water and acetone was added to the solution to separate the product as precipitate.

3-(2,4-dioxo-10-phenyl-4,10-dihydrobenzo[g]pteridin-3(2H)-yl)propane-1-sulfonic acid **5.9**

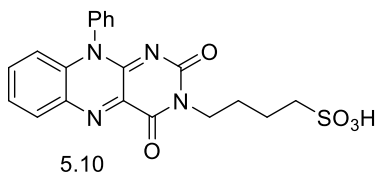


Yellow solid (55%), mp. 348-350 °C(dec). IR (cm⁻¹): 3567, 3520, 1702, 1649, 1542, 1190. ¹H NMR (500 MHz, D₂O) δ: 8.05 (d, *J* = 8.0 Hz, 1H), 7.76 – 7.64 (m, 4H), 7.61 (t, *J* = 7.6 Hz, 1H), 7.38 (d, *J* = 6.4 Hz, 2H), 7.00 (d, *J* = 8.6 Hz, 1H), 3.89 (t, *J* =

7.1 Hz, 2H), 2.90 – 2.79 (m, 2H), 1.95 (p, *J* = 7.4 Hz, 2H). ¹³C NMR (126 MHz, D₂O) δ: 160.72, 156.54, 150.02, 136.79, 136.69, 135.79, 134.72, 134.20, 131.14, 131.08, 130.92, 127.96, 127.32, 118.11, 48.65, 40.90, 22.65. HRMS (ESI) *m/z* [M-H]⁻ calculated for C₁₉H₁₆N₄O₅S 411.0769, found 411.0789.

4-(2,4-dioxo-10-phenyl-4,10-dihydrobenzo[g]pteridin-3(2H)-yl)butane-1-sulfonic acid **5.10**

Yellow solid (75%), mp. 228-230 (dec), IR (cm⁻¹): 3433, 1705, 1650. 1228. ¹H NMR (500



MHz, D₂O) δ: 8.26 (d, *J* = 8.2 Hz, 1H), 8.03 – 7.75

(m, 5H), 7.49 (dd, *J* = 7.7, 1.8 Hz, 2H), 7.15 (d, *J* =

8.6 Hz, 1H), 4.02 (t, *J* = 6.5 Hz, 2H), 3.00 (t, *J* = 7.1

Hz, 2H), 1.88 – 1.76 (m, 4H). ¹³C NMR (76 MHz,

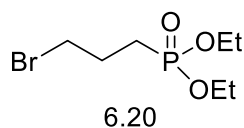
D₂O) δ: 160.40, 156.46, 149.82, 136.83, 136.48,

135.61, 134.62, 134.06, 131.10, 130.93, 127.95, 127.31, 118.10, 50.58, 41.61, 25.88,

21.63. HRMS (ESI) *m/z* [M-H]⁻ calculated for C₂₀H₁₈N₄O₅S 425.0925 found 425.0942.

Synthesis of diethyl (3-bromopropyl)phosphonate **6.20**

1,3-dibromopropane (12.2 g, 60.2 mmol) was heated to 140 °C and triethylphosphite (2.0



ml, 11.7 mmol) was added dropwise and the reaction was

heated at 140 °C for 12 h. The reaction was concentrated using

a rotary evaporator and the product was purified using flash

chromatography with two column volumes of dichloromethane followed by a gradient

elution from 10% diethyl ether in ethyl acetate to 100% ethyl acetate. Compound **6.20**

(1.9 g, 63%) was isolated as a colorless oil. ¹H NMR (500 MHz, CDCl₃) δ: 4.20-4.01 (m,

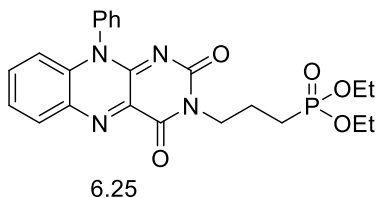
4H), 3.47 (t, *J* = 6.4 Hz, 1H), 2.20-2.09 (m, 1H), 1.98-1.83 (m, 2H), 1.32 (t, *J* = 7.1 Hz,

6H). ¹³C NMR (126 MHz, CDCl₃) δ: 61.83 (d, *J* = 6 Hz), 33.74 (d, *J* = 18 Hz), 26.09 (d, *J* =

4 Hz), 24.54 (d, *J* = 125 Hz), 16.59 (d, *J* = 6 Hz).

Synthesis of diethyl (3-(2,4-dioxo-10-phenyl-4,10-dihydrobenzo[g]pteridin-3(2H)-yl)propyl)phosphonate **6.25**

10-phenylbenzo[g]pteridine-2,4(3H,10H)-dione **6.14** (500 mg, 1.72 mmol) was heated with K_2CO_3 (600 mg, 4.3 mmol) at 105 °C for 4 h in



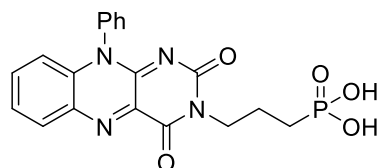
DMF (50 mL), the resultant dark yellow solid (K^+ salt of **6.14**) was filtered and rinsed with ether and dried.

The solid was then suspended in DMF (50 mL) and **6.20** (534 mg, 2.1 mmol), was added and stirred

overnight. The reaction mixture was filtered and the filtrate was dried by blowing air. The resultant solid was dissolved in DCM-water (1:1, 50 mL) and the product was extracted with DCM (3x50 mL). The organic layer was dried over $MgSO_4$ and solvent was removed and flash chromatography was used with 2% MeOH in DCM to purify the product as yellow solid (580 mg, 72% over two steps). mp. 240 °C (dec), IR (cm^{-1}): 1644, 1549, 1256, 1012. 1H NMR (500 MHz, $CDCl_3$) δ : 8.32 (d, $J = 8.0$ Hz, 1H), 7.77 – 7.52 (m, 5H), 7.30 (d, $J = 7.3$ Hz, 2H), 6.89 (d, $J = 8.5$ Hz, 1H), 4.27 – 3.99 (m, 6H), 2.16 – 1.93 (m, 2H), 1.89 – 1.75 (m, 2H), 1.29 (t, $J = 6.9$ Hz, 6H). ^{13}C NMR (125 MHz, $CDCl_3$) δ : 159.44, 155.11, 150.14, 137.87, 135.77, 135.49, 135.11, 134.28, 132.75, 130.92, 130.58, 127.63, 126.70, 117.18, 61.72 (d, $J = 6$ Hz), 42.31 (d, $J = 25$ Hz), (d, $J = 141$ Hz), 21.21, 16.6 (d, $J = 6$ Hz). ^{31}P NMR (122 MHz, $CDCl_3$) δ : 29.44. HRMS (ESI) m/z $[M+Na]^+$ calculated for $C_{23}H_{25}N_4O_5P$ 491.1455, found 491.1450.

Synthesis of (3-(2,4-dioxo-10-phenyl-4,10-dihydrobenzo[g]pteridin-3(2H)-yl)propyl) phosphonic acid **6.3**

Diethyl-(3-(2,4-dioxo-10-phenyl-4,10-dihydrobenzo[g]pteridin-3(2H)-yl)propyl) phosphonate **6.25** (300 mg, 0.64 mmol) was dissolved in dry dichloromethane (25 mL)

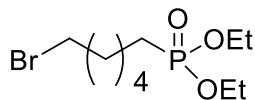


6.3

and bromotrimethylsilane (660 μ l, 3.2 mmol) was added dropwise and stirred at room temperature under argon for overnight. The solvent was removed by using rotary evaporator and methanol (20 mL) was added and stirred for 14 hr. The

solvent was removed by rotary evaporator and deionized water was added and stirred for 2 hr. A yellow solid started to form and the product **6.3** (211 mg, 80%) was isolated by filtration and washed with diethyl ether and dichloromethane. mp: 189 °C (dec). IR (cm^{-1}): 1651, 1551, 1265, 1226, 1022. ^1H NMR (500 MHz, $\text{DMSO}-d_6$) δ : 8.44 – 8.01 (m, 1H), 7.99 – 7.57 (m, 5H), 7.45 (s, 2H), 6.79 (s, 1H), 3.91 (s, 2H), 1.78 (s, 2H), 1.55 (s, 2H). ^{13}C NMR (126 MHz, $\text{DMSO}-d_6$) δ : 159.21, 154.76, 150.42, 138.71, 135.85, 134.99, 134.90, 133.96, 131.42, 130.37, 129.92, 127.84, 126.10, 116.78, 41.68, 25.89, 24.80, 21.45. ^{31}P NMR (122 MHz, $\text{DMSO}-D_6$) δ : 29.44. HRMS (ESI) m/z $[\text{M}+\text{H}]^+$ calculated for $\text{C}_{19}\text{H}_{17}\text{N}_4\text{O}_5\text{P}$ 413.1009, found 413.0997.

Synthesis of diethyl (6-bromohexyl)phosphonate **6.21**

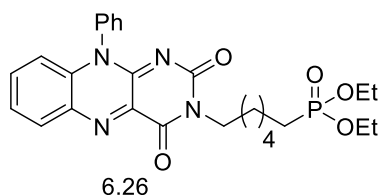


6.21

1, 6-dibromohexane (5 ml, 32.5 mmol) was heated at 140 °C and triethylphosphite (5.6 mmol, 32.5 mmol) was added drop wise using additional funnel. The reaction was heating at 140 °C for overnight and the reaction was concentrated using rotary evaporator. The product **6.21** (5.2 g, 53%) was purified as a colorless oil using column chromatography with two column volume of dichloromethane and a gradient elution with 10% hexane in ethyl acetate to 50% hexane in ethyl acetate. ¹H NMR (500 MHz, CHCl₃) δ: 4.07 – 3.98 (m, 4H), 3.33 (t, *J* = 6.8 Hz, 2H), 1.79 (p, *J* = 6.8 Hz, 2H), 1.70 – 1.61 (m, 2H), 1.56 (dtd, *J* = 15.9, 10.6, 9.7, 5.1 Hz, 2H), 1.36 (tdt, *J* = 16.5, 10.3, 5.6 Hz, 4H), 1.25 (t, *J* = 7.1 Hz, 6H). ¹³C NMR (126 MHz, CDCl₃) δ: 61.43 (d, *J* = 6 Hz), 33.73, 32.44, 29.64 (d, *J* = 16 Hz), 27.62, 25.55 (d, *J* = 140 Hz), 22.27 (d, *J* = 5 Hz), 16.49 (d, *J* = 6 Hz).

Synthesis of diethyl (6-(2,4-dioxo-10-phenyl-4,10-dihydrobenzo[*g*]pteridin-3(2H)-yl)hexyl)phosphonate **6.26**

10-phenylbenzo[*g*]pteridine-2,4(3H,10H)-dione **6.14** (2.0 g, 6.9 mmol) was heated with



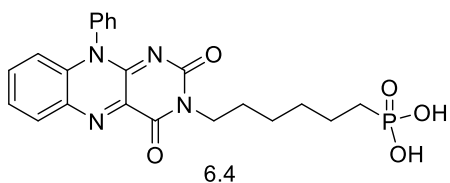
6.26

K_2CO_3 (2.6 g, 18.8 mmol) at 105 °C for 4 hours in DMF (50 mL), the resultant dark yellow solid (K salt of **6.14**) was filtered and rinse with ether and dried. The solid was then suspended in DMF (150 mL) and **6.21** (2.2 g, 7.2 mmol), was added and stirred overnight. The reaction mixture was filtered and the filtrate was dried by blowing air. The resultant solid was dissolved in DCM-water (1:1, 100 mL) and the product was extracted with DCM (3x50 ml). The organic layer was dried over $MgSO_4$ and solvent was

removed and flash chromatography was used with 2% MeOH in DCM to the product **6.26** as dark yellow solid (2.5 g, 70% in two steps). mp. 200-202 °C, IR (cm⁻¹): 1645, 1551, 1258, 1030, ¹H NMR (500 MHz, CDCl₃) δ: 8.35 – 8.28 (m, 1H), 7.71 – 7.58 (m, 5H), 7.29 (d, *J* = 7.3 Hz, 2H), 6.87 (d, *J* = 8.3 Hz, 1H), 4.14 – 3.97 (m, 6H), 1.69 (ddd, *J* = 14.8, 10.9, 7.3 Hz, 4H), 1.63 – 1.52 (m, 2H), 1.46 – 1.33 (m, 4H), 1.29 (t, *J* = 7.1 Hz, 6H). ¹³C NMR (126 MHz, CDCl₃) δ: 159.41, 155.25, 150.08, 137.95, 135.73, 135.38, 135.13, 134.28, 132.73, 130.92, 130.56, 127.67, 126.62, 117.14, 61.51 (d, *J* = 7 Hz), 42.07, 30.47 (d, *J* = 16 Hz), 27.67, 26.56, 25.74 (d, *J* = 140 Hz), 22.51 (d, *J* = 5 Hz), 16.60 (d, *J* = 6 Hz). ³¹P NMR (122 MHz, CDCl₃) δ: 33.13. HRMS (ESI) *m/z* [M+H]⁺ calculated for C₂₆H₃₁N₄O₅P 511.2110, found 511.2131.

Synthesis of (6-(2,4-dioxo-10-phenyl-4,10-dihydrobenzo[g]pteridin-3(2H)-yl)hexyl) phosphonic acid **6.4**

Diethyl-(6-(2,4-dioxo-10-phenyl-4,10-dihydrobenzo[g]pteridin-3(2H)-yl)hexyl)phosphonate

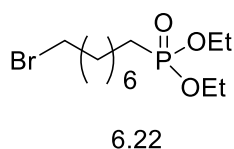


6.26 (900 mg, 1.8 mmol) was dissolved in 100 ml of dry dichloromethane and bromotrimethylsilane (1.6 ml, 8.8 mmol) was added drop wise and stirred at room

temperature under argon for overnight. The solvent was removed by using rotary evaporator and 50 ml of methanol was added and stirred for 14 hr. The solvent was removed using rotary evaporator and deionized water was added and stirred for 2 hr. A yellow solid started to form and the product **6.4** (605.3 mg, 78%) was isolated by filtration and washed with water and diethyl ether. mp. 185 °C (dec), IR (cm⁻¹): 3472, 1643, 1549, 1135, 997. ¹H NMR (500 MHz, DMSO-*d*₆) δ: 8.23 (d, *J* = 8.0 Hz, 1H), 7.79 – 7.60 (m, 5H), 7.45 (d, *J* = 7.4 Hz, 2H), 6.78 (d, *J* = 8.5 Hz, 1H), 3.86 (t, *J* = 7.2 Hz, 2H), 1.64 – 1.19 (m,

10H). ^{13}C NMR (126 MHz, $\text{DMSO-}D_6$) δ : 159.09, 154.73, 150.37, 138.63, 135.87, 135.00, 134.88, 133.99, 131.43, 130.35, 129.91, 127.86, 126.06, 116.77, 40.90, 29.87(d, $J = 16$ Hz), 28.15, 27.69 (d, $J = 142$ Hz), 27.08, 22.79 (d, $J = 4$ Hz). ^{31}P NMR (122 MHz, $\text{DMSO-}D_6$) δ : 26.94. HRMS (ESI) m/z $[\text{M}+\text{H}]^+$ calculated for $\text{C}_{22}\text{H}_{23}\text{N}_4\text{O}_5\text{P}$ 455.1479, found 455.1486.

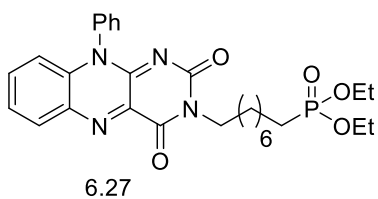
Synthesis of diethyl (8-bromooctyl)phosphonate **6.22**



1,8-dibromooctane (5.0 g, 18.4 mmol) was heated at 140 °C and triethylphosphite (1.53 g, 9.2 mmol) was added drop wise using additional funnel. The reaction was heating at 140 °C for overnight and the reaction was concentrated using rotary evaporator. The product **6.22** (2.12 g, 70%) was separated as a colorless oil using column chromatography with two column volume of dichloromethane and a gradient elution with 10% diethyl ether in ethyl acetate to ethyl acetate. ^1H NMR (500 MHz, CDCl_3) δ 4.16 – 3.97 (m, 4H), 3.43 – 3.31 (m, 2H), 1.88 – 1.75 (m, 2H), 1.76 – 1.63 (m, 2H), 1.62 – 1.48 (m, 2H), 1.45 – 1.19 (m, 14H). ^{13}C NMR (126 MHz, CDCl_3) δ : 61.48 (d, $J = 6$ Hz), 34.04, 32.82, 30.54(d, $J = 18$ Hz), 28.98, 28.36 (d, $J = 141$ Hz), 26.30, 25.18, 22.44 (d, $J = 5$ Hz), 16.57 (d, $J = 5$ Hz).

Synthesis of diethyl (8-(2,4-dioxo-10-phenyl-4,10-dihydrobenzo[g]pteridin-3(2H)-yl)octyl)phosphonate **6.27**

10-phenylbenzo[g]pteridine-2,4(3H,10H)-dione **6.14** (2.0 g, 6.9 mmol) was heated with

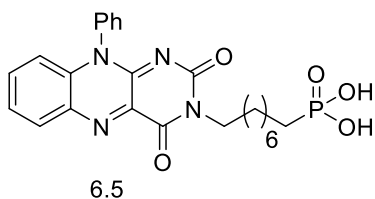


K_2CO_3 (2.6 g, 18.8 mmol) at 105 °C for 4 hr in DMF (100 mL), the resultant dark yellow solid (K salt of **6.14**) was filtered and rinse with ether and dried. The solid was then suspended in DMF (150 mL)

and **6.22** (2.2 g, 6.9 mmol), was added and stirred overnight. The reaction mixture was filtered and the filtrate was dried by blowing air. The resultant solid was dissolved in DCM-water (1:1, 100 mL) and the product was extracted with DCM (3x50 mL). The organic layer was dried over MgSO₄ and solvent was removed and flash chromatography was used with 1-2 MeOH in DCM to purify the product as yellow solid. The product **6.27** was purified as dark yellow solid (2.6 g, 71% in two steps). mp. 158-160 °C, IR (cm⁻¹): 3565, 3461, 1642, 1548, 1243, and 1019. ¹H NMR (500 MHz, CDCl₃) δ: 8.34 – 8.29 (m, 1H), 7.70 – 7.53 (m, 5H), 7.30 (d, *J* = 7.3 Hz, 2H), 6.88 (d, *J* = 8.4 Hz, 1H), 4.12 – 3.97 (m, 6H), 1.74 – 1.62 (m, 4H), 1.61 – 1.49 (m, 2H), 1.32 (m, 14H). ¹³C NMR (126 MHz, CDCl₃) δ: 159.36, 155.25, 150.05, 137.95, 135.70, 135.34, 135.12, 134.25, 132.69, 130.90, 130.53, 127.65, 126.58, 117.12, 61.48 (d, *J* = 6 Hz), 42.18, 30.63 (d, *J* = 18 Hz), 29.18, 29.03, 27.77, 26.92, 25.74 (d, *J* = 140 Hz), 22.49 (d, *J* = 6 Hz), 16.59 (d, *J* = 6 Hz). ³¹P NMR (122 MHz, DMSO-*D*₆) δ: 33.28. HRMS (ESI) *m/z* [M+Na]⁺ calculated for C₂₈H₃₅N₄O₅P 561.2237, found 561.2256.

Synthesis of (8-(2,4-dioxo-10-phenyl-4,10-dihydrobenzo[*g*]pteridin-3(2H)-yl)octyl) phosphonic acid **6.5**

diethyl (8-(2,4-dioxo-10-phenyl-4,10-dihydrobenzo[*g*]pteridin-3(2H)-yl)octyl)phosphonate



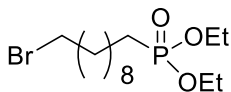
6.27 (467 mg, 0.87 mmol) was dissolved in dry dichloromethane (30 mL) and bromotrimethylsilane (572 μl, 4.3 mmol) was added dropwise and stirred at room temperature under argon for overnight. The solvent was removed by using rotary evaporator

and methanol (30 mL) was added and stirred for 14 hr. The solvent was removed using rotary evaporator and deionized water was added and stirred for 2 hr. A yellow solid started to form and the product **6.5** (293.8 mg, 70%) was isolated by filtration and washed

with water and diethyl ether. mp. 215-218 (dec), IR (cm⁻¹): 1645, 1552, 1178, 1001. ¹H NMR (500 MHz, DMSO-*d*₆) δ: 8.23 (d, *J* = 7.7 Hz, 1H), 7.83 – 7.56 (m, 5H), 7.45 (d, *J* = 6.9 Hz, 2H), 6.78 (d, *J* = 8.2 Hz, 1H), 3.85 (s, 2H), 1.62 – 1.11 (m, 14H). ¹³C NMR (126 MHz, DMSO-*D*₆) δ: 159.06, 154.71, 150.35, 138.61, 135.86, 135.00, 134.89, 133.99, 131.42, 130.36, 129.92, 127.87, 126.07, 116.78, 40.89, 30.05 (d, *J* = 16 Hz), 28.63, 27.57 (d, *J* = 136 Hz), 27.33, 26.40, 22.75, 22.73. ³¹P NMR (122 MHz, DMSO-*D*₆) δ: 27.43. HRMS (ESI) *m/z* [M+H]⁺ calculated for C₂₄H₂₇N₄O₅P 483.1792, found 483.1808.

Synthesis of diethyl (10-bromodecyl)phosphonate **6.22**

1,10-dibromodecane (18.06 g, 60.2 mmol) was heated at 140 °C and triethylphosphite (2 g, 12.04 mmol) was added drop wise using additional funnel.



6.23

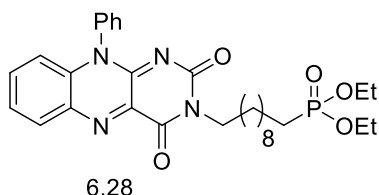
The reaction was heating at 140 °C for overnight and the reaction was concentrated using rotary evaporator. The product

6.23 (1.9 g, 47%) was separated as a colorless oil using column

chromatography with two column volume of dichloromethane and a gradient elution with 10% diethyl ether in ethyl acetate to ethyl acetate. ¹H NMR (500 MHz, CDCl₃) δ: 4.13 – 3.90 (m, 4H), 3.34 (t, *J* = 6.9 Hz, 2H), 1.78 (p, *J* = 6.9 Hz, 2H), 1.70 – 1.59 (m, 2H), 1.59 – 1.46 (m, 2H), 1.40 – 1.16 (m, 18H). ¹³C NMR (126 MHz, CDCl₃) δ: 61.43 (d, *J* = 6 Hz), 34.05, 32.84, 30.61 (d, *J* = 16 Hz), 29.38, 29.27, 29.07, 28.74, 28.17, 25.70 (d, *J* = 141 Hz), 22.42 (d, *J* = 5 Hz), 16.53 (d, *J* = 5 Hz) .

Synthesis of diethyl (10-(2,4-dioxo-10-phenyl-4,10-dihydrobenzo[g]pteridin-3(2H)-yl)decyl)phosphonate **6.28**

10-phenylbenzo[g]pteridine-2,4(3H,10H)-dione **6.14** (677 mg, 2.3 mmol) was heated with



K_2CO_3 (635 mg, 4.6 mmol) at 105 °C for 4 hr in

DMF (30 mL), the resultant dark yellow solid (K

salt of **6.14**) was filtered and rinse with ether and

dried. The solid was then suspended in DMF (50

mL) and **6.23** (1 g, 2.8 mmol), was added and

stirred overnight. The reaction mixture was filtered and the filtrate was dried by blowing

air. The resultant solid was dissolved in DCM-water (1:1, 50 mL) and the product was

extracted with DCM (3x50 mL). The organic layer was dried over $MgSO_4$ and solvent was

removed and flash chromatography was used with 1-2% MeOH in DCM to purify the

product as yellow solid **6.28** (800 mg, 62% in two steps). mp. 185 °C (dec), IR. (cm^{-1}):

3553, 3464, 2926, 1644, 1551, 1023, 955. 1H NMR (500 MHz, $CDCl_3$) δ : 8.33 (dd, $J =$

8.1, 1.2 Hz, 1H), 7.71 – 7.53 (m, 5H), 7.30 (d, $J = 7.2$ Hz, 2H), 6.88 (d, $J = 8.5$ Hz, 1H),

4.15 – 3.98 (m, 6H), 1.72 – 1.63 (m, 4H), 1.61 – 1.51 (m, 2H), 1.39 – 1.24 (m, 18H). ^{13}C

NMR (126 MHz, $CDCl_3$) δ : 159.34, 155.23, 150.03, 137.95, 135.67, 135.31, 135.11,

134.24, 132.67, 130.89, 130.51, 127.64, 126.55, 117.10, 61.44 (d, $J = 6$ Hz), 42.21,

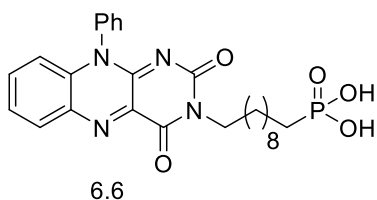
30.69 (d, $J = 18$ Hz), 29.49, 29.40, 29.38, 29.15, 27.78, 26.98, 25.75 (d, $J = 141$ Hz),

22.50 (d, $J = 5$ Hz), 16.58 (d, $J = 6$ Hz). ^{31}P NMR (122 MHz, $CDCl_3$) δ : 33.34. HRMS

(ESI) m/z $[M+H]^+$ calculated for $C_{30}H_{39}N_4O_5P$ 567.2731, found 566.2729.

Synthesis of (10-(2,4-dioxo-10-phenyl-4,10-dihydrobenzo[g]pteridin-3(2H)-yl)decyl) phosphonic acid **6.6**

Diethyl(10-(2,4-dioxo-10-phenyl-4,10-dihydrobenzo[g]pteridin-3(2H)-yl)decyl) phosphonate **6.28** (593 mg, 1.05 mmol) was dissolved in dry

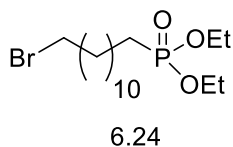


dichloromethane (30 mL) and bromotrimethylsilane (691 μ l, 5.24 mmol) was added dropwise and stirred at room temperature under argon for overnight. The solvent was removed by using rotary evaporator

and methanol (30 mL) was added and stirred for 14 hr. The solvent was removed using rotary evaporator and deionized water was added and stirred for 2 hr. A yellow solid started to form and the product **6.6** (470 mg, 88%) was isolated by filtration and washed with water and diethyl ether. mp. 185 °C (dec) IR (cm^{-1}): 2925, 2850, 1645, 1549. ^1H NMR (500 MHz, $\text{DMSO-}d_6$) δ 8.22 (d, $J = 7.5$ Hz, 1H), 7.84 – 7.51 (m, 5H), 7.45 (d, $J = 6.7$ Hz, 2H), 6.78 (d, $J = 8.2$ Hz, 1H), 3.85 (s, 2H), 1.63 – 1.09 (m, 18H). ^{13}C NMR (126 MHz, $\text{DMSO-}D_6$) δ 159.59, 155.24, 150.88, 139.15, 136.39, 135.53, 135.42, 134.52, 131.95, 130.88, 130.44, 128.39, 126.59, 117.31, 41.42, 30.60 (d, $J = 15$ Hz), 29.49, 29.40, 29.35, 29.25, 28.12 (d, $J = 136$ Hz), 27.87, 26.96, 23.30 (d, $J = 5$ Hz). ^{31}P NMR (122 MHz, $\text{DMSO-}D_6$) δ 27.28. HRMS (ESI) m/z $[\text{M}+\text{H}]^+$ calculated for $\text{C}_{26}\text{H}_{31}\text{N}_4\text{O}_5\text{P}$ 511.2105, found 511.2104.

Synthesis of diethyl (12-bromododecyl)phosphonate (**6.24**)

1,12-dibromododecane (19.75 g, 60.2 mmol) was heated at 140 °C and triethylphosphite (2 g, 12.04 mmol) was added drop wise using additional funnel.

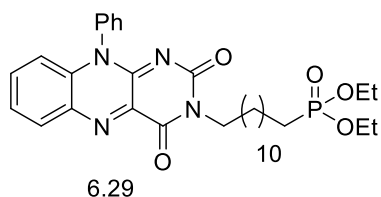


The reaction was heating at 140 °C for overnight and the reaction was concentrated using rotary evaporator. The product **6.24** (2.32 g, 32%) was separated as a colorless oil

using column chromatography with two column volume of dichloromethane and a gradient elution with 10% diethyl ether in ethyl acetate to ethyl acetate. ¹H NMR (500 MHz, CDCl₃) δ: 4.14 – 3.94 (m, 4H), 3.37 (t, *J* = 6.9 Hz, 2H), 1.82 (p, *J* = 7.0 Hz, 2H), 1.74 – 1.62 (m, 2H), 1.61 – 1.48 (m, 2H), 1.41 – 1.20 (m, 22H). ¹³C NMR (126 MHz, CDCl₃) δ: 61.44 (d, *J* = 6 Hz), 34.13, 32.89, 30.68(d, *J* = 16 Hz), 29.58, 29.54, 29.48, 29.41, 29.15, 28.82, 28.23, 25.76 (d, *J* = 140 Hz), 22.46 (d, *J* = 5 Hz), 16.56 (d, *J* = 6 Hz).

Synthesis of diethyl (12-(2,4-dioxo-10-phenyl-4,10-dihydrobenzo[g]pteridin-3(2H)-yl)dodecyl)phosphonate **6.29**

10-phenylbenzo[g]pteridine-2,4(3H,10H)-dione **6.14** (560 mg, 1.95 mmol) was heated with K₂CO₃ (550 mg, 3.98 mmol) at 105 °C for 4 hr



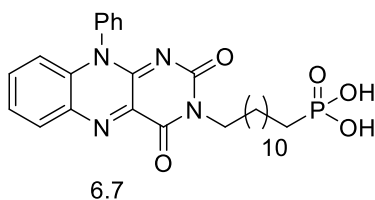
in DMF (50 mL), the resultant dark yellow solid (K salt of **6.14**) was filtered and rinse with ether and dried. The solid was then suspended in DMF (50 mL) and **6.24** (900 mg, 2.33 mmol), was added

and stirred overnight. The reaction mixture was filtered and the filtrate was dried by blowing air. The resultant solid was dissolved in DCM-water (1:1, 50 mL) and the product was extracted with DCM (3x50 ml). The organic layer was dried over MgSO₄ and solvent was removed and flash chromatography was used with 2-5% MeOH in DCM to purify the

product as yellow solid. The product **6.29** was purified as dark yellow solid (860 mg, 74% in two steps). mp. 150-152 °C. IR (cm⁻¹): 3578, 3462, 2920, 1644, 1551, 1023, 953. ¹H NMR (500 MHz, CDCl₃) δ: 8.35 – 8.26 (m, 1H), 7.72 – 7.49 (m, 5H), 7.29 (d, *J* = 7.4 Hz, 2H), 6.87 (d, *J* = 8.4 Hz, 1H), 4.15 – 3.94 (m, 6H), 1.76 – 1.62 (m, 4H), 1.62 – 1.49 (m, 2H), 1.36 – 1.17 (m, 22H). ¹³C NMR (126 MHz, CDCl₃) δ: 159.33, 155.24, 150.03, 137.95, 135.67, 135.31, 135.11, 134.23, 132.67, 130.89, 130.51, 127.64, 126.56, 117.10, 61.46, (d, *J* = 6 Hz), 42.24, 30.71 (d, *J* = 16 Hz), 29.63, 29.57, 29.47, 29.43, 29.19, 27.80, 27.01, 25.76 (d, *J* = 140 Hz), 22.52, 22.48, 16.58 (d, *J* = 5 Hz). ³¹P NMR (122 MHz, CDCl₃) δ: 33.36. HRMS (ESI) *m/z* [M+H]⁺ calculated for C₃₂H₄₃N₄O₅P 595.3044, found 595.3058.

Synthesis of (12-(2,4-dioxo-10-phenyl-4,10-dihydrobenzo[*g*]pteridin-3(2H)-yl)dodecyl) phosphonic acid **6.7**

Diethyl (12-(2,4-dioxo-10-phenyl-4,10-dihydrobenzo[*g*]pteridin-3(2H)-yl)dodecyl)phospho-



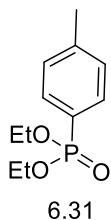
-nate **6.29** (845 mg, 1.42 mmol) was dissolved in 50 ml of dry dichloromethane and bromotrimethylsilane (938 μl, 7.10 mmol) was added dropwise and stirred at room temperature under argon for overnight. The solvent was removed by

using rotary evaporator and 30 ml of methanol was added and stirred for 14 hr. The solvent was removed using rotary evaporator and deionized water was added and stirred for 2 hr. A yellow solid started to form and the product **6.7** (685 mg, 90%) was isolated by filtration and washed with water and diethyl ether. mp. 176-178 °C (dec). IR (cm⁻¹): 2920, 2850, 1648, 1553. ¹H NMR (500 MHz, DMSO-*d*₆) δ: 8.22 (d, *J* = 7.7 Hz, 1H), 7.99 – 7.55 (m, 5H), 7.45 (d, *J* = 7.1 Hz, 2H), 6.78 (d, *J* = 8.3 Hz, 1H), 3.85 (s, 2H), 1.60 – 1.11 (m,

22H). ^{13}C NMR (126 MHz, $\text{DMSO-}D_6$) δ : 159.59, 155.25, 150.88, 139.15, 136.39, 135.53, 135.42, 134.52, 131.96, 130.89, 130.44, 128.39, 126.60, 117.31, 41.41, 30.69, 30.56, 29.58, 29.43, 29.37, 29.26, 28.13(d, $J = 137$ Hz), 27.86, 26.96, 23.31, 23.28. ^{31}P NMR (122 MHz, $\text{DMSO-}D_6$) δ : 27.35. HRMS (ESI) m/z $[\text{M}+\text{H}]^+$ calculated for $\text{C}_{28}\text{H}_{35}\text{N}_4\text{O}_5\text{P}$ 539.2418, found 539.2432.

Synthesis of diethyl p-tolylphosphonate **6.31**¹⁶⁶

Diethyl p-tolylphosphonate **6.31** was synthesized by following a known procedure.¹⁶⁶The



product was isolated with small amount of the starting material and the

resultant crude material was used for the following bromination. Both ^1H

NMR and ^{13}C NMR indicated the formation of the product **6.31**. ^1H NMR

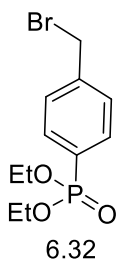
(500 MHz, CDCl_3) δ : 7.81 – 7.57 (m, 2H), 7.27 – 7.17 (m, 2H), 4.22 –

3.87 (m, 4H), 2.36 (s, 3H), 1.46 – 1.10 (m, 6H). ^{13}C NMR (126 MHz,

CDCl_3) δ : 143.00 (d, $J = 3$ Hz), 131.90 (d, $J = 11$ Hz), 129.27 (d, $J = 15$ Hz), 125.08 (d, $J = 190$ Hz), 62.02 (d, $J = 5$ Hz), 21.71, 16.39 (d, $J = 6$ Hz).

Synthesis of diethyl (4-(bromomethyl)phenyl)phosphonate **6.32**

Diethyl (4-(bromomethyl)phenyl)phosphonate **6.32** was also synthesized also



synthesized by following the previous reference with the 6.31 as the

starting material. After bromination, the product **6.32** was also isolated

with a small amount of impurity and the isolated material was used as an

alkylating agent in the following step. Both ^1H NMR and ^{13}C NMR

indicated the formation of mono brominated product **6.32**. ^1H NMR (500

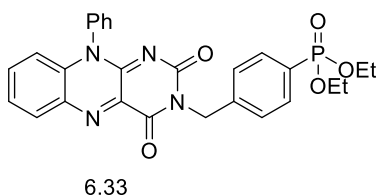
MHz, CDCl_3) δ 7.77 (dd, $J = 13.1, 8.1$ Hz, 2H), 7.68 (dd, $J = 13.1, 8.0$ Hz,

1H), 7.47 (dd, $J = 8.0, 3.7$ Hz, 2H), 7.28 – 7.21 (m, 1H), 4.47 (s, 2H), 4.26 – 3.92 (m, 5H),

1.43 – 1.19 (m, 8H). ^{13}C NMR (126 MHz, CDCl_3) δ 147.90, 139.92, 129.65, 128.20, 114.91 (d, $J = 191$ Hz), 62.01 (d, $J = 5$ Hz), 32.77, 16.51 (d, $J = 6$ Hz).

Synthesis of diethyl (4-((2,4-dioxo-10-phenyl-4,10-dihydrobenzo[g]pteridin-3(2H)-yl)methyl)phenyl)phosphonate **6.33**

10-phenylbenzo[g]pteridine-2,4(3H,10H)-dione **6.14** (484 mg, 1.67 mmol) was heated



with K_2CO_3 (346 mg, 2.51 mmol) in DMF at 90°C

for 4 h, then the precipitate was filtered and used for the next step. The resultant solid was stirred with

6.32 (615 mg, 2 mmol) in DMF for 12 hours at room

temperature. The reaction mixture was filtered and

the filtrate was dried by blowing air. The resultant solid was dissolved in DCM-water (1:1)

and the product was extracted with 3x50 ml of DCM. The organic layer was dried over

MgSO_4 and solvent was removed and flash chromatography was used with 3-5% MeOH

in DCM to purify the product as yellow solid. The product was isolated as dark yellow

solid **6.33** (457 mg, 53%). mp. $288\text{--}290^\circ\text{C}$. IR (cm^{-1}): 1650, 1548, 1020. ^1H NMR (500

MHz, CDCl_3) δ 8.31 (d, $J = 7.9$ Hz, 1H), 7.77 – 7.54 (m, 9H), 7.28 (d, $J = 7.3$ Hz, 2H),

6.89 (d, $J = 8.5$ Hz, 1H), 5.28 (s, 2H), 4.20 – 3.90 (m, 4H), 1.27 (t, $J = 7.0$ Hz, 6H). ^{13}C

NMR (126 MHz, CDCl_3) δ 159.67, 155.27, 150.37, 141.54, 138.09, 136.09, 135.94,

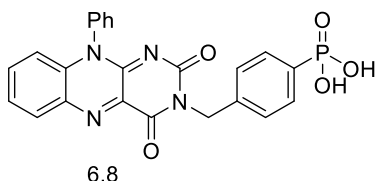
135.28, 134.51, 133.03, 132.39, 132.31, 131.18, 130.88, 129.88, 129.76, 127.83, 127.10,

117.48, 62.41 (d, $J = 5$ Hz), 45.22, 16.68 (d, $J = 6$ Hz). ^{31}P NMR (122 MHz, CDCl_3) δ

19.45. HRMS (ESI) m/z $[\text{M}+\text{H}]^+$ calculated for $\text{C}_{27}\text{H}_{25}\text{N}_4\text{O}_5\text{P}$ 517.1635, found 517.1636.

Synthesis of (4-((2,4-dioxo-10-phenyl-4,10-dihydrobenzo[g]pteridin-3(2H)-yl)methyl)phenyl)phosphonic acid **6.8**

Diethyl (4-((2,4-dioxo-10-phenyl-4,10-dihydrobenzo[g]pteridin-3(2H)-yl)methyl)phenyl)



phosphonate **6.33** (310mg, 0.6 mmol) was

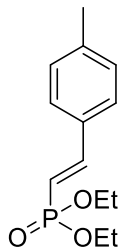
dissolved in 50 ml of dry dichloromethane and bromotrimethylsilane (400 μ l, 3.0 mmol) was added

dropwise and stirred at room temperature under

argon for overnight. The solvent was removed by using rotary evaporator and 30 ml of methanol was added and stirred for 14 hr. The solvent was removed using rotary evaporator and deionized water was added and stirred for 2 hr. A yellow solid started to form and the product **6.8** (221 mg, 85%) was isolated by filtration and washed with water and diethyl ether. mp. 356- 358 $^{\circ}$ C, IR (cm^{-1}): 3189, 1645, 1548, 991, 957. ^1H NMR (500 MHz, $\text{DMSO-}d_6$) δ : 8.20 (s, 1H), 7.77 – 7.33 (m, 11H), 6.77 (s, 1H), 5.08 (s, 2H). ^{13}C NMR (126 MHz, $\text{DMSO-}D_6$) δ : 159.81, 155.16, 151.10, 140.66, 139.28, 136.36, 135.60, 134.49, 131.99, 131.07, 130.99, 130.91, 130.50, 128.35, 127.71, 127.60, 126.78, 117.39, 44.49. ^{31}P NMR (122 MHz, $\text{DMSO-}D_6$) δ : 13.30. HRMS (ESI) m/z $[\text{M}+\text{H}]^+$ calculated for $\text{C}_{23}\text{H}_{17}\text{N}_4\text{O}_5\text{P}$ 461.1009, found 461.1005.

Synthesis of diethyl (E)-(4-methylstyryl)phosphonate **6.36**¹⁶⁶

Tetraethyl methylenediphosphonate **6.35** (4.79 g, 16.6 mmol) was dissolved in 60 mL of dry THF under argon. *n*-BuLi (2.5 M in hexane, 7.3 ml, 18.3 mmol)



6.36

was added slowly at -78 °C and the reaction was stirred for 20 min.

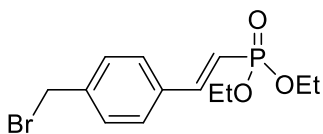
The reaction was warmed to room temperature and 4-methyl benzaldehyde **6.34** (2.0 g, 16.6 mmol) was added and stirred overnight at room temperature. Diethyl ether (100 mL) and 100 ml of

NaHCO₃ (1.0 g in 100 ml H₂O) was added and extracted into (100 ml × 2) Et₂O. The product **6.36** (3.8 g, 90%) was purified using flash

chromatography using 2% methanol in ethyl acetate as eluent. ¹H NMR (500 MHz, CDCl₃) δ: 7.47 (dd, *J* = 22.6, 17.5 Hz, 1H), 7.39 (d, *J* = 8.0 Hz, 2H), 7.18 (d, *J* = 7.9 Hz, 2H), 6.19 (dd, *J* = 17.7 Hz, 1H), 4.25-4.01 (m, 4H), 2.36 (s, 3H), 1.34 (t, *J* = 7.1 Hz, 6H). ¹³C NMR (126 MHz, CDCl₃) δ: 148.91 (d, *J* = 6 Hz), 140.74, 132.28 (d, *J* = 24 Hz), 129.69, 127.82, 112.68 (d, *J* = 192 Hz), 61.88 (d, *J* = 5 Hz), 21.55, 16.54 (d, *J* = 6 Hz).

Synthesis of diethyl (E)-(4-(bromomethyl)styryl)phosphonate **6.37**¹⁶⁵

Diethyl (E)-(4-methylstyryl)phosphonate **6.36** (3.74 g, 14.7 mmol), *N*-bromosuccinimide (2.61 g, 14.7 mmol) and 2,2'-azobis(2-methylpropionitrile)



6.37

(241 mg, 1.47 mmol) was added to 60 ml of carbon tetrachloride and refluxed at 90 °C overnight. The reaction mixture was cooled by an ice-water bath and

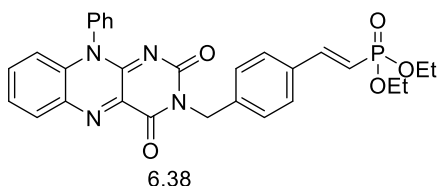
filtered to remove the ppt. The filtrate was washed with

50 mL of water and 50 ml of brine. The CCl₄ layer was dried with anhydrous MgSO₄ and filtered. The solvent was removed using rotary evaporator and the flash chromatography was used to purify using 75% ethyl acetate with 25% hexane. The isolated product **6.37**

(2.3 g, 47%) was mixed with a small amount of starting material and the mixture was used for next experiment without further purification. ^1H NMR (500 MHz, CDCl_3) δ : 7.69-7.29 (m, 6H), 6.26 (t, $J = 17.4$ Hz, 1H), 4.48 (s, 2H), 4.21-4.09 (m, 4H), 1.35 (t, $J = 6.9$ Hz, 6H). ^{13}C NMR (126 MHz, CDCl_3) δ : 147.91 (d, $J = 7$ Hz), 139.96, 135.07 (d, $J = 24$ Hz), 129.68, 128.23, 114.94 (d, $J = 191$ Hz), 62.03 (d, $J = 6$ Hz), 32.80, 16.53 (d, $J = 6$ Hz).

Synthesis of diethyl (E)-4-((2,4-dioxo-10-phenyl-4,10-dihydrobenzo[g]pteridin-3(2H)-yl)methyl)styryl)phosphonate **6.38**

10-phenylbenzo[g]pteridine-2,4(3H,10H)-dione **6.14** (2.0 g, 6.9 mmol) was heated with



K_2CO_3 (2.6 g, 18.8 mmol) at 105 °C for 4 hr in

DMF, the resultant dark yellow solid (K^+ salt of

6.14) was filtered and rinse with diethyl ether and dried. The solid was then suspended in

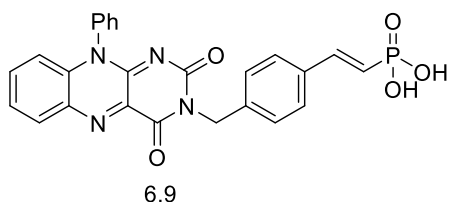
DMF (150 mL) and **6.37** (2.3 g, 6.9 mmol), was

added and stirred overnight. The reaction mixture was filtered and the filtrate was dried by blowing air. The resultant solid was dissolved in DCM-water (1:1, 100 mL) and the product was extracted with DCM (3x50 ml). The organic layer was dried over MgSO_4 and solvent was removed and flash chromatography was used with 5% MeOH in DCM to purify the product as yellow solid. The product **6.38** was purified as dark yellow solid with some impurity. The impurity was removed washing the solid with hexane, ether and ethyl acetate. The final product was yellow solid (2.01 g, 54%). mp. 296- 298 °C (dec), IR (cm^{-1}): 1649, 1548, 1245, 1053, 1024. ^1H NMR (301 MHz, CDCl_3) δ : 8.32 (d, $J = 8.0$ Hz, 1H), 7.70 – 7.49 (m, 7H), 7.48 – 7.34 (m, 3H), 7.34 – 7.26 (m, 2H), 6.89 (d, $J = 8.5$ Hz, 1H), 6.20 (dd, $J = 17.6$ Hz, 1H), 5.26 (s, 2H), 4.19 – 4.03 (m, 4H), 1.33 (t, $J = 7.0$ Hz, 6H). ^{13}C

NMR (76 MHz, CDCl₃) δ: 159.39, 155.08, 150.08, 148.57 (d, *J* = 11 Hz), 139.07, 137.92, 135.80, 135.61, 135.05, 134.25, 132.77, 130.92, 130.61, 130.24, 127.85, 127.59, 126.79, 117.21, 115.17, 112.64, 61.96 (d, *J* = 4 Hz), 44.91, 16.53 (d, *J* = 10 Hz). ³¹P NMR (122 MHz, CDCl₃) δ: 20.24. HRMS (ESI) *m/z* [M+Na]⁺ calculated for C₂₉H₂₇N₄O₅P 565.1611, found 565.1622.

Synthesis of (E)-4-((2,4-dioxo-10-phenyl-4,10-dihydrobenzo[g]pteridin-3(2H)-yl)methylstyryl)phosphonic acid **6.9**

Diethyl (E)-4-((2,4-dioxo-10-phenyl-4,10-dihydrobenzo[g]pteridin-3(2H)-yl)methylstyryl)

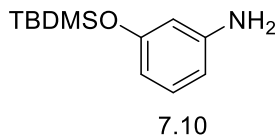


phosphonate **6.38** (1.0 g, 1.84 mmol) was dissolved in 100 ml of dry dichloromethane and bromotrimethylsilane (1.22 ml, 9.2 mmol) was added dropwise and stirred at room temperature under argon for overnight. The

solvent was removed by using rotary evaporator and 30 ml of methanol was added and stirred for overnight. The solvent was removed using rotary evaporator and deionized water was added and stirred for 2-3 hours. A yellow solid started to form and the product **6.9** (870 mg, 97%) was isolated by filtration and washed with water and diethyl ether. mp. 254-256 °C. IR (cm⁻¹): 1641, 1545, 1177, 985. ¹H NMR (500 MHz, DMSO-*d*₆) δ: 8.40 – 8.11 (m, 1H), 7.73 (t, *J* = 26.2 Hz, 5H), 7.60 – 7.27 (m, 6H), 7.15 (t, *J* = 18.8 Hz, 1H), 6.80 (d, *J* = 7.1 Hz, 1H), 6.46 (t, *J* = 15.6 Hz, 1H), 5.09 (s, 2H). ¹³C NMR (126 MHz, DMSO-*D*₆) δ: 159.29, 154.67, 150.56, 142.53 (d, *J* = 6 Hz), 138.75, 138.56, 135.85, 135.08, 135.06, 134.40, 134.22, 133.98, 131.45, 130.38, 129.96, 127.99, 127.82, 127.30, 126.23, 116.86, 43.89. ³¹P NMR (122 MHz, DMSO-*D*₆) δ: 13.94. HRMS (ESI) *m/z* [M+H]⁺ calculated for C₂₅H₁₉N₄O₅P 487.1166, found 487.1188.

Synthesis of 3-((tert-butyldimethylsilyl)oxy)aniline **7.10**¹⁶⁰

A mixture of 3-aminophenol **7.9** (2.0 g, 18.32 mmol) and imidazole (2.5 g, 36.7 mmol)



was dissolved in dry THF (100 mL) and the solution was stirred for half an hour followed by addition of tert-butylchlorodimethylsilane (4.14 g, 27.5 mmol) in portions. A white solid forms immediately and the mixture was stirred for

6 more hours under argon at room temperature and the reaction was monitored by TLC.

After 6 hours, the reaction was quenched with water (100 mL). The reaction mixture was

extracted with diethyl ether (4 x 50 ml) and the organic fractions were combined and

dried over Na₂SO₄. After removing the diethyl ether using rotary evaporator and the

product was separated as a colorless liquid **7.10** (3.8 g, 93%) by using silica gel

chromatography with 5% ethyl acetate and 95% hexane as eluent. Colorless oil: ¹H NMR

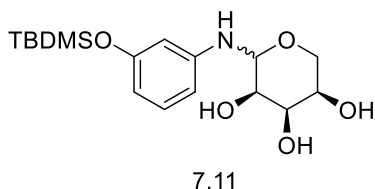
(500 MHz, DMSO-D₆) δ: 6.84 (t, *J* = 7.9 Hz, 1H), 6.16 (d, *J* = 7.9 Hz, 1H), 6.09 (s, 1H),

5.98 (dd, *J* = 7.9, 1.5 Hz, 1H), 5.00 (s, 2H), 0.94 (s, 9H), 0.15 (s, 6H). ¹³C NMR (126

MHz, DMSO-D₆) δ: 155.85, 150.03, 129.44, 107.61, 107.26, 105.41, 25.58, 17.88, -4.46.

Synthesis of (3R,4R,5R)-2-((3-((tert-butyldimethylsilyl)oxy)phenyl)amino) tetrahydro-2H-pyran-3,4,5-triol **7.11**¹⁵⁸

A mixture of compound **7.10** (1.79 g, 8.0 mmol) and D-(-) ribose (1.3 g, 8.7 mmol) were



dissolved in 30 mL of methanol and the mixture

was refluxed under Ar. After six hours, the solvent

was removed using rotary evaporator and the

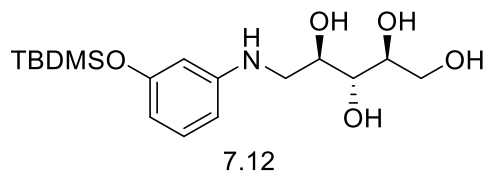
resultant solid was purified using flash

chromatography with 5% methanol and 95% DCM. The product **7.11** (2.3 g, 81%) was

isolated as a white hygroscopic solid. White solid: ^1H NMR (500 MHz, CD_3OD) δ : 7.00 (td, $J = 8.0, 3.7$ Hz, 1H), 6.40 (d, $J = 8.0$ Hz, 1H), 6.31 (dt, $J = 13.1, 2.0$ Hz, 1H), 6.23 (d, $J = 7.8$ Hz, 1H), 4.83 (d, $J = 7.9$ Hz, 1H), 4.11 (br, 1H), 3.95 – 3.44 (m, 5H), 1.00 (s, 9H), 0.20 (s, 6H). ^{13}C NMR (126 MHz, CD_3OD) some overlapping of ^{13}C peaks (may be rotational isomer or cis/trans) δ : 157.85, 157.81, 149.55, 148.55, 130.69, 130.63, 111.27, 108.69, 107.00, 106.94, 83.71, 83.54, 71.87, 69.04, 64.61, 26.21, 19.08, -4.23. HRMS (ESI) m/z $[\text{M}+\text{Na}]^+$ calculated for $\text{C}_{17}\text{H}_{29}\text{NO}_5\text{Si}$ 378.1707, found 378.1700.

Synthesis of (2S,3R,4R)-5-((3-((tert-butyldimethylsilyloxy)phenyl)amino)pentane-1,2,3,4-tetraol **7.12**¹⁵⁸

In a solution of compound **7.11** (2.0 g, 5.6 mmol) in 20 mL of ethanol, NaBH_4 (0.43 g,

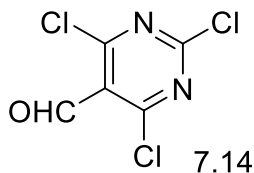


11.0 mmol) was added in portionwise at 0 °C and after the addition of NaBH_4 , the mixture was heated at 50 °C for 16 hours under argon. The reaction was quenched

with 100 mL of saturated NH_4Cl and extracted with DCM (5 x 50 ml). The DCM has been removed using rotary evaporator and the product was isolated as a white sticky solid **7.12** (1.5 g, 75%) by using column chromatography with 10% methanol in DCM. White sticky solid, ^1H NMR (500 MHz, CD_3OD) δ : 6.97 (t, $J = 8.0$ Hz, 1H), 6.34 (dd, $J = 8.0, 1.5$ Hz, 1H), 6.22 (t, $J = 1.9$ Hz, 1H), 6.15 (dd, $J = 7.9, 1.6$ Hz, 1H), 3.93 (td, $J = 7.8, 3.4$ Hz, 1H), 3.84 – 3.74 (m, 2H), 3.70 – 3.61 (m, 2H), 3.44 (dd, $J = 12.9, 3.3$ Hz, 1H), 3.12 (dd, $J = 12.9, 7.9$ Hz, 1H), 1.00 (s, 9H), 0.19 (s, 6H). ^{13}C NMR (126 MHz, CD_3OD) δ : 157.88, 151.66, 130.65, 110.12, 108.13, 106.21, 74.72, 74.32, 72.23, 64.58, 47.55, 26.21, 19.05, -4.24. HRMS (ESI) m/z $[\text{M}+\text{Na}]^+$ calculated for $\text{C}_{17}\text{H}_{31}\text{NO}_5\text{Si}$ 380.1864, found 380.1871.

Synthesis of 2,4,6-trichloropyrimidine-5-carbaldehyde **7.14**¹⁶¹

8.45 g of barbituric acid **7.13** (66 mmol) was dissolved in 40 ml of POCl₃ and 5 mL of

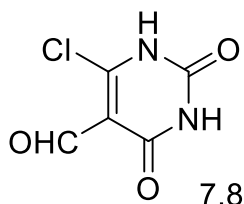


DMF (65 mmol) was added dropwise at 0 °C and the mixture was stirred at 0 °C an hour followed by refluxing for 16 hours at 130 °C. The reaction was concentrated using rotary evaporator and the thick reaction mixture was poured in ice-

water and stirred to form a beige solid. After filtration, the resultant crude solid was purified using silica gel with 10% ethyl acetate in hexane to get the product as white solid **7.14** (8.6 g, 61.6%). ¹H NMR (500 MHz, CDCl₃) δ: 10.39 (s, 1H). ¹³C NMR (126 MHz, CDCl₃) δ: 184.70, 164.18, 161.69, 123.10.

Synthesis of 6-chloro-2,4-dioxo-1,2,3,4-tetrahydropyrimidine-5-carbaldehyde **7.8**¹⁶²

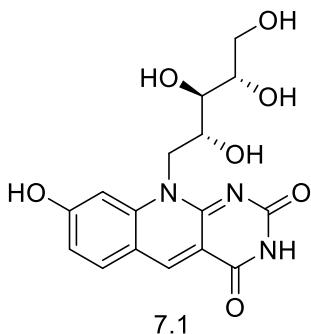
A mixture of compound **7.14** (1.0 g, 4.73 mmol) and K₂CO₃ (0.65 g, 4.73 mmol) was added to ethanol: water (2:1, 40 mL) and the solution was



stirred for 4 hours at room temperature. The reaction was neutralized with CH₃COOH (3-4 mL) and the reaction was concentrated with rotary evaporator and kept at 4 °C for 3 days. The product was isolated as white crystalline solid **7.8**

(760 mg, 91%) White solid, ¹H NMR (500 MHz, DMSO-D₆) δ: 10.04 (s, 1H). ¹³C NMR (126 MHz, DMSO-D₆) δ: 189.11, 171.50, 160.75, 159.07, 111.97

Synthesis of 8-hydroxy-10-((2R,3R,4S)-2,3,4,5-tetrahydroxypentyl)pyrimido[4,5-b]quinoline-2,4(3H,10H)-dione **7.1**

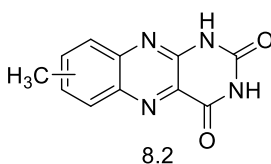


A mixture of compound **7.8** (1.02 g, 2.9 mmol) and **7.12** (0.31 g, 1.8 mmol) were mixed with DMF (10 mL). And the mixture was heated at 130 °C for 90 min and the reaction was cooled at room temperature. About 20 mL of diethyl ether was added and the mixture was stirred and kept in freezer. The product was formed as golden yellow solid **7.1** (390 mg, 60.3%) Golden yellow solid, ¹H NMR (500 MHz, DMSO-D₆) δ: 11.24 (s, 1H), 10.97 (s, 1H), 8.88 (s, 1H), 8.02 (d, *J* = 8.7 Hz, 1H), 7.39 (s, 1H), 7.03 (d, *J* = 8.5 Hz, 1H), 5.11 (d, *J* = 4.9 Hz, 1H), 4.94 (d, *J* = 5.2 Hz, 1H), 4.79 (d, *J* = 4.1 Hz, 2H), 4.65 (d, *J* = 13.1 Hz, 1H), 4.52 – 4.43 (m, 1H), 4.23 (s, 1H), 3.71 – 3.53 (m, 3H), 3.49 – 3.40 (m, 1H). ¹³C NMR (126 MHz, DMSO-D₆) δ: 164.48, 162.52, 158.19, 156.63, 144.06, 141.46, 133.71, 115.43, 115.34, 110.67, 102.21, 73.86, 72.77, 69.58, 63.38, 47.81, 39.52. HRMS (ESI) *m/z* [M-H]⁻ calculated for C₁₆H₁₇N₃O₇ 362.0994, found 362.0973.

General synthesis of 8.1-8.9

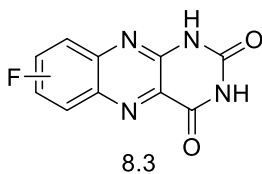
The derivative of *o*-phenylenediamine (0.7-0.8 mmol, 1 equiv) was stirred with alloxan monohydrate (0.7-0.8 mmol, 1 equiv) and boric acid (1.2 equiv) in acetic acid (20 ml) at room temperature for 6-8 hours. A solid formed in the reaction which was separated by filtration and washed with diethyl ether. NMR of some of these compounds indicate the presence of acetic acid.

7-methylbenzo[g]pteridine-2,4(1H,3H)-dione and 8-methylbenzo[g]pteridine-2,4(1H,3H)-dione **8.2** (isolated as mixture of two products)



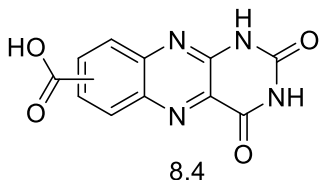
Light yellow solid, (230 mg, 85%), ¹H NMR (500 MHz, DMSO-*d*₆) δ: 11.76 (s, 2H), 8.21 – 7.22 (m, 3H). ¹³C NMR (126 MHz, DMSO-*D*₆) δ: 161.07, 150.64, 147.44, 146.90, 144.81, 143.29, 141.56, 139.83, 139.01, 136.17, 131.73, 131.30, 130.19, 129.11, 127.06, 126.17, 22.21, 21.59.

7-fluorobenzo[g]pteridine-2,4(1H,3H)-dione and 8-fluorobenzo[g]pteridine-2,4(1H,3H)-dione **8.3** (isolated as mixture of two products)



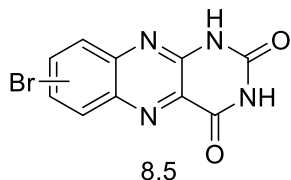
Light yellow solid, (210 mg, 86%), ¹H NMR (500 MHz, DMSO-*d*₆) δ: 11.96 (d, 2H), 11.75 (s, 2H), 8.27 – 8.12 (m, 1H), 8.03 – 7.89 (m, 2H), 7.89 – 7.75 (m, 1H), 7.75 – 7.52 (m, 2H). ¹³C NMR (126 MHz, DMSO-*D*₆) δ: 165.84, 163.82, 162.30, 160.83, 160.76, 160.32, 150.60, 147.94, 147.10, 144.44, 144.32, 140.41, 140.00, 139.90, 137.04, 133.49, 133.40, 132.91, 131.76, 129.83, 129.75, 124.12, 123.91, 119.40, 119.19, 113.88, 113.71, 111.22, 111.04.

2,4-dioxo-1,2,3,4-tetrahydrobenzo[g]pteridine-8-carboxylic acid and 2,4-dioxo-1,2,3,4-tetrahydrobenzo[g]pteridine-8-carboxylic acid **8.4** (isolated as mixture of two products)



Light greenish solid, (400 mg, 70%) ^1H NMR (500 MHz, $\text{DMSO-}d_6$) δ : 12.40 – 11.63 (m, 2H), 9.03 – 7.46 (m, 3H). ^{13}C NMR (126 MHz, $\text{DMSO-}D_6$) δ : 166.96, 160.75, 160.70, 150.59, 148.55, 148.05, 145.26, 142.45, 141.30, 138.72, 134.99, 134.02, 133.67, 132.71, 132.42, 131.09, 130.67, 129.03, 127.92, 127.83, 40.53, 40.36, 40.20, 40.03, 39.87, 39.70, 39.53.

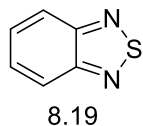
7-bromobenzo[g]pteridine-2,4(1H,3H)-dione and 8-bromobenzo[g]pteridine-2,4(1H,3H)-dione **8.5** (isolated as mixture of two products)



Light purple solid, (320 mg, 70%), ^1H NMR (500 MHz, $\text{DMSO-}d_6$) δ : 12.29 – 11.62 (m, 2H), 8.43 – 7.52 (m, 3H). ^{13}C NMR (126 MHz, $\text{DMSO-}D_6$) δ : 160.74, 150.58, 148.05, 147.66, 143.52, 141.82, 139.80, 138.31, 138.24, 134.14, 133.19, 132.92, 132.71, 132.42, 129.53, 129.29, 129.09, 126.18.

Compound 8.6, 8.7, 8.8 and 8.9 were synthesized by following the published report.¹¹⁶

Benzo[c][1,2,5]thiadiazole **8.19**¹⁶⁷

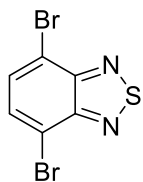


8.19

Yellowish red solid, (3.6 g, 83%), mp: 40-42 °C (lit. mp. 42-43 °C)¹⁸⁵ ¹H

NMR (500 MHz, CDCl₃) δ: 8.01 (dd, *J* = 6.8, 3.2 Hz, 2H), 7.59 (dd, *J* = 6.8, 3.2 Hz, 2H).¹³C NMR (126 MHz, CDCl₃) δ: 154.90, 129.42, 121.66,

4,7-dibromobenzo[c][1,2,5]thiadiazole **8.20**¹⁶⁸

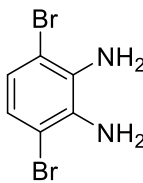


8.20

Beige solid, (1.2 g, 93%), mp: 191-193 °C (lit. mp. 189 – 190 °C)¹²⁰ ¹H

NMR (500 MHz, CDCl₃) δ: 7.72 (s, 2H).¹³C NMR (126 MHz, CDCl₃) δ: 153.10, 132.50, 114.05.

3,6-dibromobenzene-1,2-diamine **8.21**¹⁶⁹

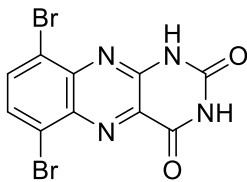


8.21

White solid, (900 mg, 82%), mp: 90 - 92 °C (lit. mp. 92 – 94 °C).¹⁶⁸ ¹H

NMR (500 MHz, CDCl₃) δ: 7.73 (s, 1H).¹³C NMR (126 MHz, CDCl₃) δ: 153.13, 132.52, 114.07.

6,9-dibromobenzo[g]pteridine-2,4(1H,3H)-dione **8.12**



8.12

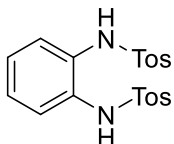
Light yellow solid, (310 mg, 80%), mp. >400 °C. IR (cm⁻¹):

3305, 3069, 1702, 1568. ¹H NMR (301 MHz, DMSO-*d*₆) δ: 12.27 (s, 1H), 11.89 (s, 1H), 8.14 (s, 1H), 8.02 (s, 1H). ¹³C

NMR (126 MHz, DMSO-*D*₆) δ: 160.20, 150.50, 148.62, 141.65, 137.56, 136.79, 133.81, 132.20, 124.83, 121.03,

40.54, 40.37, 40.21, 40.04, 39.87, 39.71, 39.54. HRMS (ESI) *m/z* [M-H]⁻ calculated for C₁₀H₄Br₂N₄O₂ 370.8608, found 370.8623.

N,N'-(1,2-phenylene)bis(4-methylbenzenesulfonamide) **8.14**¹⁷⁰



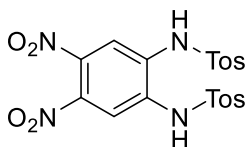
8.14

White solid, (12 g, 95%), mp. 204-205 °C, (lit. mp. 204 - 207 °C).¹⁸⁷

¹H NMR (500 MHz, CDCl₃) δ: 7.56 (d, *J* = 8.3 Hz, 4H), 7.21 (d, *J* = 8.1 Hz, 4H), 7.03 (dd, *J* = 6.0, 3.5 Hz, 2H), 6.95 (dd, *J* = 5.9, 3.6 Hz, 2H), 2.39 (s, 6H).¹³C NMR (126 MHz, DMSO-*D*₆) δ: 144.20, 136.59,

130.27, 130.20, 127.46, 126.40, 123.90, 39.88, 39.71, 39.55, 21.55.

N,N'-(4,5-dinitro-1,2-phenylene)bis(4-methylbenzenesulfonamide) **8.15**¹⁷⁰

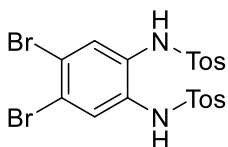


8.15

Light yellow solid, (2.1g, 92%), mp. 233-236 °C, (lit. mp. 248 -

250 °C)¹⁸⁸. ¹H NMR (500 MHz, DMSO-*d*₆) δ: 7.72 (s, 2H), 7.65 (d, *J* = 7.7 Hz, 4H), 7.33 (d, *J* = 7.6 Hz, 4H), 2.33 (s, 6H).¹³C NMR (126 MHz, DMSO-*D*₆) δ: 144.69, 137.35, 136.56, 134.42, 130.50, 127.42, 115.80, 21.57.

N,N'-(4,5-dibromo-1,2-phenylene)bis(4-methylbenzenesulfonamide) **8.16**¹⁷⁰



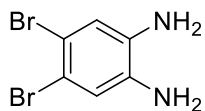
8.16

White solid (1.2 g, 65%), mp. 220 - 222 °C, (lit. mp. 218 - 220

°C)¹⁸⁹. ¹H NMR (500 MHz, CDCl₃) δ: 7.59 (d, *J* = 8.2 Hz, 4H), 7.28 (d, *J* = 8.1 Hz, 4H), 7.20 (s, 2H), 6.75 (s, 2H), 2.42 (s, 6H).¹³C NMR (126 MHz, DMSO-*D*₆) δ 144.69, 136.17, 130.59, 130.48, 127.47, 127.24, 120.04, 21.58.

4,5-dinitrobenzene-1,2-diamine **8.17** was synthesized by a known procedure.¹⁷¹ The compound was used for the next step without further purification due to the reported instability.

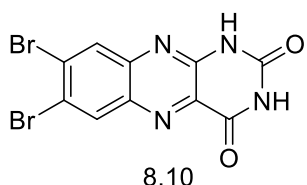
4,5-dibromobenzene-1,2-diamine **8.18**¹⁷²



8.18

Beige solid, (1.2 g, 65%), mp. 150-151 °C, (lit. mp. 150 - 151 °C)¹⁹⁰. ¹H NMR (500 MHz, DMSO-*d*₆) δ: 6.77 (s, 2H), 4.88 (s, 4H). ¹³C NMR (126 MHz, DMSO-*D*₆) δ: 136.87, 117.66, 109.17.

7,8-dibromobenzo[g]pteridine-2,4(1H,3H)-dione **8.10**

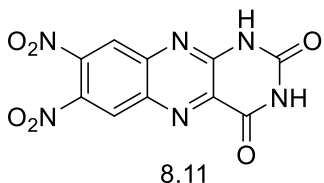


8.10

Light yellow solid, (250 mg, 70%), mp. >400 °C. IR (cm⁻¹): 3067, 1705, 1440. ¹H NMR (500 MHz, DMSO-*d*₆) δ: 12.04 (s, 1H), 11.83 (s, 2H), 8.56 (s, 1H), 8.29 (s, 1H). ¹³C NMR (126 MHz, DMSO-*D*₆) δ: 160.55, 150.53, 148.23, 142.46, 138.97, 134.35, 133.74, 131.49, 129.60, 123.78. HRMS

(ESI) m/z [M+H]⁺ calculated for C₁₀H₄Br₂N₄O₂ 370.8608, found 370.8622.

7,8-dinitrobenzo[g]pteridine-2,4(1H,3H)-dione **8.11**



8.11

Light yellow solid, (210 mg, 75% in two steps), mp. 304 °C (dec). IR (cm⁻¹): 3054, 1698, 1538. ¹H NMR (500 MHz, DMSO-*d*₆) δ: 12.51 (s, 1H), 12.05 (s, 2H), 9.08 (s, 1H), 8.70 (s, 1H). ¹³C NMR (126 MHz, DMSO-*D*₆) δ: 160.04, 150.42, 150.36, 144.76, 144.44, 139.86,

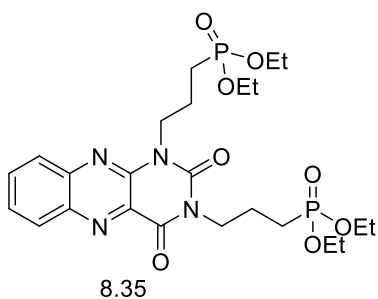
138.83, 137.10, 129.45, 125.36. HRMS (ESI) m/z [M-H]⁻ calculated for C₁₀H₄N₆O₆ 303.0120, found 303.0132.

General synthesis of **8.35-8.39**

Benzo[g]pteridine-2,4(1H,3H)-dione **8.1** (500 mg, 2.3 mmol) was heated with K_2CO_3 (1.3 g, 9.2 mmol) at 110 °C for 6 hours and the resultant solid was stirred with 2.2 equivalent of bromophosphonates in DMF at room temperature for overnight. The reaction mixture was filtered and the filtrate was dried by blowing air. The resultant solid was dissolved in DCM-water (1:1, 50 mL) and the product was extracted with DCM (3x50 ml). The organic layer was dried over $MgSO_4$ and solvent was removed and flash chromatography was used with 2% MeOH in DCM to purify the product as greenish yellow liquid.

Tetraethyl ((2,4-dioxobenzo[g]pteridine-1,3(2H,4H)-diyl)bis(propane-3,1-diyl)bis (phosphonate) **8.35**

Greenish yellow liquid, (1.02 g, 75%), IR (cm^{-1}): 2980, 2934, 1720, 1560, 1219,

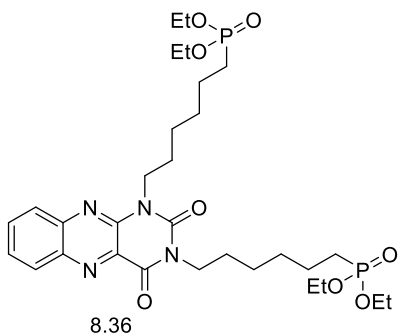


1022,955. 1H NMR (500 MHz, $CDCl_3$) δ : 8.29 (d, $J = 8.5$ Hz, 1H), 7.99 (d, $J = 8.5$ Hz, 1H), 7.87 (t, $J = 7.1$ Hz, 1H), 7.73 (t, $J = 7.2$ Hz, 1H), 4.48 (t, $J = 7.3$ Hz, 2H), 4.22 (t, $J = 7.2$ Hz, 2H), 4.17 – 3.96 (m, 8H), 2.17 – 1.96 (m, 5H), 1.95 – 1.77 (m, 4H), 1.34 – 1.17 (m, 12H). ^{13}C NMR (126 MHz, $CDCl_3$) δ :

159.65, 150.20, 144.94, 143.39, 140.18, 134.04, 130.87, 129.69, 129.37, 127.97, 61.76 (d, $J = 6$ Hz), 43.02 (d, $J = 29$ Hz), 42.87 (d, $J = 29$ Hz), 23.49 (d, $J = 142$ Hz), 23.46 (d, $J = 142$ Hz), 21.20 (d, $J = 4$ Hz), 21.01 (d, $J = 4$ Hz), 16.55 (d, $J = 6$ Hz). ^{31}P NMR (122 MHz, $CDCl_3$) δ : 31.54, 31.52. HRMS (ESI) m/z $[M+Na]^+$ calculated for $C_{24}H_{36}N_4O_8P_2$ 593,1901 found 593.1898.

Tetraethyl ((2,4-dioxobenzo[g]pteridine-1,3(2H,4H)-diyl)bis(hexane-6,1-diyl))bis
(phosphonate) **8.36**

Greenish yellow liquid (1.2 g, 78%), IR (cm⁻¹): 2934, 1673, 1560, 1023, 956. ¹H NMR

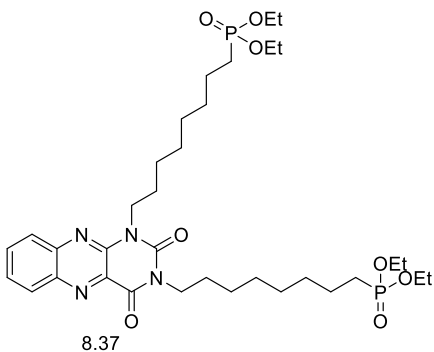


(500 MHz, CDCl₃) δ: 8.29 (d, *J* = 8.7 Hz, 1H), 7.99 (d, *J* = 8.5 Hz, 1H), 7.86 (ddd, *J* = 8.4, 7.0, 1.2 Hz, 1H), 7.72 (td, *J* = 7.6, 7.0, 1.1 Hz, 1H), 4.46 – 4.31 (m, 2H), 4.20 – 4.10 (m, 2H), 4.10 – 3.97 (m, 8H), 1.80 – 1.53 (m, 12H), 1.50 – 1.36 (m, 8H), 1.32 – 1.21 (m, 12H). ¹³C NMR (126 MHz, CDCl₃) δ:

159.64, 150.20, 145.08, 143.49, 140.08, 133.84, 130.84, 129.82, 129.15, 127.98, 61.48 (d, *J* = 6 Hz), 42.69, 42.52, 30.33 (d, *J* = 18 Hz), 30.29 (d, *J* = 18 Hz), 27.67, 27.37, 26.52, 26.44, 25.21 (d, *J* = 141 Hz), 25.19 (d, *J* = 141 Hz), 22.45 (d, *J* = 4 Hz), 22.44 (d, *J* = 4 Hz), 16.55 (d, *J* = 5 Hz). ³¹P NMR (122 MHz, CDCl₃) δ: 33.03, 32.99. HRMS (ESI) *m/z* [M+H]⁺ calculated for C₃₀H₄₈N₄O₈P₂ 655.3020, found 655.3045.

Tetraethyl ((2,4-dioxobenzo[g]pteridine-1,3(2H,4H)-diyl)bis(octane-8,1-diyl))bis
(phosphonate) **8.37**

Greenish yellow liquid (1.3 g, 81%), IR (cm⁻¹):2981, 2930, 1721, 1276, 1228, 1024, 956.

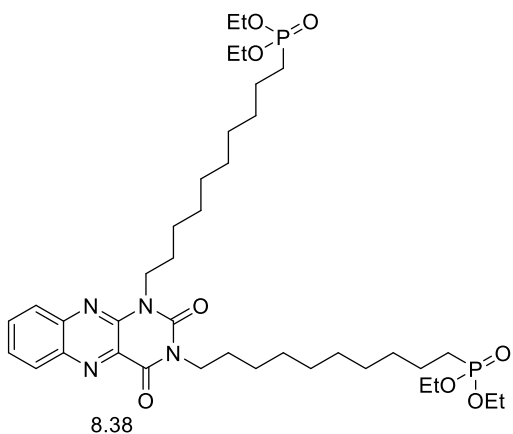


¹H NMR (500 MHz, CDCl₃) δ: 8.29 (d, *J* = 8.0 Hz, 1H), 7.98 (d, *J* = 8.2 Hz, 1H), 7.89 – 7.82 (m, 1H), 7.71 (ddd, *J* = 8.2, 7.0, 1.1 Hz, 1H), 4.43 – 4.36 (m, 2H), 4.16 – 4.11 (m, 2H), 4.10 – 3.98 (m, 8H), 1.78 – 1.64 (m, 8H), 1.59 – 1.51 (m, 4H), 1.42 – 1.27 (m, 28H). ¹³C NMR (126 MHz, CDCl₃) δ: 159.66, 150.21, 145.11,

143.51, 140.06, 133.79, 130.85, 129.87, 129.09, 127.97, 61.45 (d, $J = 6$ Hz), 42.79, 42.64, 30.62 (d, $J = 19$ Hz), 30.67, 29.07, 29.04, 27.81, 27.53, 26.91, 26.84, 26.26 (d, $J = 139$ Hz), 25.24 (d, $J = 139$ Hz),, 22.48, 22.44, 16.57 (d, $J = 6$ Hz). ^{31}P NMR (122 MHz, CDCl_3) δ : 33.27, 33.23. HRMS (ESI) m/z $[\text{M}+\text{H}]^+$ calculated for $\text{C}_{34}\text{H}_{56}\text{N}_4\text{O}_8\text{P}_2$ 711.3646, found 711.3677.

Tetraethyl ((2,4-dioxobenzo[*g*]pteridine-1,3(2H,4H)-diyl)bis(decane-10,1-diyl))bis (phosphonate) **8.38**

Greenish yellow liquid (1.4 g, 79%), IR (cm^{-1}): 2927, 2854, 1721, 1676, 1560, 1231,



1025, 957. ^1H NMR (500 MHz, CDCl_3) δ :

8.20 (d, $J = 8.4$ Hz, 1H), 7.91 (d, $J = 8.4$

Hz, 1H), 7.78 (t, $J = 7.2$ Hz, 1H), 7.64 (t,

$J = 7.2$ Hz, 1H), 4.37 – 4.28 (m, 2H),

4.10 – 4.03 (m, 2H), 4.02 – 3.94 (m,

8H), 1.72 – 1.57 (m, 8H), 1.52 – 1.44

(m, 5H), 1.31 – 1.16 (m, 38H). ^{13}C NMR

(126 MHz, CDCl_3) δ : 159.46, 150.04,

144.96, 143.32, 139.85, 133.59, 130.64,

129.72, 128.91, 127.80, 61.28 (d, $J = 6$ Hz), 42.64, 42.50, 30.50 (d, $J = 16$ Hz), 29.35,

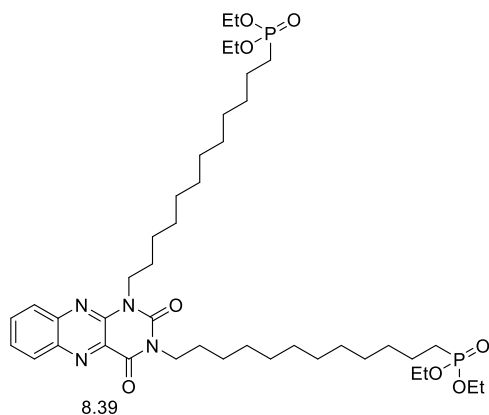
29.32, 29.22, 29.20, 29.13, 29.11, 28.98, 28.97, 27.66, 27.38, 26.80, 26.71, 25.57 (d, $J =$

139 Hz), 22.32, 22.28, 16.40 (d, $J = 6$ Hz). ^{31}P NMR (122 MHz, CDCl_3) δ : 33.32, 33.29.

HRMS (ESI) m/z $[\text{M}+\text{Na}]^+$ calculated for $\text{C}_{38}\text{H}_{64}\text{N}_4\text{O}_8\text{P}_2$ 789.4092, found 789.4120.

Tetraethyl ((2,4-dioxobenzo[g]pteridine-1,3(2H,4H)-diyl)bis(dodecane-12,1-diyl))bis (phosphonate) **8.39**

Greenish yellow liquid (1.6 g, 85%), IR (cm⁻¹): 2924, 2853, 1722, 1560, 1054, 956. ¹H



NMR (500 MHz, CDCl₃) δ: 8.26 (d, *J* = 8.4

Hz, 1H), 7.96 (d, *J* = 8.4 Hz, 1H), 7.83

(ddd, *J* = 8.3, 6.9, 1.1 Hz, 1H), 7.69 (ddd,

J = 8.1, 6.8, 1.0 Hz, 1H), 4.41 – 4.35 (m,

2H), 4.14 – 4.09 (m, 2H), 4.08 – 3.98 (m,

8H), 1.80 – 1.61 (m, 8H), 1.58 – 1.47 (m,

4H), 1.35 – 1.17 (m, 44H). ¹³C NMR (126

MHz, CDCl₃) δ: 159.61, 150.18, 145.09,

143.47, 139.98, 133.70, 130.78, 129.83, 129.03, 127.92, 61.42 (d, *J* = 6 Hz), 42.79,

42.66, 30.64 (d, *J* = 18 Hz) 29.58, 29.56, 29.52, 29.40, 29.31, 29.29, 29.12, 27.80, 27.51,

26.94, 26.85, 25.67 (d, *J* = 139 Hz), 22.44, 22.39, 16.52 (d, *J* = 6 Hz). ³¹P NMR (122

MHz, CDCl₃) δ: 33.36, 33.32. HRMS (ESI) *m/z* [M+H]⁺ calculated for C₄₂H₇₂N₄O₈P₂

823.4898, found 823.4922.

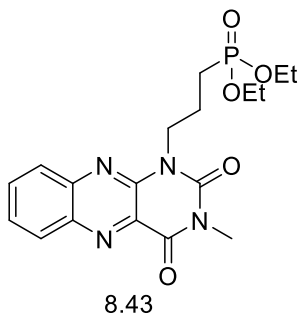
General synthesis of 8.43-8.47

3-methyl alloxazine **8.41** (300 mg, 1.3 mmol) was heated with K₂CO₃ (363 mg, 2mmol) at 80 °C for overnight to form the salt of the **8.41**. After filtration the solid was stirred with 2 equivalent of the bromophosphonates for 6-8 hours at room temperature. The reaction mixture was filtered and the filtrate was dried by blowing air. The resultant solid was dissolved in DCM-water (1:1, 30 mL) and the product was extracted with DCM (3×50 mL). The organic layer was dried over MgSO₄. The compounds were separated as light yellow solid using flash chromatography with 1-2% MeOH in DCM.

Diethyl (3-(3-methyl-2,4-dioxo-3,4-dihydrobenzo[g]pteridin-1(2H)-yl)propyl)phosphonate

8.43

Light yellow solid (370 mg , 70%), mp.140-142 °C. IR (cm⁻¹): 1722, 1668, 1557, 1026. ¹H



NMR (301 MHz, CDCl₃) δ: 8.35 (d, *J* = 8.4 Hz, 1H), 8.03

(d, *J* = 8.4 Hz, 1H), 7.91 (t, *J* = 7.6 Hz, 1H), 7.77 (t, *J* = 7.6

Hz, 1H), 4.54 (t, *J* = 7.2 Hz, 2H), 4.21 – 3.98 (m, 4H), 3.60

(s, 3H), 2.26 – 2.06 (m, 2H), 1.99 – 1.81 (m, 2H), 1.31 (t, *J*

= 7.1 Hz, 5H). ¹³C NMR (126 MHz, CDCl₃) δ: 159.85,

150.51, 144.88, 143.38, 140.20, 134.03, 130.90, 129.66,

129.38, 127.98, 61.79 (d, *J* = 6 Hz), 43.06 (d, *J* = 21 Hz),

29.29, 23.47 (d, *J* = 144 Hz), 21.07 (d, *J* = 4 Hz), 16.57 (d, *J* = 6 Hz). ³¹P NMR (122 MHz,

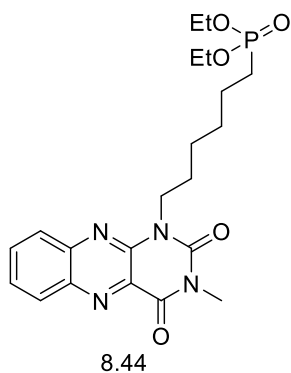
CDCl₃) δ: 31.51. HRMS (ESI) *m/z* [M+H]⁺ calculated for C₁₈H₂₃N₄O₅P 407.1479, found

407.1477.

Diethyl (6-(3-methyl-2,4-dioxo-3,4-dihydrobenzo[g]pteridin-1(2H)-yl)hexyl) phosphonate

8.44

Light yellow solid (397 mg , 68%), mp. 82 °C IR (cm⁻¹):2927, 1722, 1670, 1559, 1081,



951. ¹H NMR (500 MHz, CDCl₃) δ: 8.34 (d, *J* = 8.4 Hz, 1H),

8.02 (d, *J* = 8.4 Hz, 1H), 7.89 (t, *J* = 7.3 Hz, 1H), 7.75 (t, *J*

= 7.6 Hz, 1H), 4.48 – 4.36 (m, 2H), 4.16 – 3.96 (m, 4H),

3.59 (s, 3H), 1.83 – 1.59 (m, 8H), 1.52 – 1.45 (m, 4H), 1.30

(t, *J* = 7.1 Hz, 6H). ¹³C NMR (126 MHz, CDCl₃) δ: 159.97,

150.47, 145.04, 143.51, 140.12, 133.90, 130.90, 129.72,

129.23, 128.03, 61.51,(d, *J* = 6 Hz) 42.77, 30.34 (d, *J* = 18

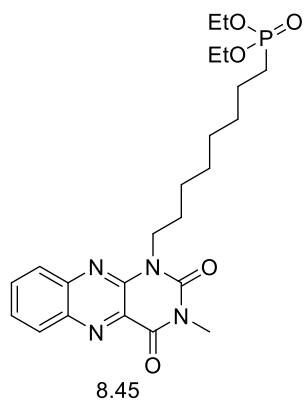
Hz), 29.25, 27.41, 26.44, 25.75 (d, $J = 141$ Hz), 22.46 (d, $J = 5$ Hz), 16.58 (d, $J = 6$ Hz).

^{31}P NMR (122 MHz, CDCl_3) δ : 32.96. HRMS (ESI) m/z $[\text{M}+\text{H}]^+$ calculated for $\text{C}_{21}\text{H}_{29}\text{N}_4\text{O}_5\text{P}$ 449.1948, found 449.1947.

Diethyl (8-(3-methyl-2,4-dioxo-3,4-dihydrobenzo[*g*]pteridin-1(2H)-yl)octyl) phosphonate

8.45

Light yellow solid (403 mg, 65%), mp. 84 °C IR (cm^{-1}): 2908, 1722, 1670, 1557, 1014,



955. ^1H NMR (500 MHz, CDCl_3) δ : 8.34 (d, $J = 8.5$ Hz,

1H), 8.02 (d, $J = 7.8$ Hz, 1H), 7.89 (ddd, $J = 8.4, 6.9, 1.3$

Hz, 1H), 7.75 (ddd, $J = 8.3, 6.9, 1.2$ Hz, 1H), 4.49 – 4.39

(m, 2H), 4.17 – 3.99 (m, $J = 8.4, 7.8$ Hz, 4H), 3.60 (s,

3H), 1.85 – 1.67 (m, 5H), 1.60 (s, 2H), 1.48 – 1.31 (m,

12H), 1.31 (t, $J = 7.0$ Hz, 8H). ^{13}C NMR (126 MHz,

CDCl_3) δ : 160.00, 150.47, 145.07, 143.54, 140.10,

133.88, 130.89, 129.72, 129.20, 128.03, 61.55, 42.89,

30.72, 30.59, 29.24, 29.10, 29.08, 27.57, 26.83, 22.50, 16.59 (d, $J = 3$ Hz). ^{31}P NMR (122

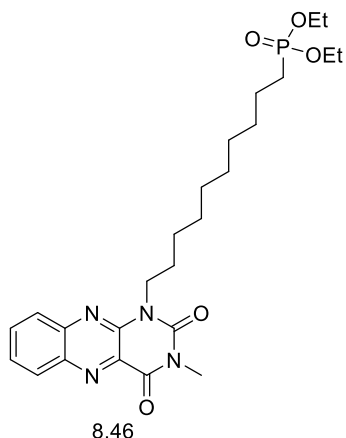
MHz, CDCl_3) δ : 33.20. HRMS (ESI) m/z $[\text{M}+\text{H}]^+$ calculated for $\text{C}_{23}\text{H}_{33}\text{N}_4\text{O}_5\text{P}$ 477.2261,

found 477.2261.

Diethyl (10-(3-methyl-2,4-dioxo-3,4-dihydrobenzo[g]pteridin-1(2H)-yl)decyl) phosphonate

8.46

Light yellow solid (460 mg, 70%), mp. 84 °C IR (cm⁻¹): 2912, 2850, 1722, 1671, 1557,



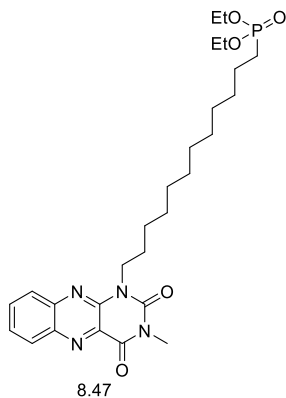
1014, 959. ¹H NMR (500 MHz, CDCl₃) δ: 8.32 (d, *J* = 8.4 Hz, 1H), 8.01 (d, *J* = 8.4 Hz, 1H), 7.89 (t, *J* = 7.2 Hz, 1H), 7.74 (t, *J* = 7.3 Hz, 1H), 4.48 – 4.37 (m, 2H), 4.16 – 3.97 (m, *J* = 8.9, 7.5 Hz, 4H), 3.59 (s, 3H), 1.78 (p, *J* = 7.5 Hz, 3H), 1.77 – 1.63 (m, 2H), 1.63 – 1.50 (m, 2H), 1.49 – 1.25 (m, 18H). ¹³C NMR (126 MHz, CDCl₃) δ: 160.02, 150.49, 145.10, 143.56, 140.10, 133.88, 130.89, 129.74, 129.21, 128.04,

61.54 (d, *J* = 5 Hz), 42.95, 30.72 (d, *J* = 18 Hz), 29.54, 29.44, 29.33, 29.25, 29.19, 27.60, 26.90, 22.50 (d, *J* = 5 Hz), 16.60 (d, *J* = 5 Hz). ³¹P NMR (122 MHz, CDCl₃) δ: 33.28.

HRMS (ESI) *m/z* [M+H]⁺ calculated for C₂₅H₃₇N₄O₅P 505.2574, found 505.2571.

Diethyl (12-(3-methyl-2,4-dioxo-3,4-dihydrobenzo[g]pteridin-1(2H)-yl)dodecyl) phosphonate **8.47**

Light yellow solid (499 mg, 72%), mp. 89 °C, IR (cm⁻¹): 2915, 2850, 1722, 1671, 1557,



1048, 957. ¹H NMR (500 MHz, CDCl₃) δ: 8.34 (d, *J* = 8.4 Hz, 1H), 8.02 (d, *J* = 8.4 Hz, 1H), 7.89 (t, *J* = 7.6 Hz, 1H), 7.75 (t, *J* = 7.6 Hz, 1H), 4.53 – 4.35 (m, 2H), 4.09 (s, 4H), 3.60 (s, 3H), 2.00 – 1.52 (m, 6H), 1.49 – 1.21 (m, 20H). ¹³C NMR (126 MHz, CDCl₃) δ: 160.05, 150.51, 145.13, 143.59, 140.13, 133.88, 130.93, 129.77, 129.21, 128.06, 61.59, 42.99, 30.84, 29.69, 29.63, 29.51, 29.39, 29.28, 29.24, 27.63, 26.93, 22.56, 16.65. ³¹P NMR (122 MHz, CDCl₃) δ:

33.30. HRMS (ESI) m/z $[M+H]^+$ calculated for $C_{27}H_{41}N_4O_5P$ 533.2887, found 533.2883.

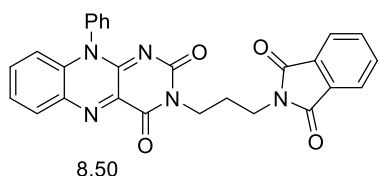
Synthesis of 3-(3-aminopropyl)-10-phenylbenzo[g]pteridine-2,4(3H,10H)-dione **8.51**

10-phenylbenzo[g]pteridine-2,4(3H,10H)-dione **8.48** (2.3 g, 8.0 mmol) was heated with K_2CO_3 (3 g, 22 mmol) was heated at 105 °C in DMF for 4 hours and the resultant solid was filtered and stirred with N-(3-bromopropyl) phthalimide (2.5 g, 9.3 mmol) in DMF (100 mL) at 70 °C for overnight. A solid started to form after 2 hours. After overnight, DMF was removed by rotary evaporator and the resultant solid was dissolve in DCM and washed with water. The organic part was dried over $MgSO_4$ and the product was purified using flash chromatography with 1-2% MeOH in DCM. The product formed as a bright yellow solid **8.50** (3.7 g, 97%)

3-(3-(1,3-dioxisoindolin-2-yl)propyl)-10-phenylbenzo[g]pteridine-2,4(3H,10H)-dione (1.0 g, 2.1 mmol) **8.50** was heated with 100 ml of conc. HCl at 90 °C for 12 hour and the reaction turned clear. The reaction was dried using rotary evaporator. The sticky solid was dissolve in minimal amount of acetone and a yellow solid started to form upon the addition of ethanol. The solid was filtered and washed with ether and dried under high vacuum. The product **8.51** was purified as a dark yellow solid (XXX mg, 95%).

3-(3-(1,3-dioxisoindolin-2-yl)propyl)-10-phenylbenzo[g]pteridine-2,4(3H,10H)-dione **8.50**

Light yellow solid (3.7g, 97%), mp. 324 °C. IR (cm^{-1}): 3053, 1704, 1650, 1545. 1H NMR



(500 MHz, $CDCl_3$) δ : 8.32 (d, J = 8.1 Hz, 1H), 7.83

(dd, J = 5.4, 3.1 Hz, 2H), 7.73 – 7.55 (m, 7H), 7.31

(d, J = 7.3 Hz, 2H), 6.90 (d, J = 8.5 Hz, 1H), 4.18 (t,

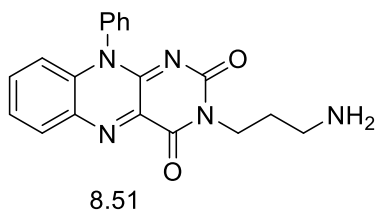
J = 7.2 Hz, 2H), 3.81 (t, J = 7.1 Hz, 2H), 2.13 (p, J =

7.1 Hz, 2H). ^{13}C NMR (126 MHz, $CDCl_3$) δ : 168.47, 159.43, 155.10, 150.16, 137.91,

135.78, 135.44, 135.14, 134.30, 133.98, 132.77, 132.29, 130.92, 130.56, 127.67, 126.66, 123.37, 117.18, 39.82, 36.04, 27.39. HRMS (ESI) m/z $[M+H]^+$ calculated for $C_{27}H_{19}N_5O_4$ 478.1510, found 478.1509.

3-(3-aminopropyl)-10-phenylbenzo[g]pteridine-2,4(3H,10H)-dione **8.51**

Light yellow solid (695 mg, 95%), mp. 280-282 °C (dec), IR (cm^{-1}): 3571, 3490, 1701,

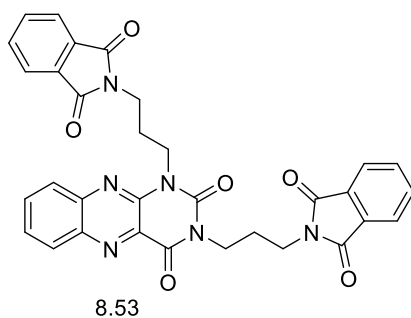


1656, 1587. 1H NMR (500 MHz, $DMSO-d_6$) δ : 8.22 (dd, $J = 8.1, 1.2$ Hz, 1H), 7.81 (s, 3H), 7.78 – 7.59 (m, 5H), 7.43 – 7.36 (m, 2H), 6.78 (d, $J = 8.5$ Hz, 1H), 3.91 (t, $J = 6.9$ Hz, 2H), 2.89 – 2.76 (m, 2H), 1.86 (p, $J = 7.2$ Hz, 2H). ^{13}C NMR (126 MHz, D_2O)

δ : 161.19, 156.85, 150.16, 136.85, 136.71, 136.05, 134.74, 134.30, 131.21, 131.09, 130.90, 128.09, 127.26, 118.12, 38.84, 37.08, 25.17. HRMS (ESI) m/z $[M+H]^+$ calculated for $C_{19}H_{17}N_5O_2$ 348.1455, found 348.1441.

Synthesis of 2,2'-((2,4-dioxobenzo[g]pteridine-1,3(2H,4H)-diyl)bis(propane-3,1-diyl))bis(isoindoline-1,3-dione) **8.53**

Benzo[g]pteridine-2,4(1H,3H)-dione **8.1** (500 mg, 2.34 mmol) was heated with K_2CO_3



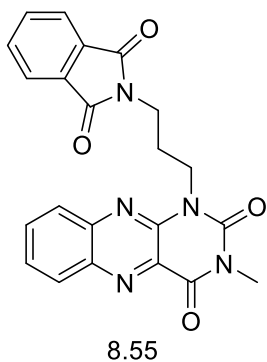
(1.3 g, 9.34 mmol) in DMF at 110 °C for 6 hours and the resultant potassium salt was filtered and stirred with N-(3-bromopropyl) phthalimide **8.52** (1.57 g, 5.88 mmol) in DMF at room temperature for 48 hours. The reaction turned cloudy and the reaction was filtered and the resultant solid was dissolved in DCM and washed with water. The

organic layer was dried over $MgSO_4$ and the product was purified using flash chromatography with 2% MeOH in DCM as a light yellow solid **8.53** (1.1 g, 80%). mp.

202- 204 °C. IR (cm⁻¹): 1703, 1681, 1667, 718. ¹H NMR (500 MHz, CDCl₃) δ: 8.26 (d, *J* = 8.2 Hz, 1H), 7.85 – 7.76 (m, 5H), 7.75 – 7.65 (m, 6H), 4.54 – 4.43 (m, 2H), 4.29 – 4.18 (m, 2H), 3.83 (dt, *J* = 19.2, 6.9 Hz, 4H), 2.27 (p, *J* = 6.9 Hz, 2H), 2.18 (p, *J* = 7.0 Hz, 2H). ¹³C NMR (126 MHz, CDCl₃) δ: 168.45, 168.43, 159.63, 150.21, 144.99, 143.31, 140.16, 134.12, 134.04, 133.90, 132.22, 132.15, 130.89, 129.85, 129.25, 127.90, 123.41, 123.38, 40.52, 40.43, 35.80, 27.15, 26.71. HRMS (ESI) *m/z* [M+H]⁺ calculated for C₃₂H₂₄N₆O₆ 589.1830, found 589.1827.

Synthesis of 1-(3-(1,3-dioxisoindolin-2-yl)propyl)-3-methylbenzo[g]pteridine-2,4(1H,3H)-dione **8.55**

10-phenylbenzo[g]pteridine-2,4(3H,10H)-dione **8.41** (300 mg, 1.31 mmol) was heated



with K₂CO₃ (363 mg, 2.6 mmol) in DMF at 85 °C for 6 hours.

The potassium salt of **8.41** will form which was filtered and stirred with N-(3-bromopropyl) phthalimide **8.52** (421 mg, 1.7 mmol) in DMF (20 mL) at room temperature for overnight.

The solvent was removed by rotary evaporator and the resultant solid was washed with DCM. The organic layer was concentrated and sonicated with addition of hexane to

precipitate out the product as a light yellow solid **8.55** (496 mg, 46%). mp. 220 °C IR (cm⁻¹): 1709, 1672, 1556, 721. ¹H NMR (500 MHz, CDCl₃) δ: 8.31 – 8.27 (m, 1H), 7.83 – 7.75 (m, 3H), 7.74 – 7.66 (m, 4H), 4.57 – 4.48 (m, 2H), 3.86 (t, *J* = 6.9 Hz, 2H), 2.27 (p, *J* = 7.0 Hz, 2H). ¹³C NMR (126 MHz, CDCl₃) δ: 168.45, 168.43, 159.63, 150.21, 144.99, 143.31, 140.16, 134.12, 134.04, 133.90, 132.22, 132.15, 130.89, 129.85, 129.25, 127.90, 123.41, 123.38, 40.52, 40.43, 35.80, 27.15, 26.71. HRMS (ESI) *m/z* [M+H]⁺ calculated for C₂₂H₁₇N₅O₄ 416.1353, found 416.1357.

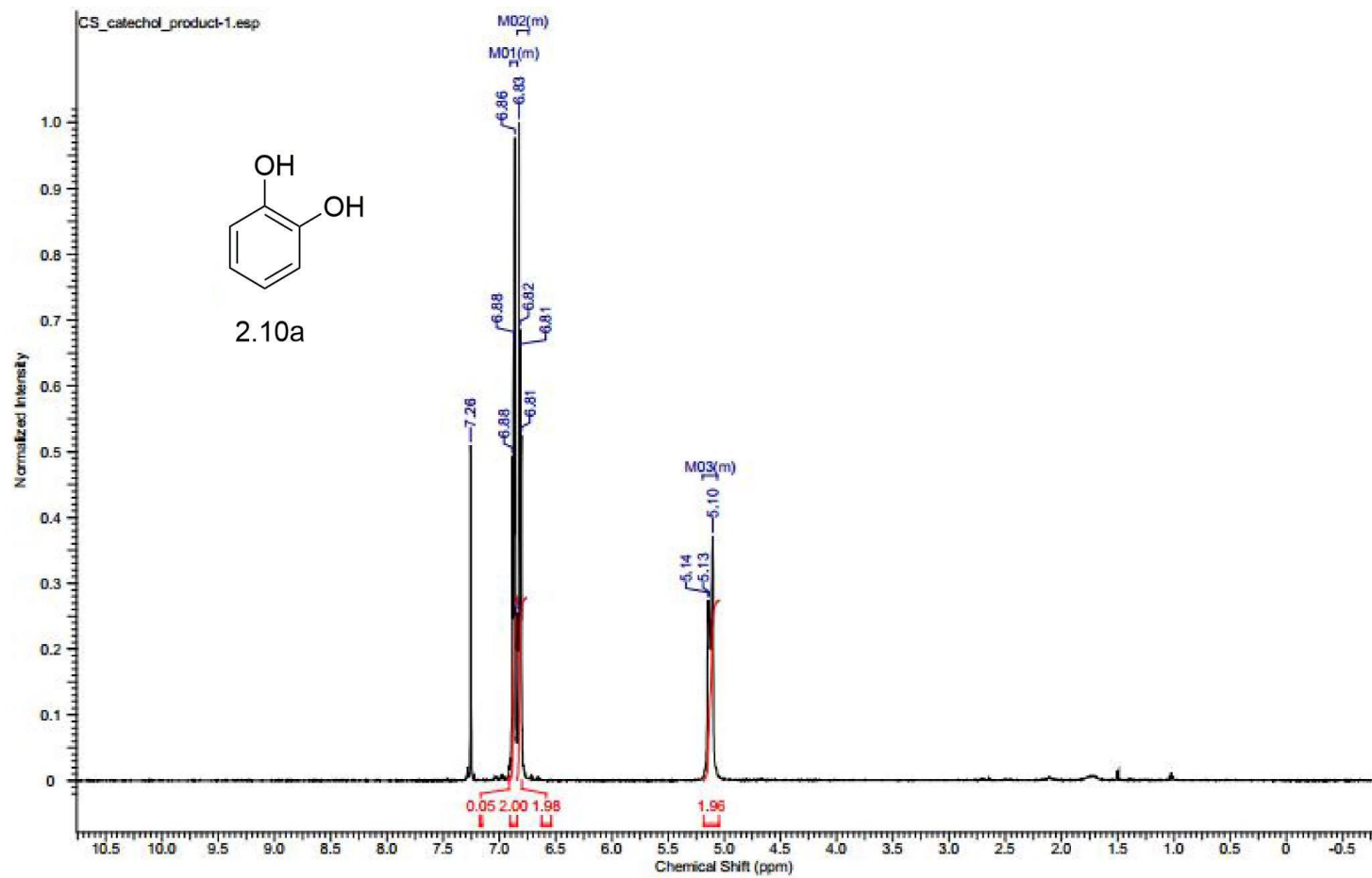
MTT Assay protocol

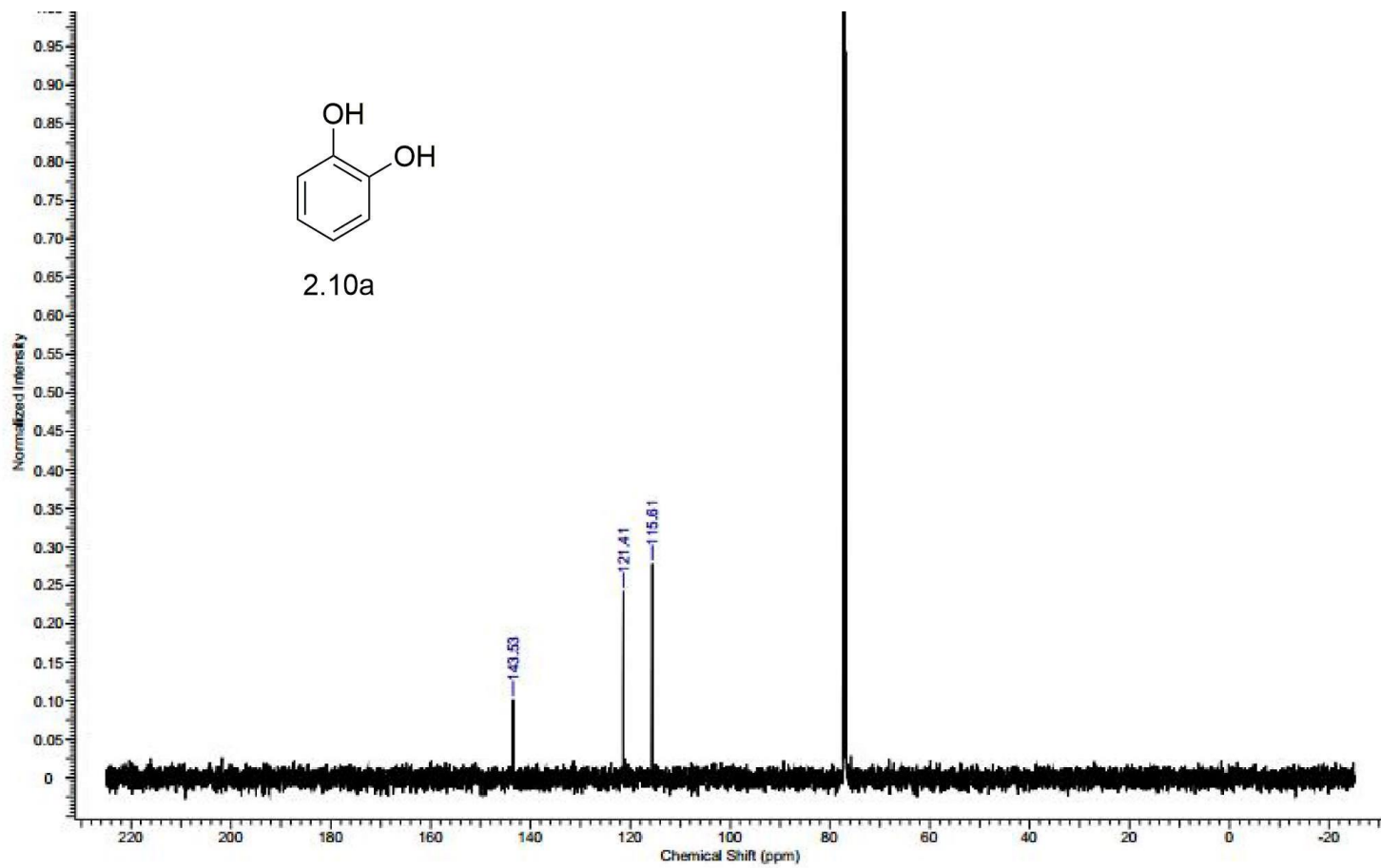
Procedure:

Human Breast Cancer Cells, MCF7 and normal human breast epithelial cells, MCF10 were obtained from ATCC (American Type Culture Collection) and grown in Dulbecco's modified Eagles media (DMEM) supplemented with 10% heat-inactivated Fetal Bovine Serum (FBS), 2 mM L-glutamine and Penicillin/Streptomycin (100 units and 0.1 mg/mL) in a humidified CO₂ incubator maintained at 5% CO₂. The cytotoxicity of all the compounds was determined by using an MTT (3-(4,5-dimethylthiazol-2-yl)-2,5-diphenyltetrazolium bromide) assay as previously described. In brief, ~10,000 MCF7 or MCF10 cells were seeded into each well of a 96-well micro-titer plate and incubated for 24 h in 180 µL of DMEM media with appropriate amounts of supplements. The cells were exposed to varying concentrations of each test compound (0.18 µM to 100 µM final concentrations with total volume in each well-being 200 µL), described in **Table 4.1 and 4.2**. Control wells were treated with equivalent amounts of DMSO (the solvent used for dissolving the stock solutions of test compounds). Cells were then incubated for 96 h inside the tissue culture incubator. At the end of 96 h incubation of the cells with the test compounds, 20 µL of MTT solution (5 mg/mL in PBS, (Phosphate buffer saline pH -7.4) was added to each well, followed by incubation for an additional 3-4 h. After the incubation ended, media was decanted off, 100 µL of DMSO was added into each well, followed by gentle shaking for 1 h at room temperature (in dark) to dissolve the precipitated formazan crystals. Cell viability was assayed by measuring the formazan absorption at 560 nm using a 96 well plate reader, Flowstar-Omega (BMG Labtech). The absorbance values at 560 nm values of drug treated MCF7 or MCF10 cells were normalized to the absorbance values of MCF7 or MCF10 cells that were treated with the solvent DMSO, respectively (with similar dilution pattern as described above). The percent cell

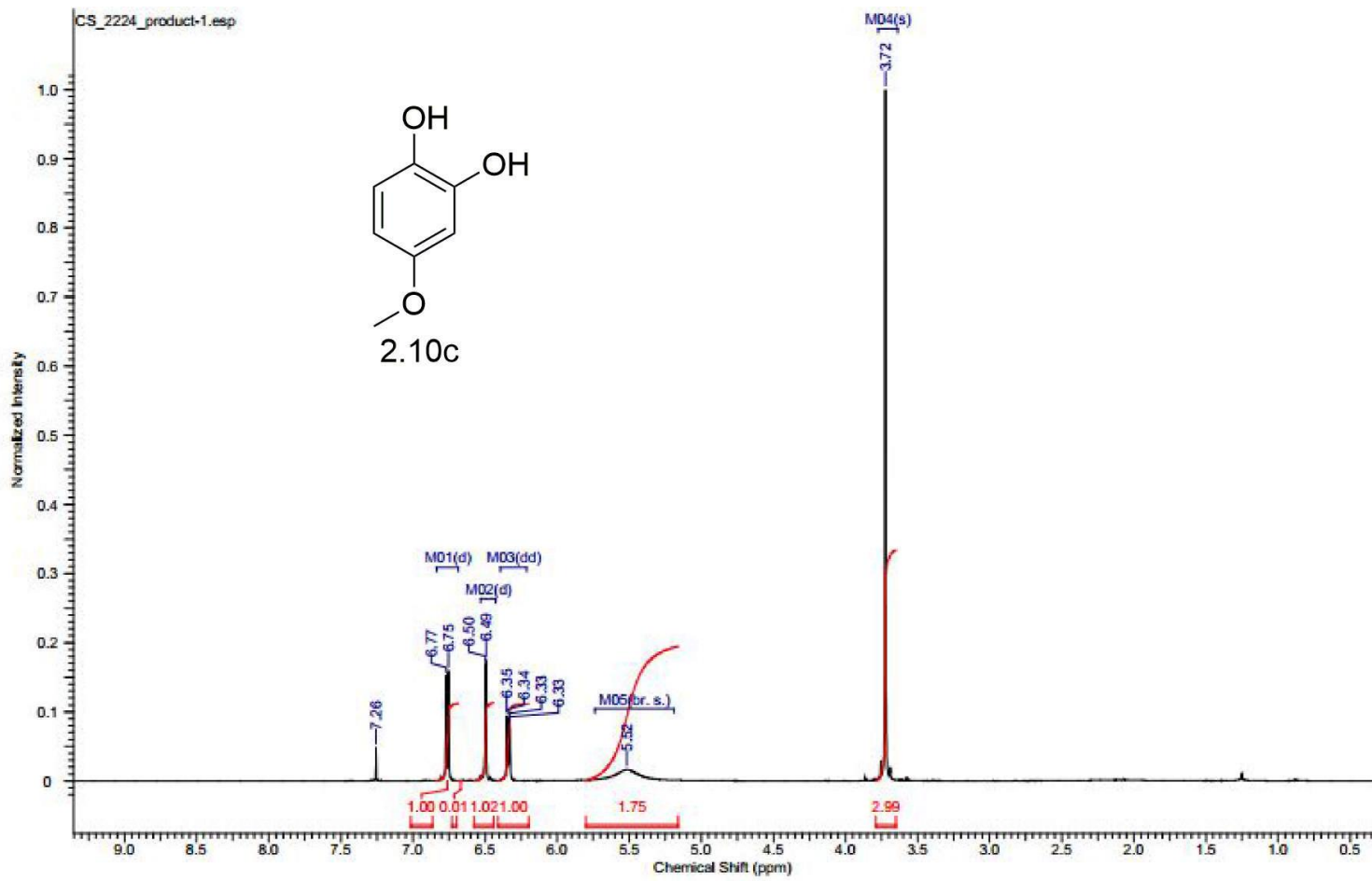
viability, as a function of test compound concentration was plotted and IC_{50} of the compounds were elucidated. The concentration of the compounds at which the conversion of MTT to formazan by viable cells is reduced to 50% in comparison to control cells is defined as the IC_{50} . Each experiment was performed in five parallel replicates and experiments were repeated at least three times.

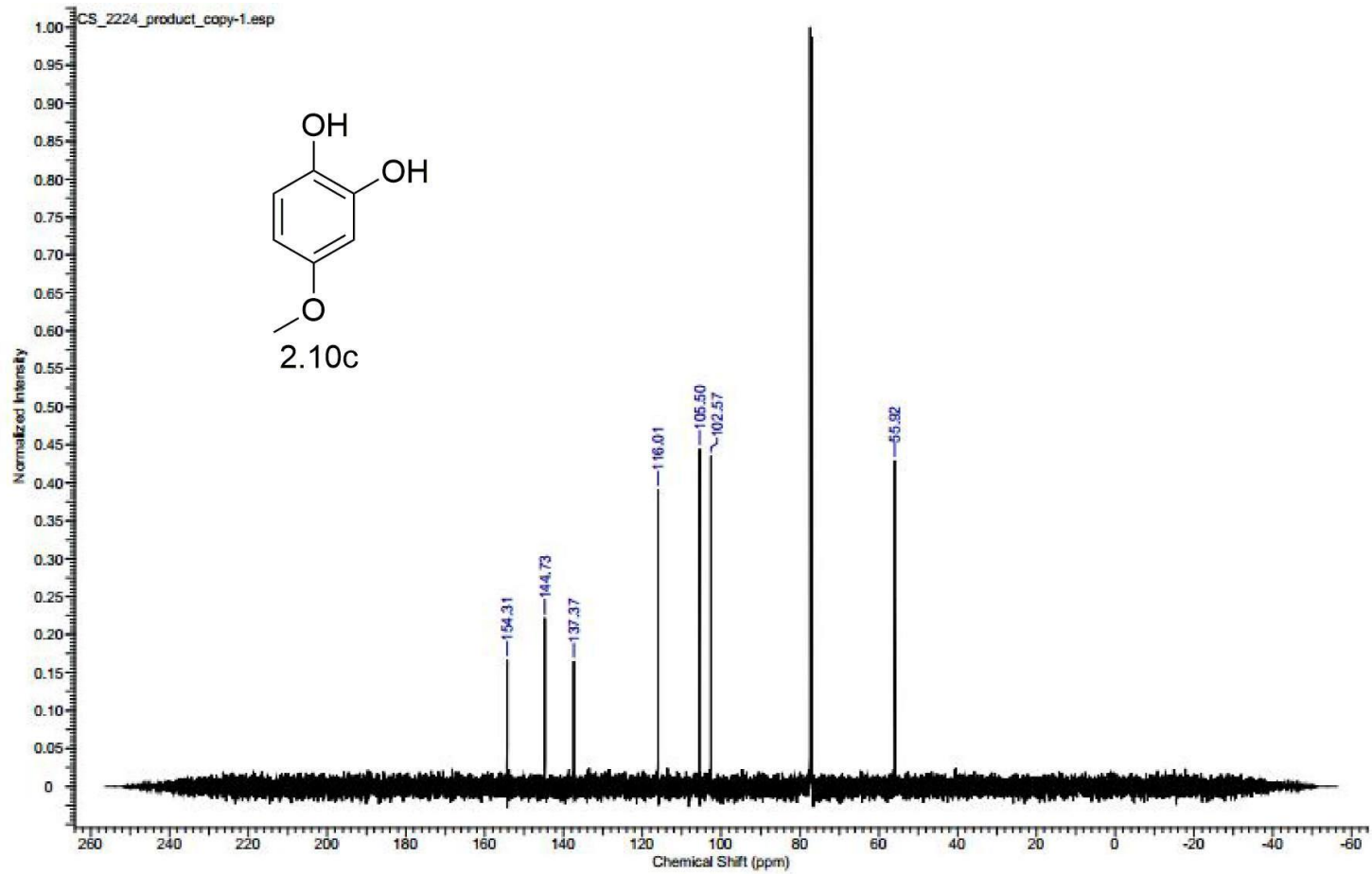
Appendix C
NMR spectra of compounds

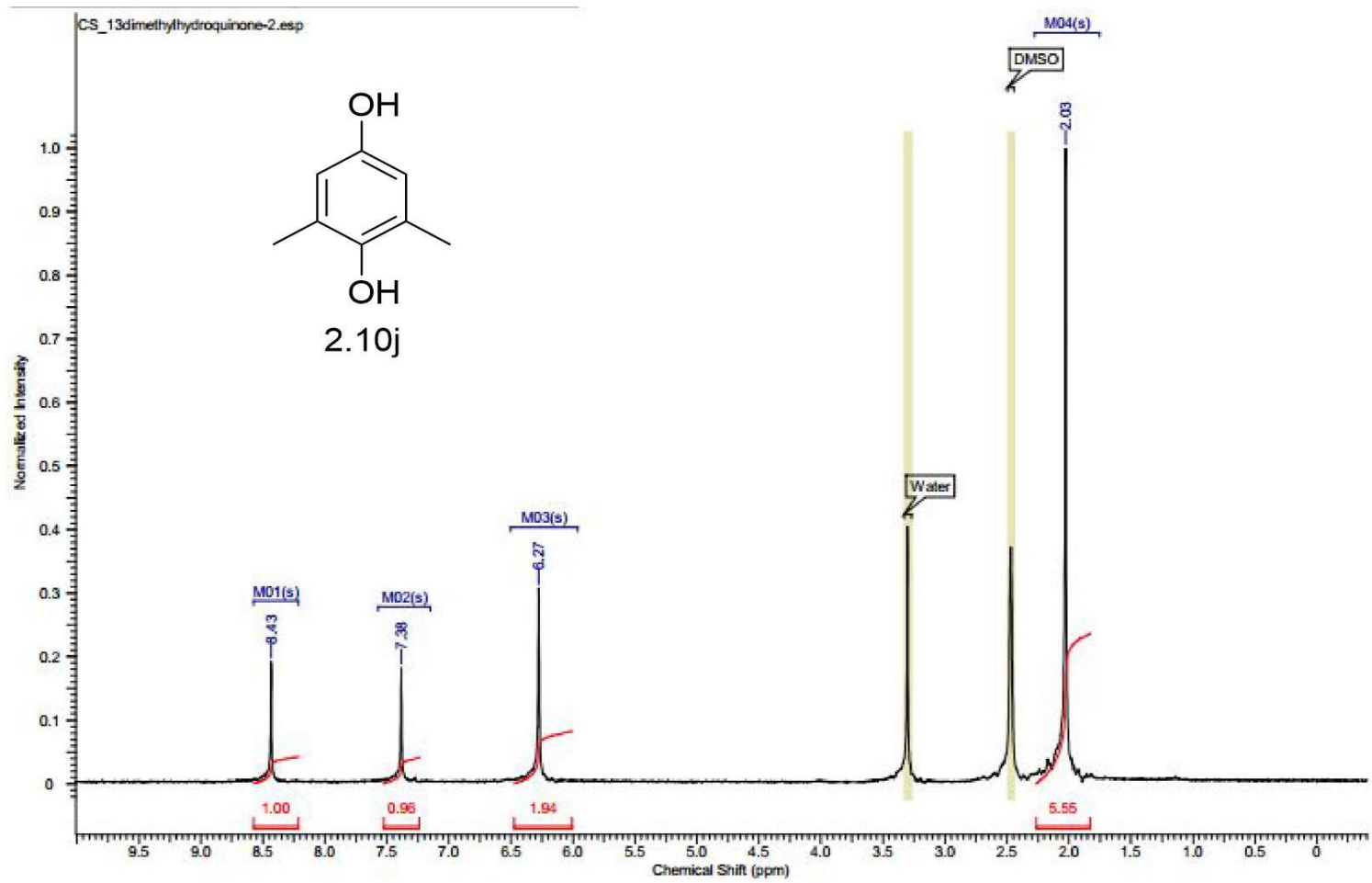


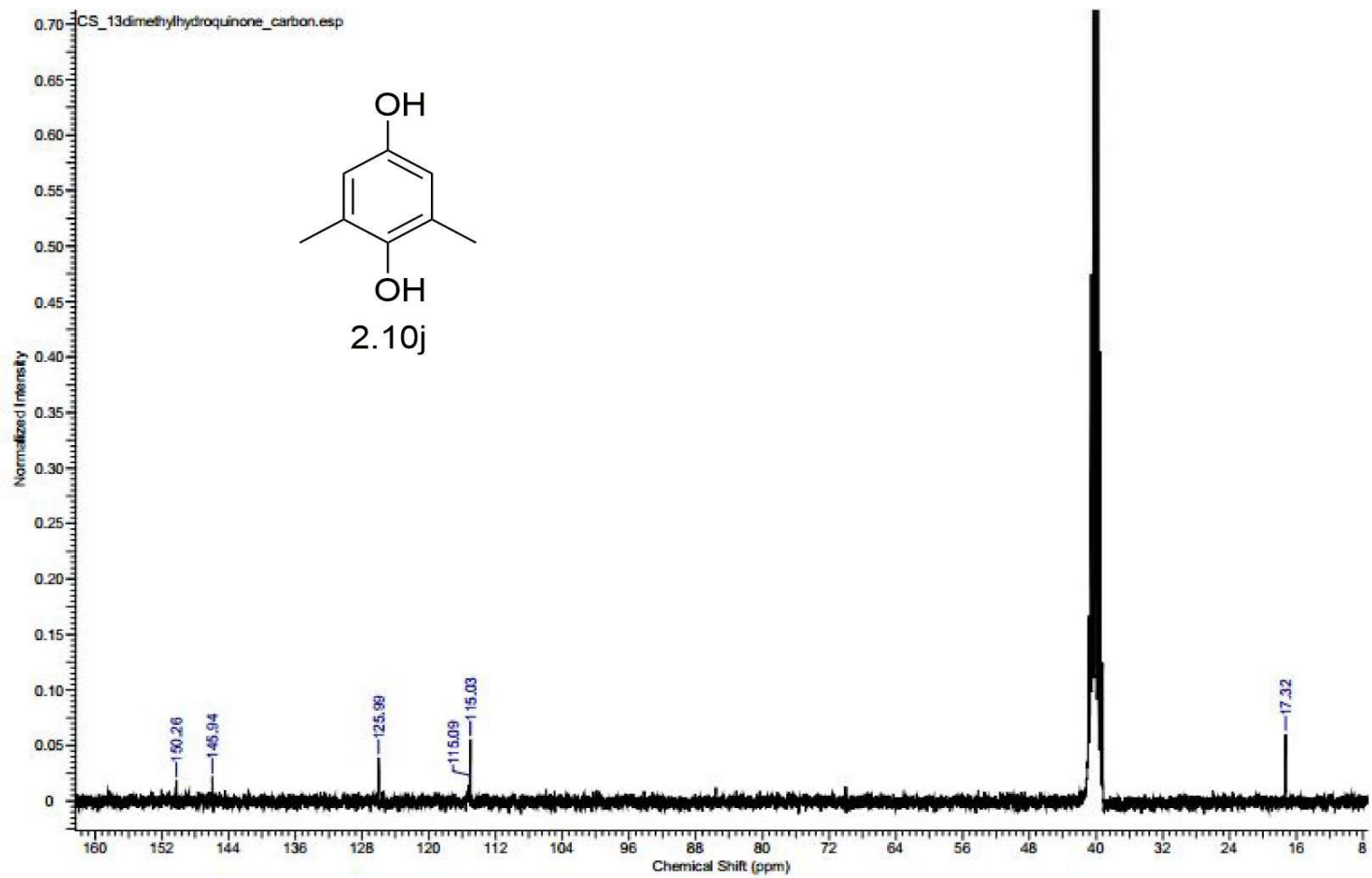


200

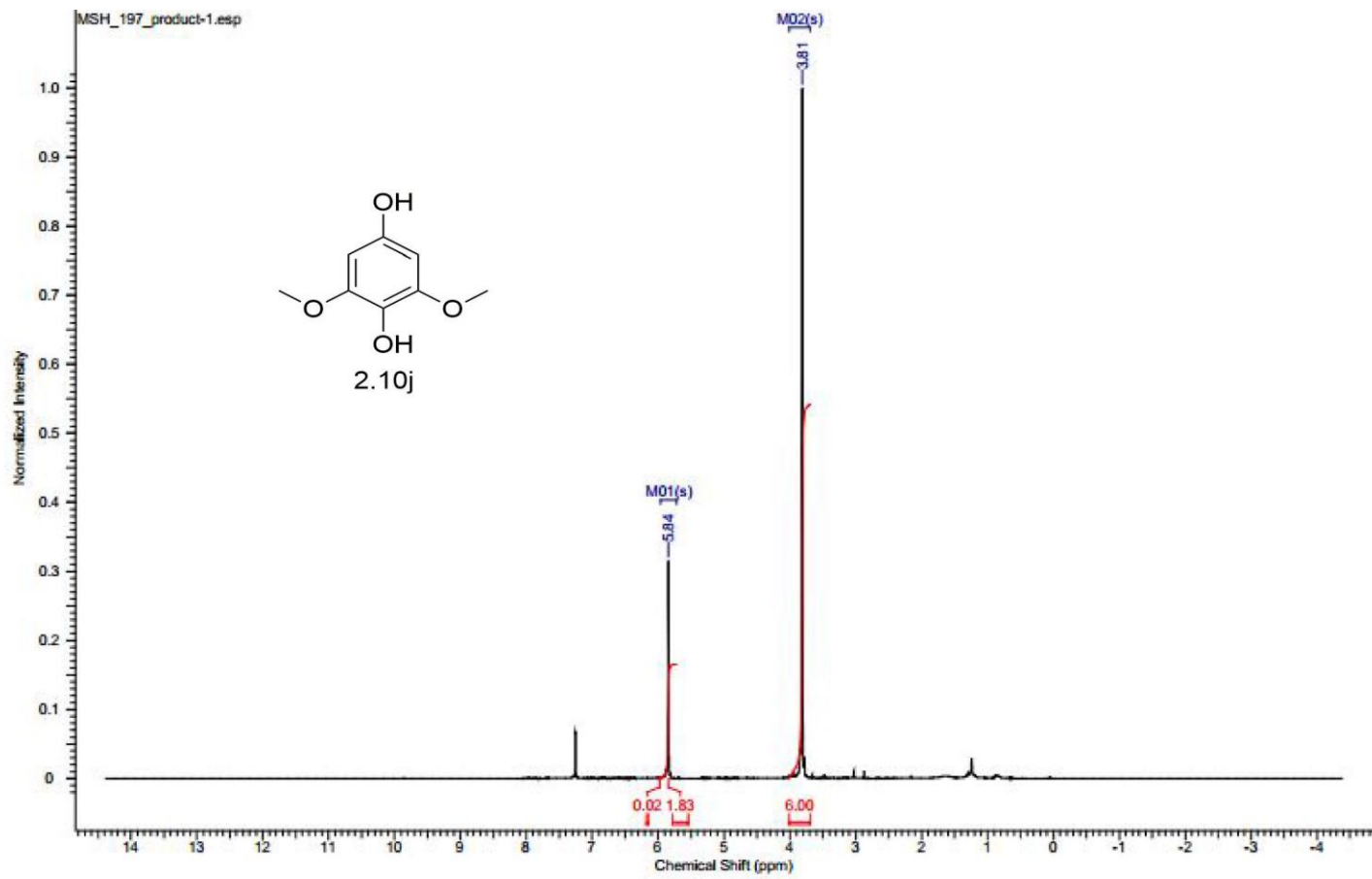


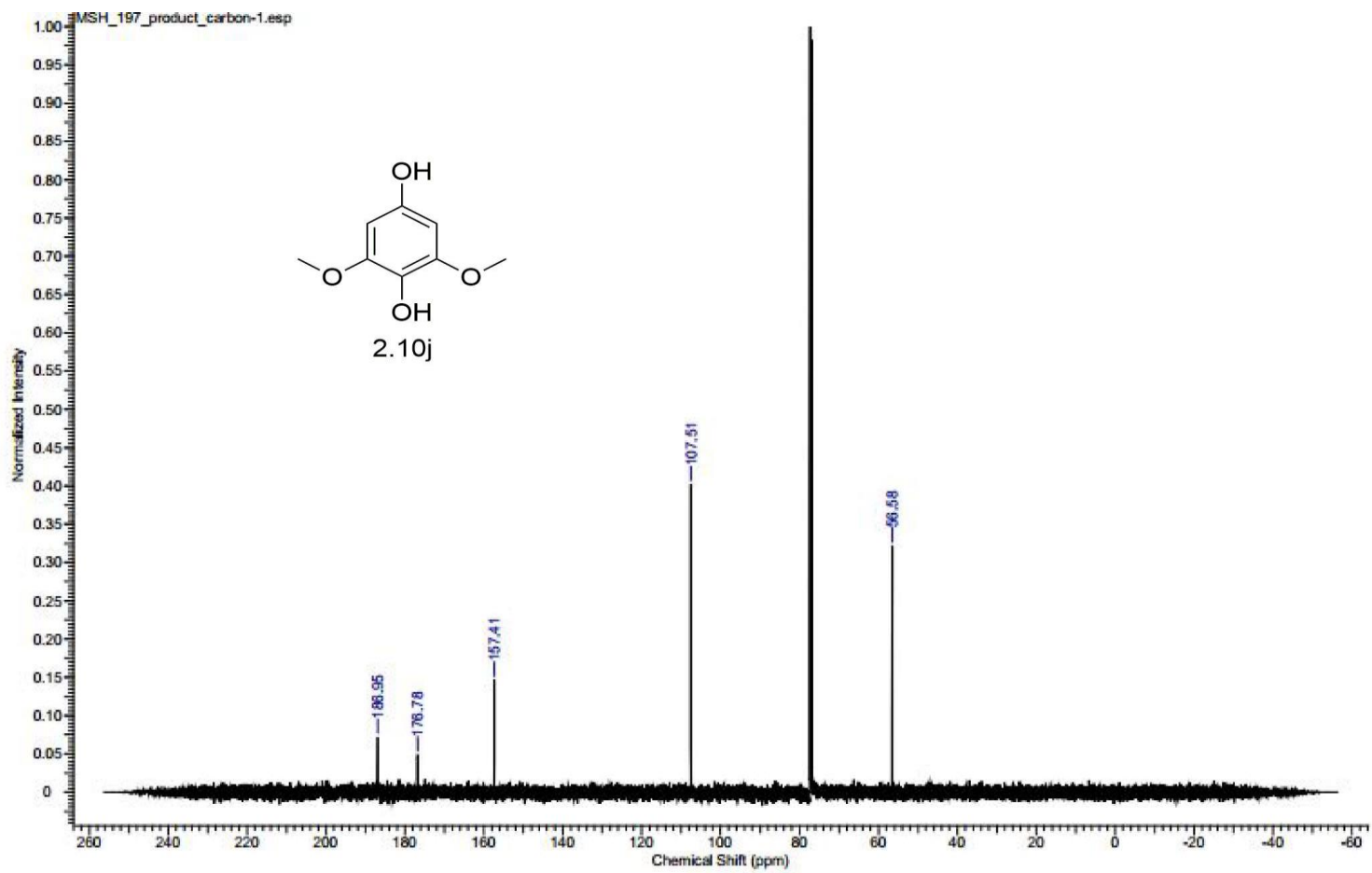




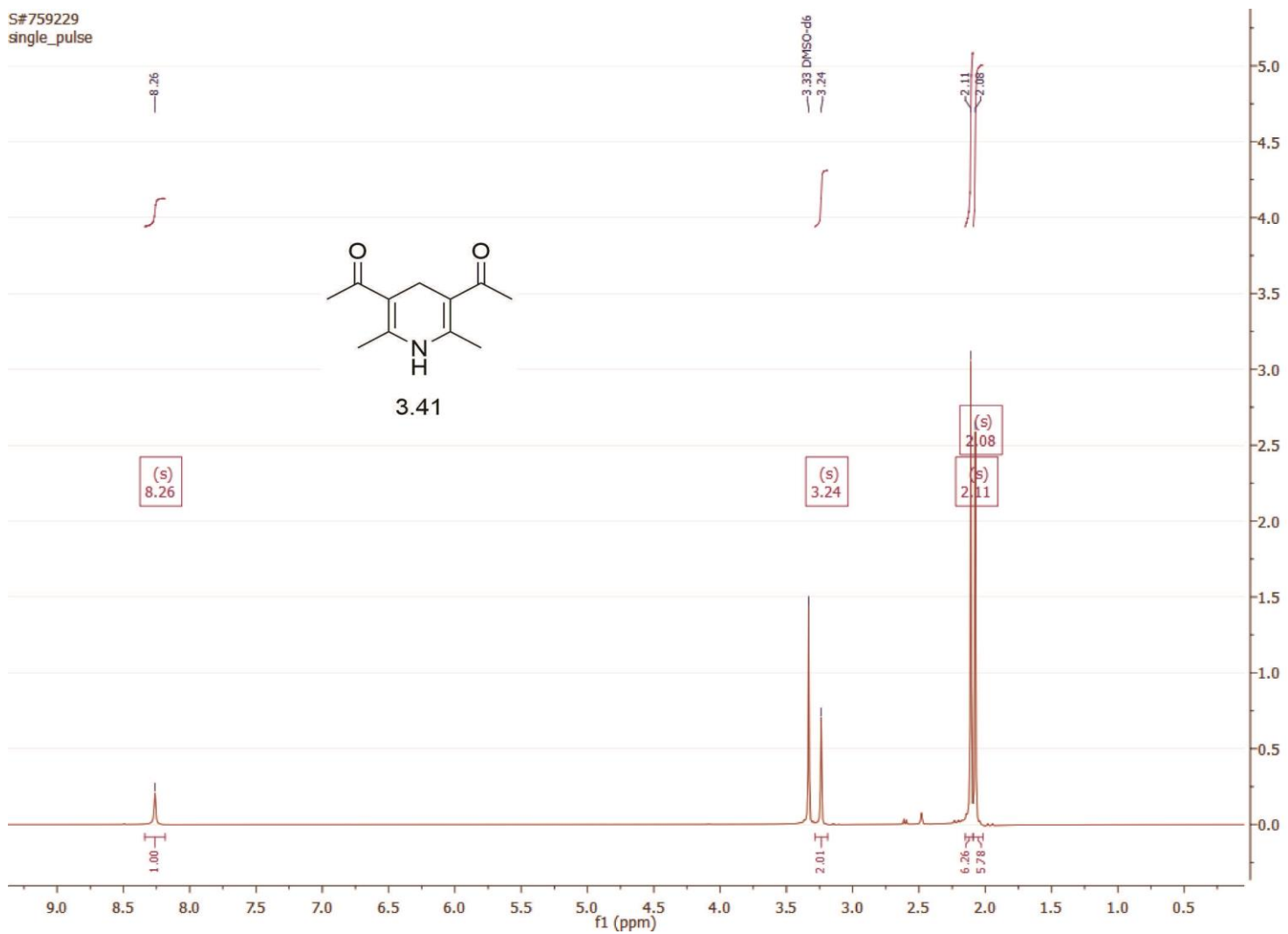


204



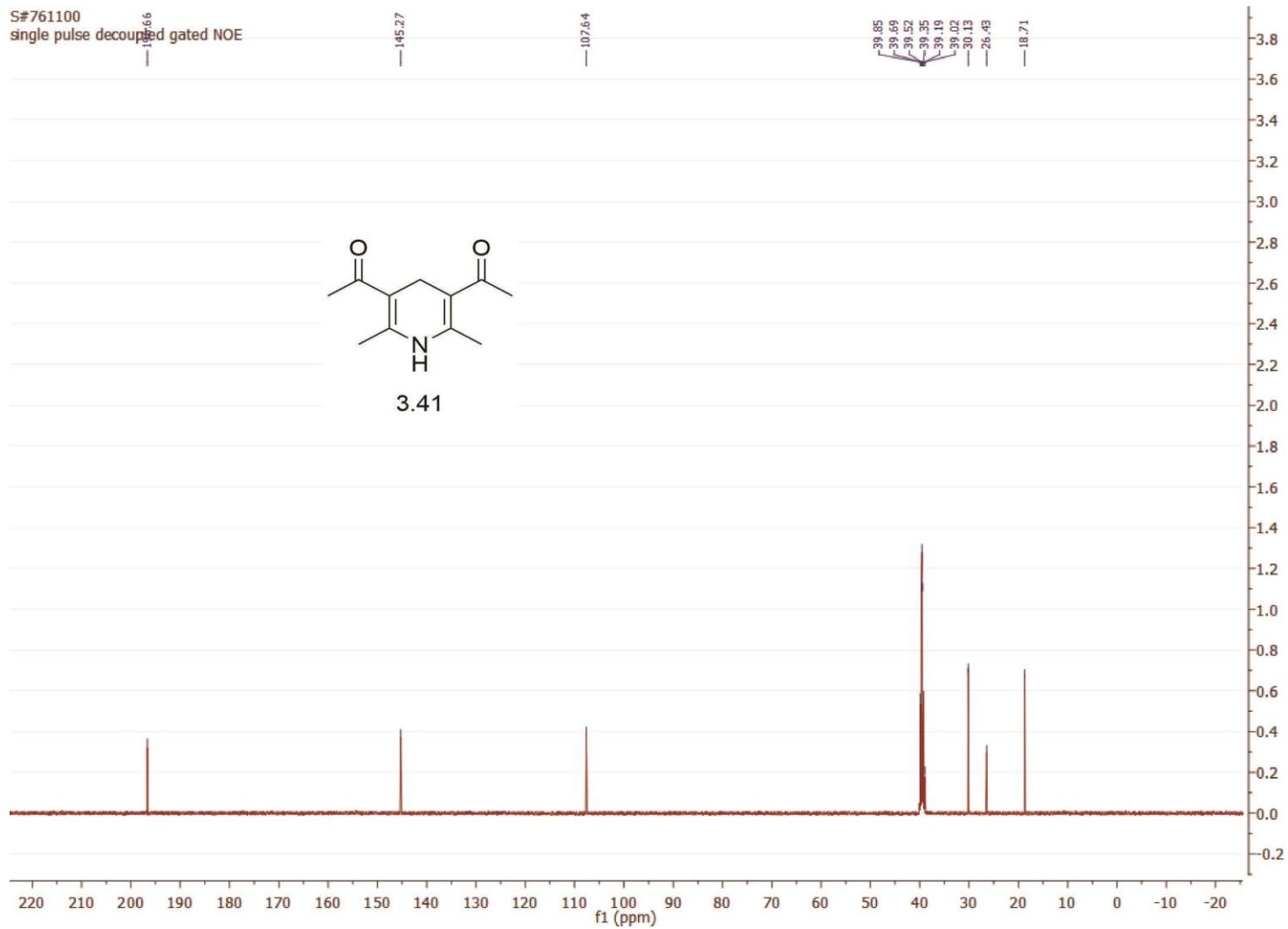


S#759229
single_pulse

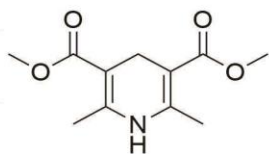


206

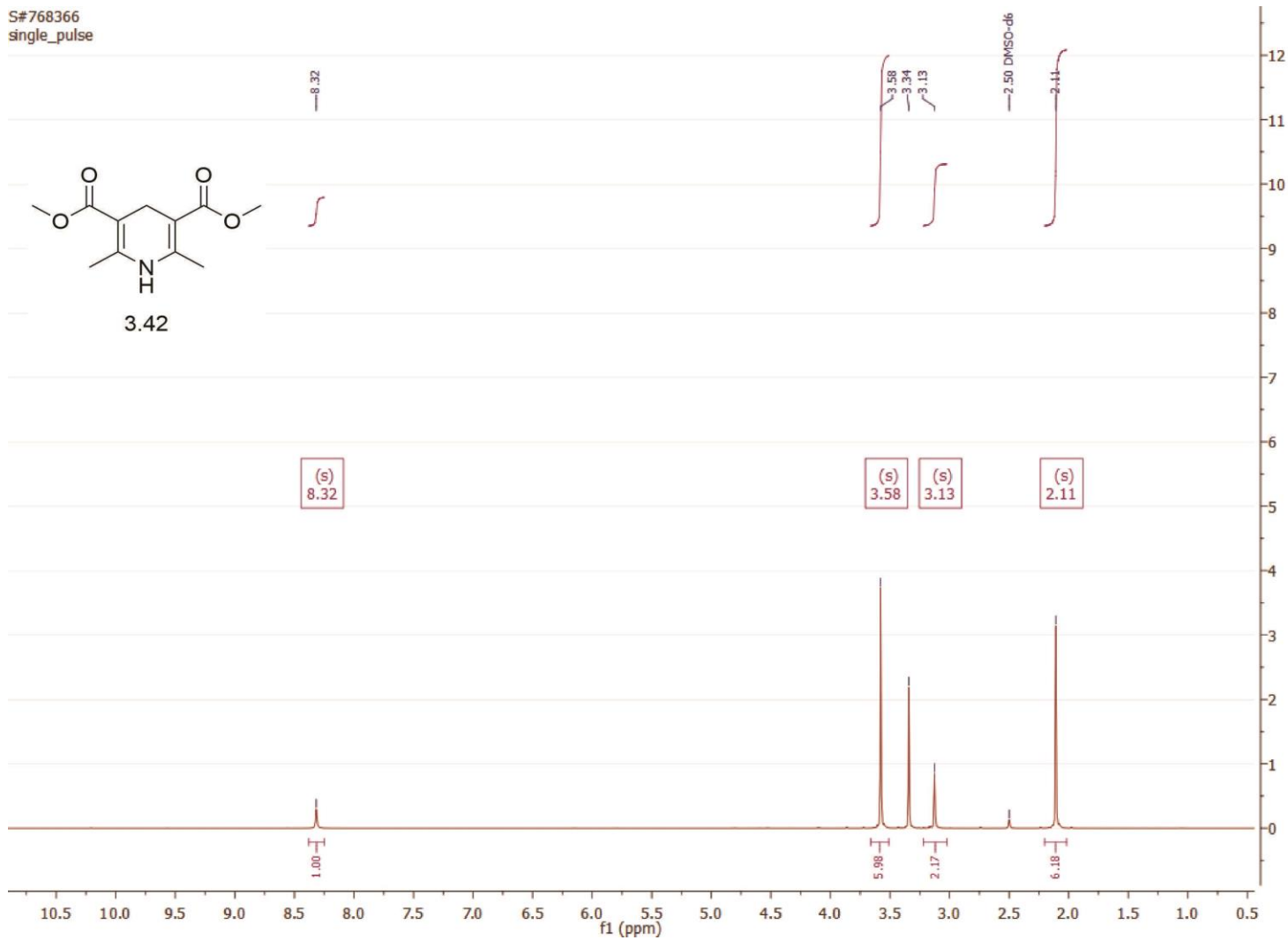
S#761100
single pulse decoupled gated NOE



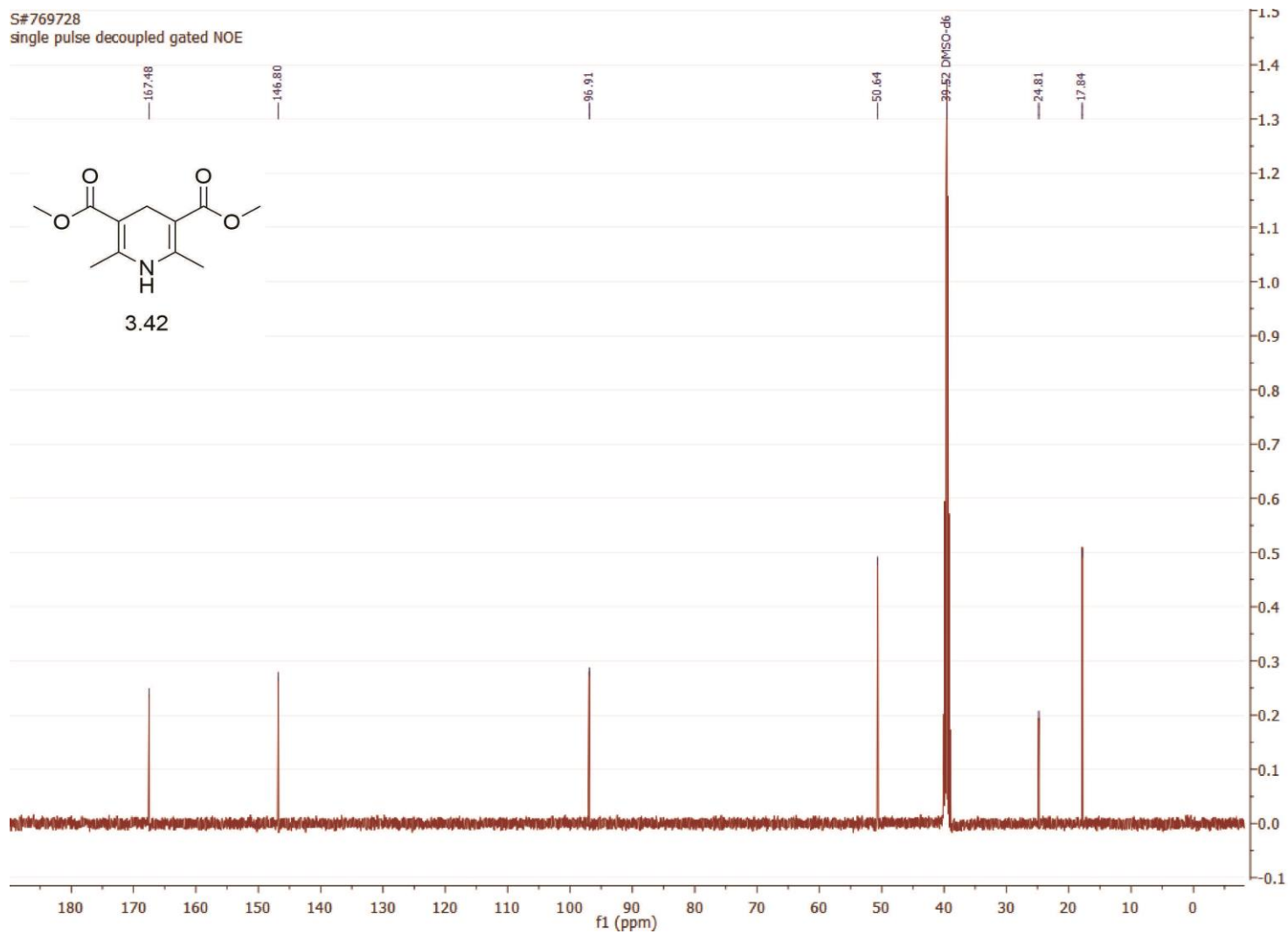
S#768366
single_pulse

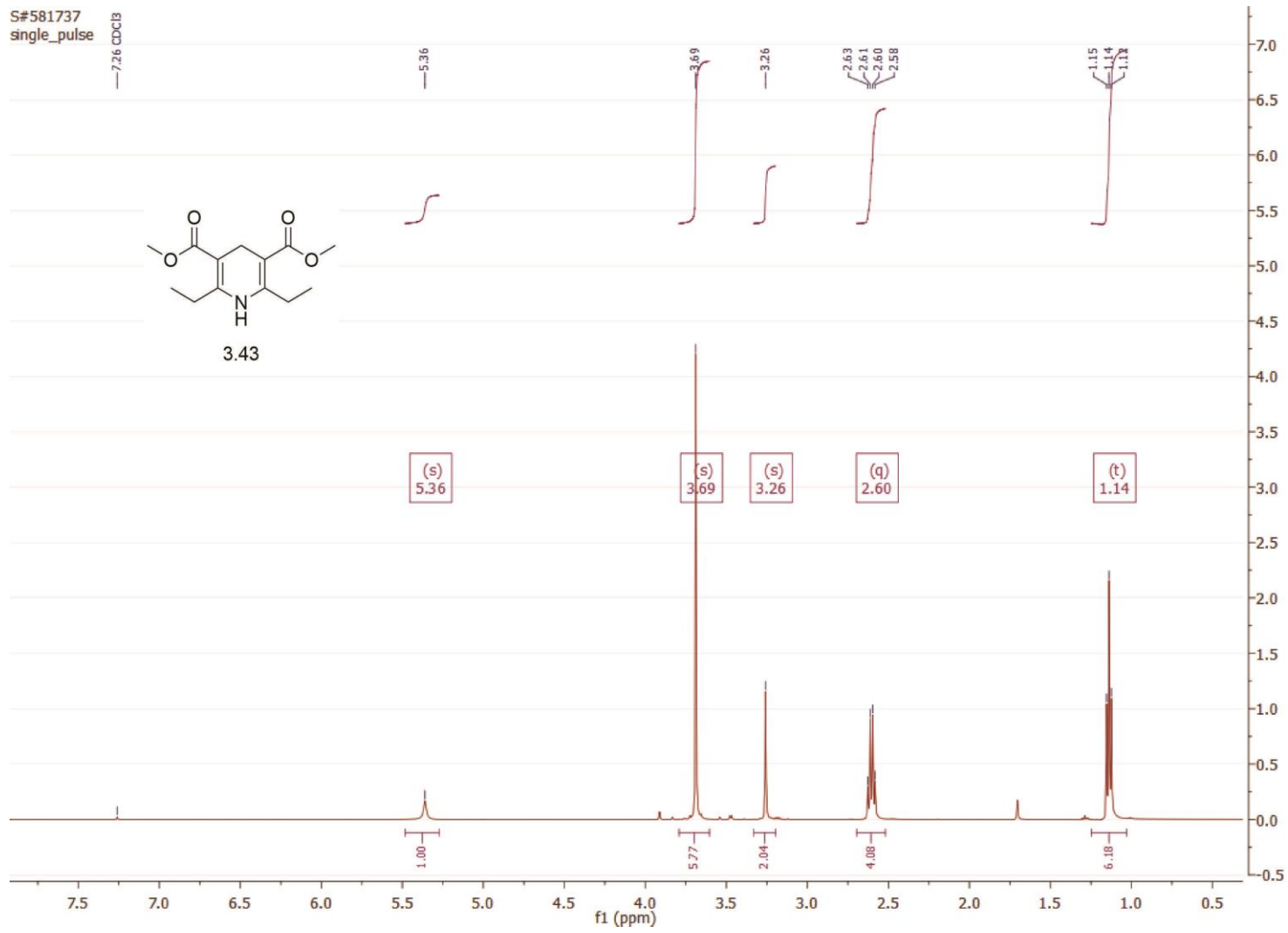


3.42

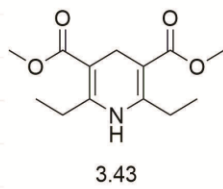
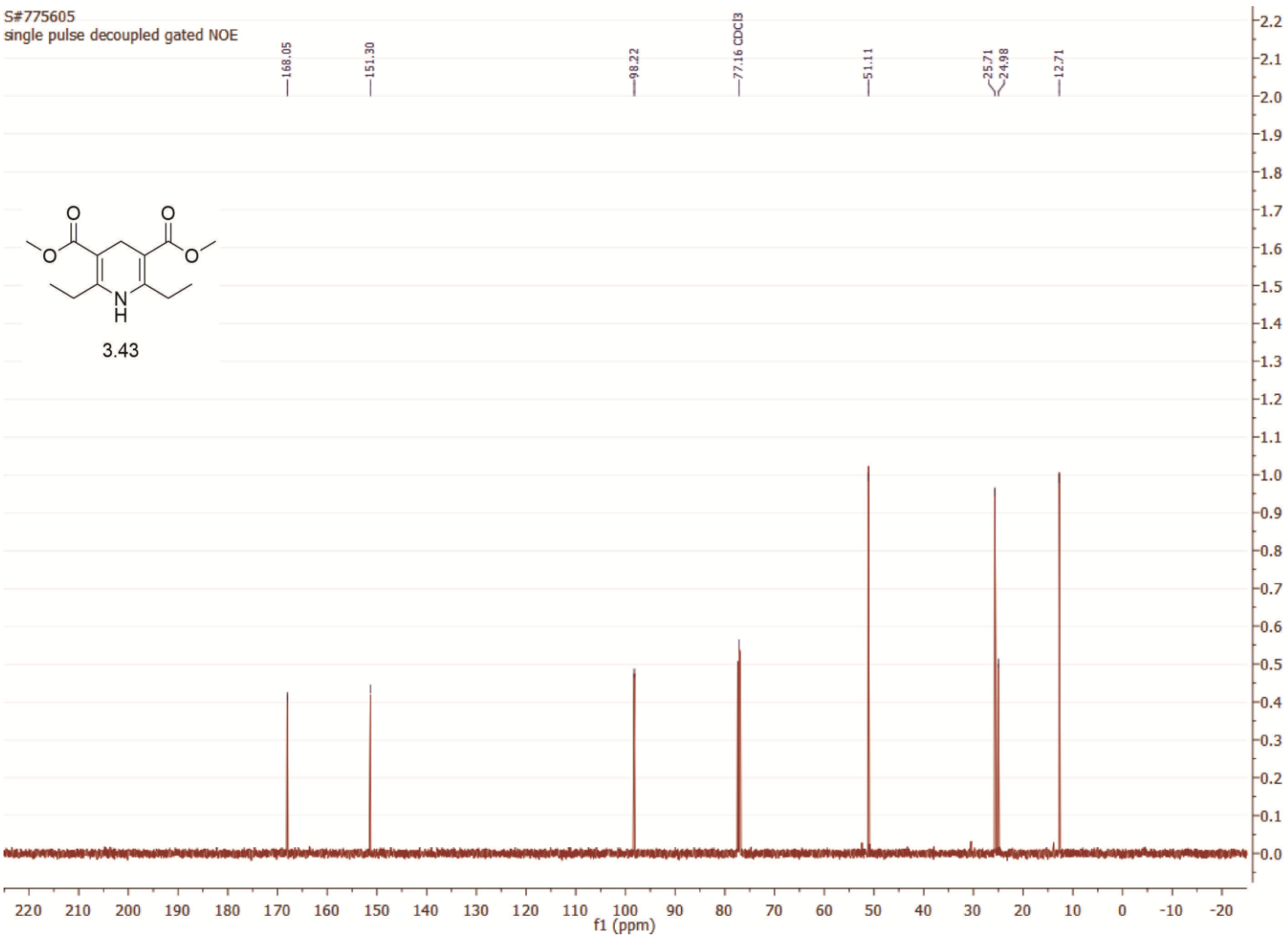


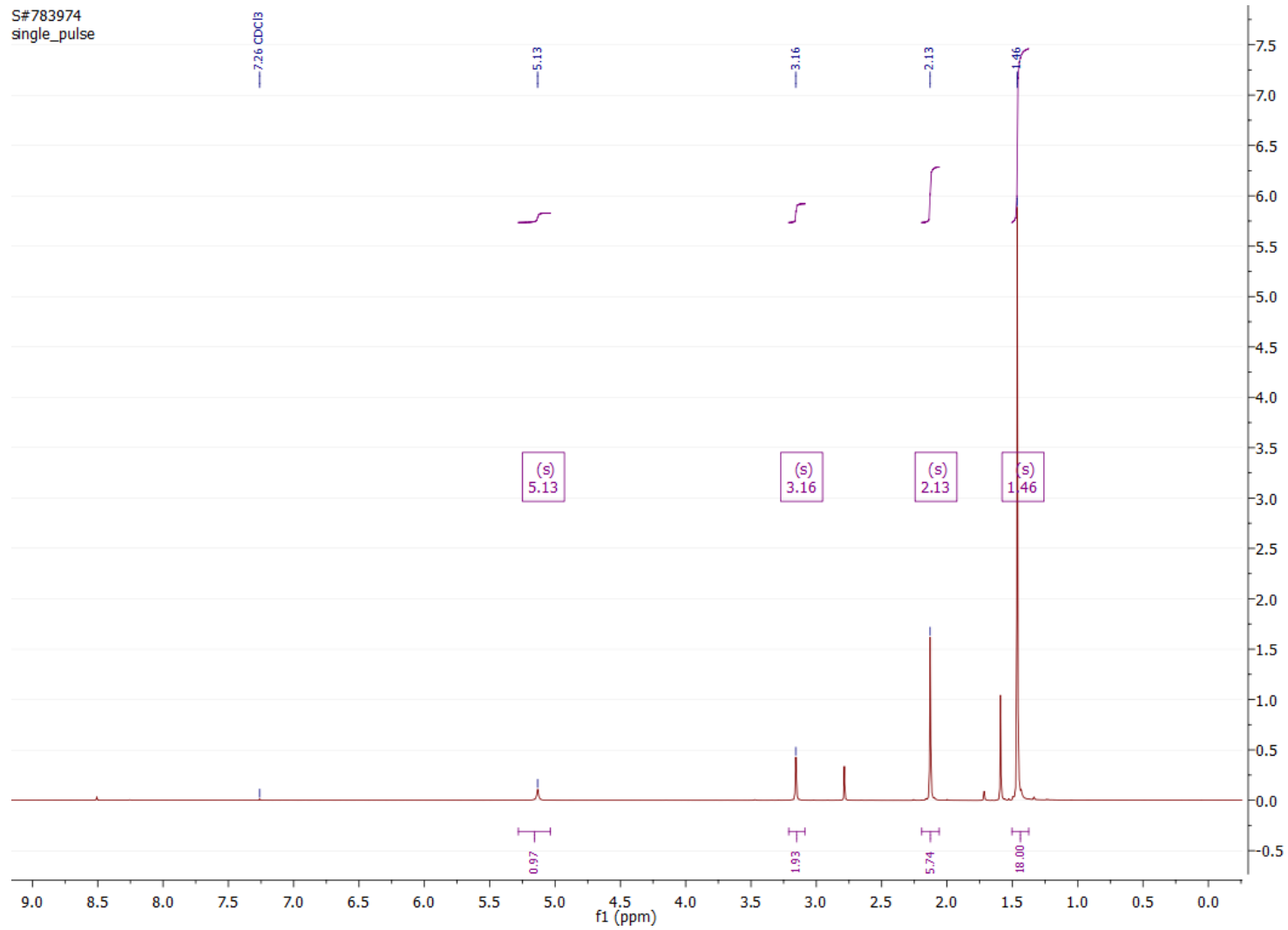
S#769728
single pulse decoupled gated NOE



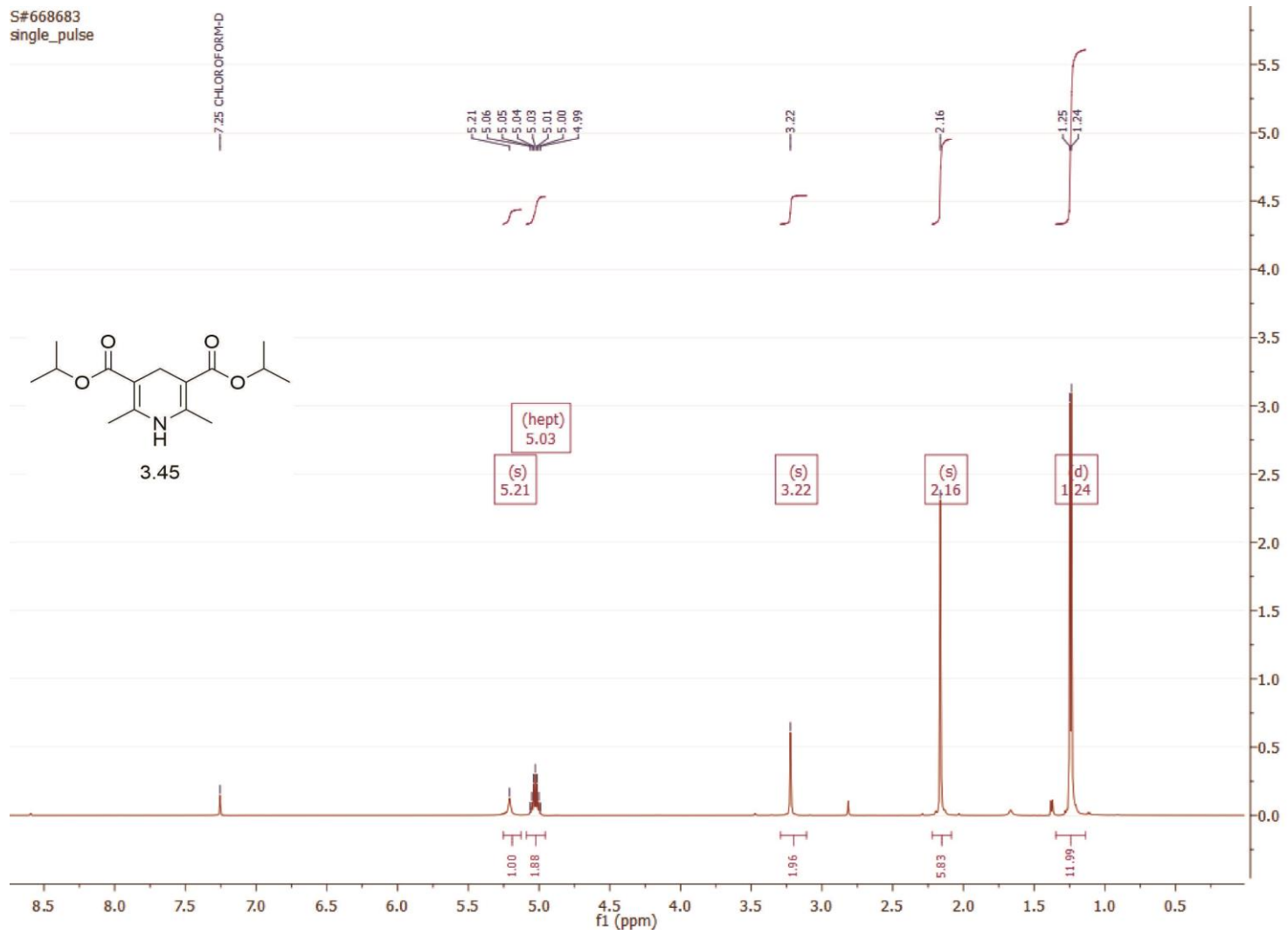


S#775605
single pulse decoupled gated NOE



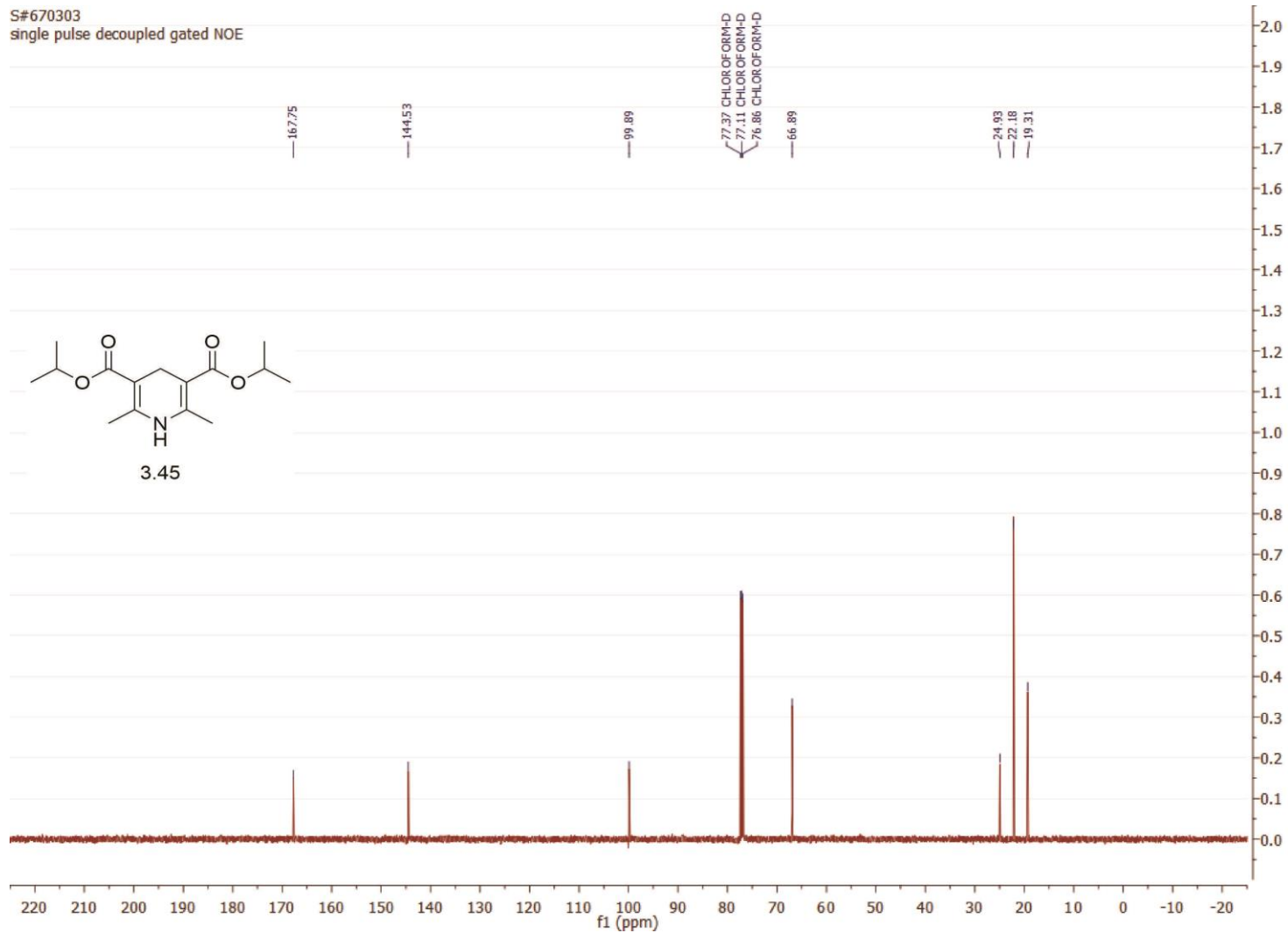


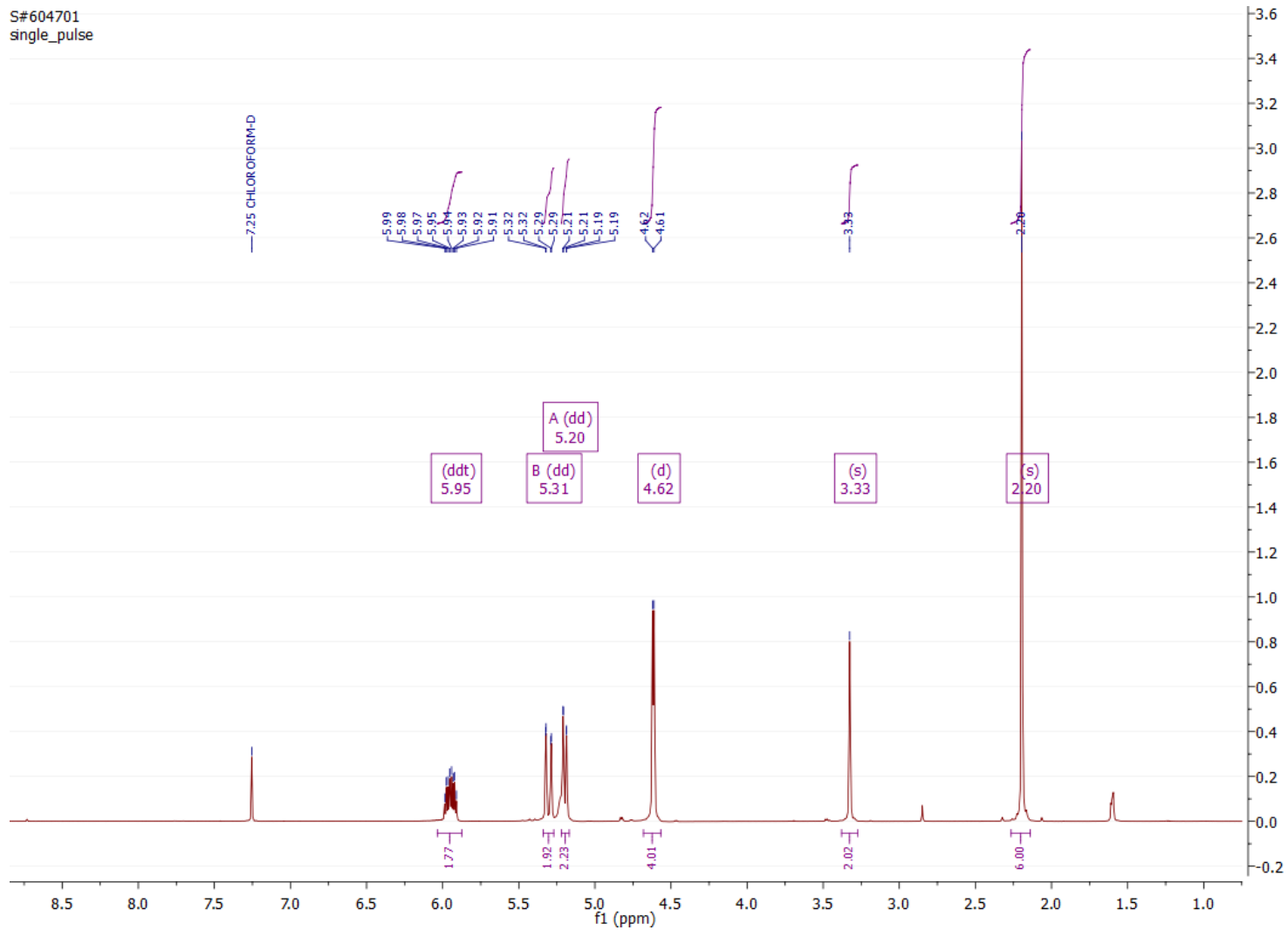
214



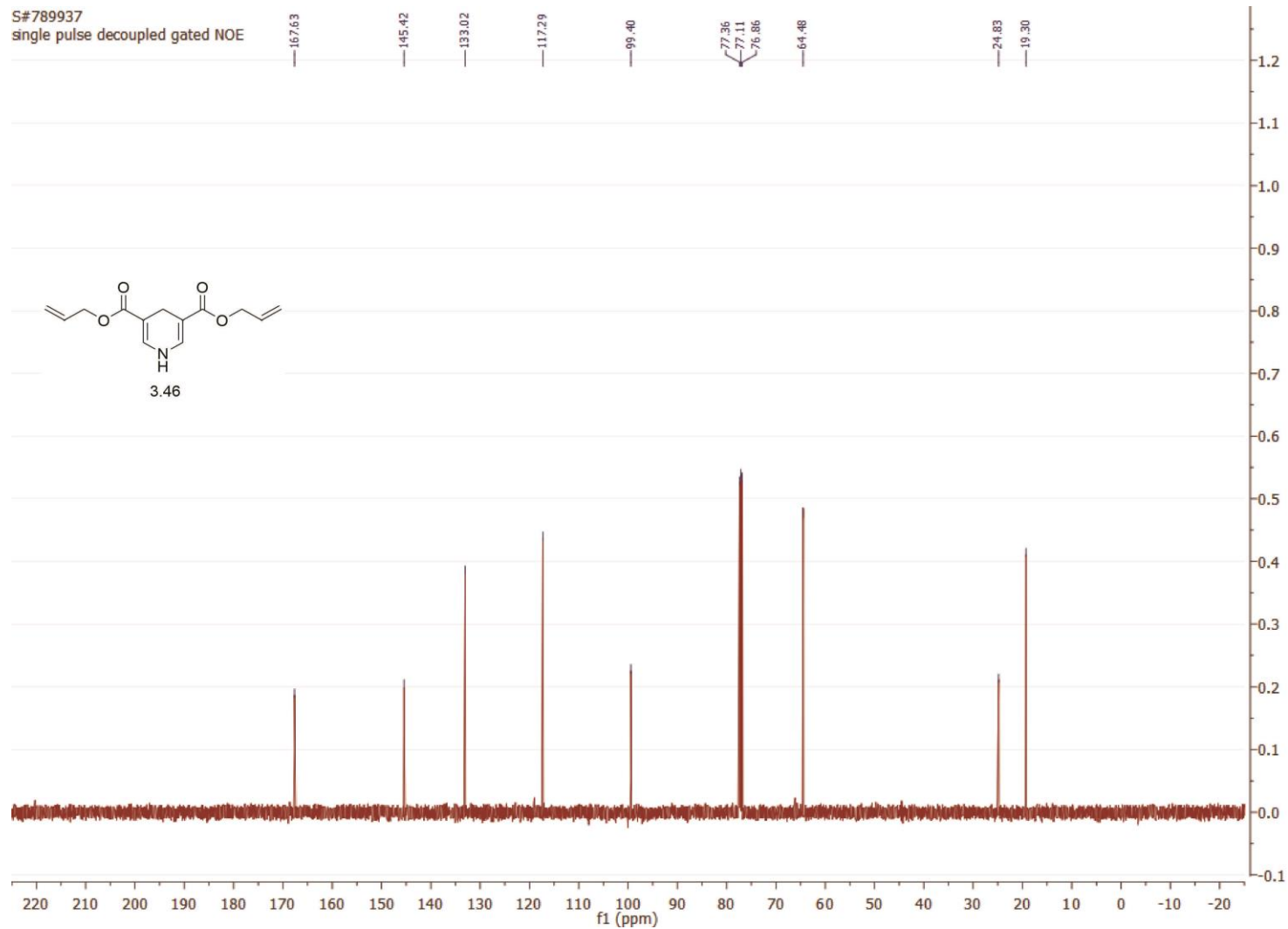
215

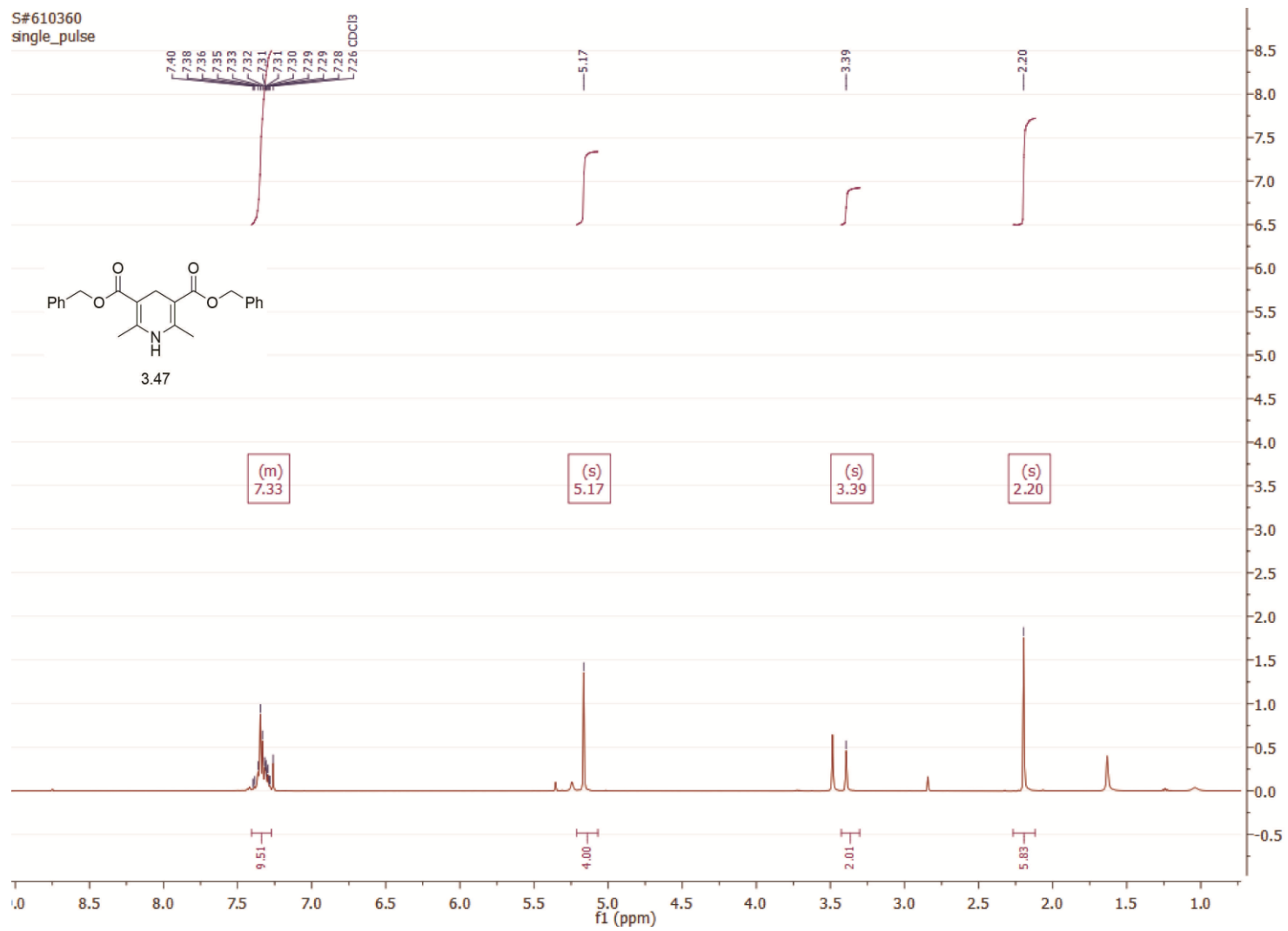
S#670303
single pulse decoupled gated NOE



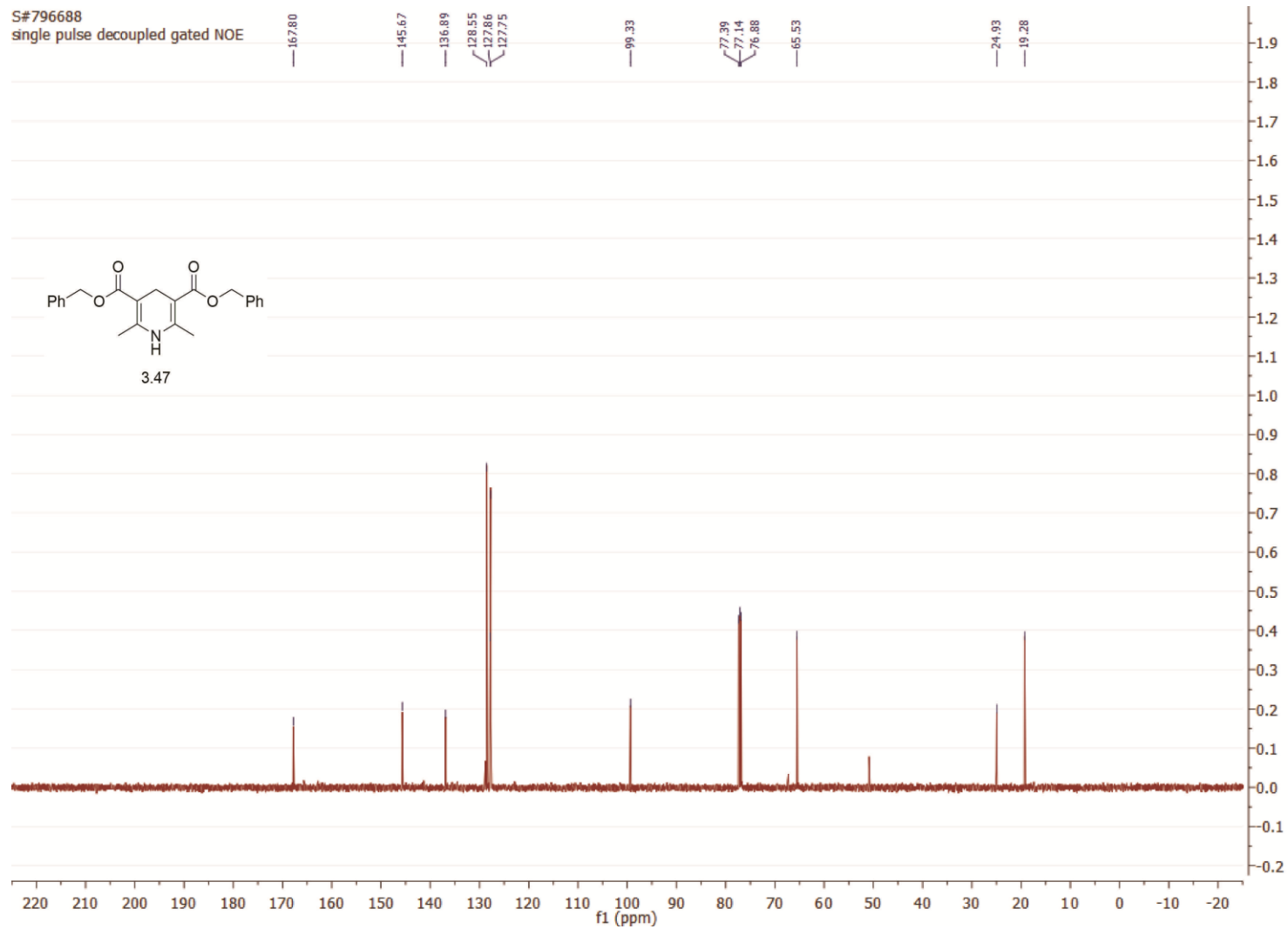


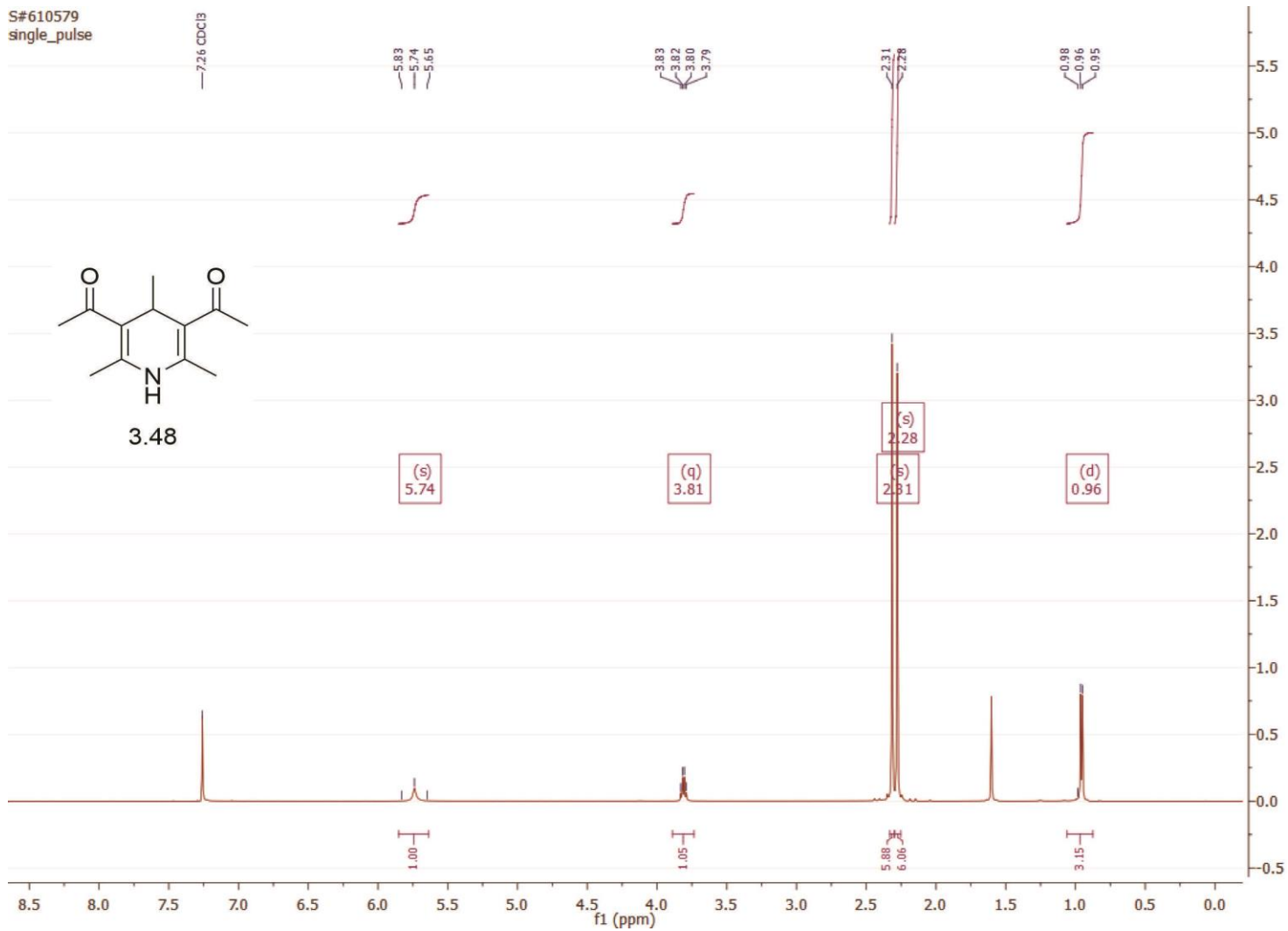
S#789937
single pulse decoupled gated NOE



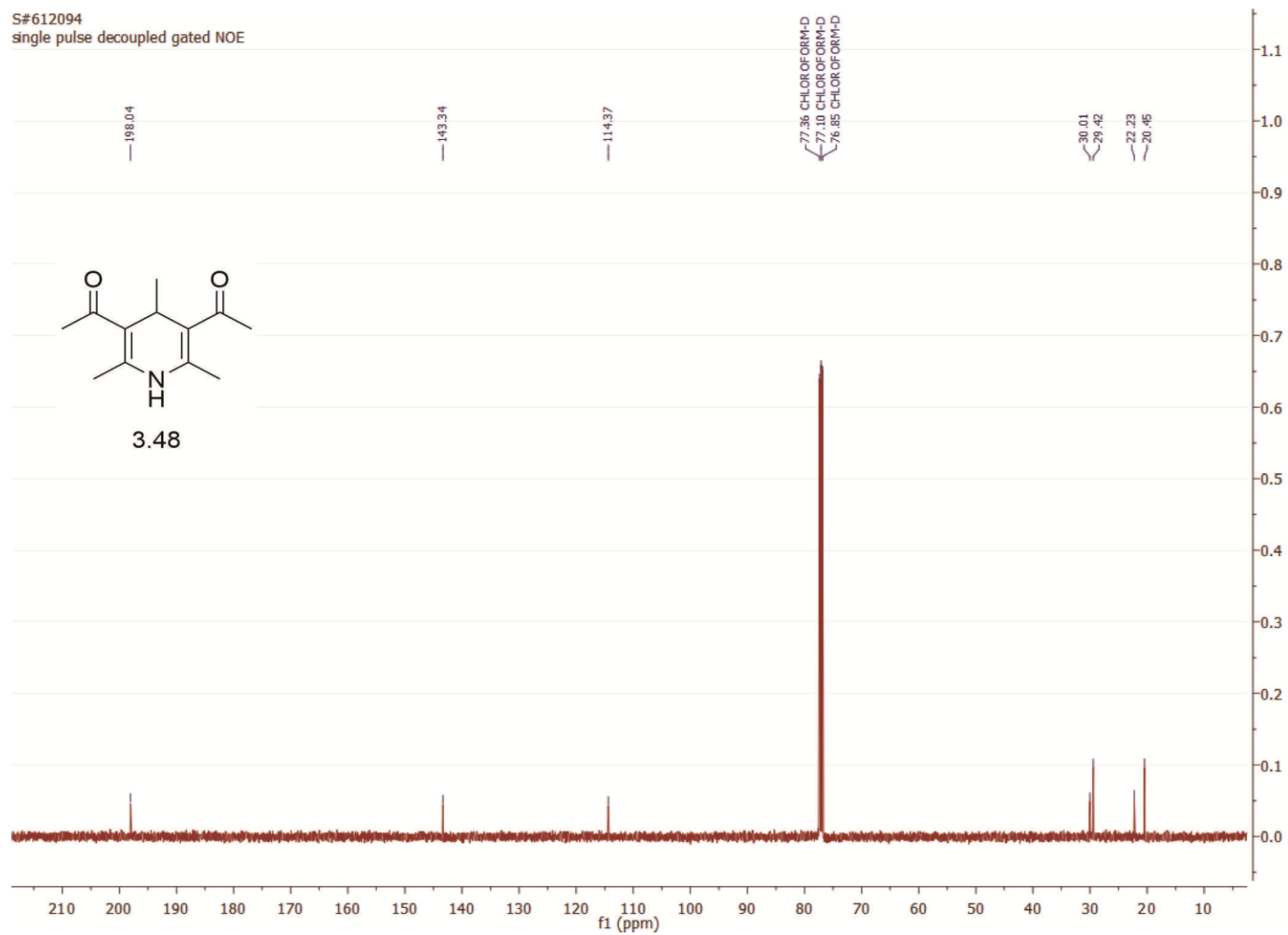


219





S#612094
single pulse decoupled gated NOE



221

S#621263
single_pulse

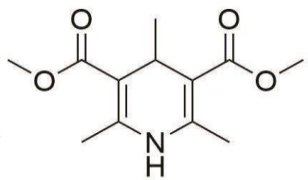
7.26 CDCl3

5.67

3.82
3.80
3.78
3.71

2.27

0.96
0.94
0.91



3.49

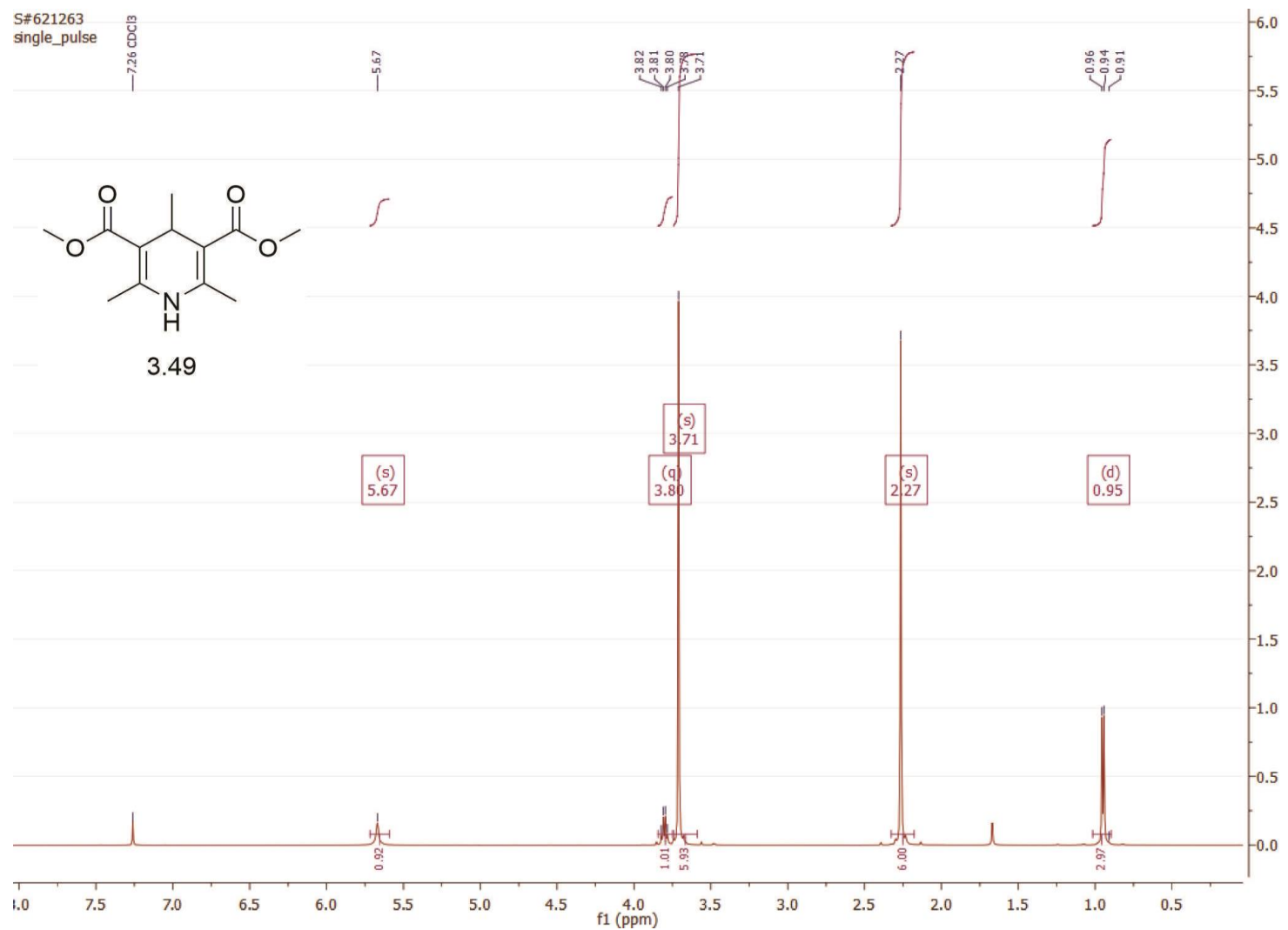
(s)
5.67

(q)
3.80

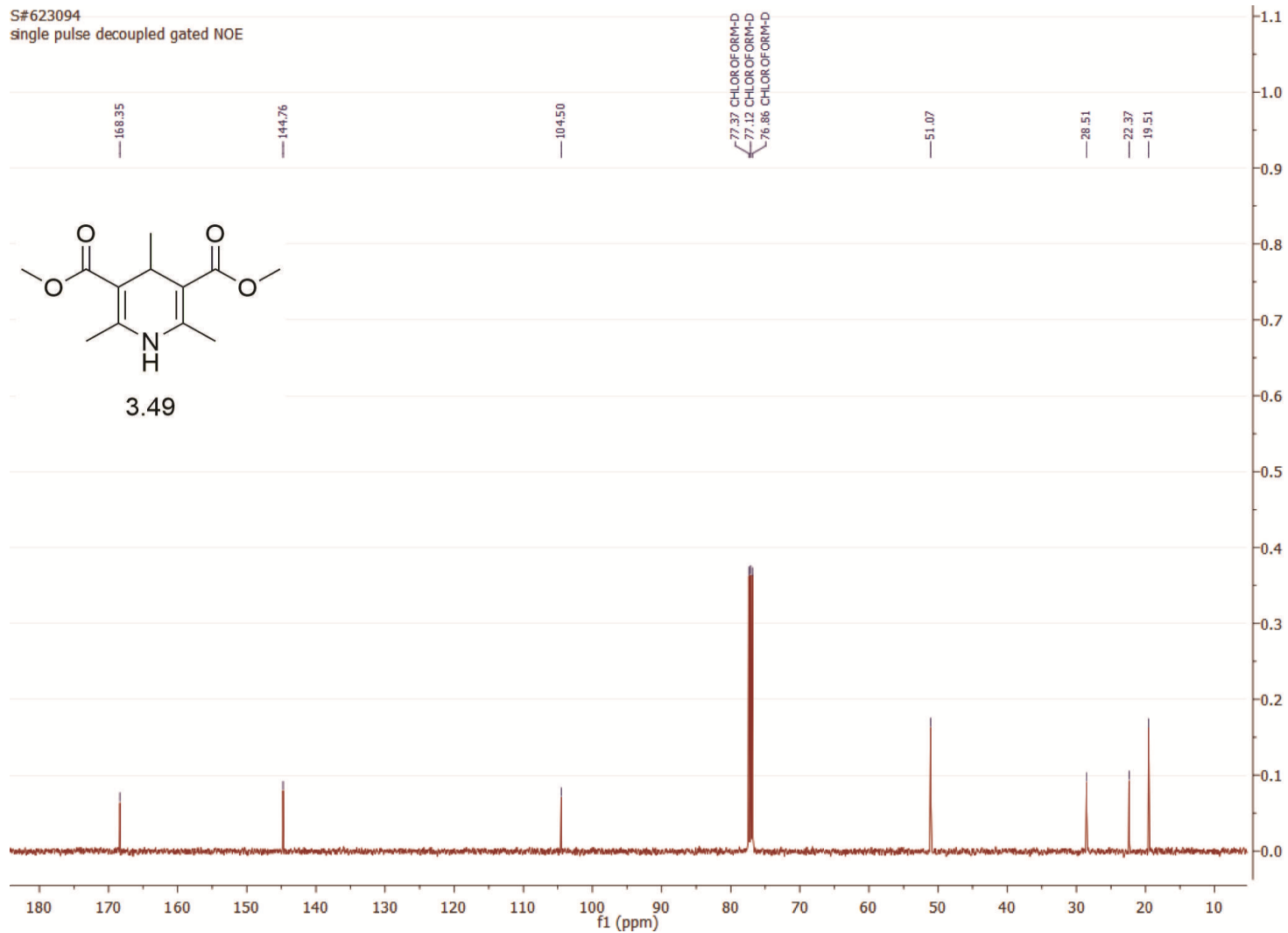
(s)
3.71

(s)
2.27

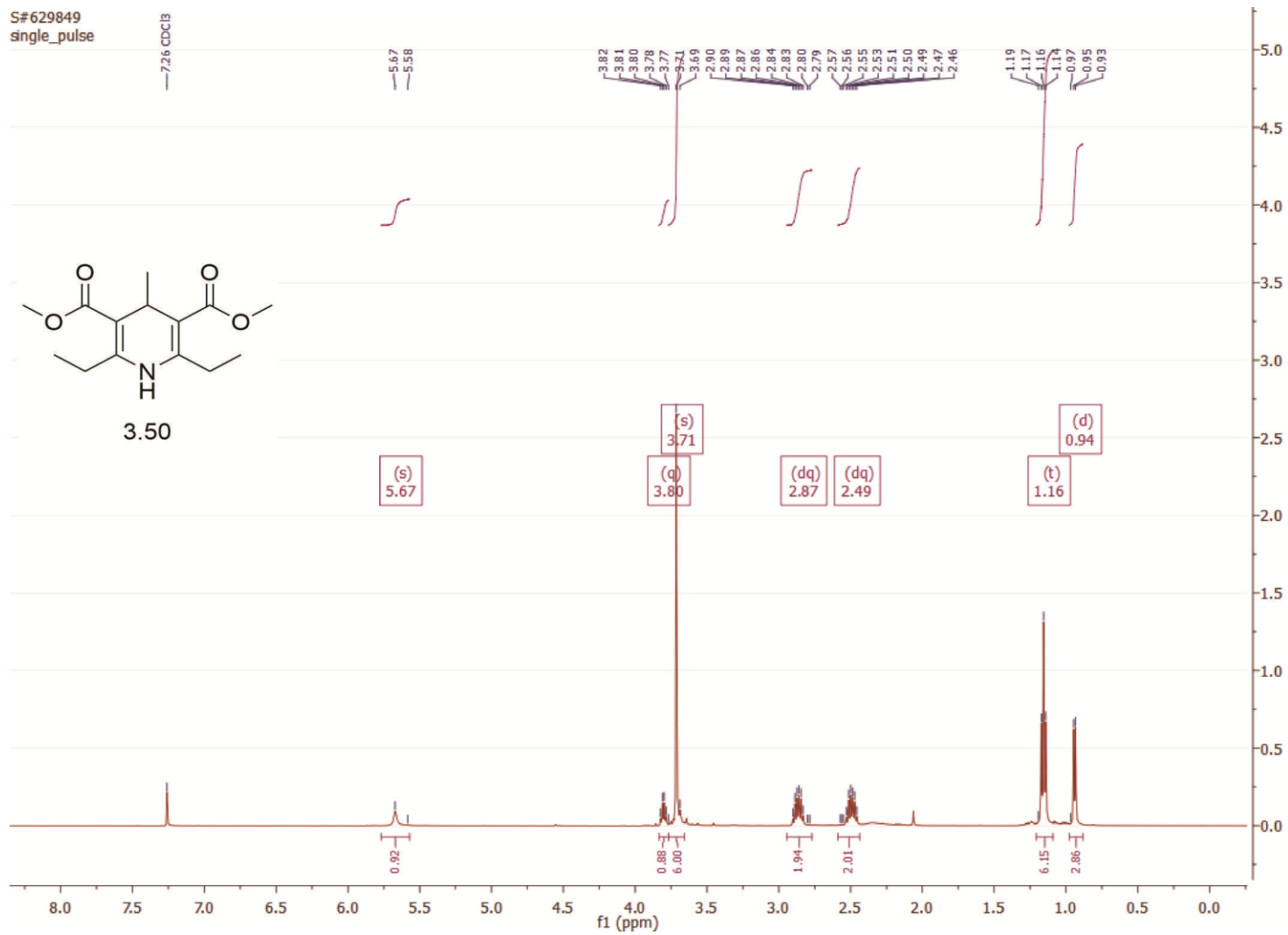
(d)
0.95



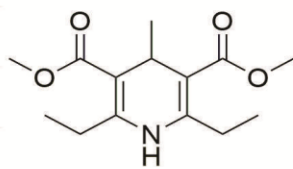
S#623094
single pulse decoupled gated NOE



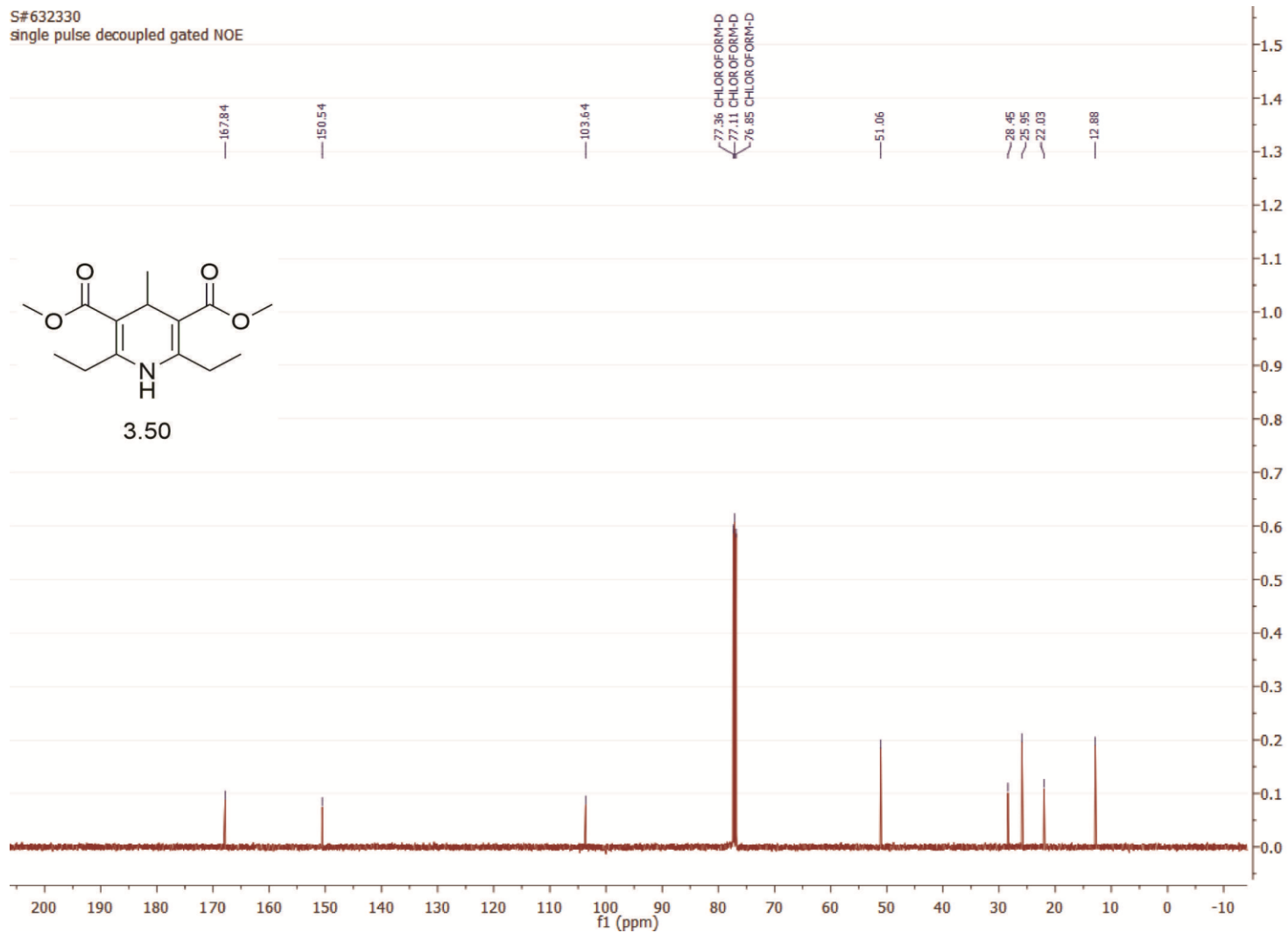
223



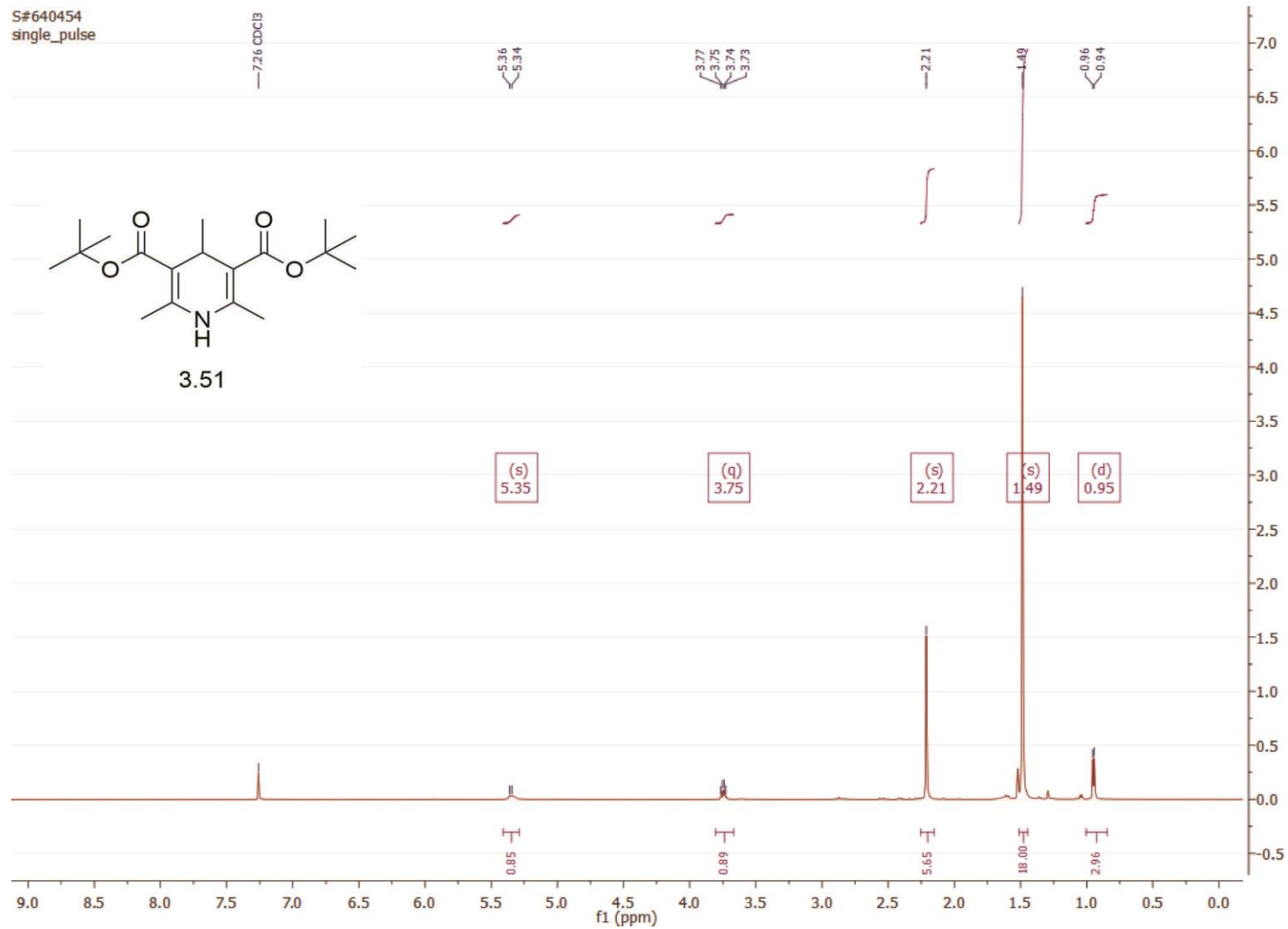
S#632330
single pulse decoupled gated NOE



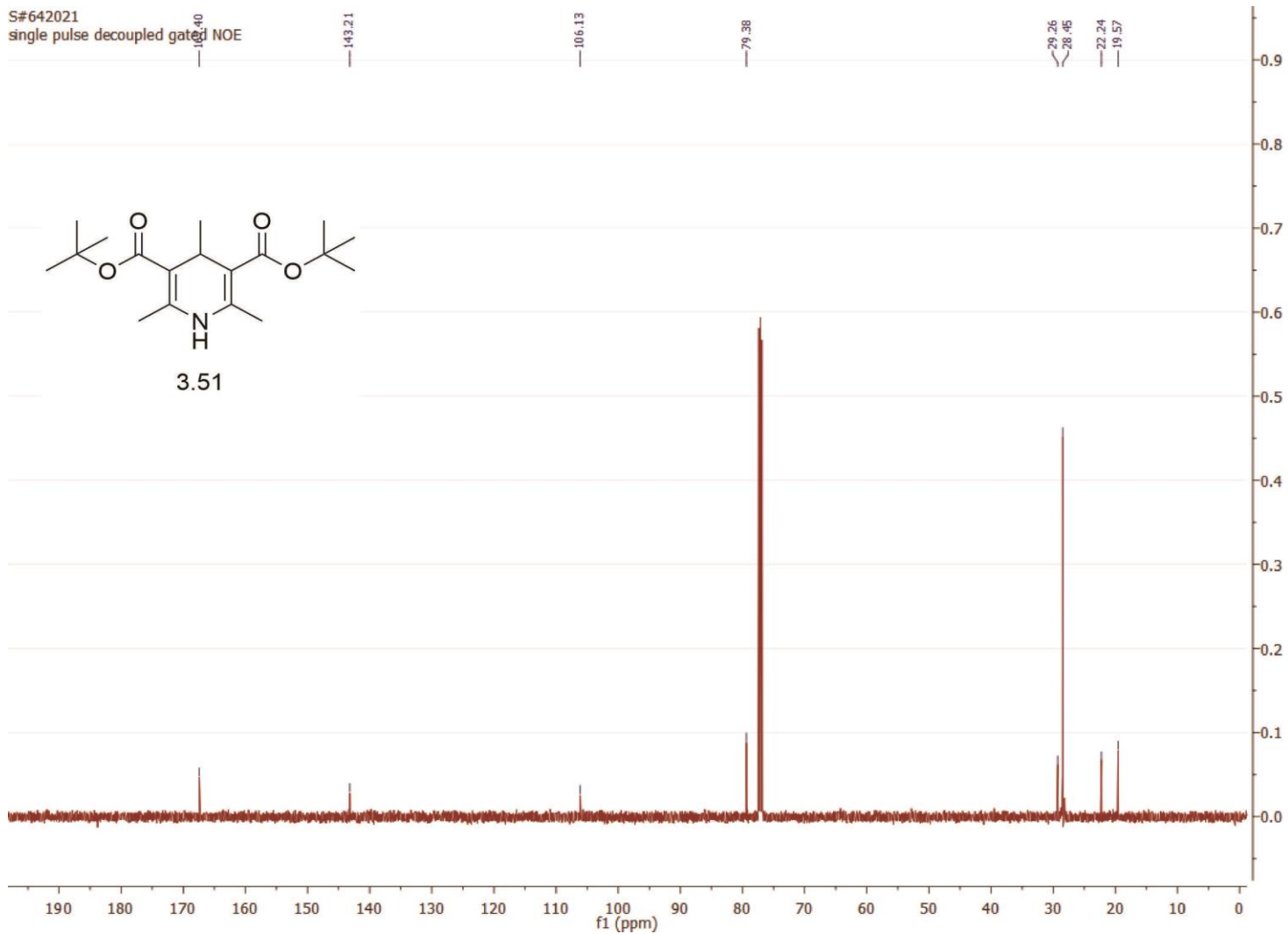
3.50



226

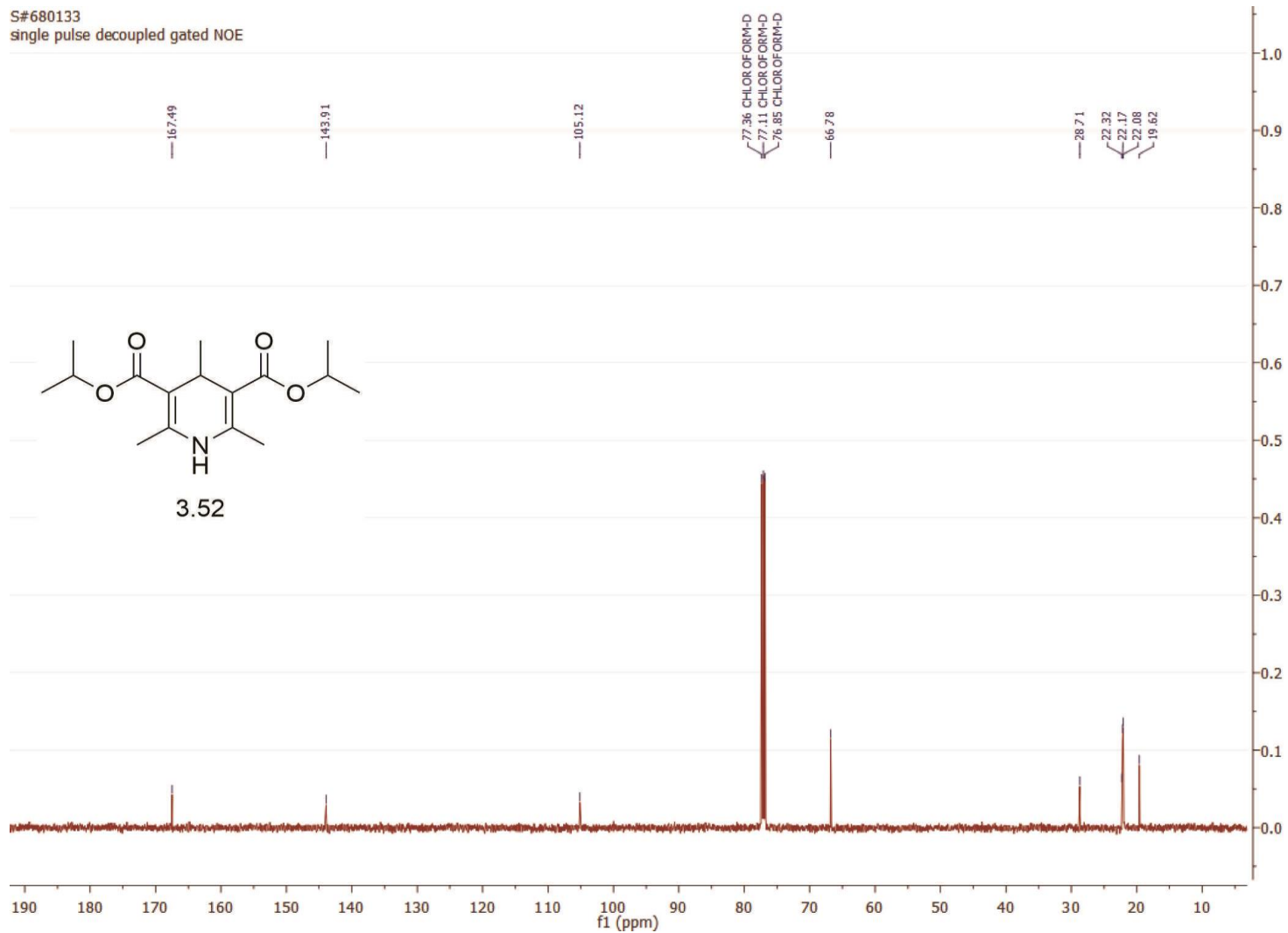


S#642021
single pulse decoupled gated NOE

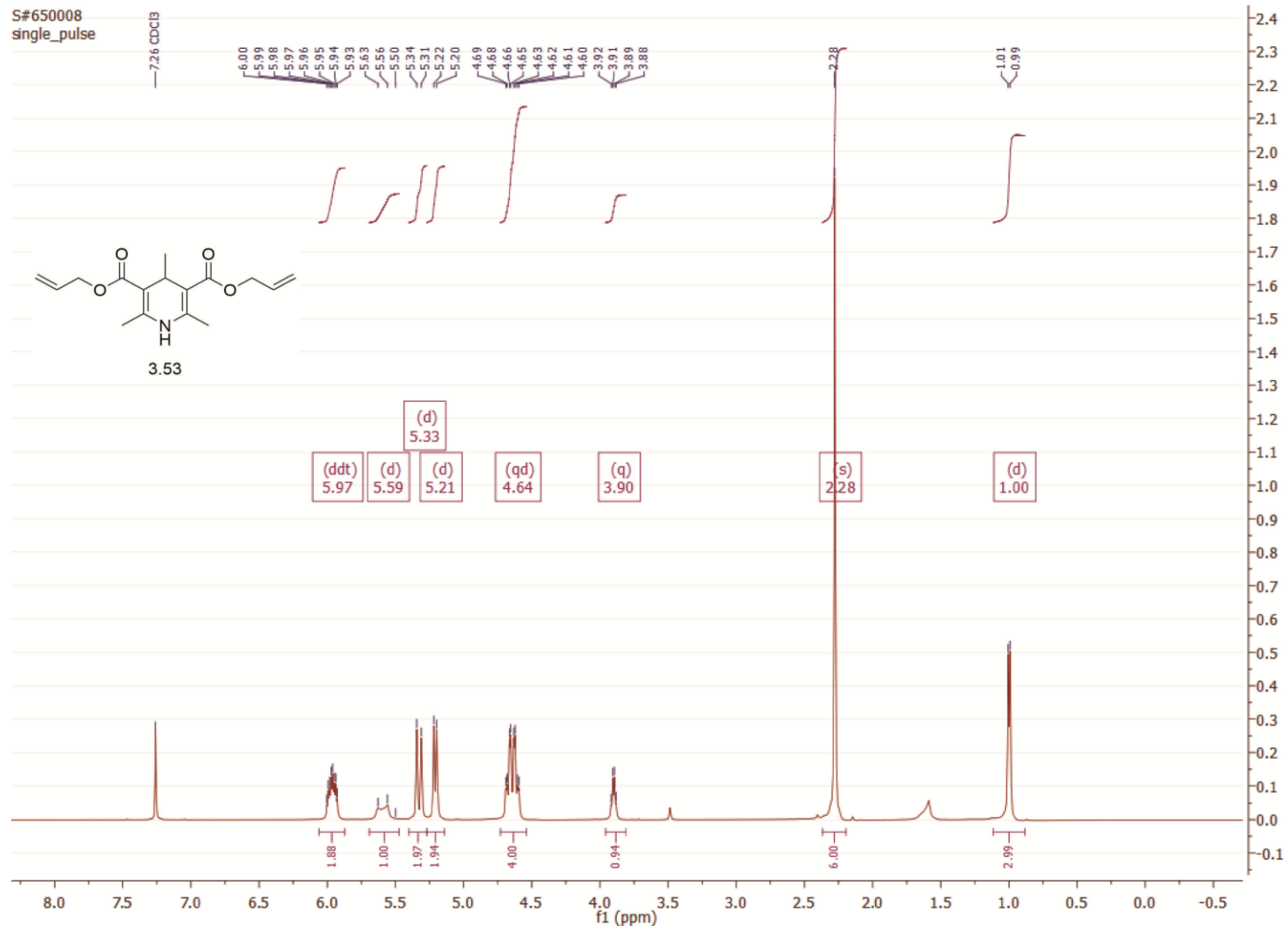




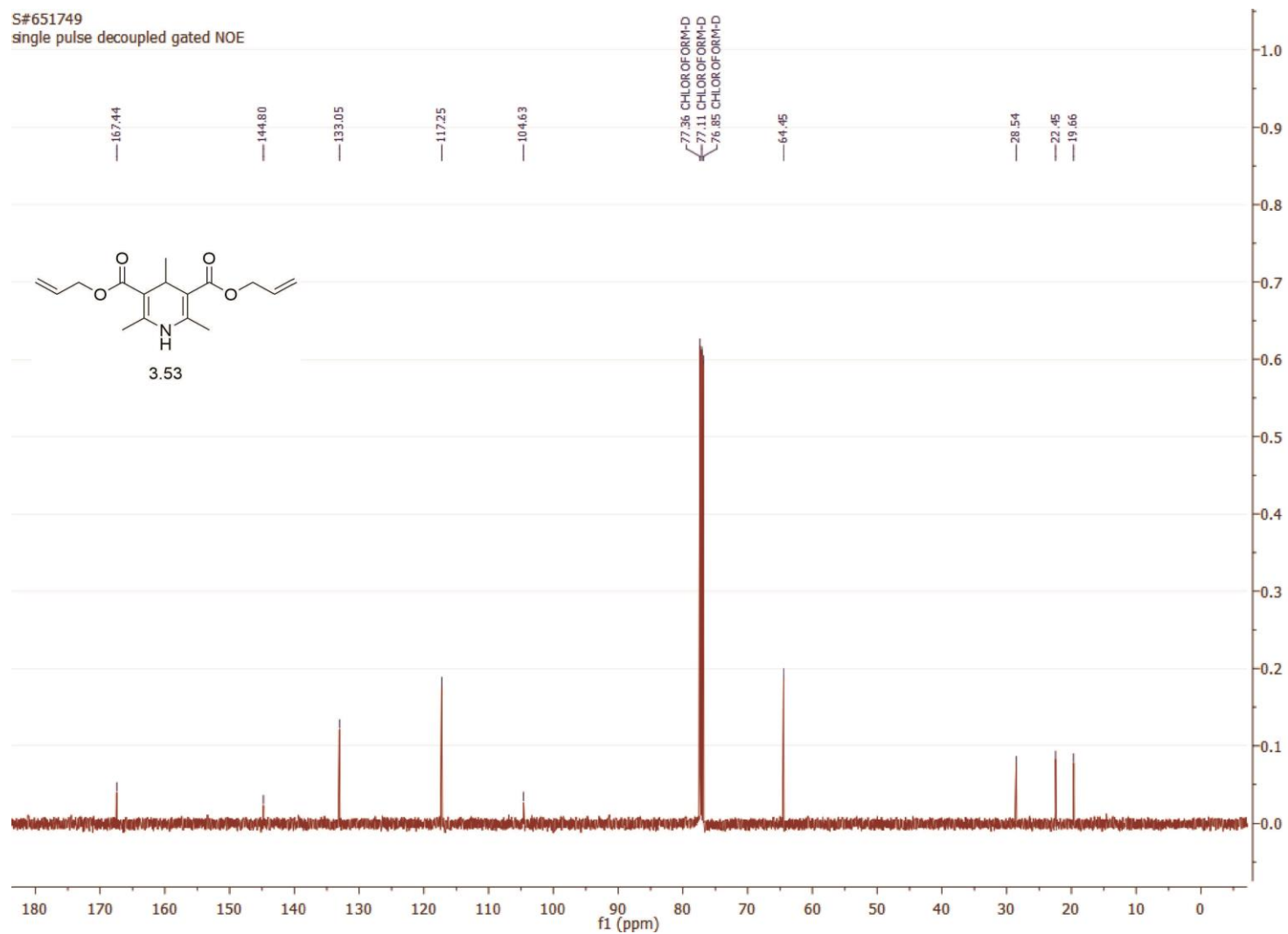
S#680133
single pulse decoupled gated NOE



230

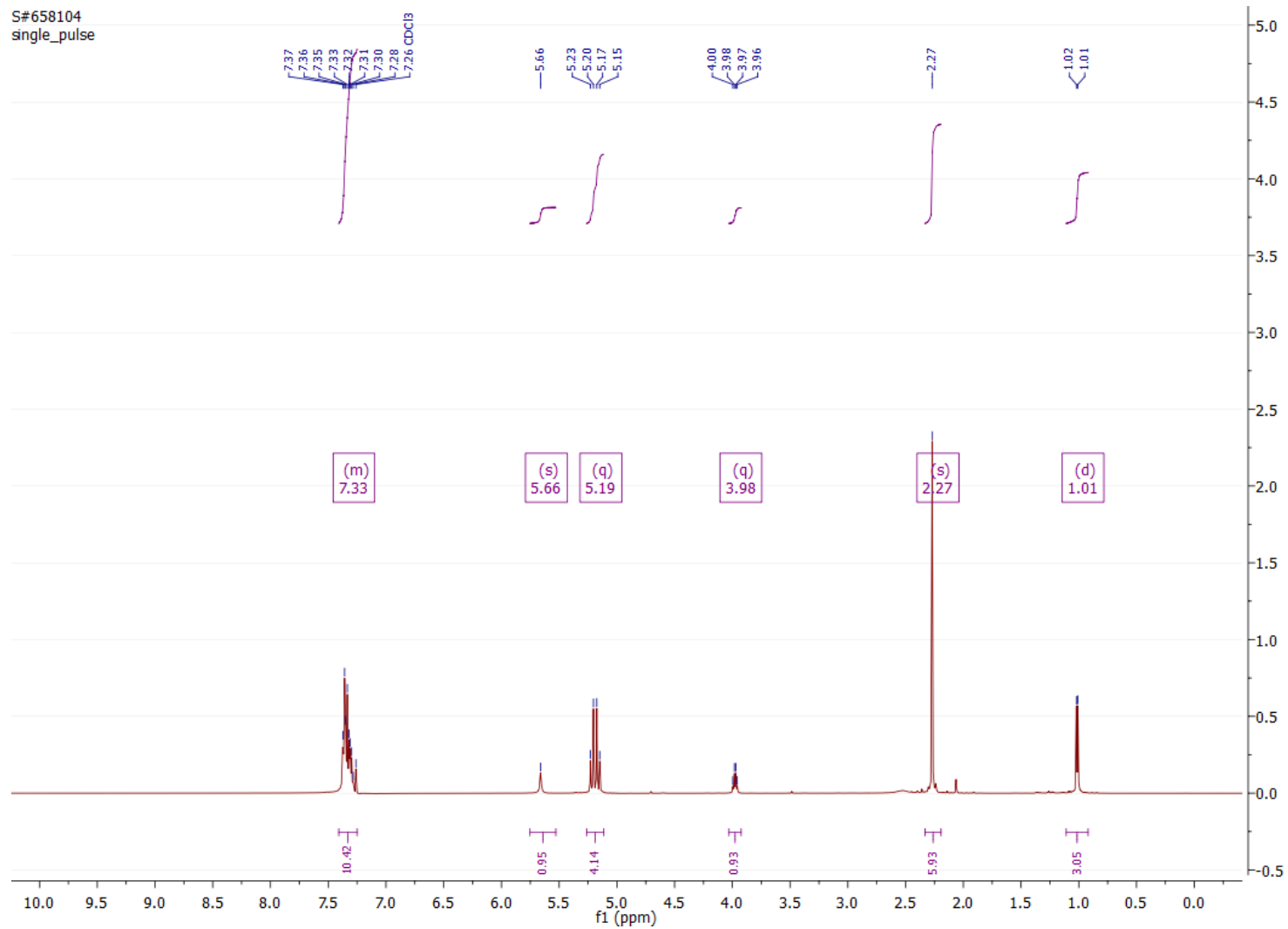


S#651749
single pulse decoupled gated NOE

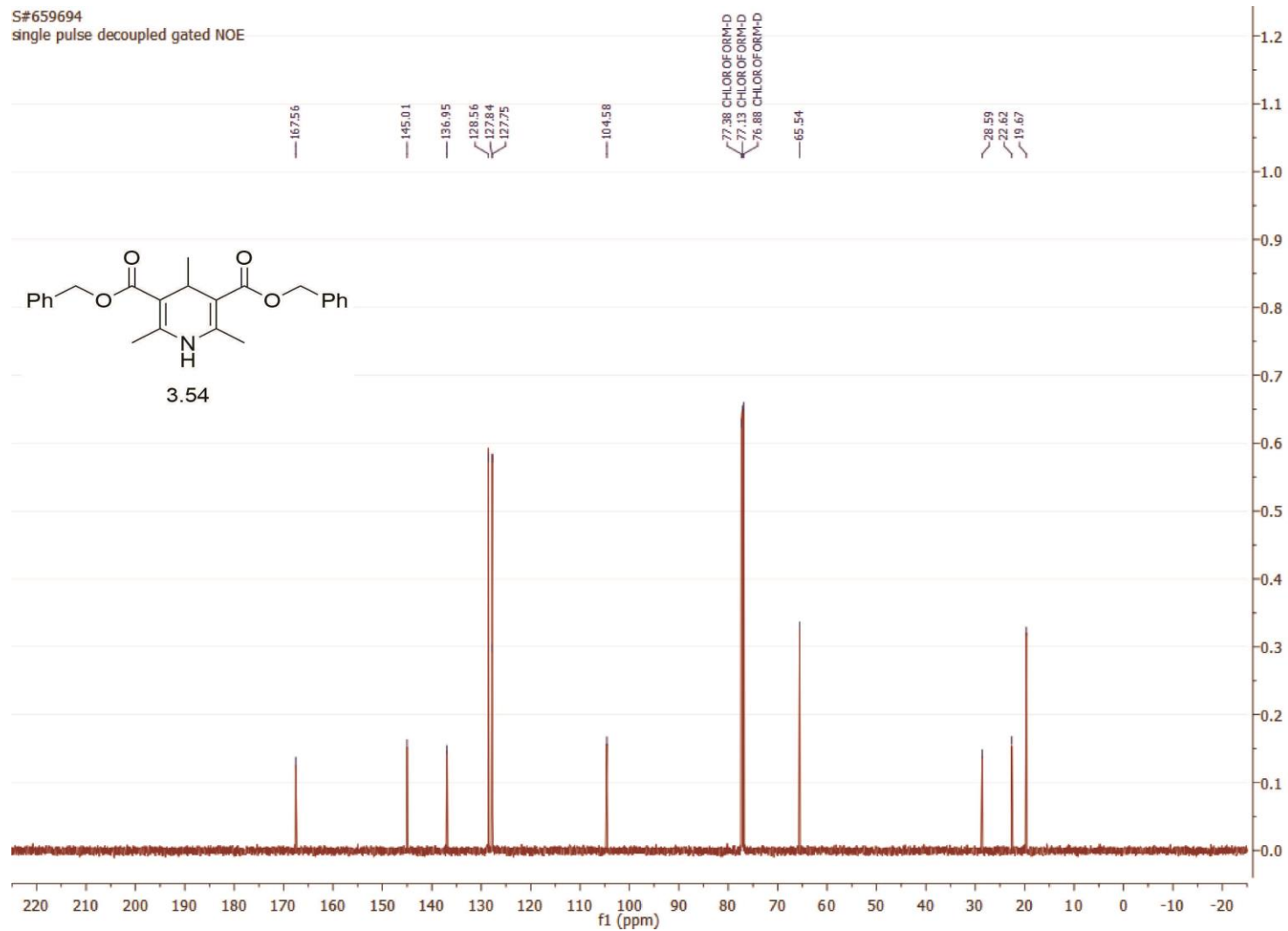
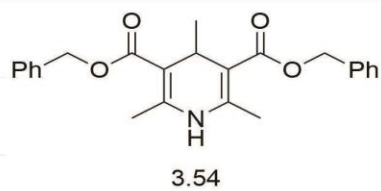


231

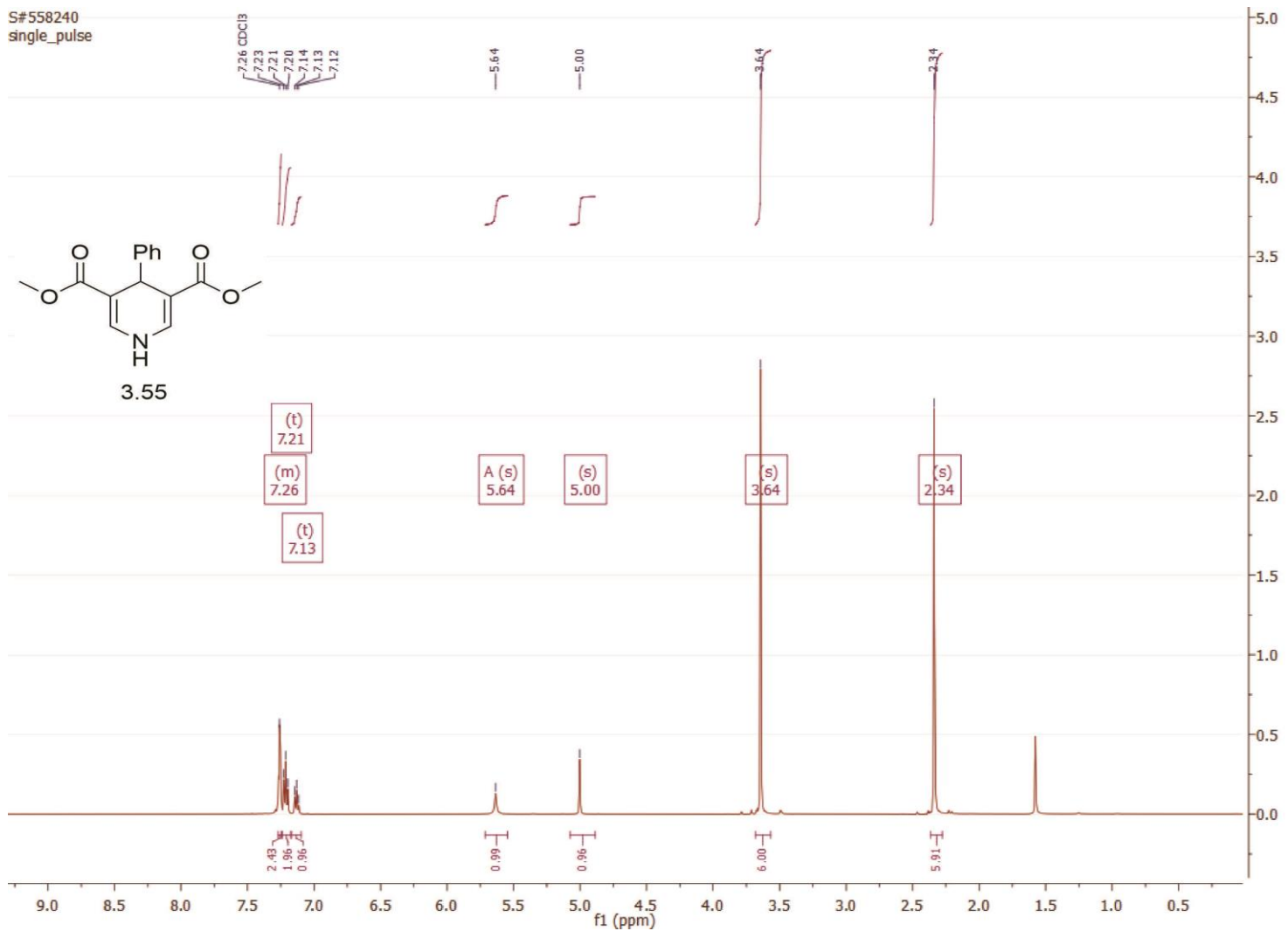
232



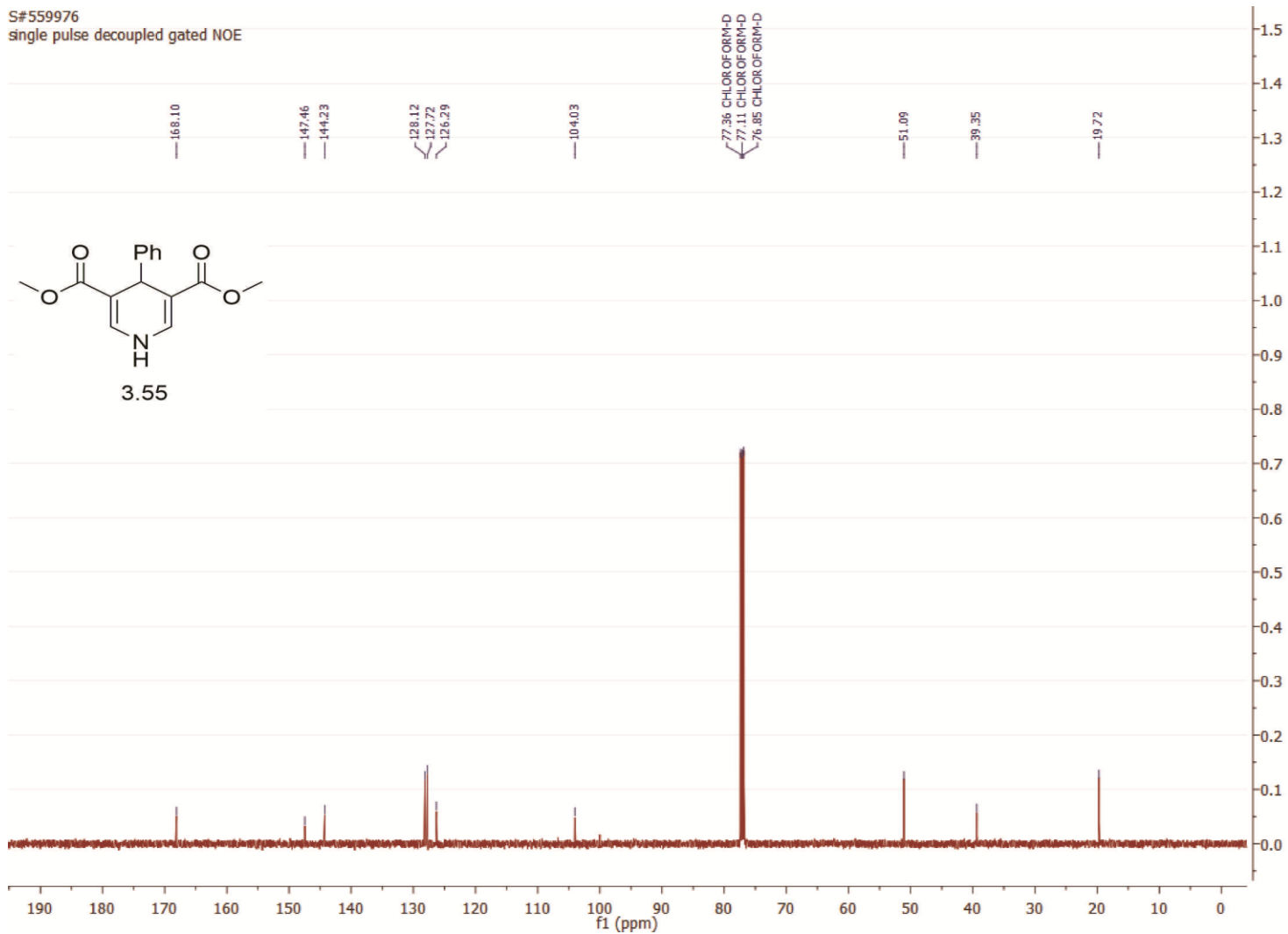
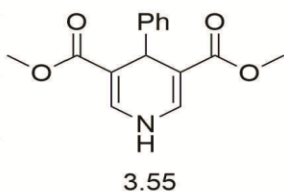
S#659694
single pulse decoupled gated NOE

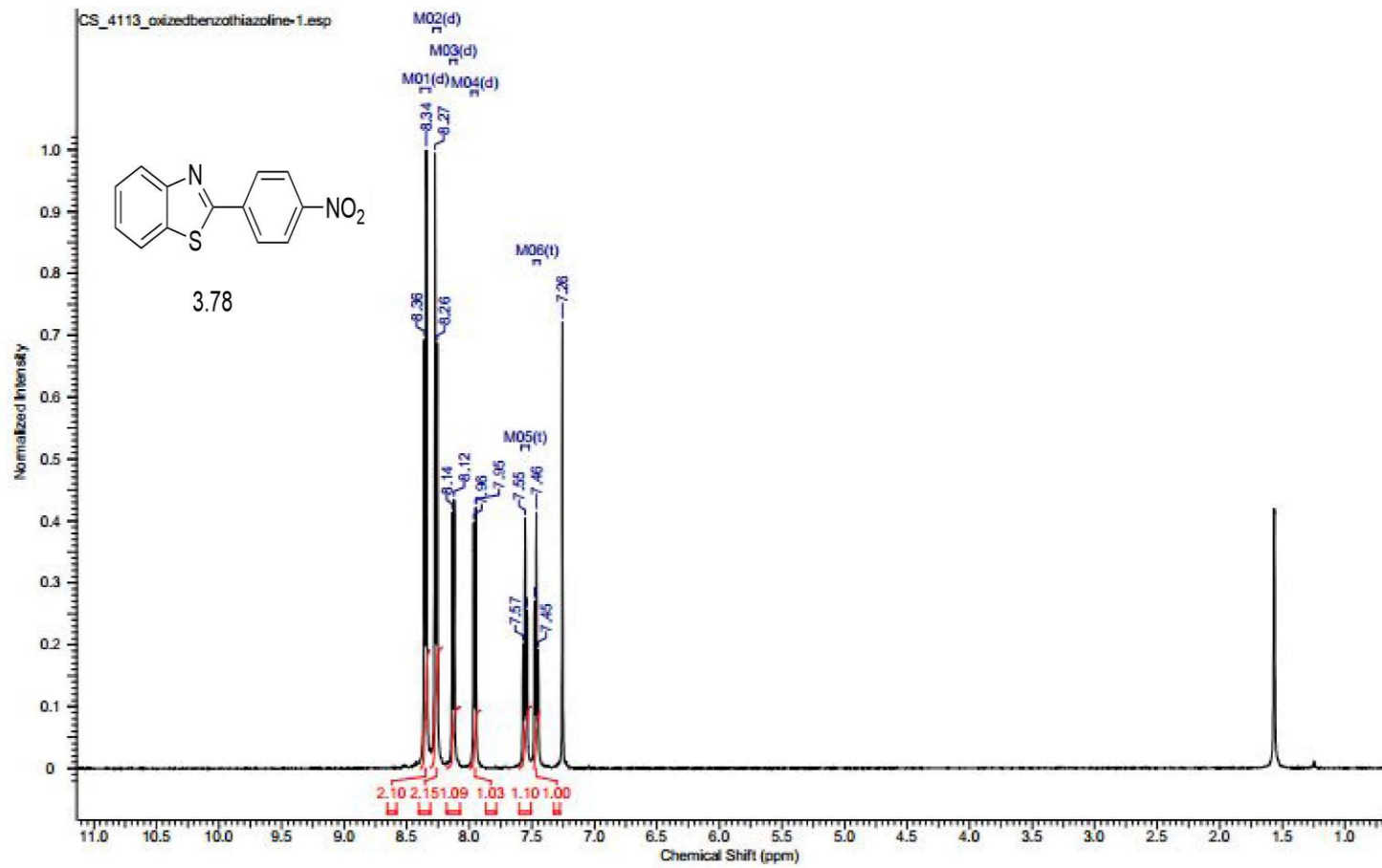


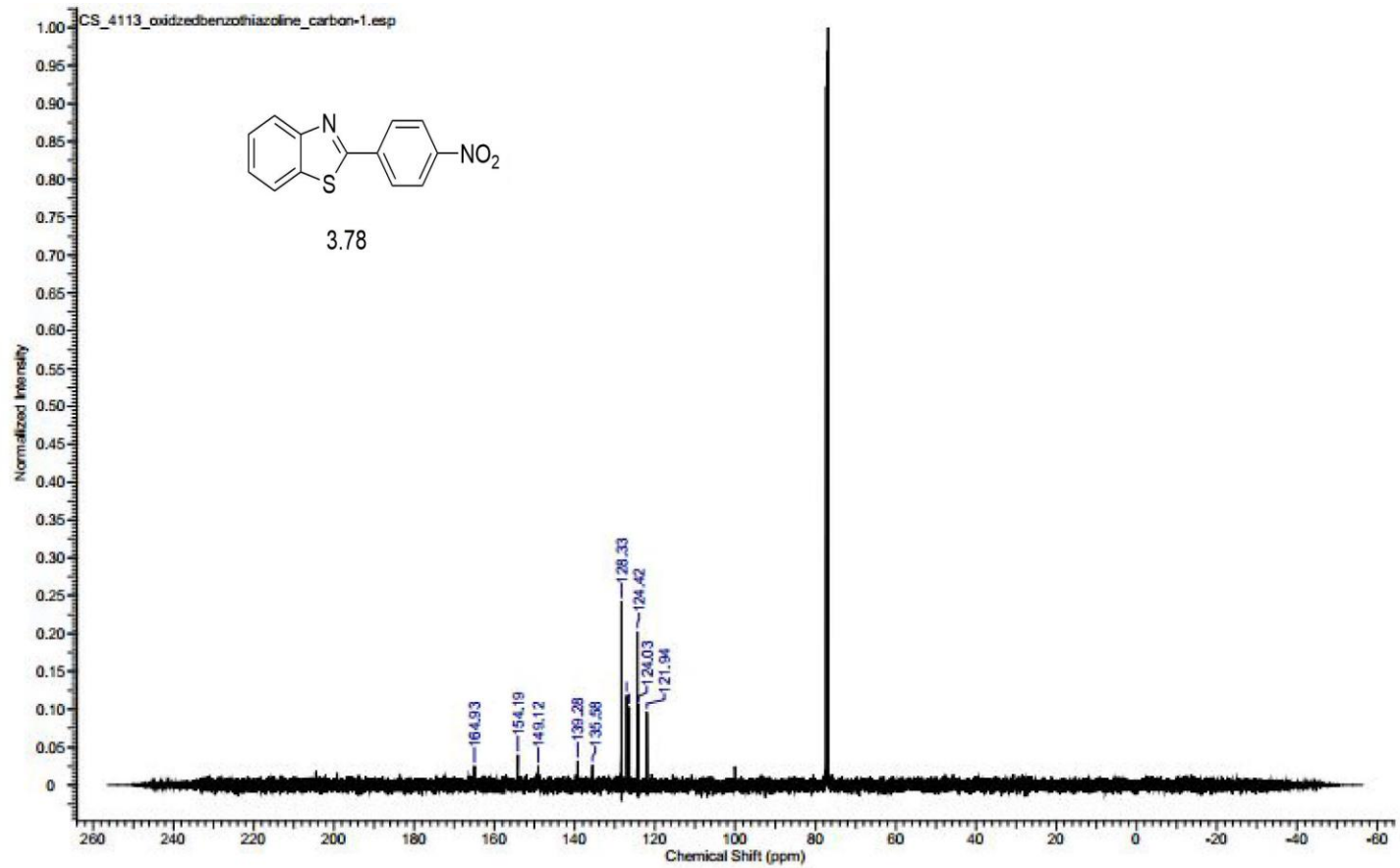
234

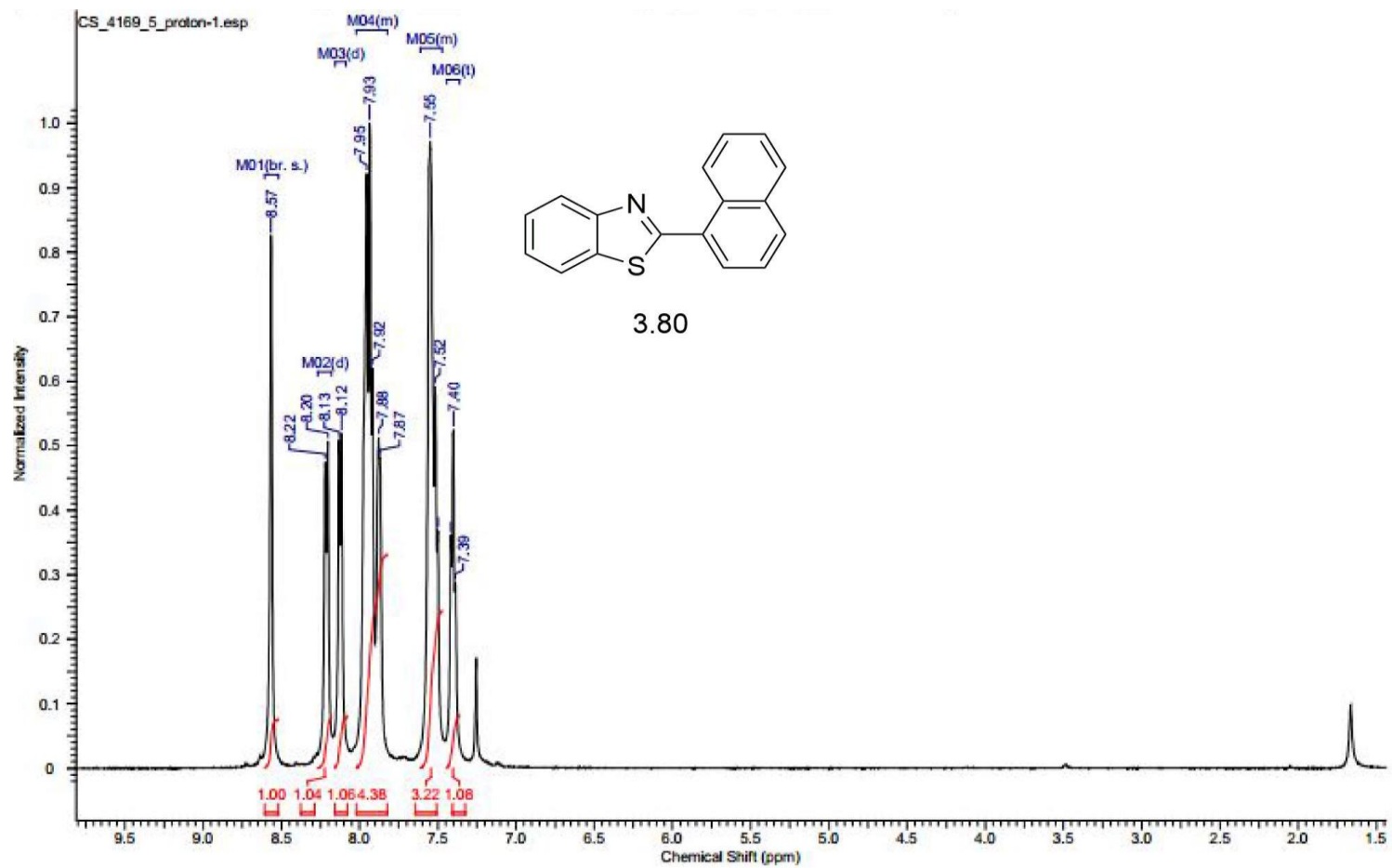


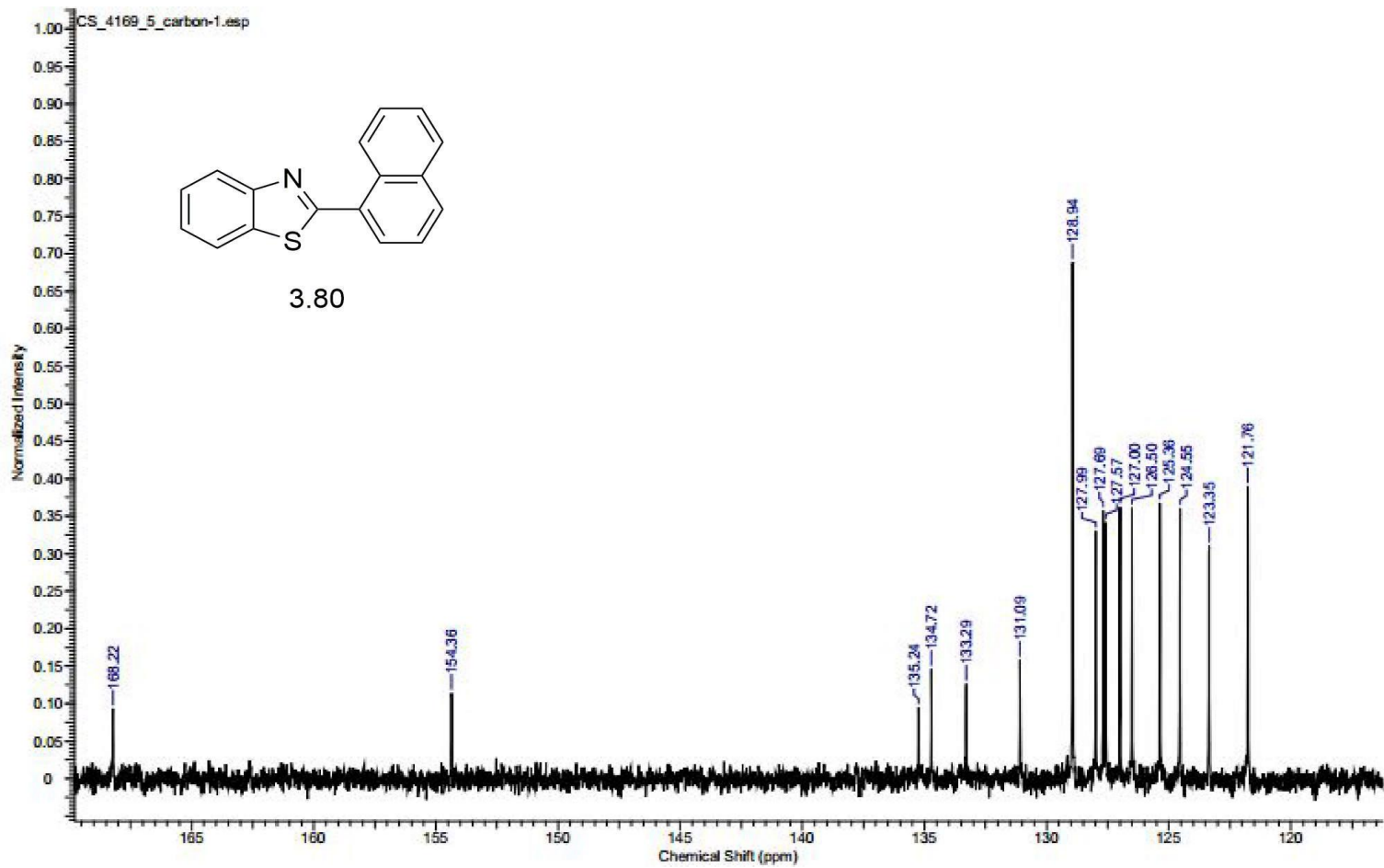
S#559976
single pulse decoupled gated NOE

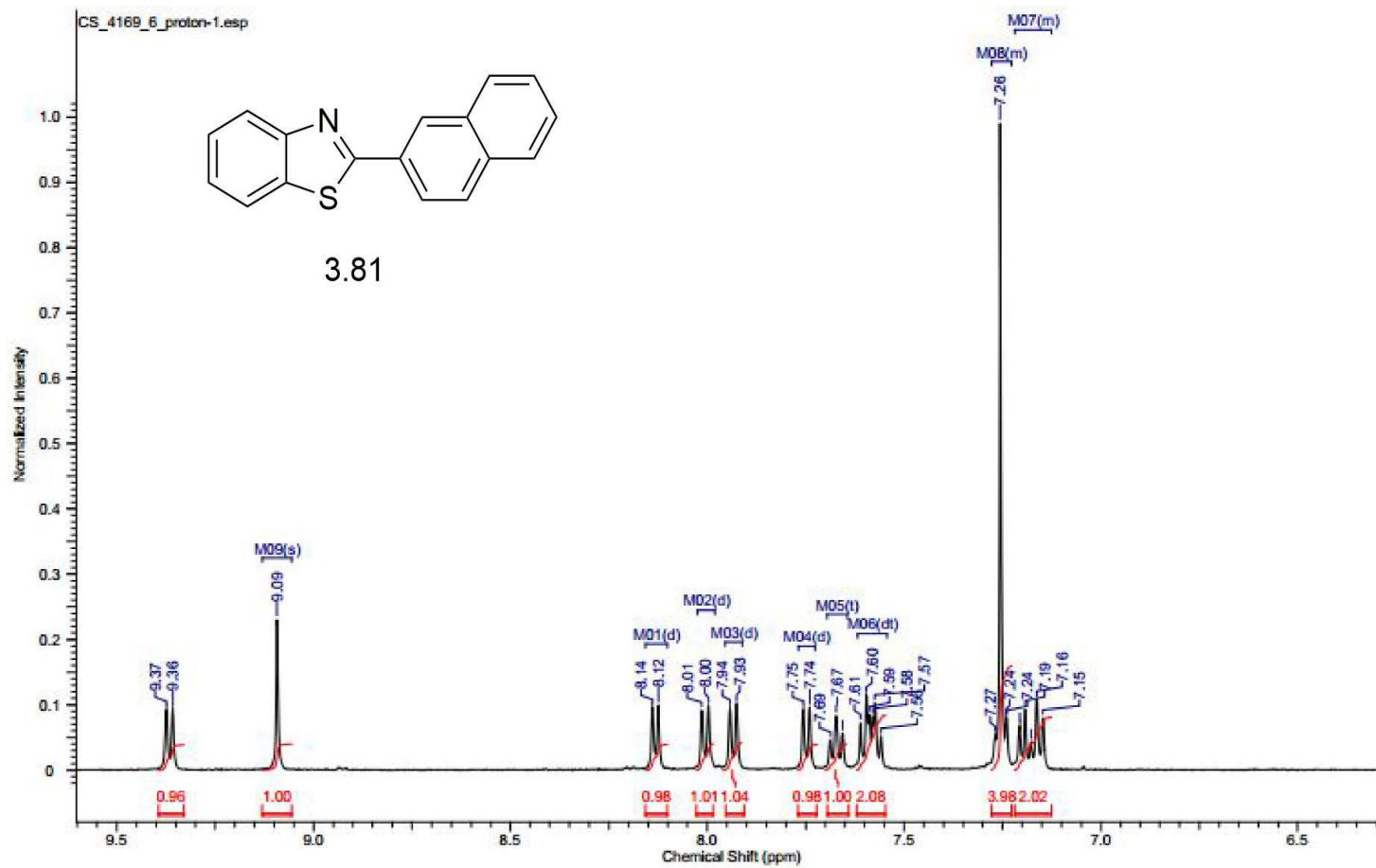


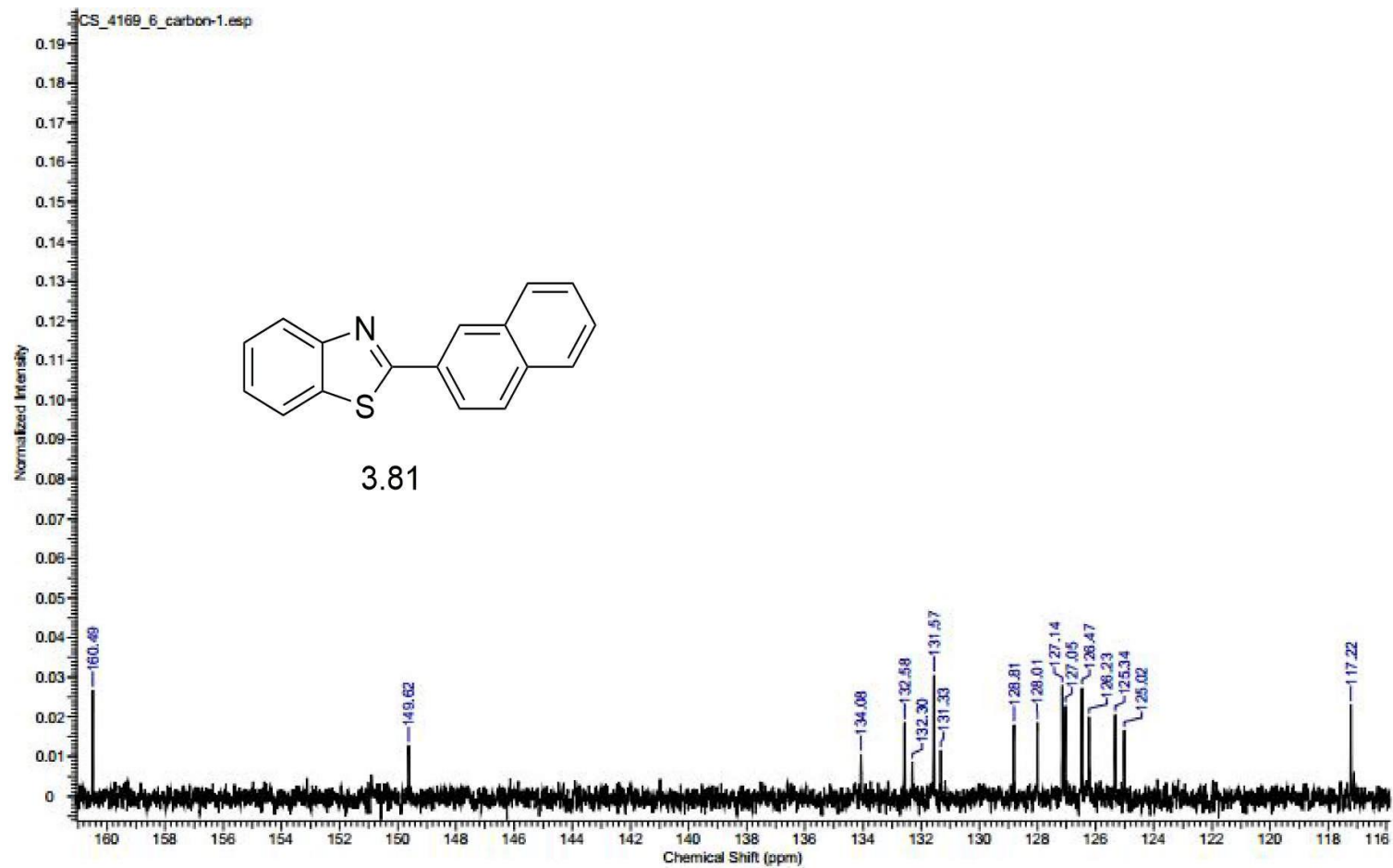




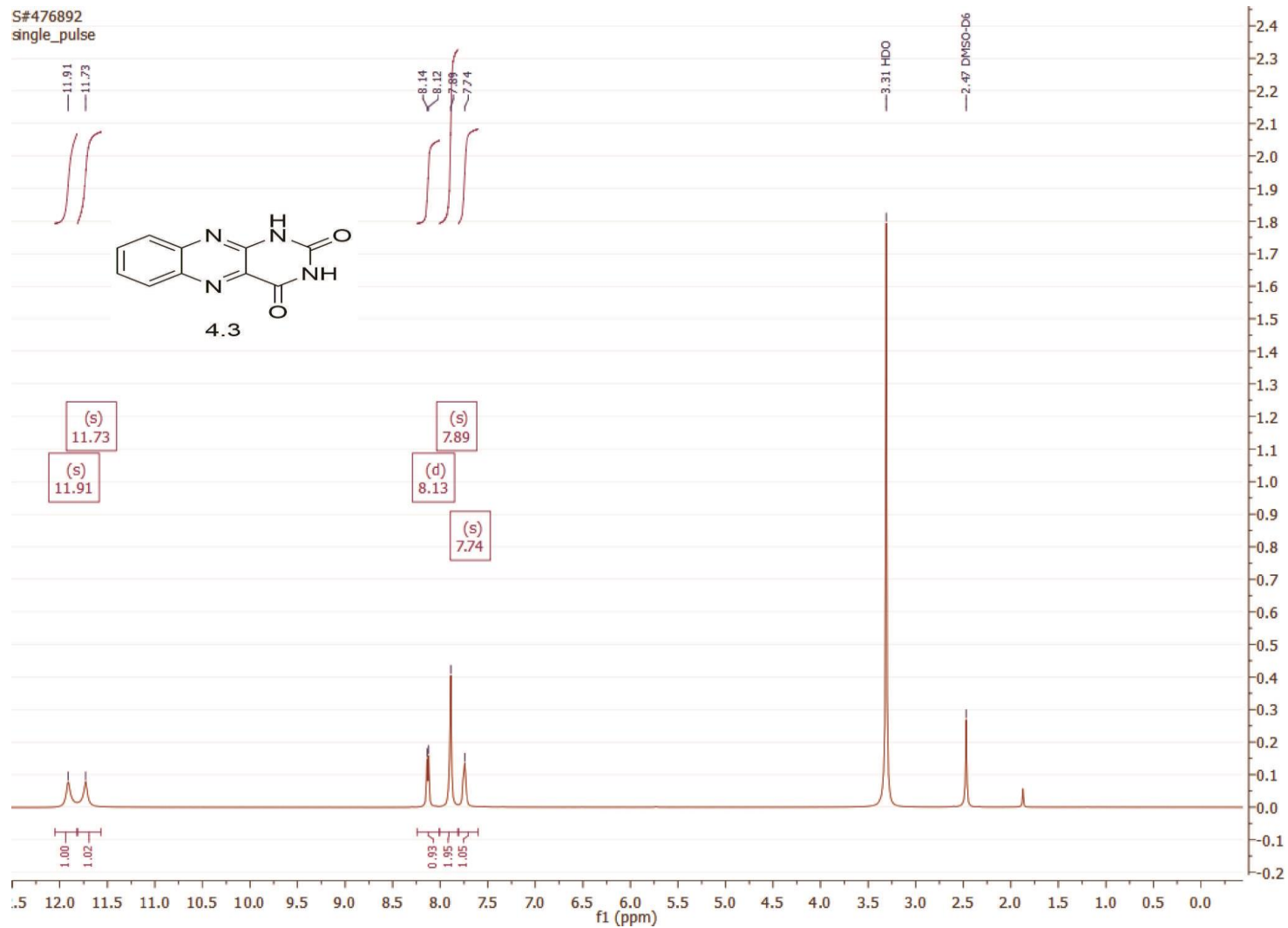




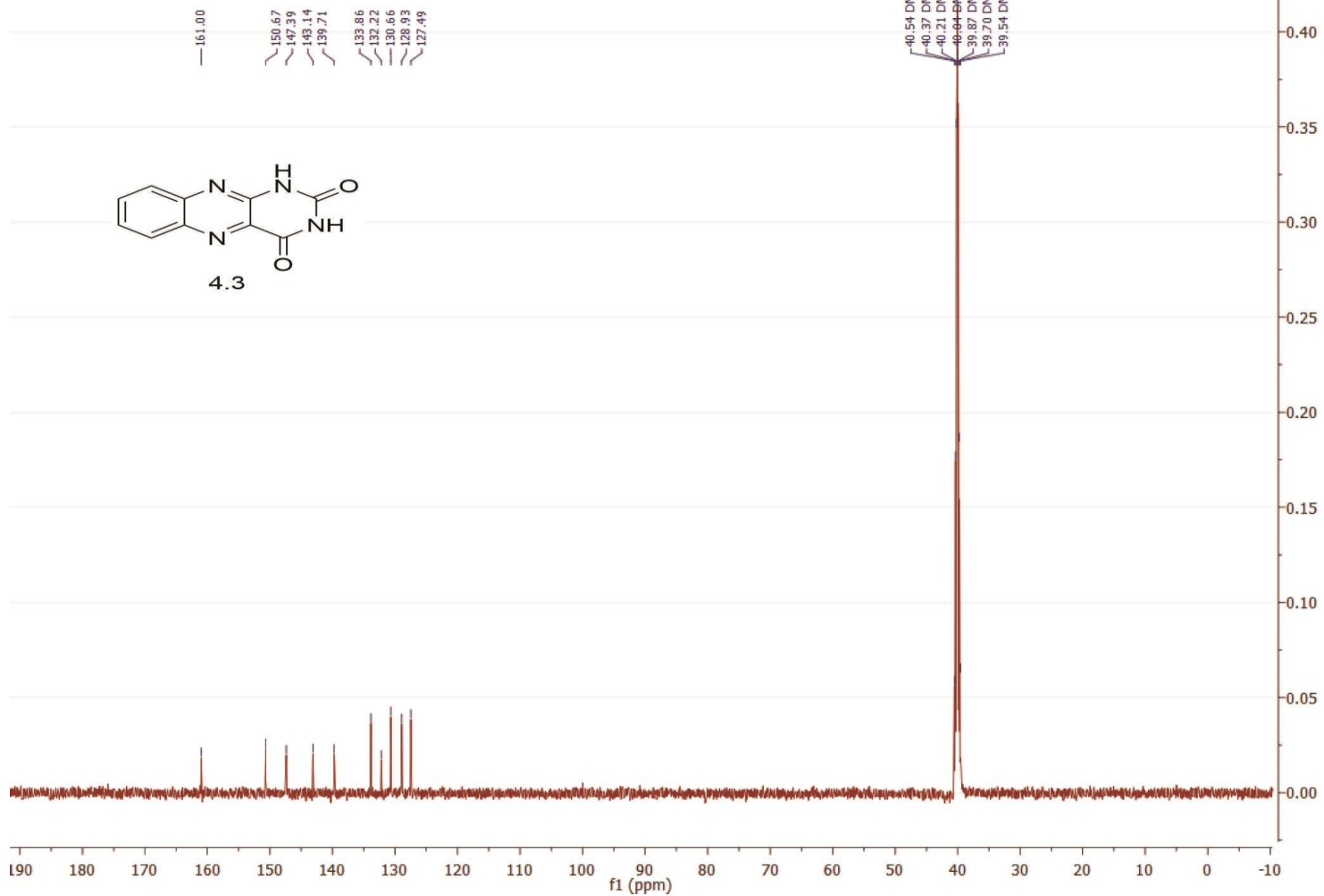




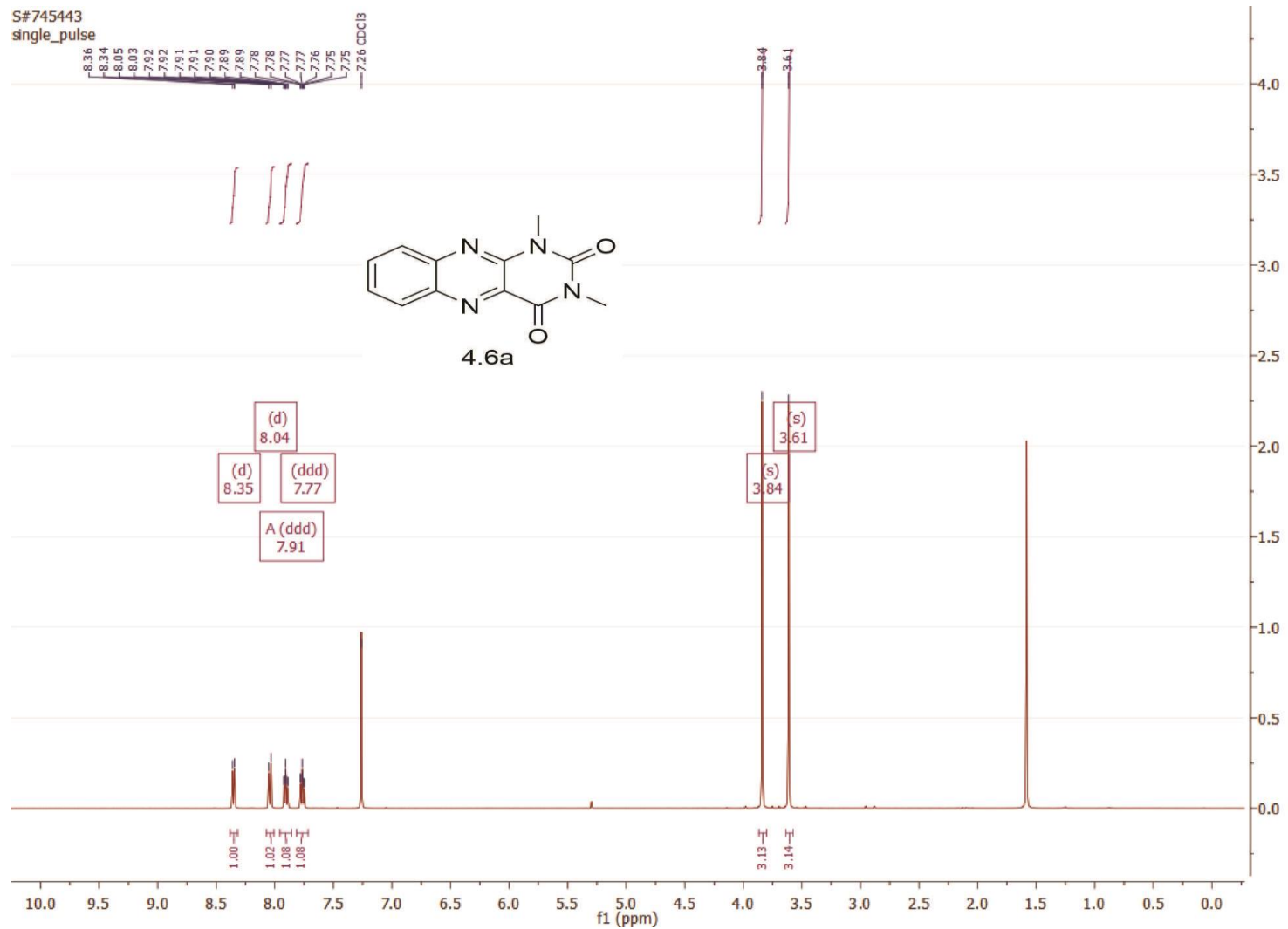
242



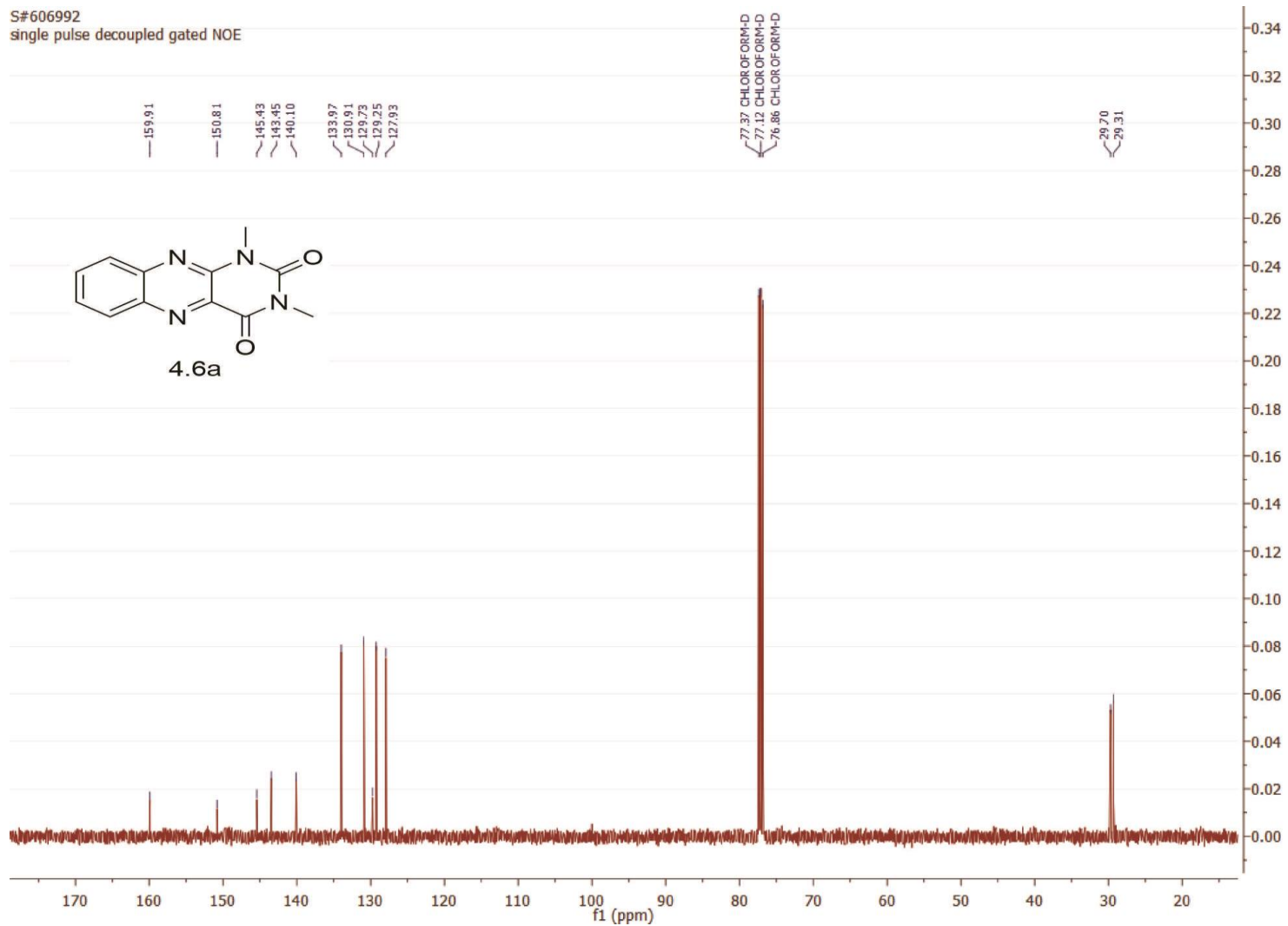
S#477648
single pulse decoupled gated NOE



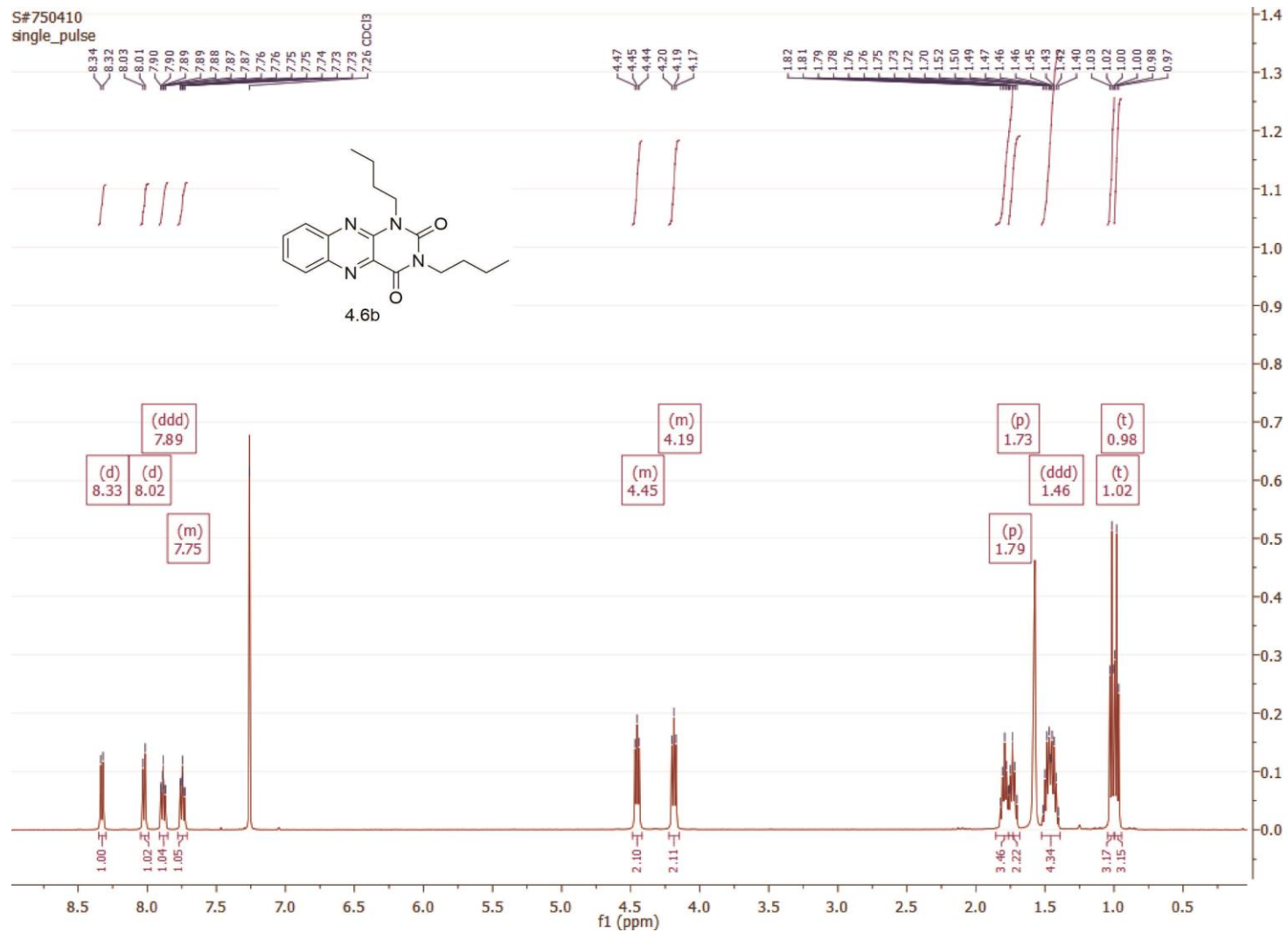
244



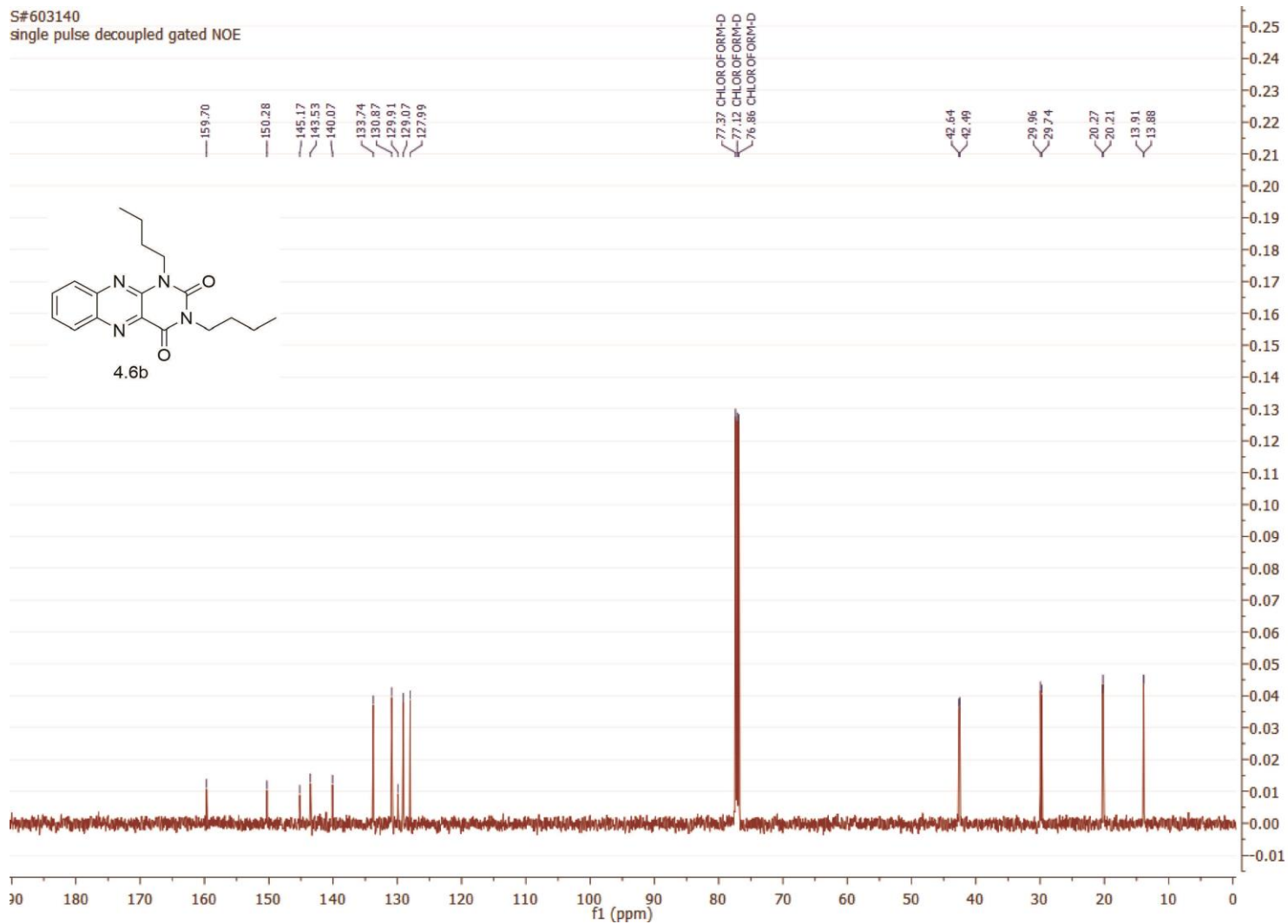
S#606992
single pulse decoupled gated NOE



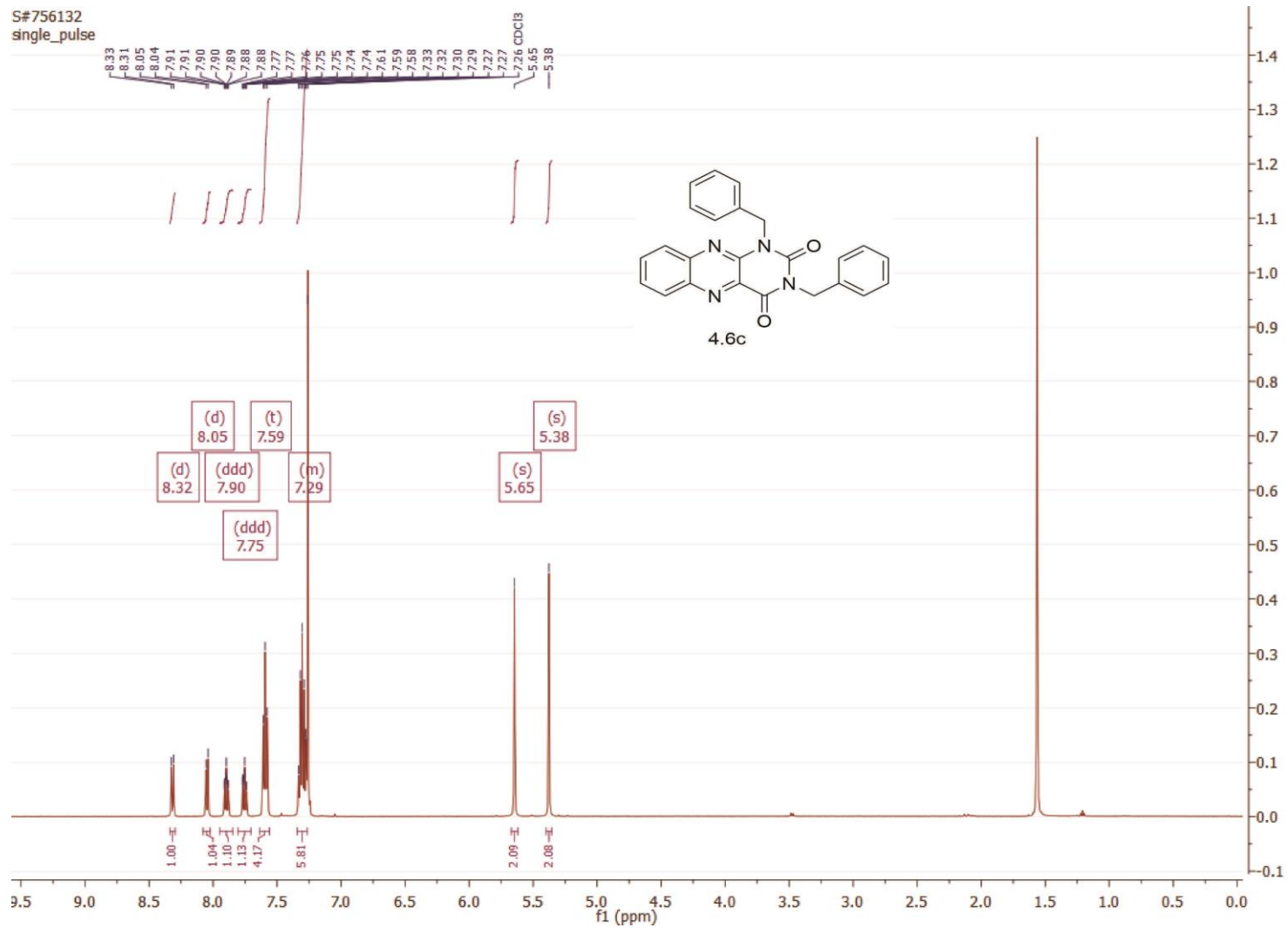
246



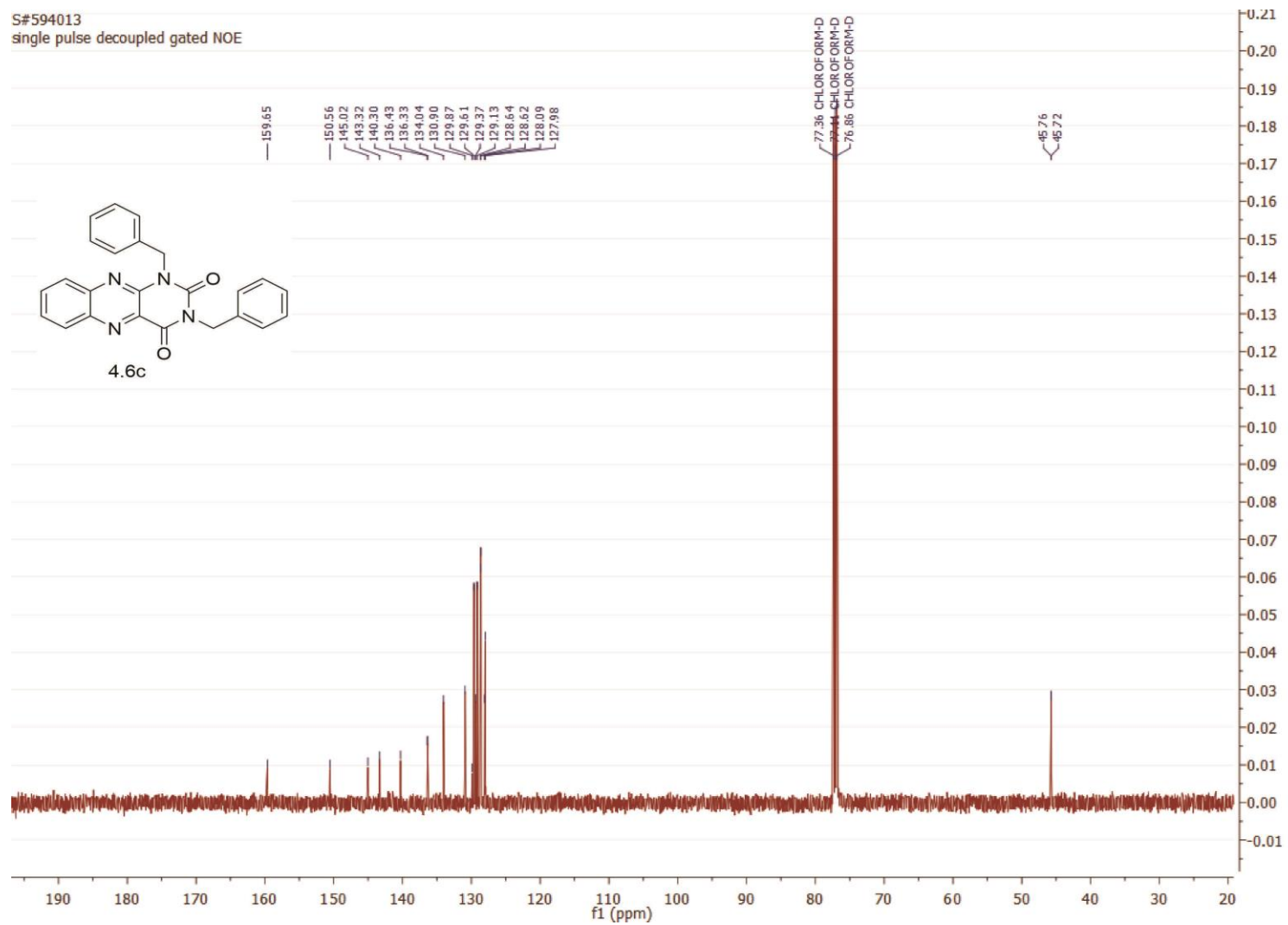
S#603140
single pulse decoupled gated NOE



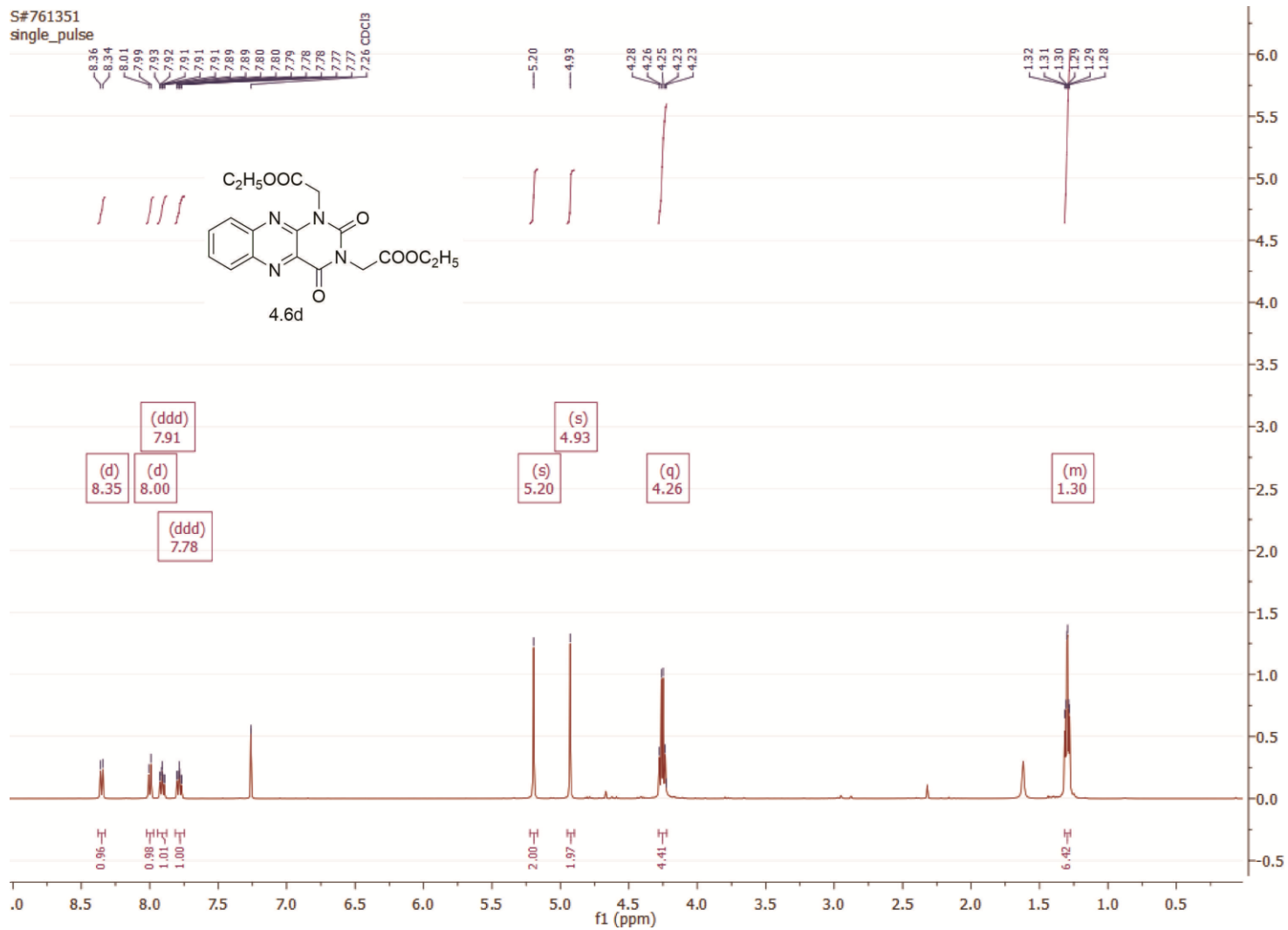
248



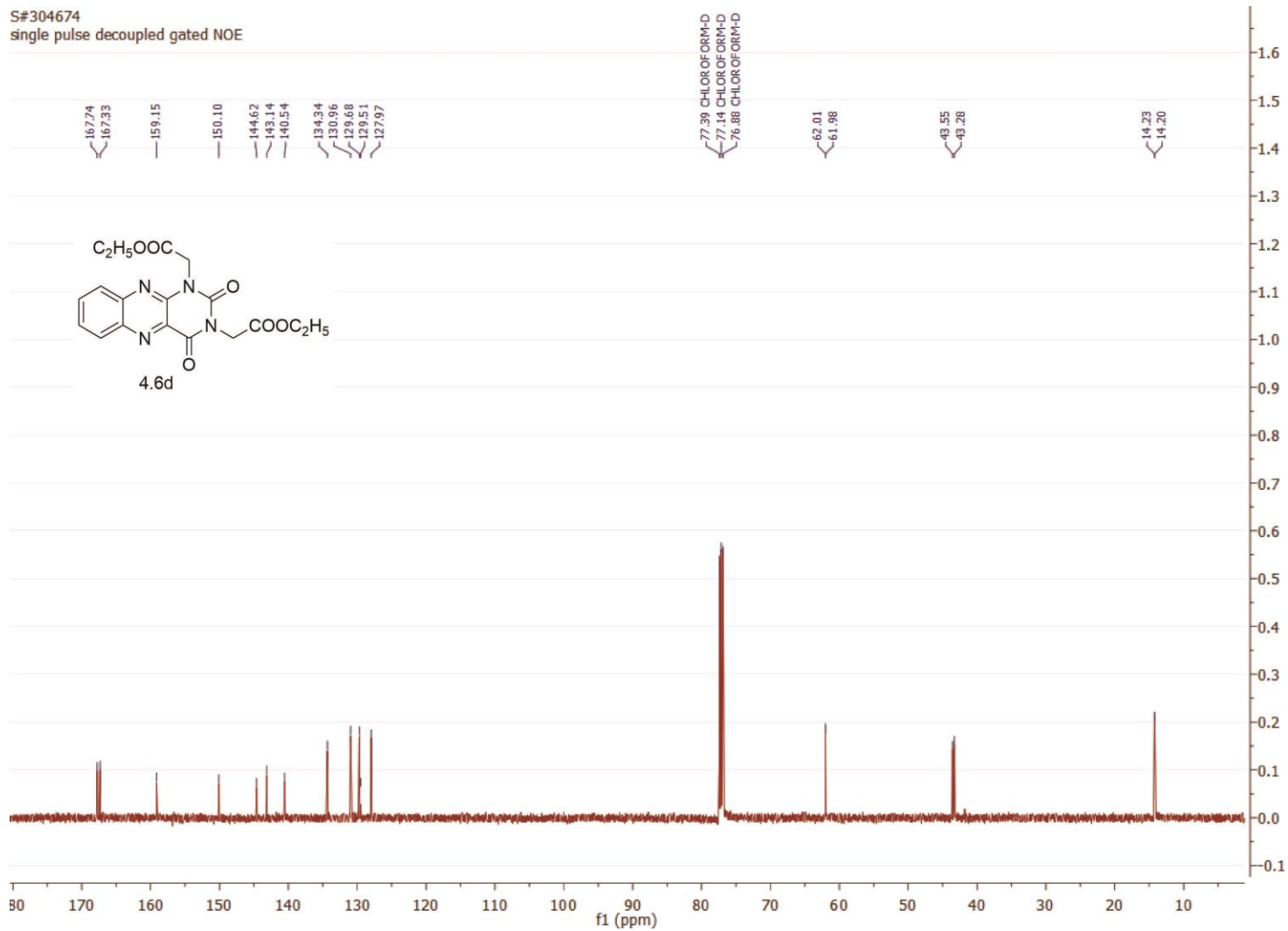
S#594013
single pulse decoupled gated NOE



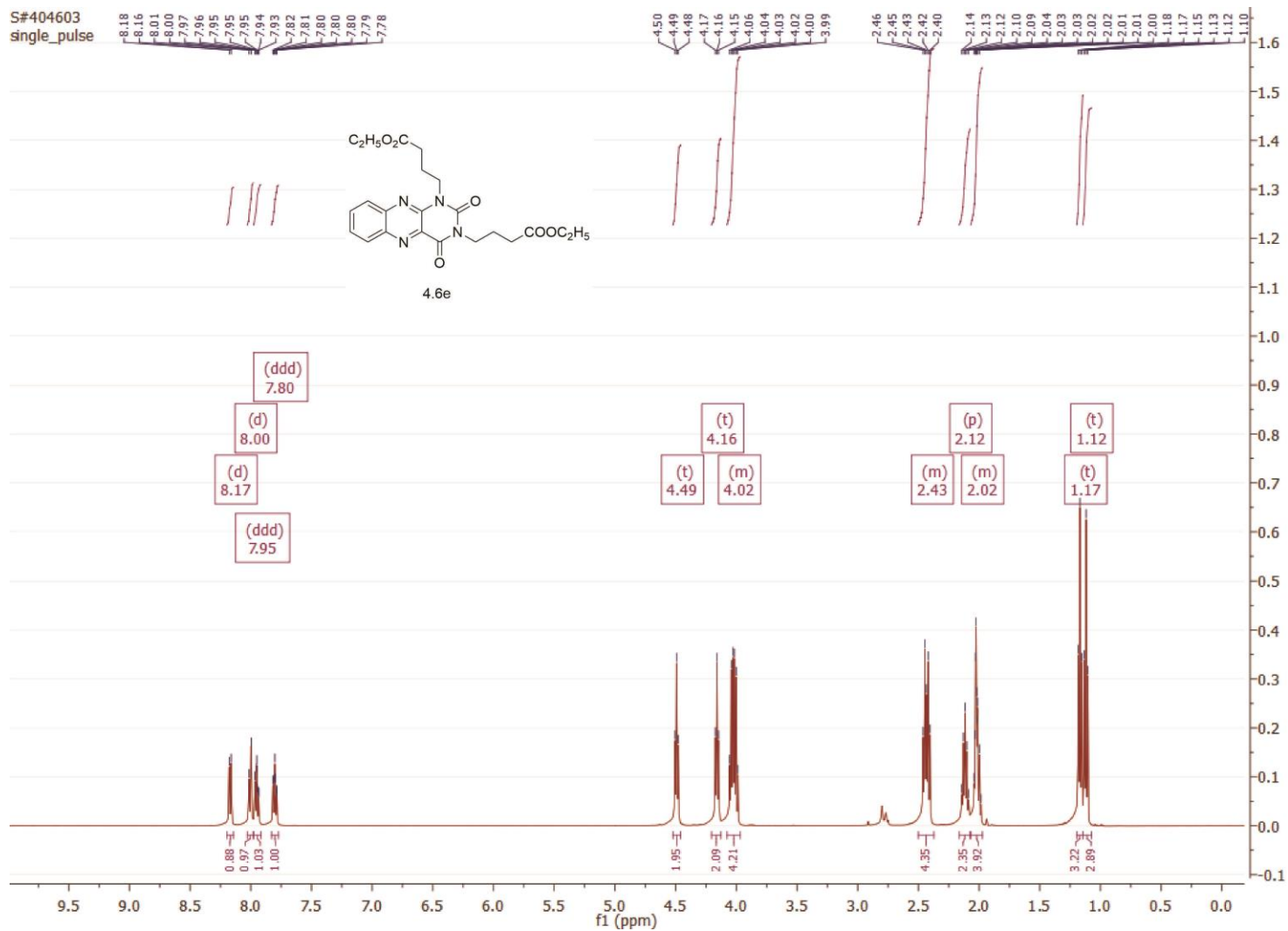
250



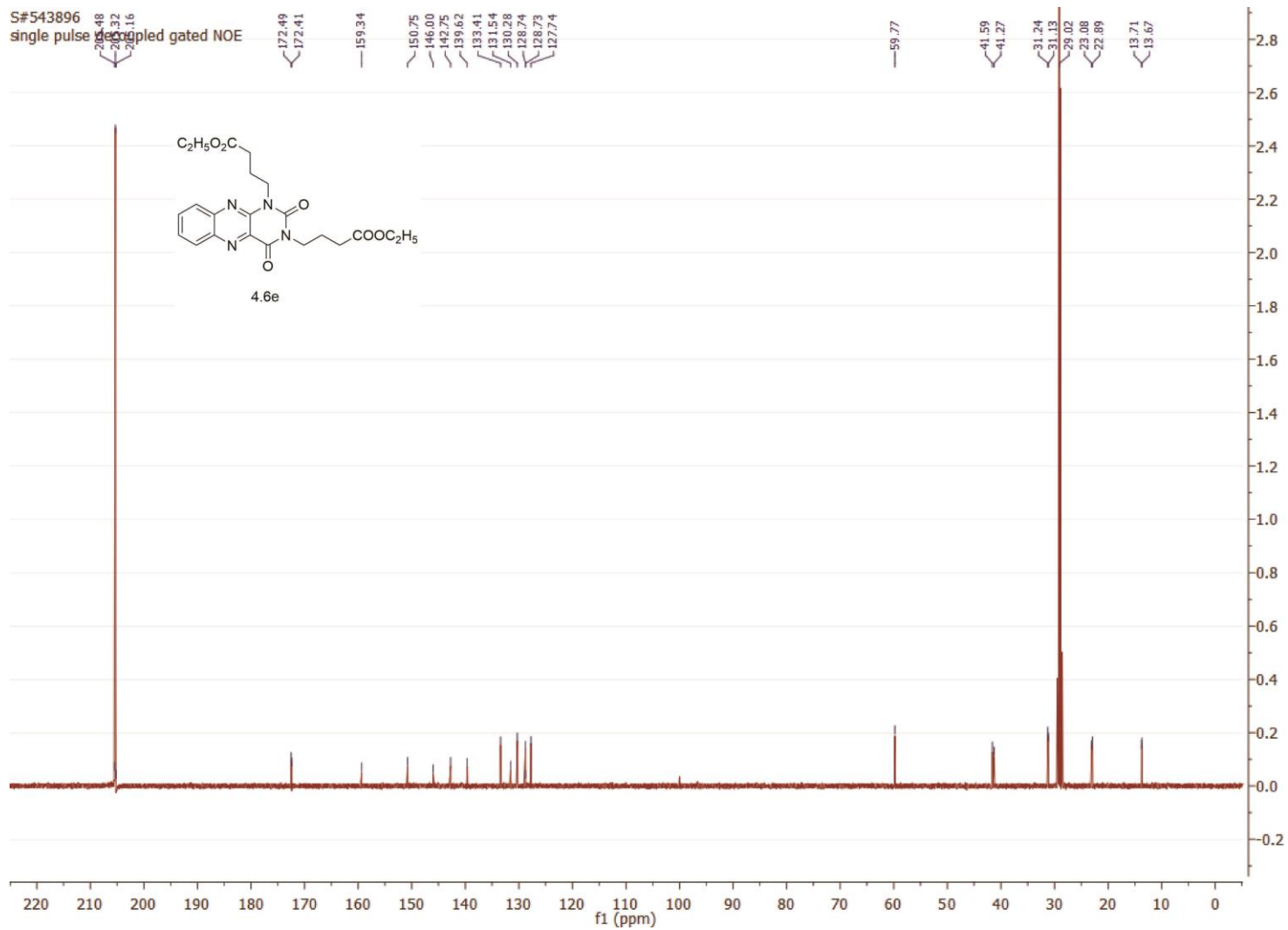
S#304674
single pulse decoupled gated NOE



252

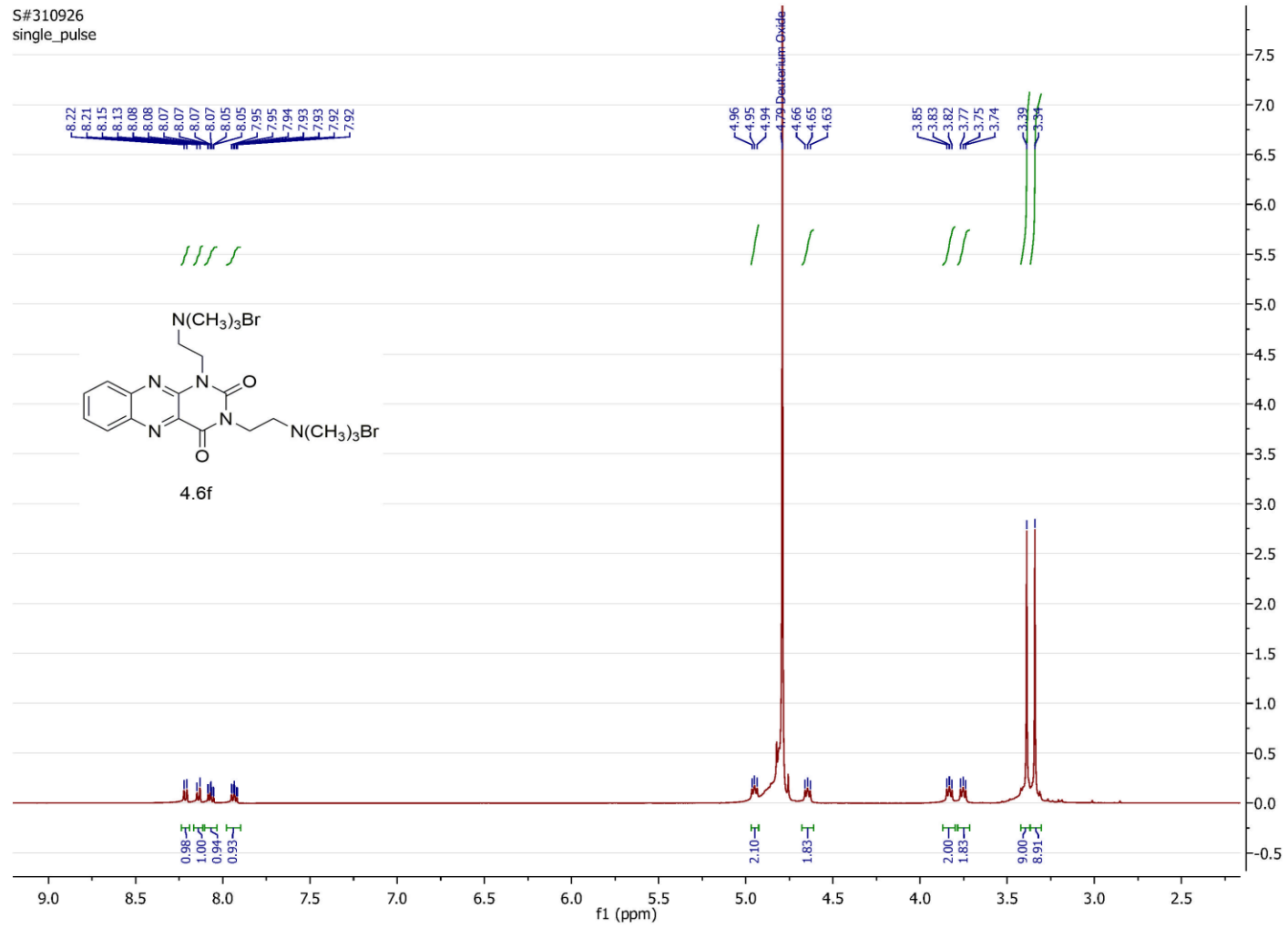


253

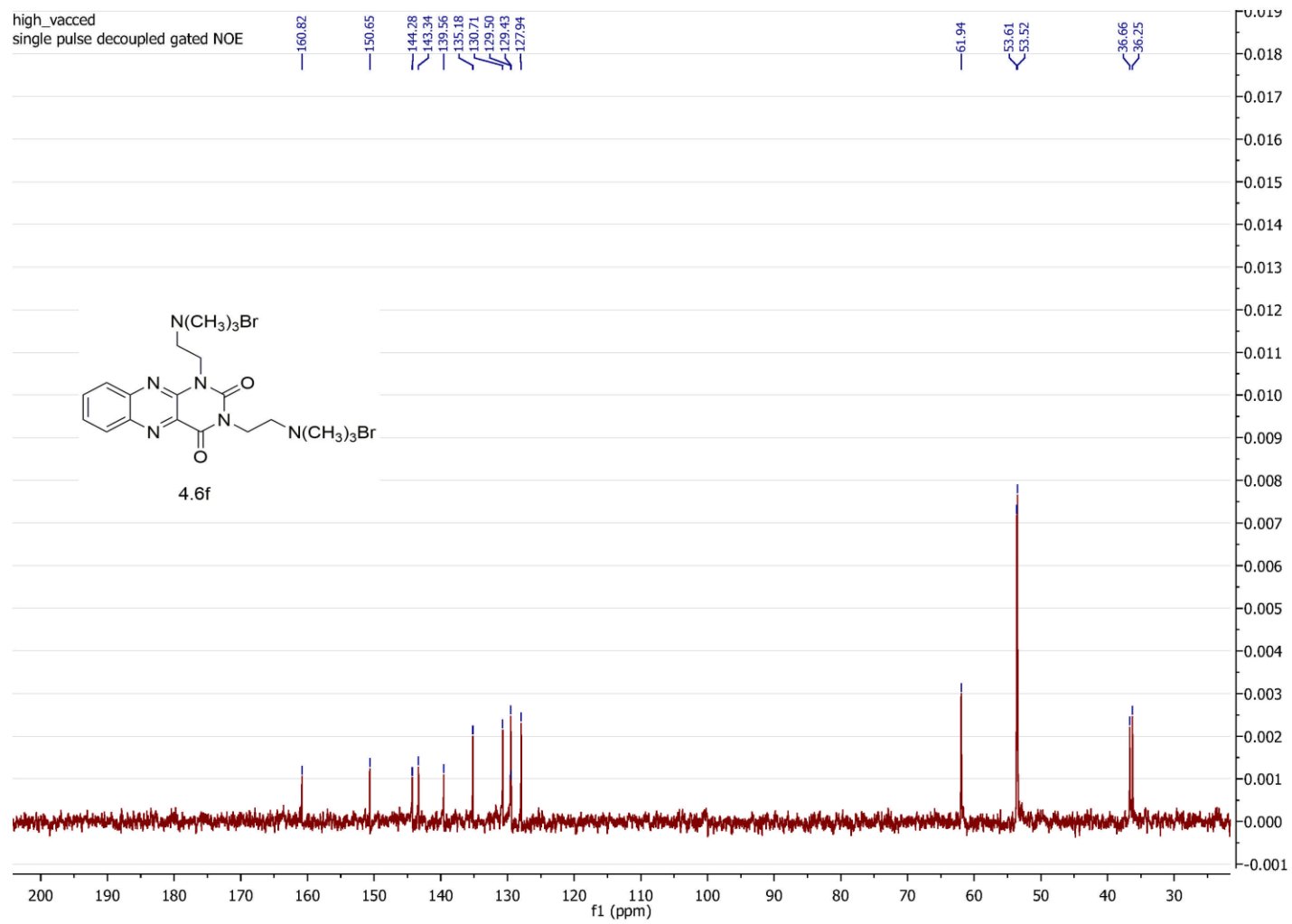


254

S#310926
single_pulse

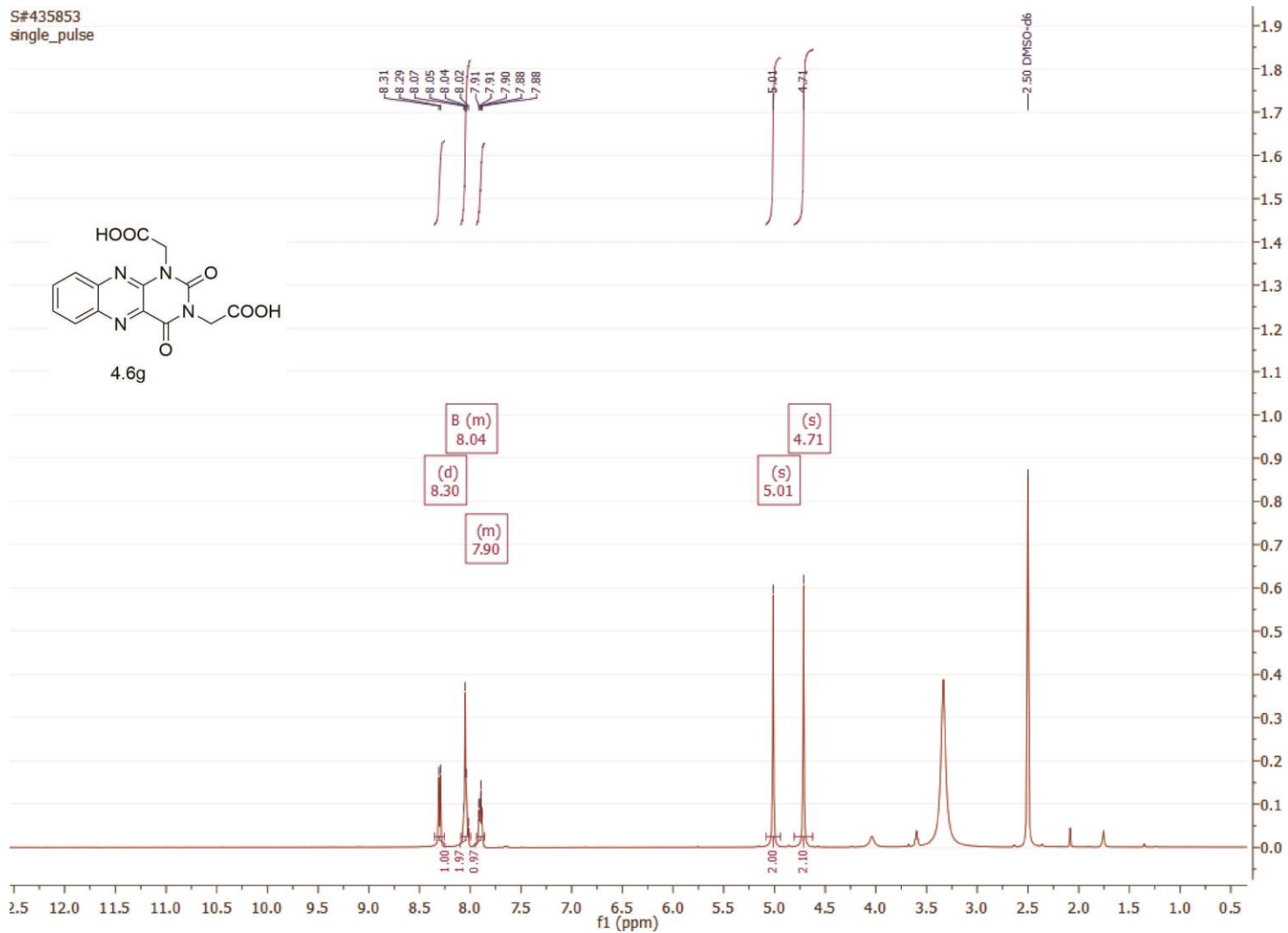
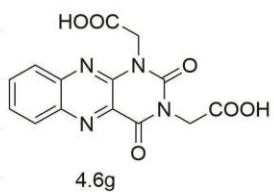


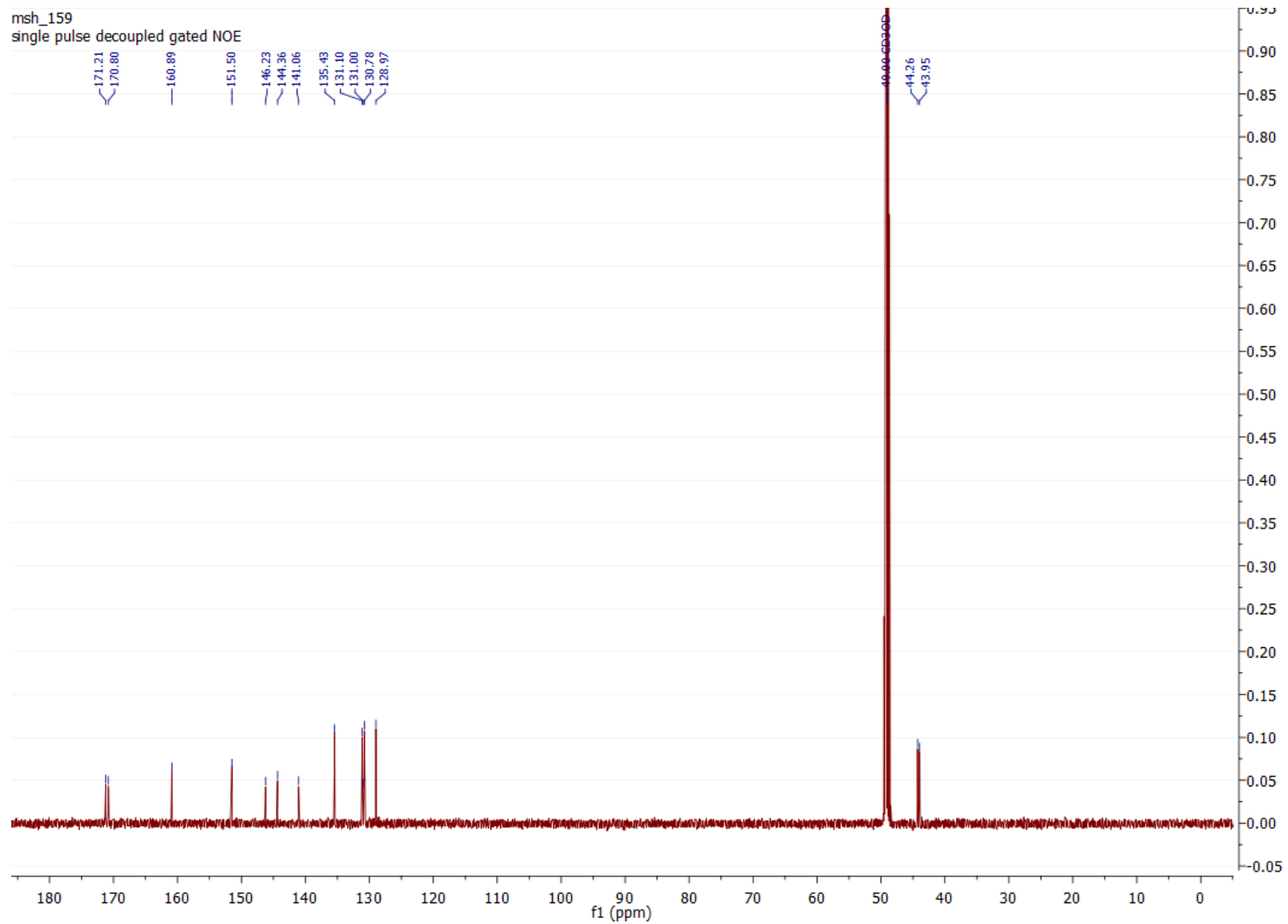
255



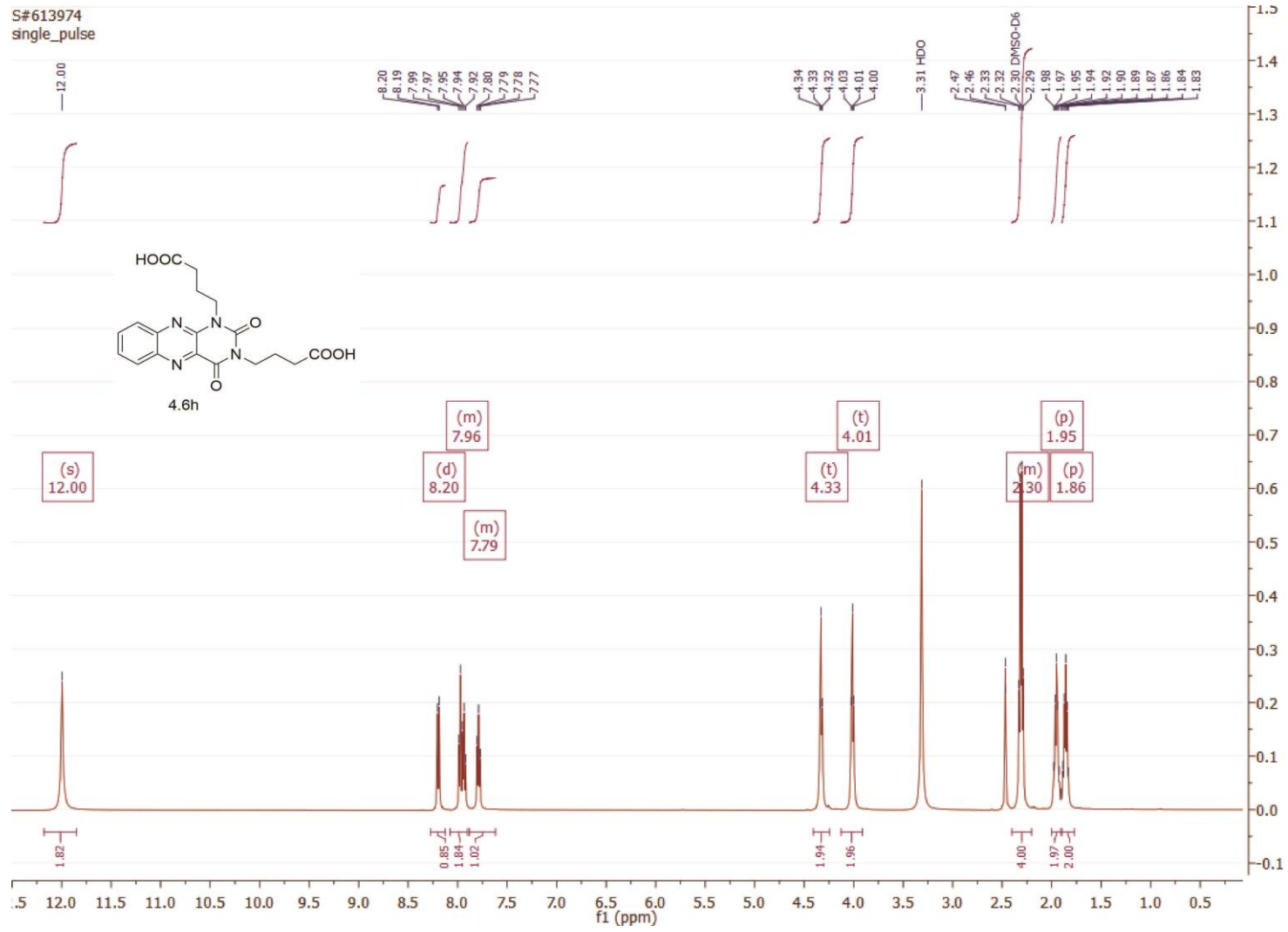
256

S#435853
single_pulse

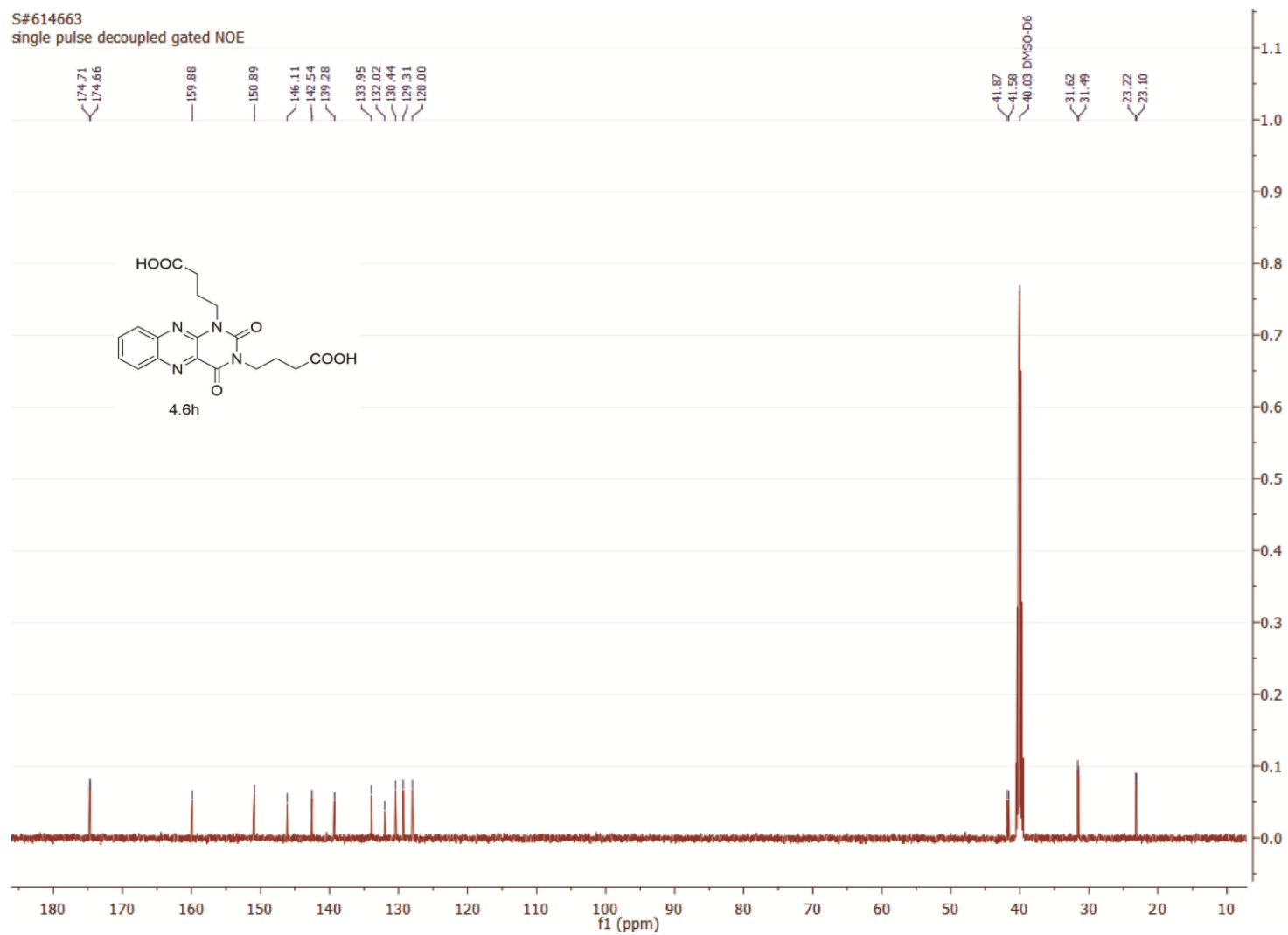




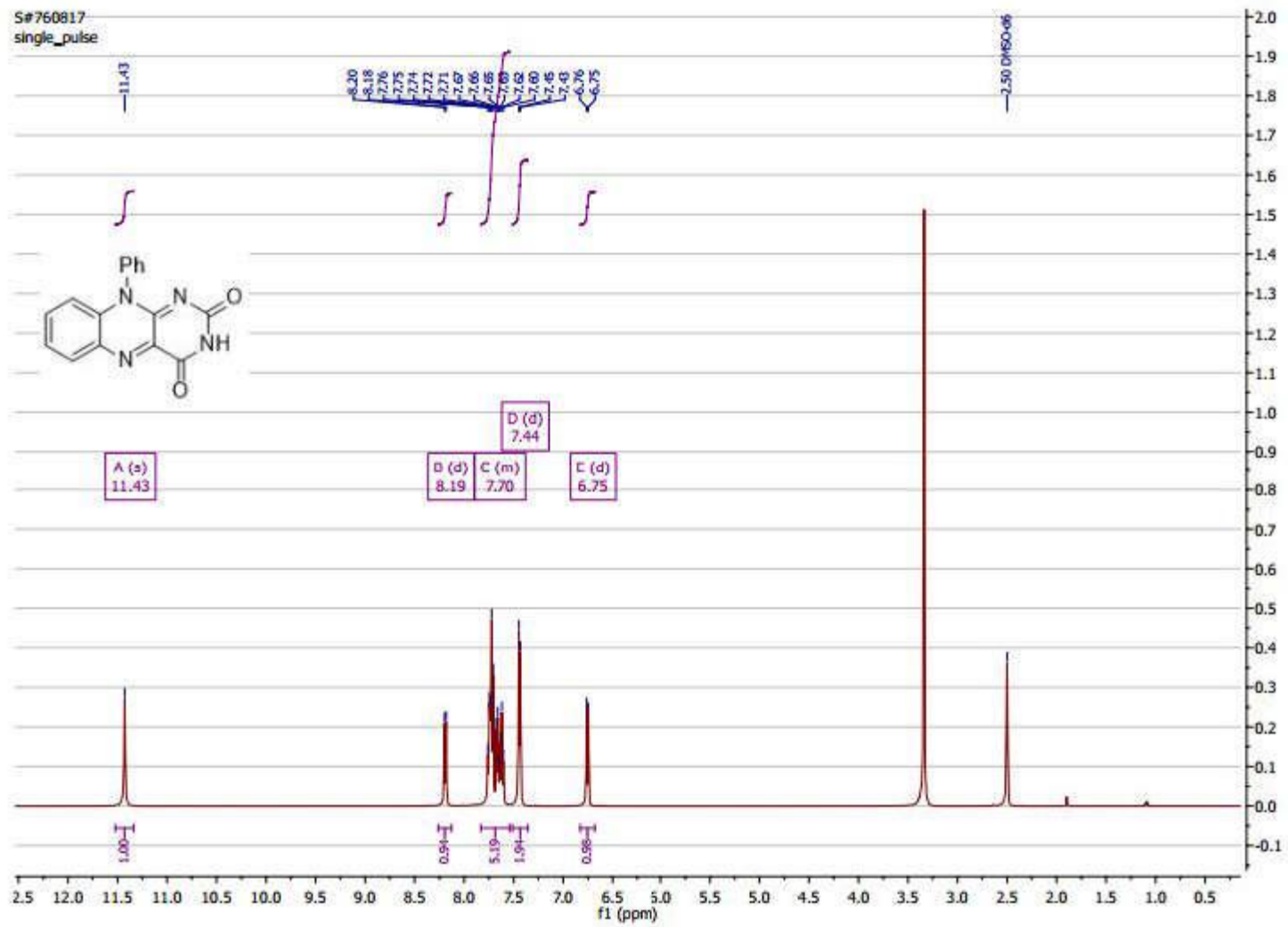
258



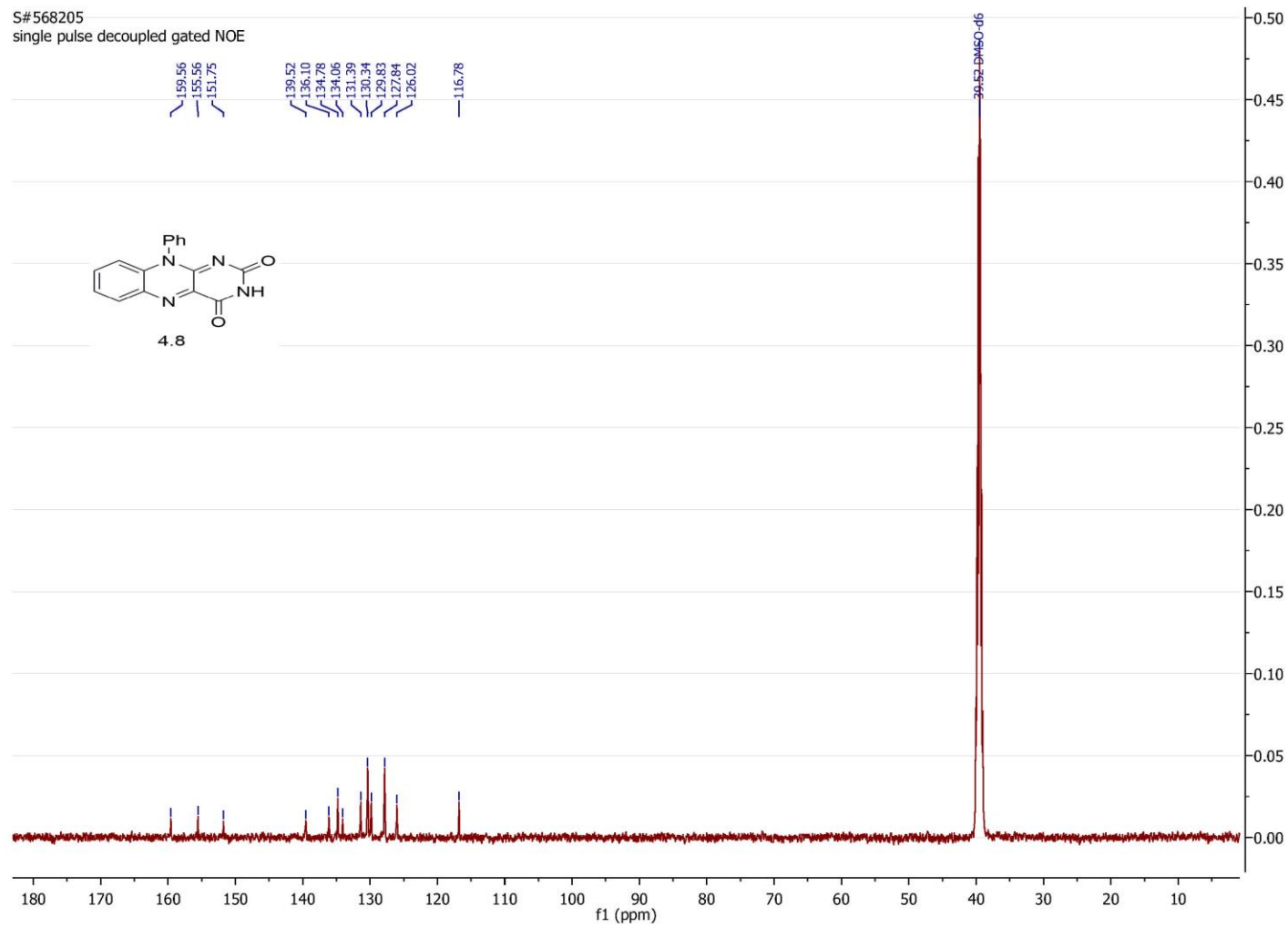
S#614663
single pulse decoupled gated NOE

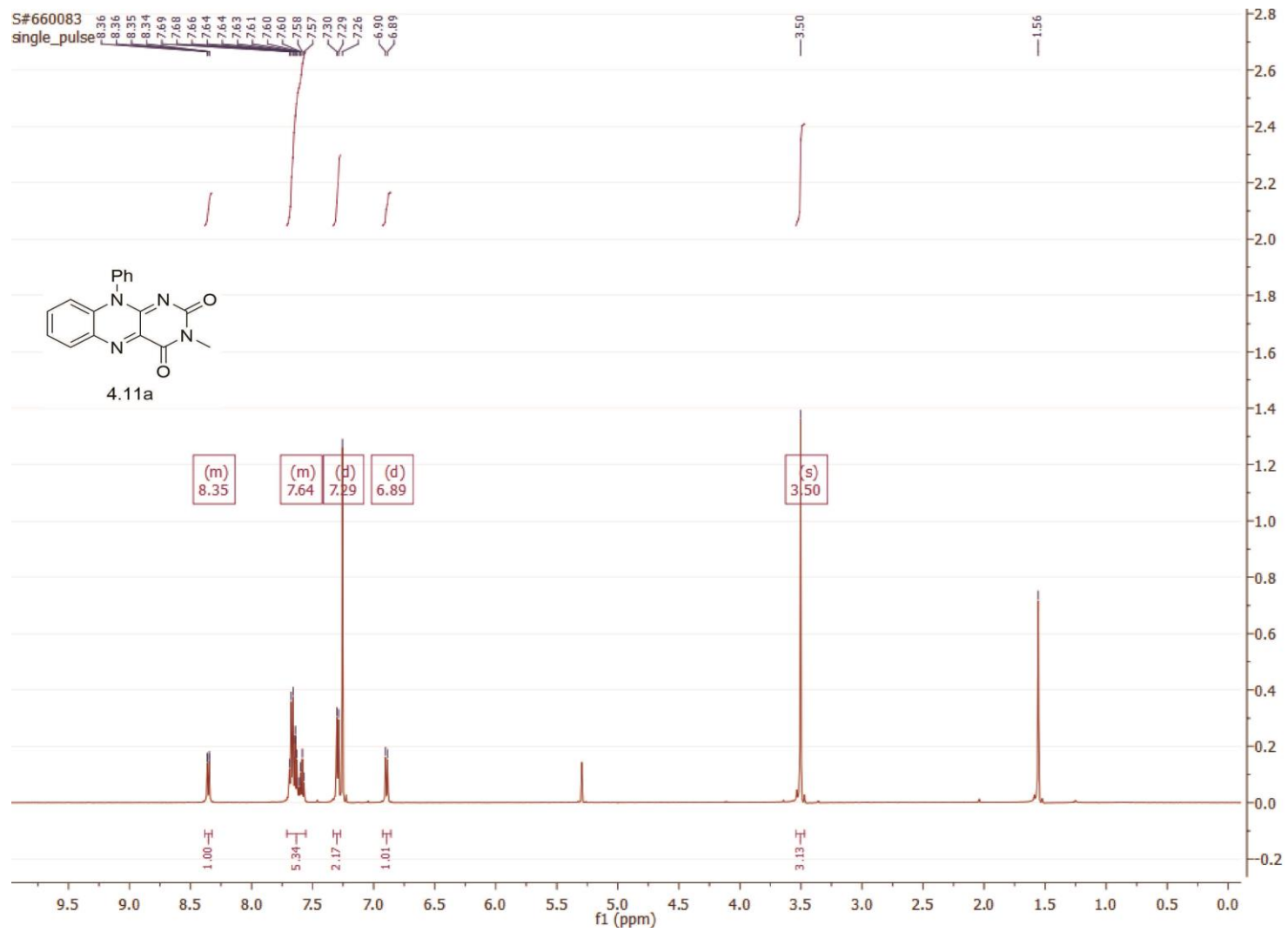


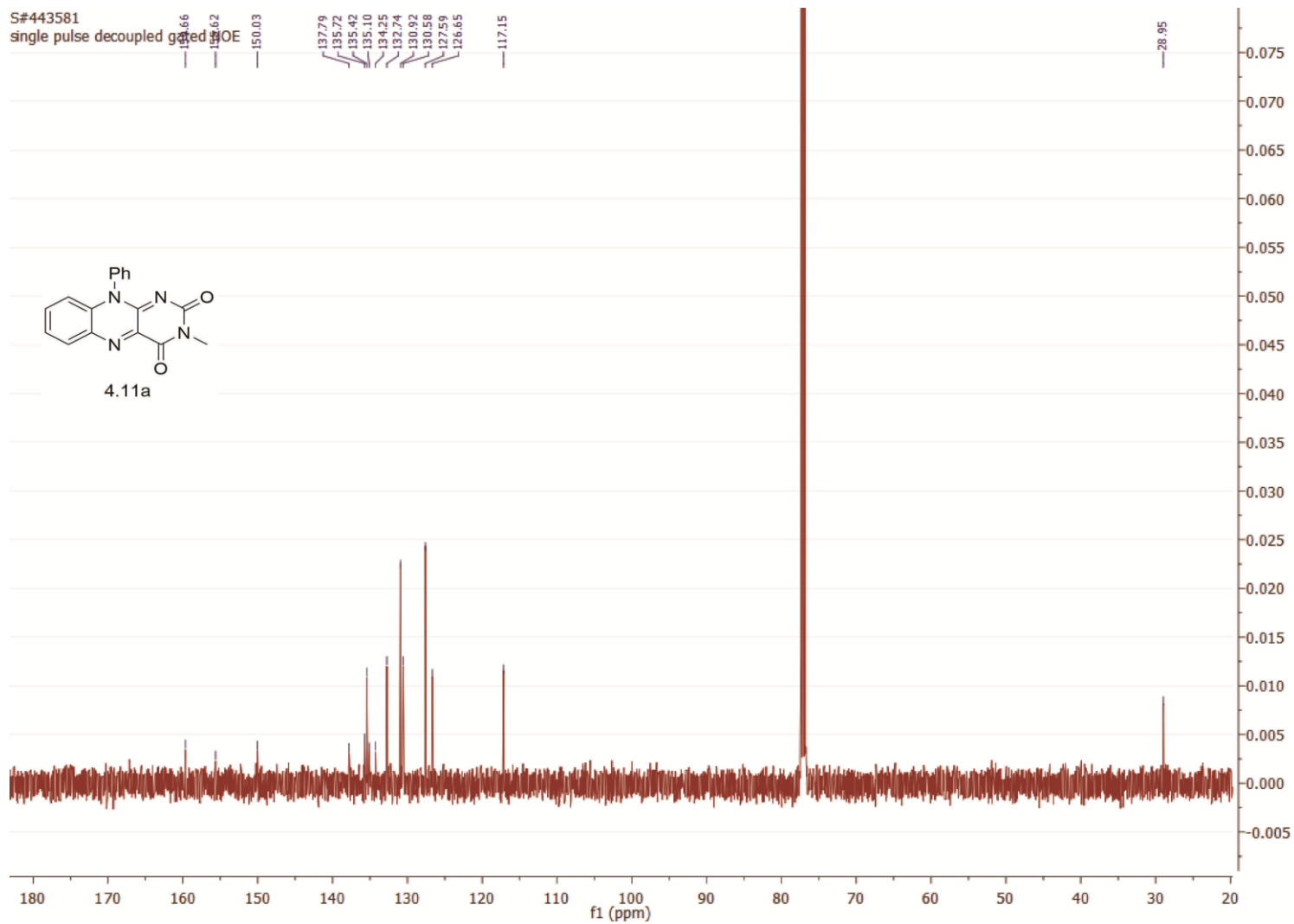
259



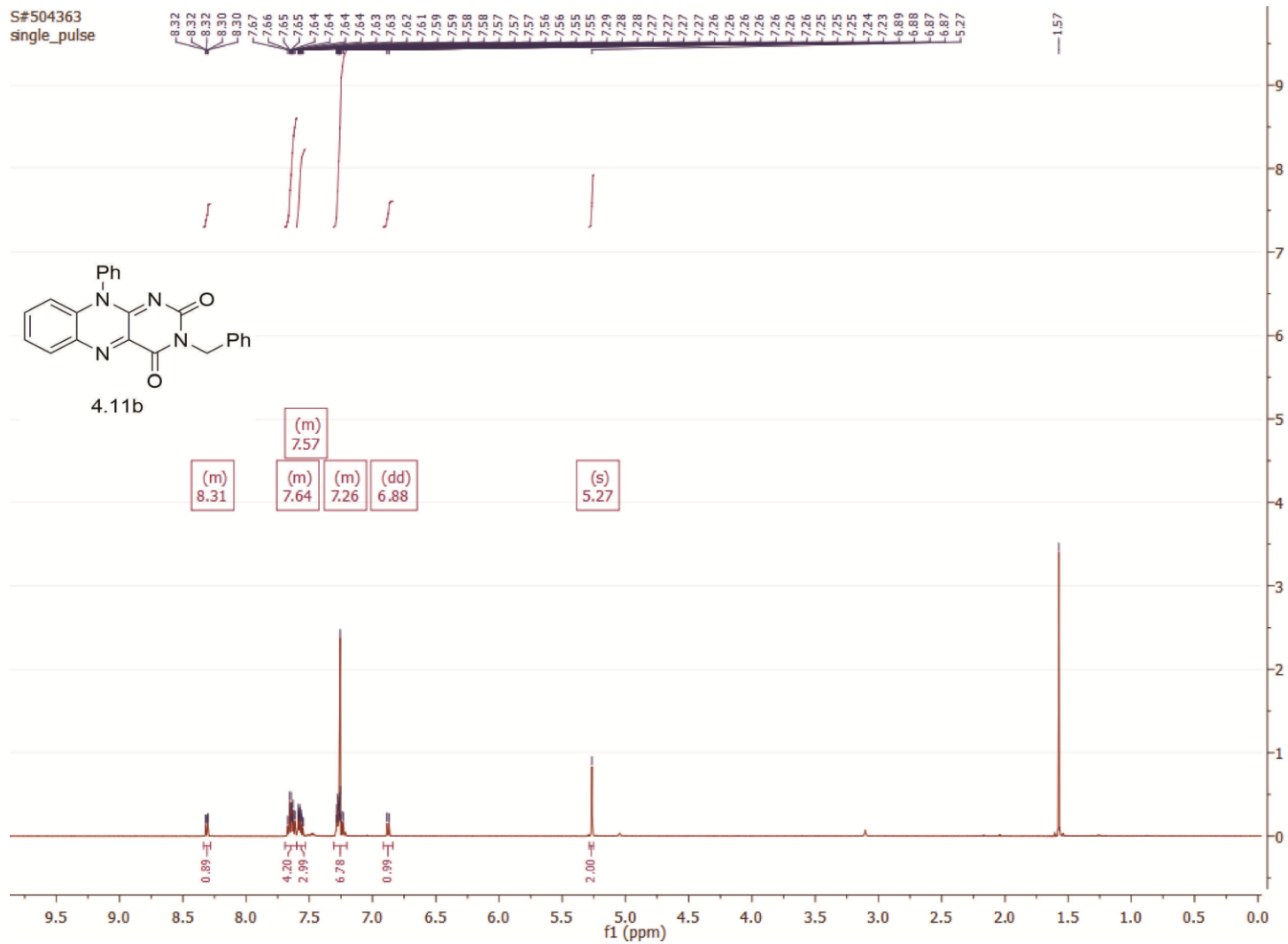
S#568205
single pulse decoupled gated NOE



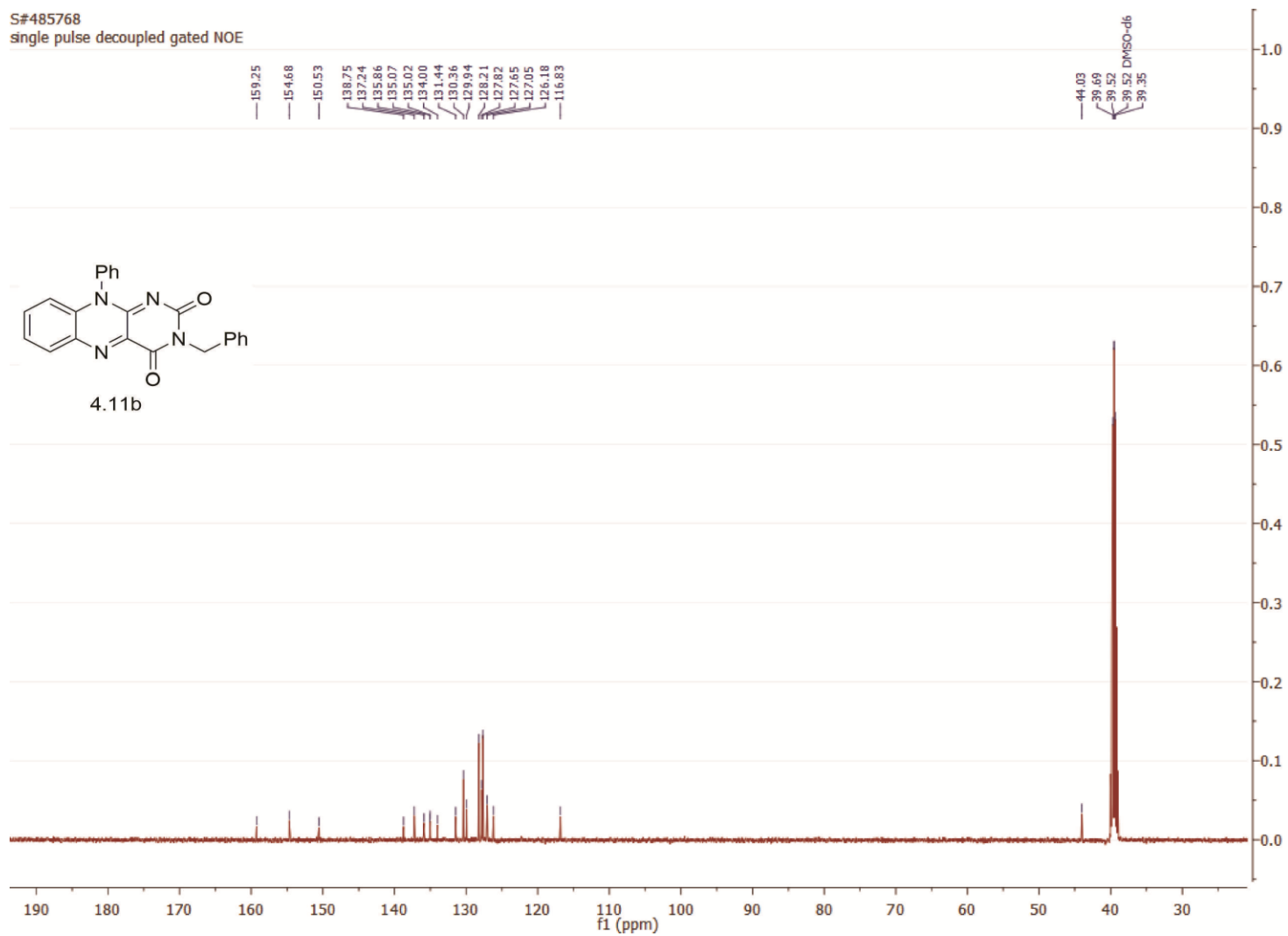


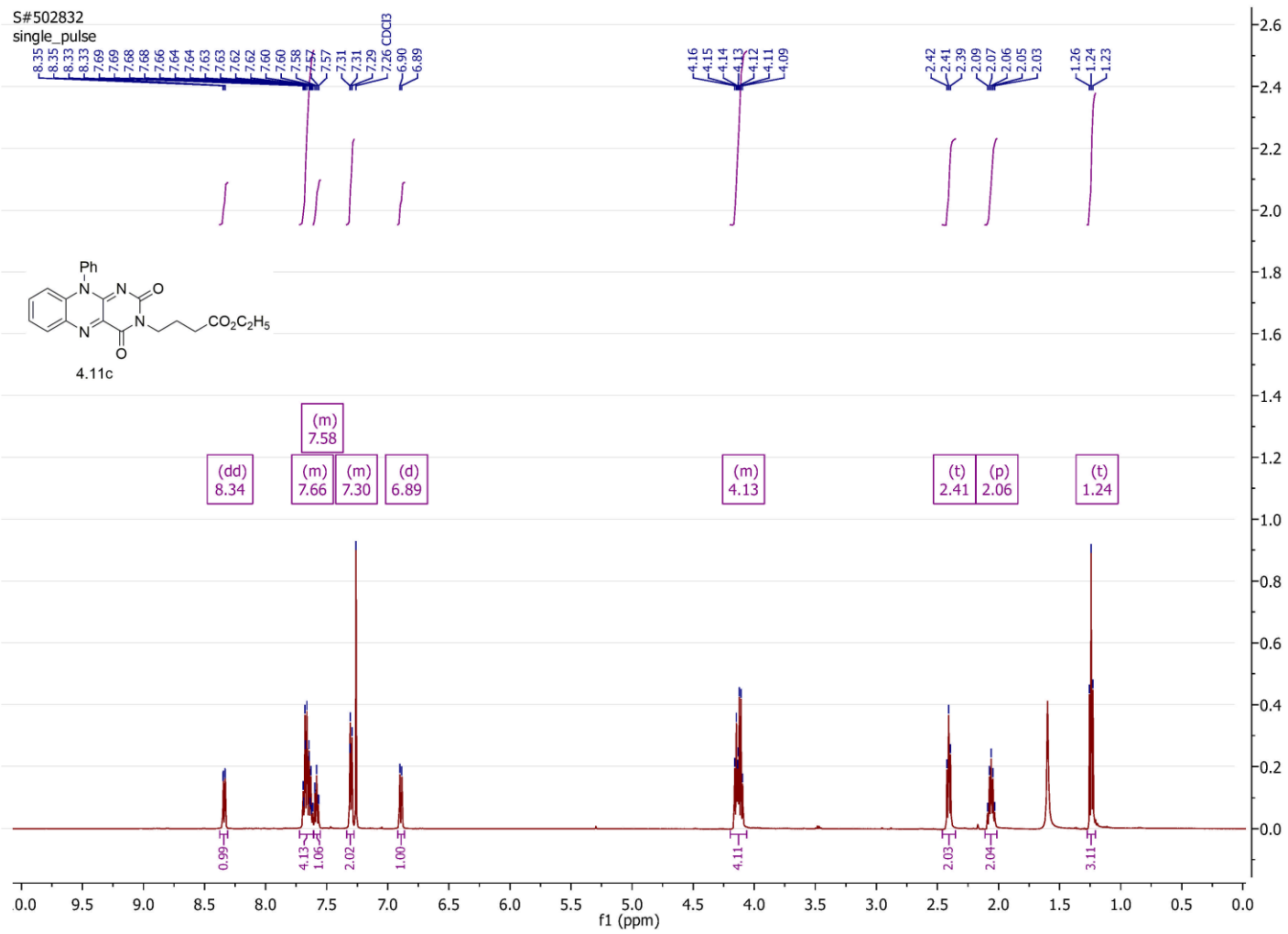


264

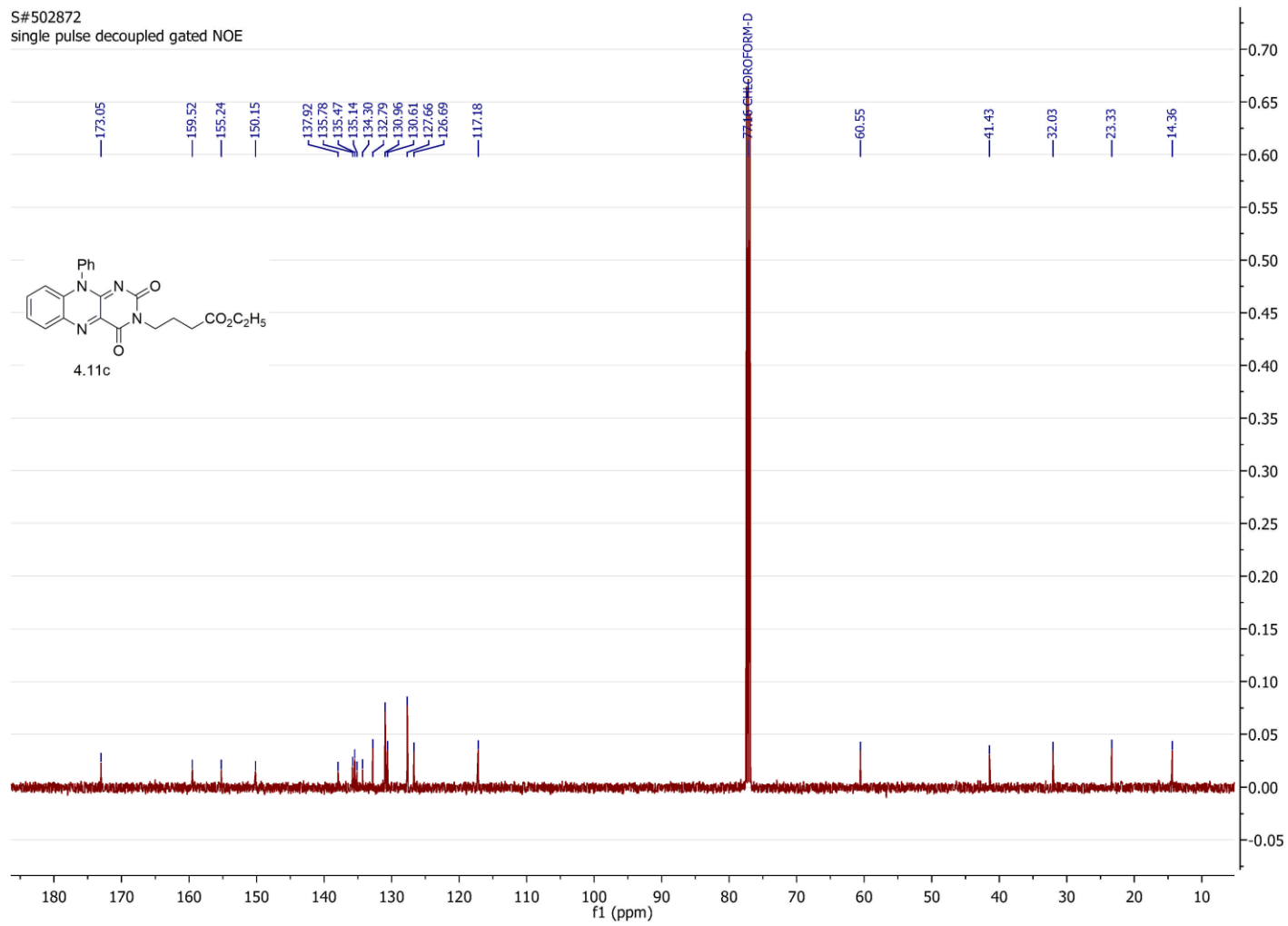


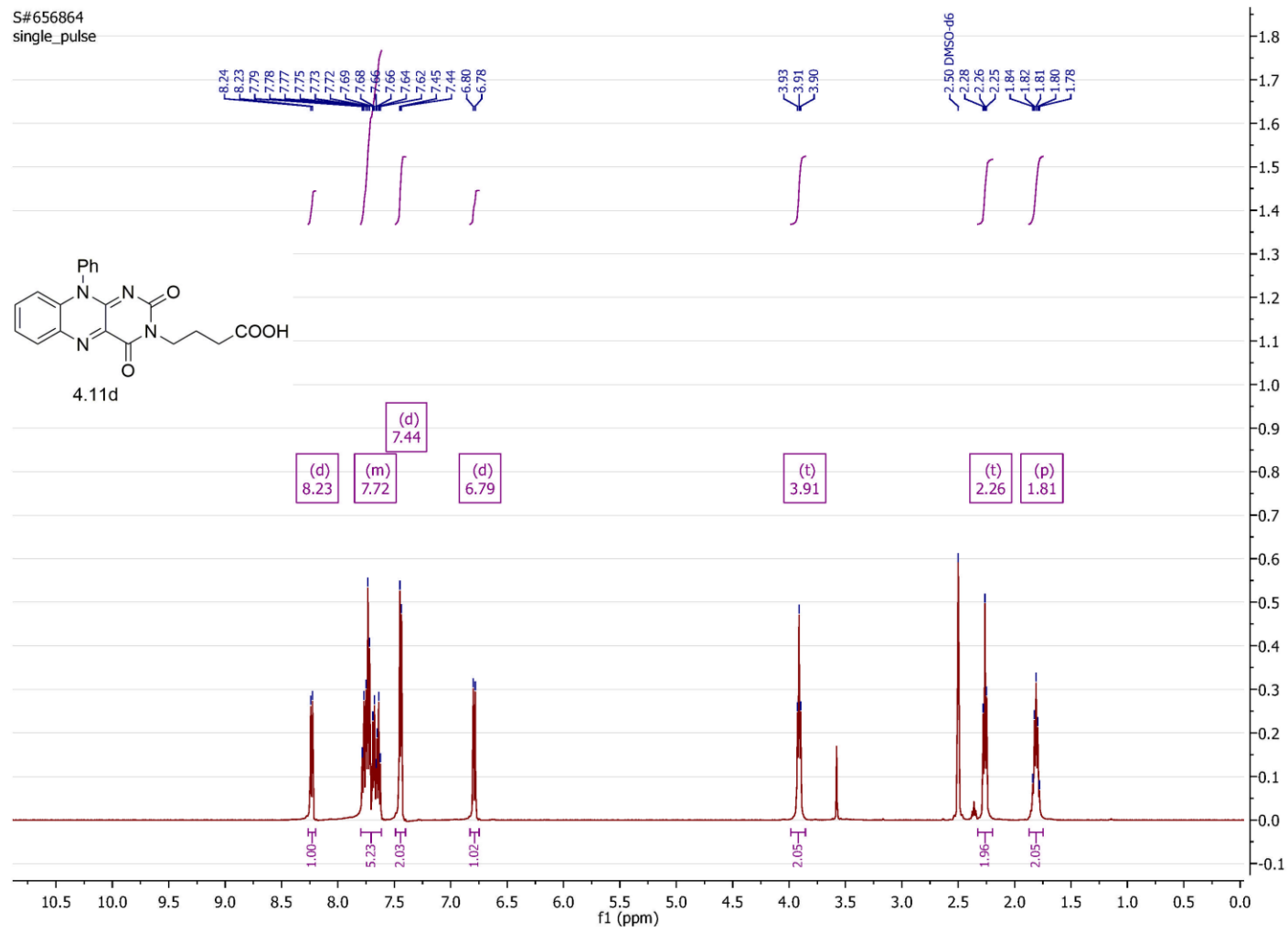
S#485768
single pulse decoupled gated NOE

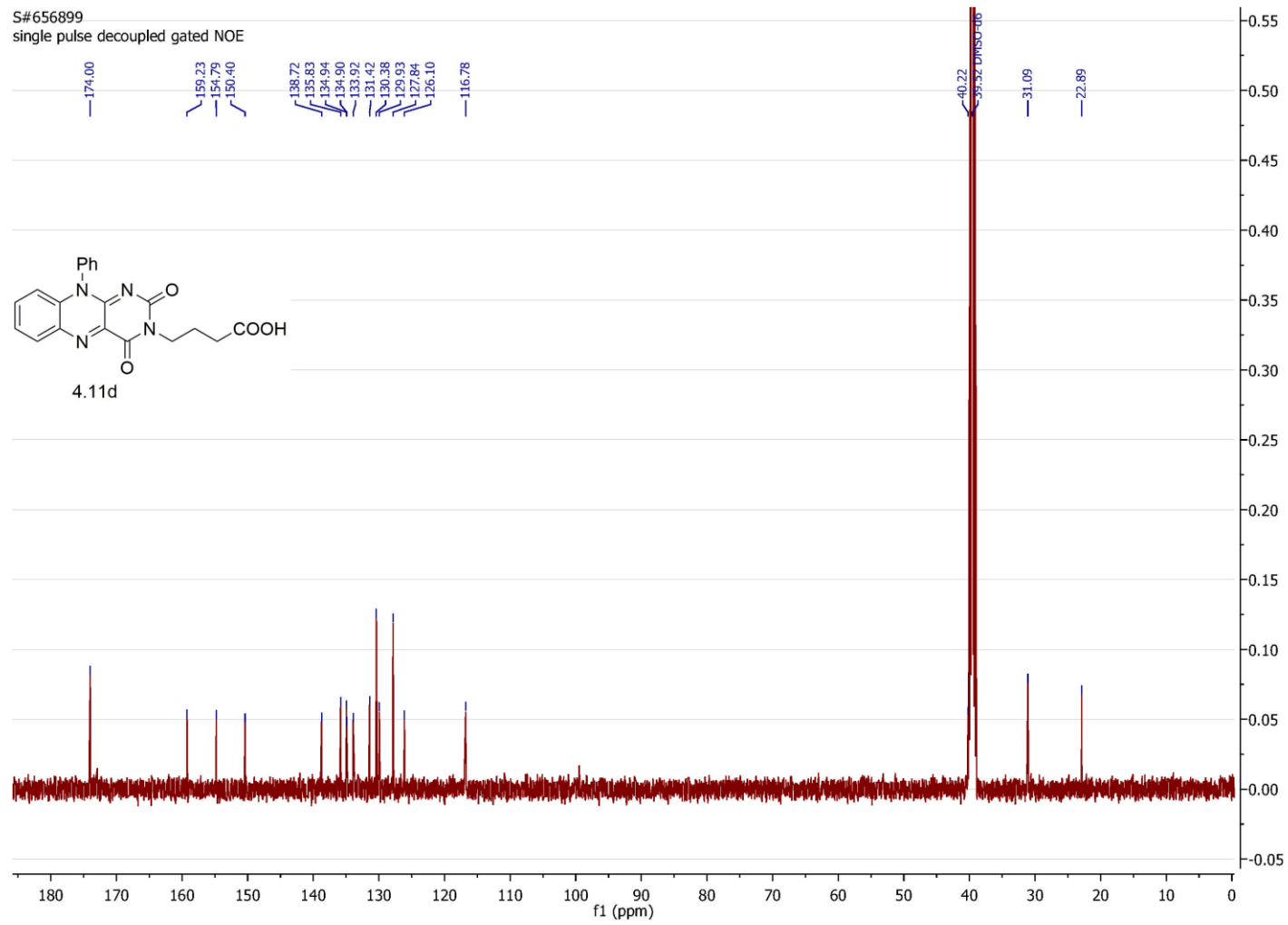




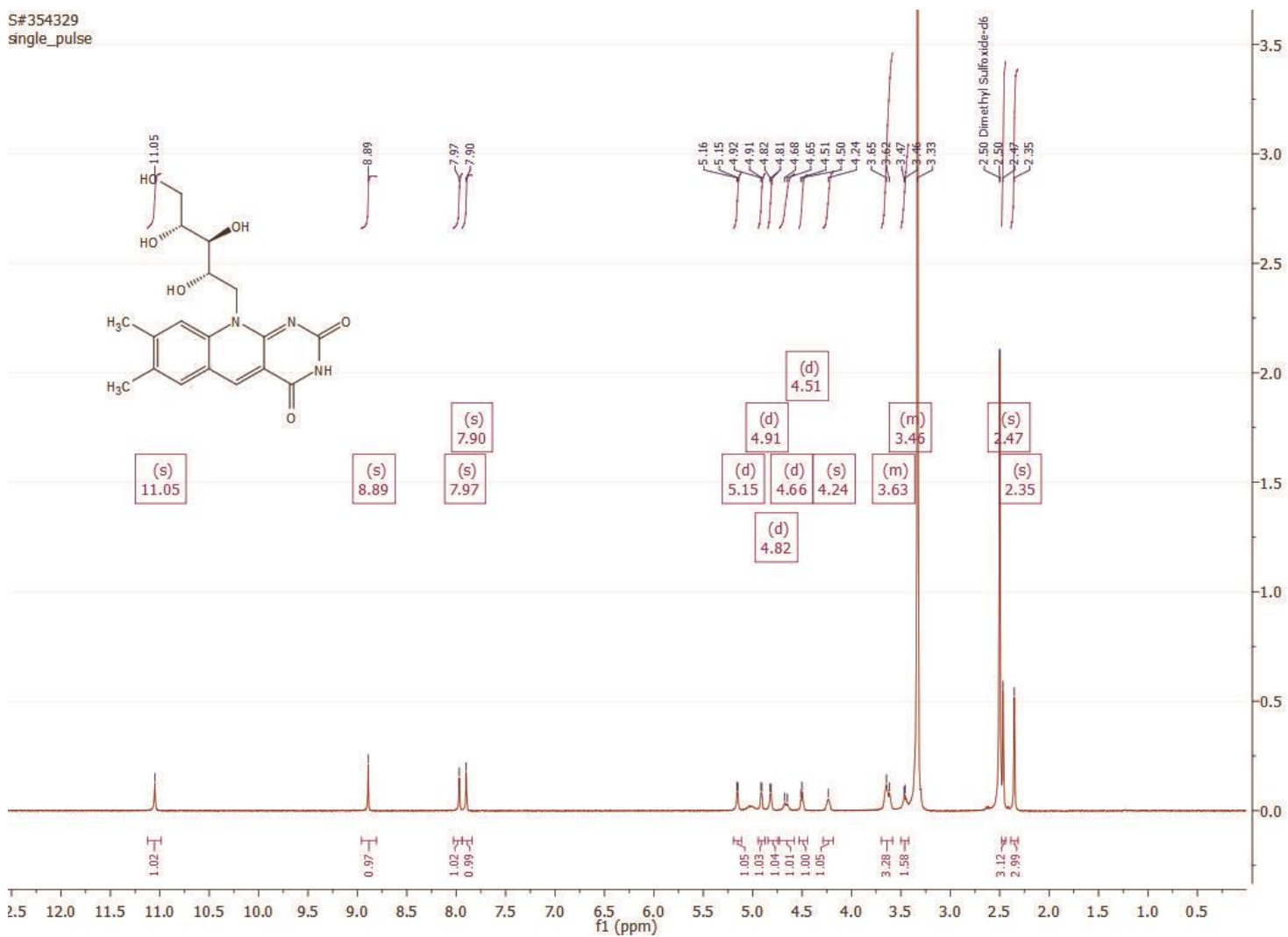
S#502872
single pulse decoupled gated NOE





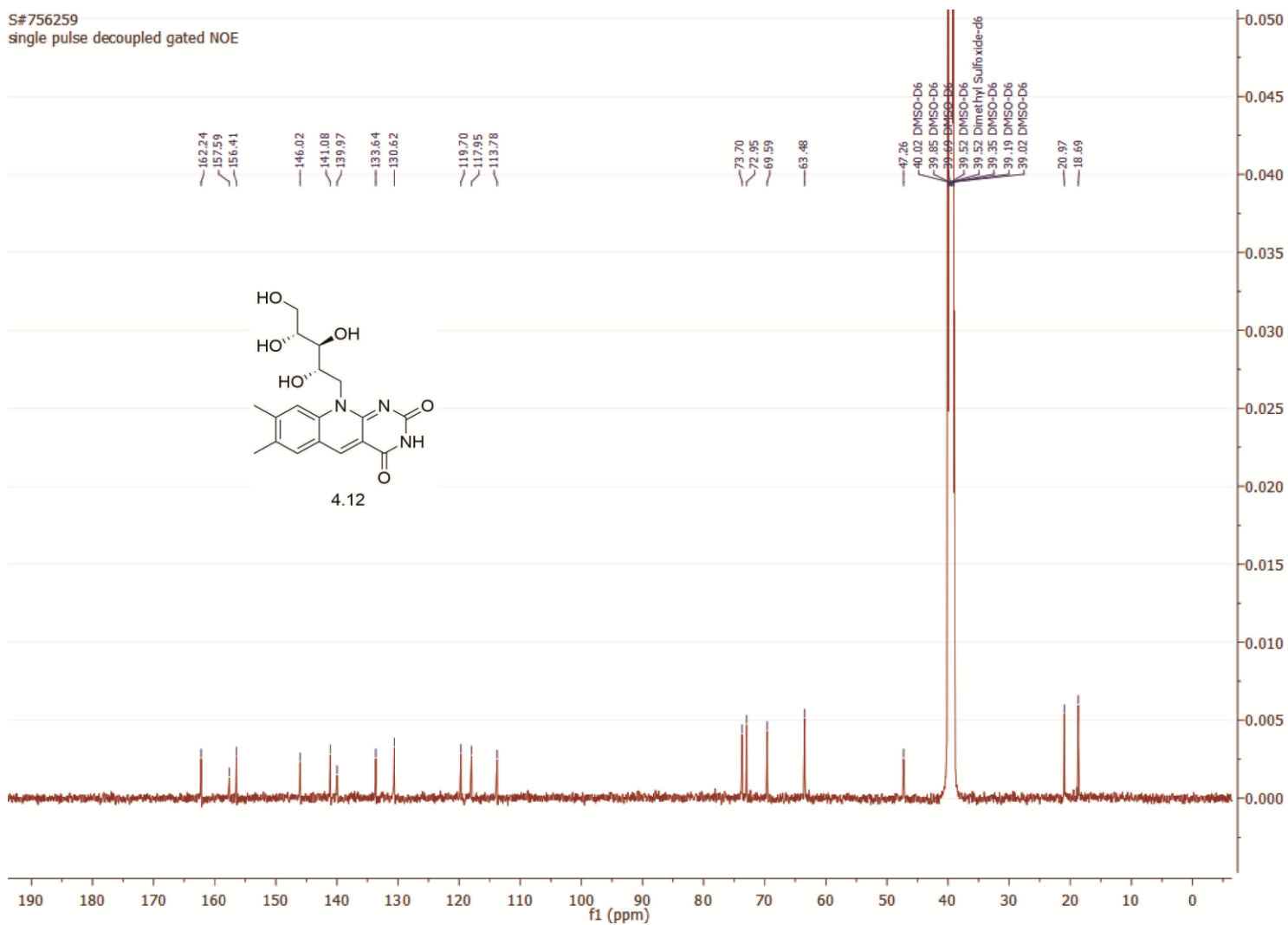


S#354329
single_pulse



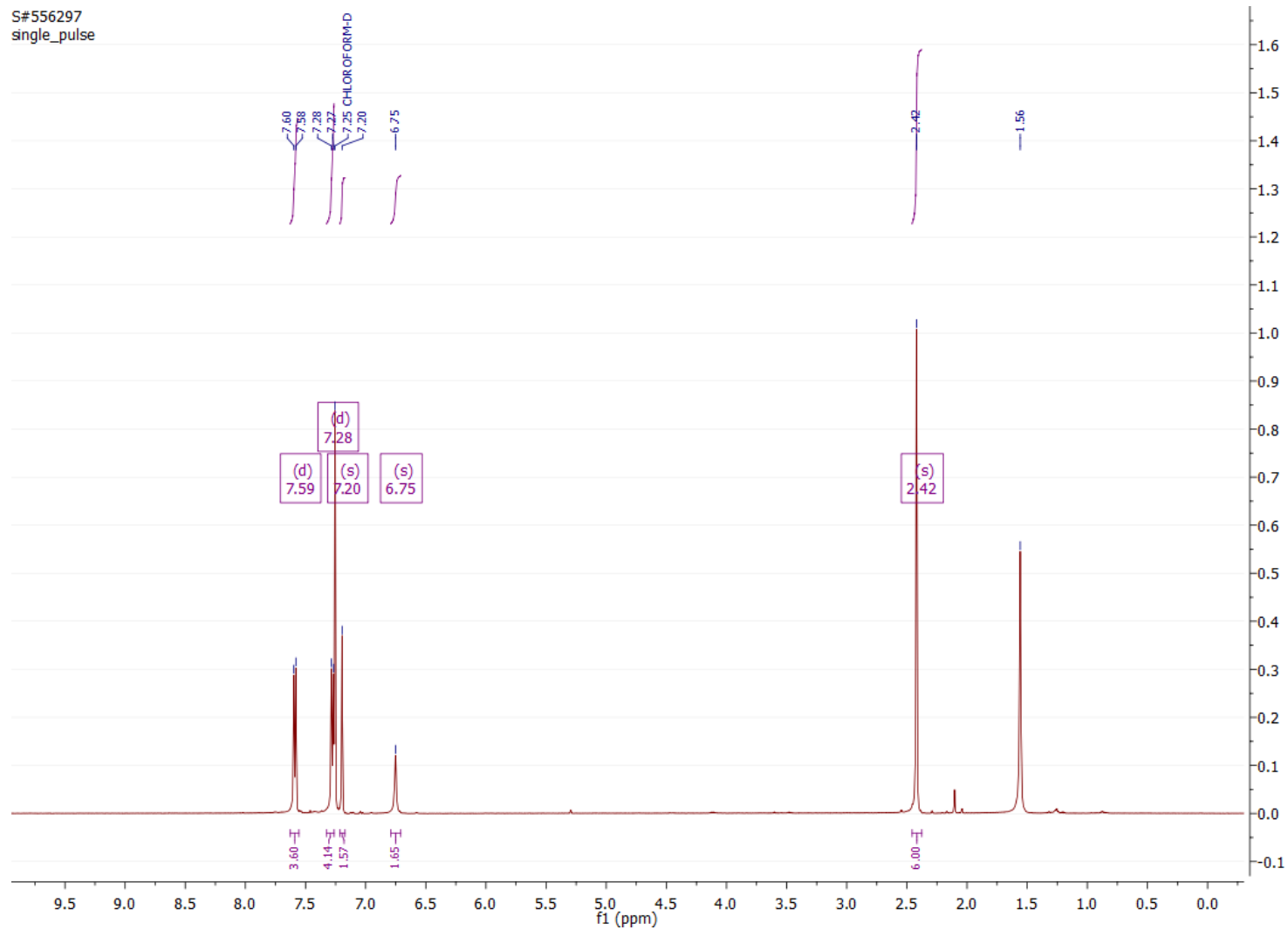
270

S#756259
single pulse decoupled gated NOE



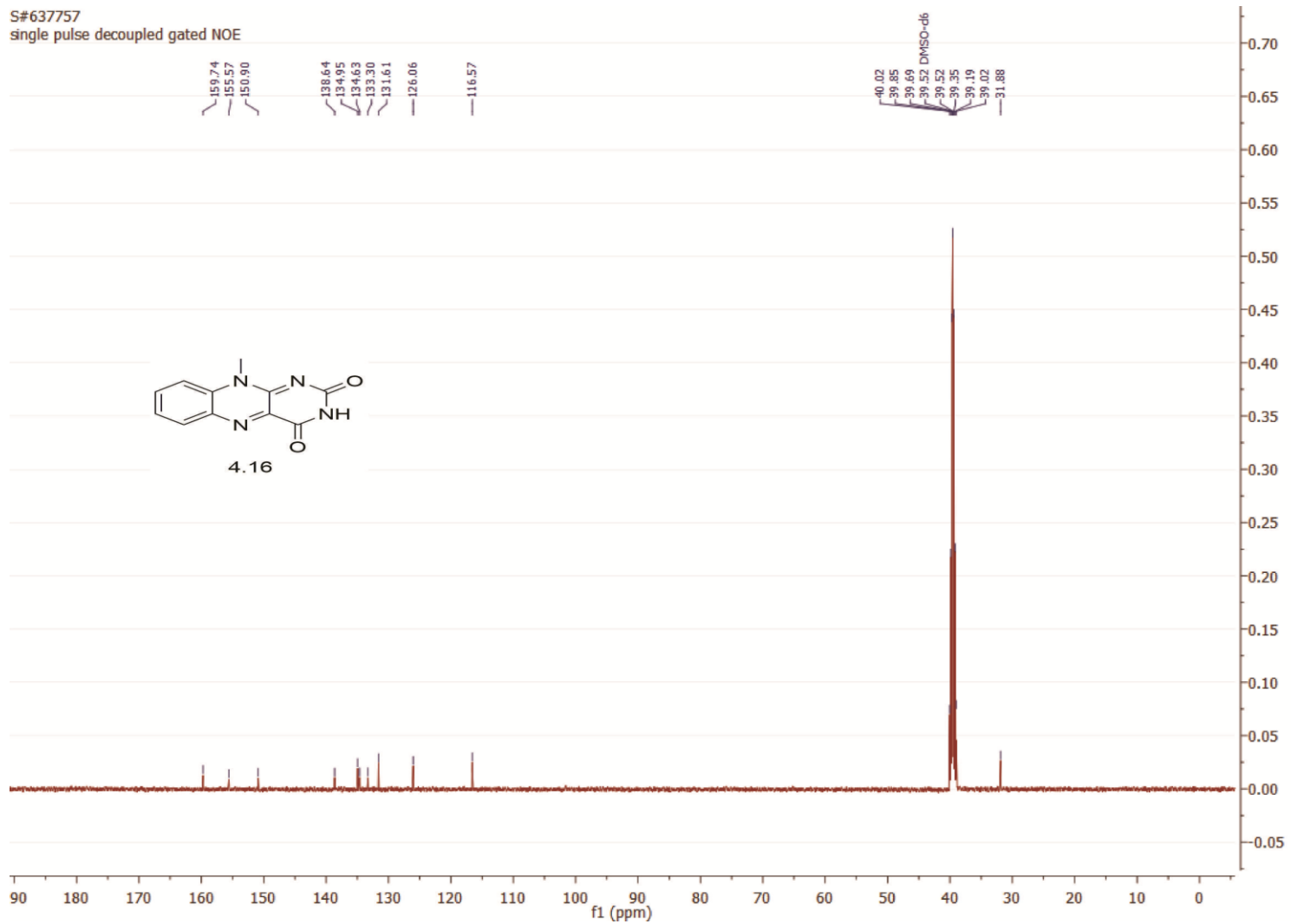
271

S#556297
single_pulse

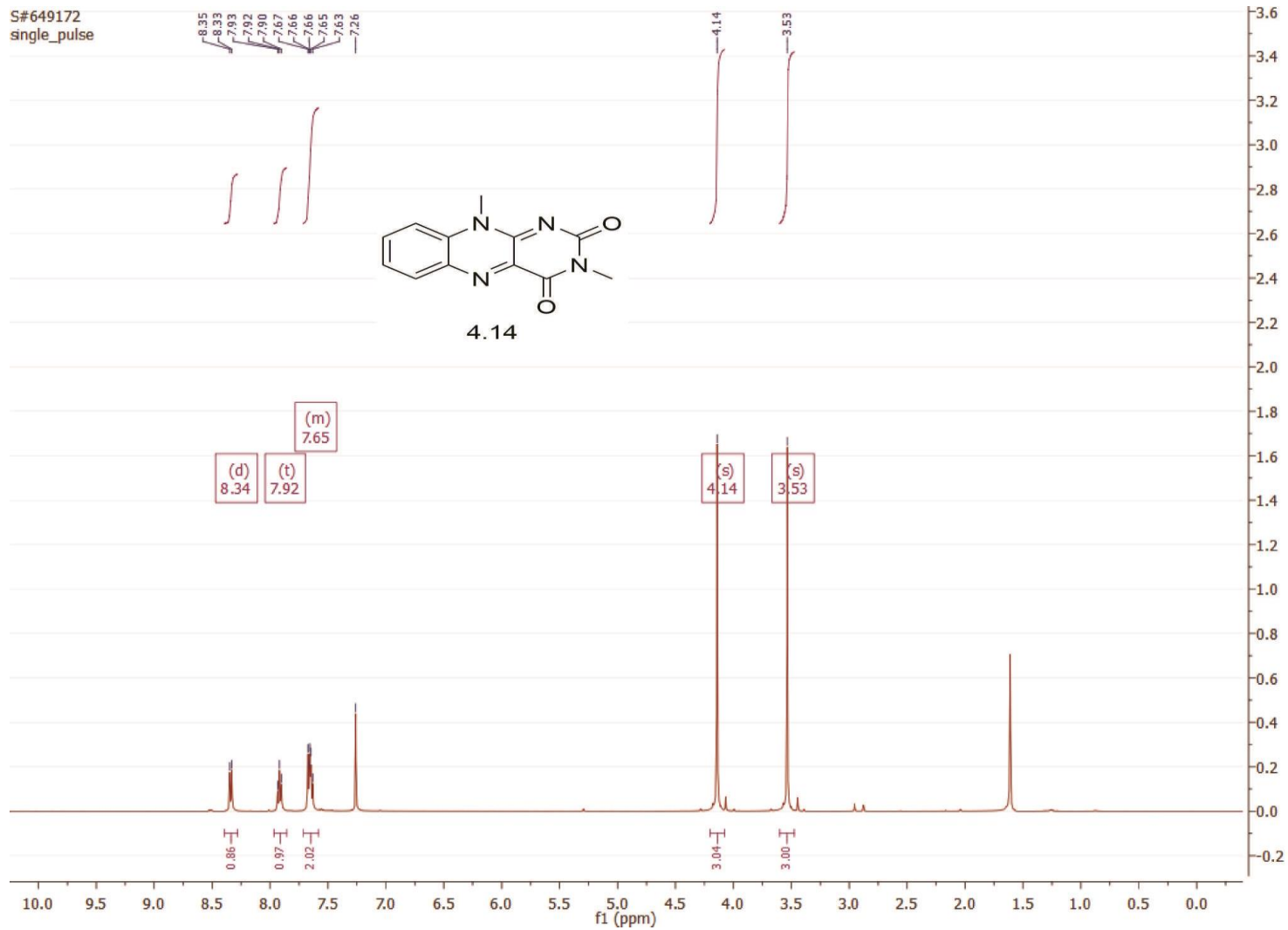


272

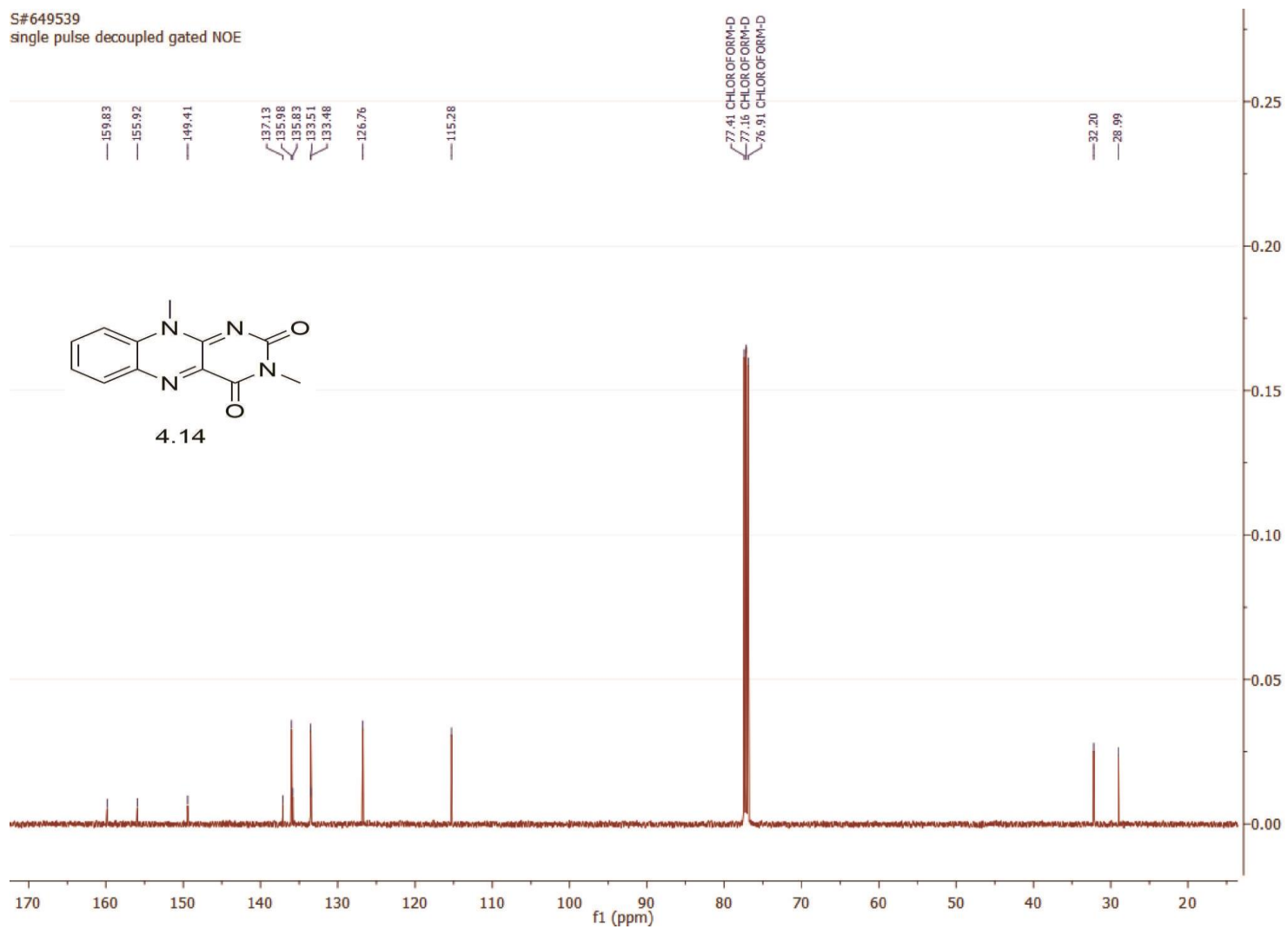
273



274

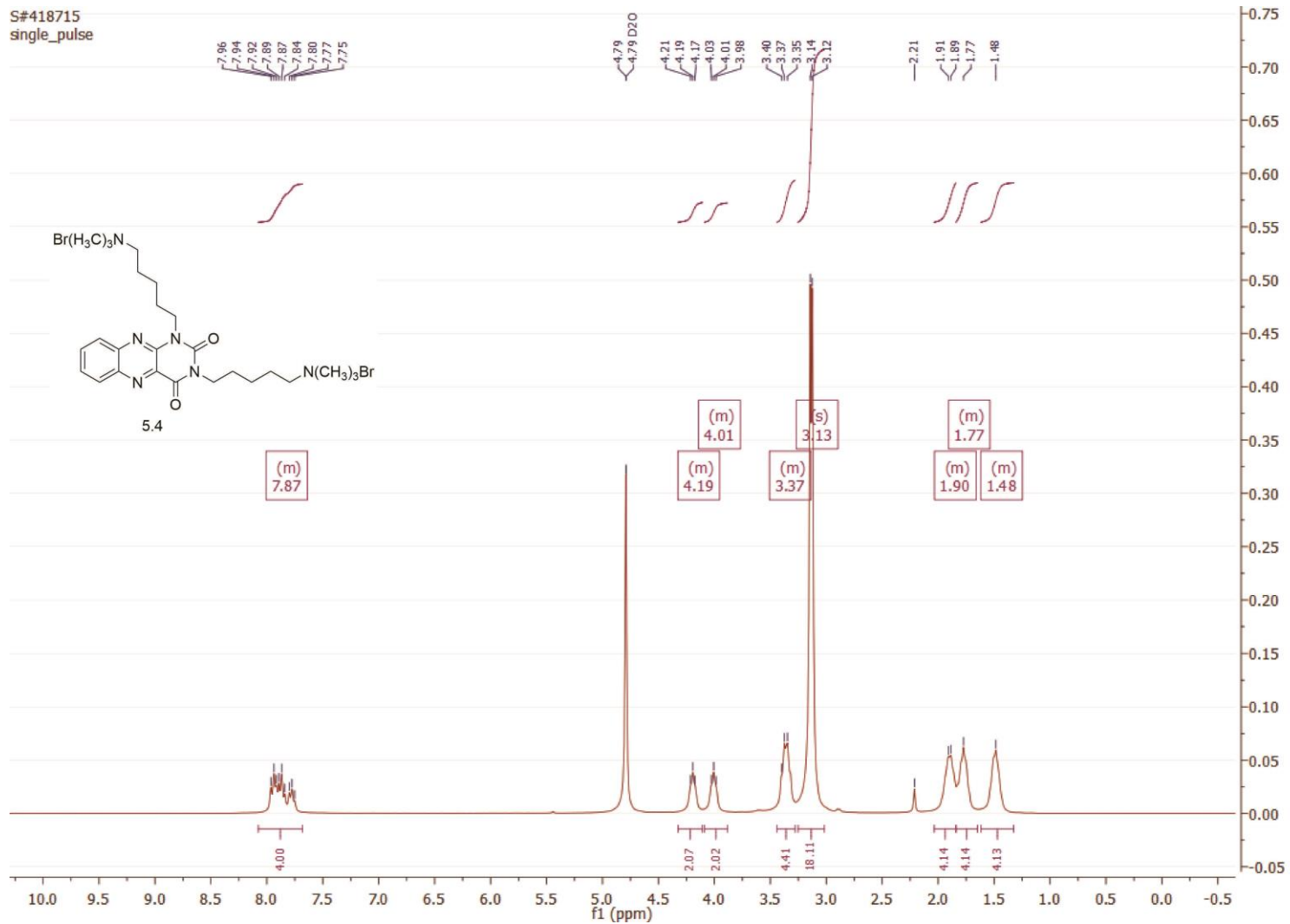


S#649539
single pulse decoupled gated NOE



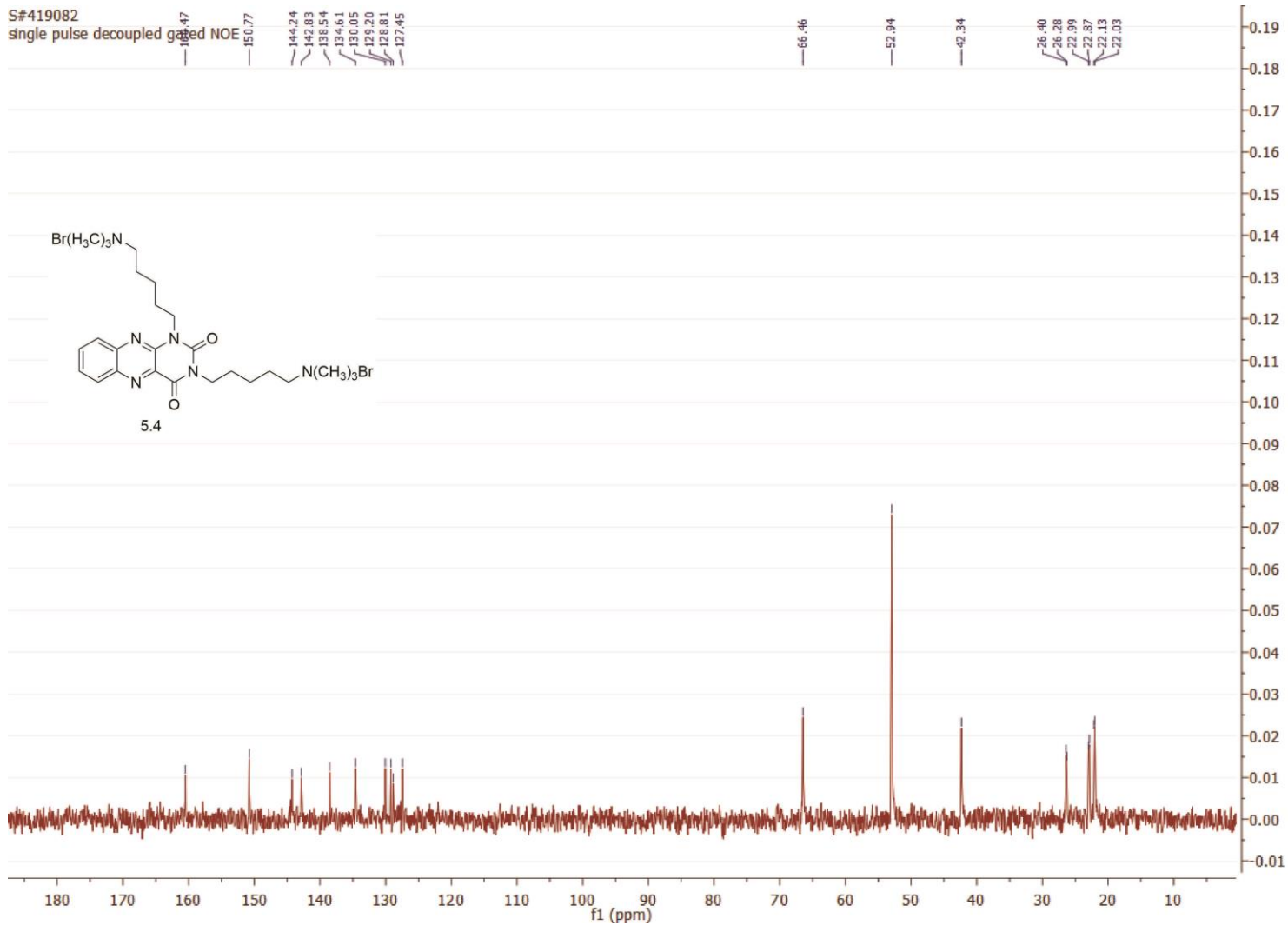
275

276

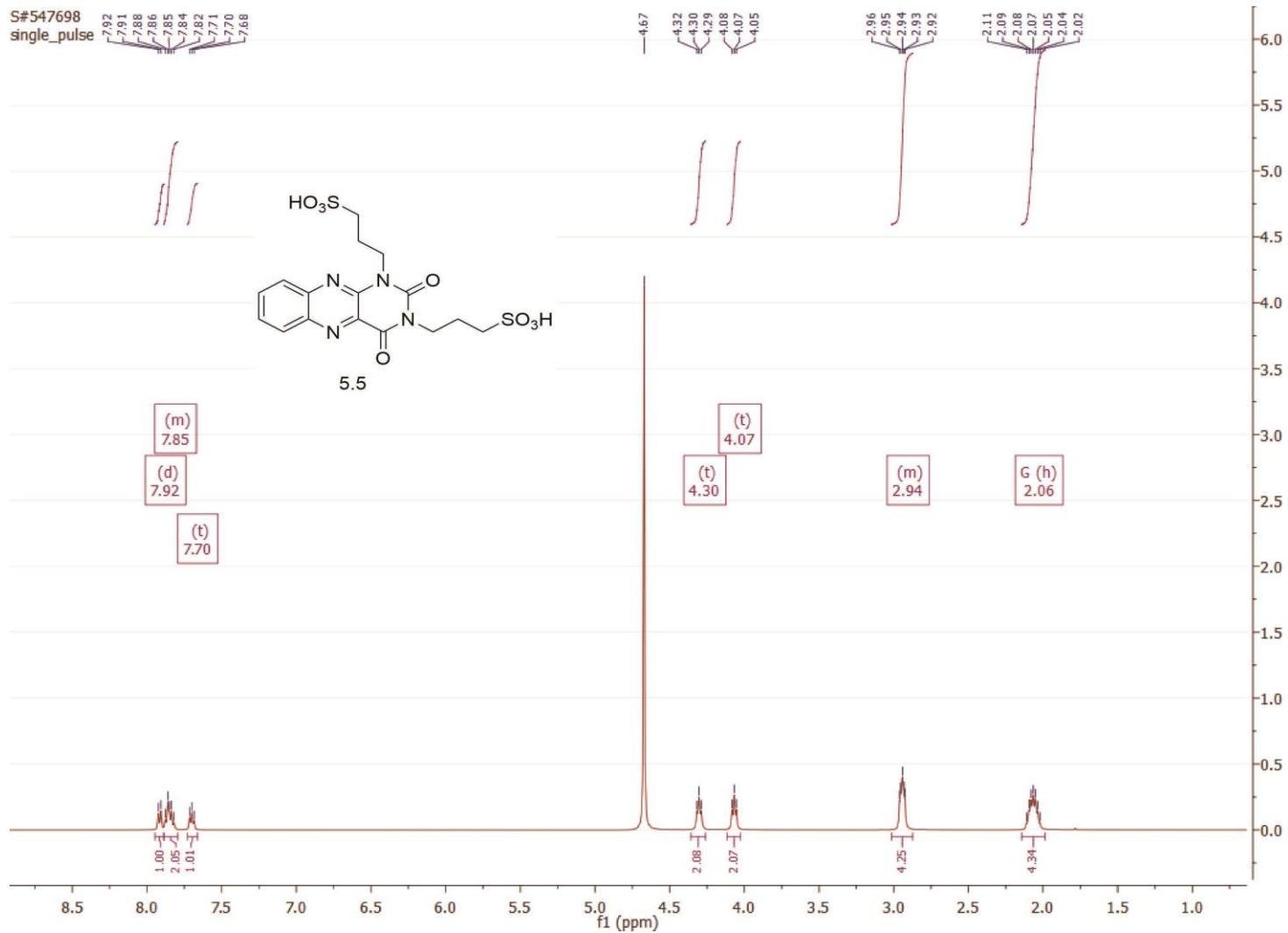


S#419082

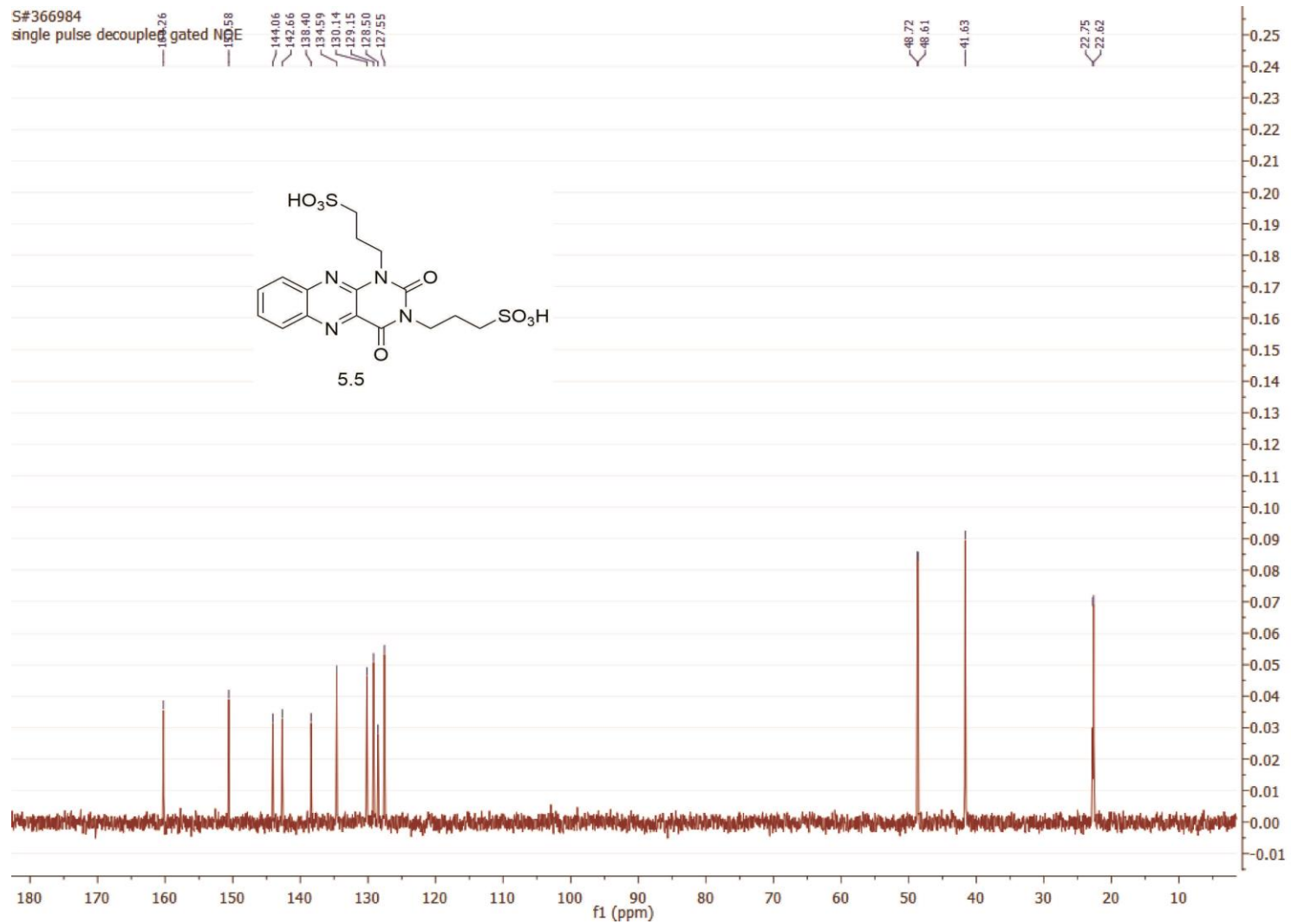
single pulse decoupled gated NOE



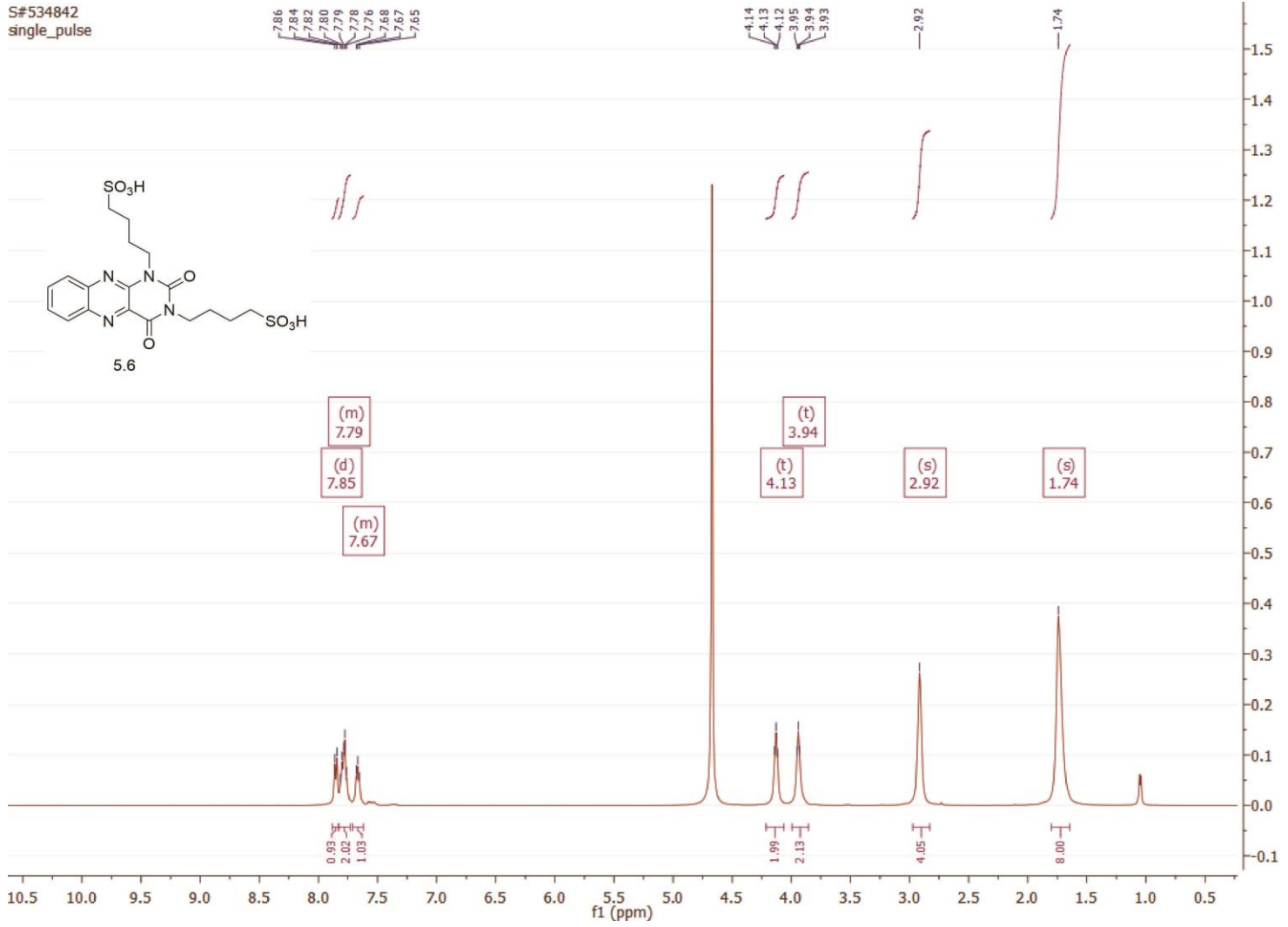
278



279



S#534842
single_pulse



280

S#534876

single pulse decoupled

151.59
147.78
144.29
142.89
138.58
134.54
130.05
128.17
127.53

50.65

42.24

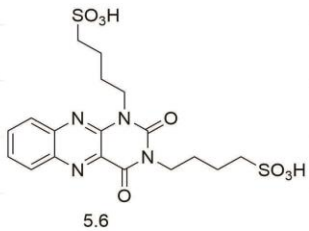
42.05

25.98

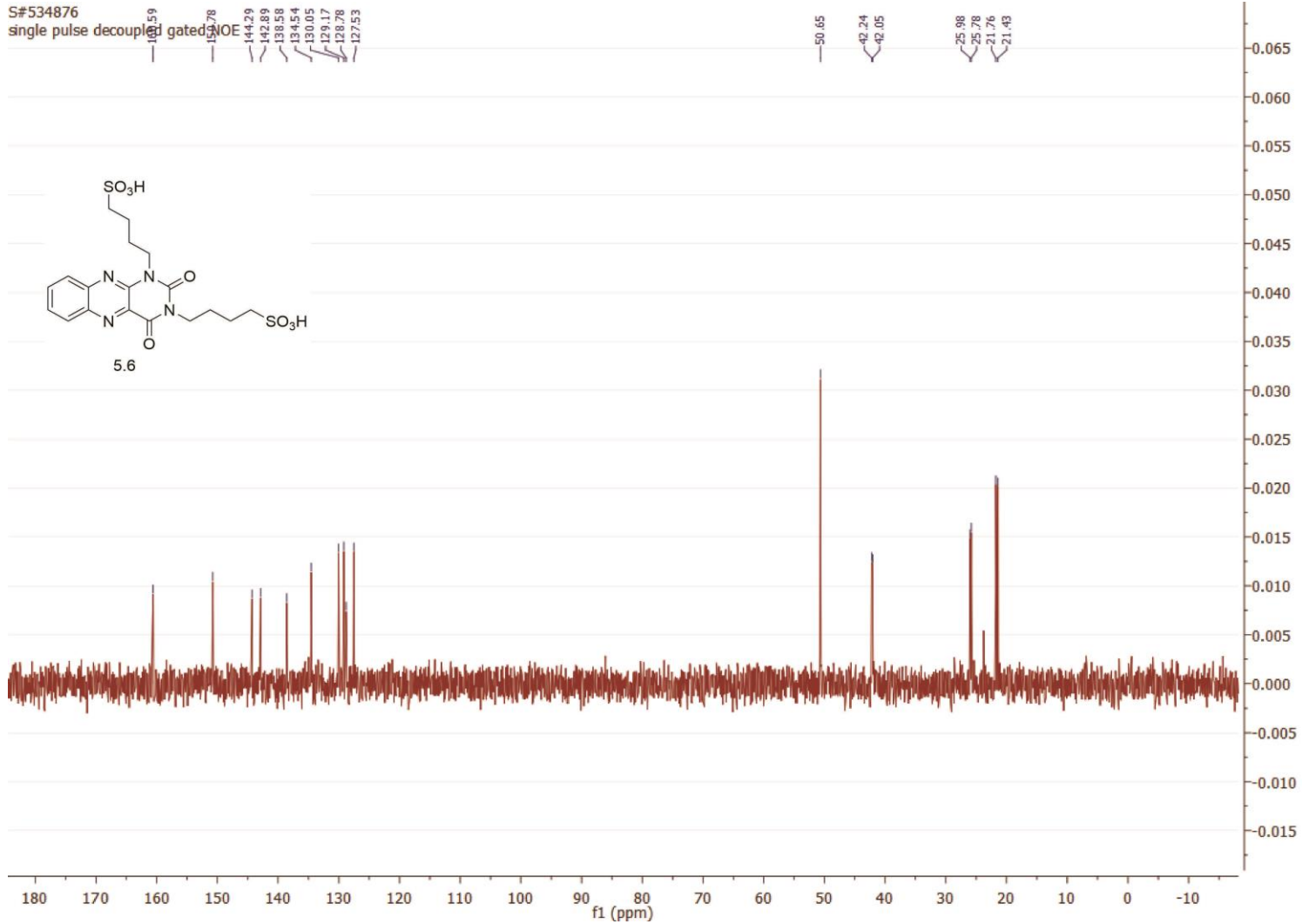
25.78

21.76

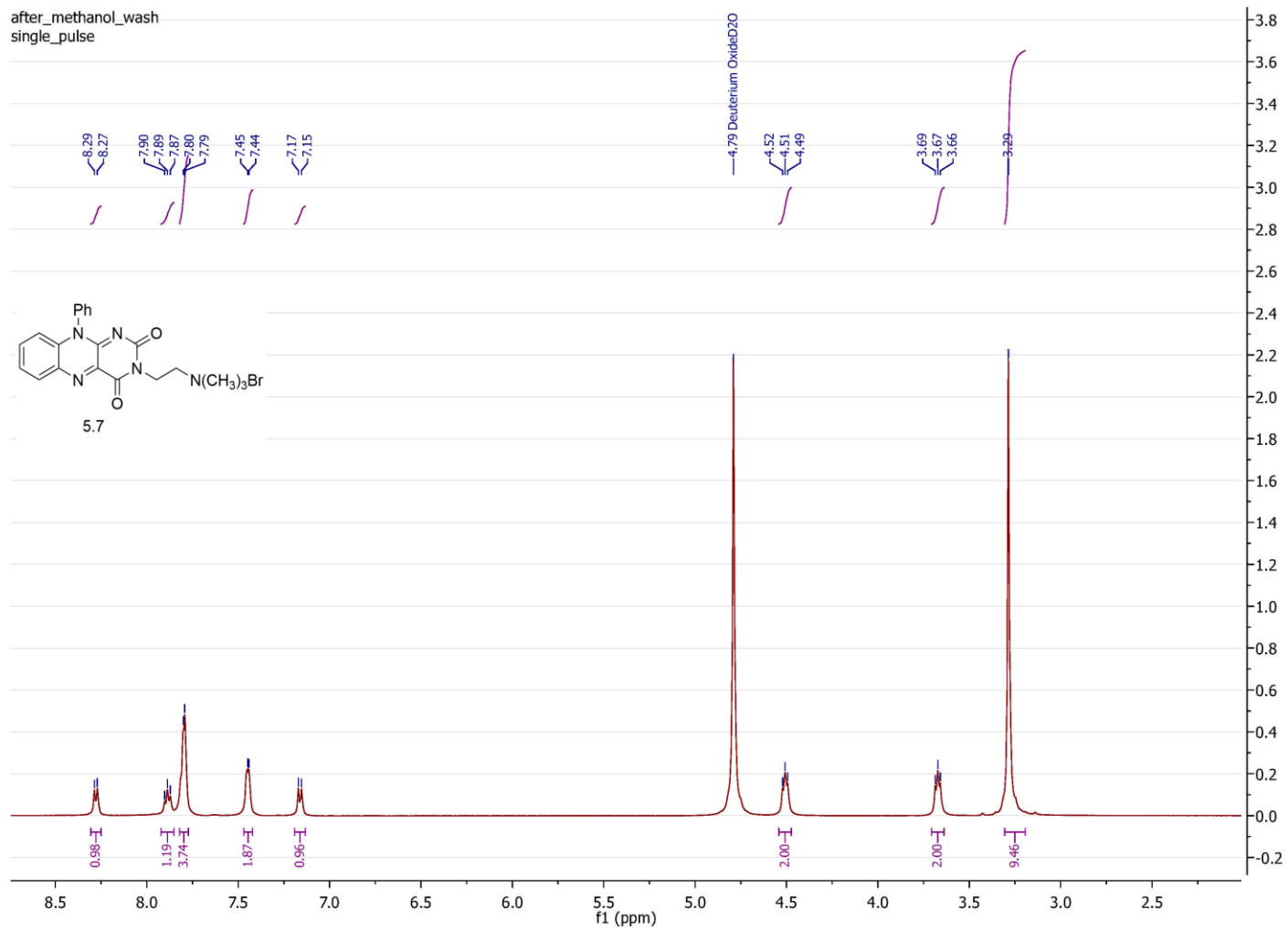
21.49

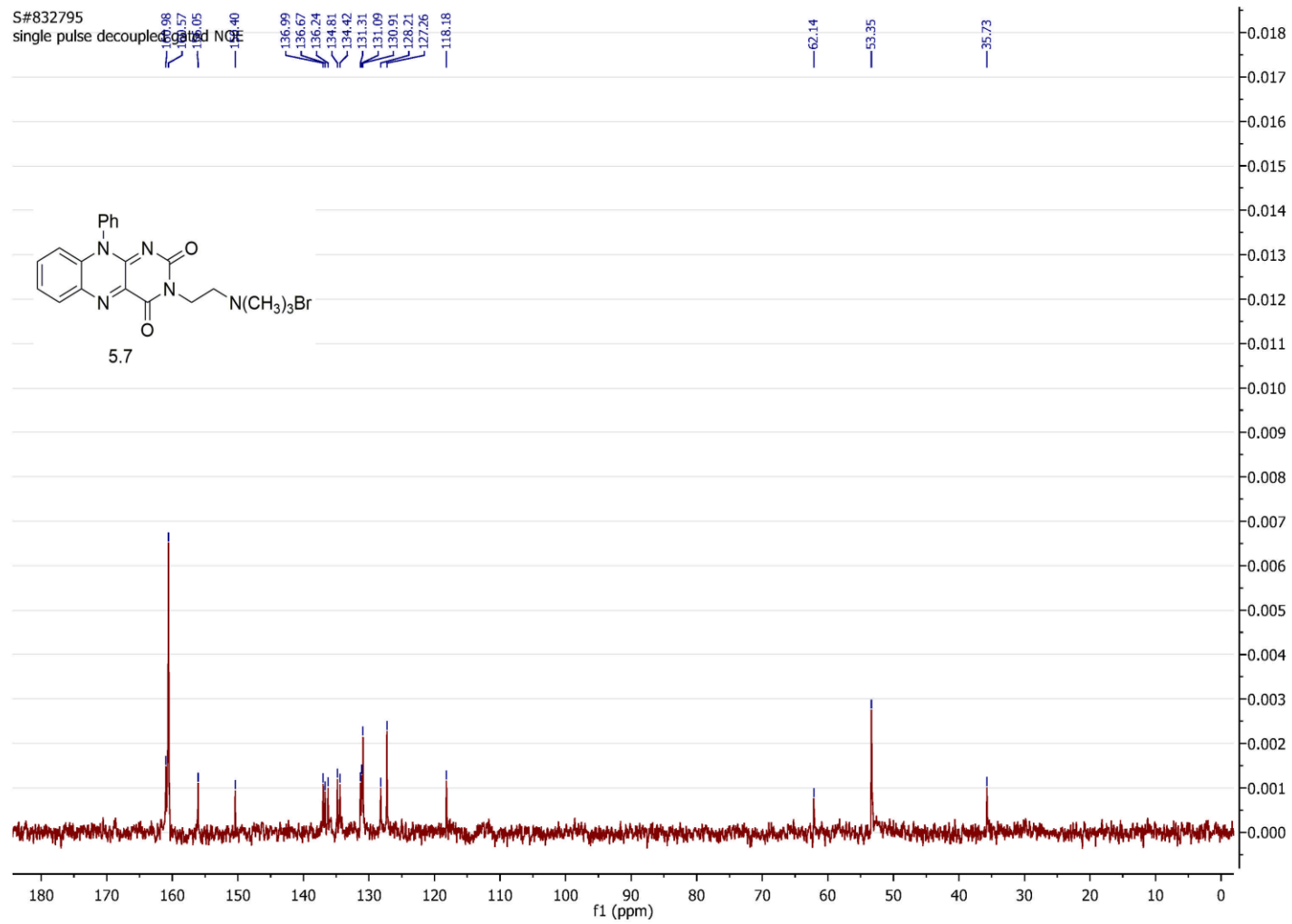


281



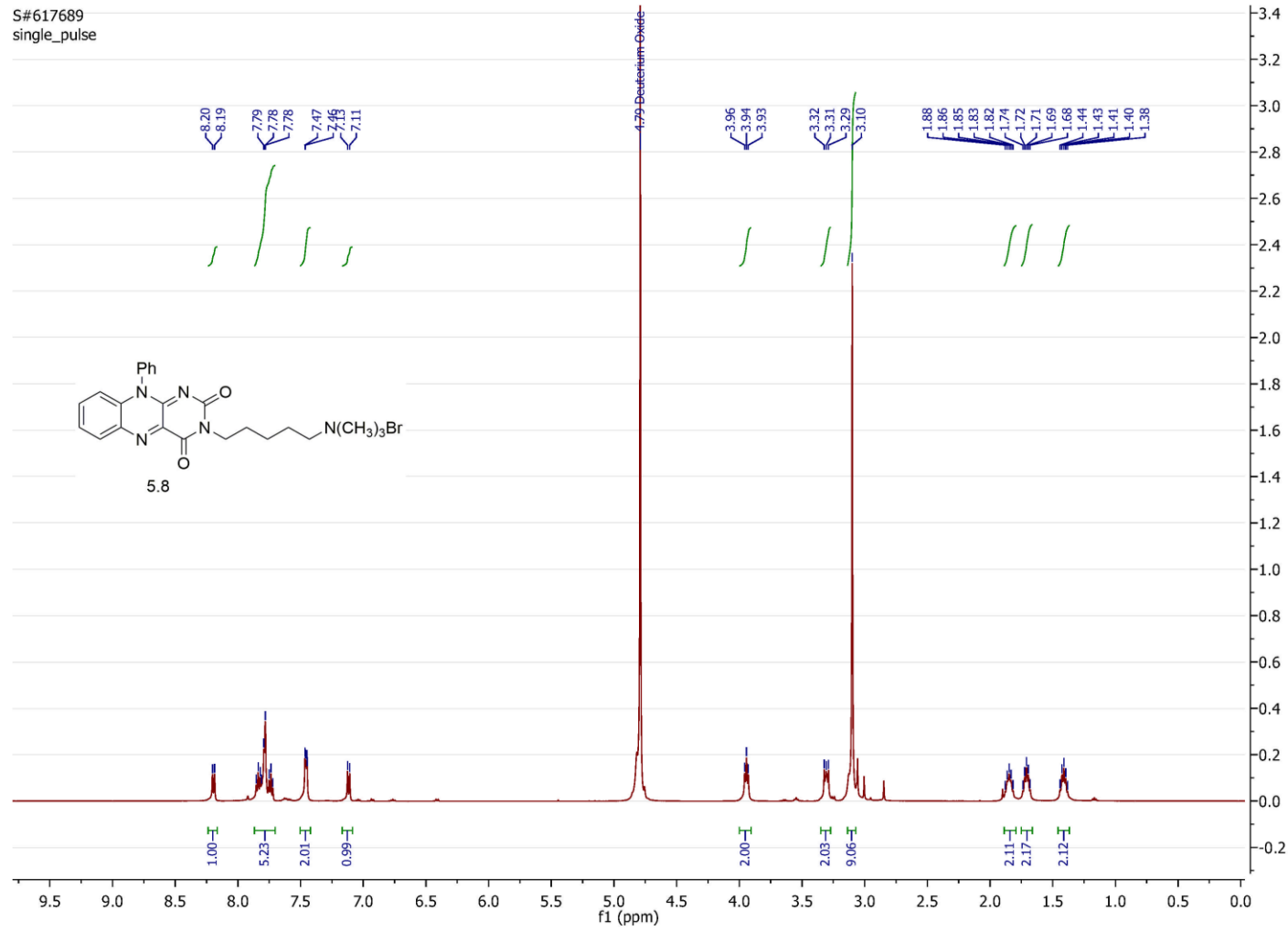
282



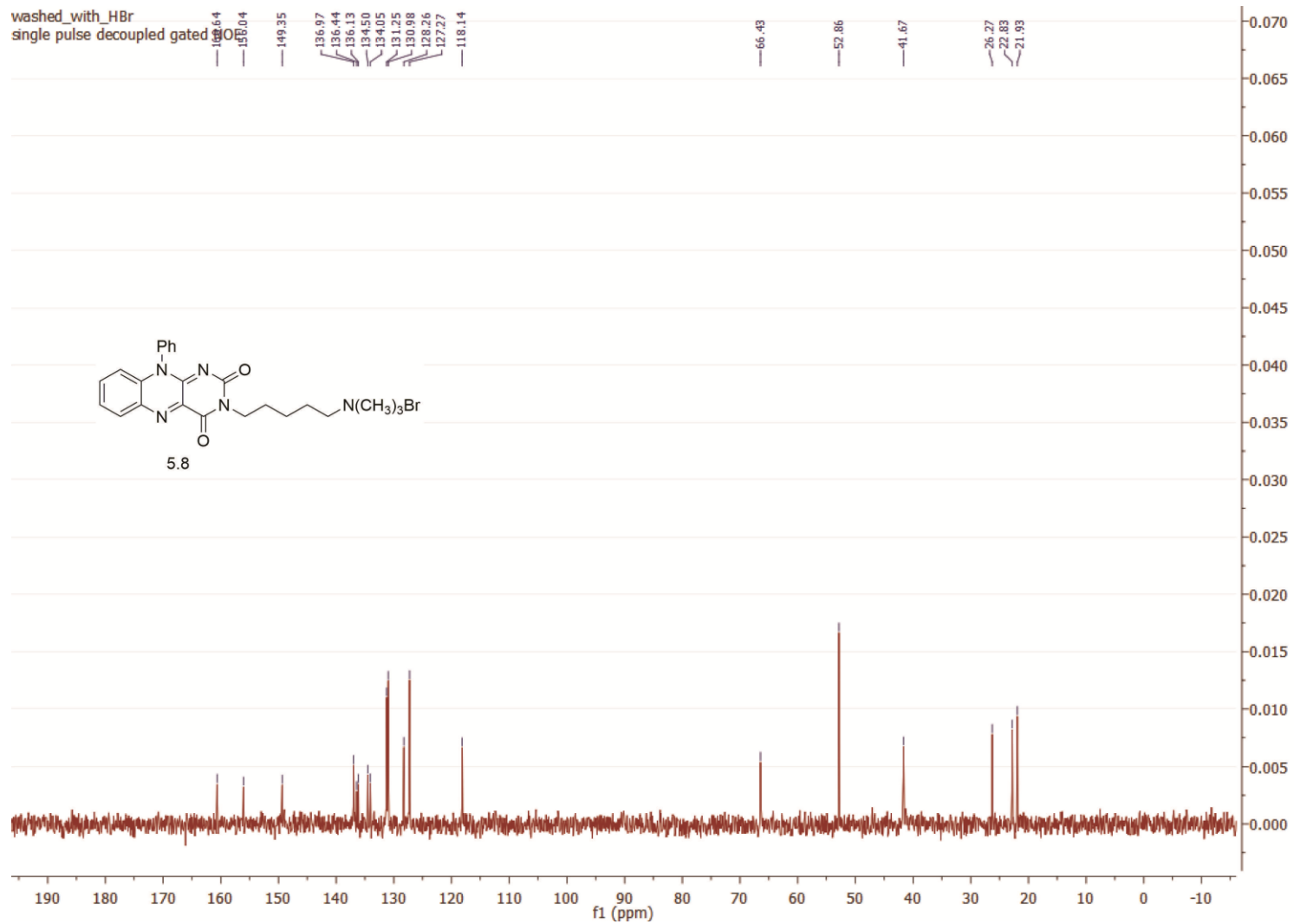


284

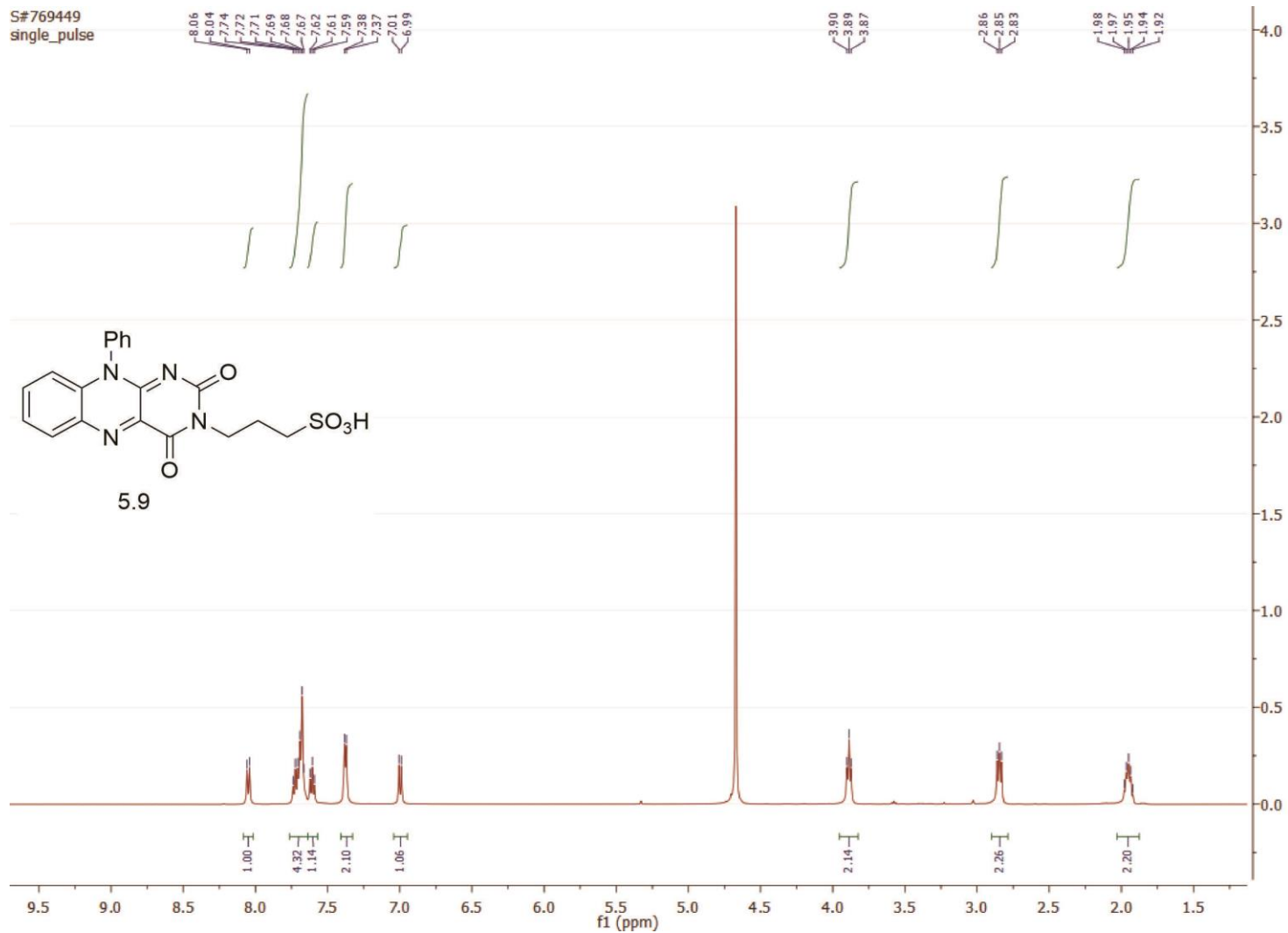
S#617689
single_pulse



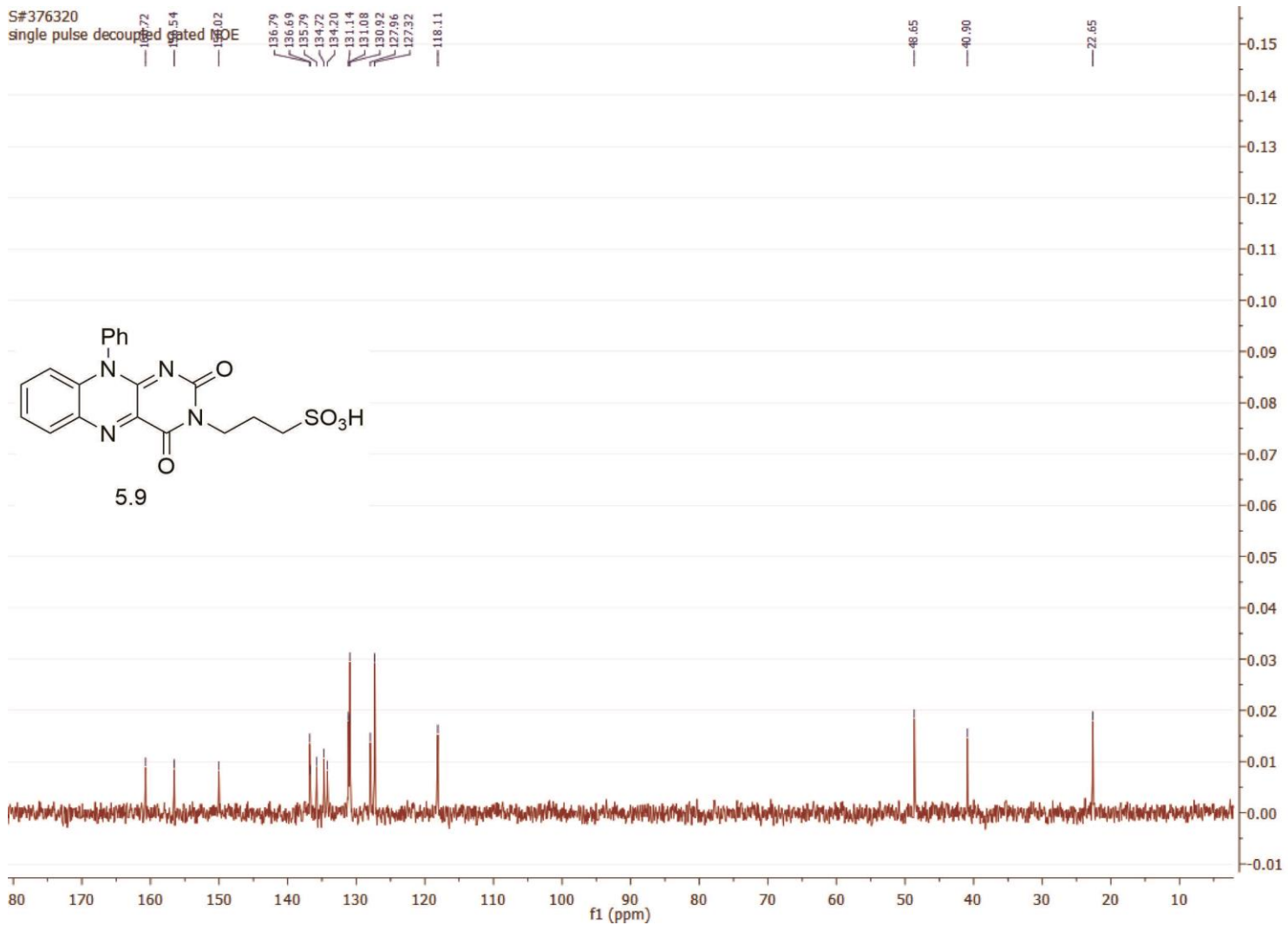
285



286

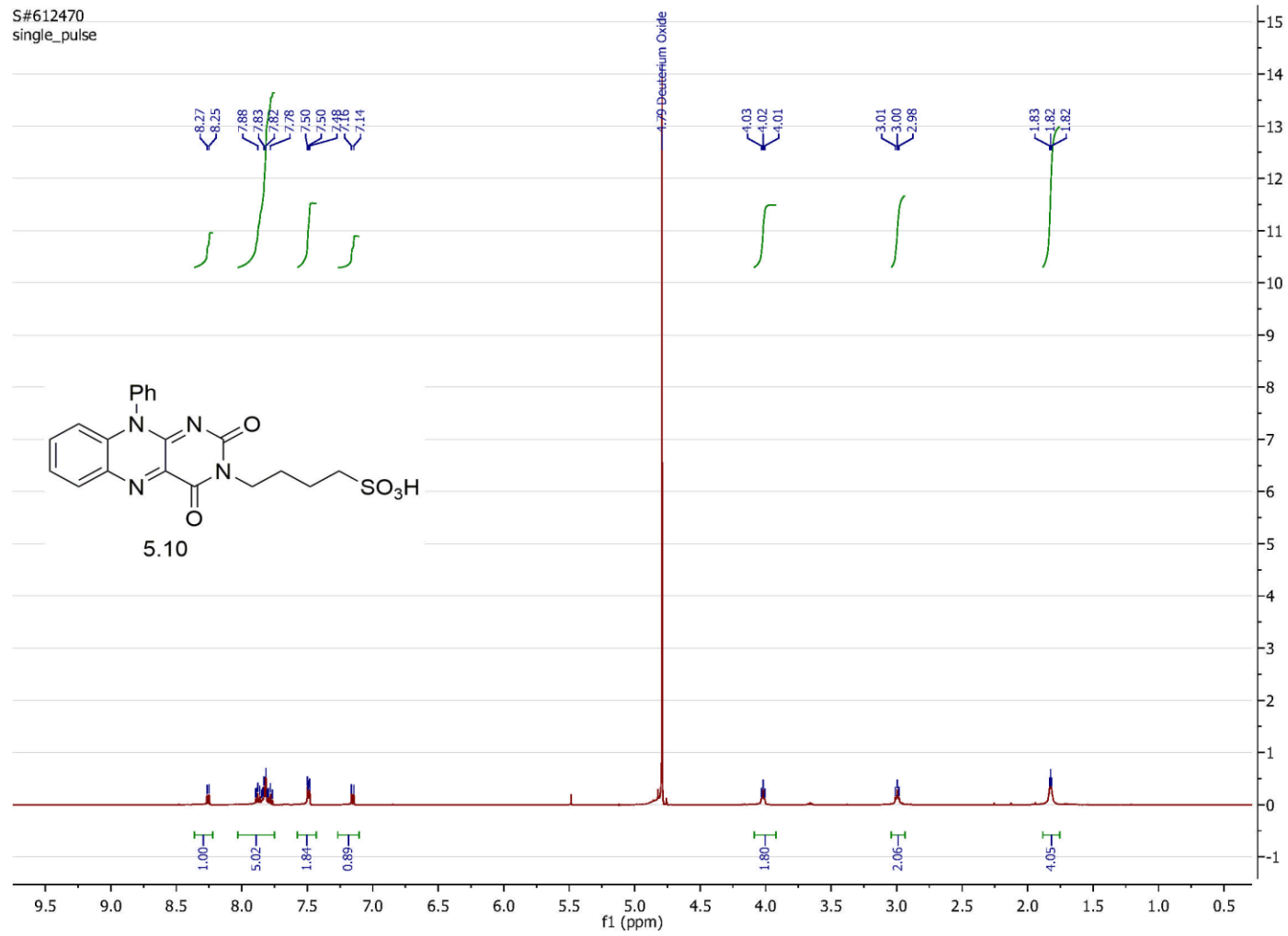


S#376320
single pulse decoupled gated 150E

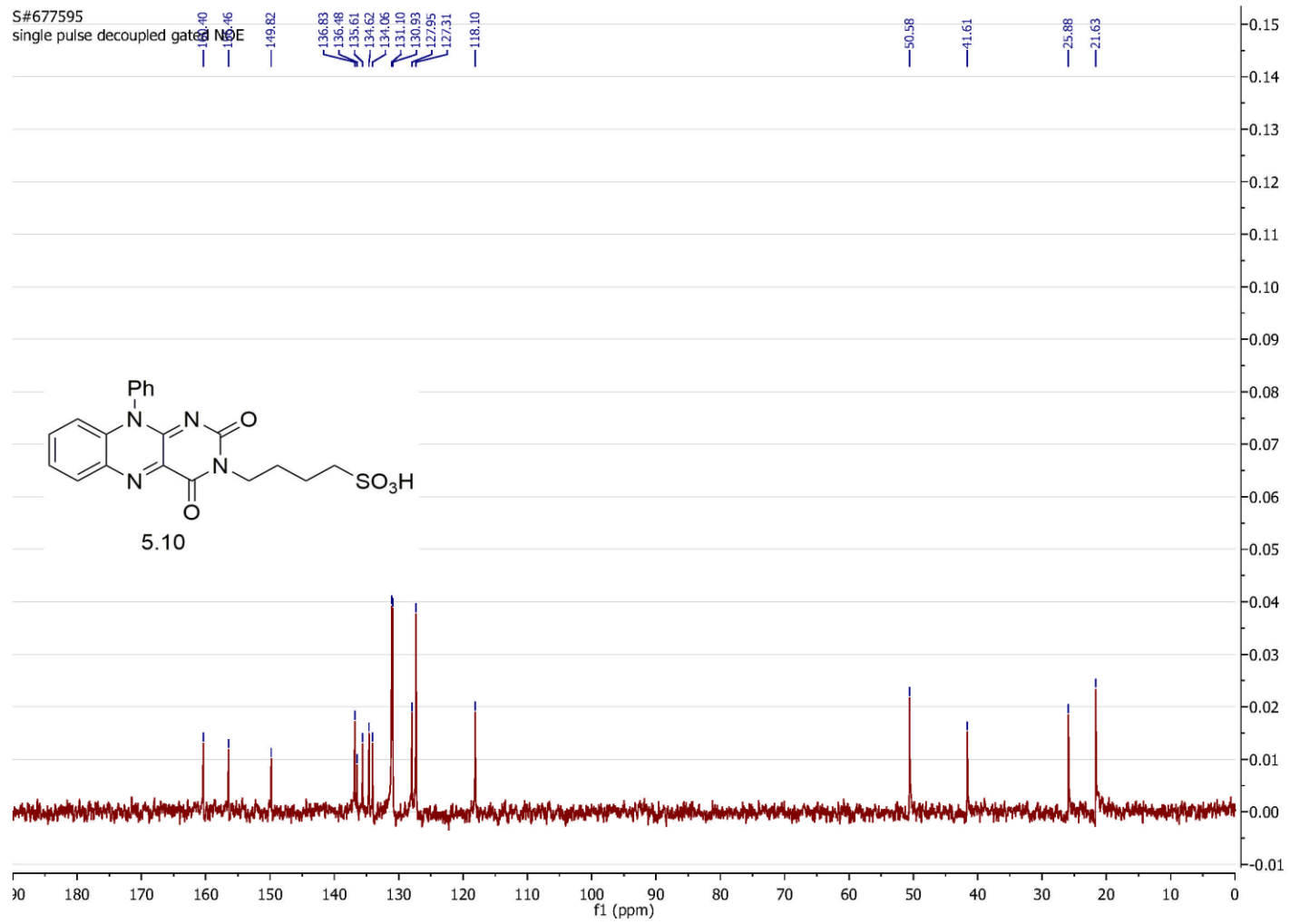


288

S#612470
single_pulse

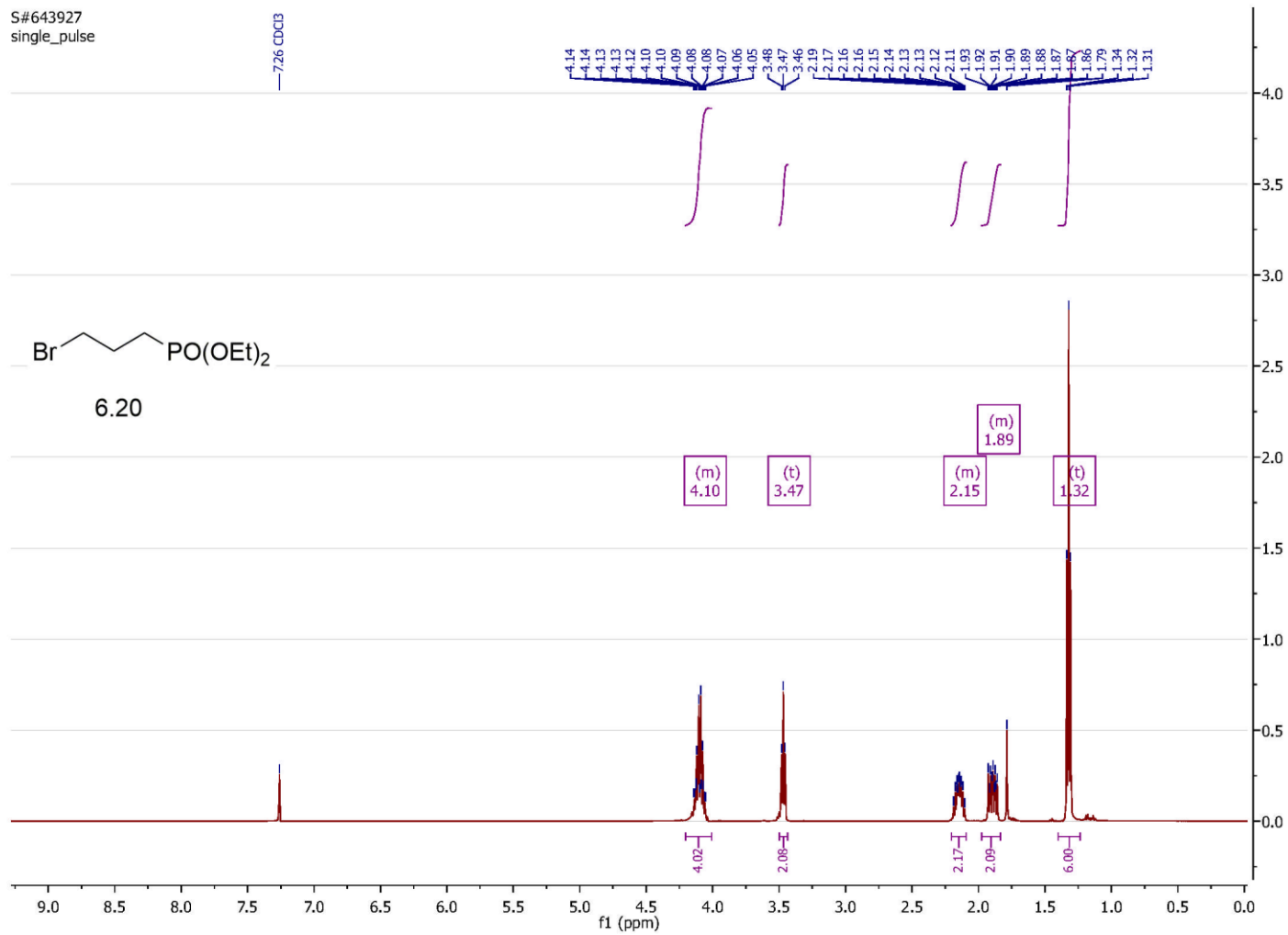


289

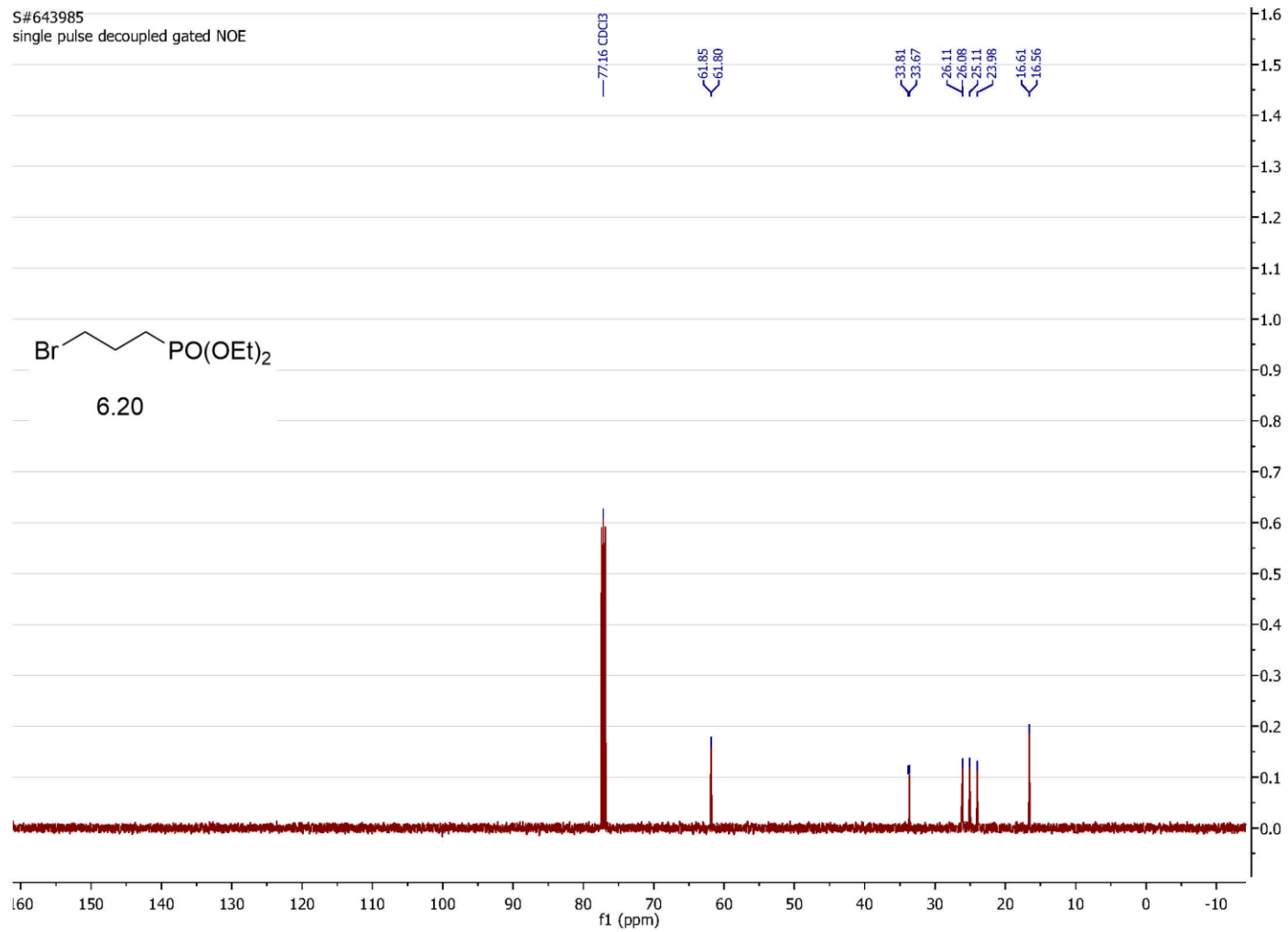


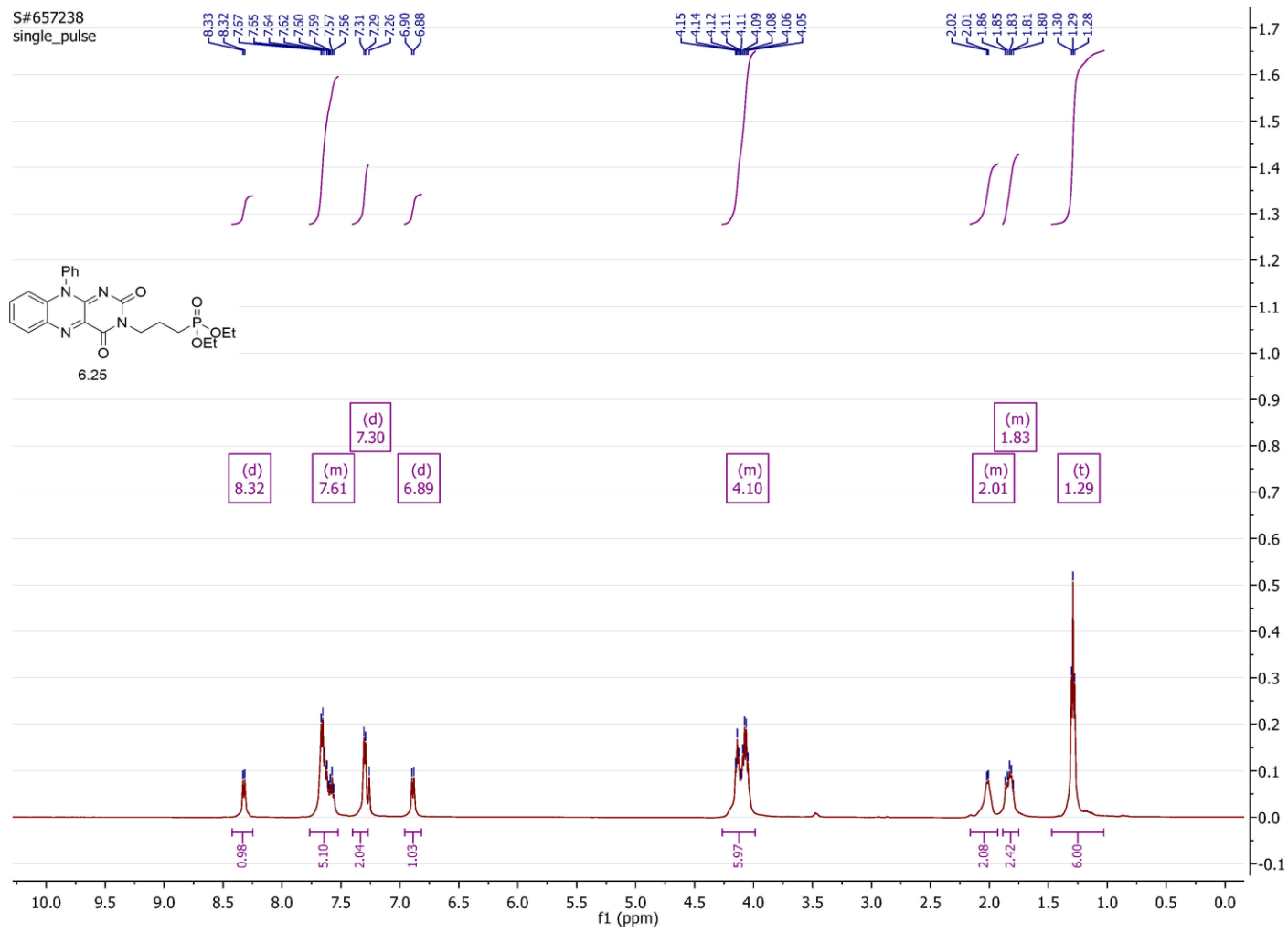
290

S#643927
single_pulse

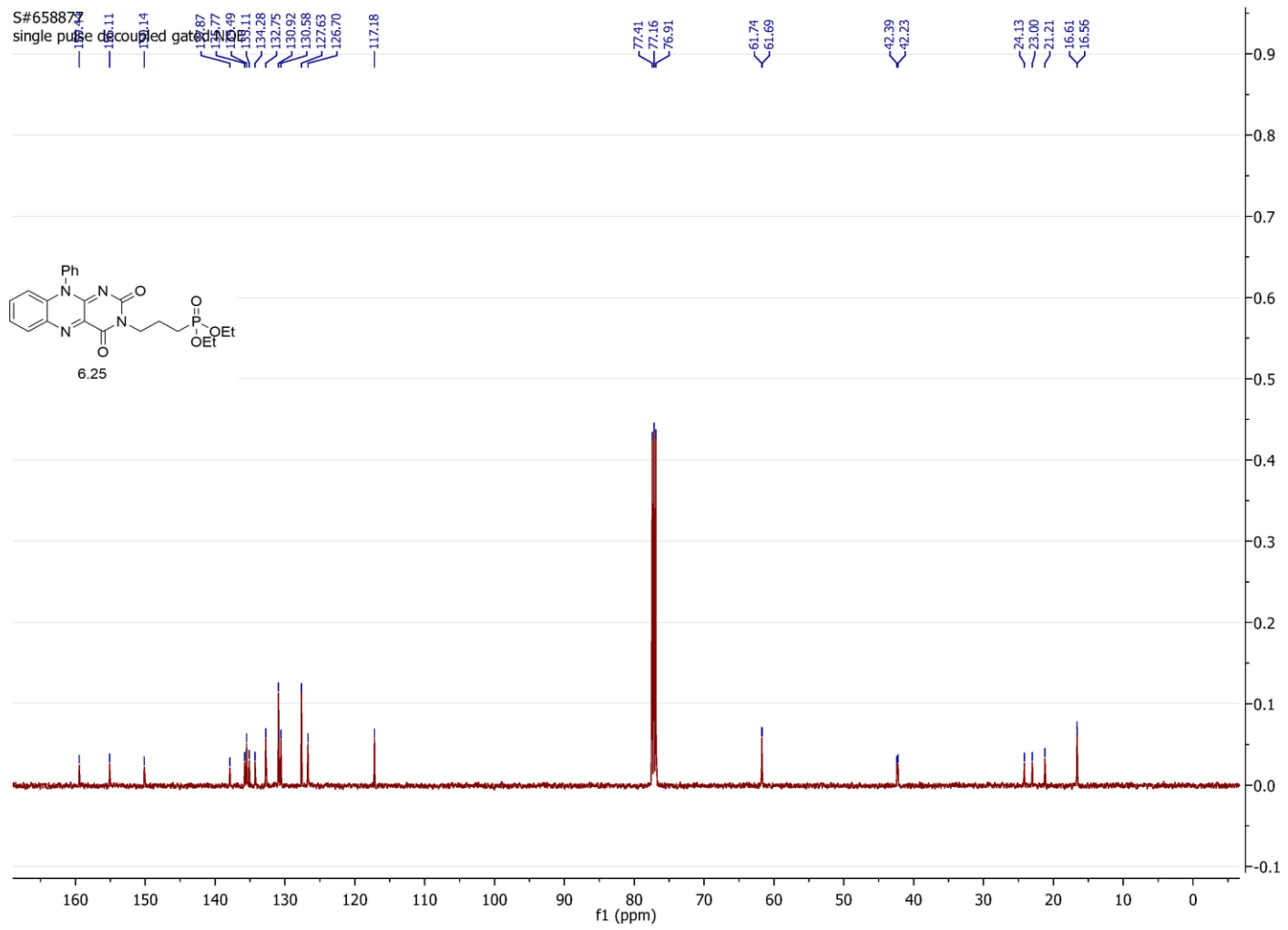


S#643985
single pulse decoupled gated NOE

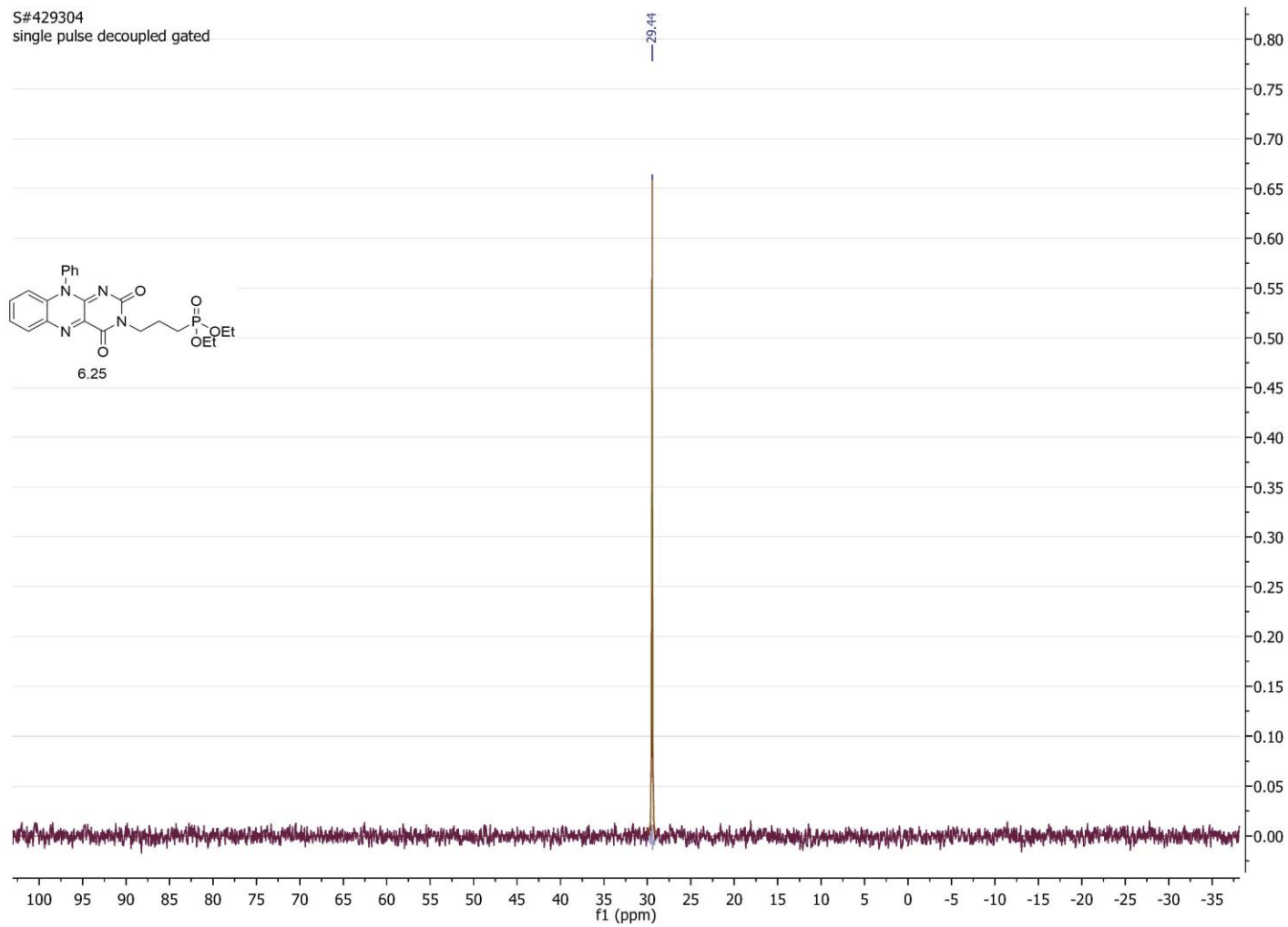




293

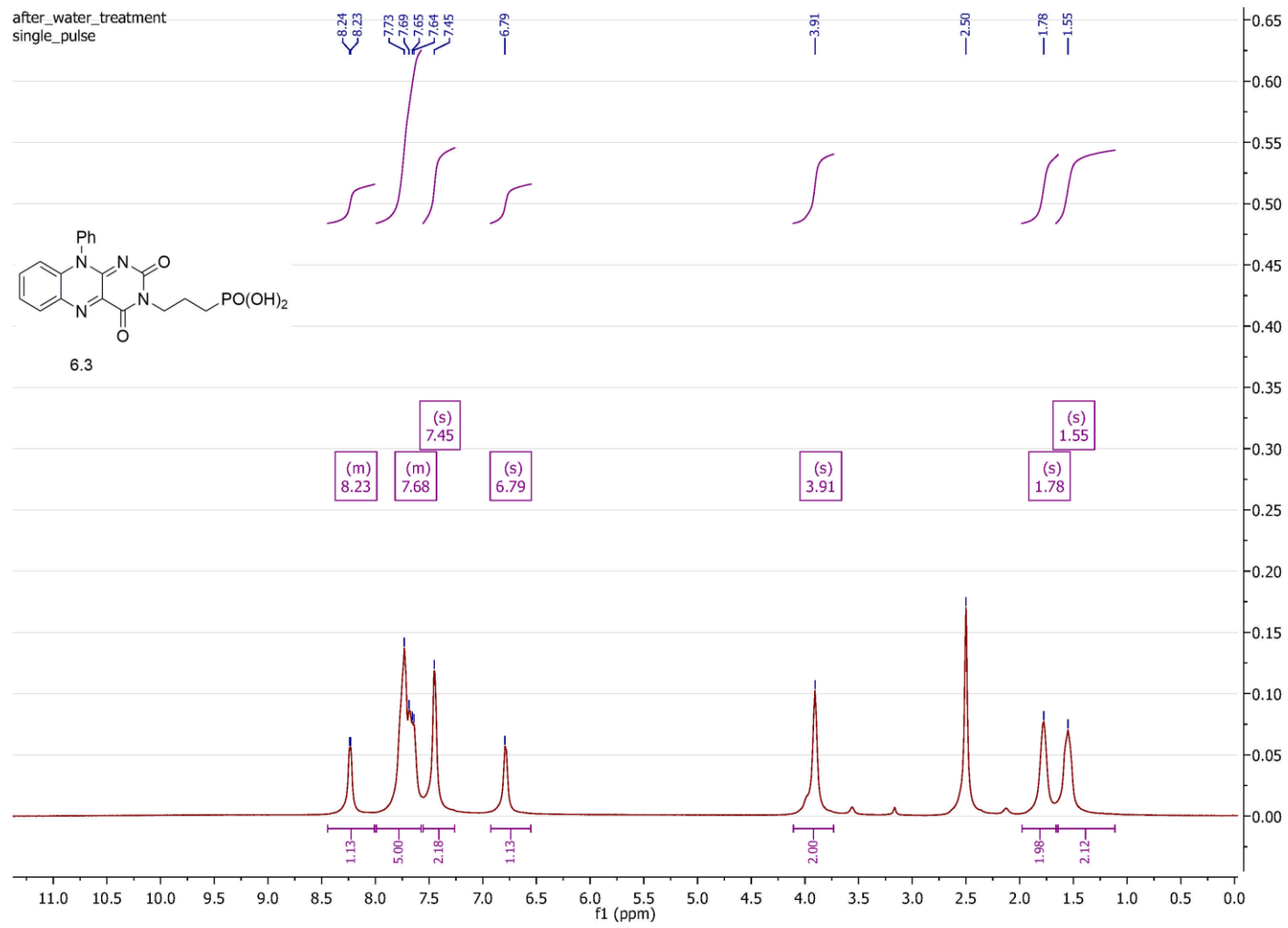


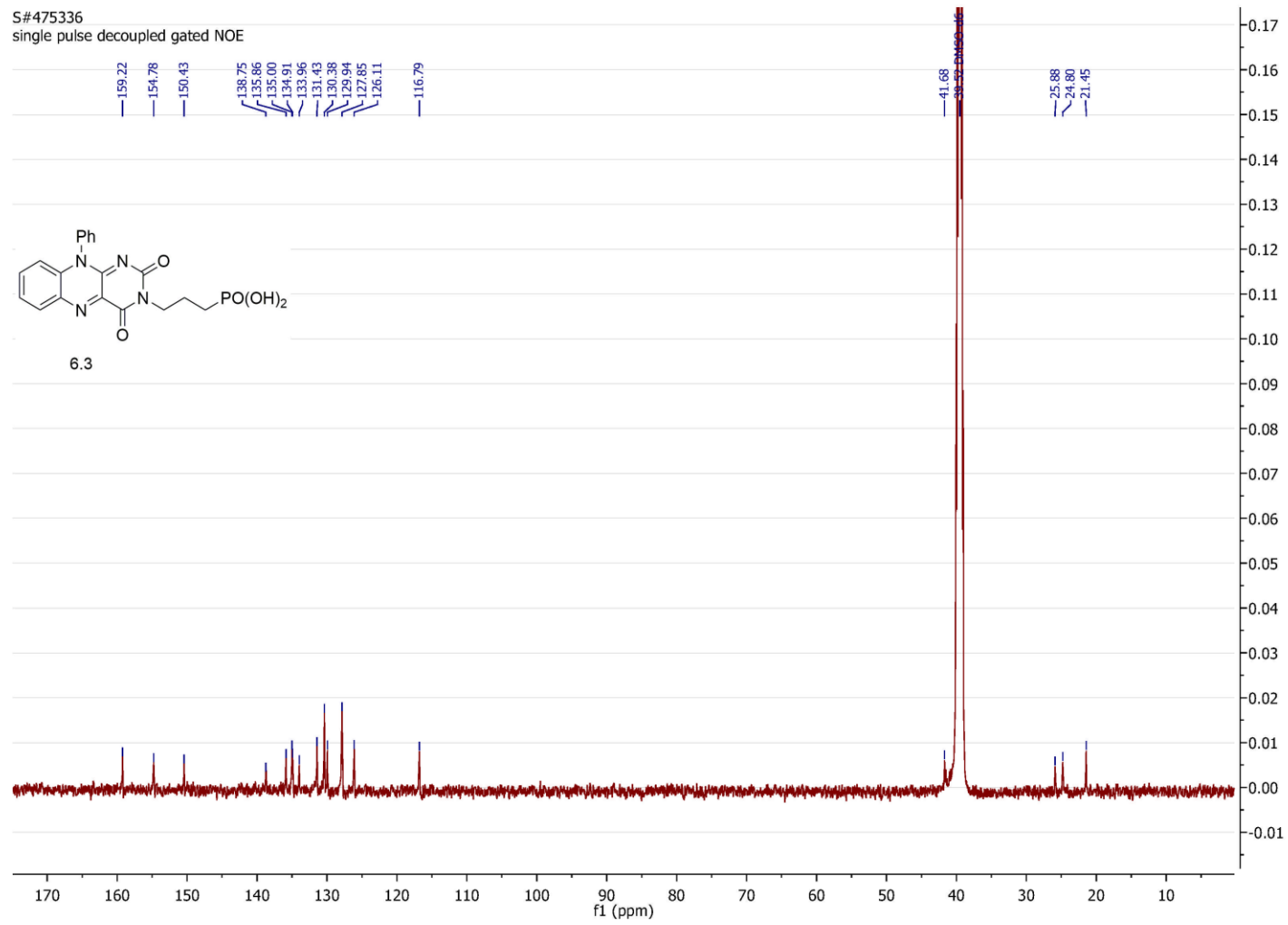
S#429304
single pulse decoupled gated



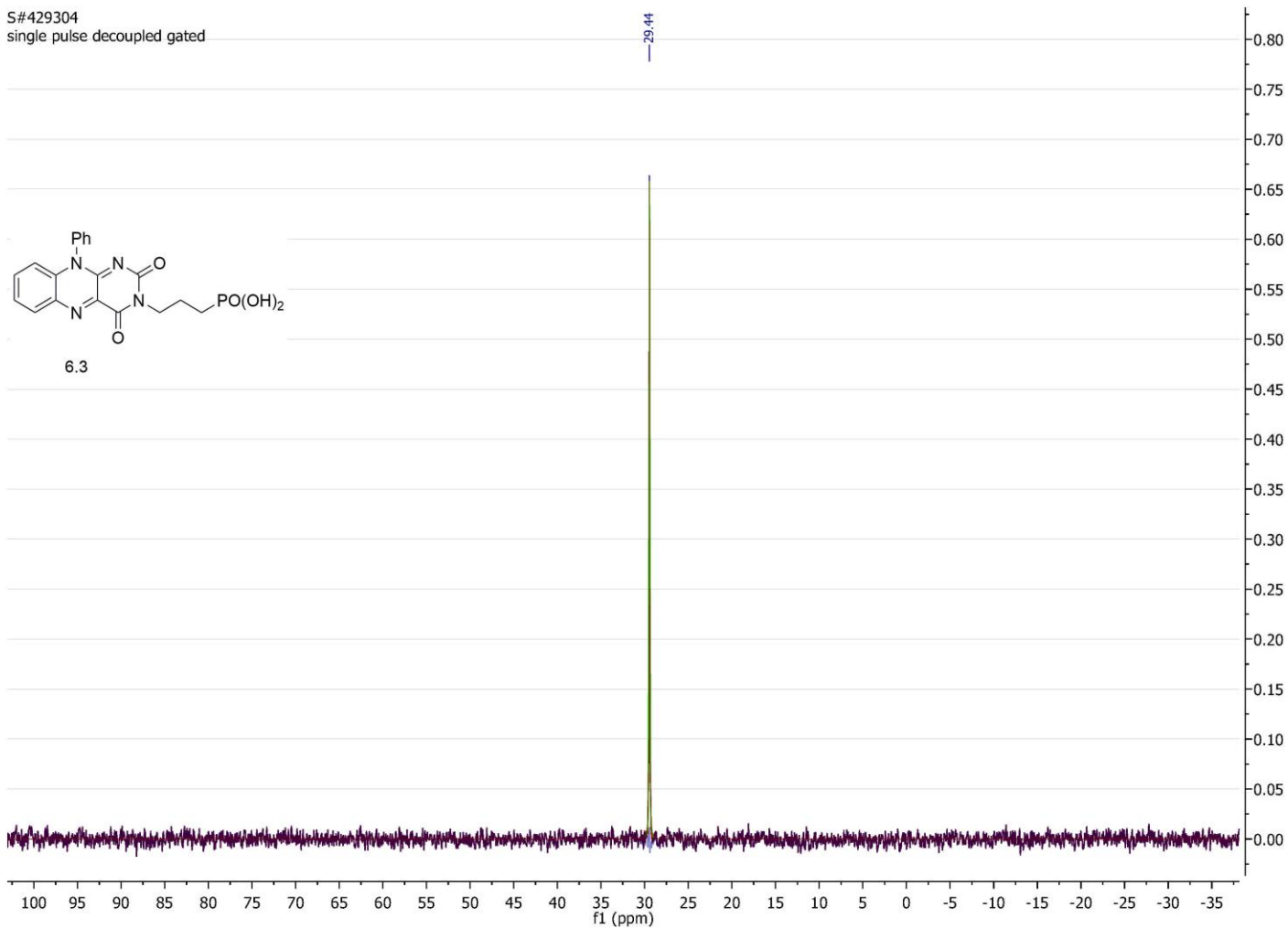
294

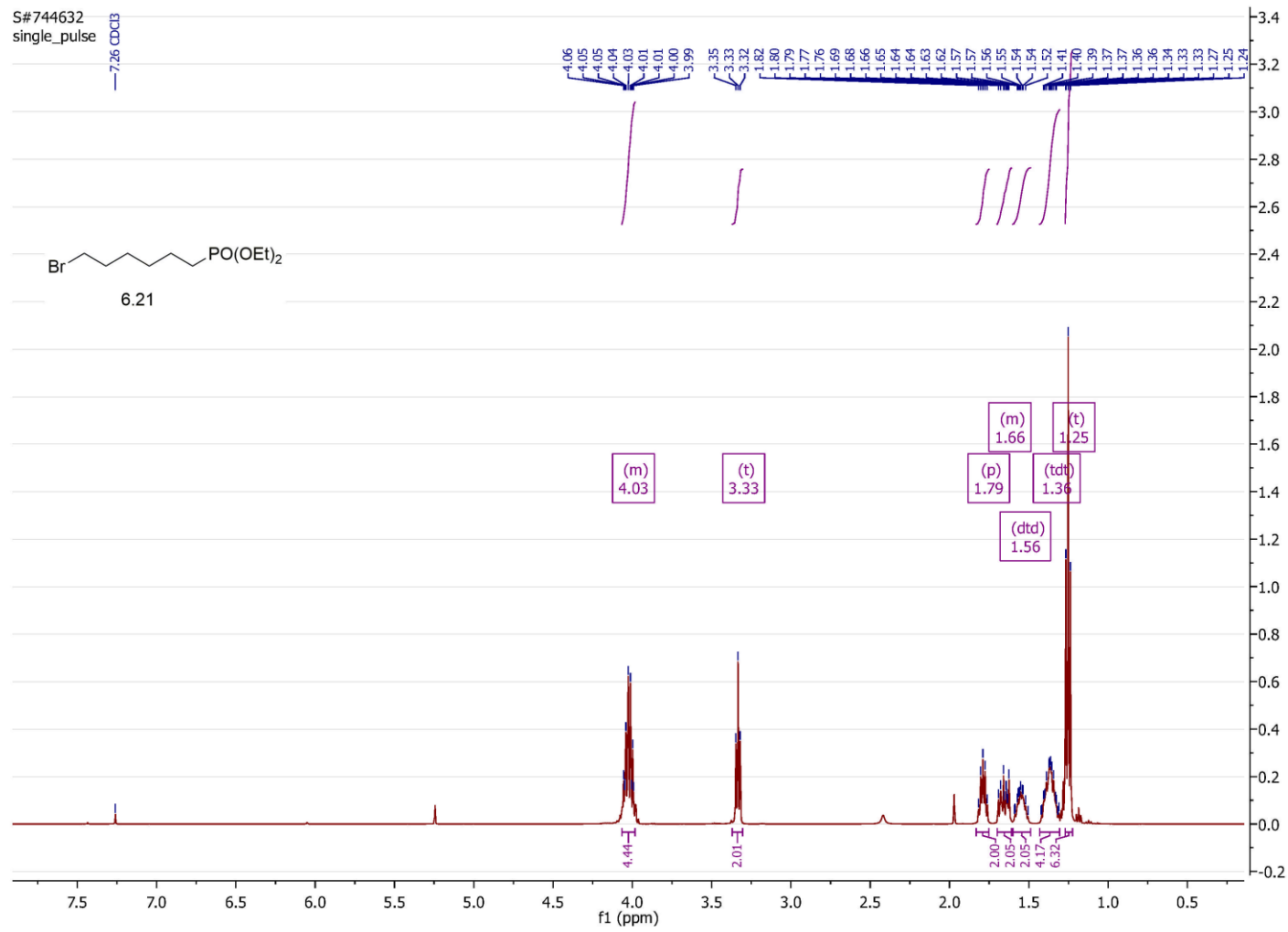
295

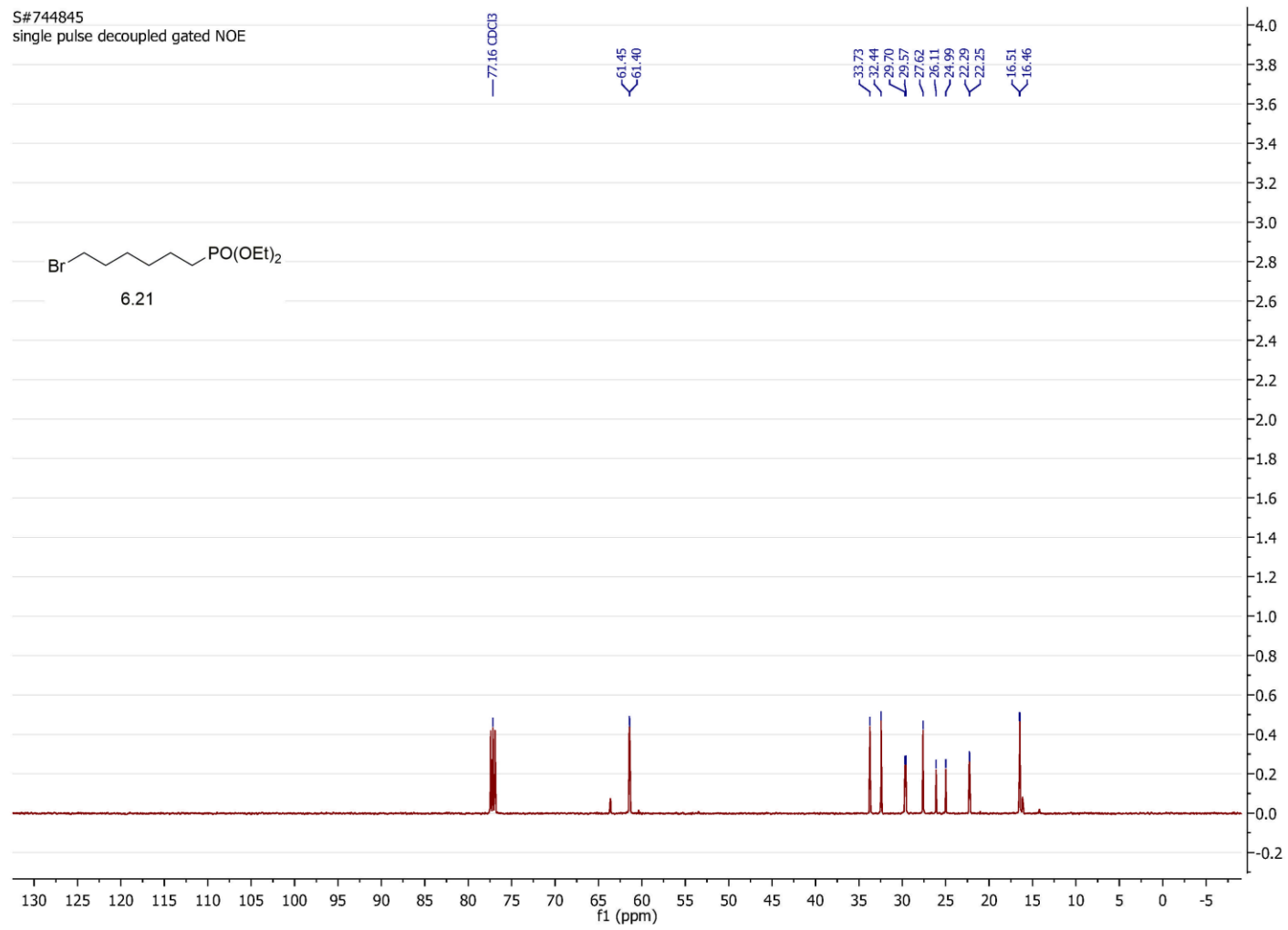




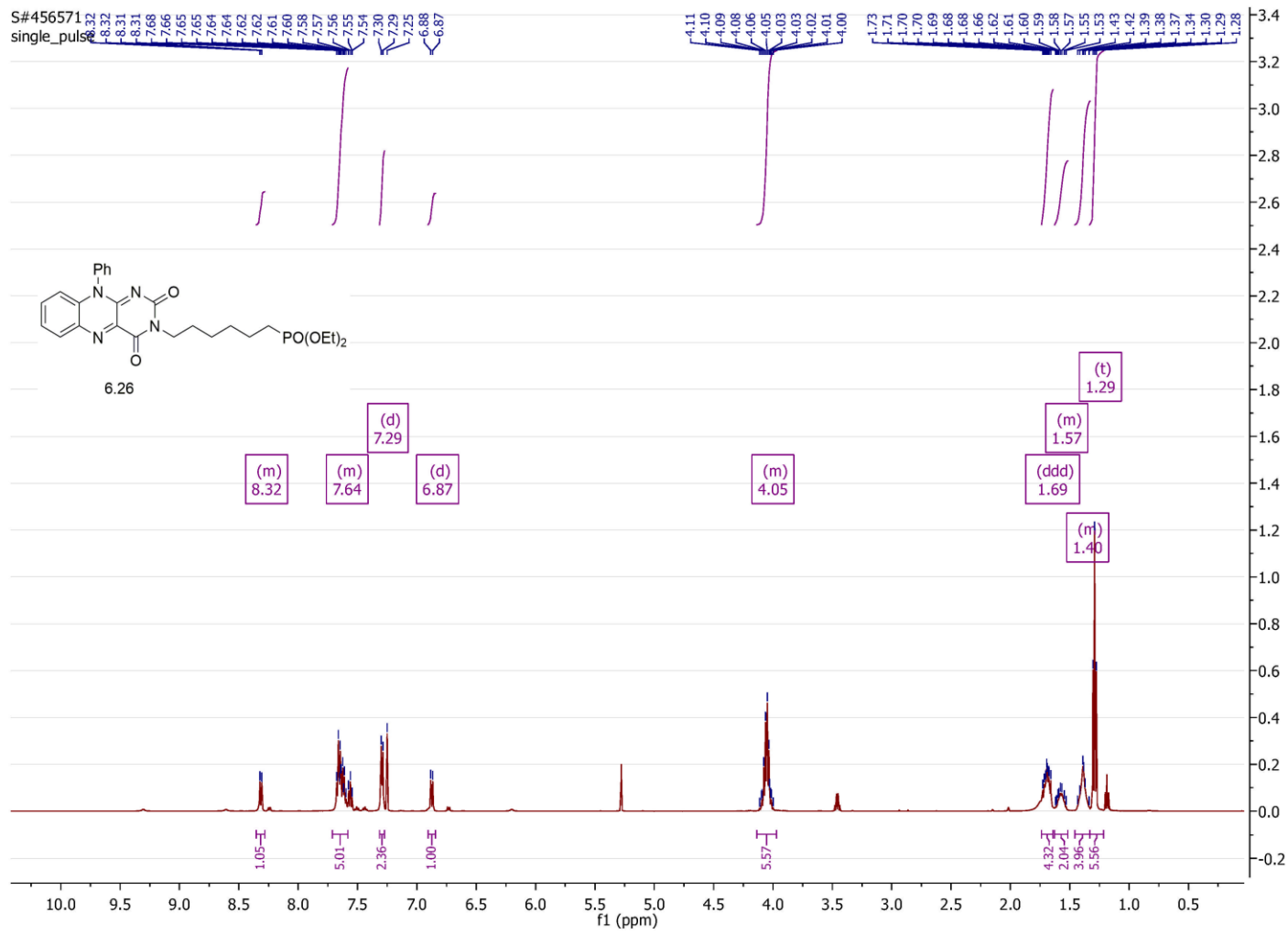
S#429304
single pulse decoupled gated



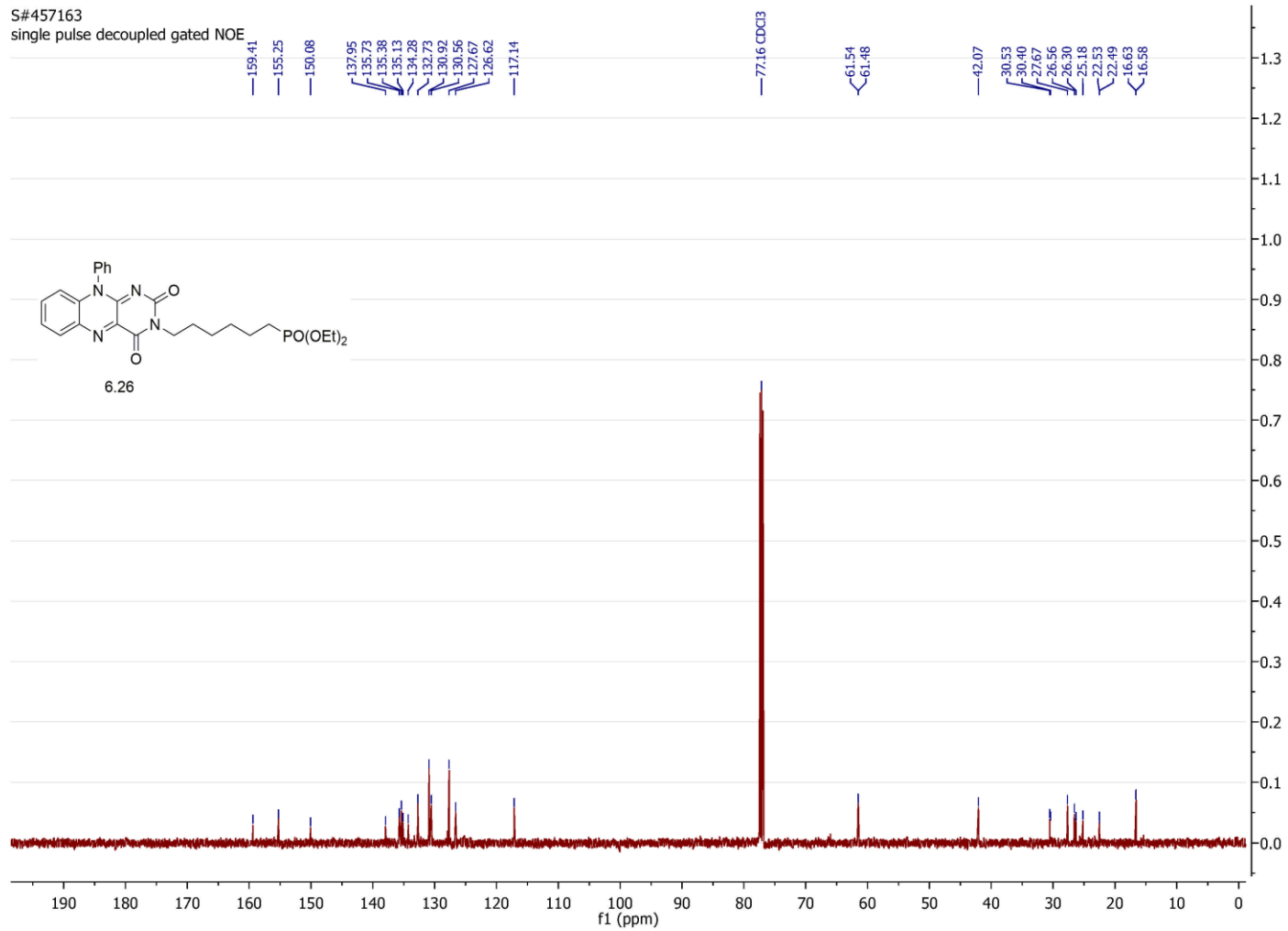




300

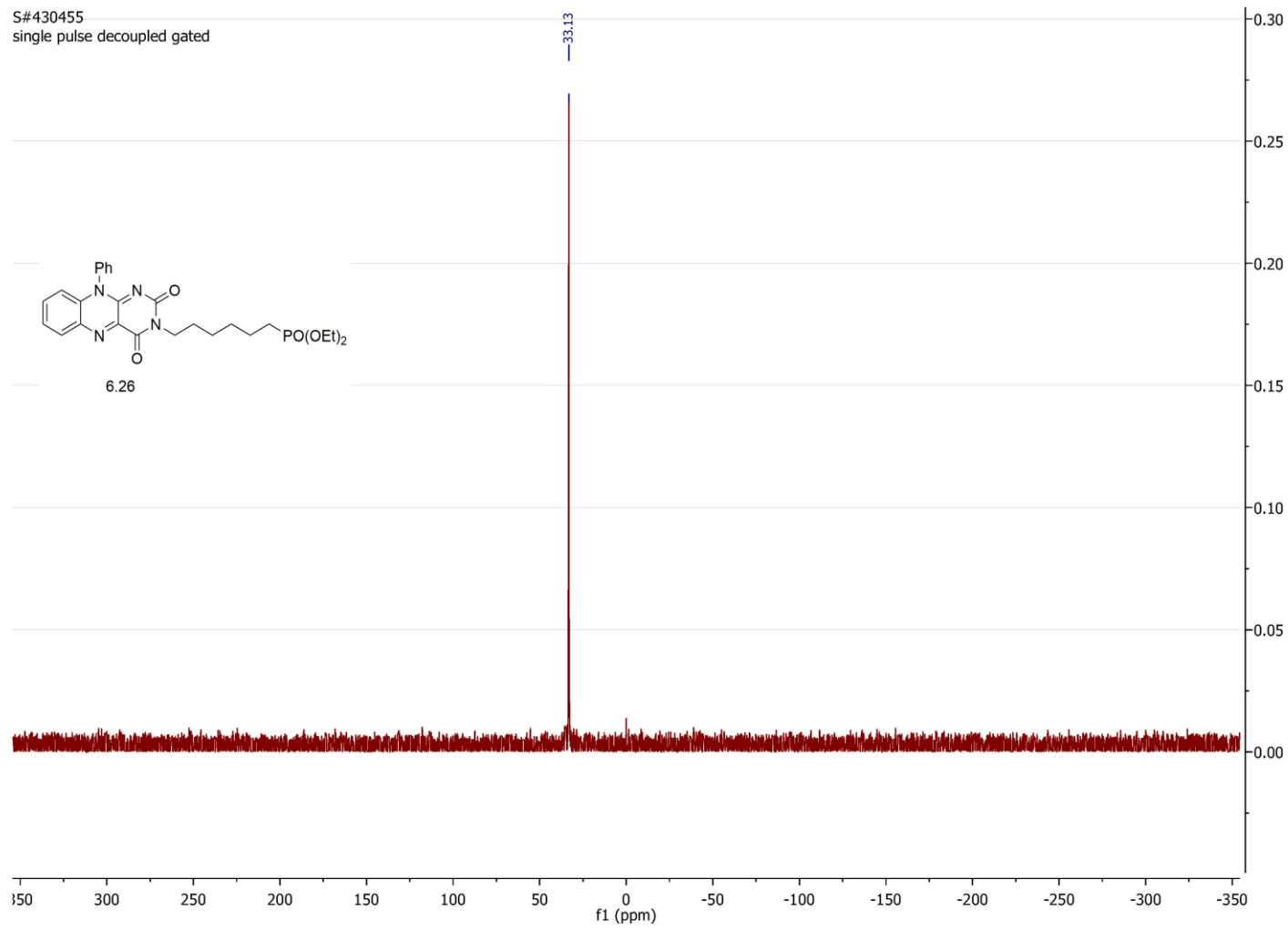


S#457163
single pulse decoupled gated NOE



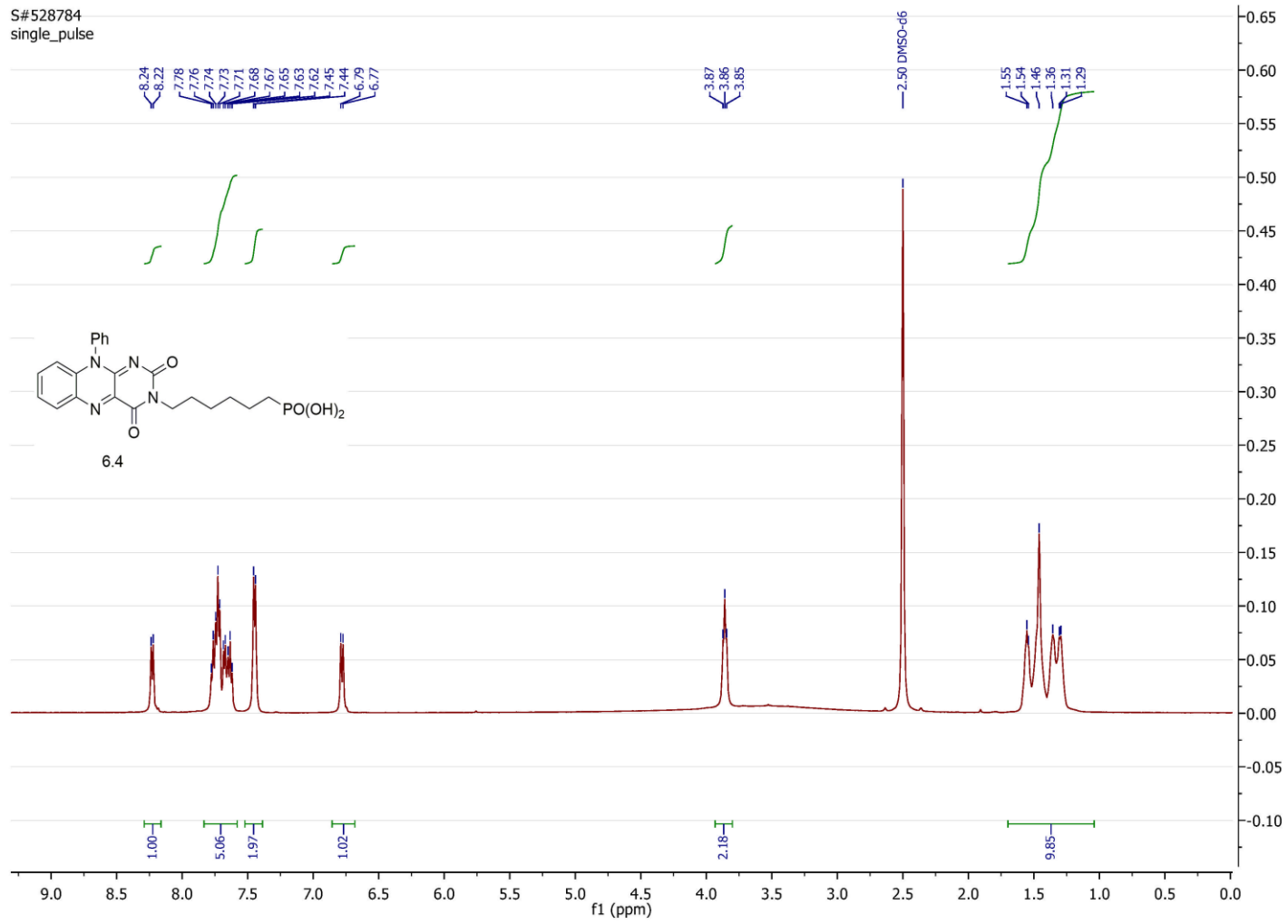
301

S#430455
single pulse decoupled gated

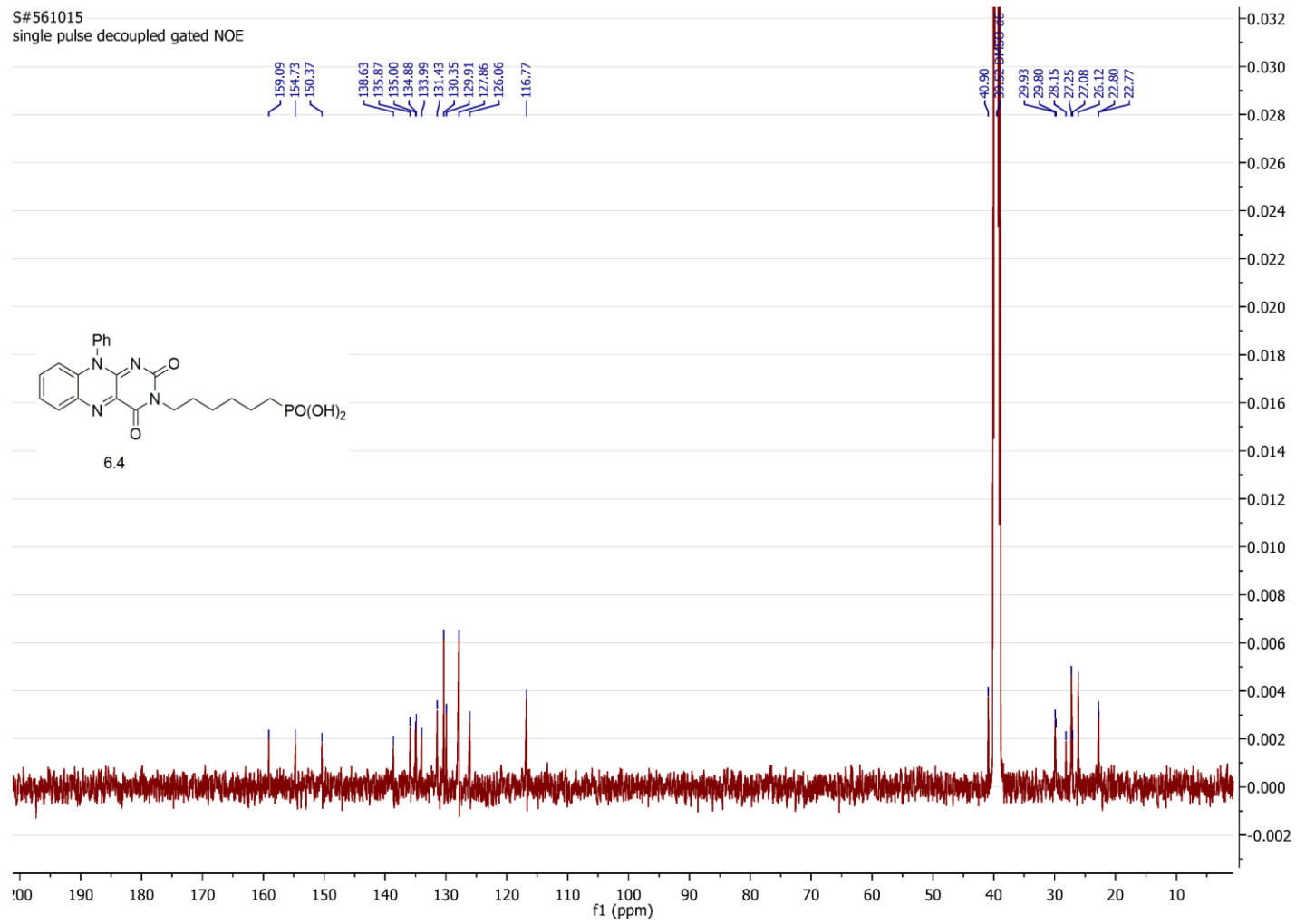


302

303

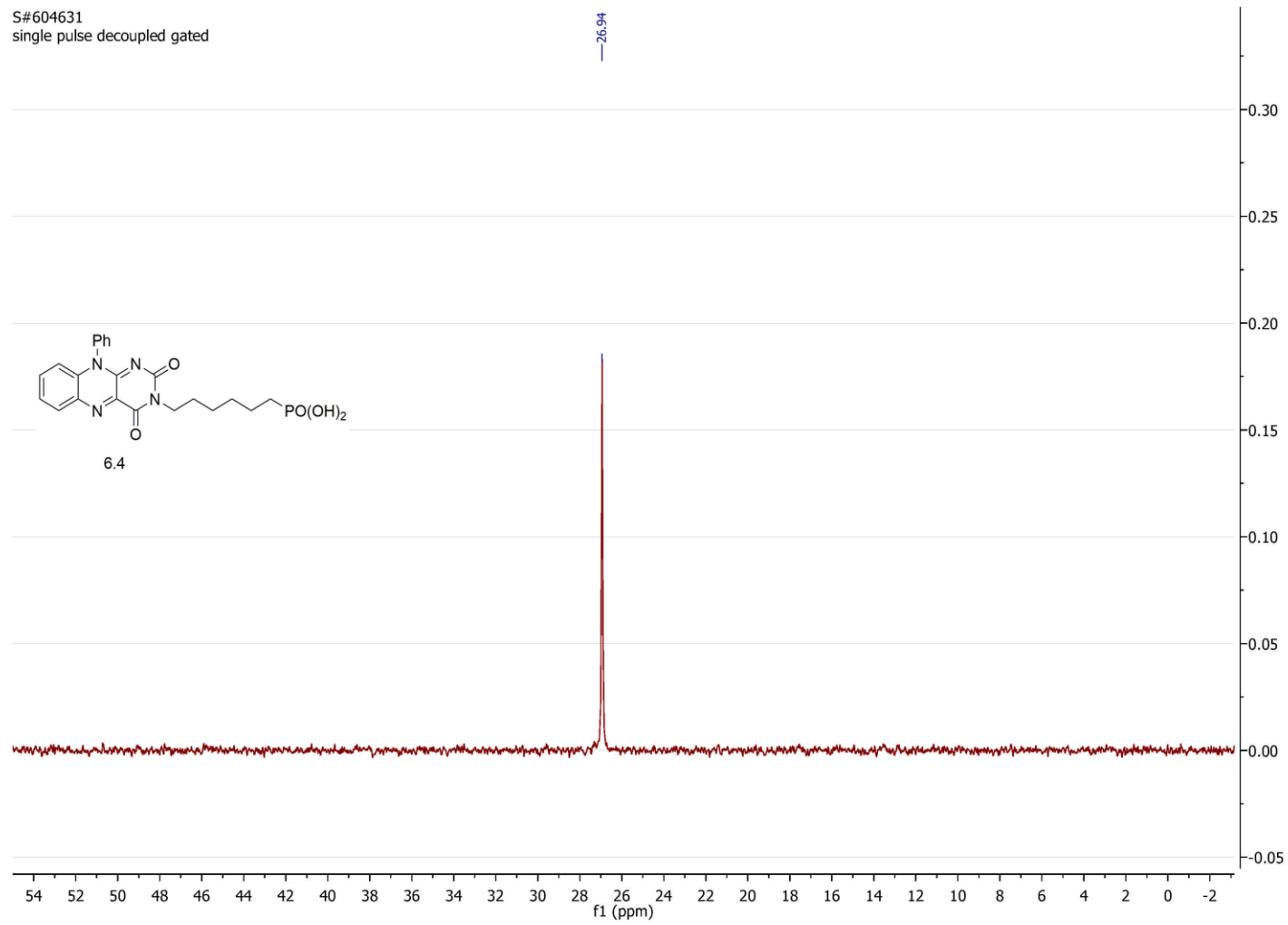


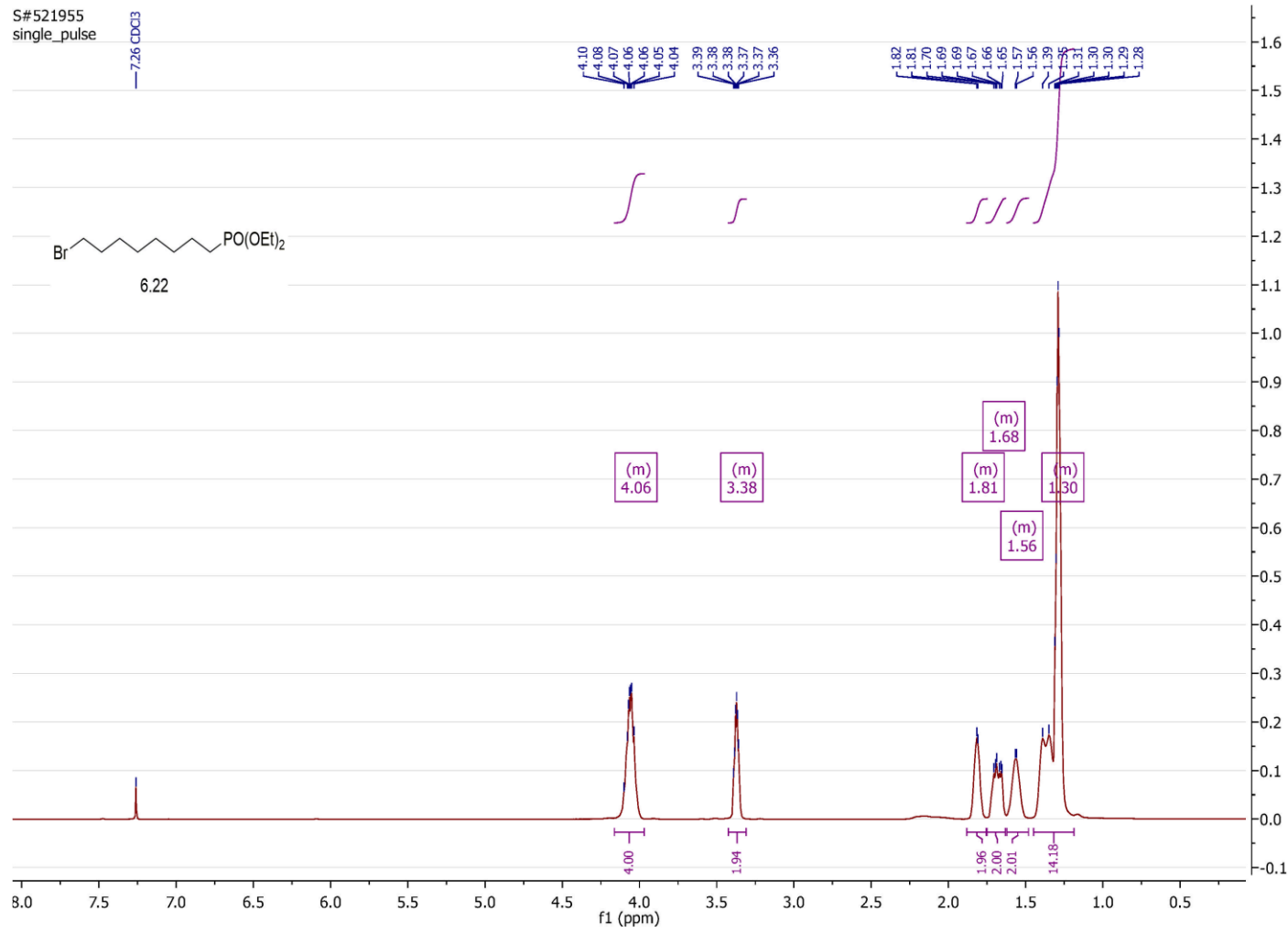
304



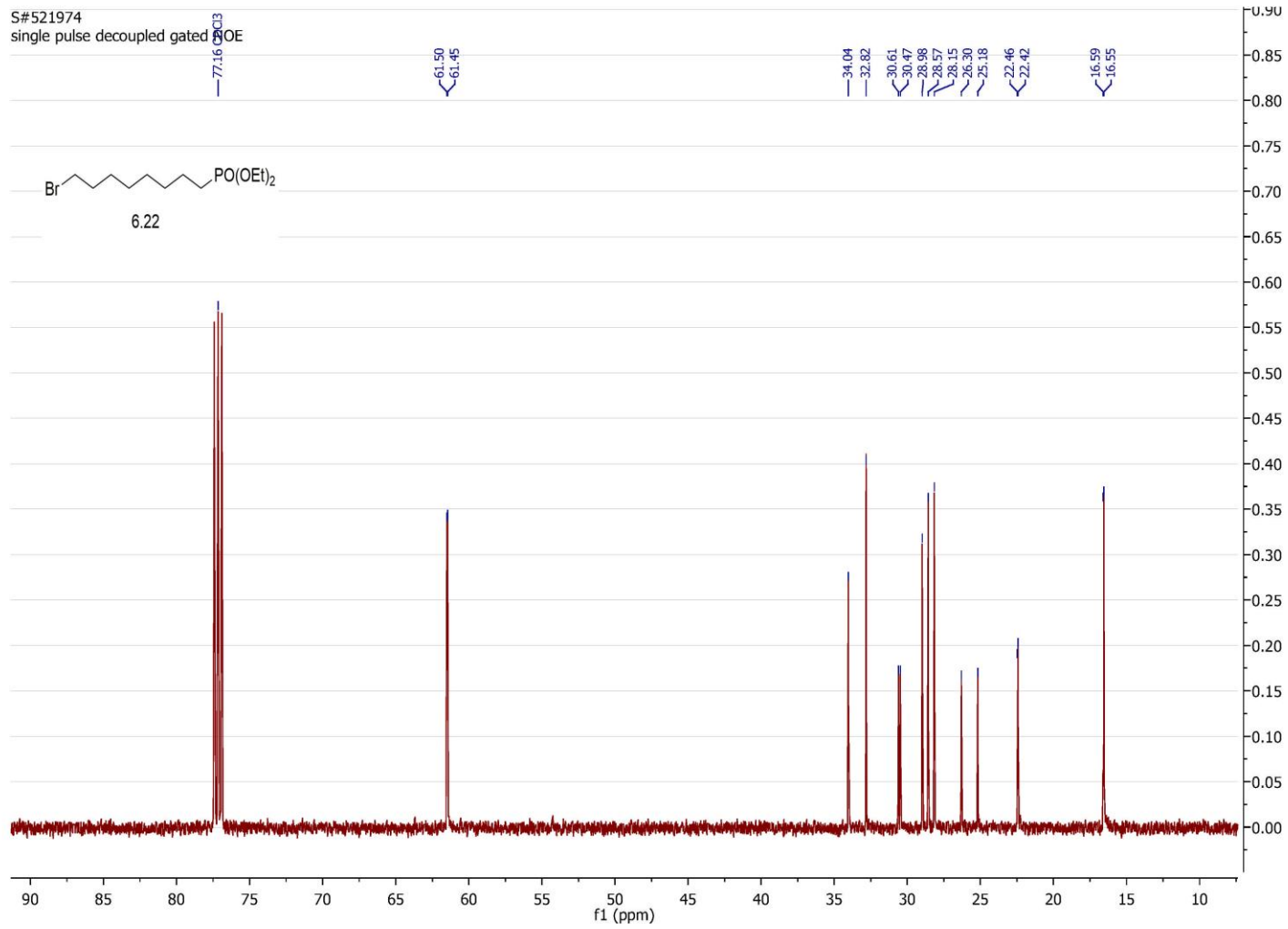
S#604631
single pulse decoupled gated

26.94

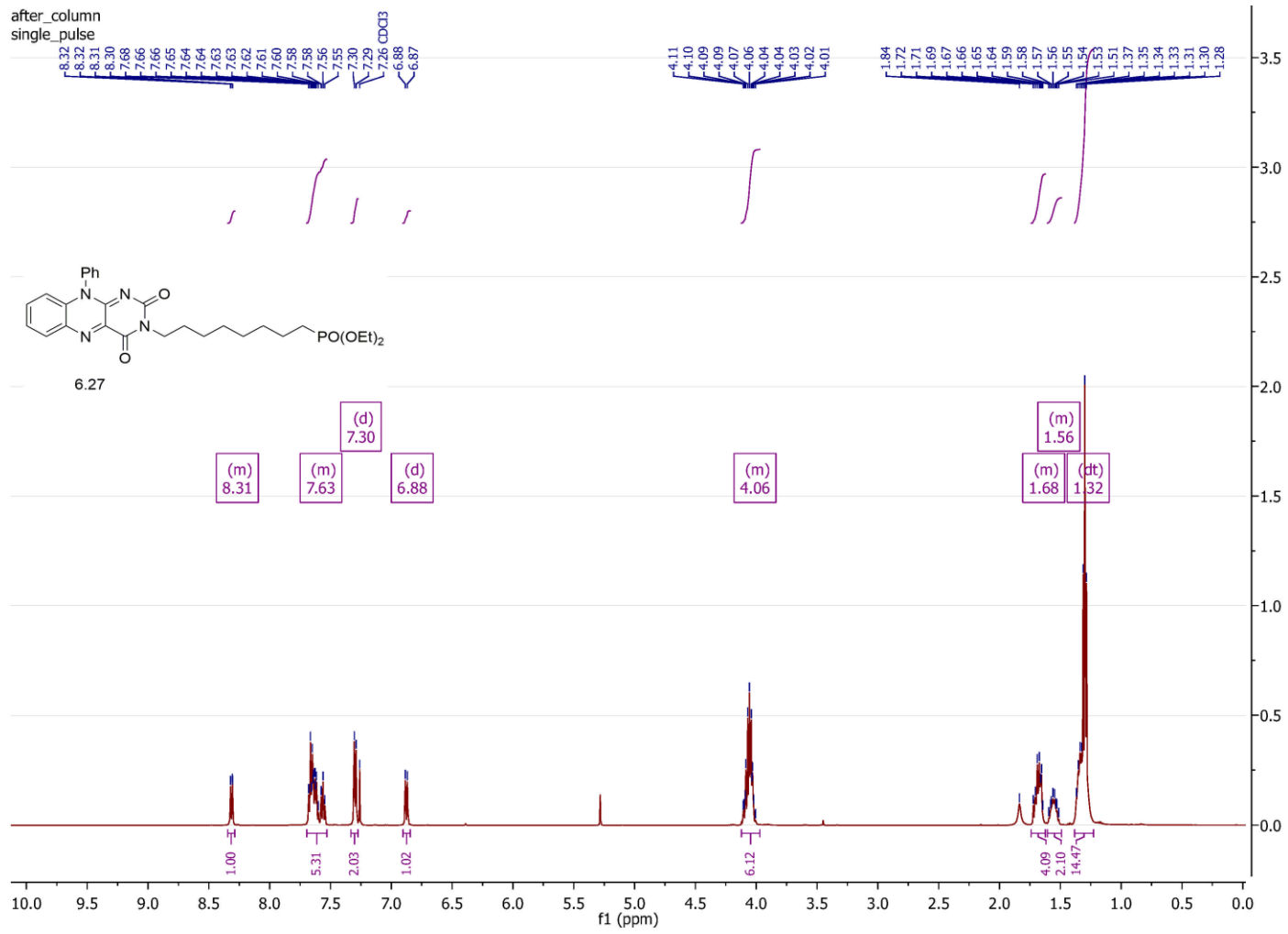




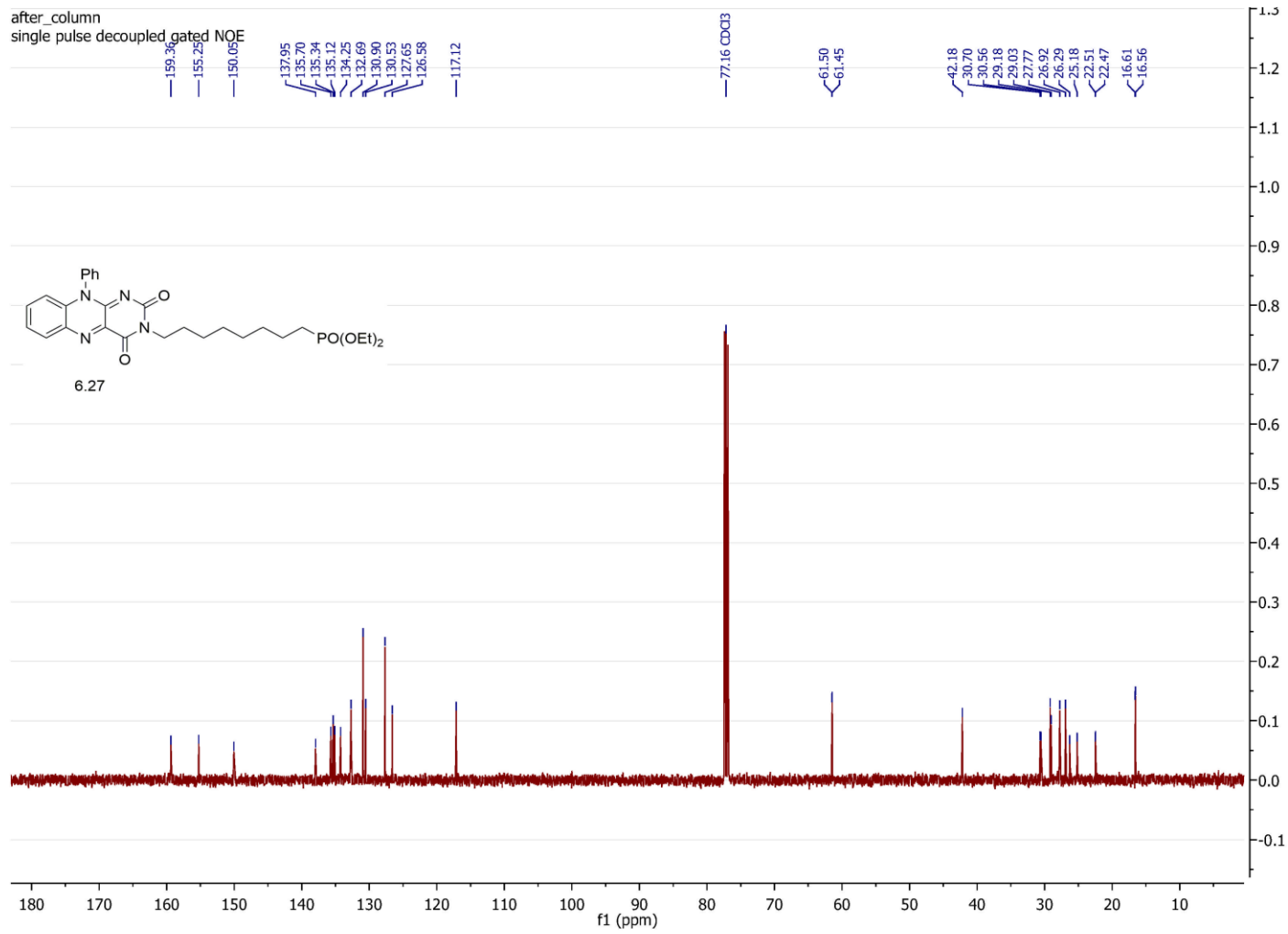
307



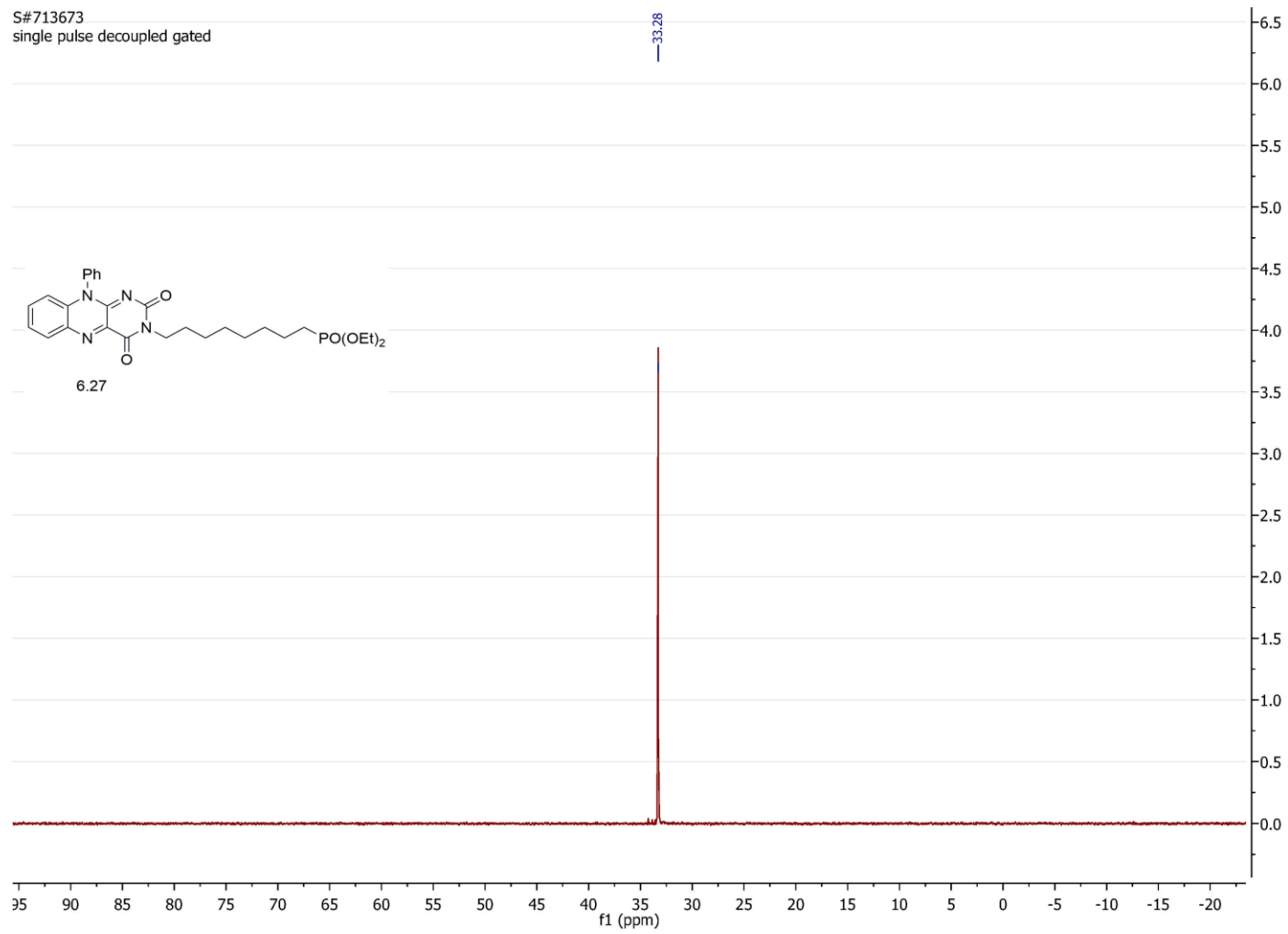
308



309

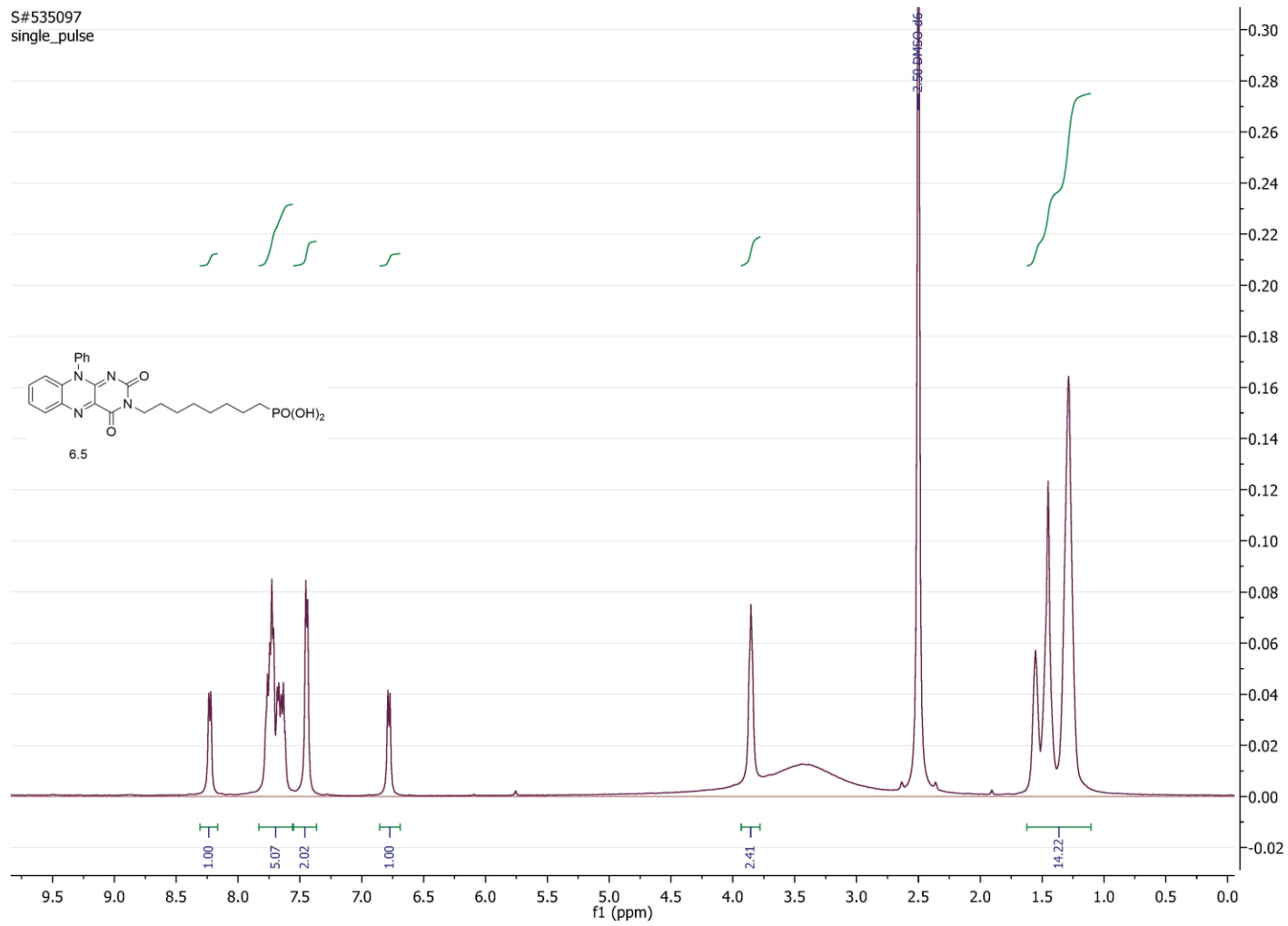


S#713673
single pulse decoupled gated

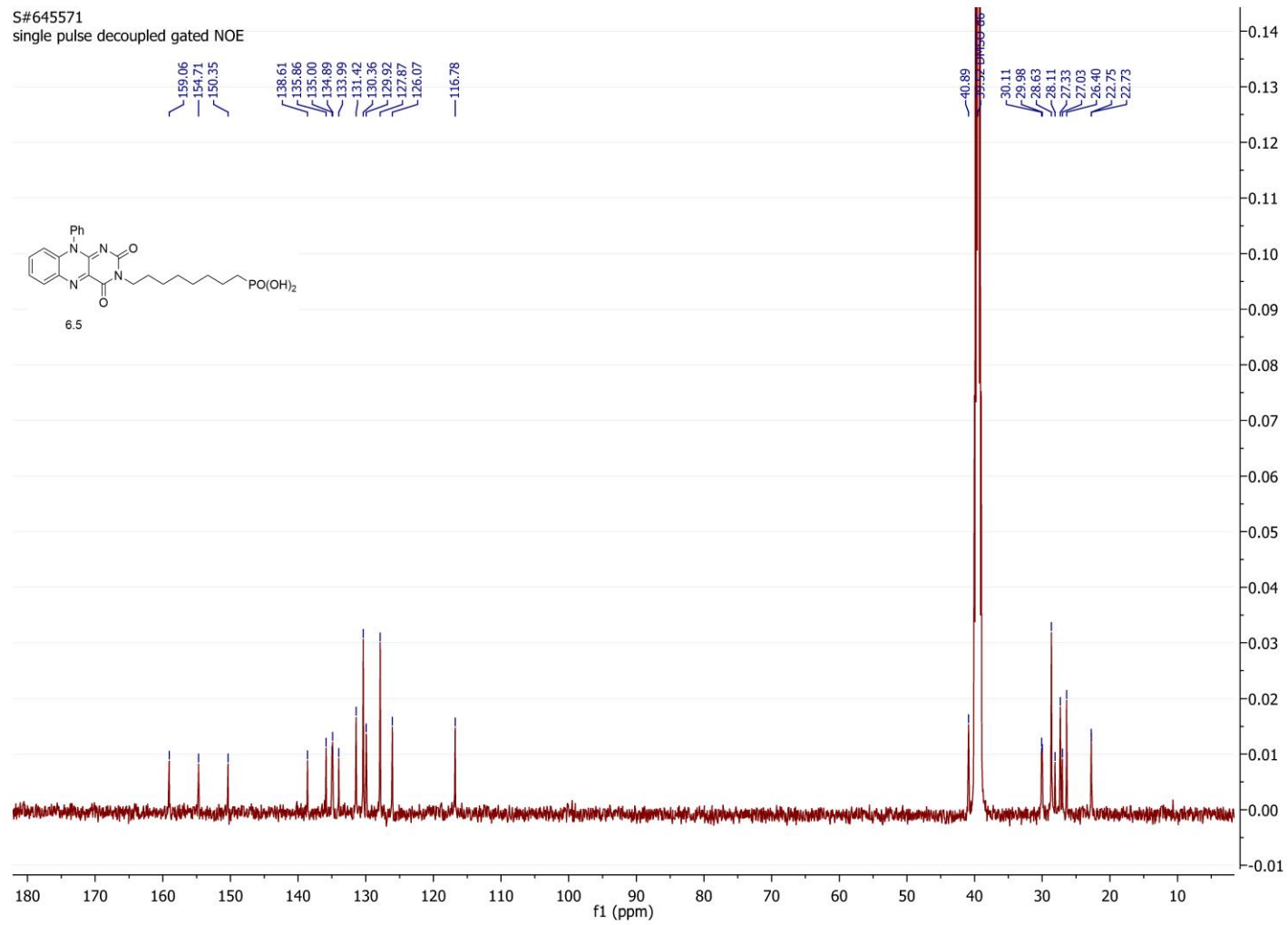


310

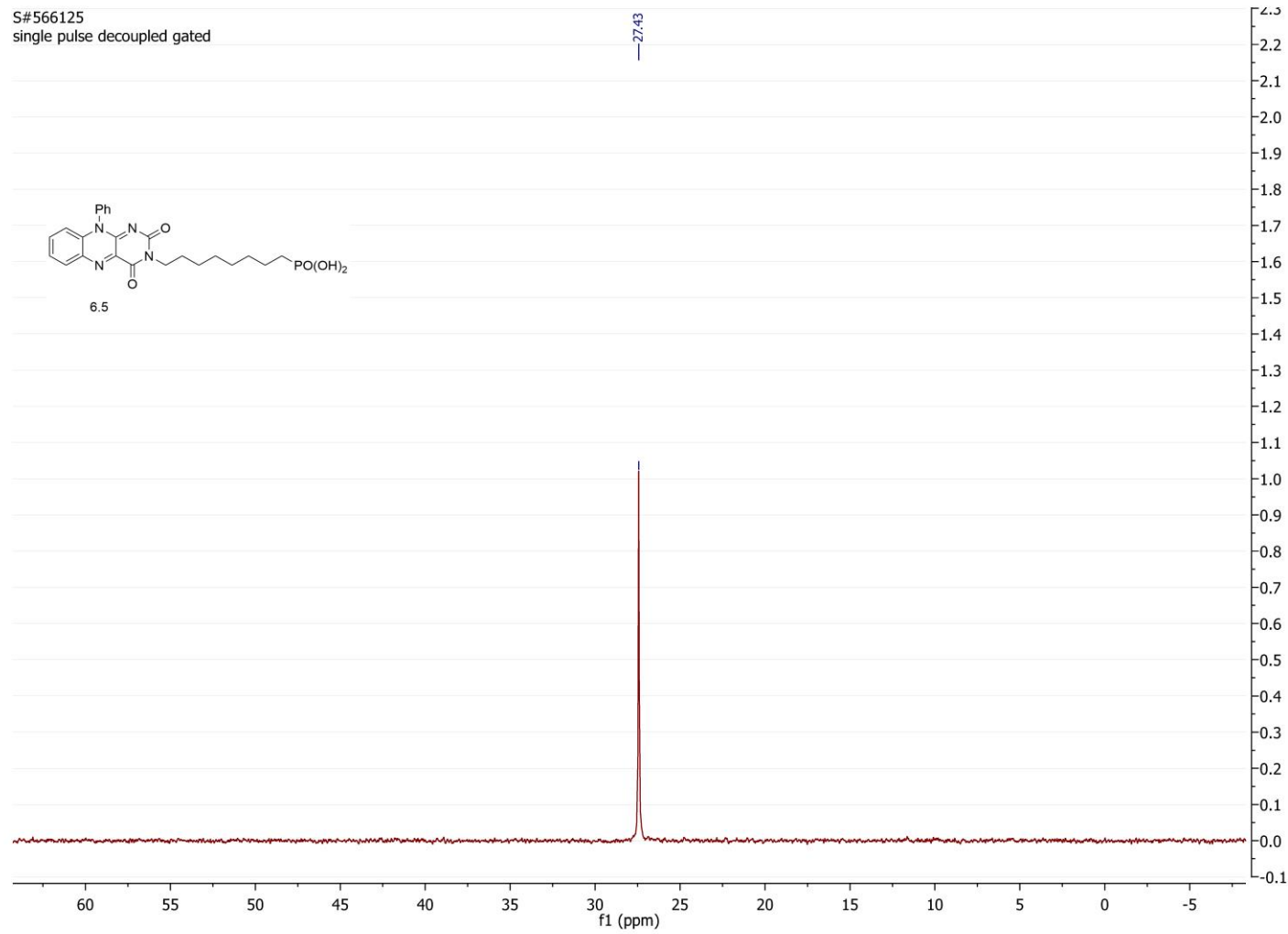
S#535097
single_pulse



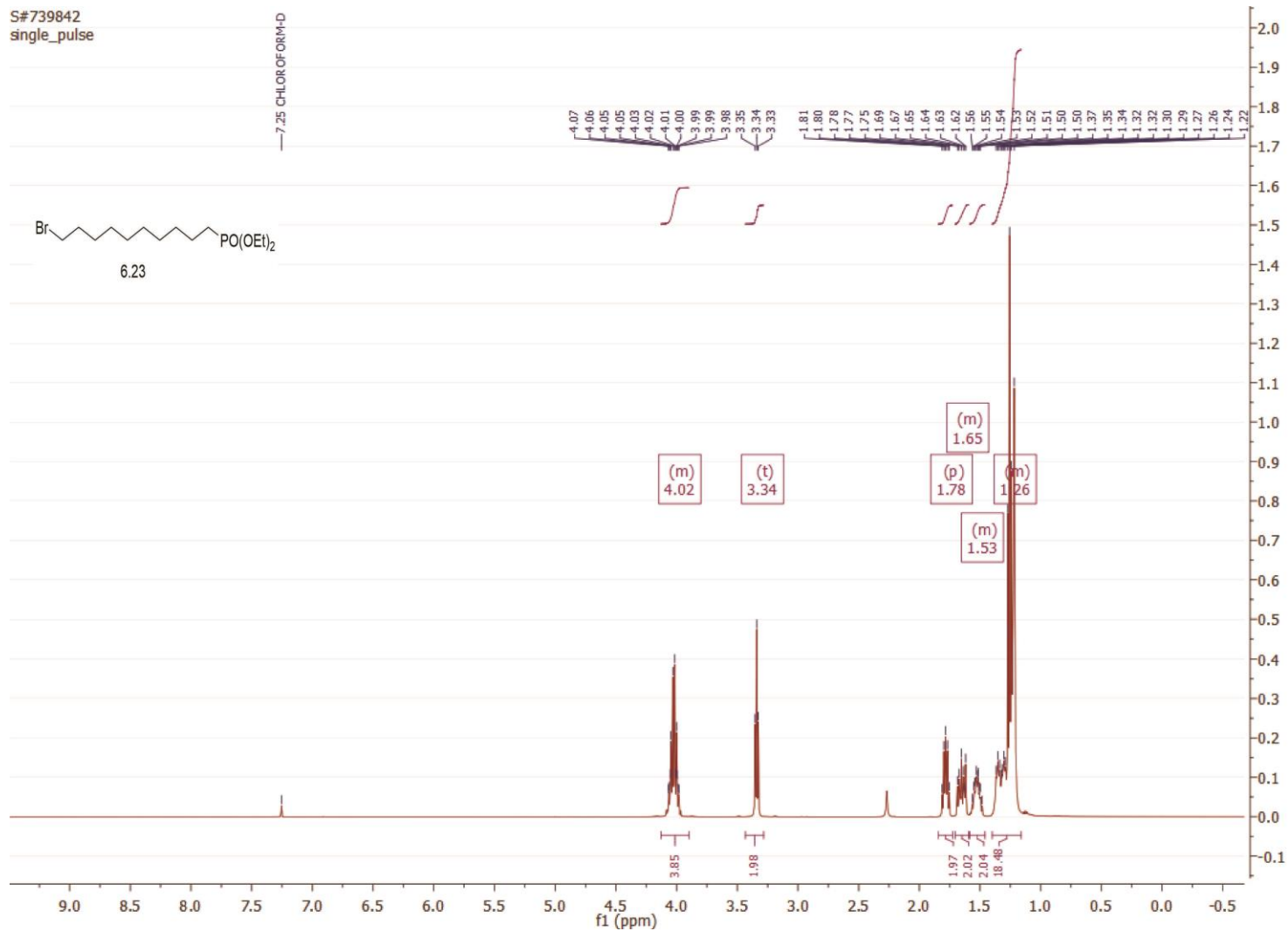
311

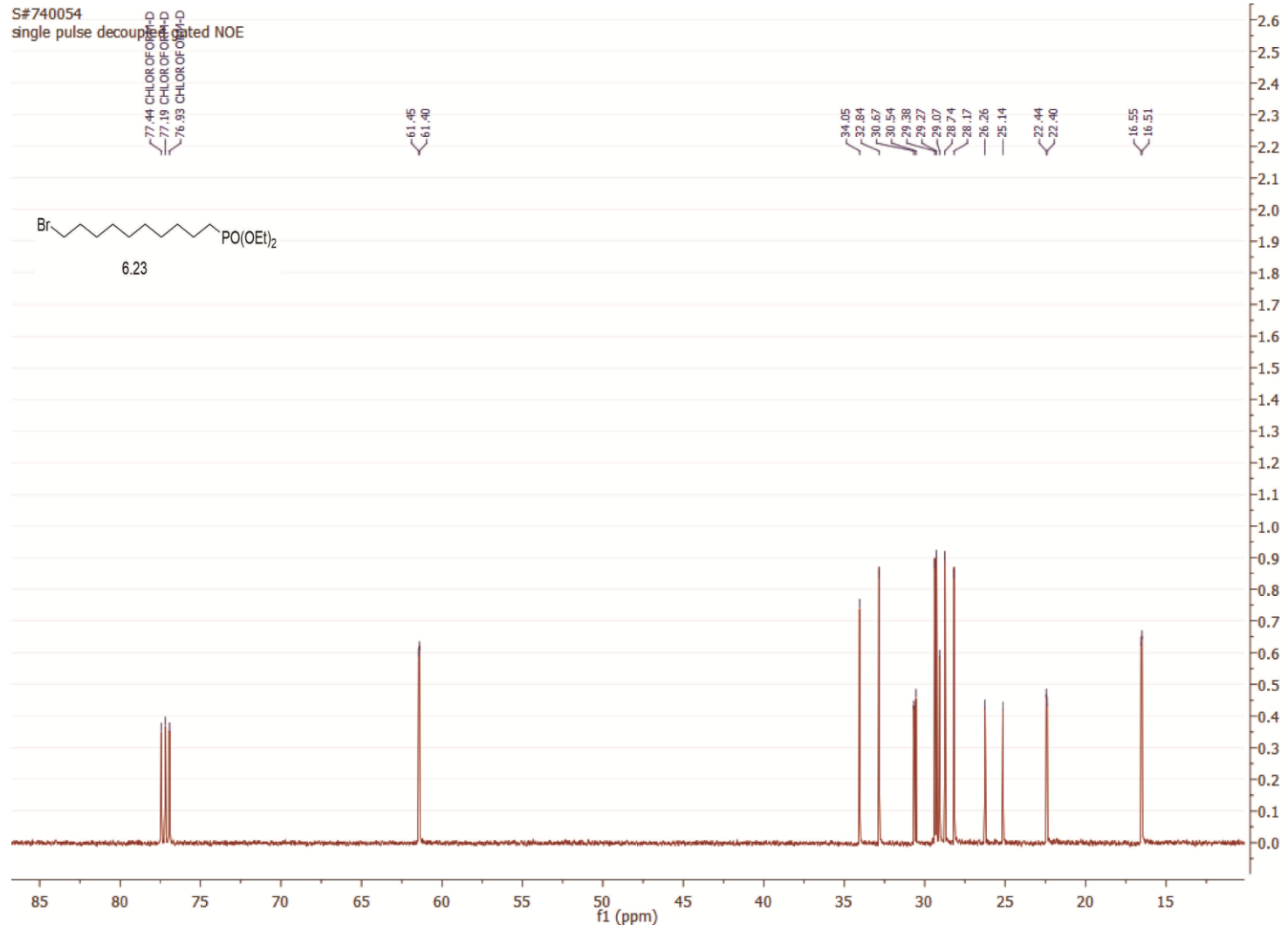


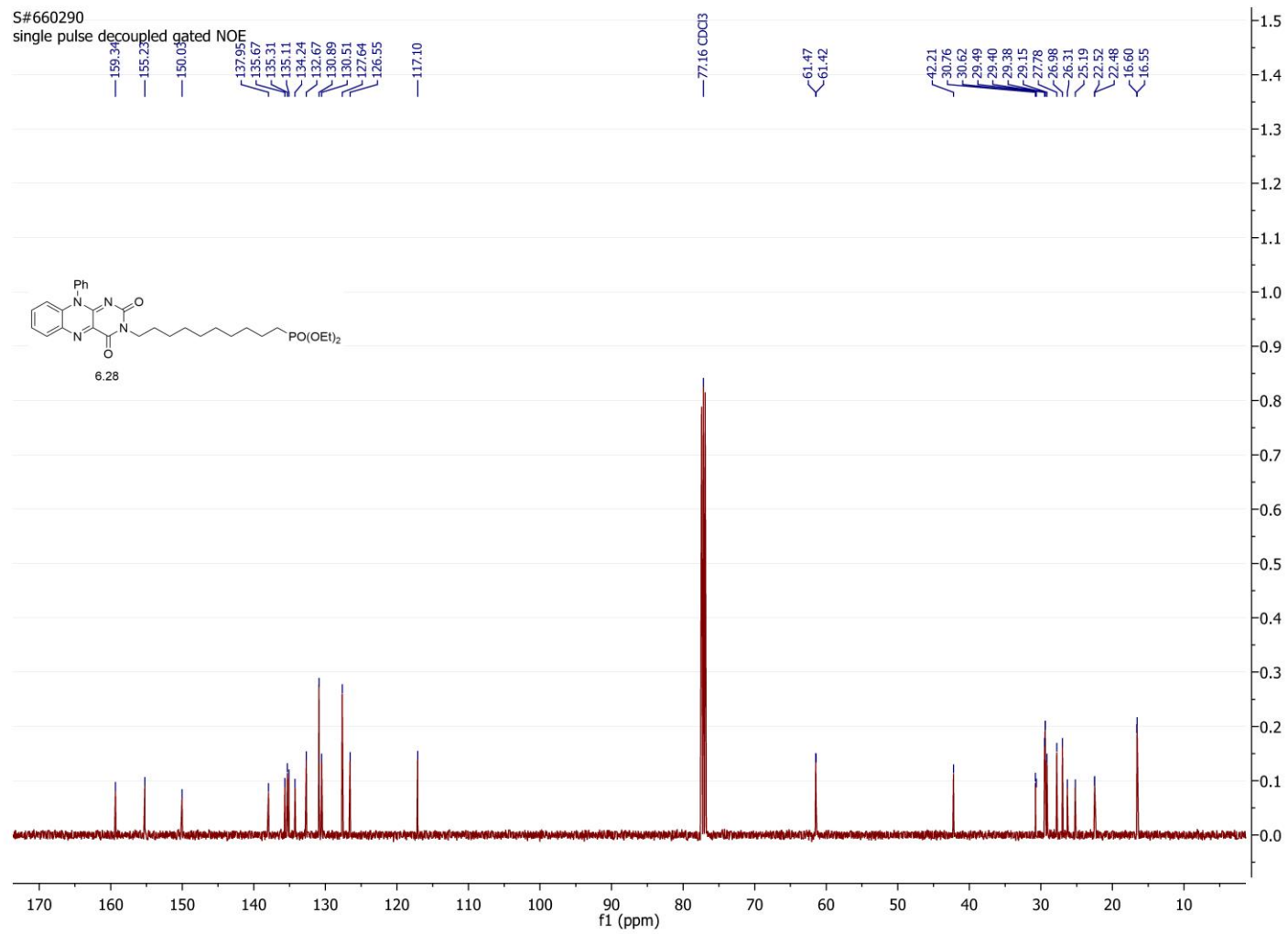
S#566125
single pulse decoupled gated



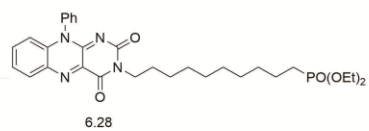
313





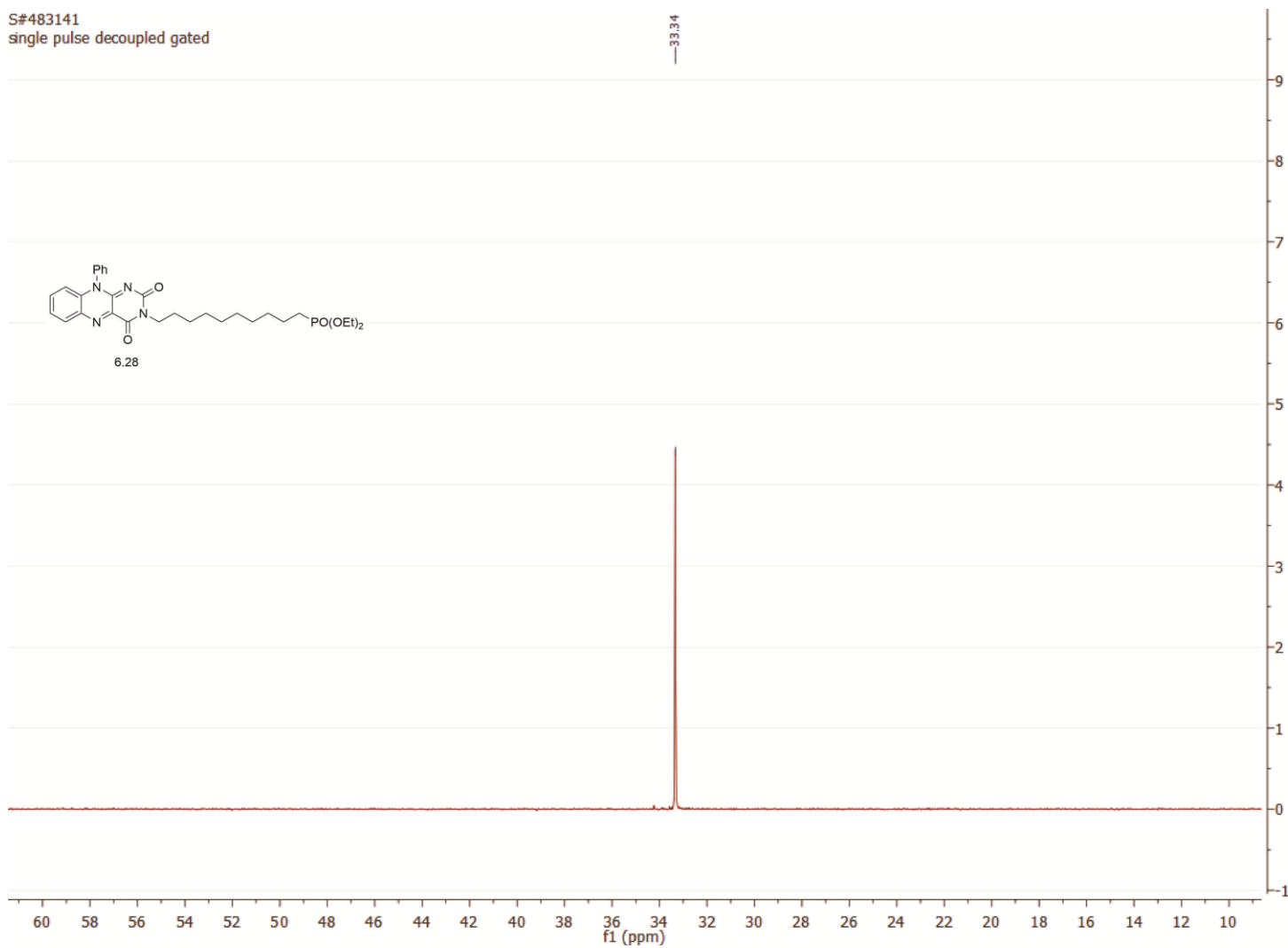


S#483141
single pulse decoupled gated

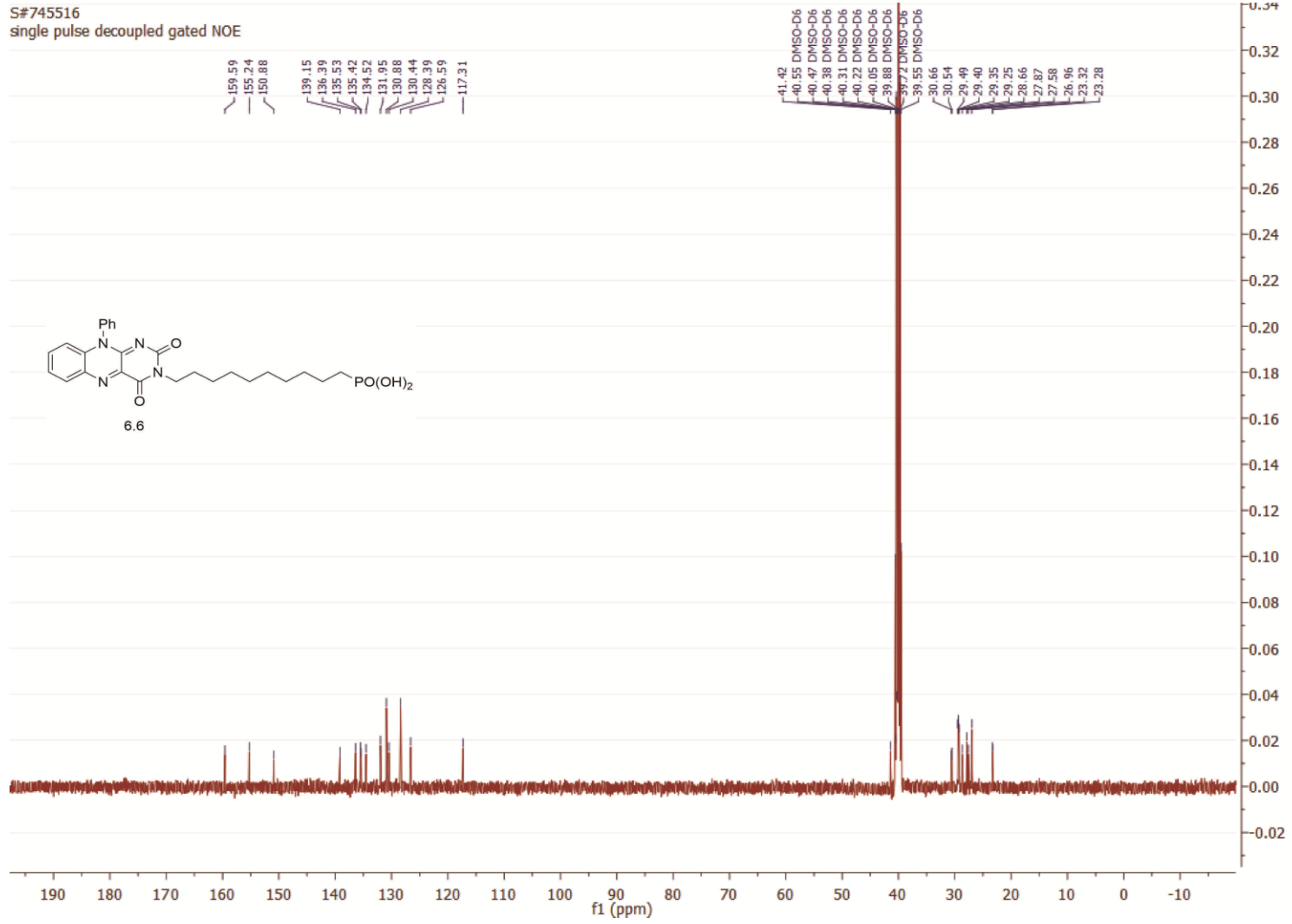


33.34

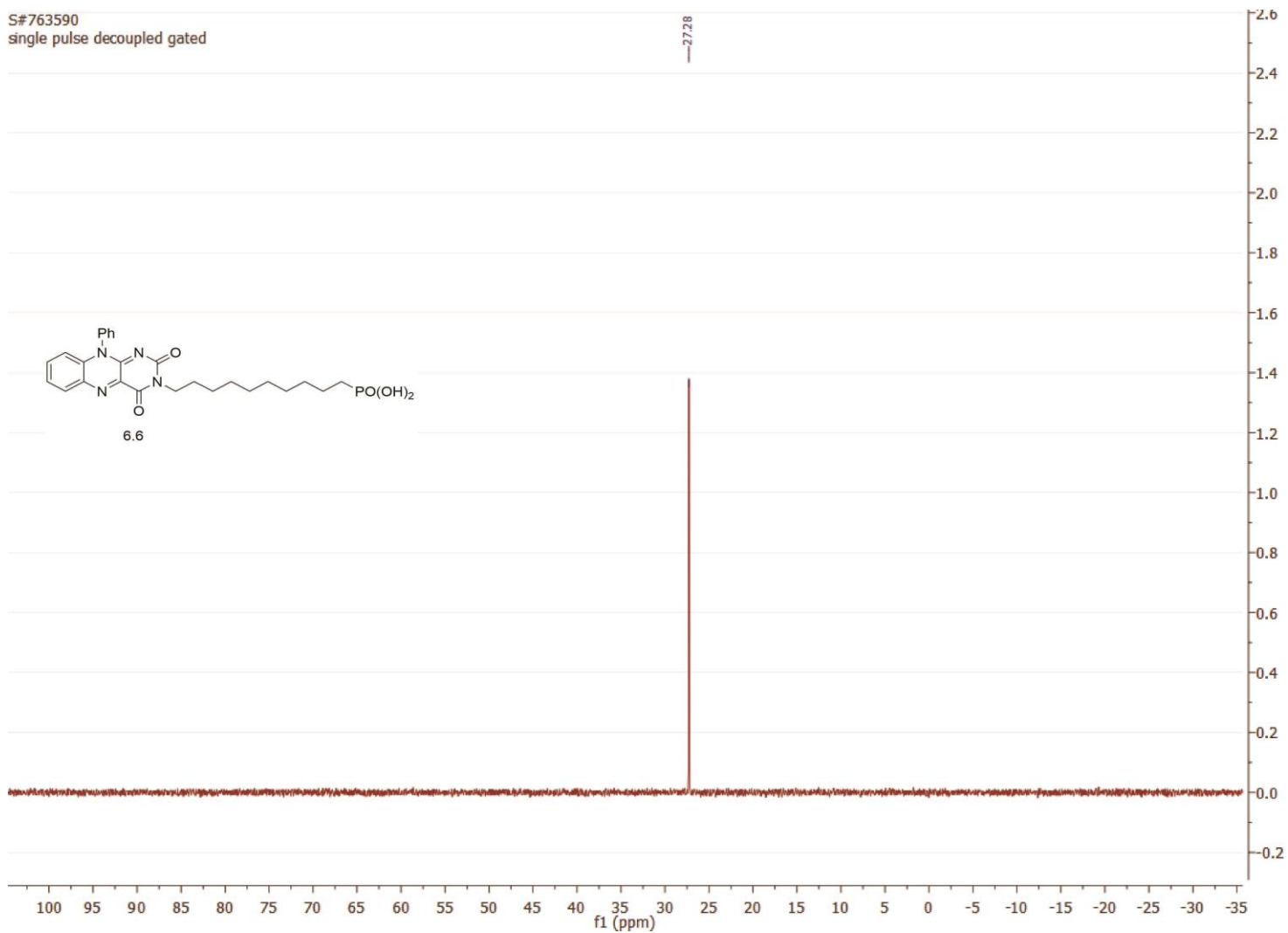
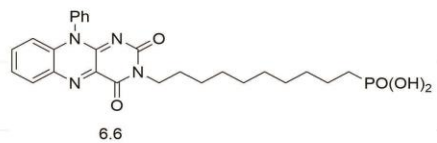
318



S#745516
single pulse decoupled gated NOE



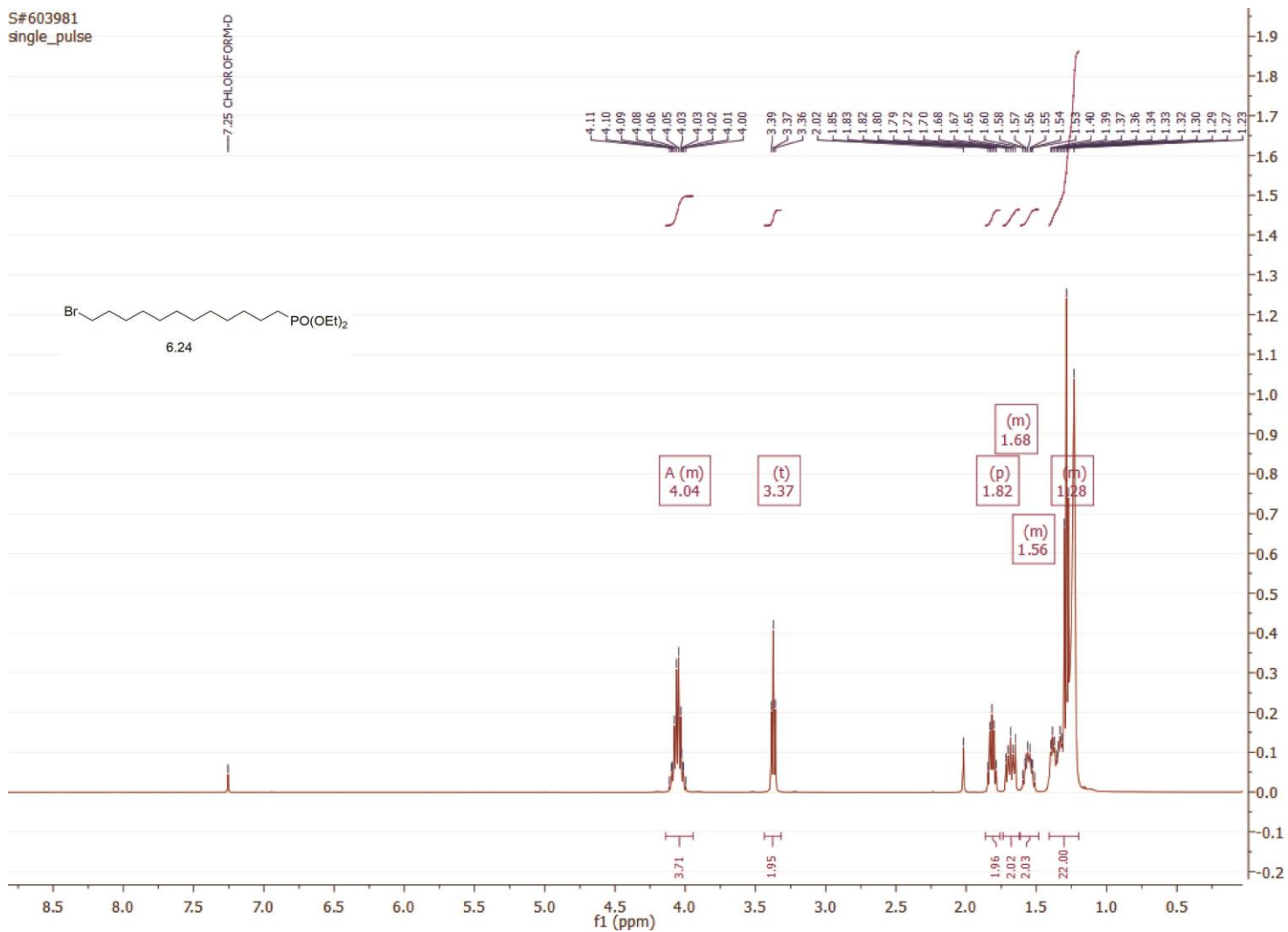
S#763590
single pulse decoupled gated



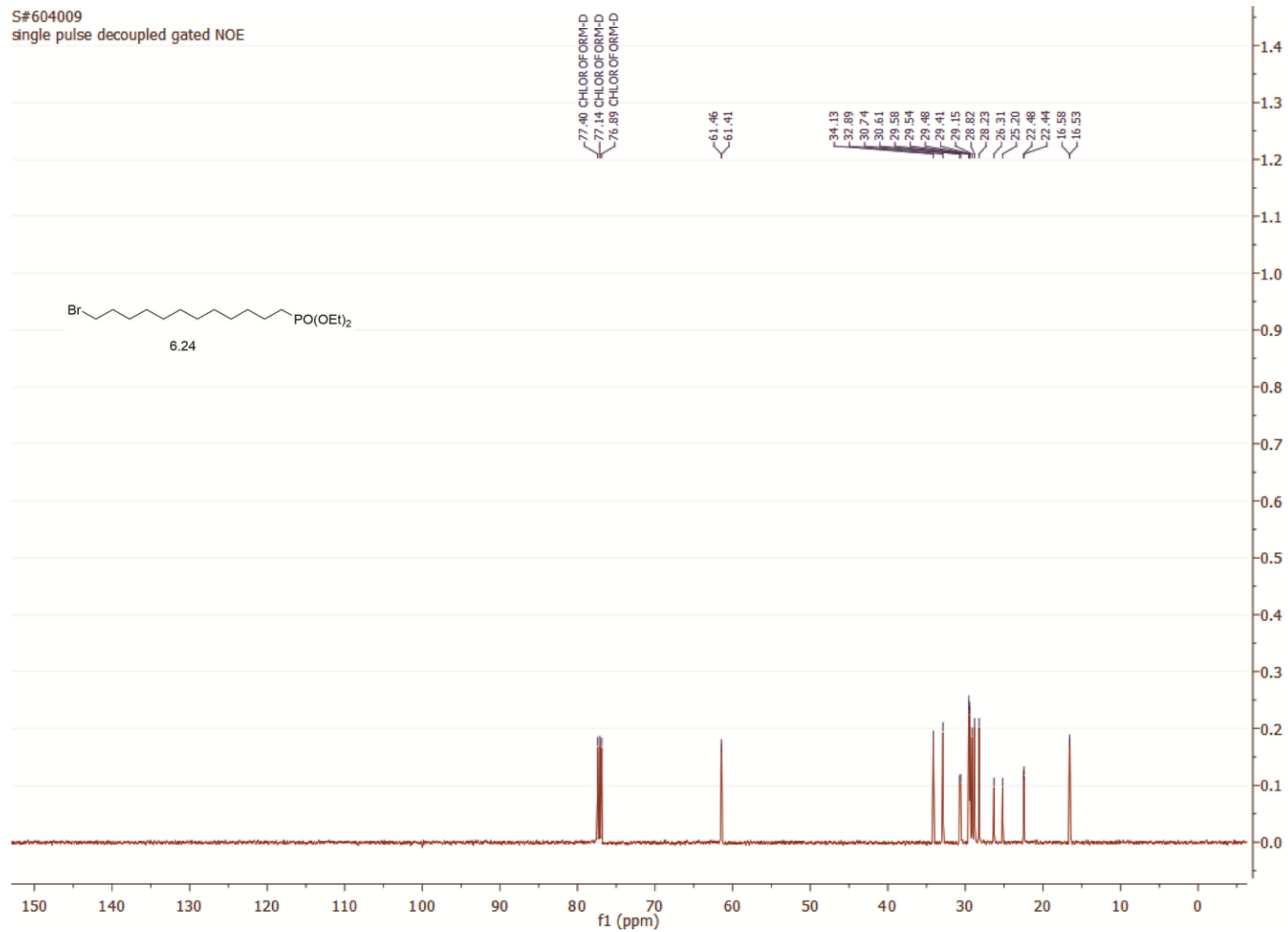
321

S#603981
single_pulse

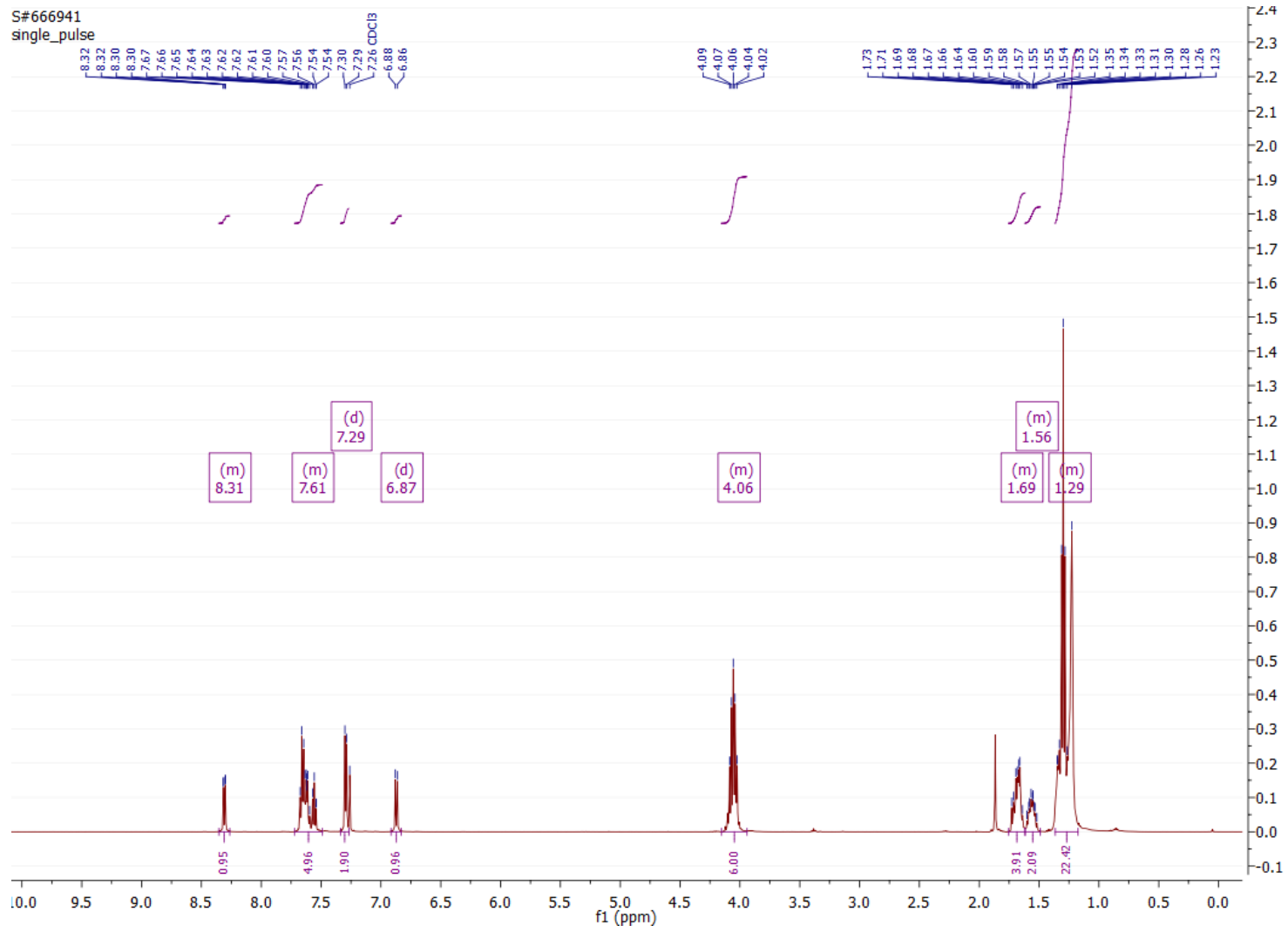
7.25 CHLOROFORM-D



S#604009
single pulse decoupled gated NOE

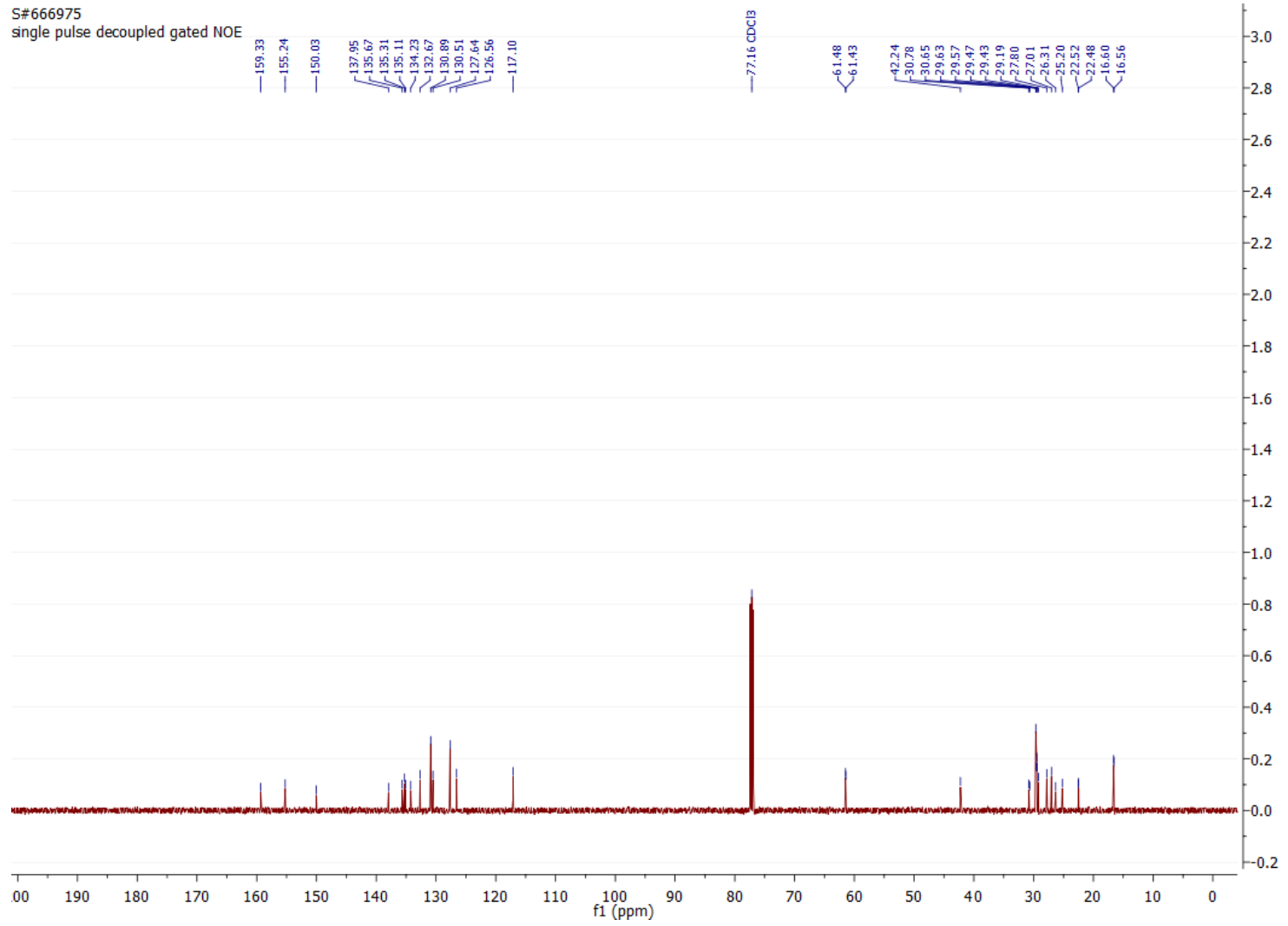


324



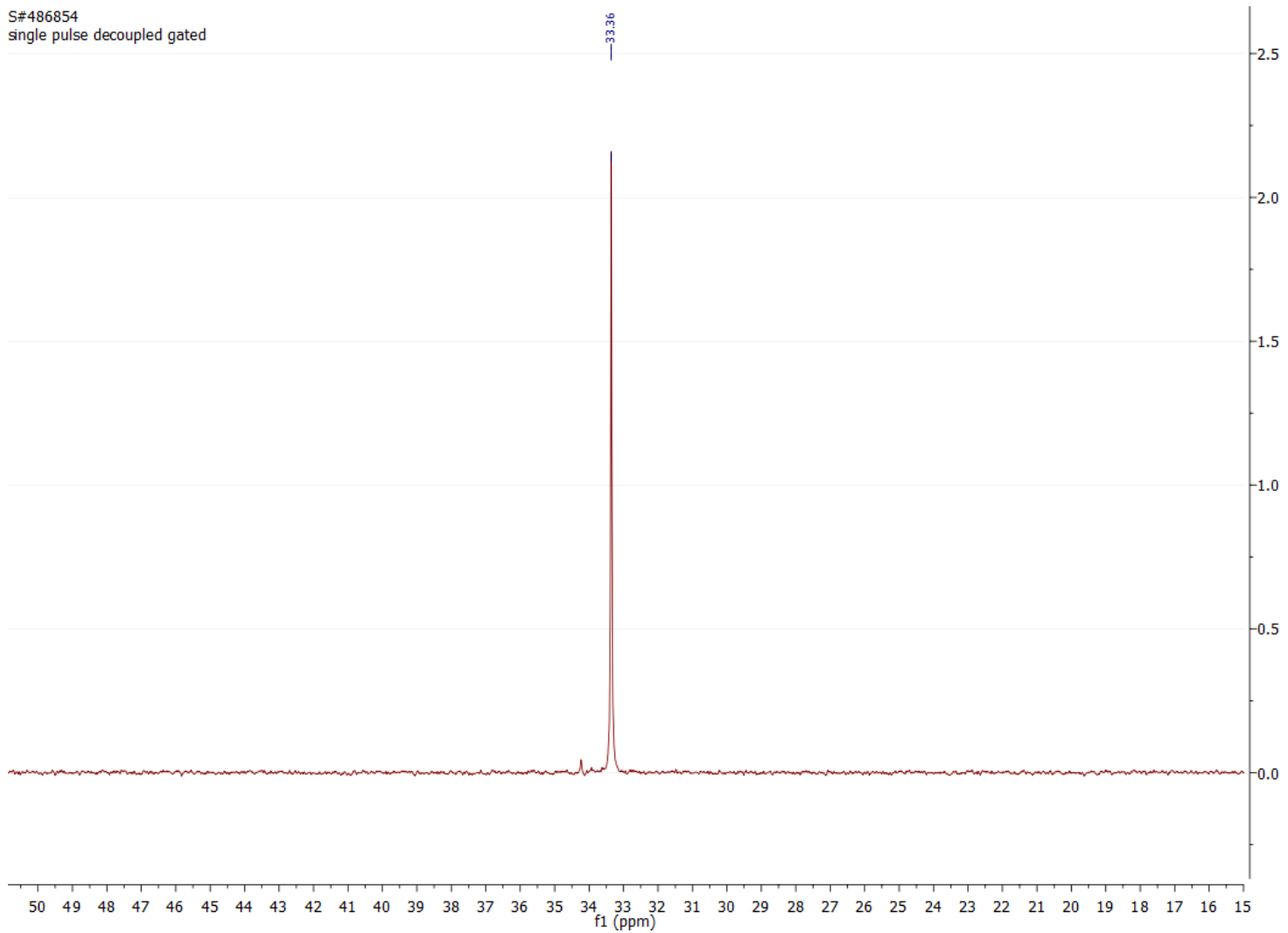
325

S#666975
single pulse decoupled gated NOE

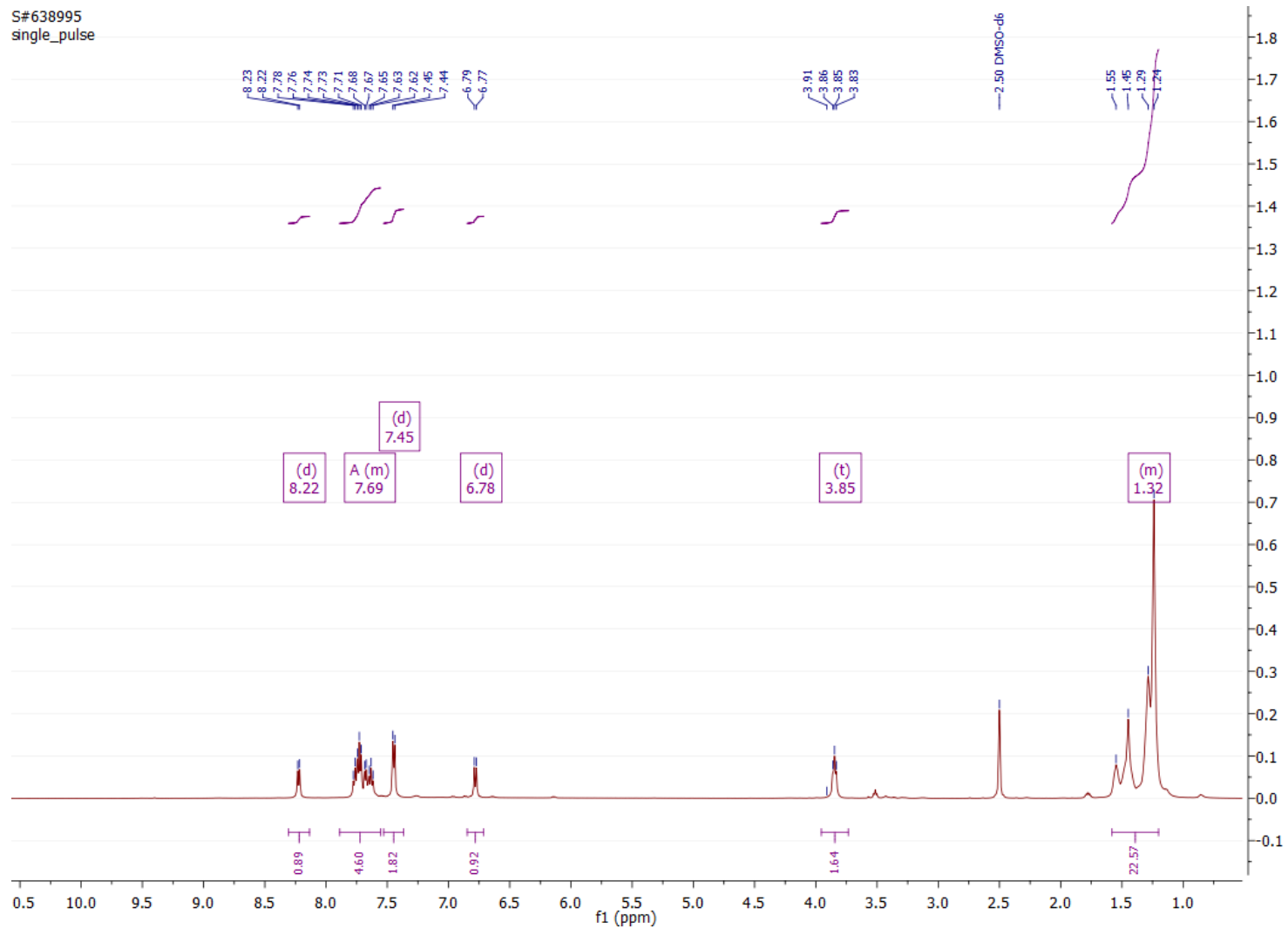


S#486854
single pulse decoupled gated

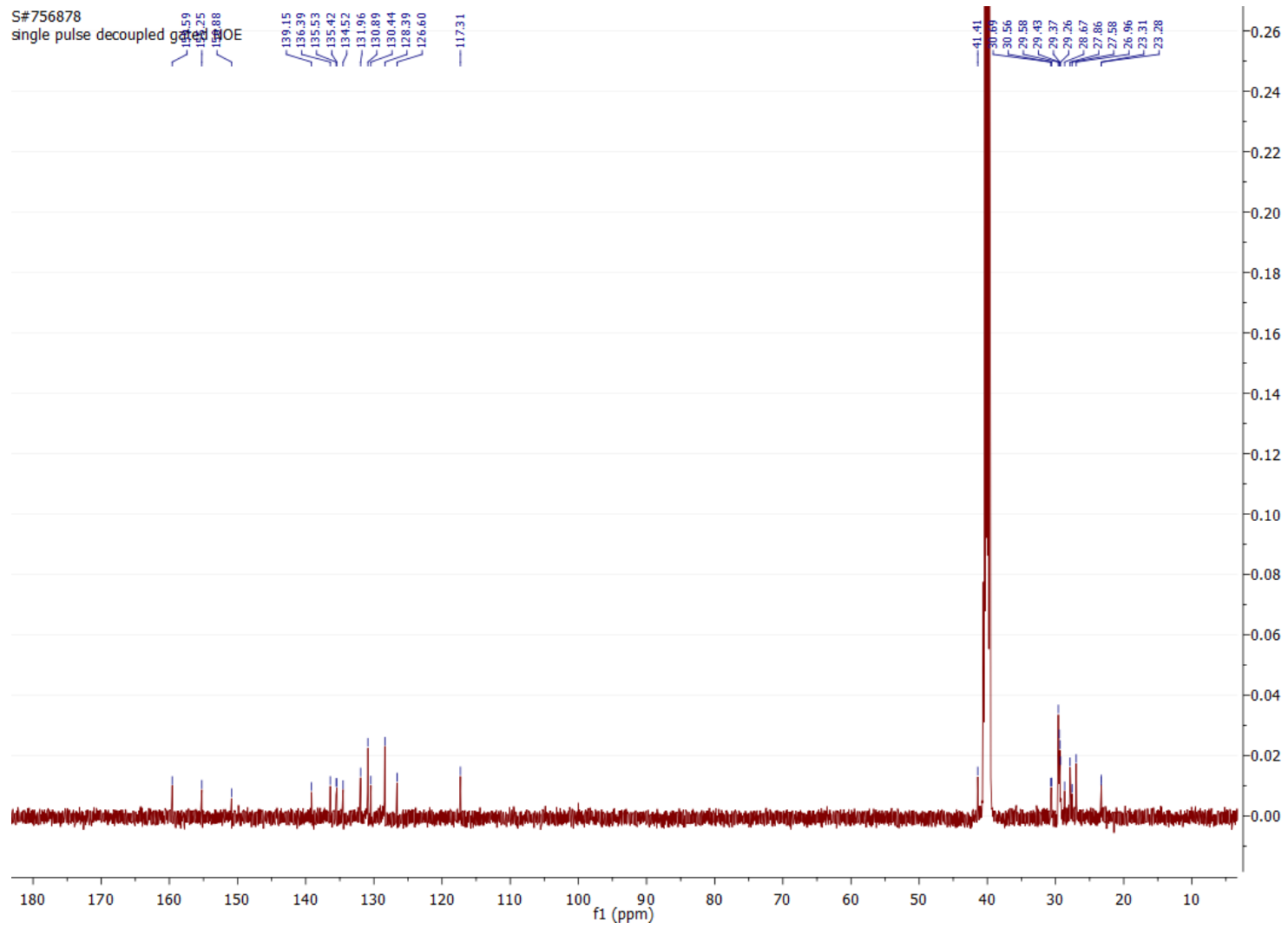
326



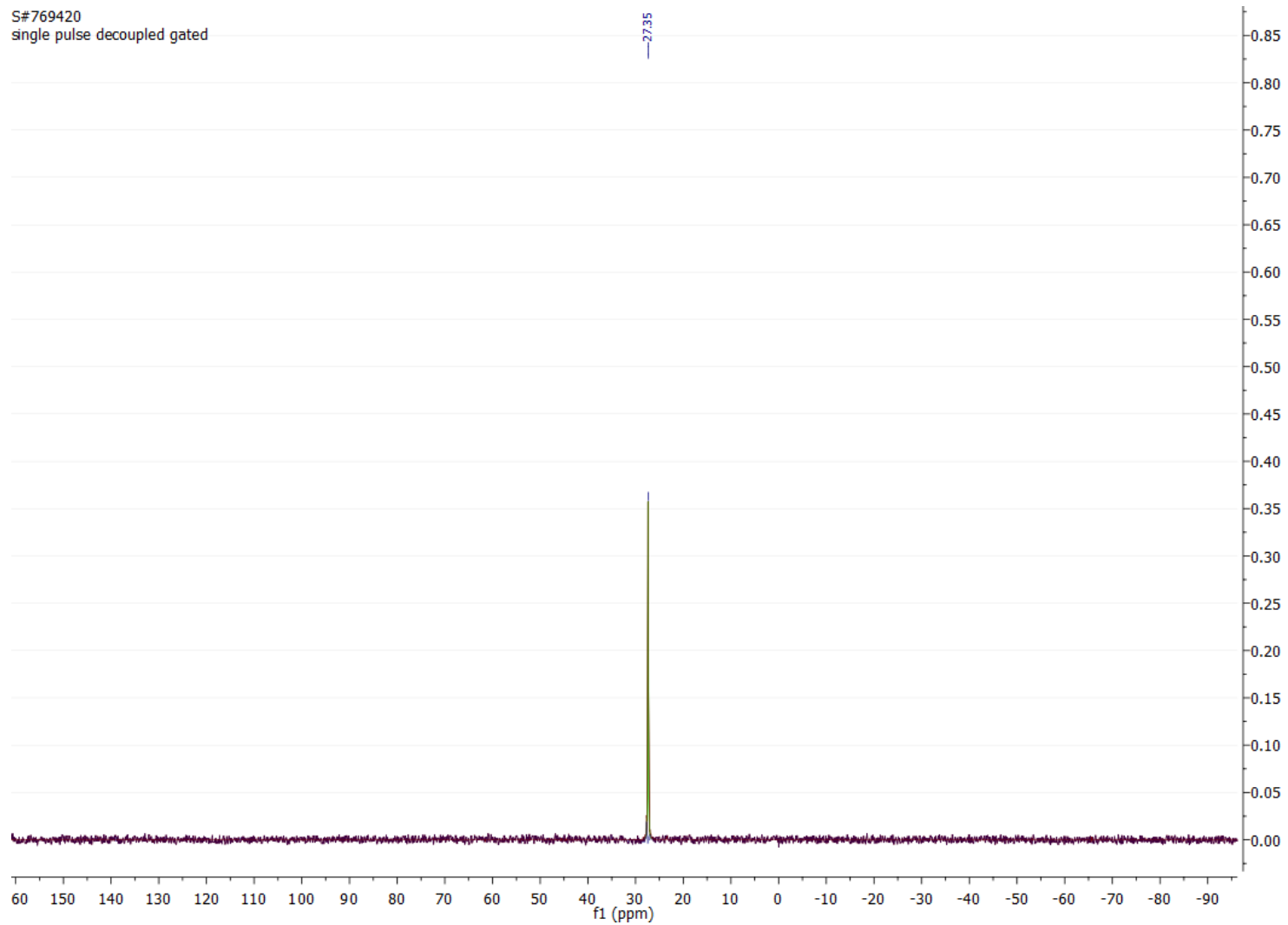
327



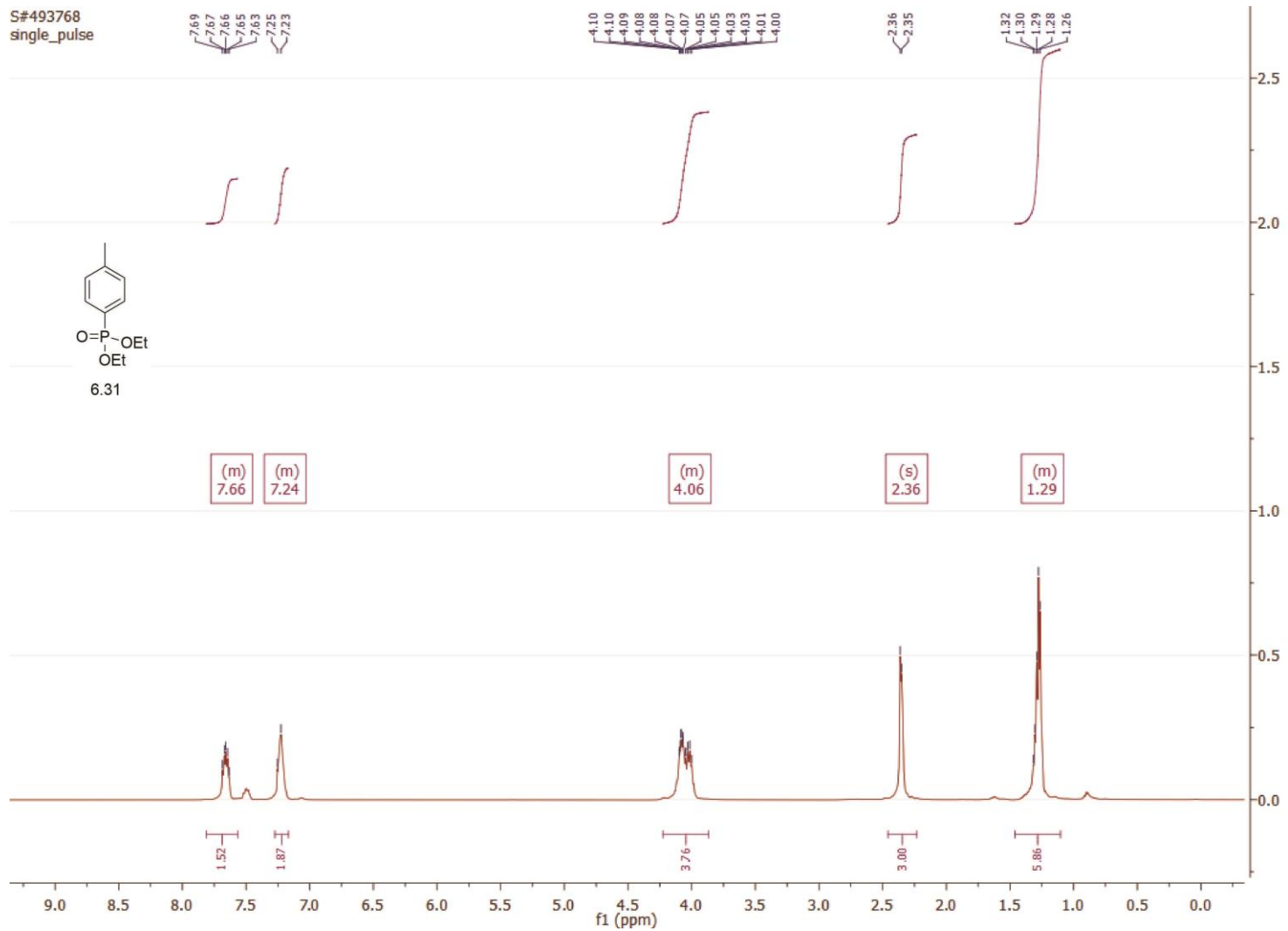
328



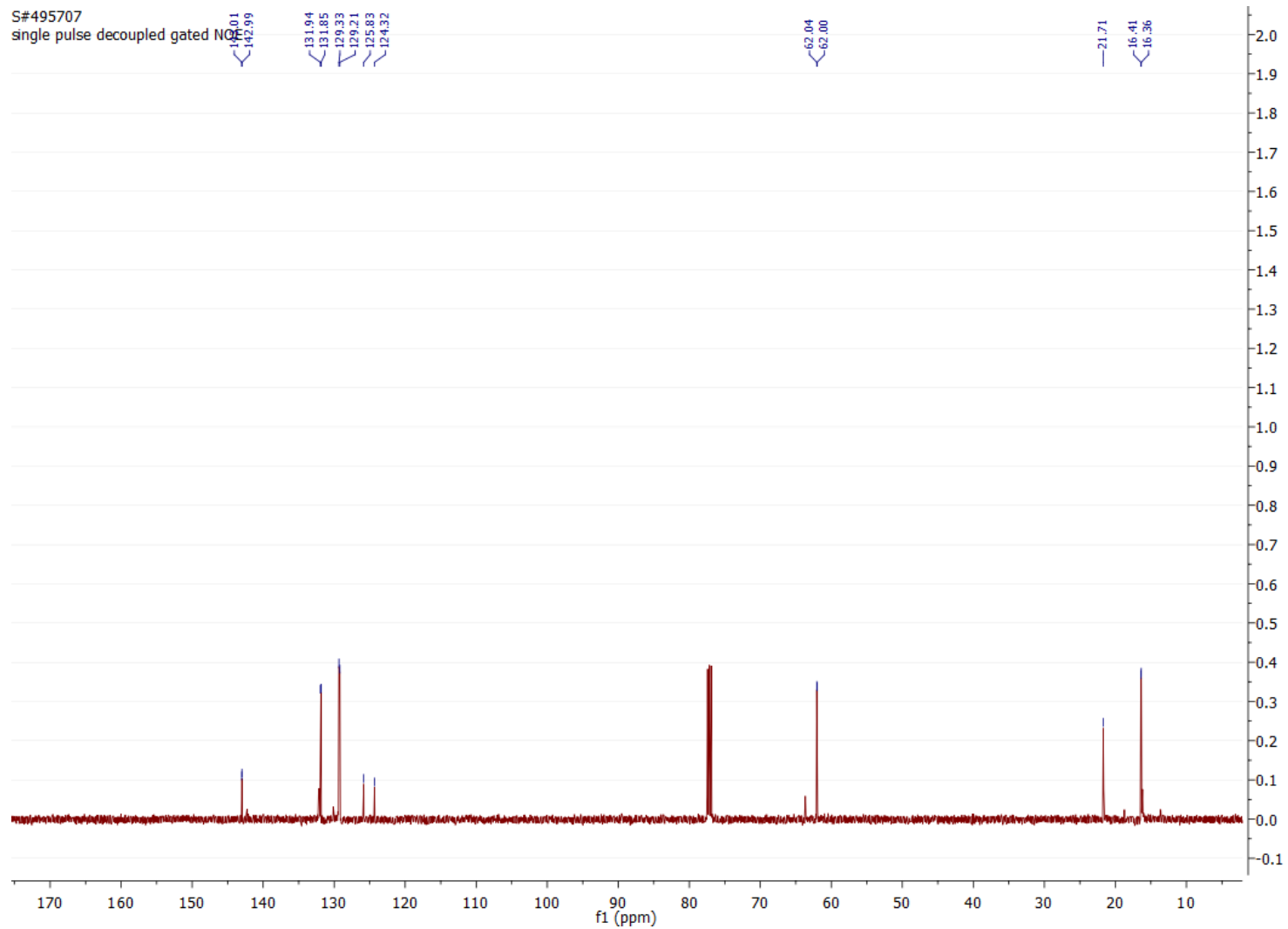
S#769420
single pulse decoupled gated



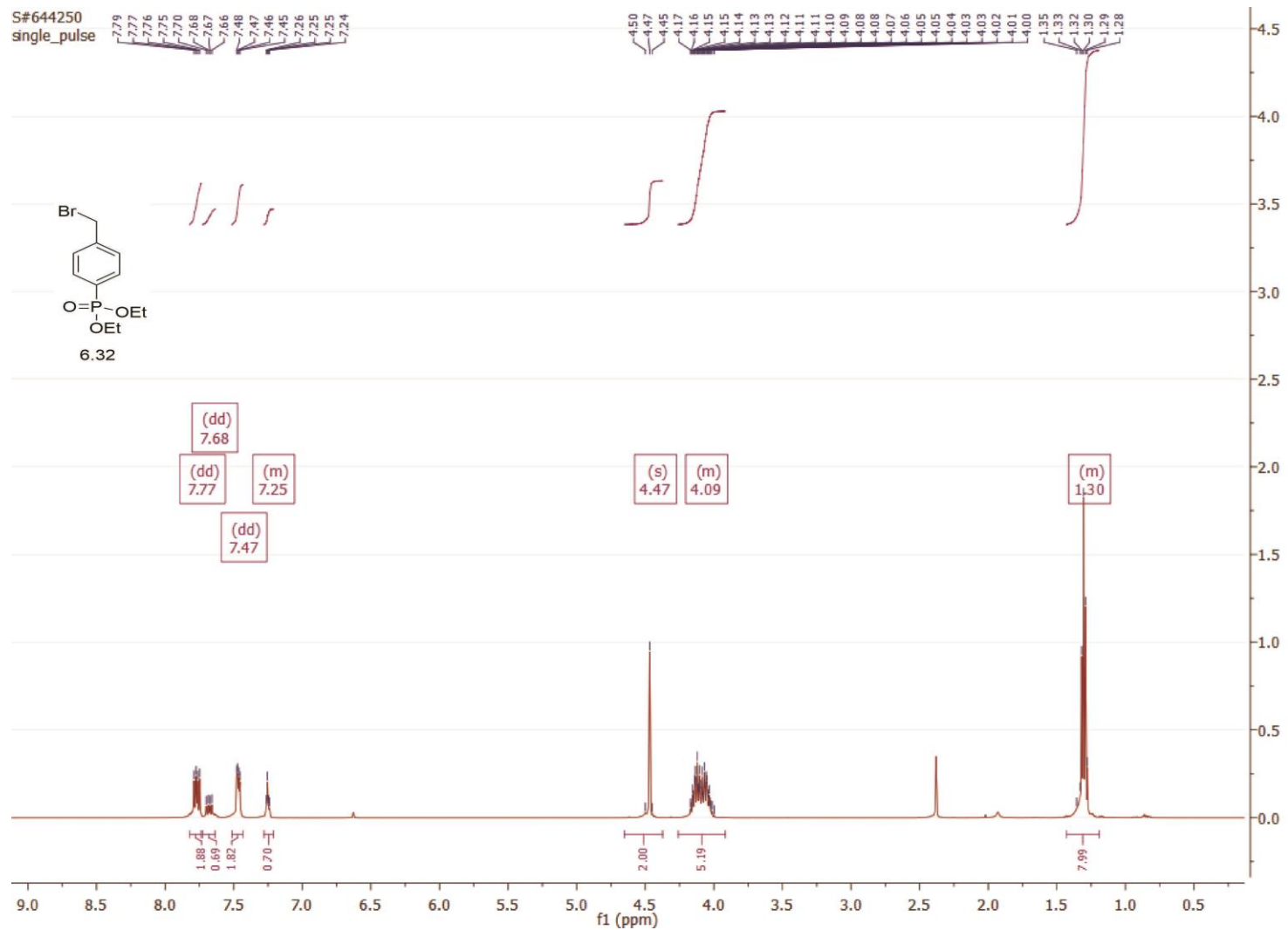
330



331

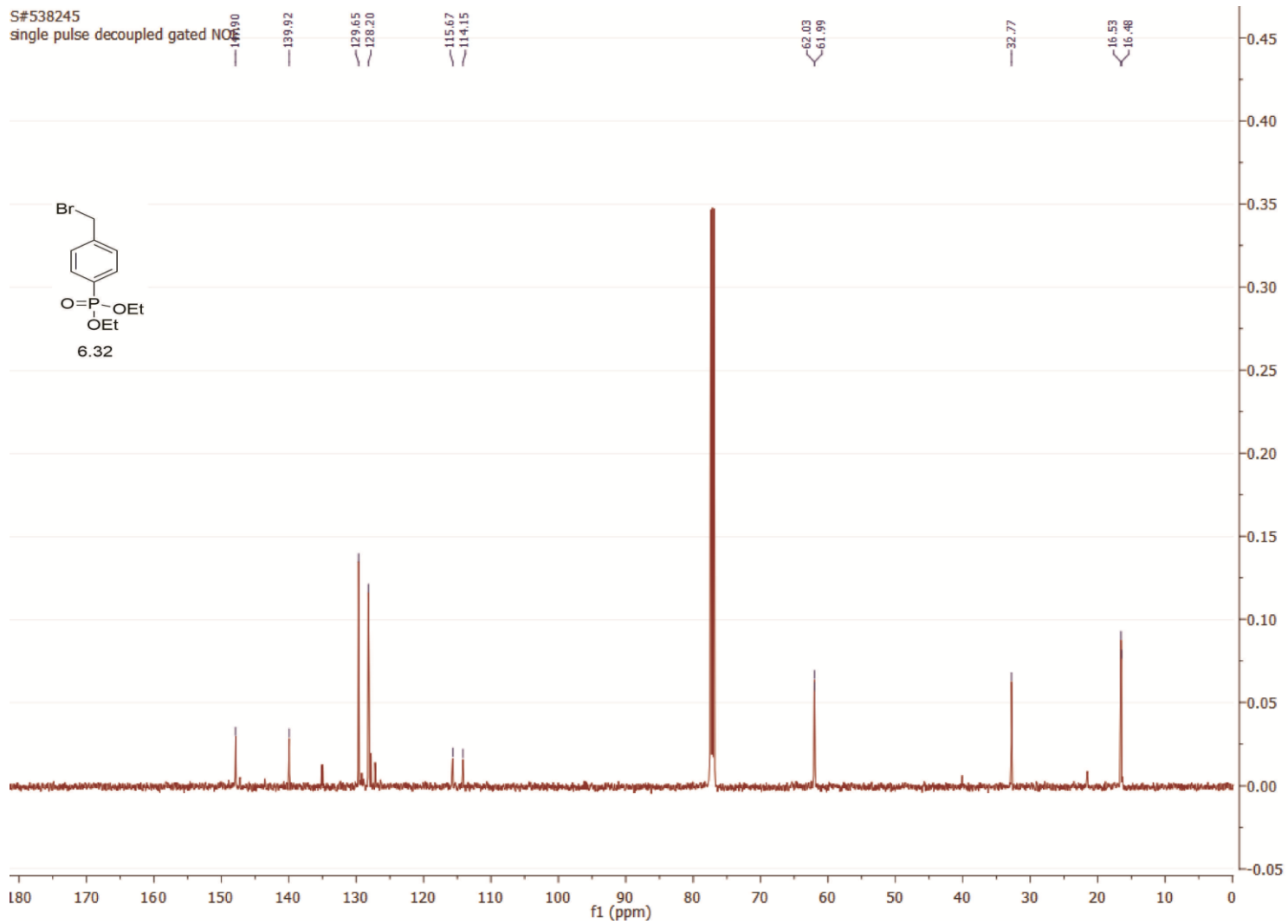


332



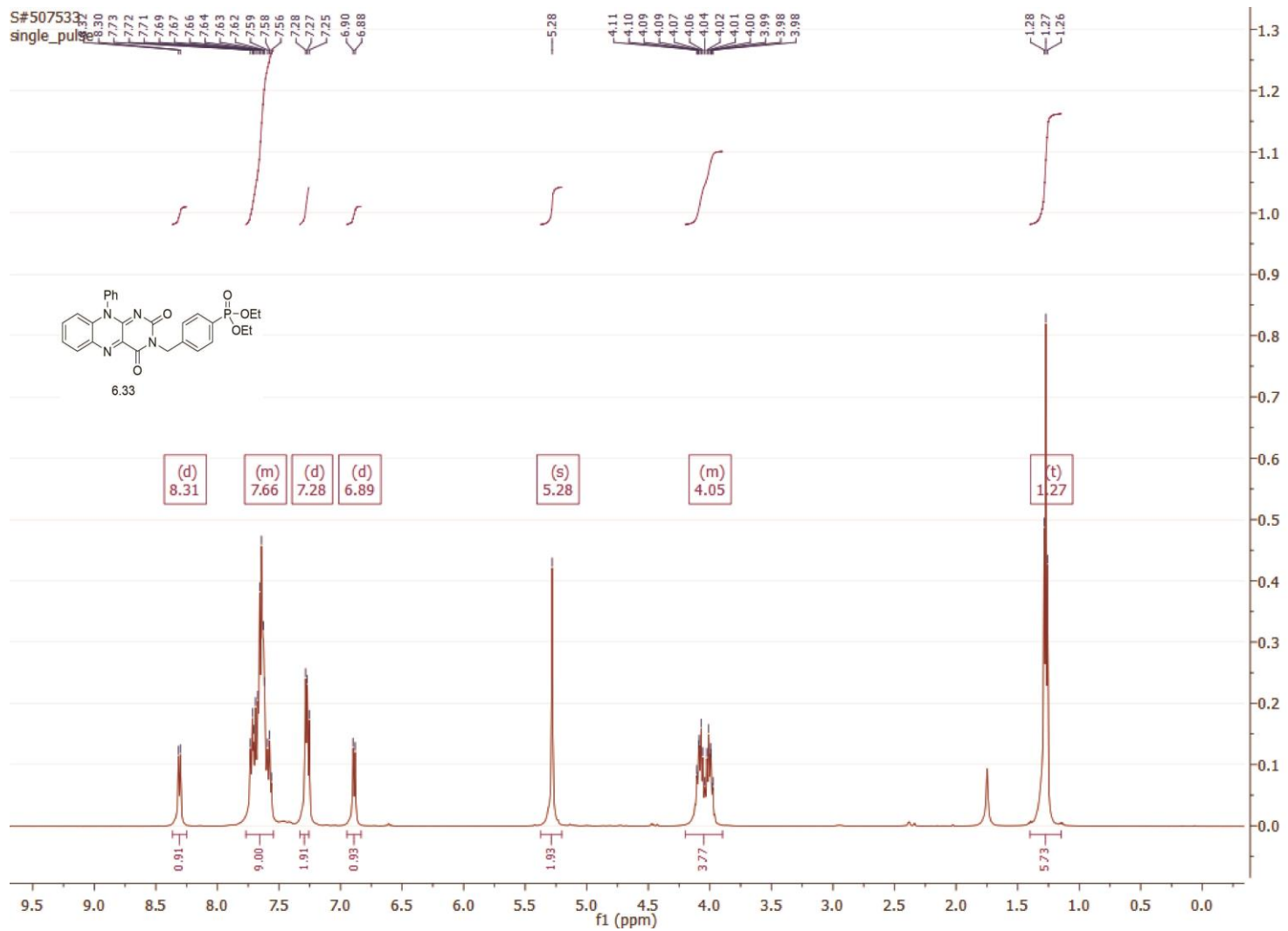
S#538245

single pulse decoupled gated NO

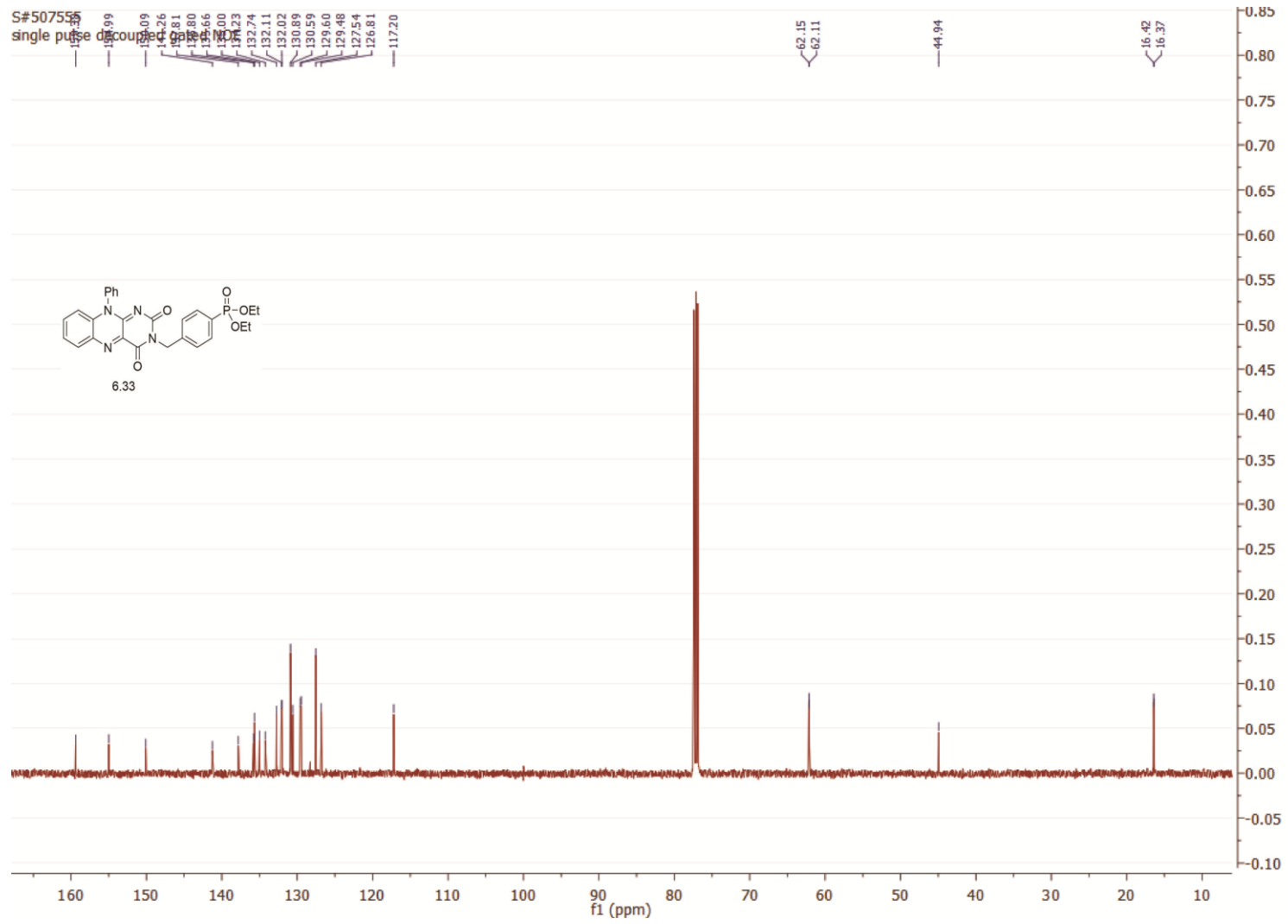


333

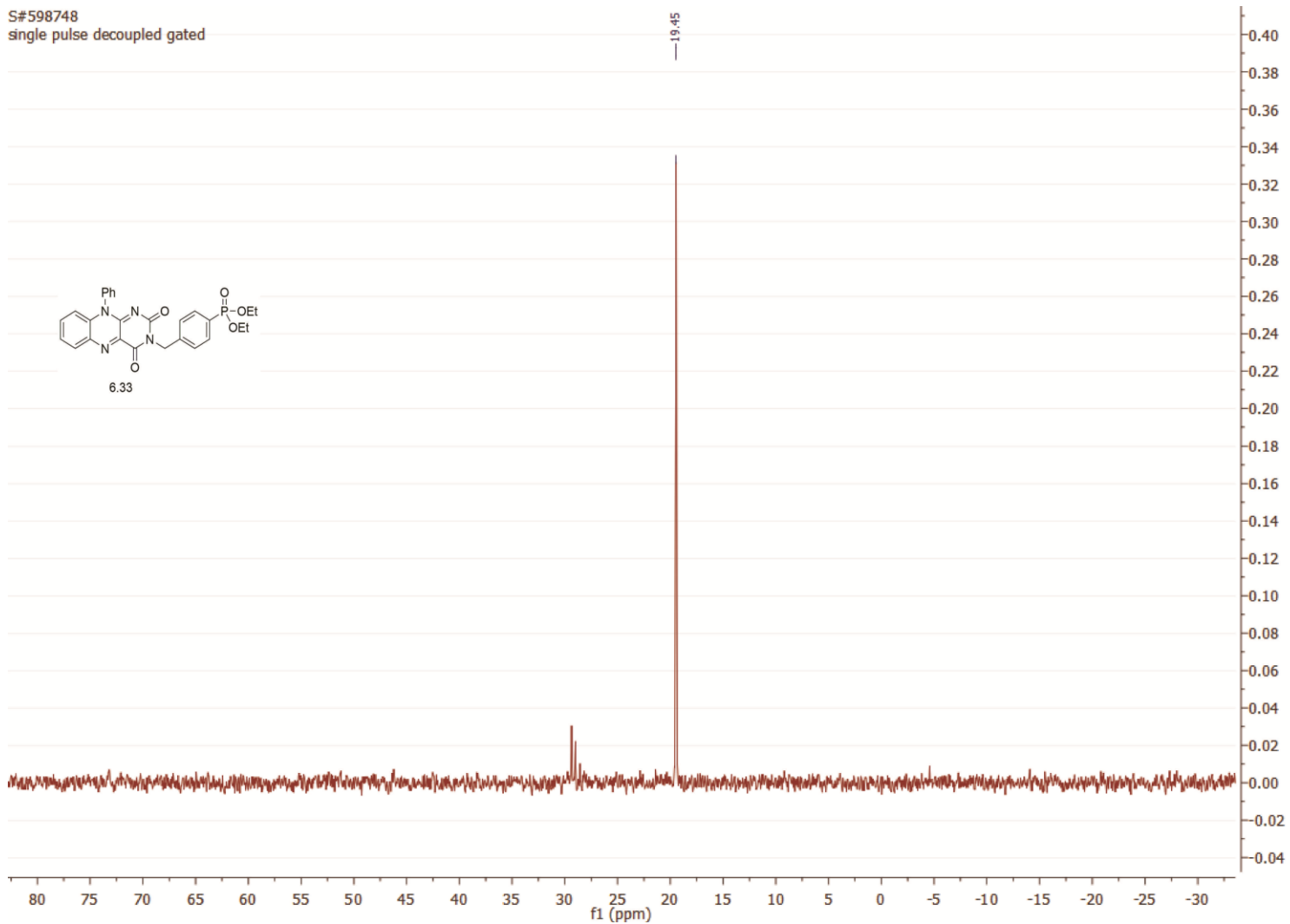
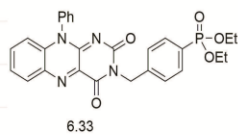
334



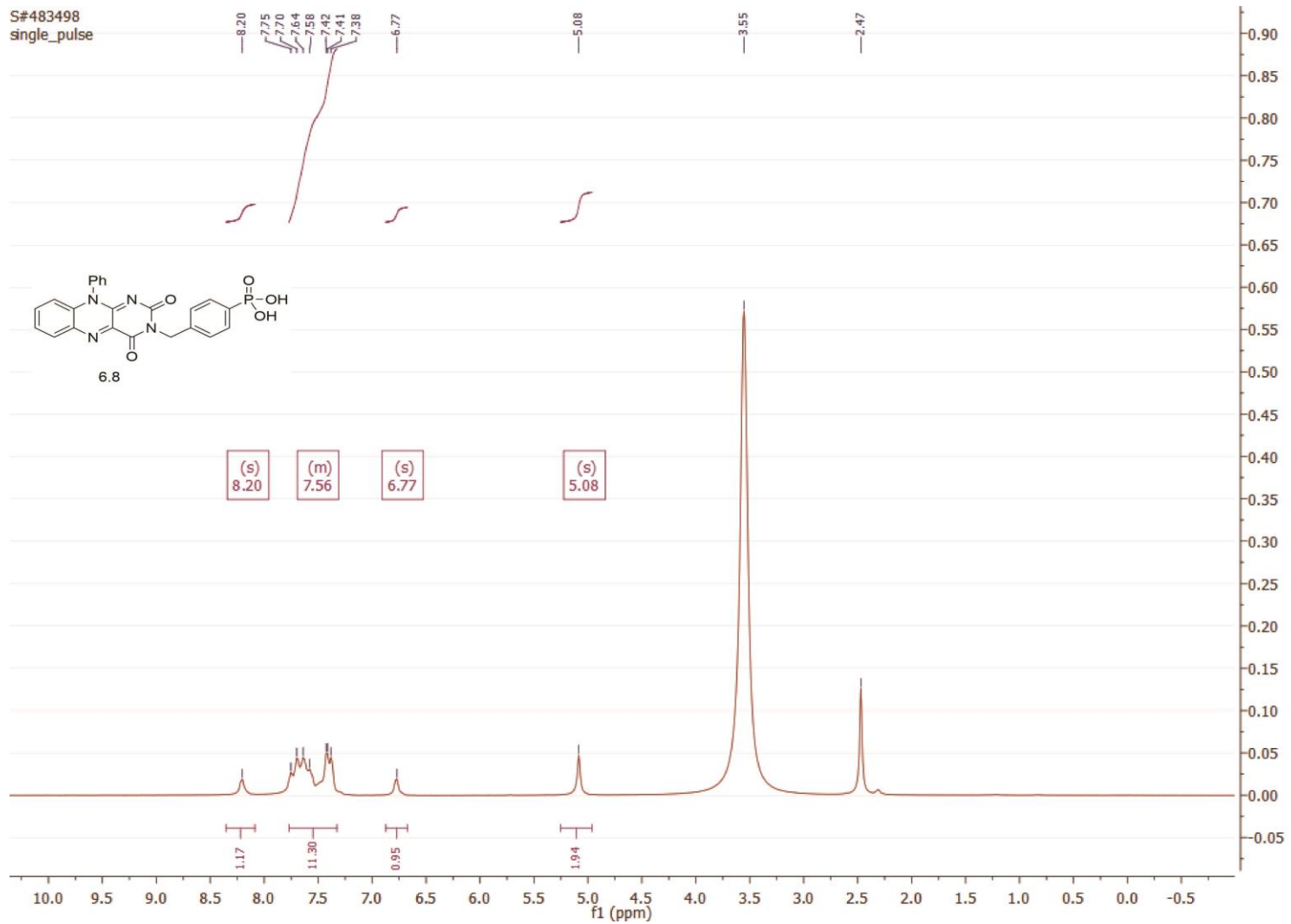
335



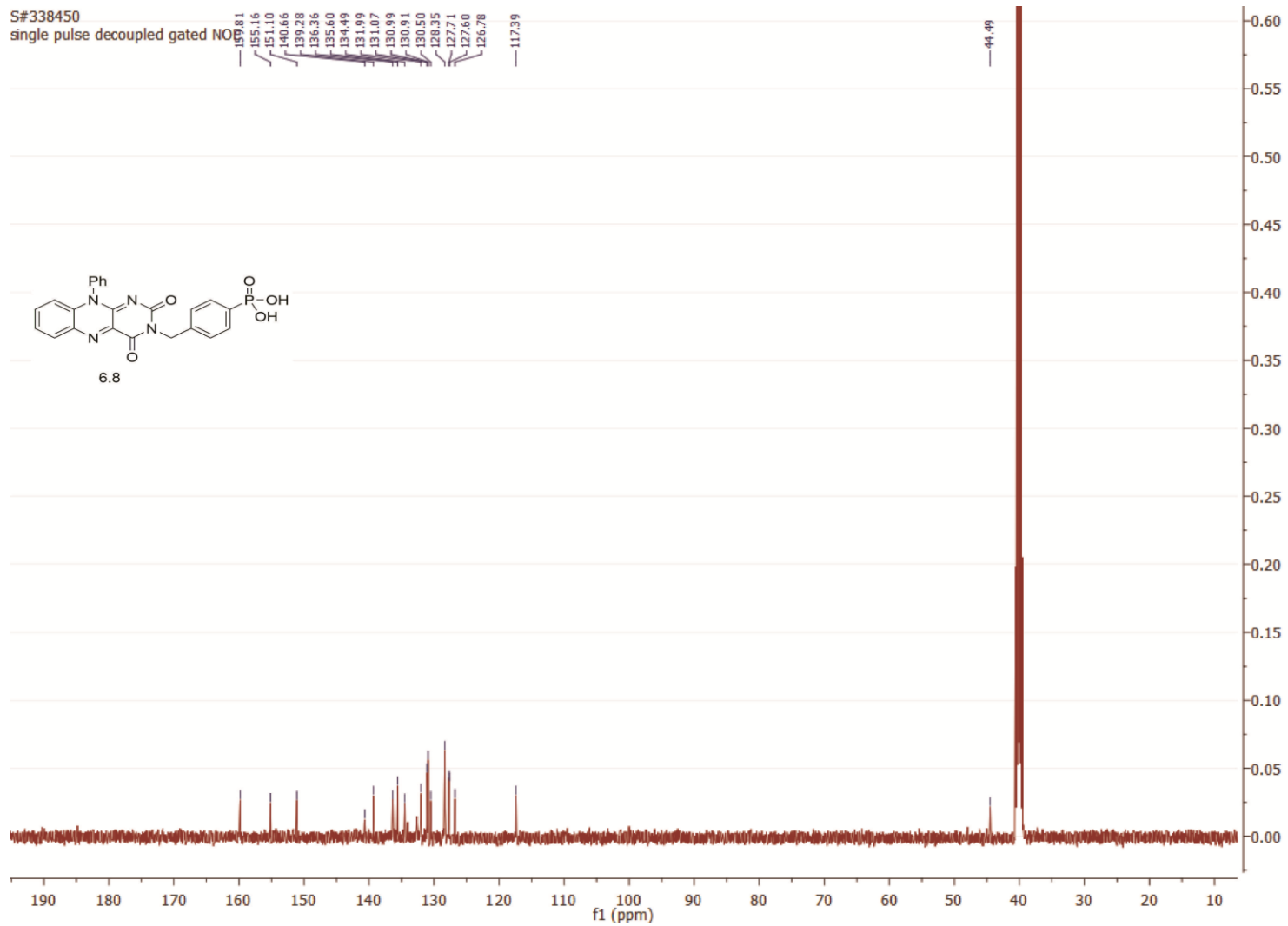
S#598748
single pulse decoupled gated



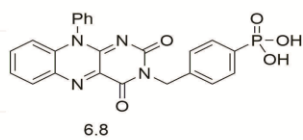
337



338

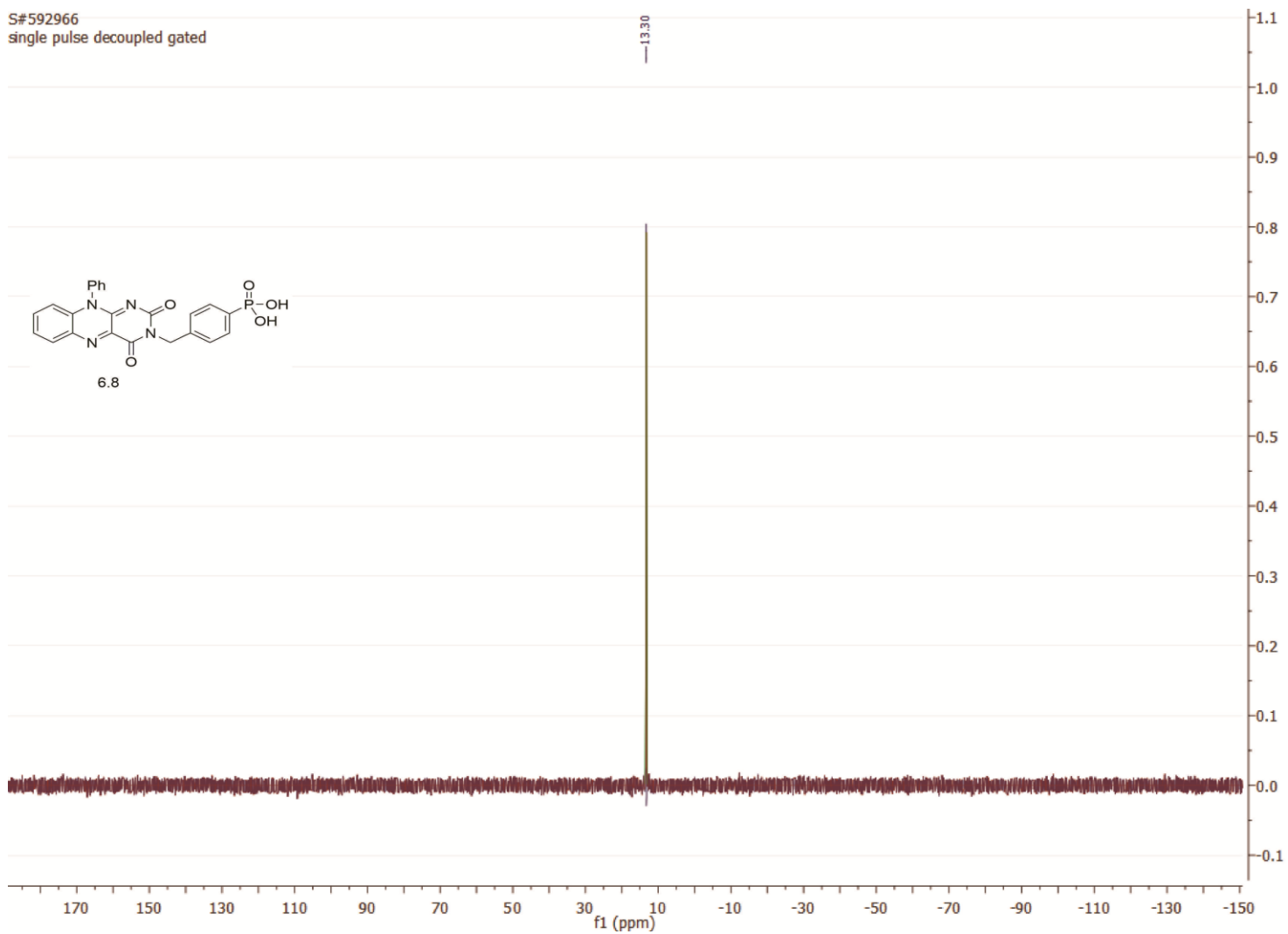


S#592966
single pulse decoupled gated

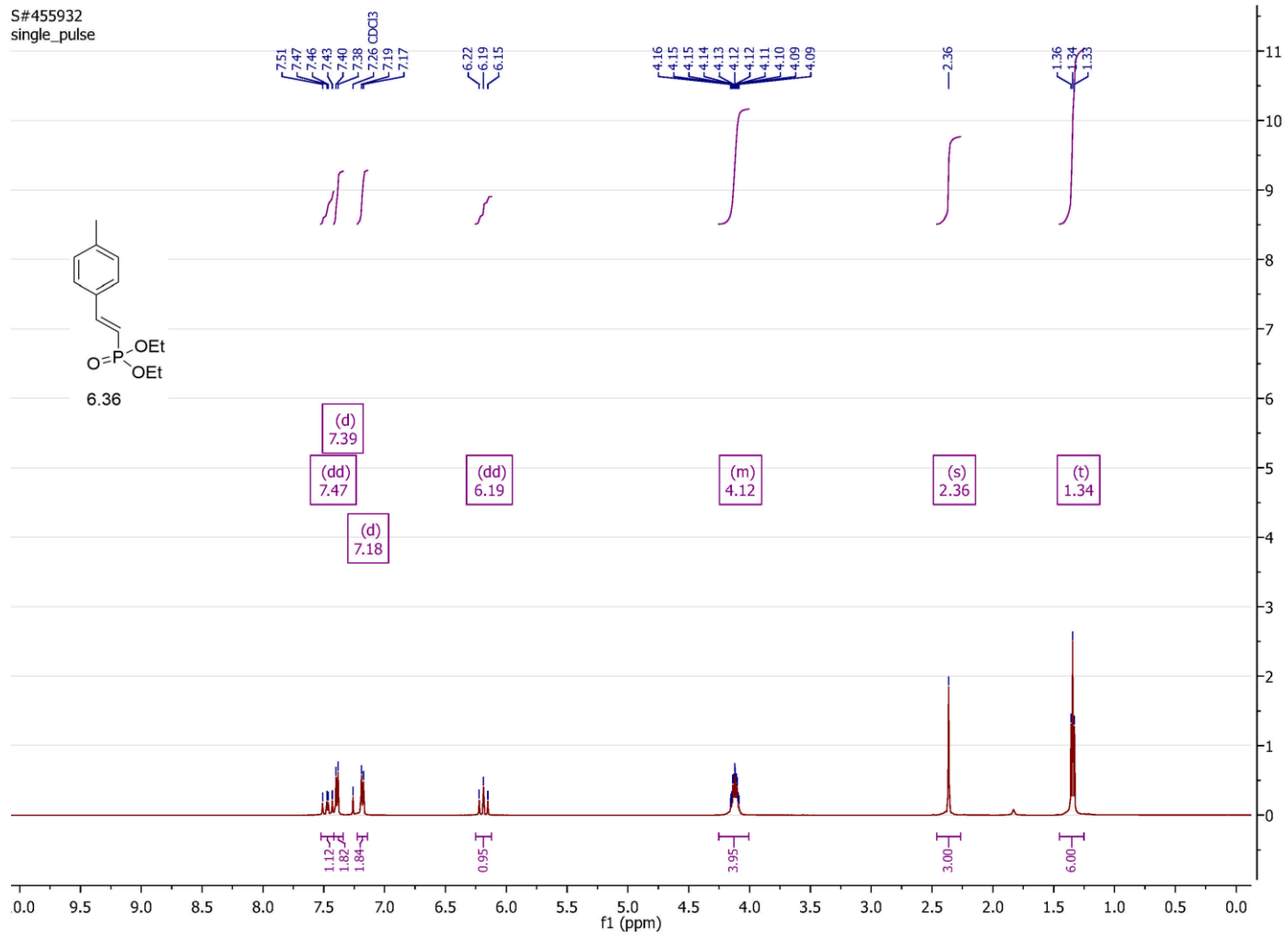


13.30

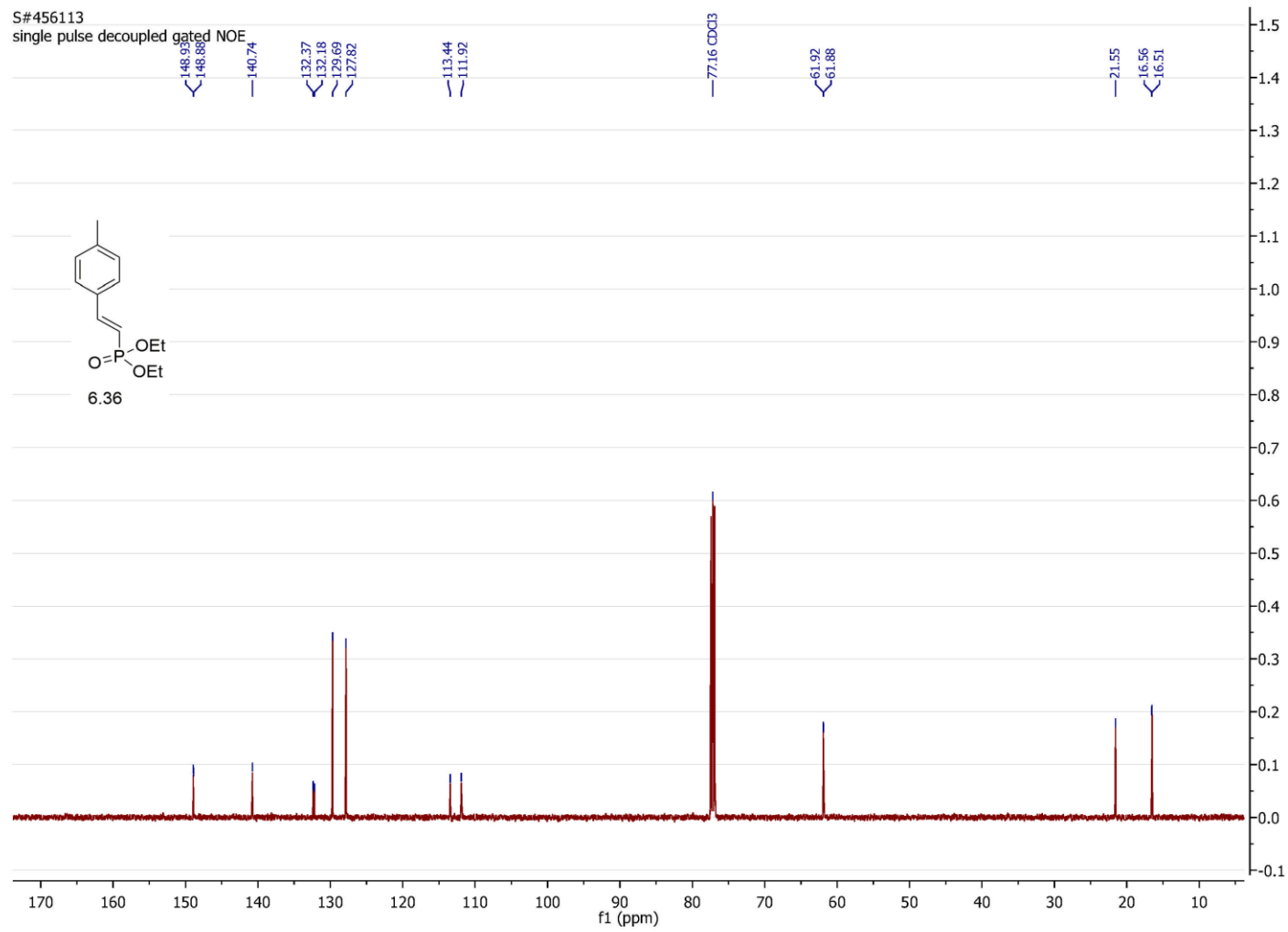
339



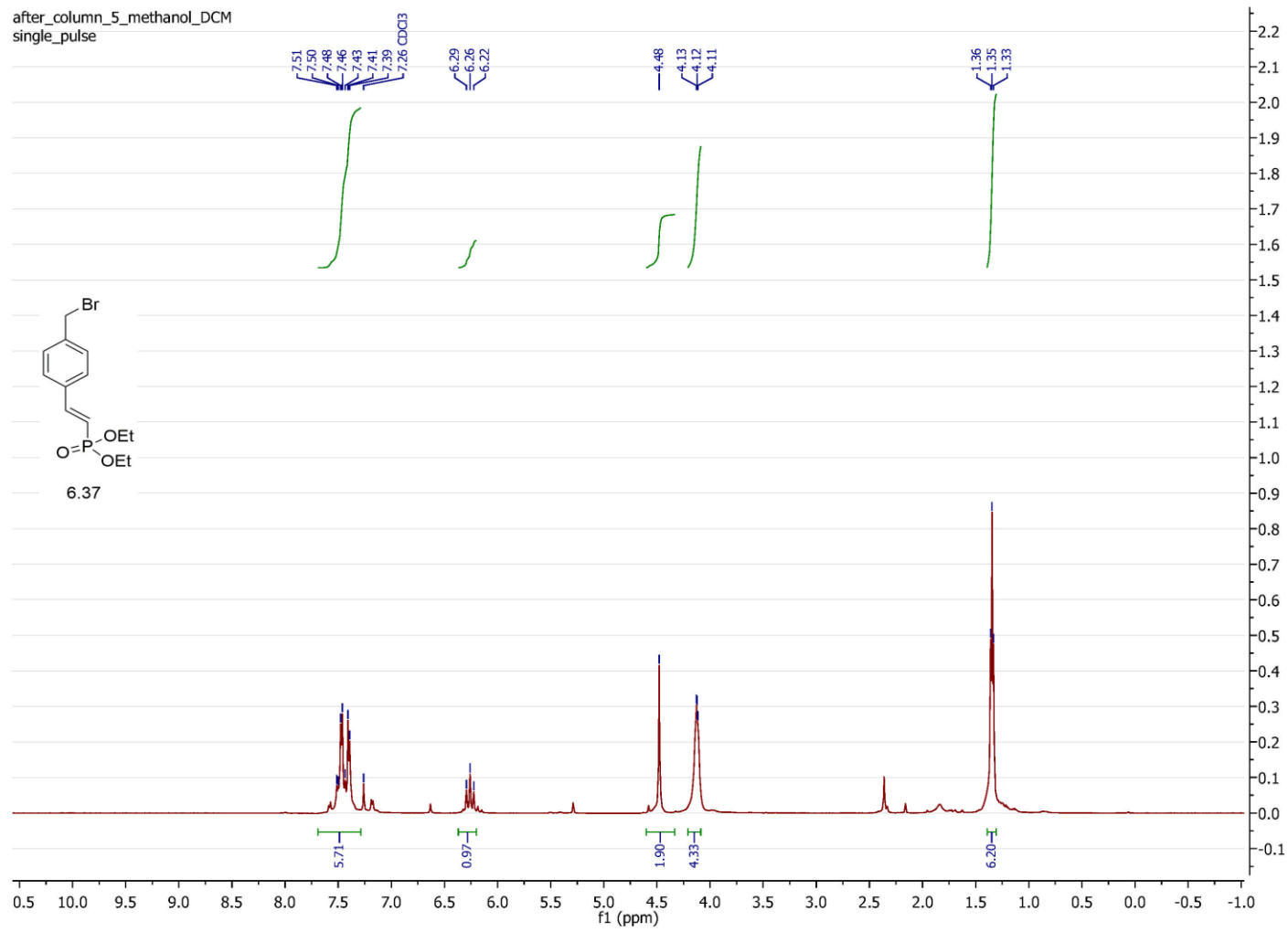
340



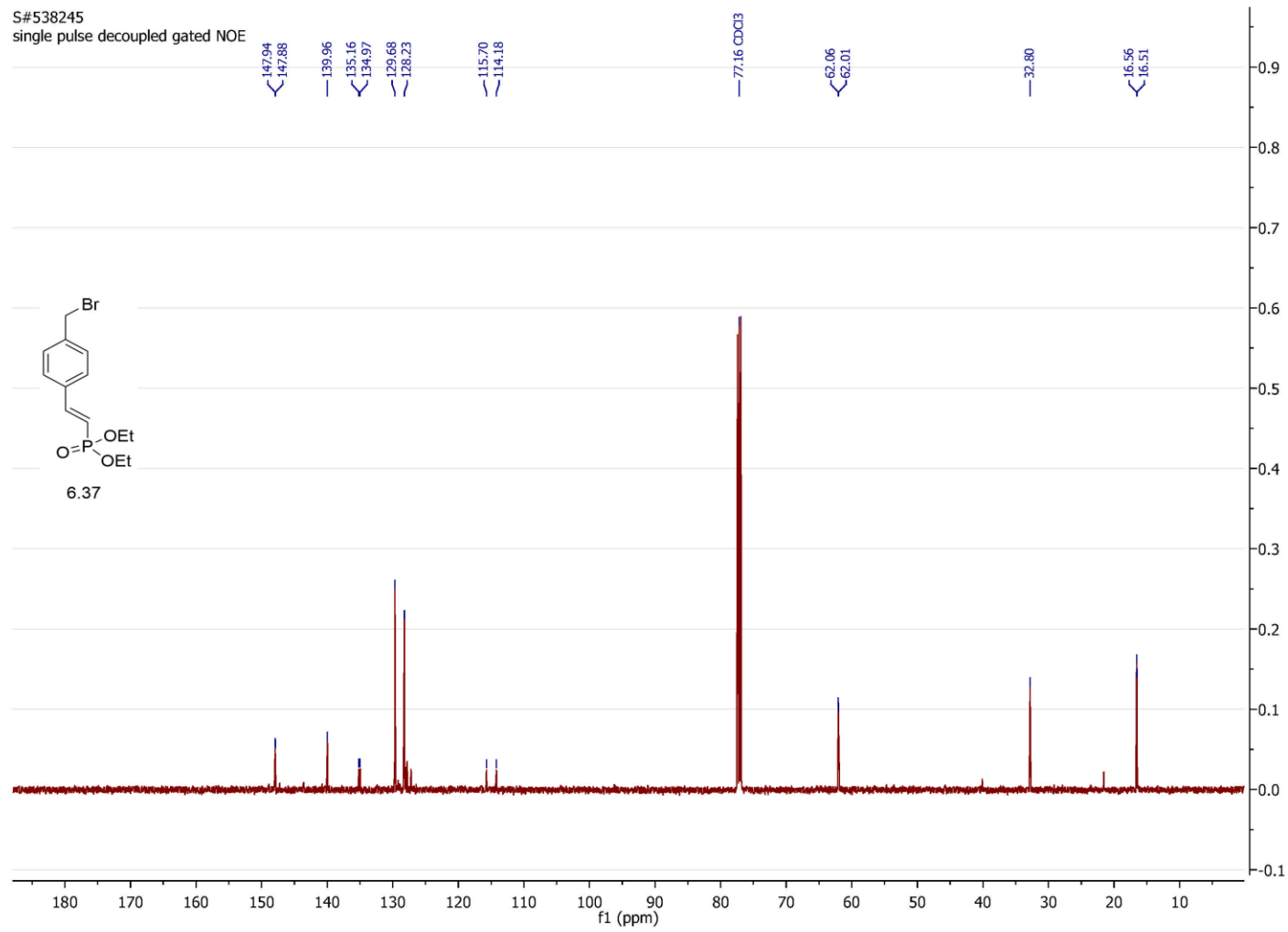
341



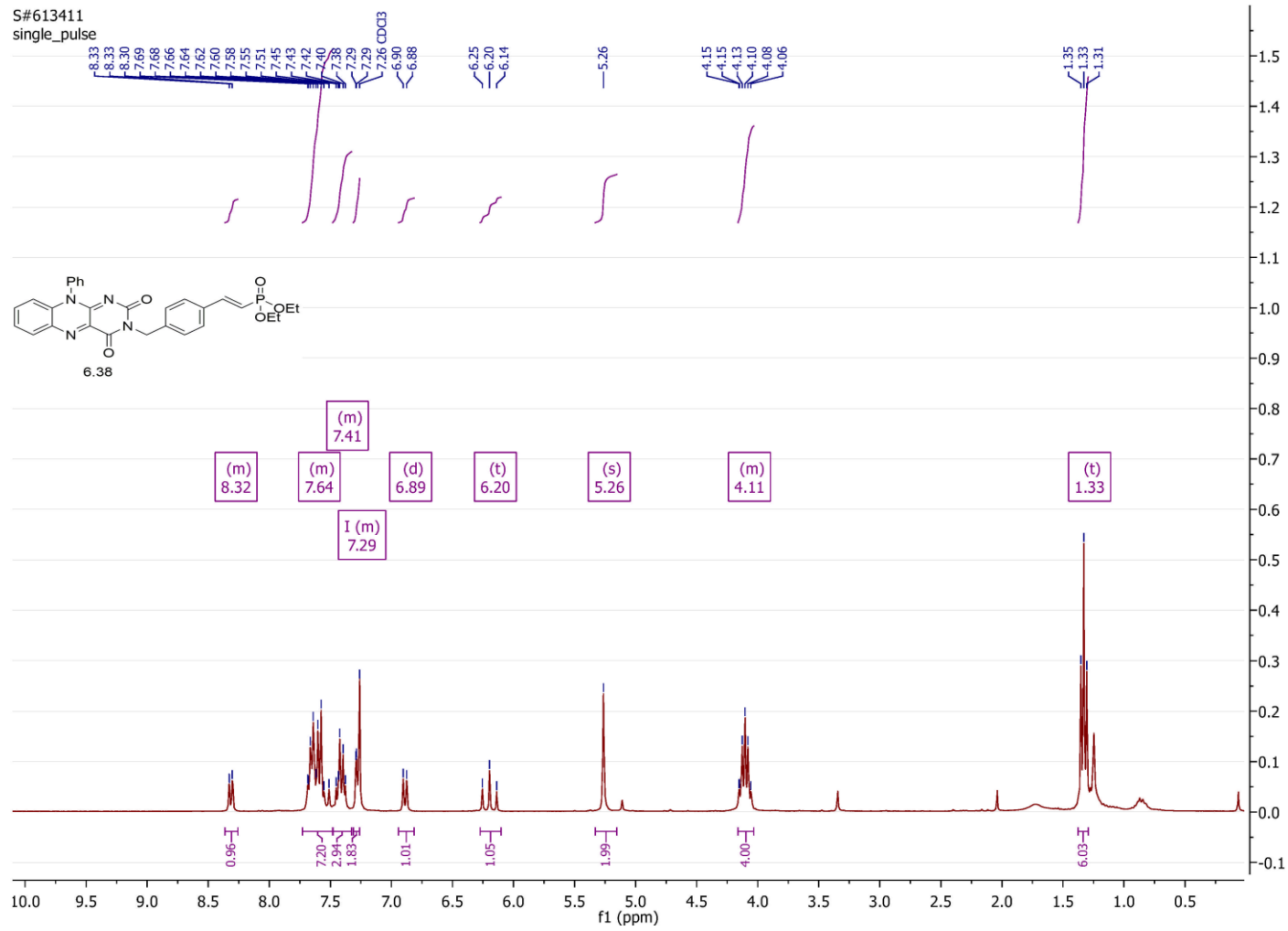
342



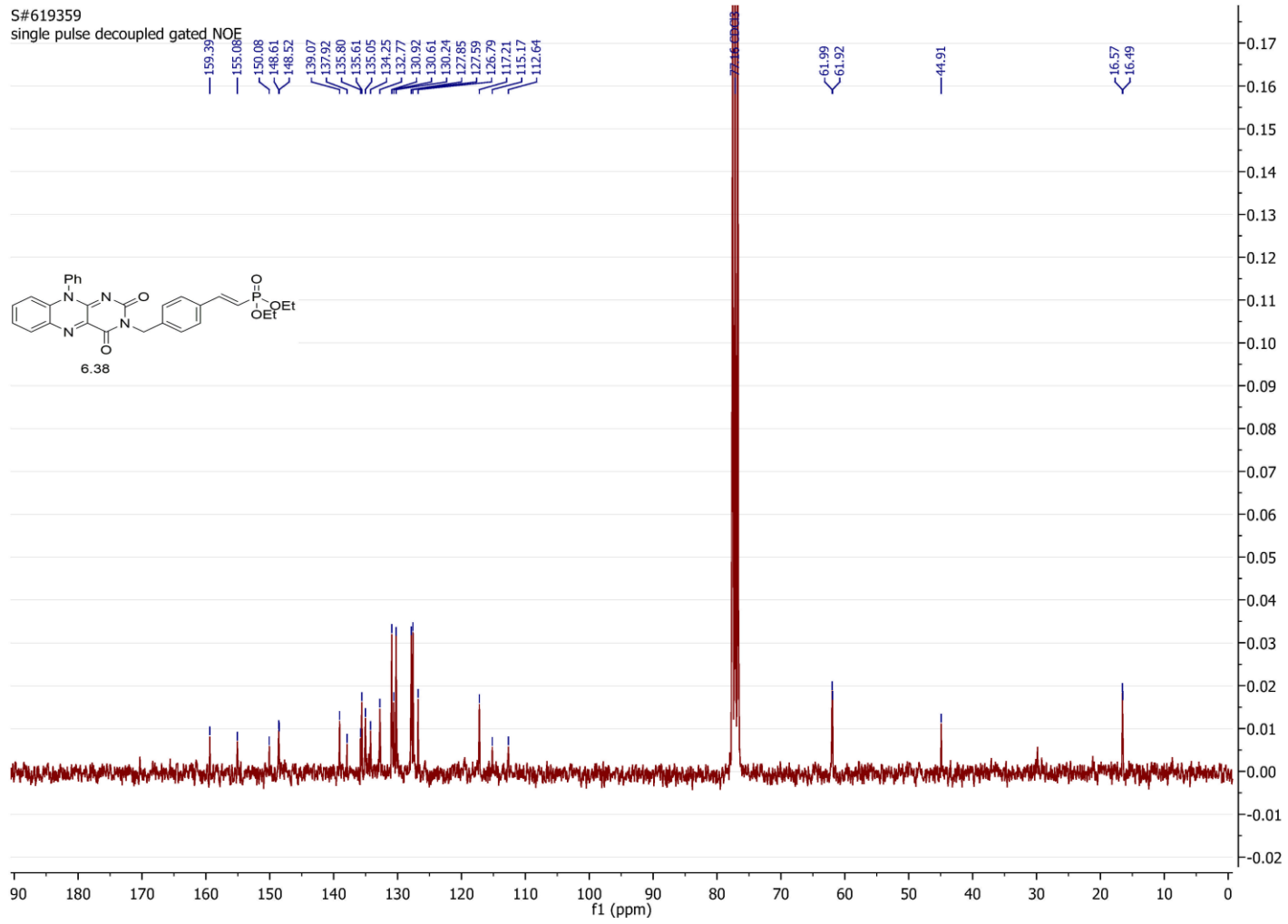
343



344

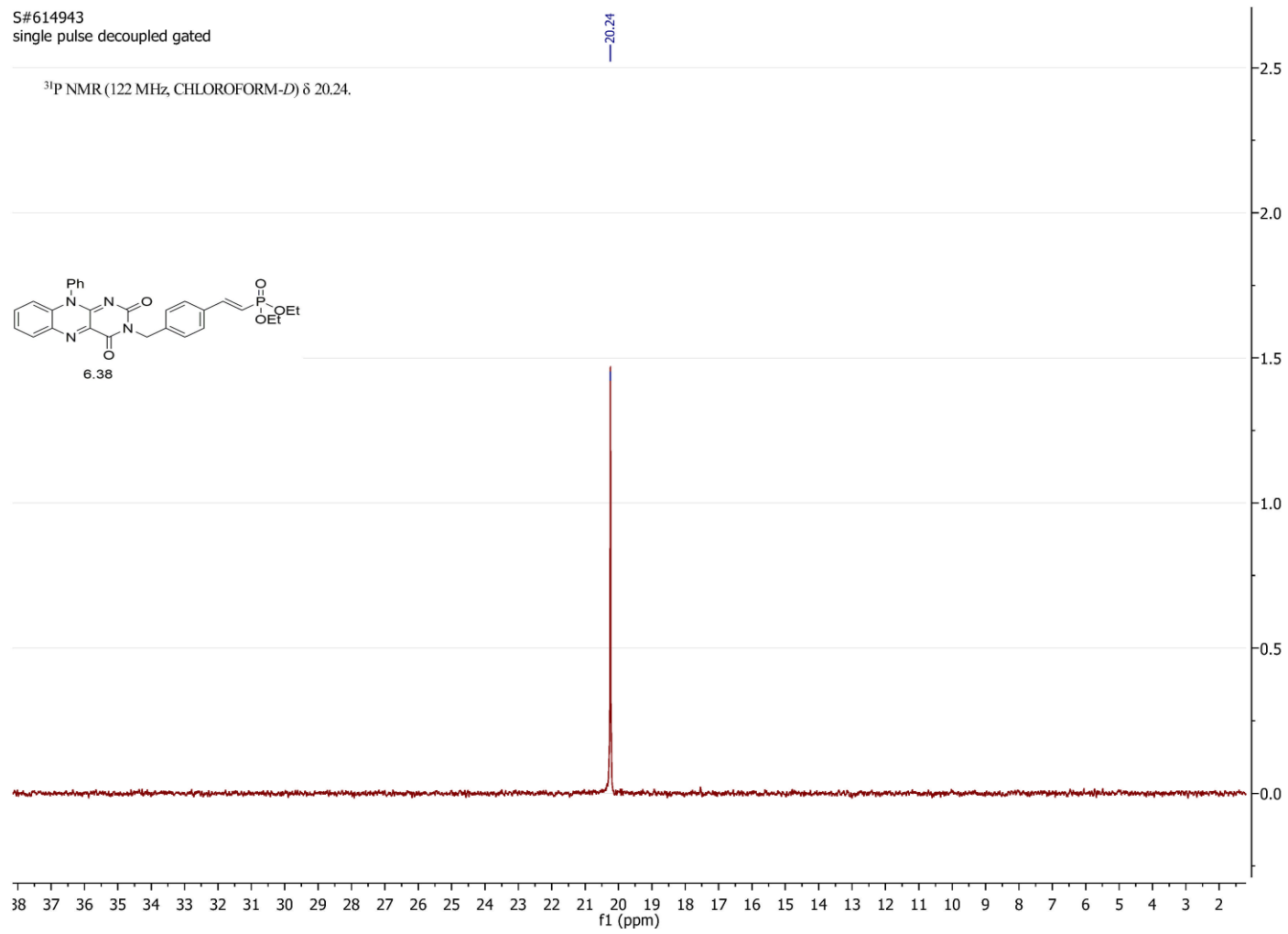
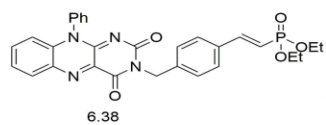


345



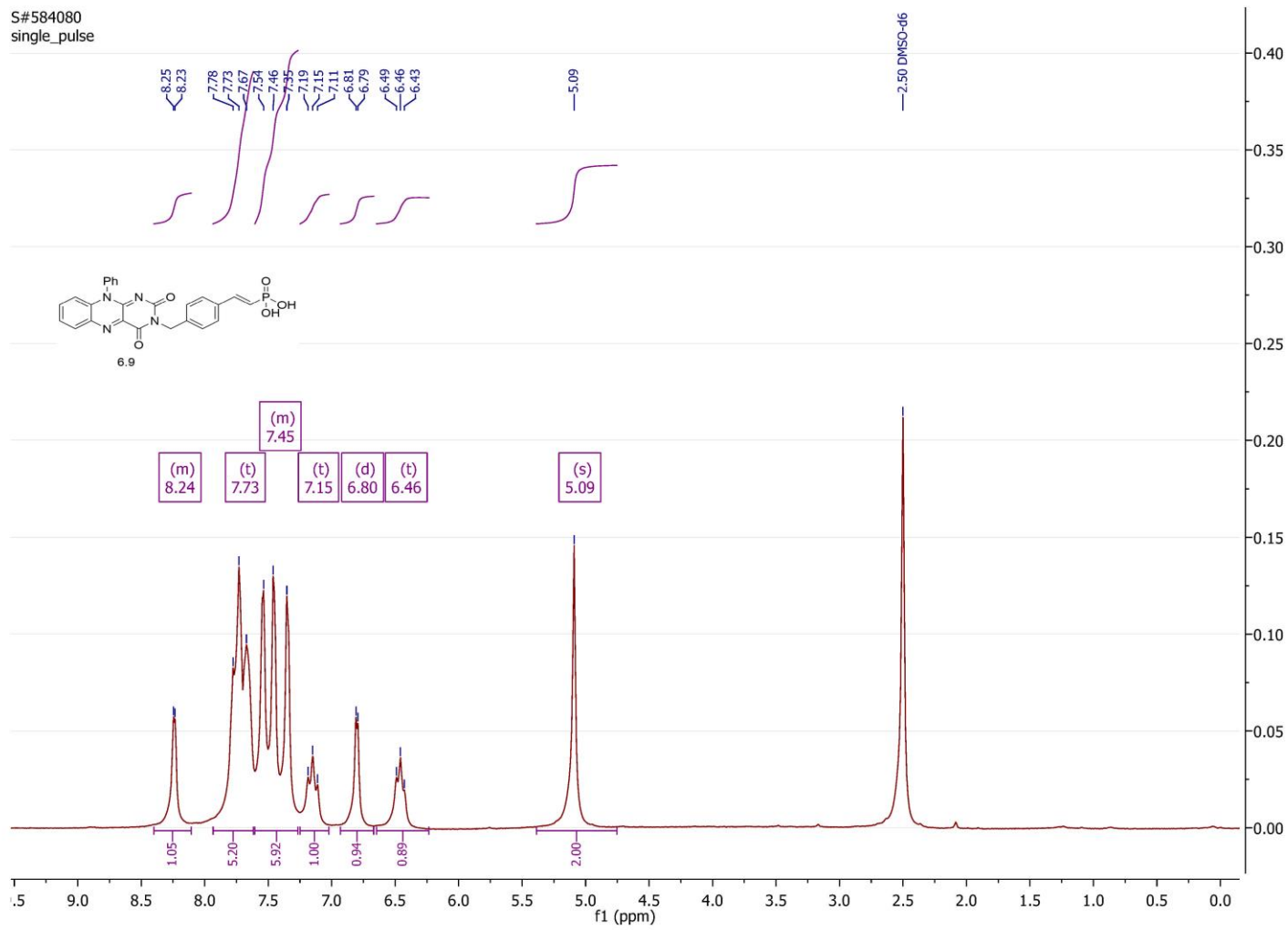
S#614943
single pulse decoupled gated

^{31}P NMR (122 MHz, CHLOROFORM-*D*) δ 20.24.

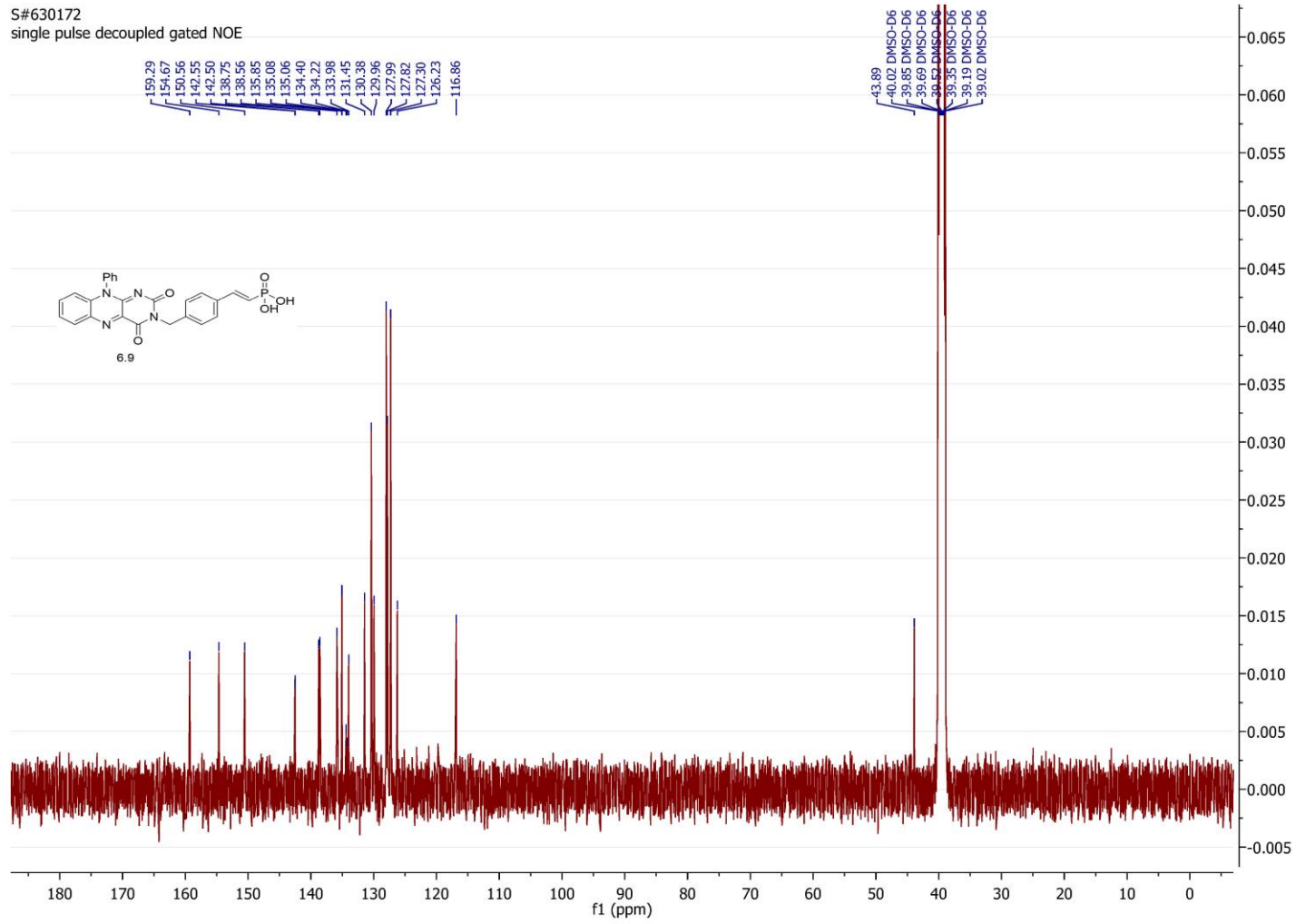


346

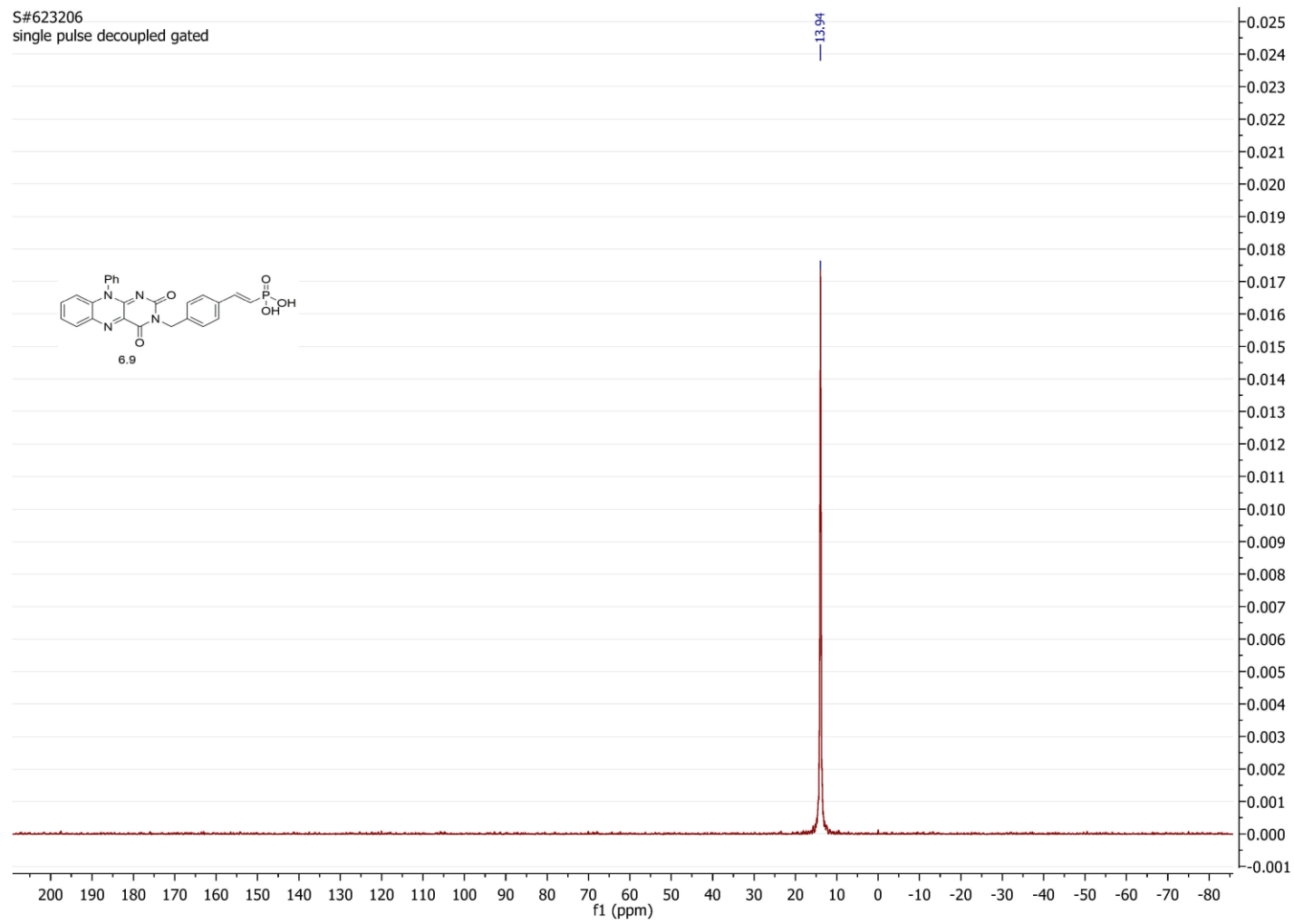
347



S#630172
single pulse decoupled gated NOE

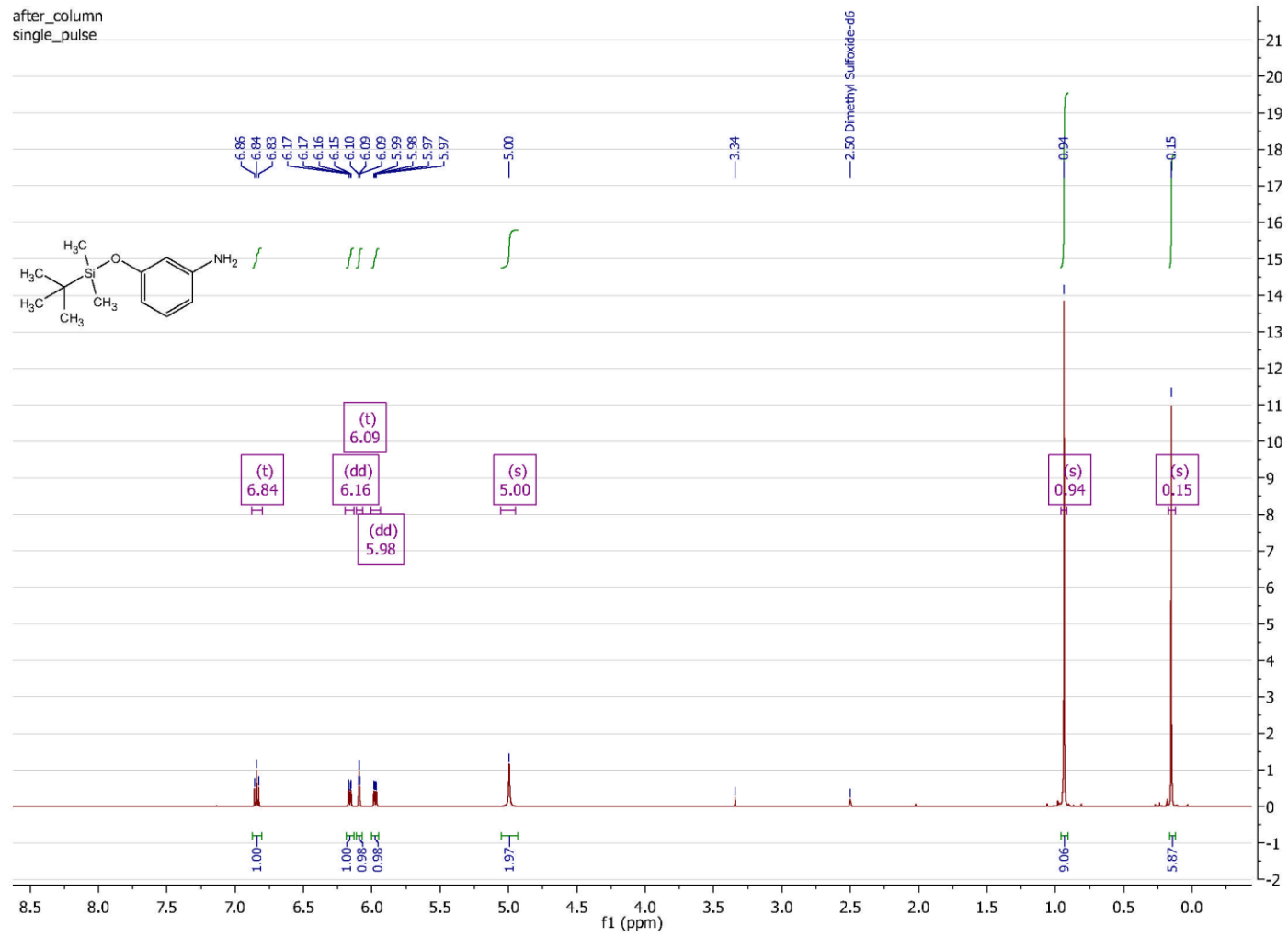


S#623206
single pulse decoupled gated

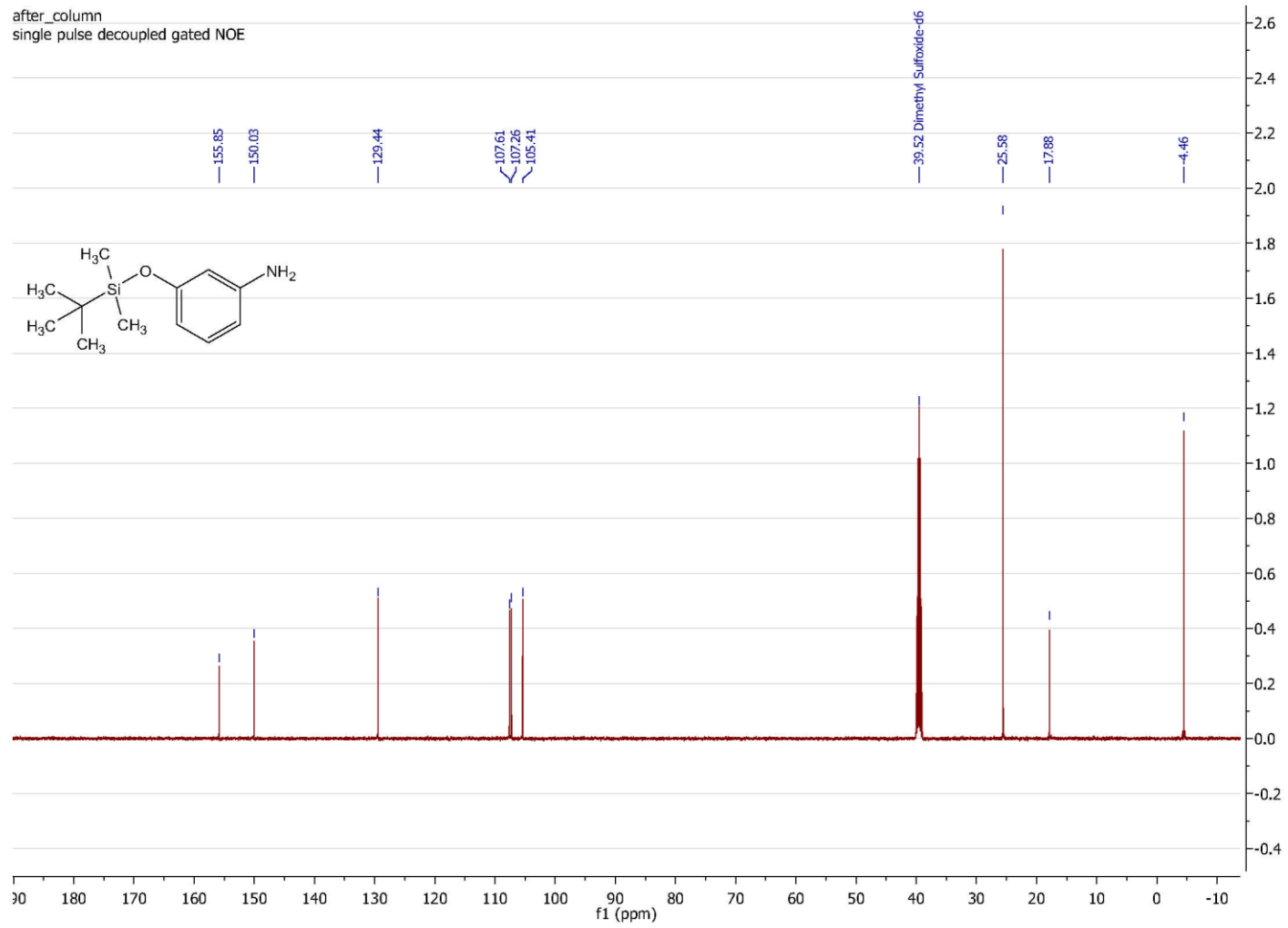


349

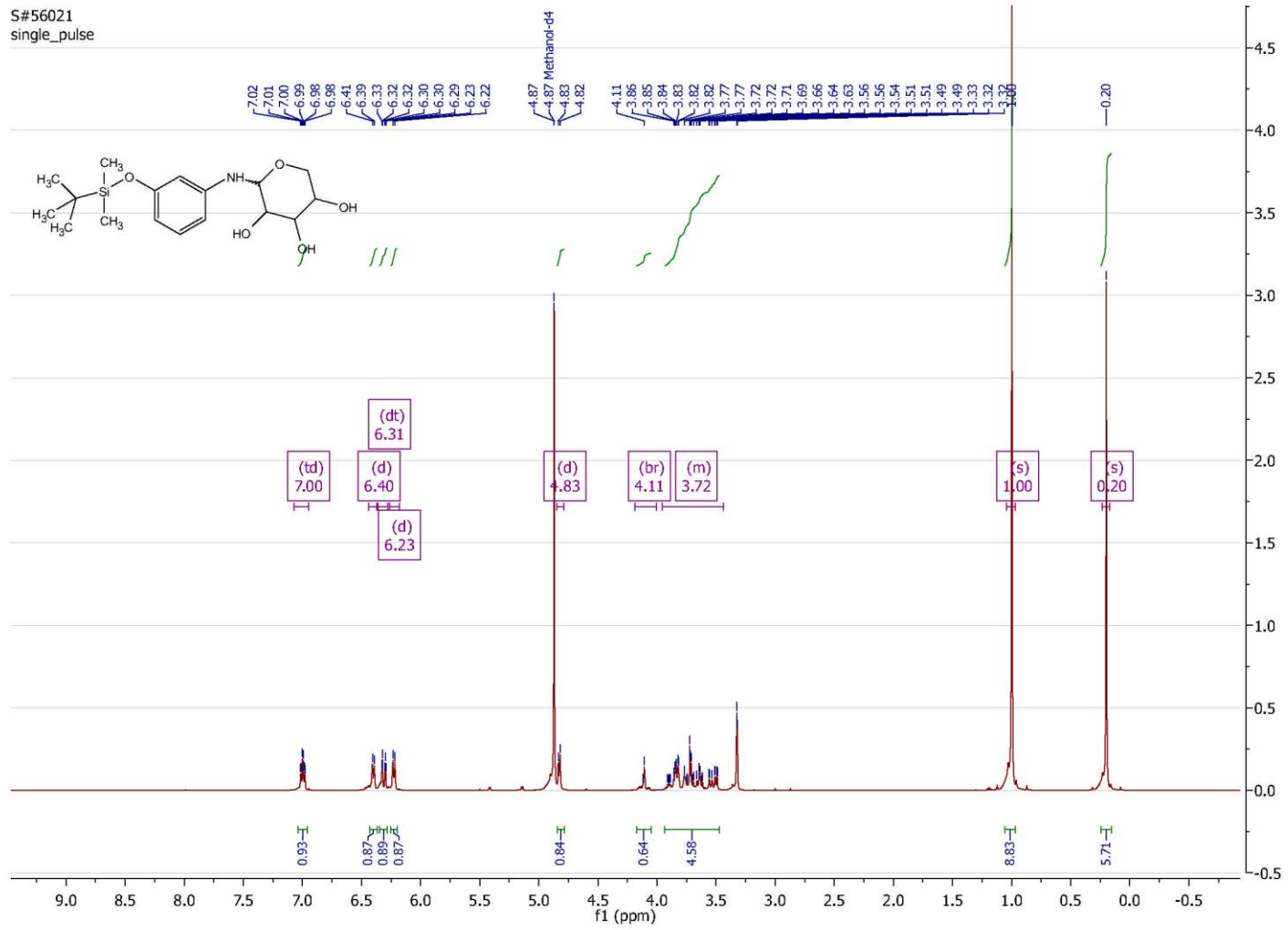
350



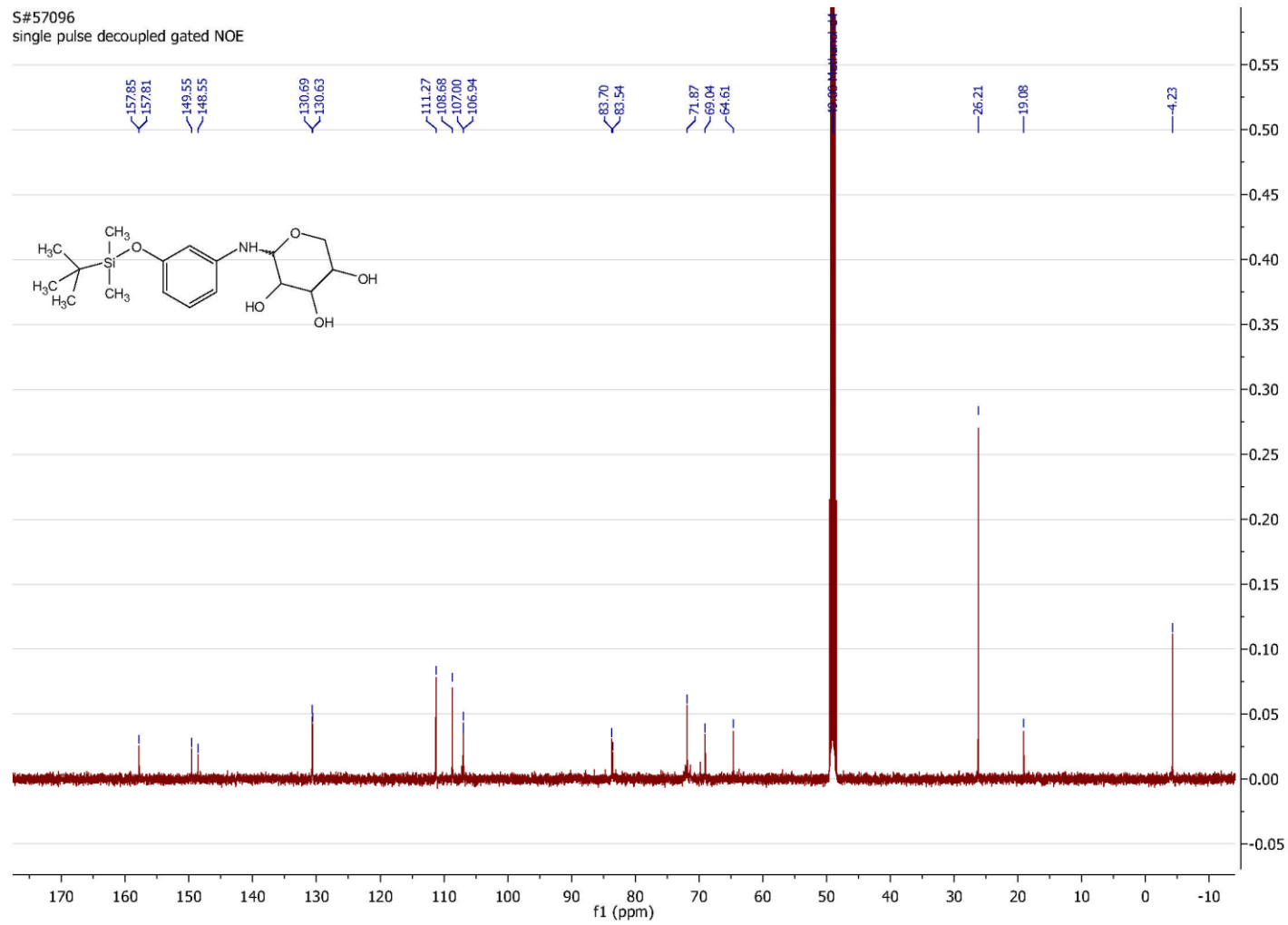
351



352

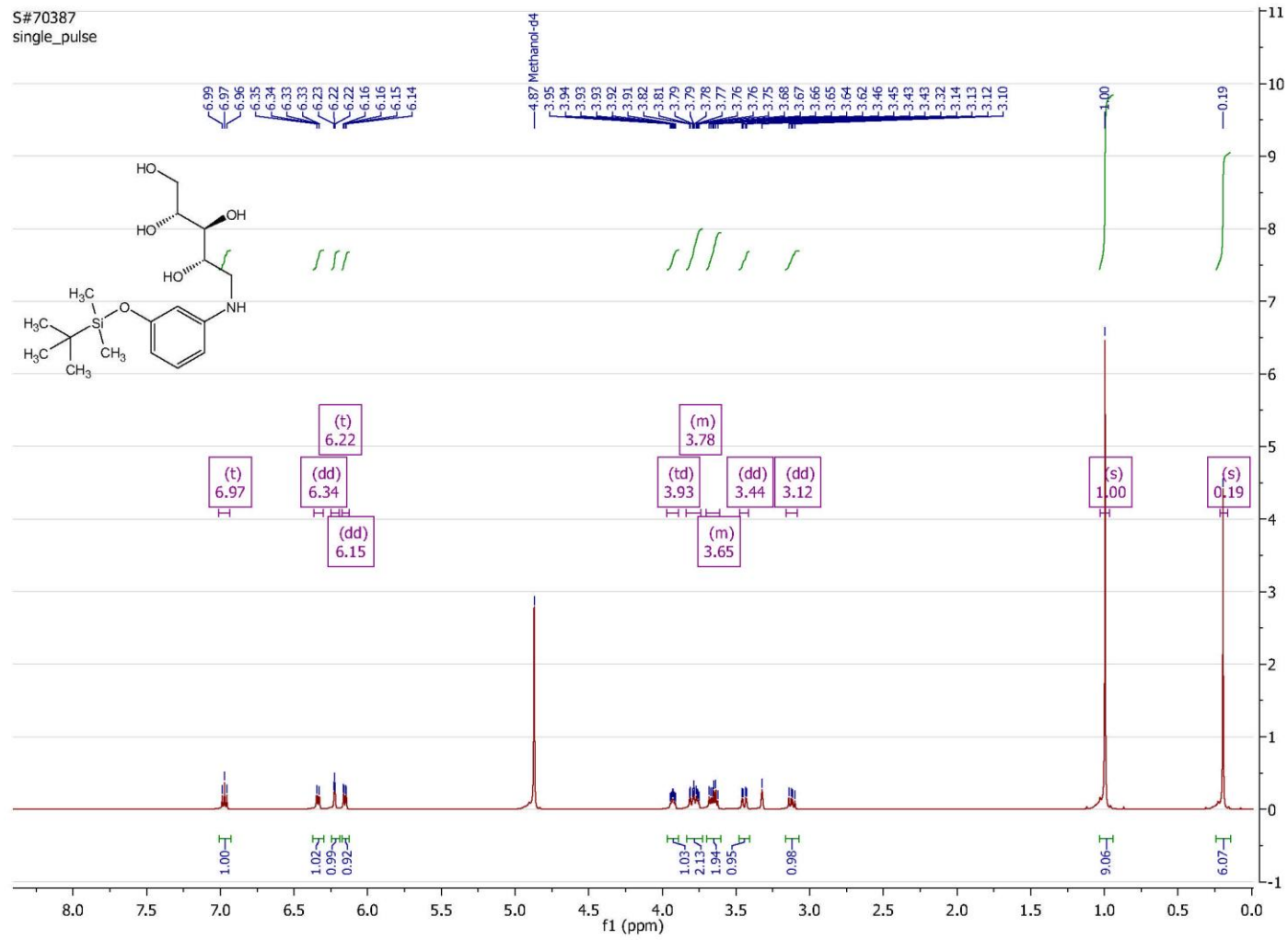


S#57096
single pulse decoupled gated NOE

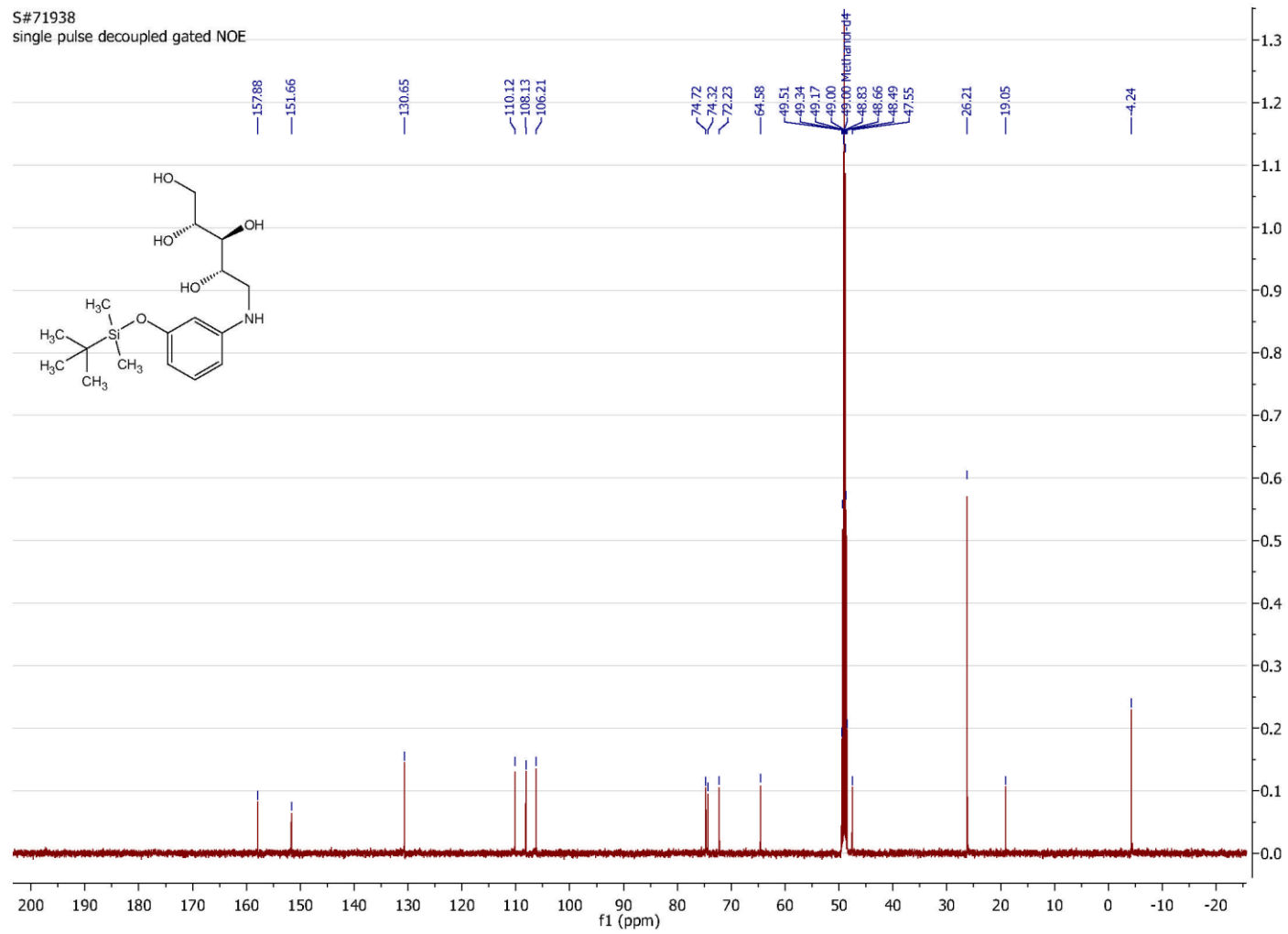


353

354



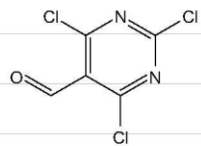
S#71938
single pulse decoupled gated NOE



355

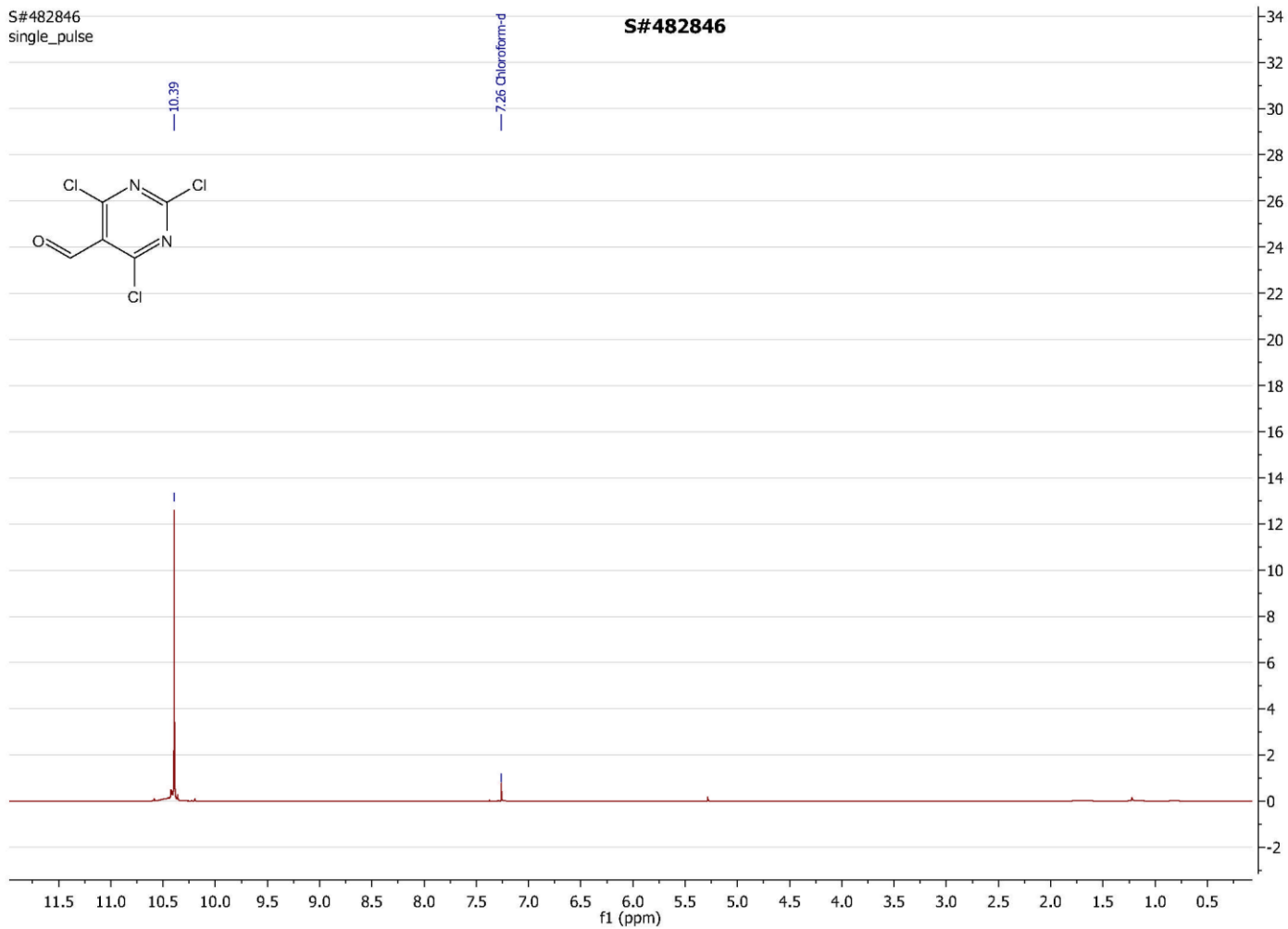
S#482846
single_pulse

S#482846



10.39

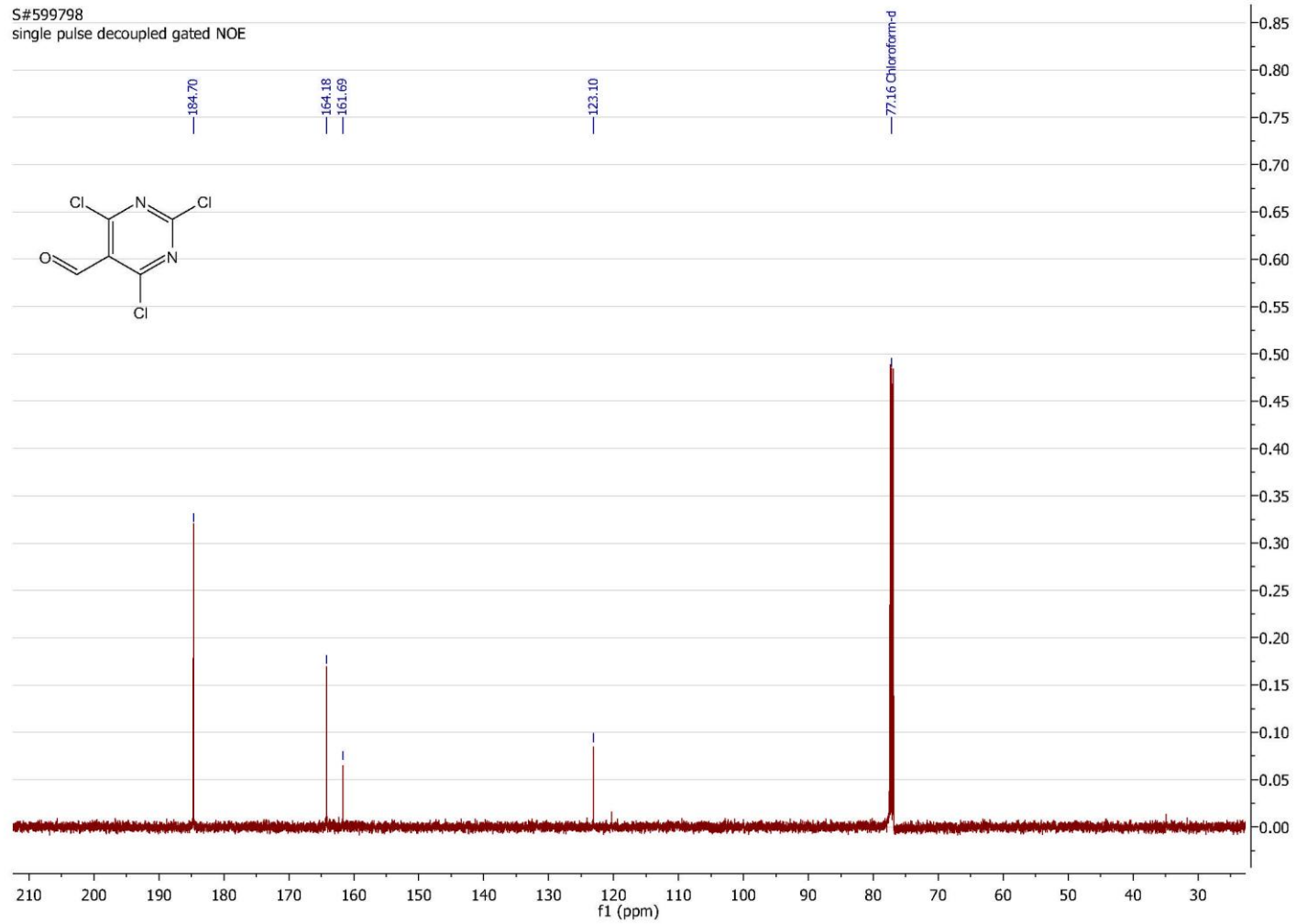
7.26 Chloroform-d



356

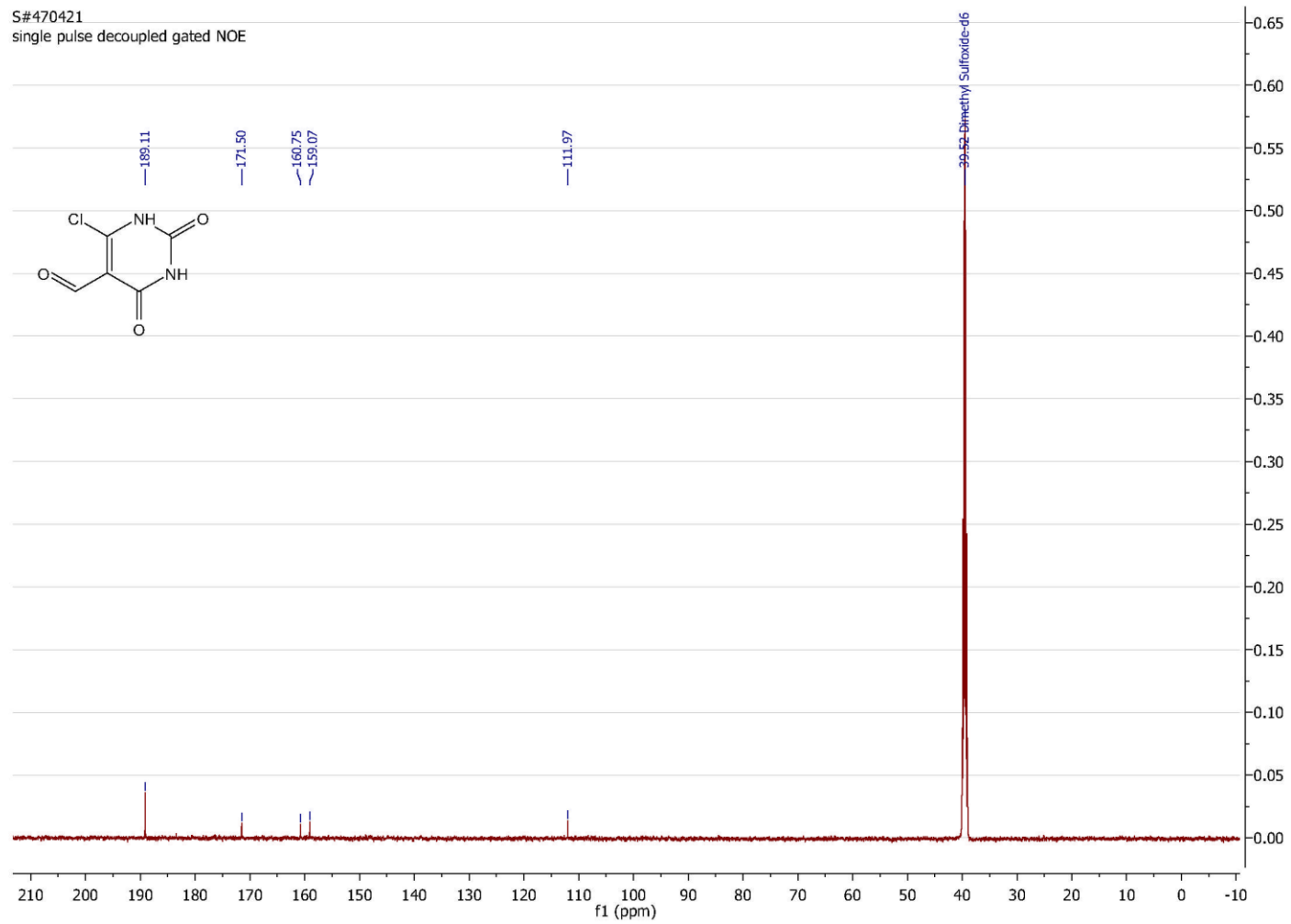
357

S#599798
single pulse decoupled gated NOE



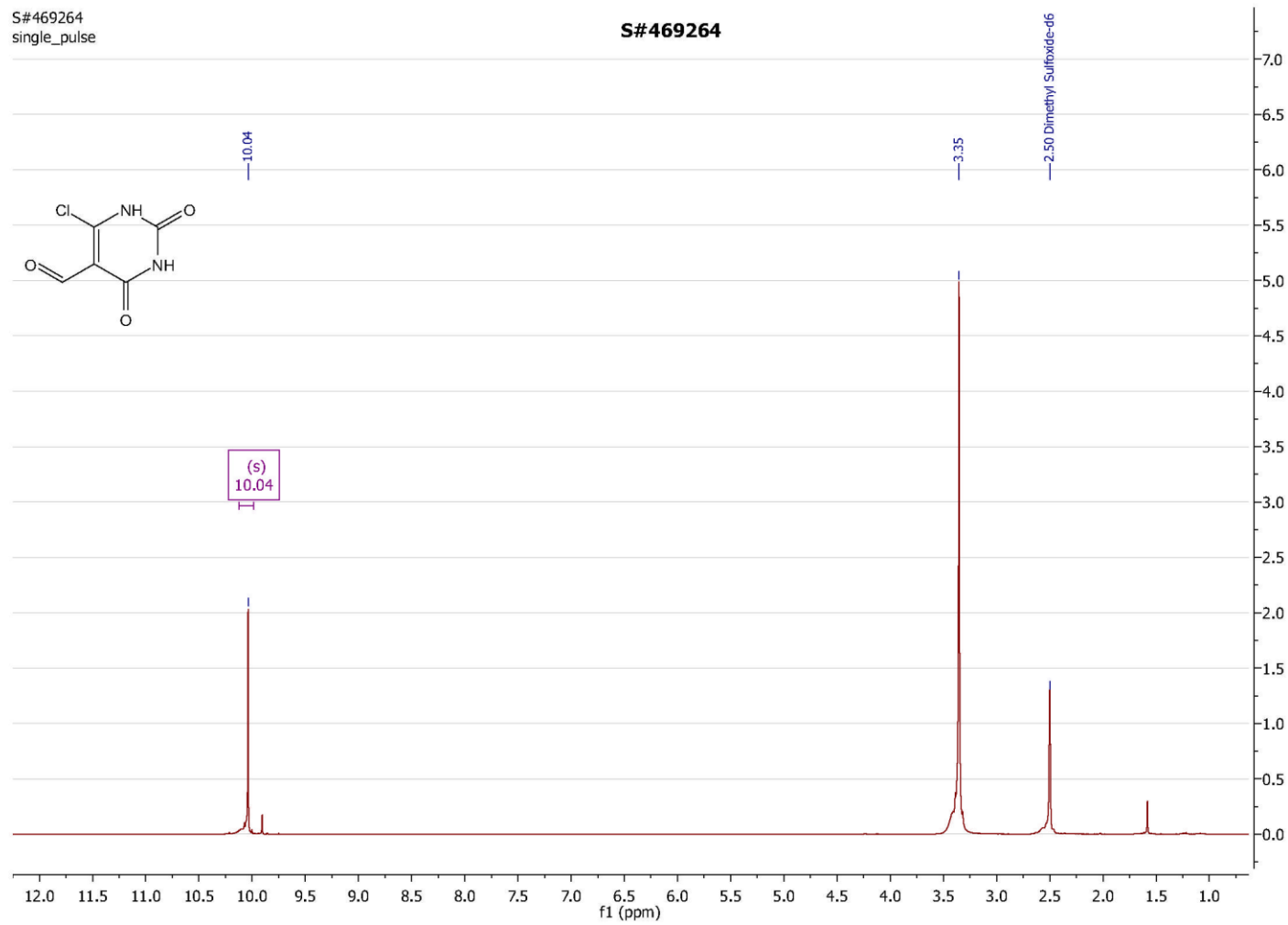
358

S#470421
single pulse decoupled gated NOE



S#469264
single_pulse

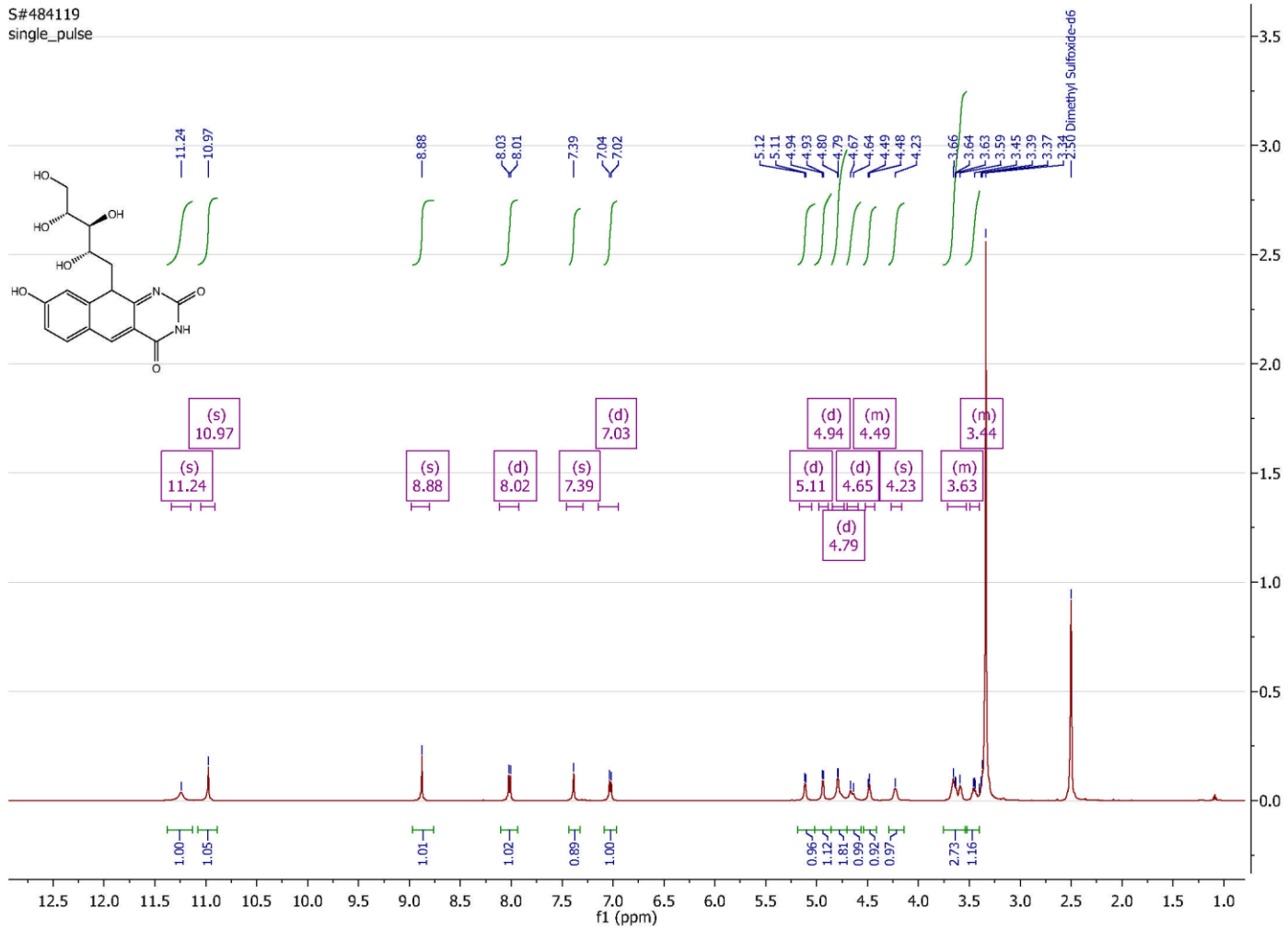
S#469264



359

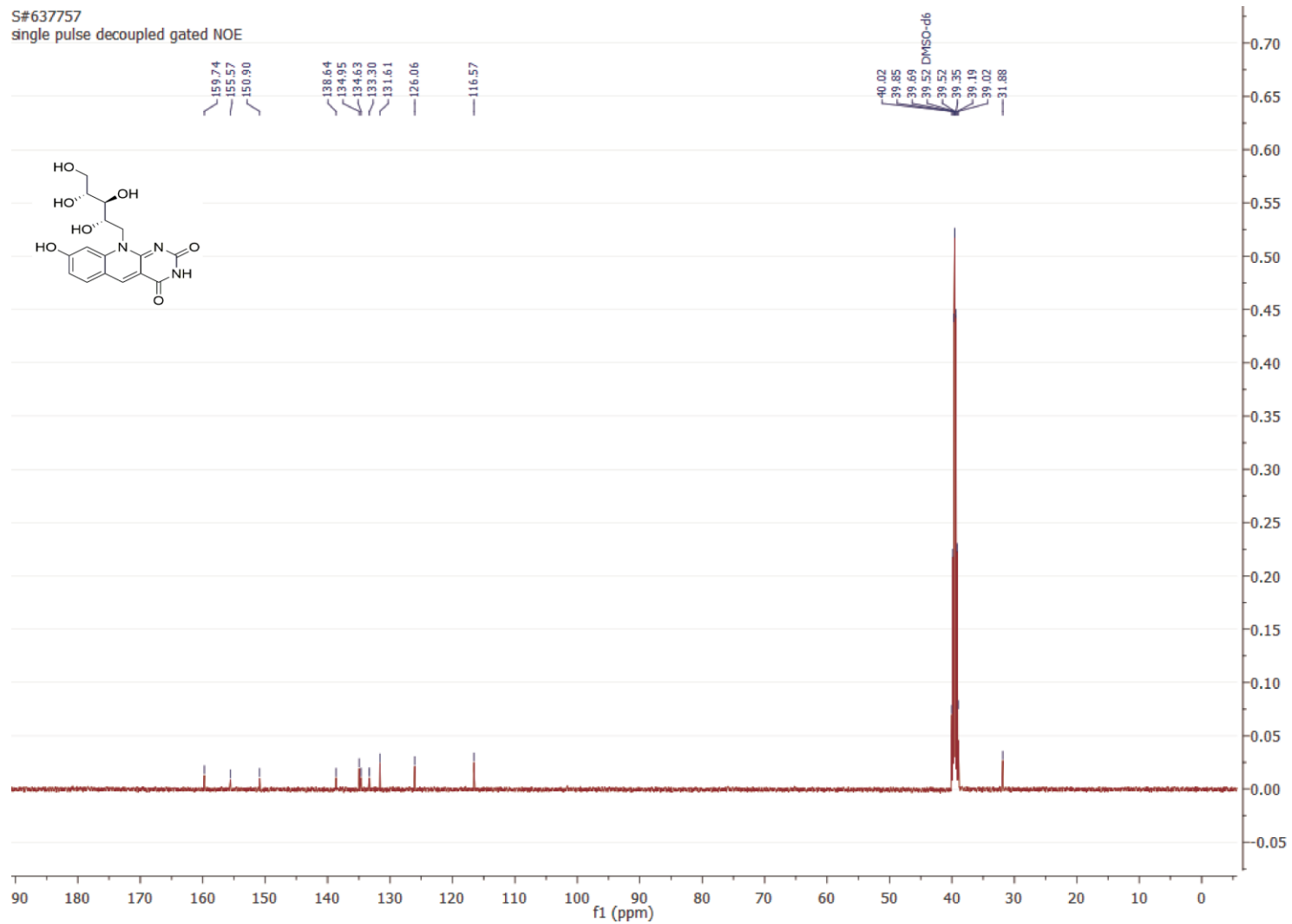
360

S#484119
single_pulse

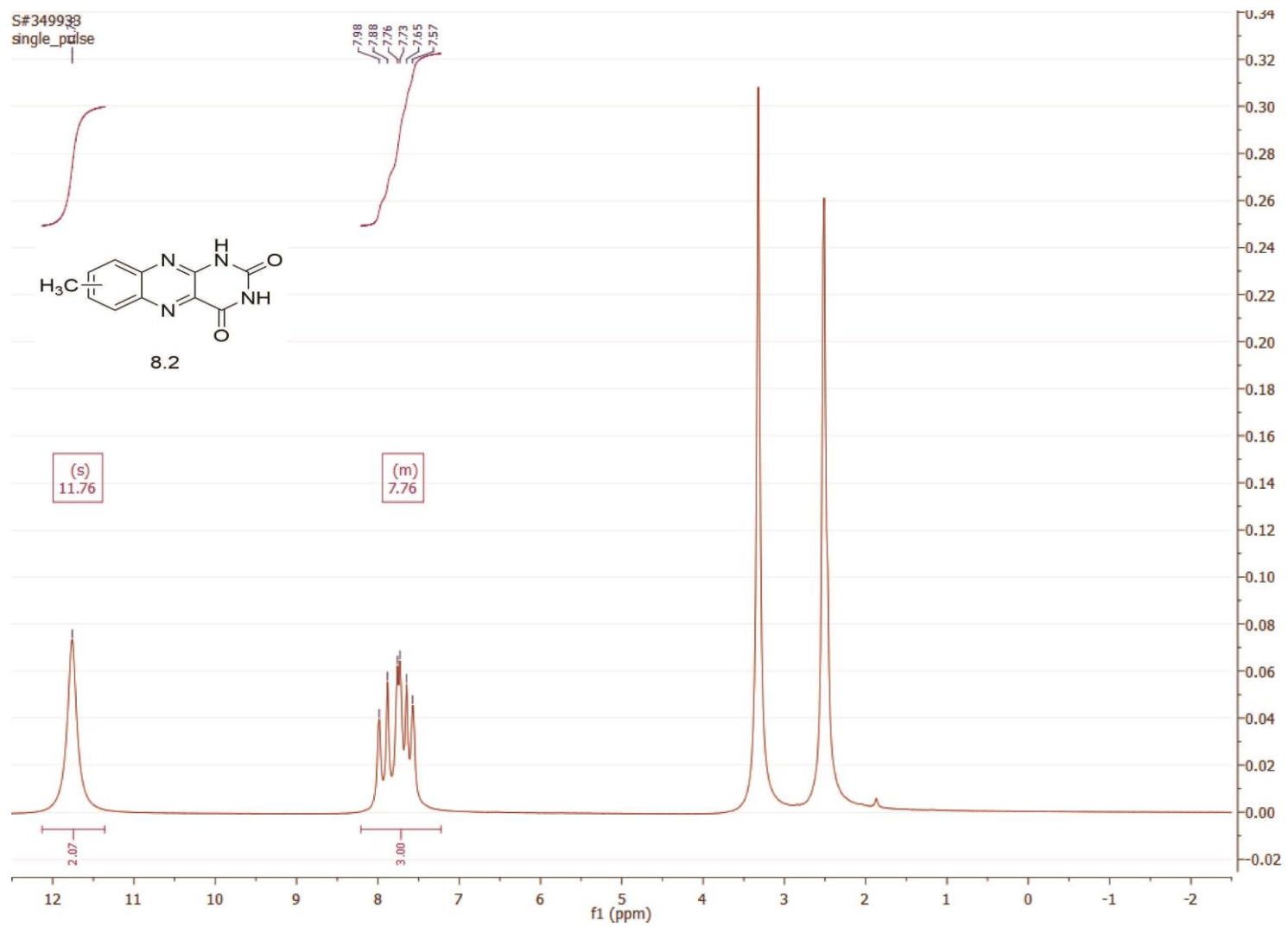


361

S#637757
single pulse decoupled gated NOE

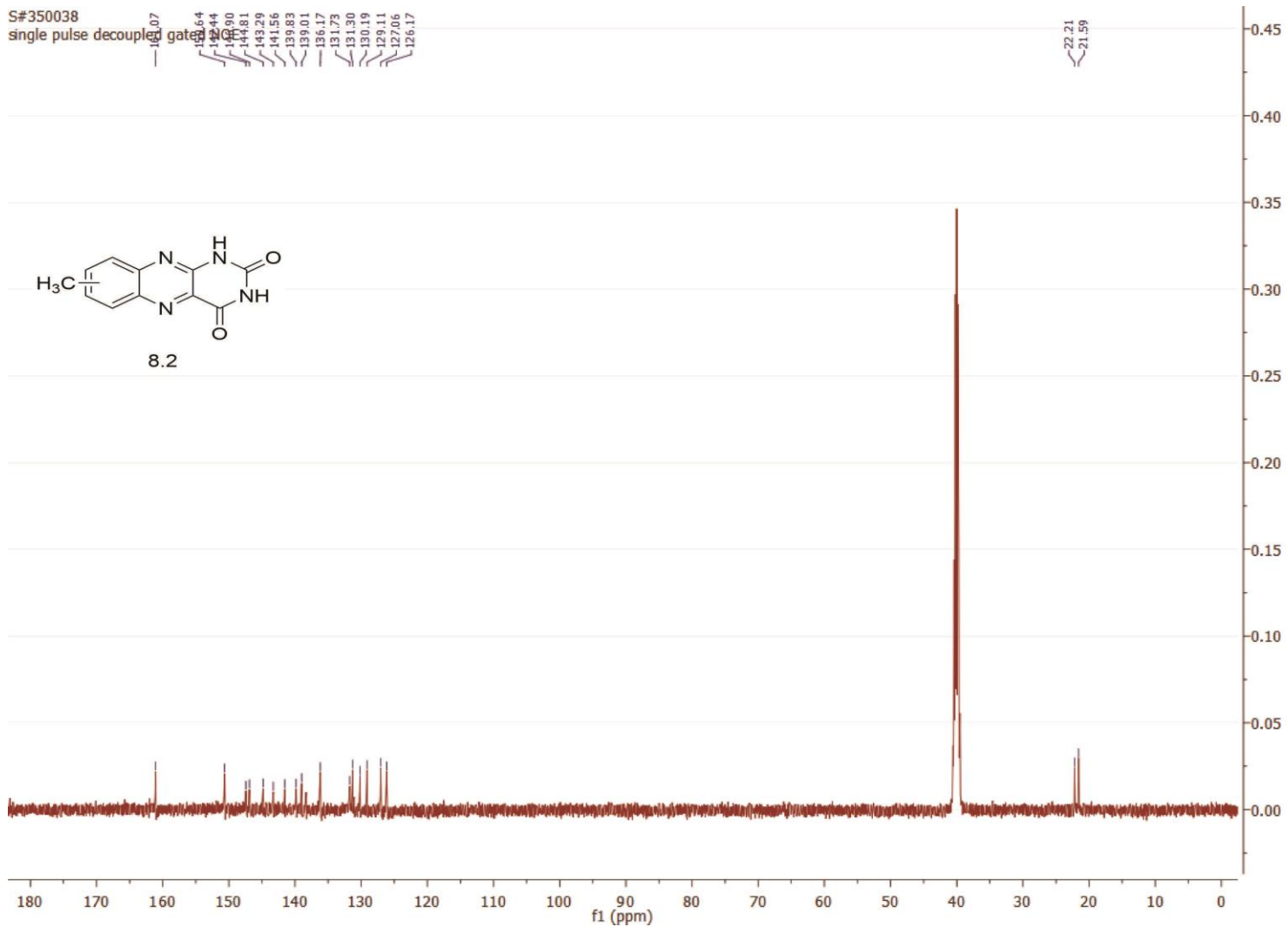


362



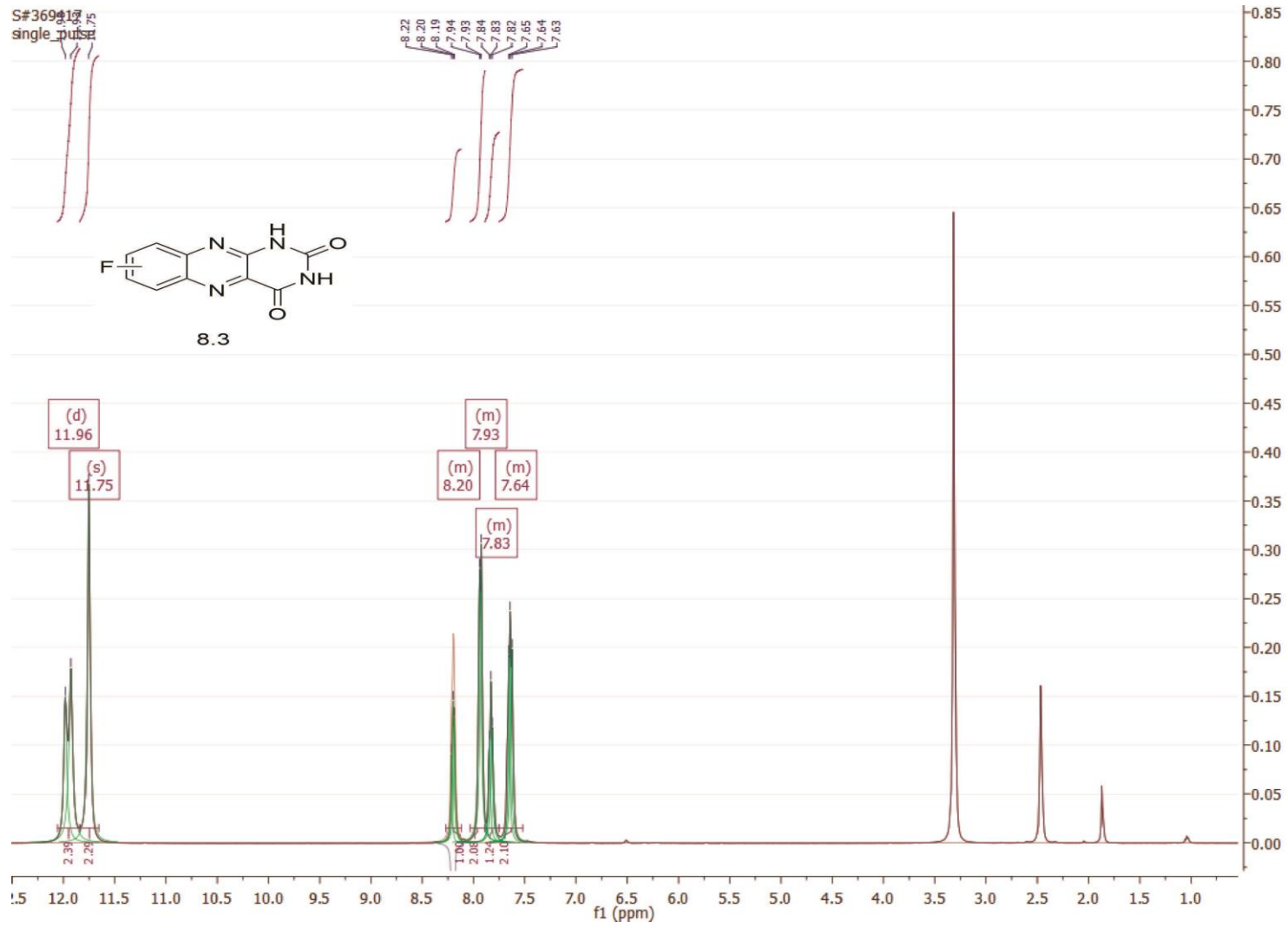
S#350038

single pulse decouple gated

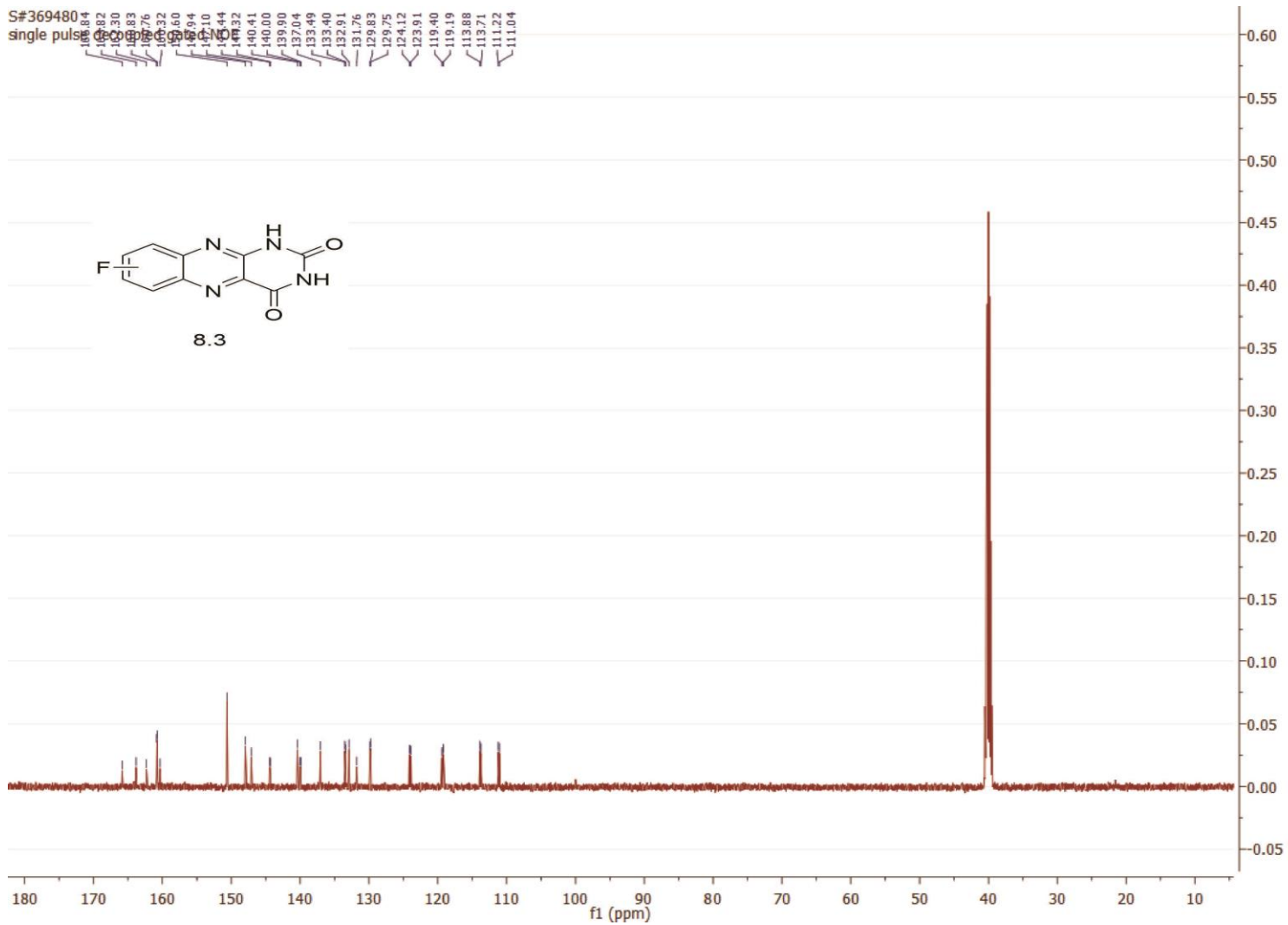


363

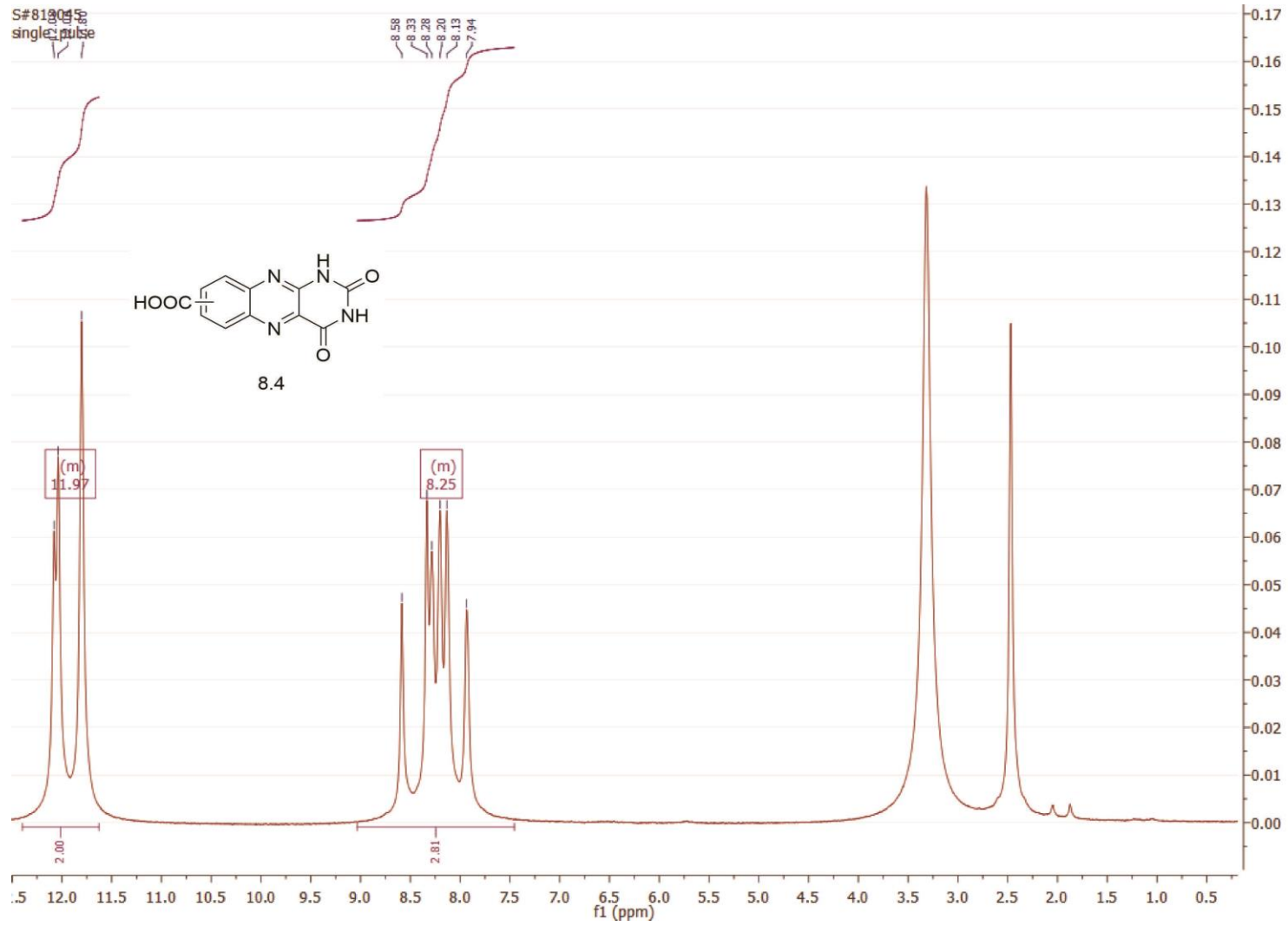
364



365

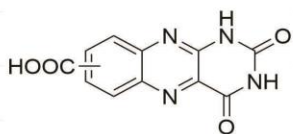


366

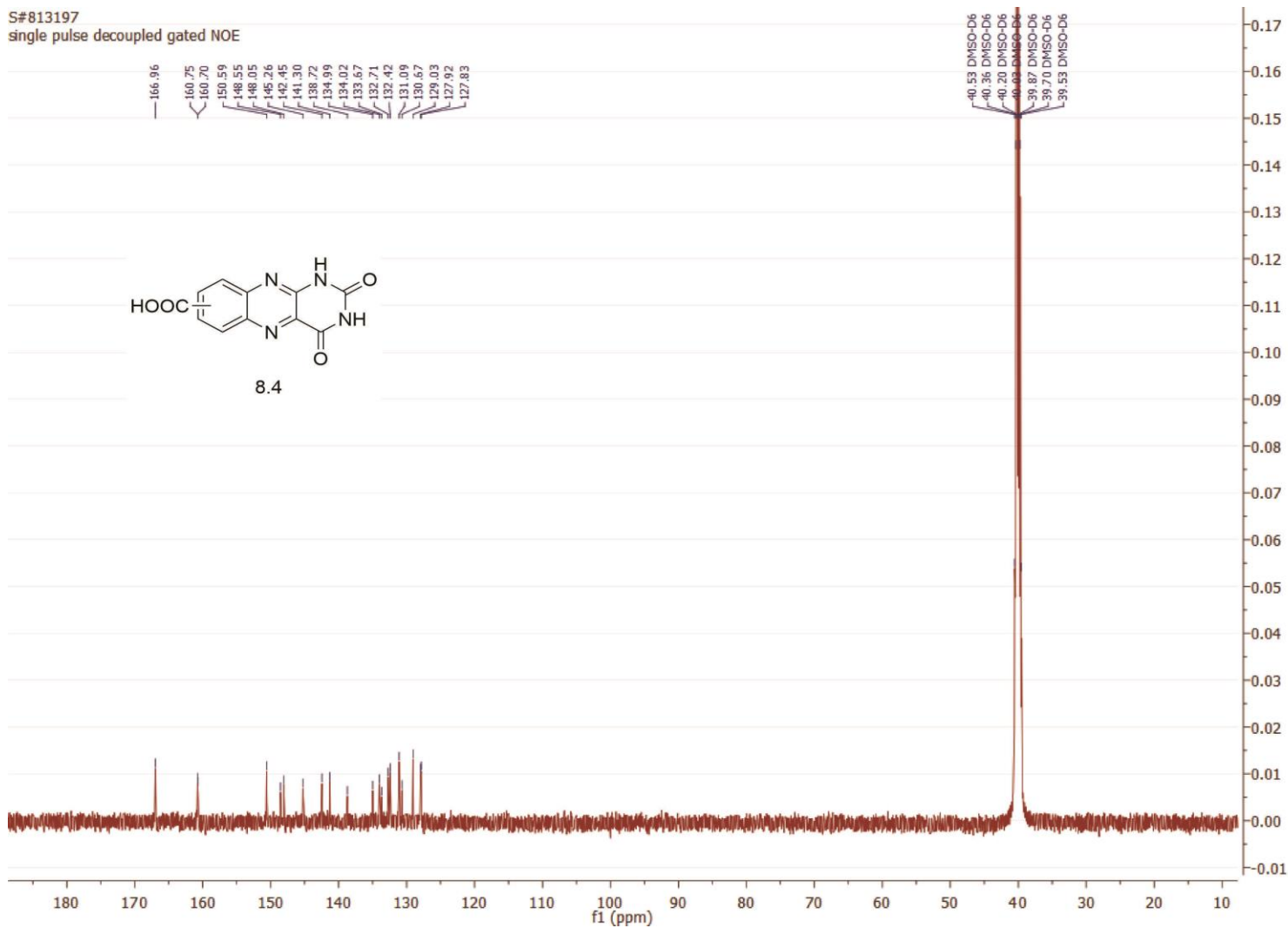


S#813197

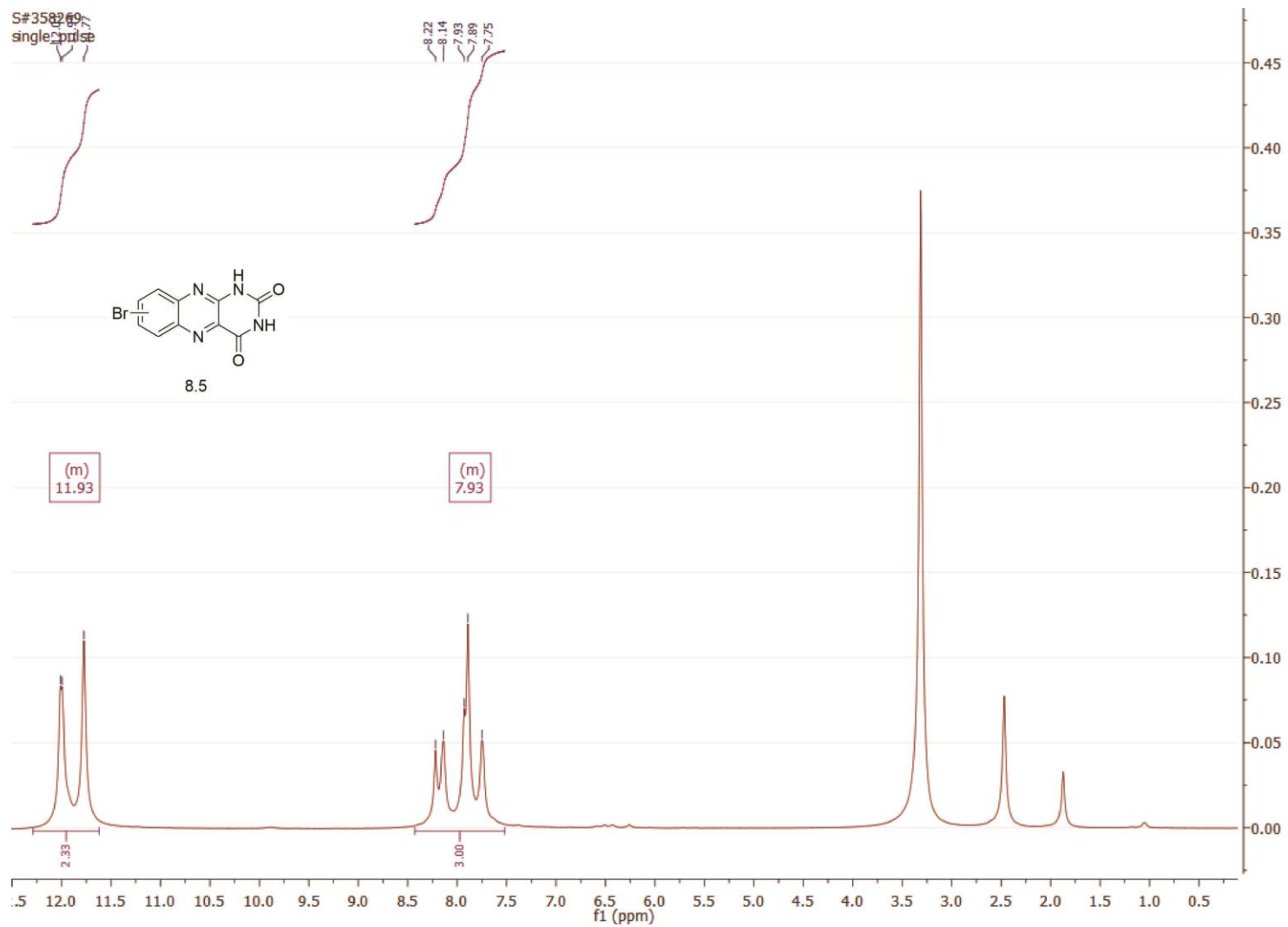
single pulse decoupled gated NOE



8.4

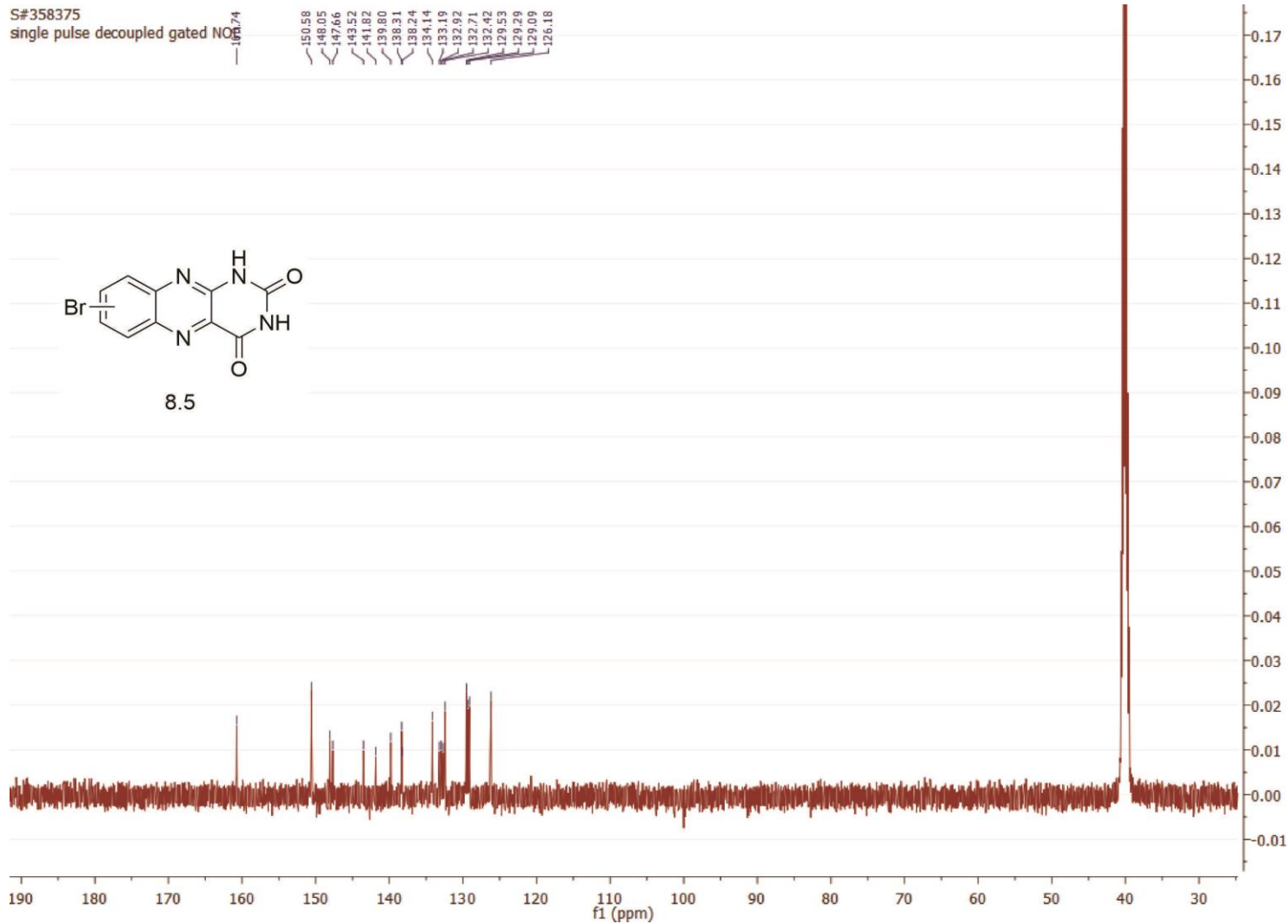
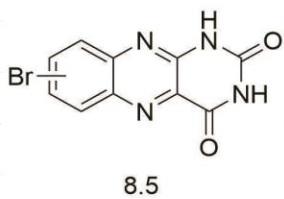


368



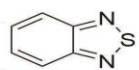
369

S#358375
single pulse decoupled gated NO

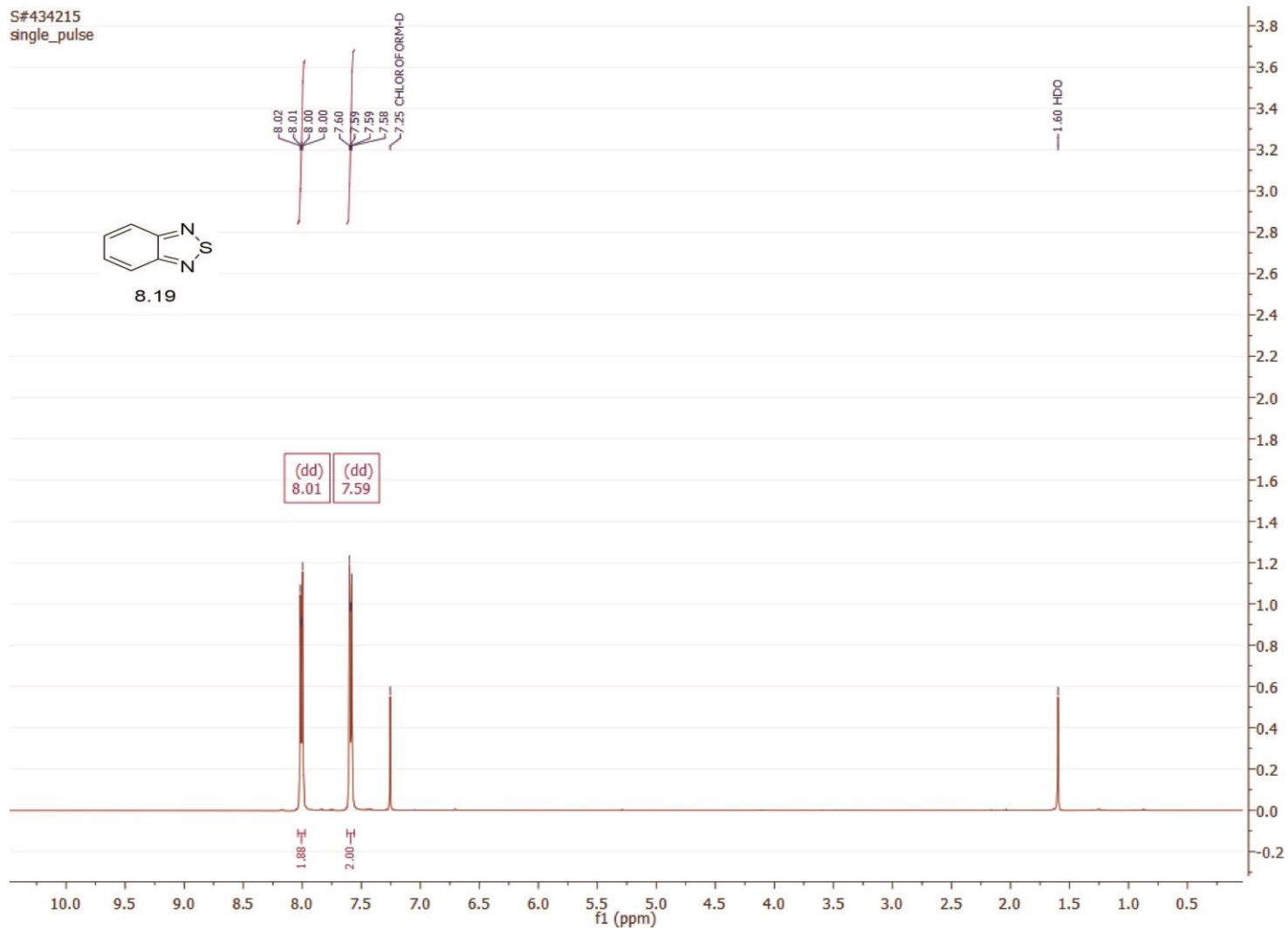


370

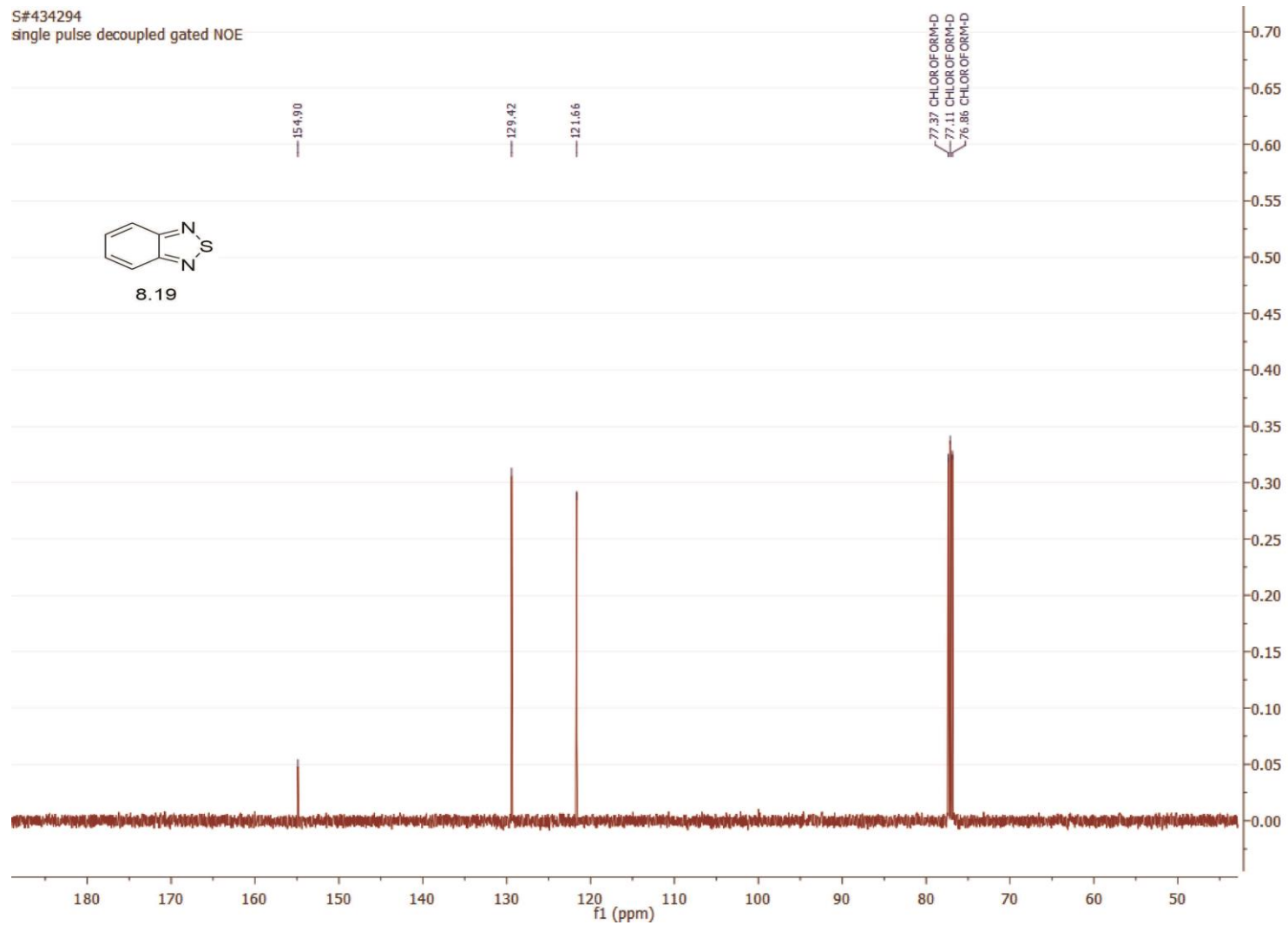
S#434215
single_pulse



8.19

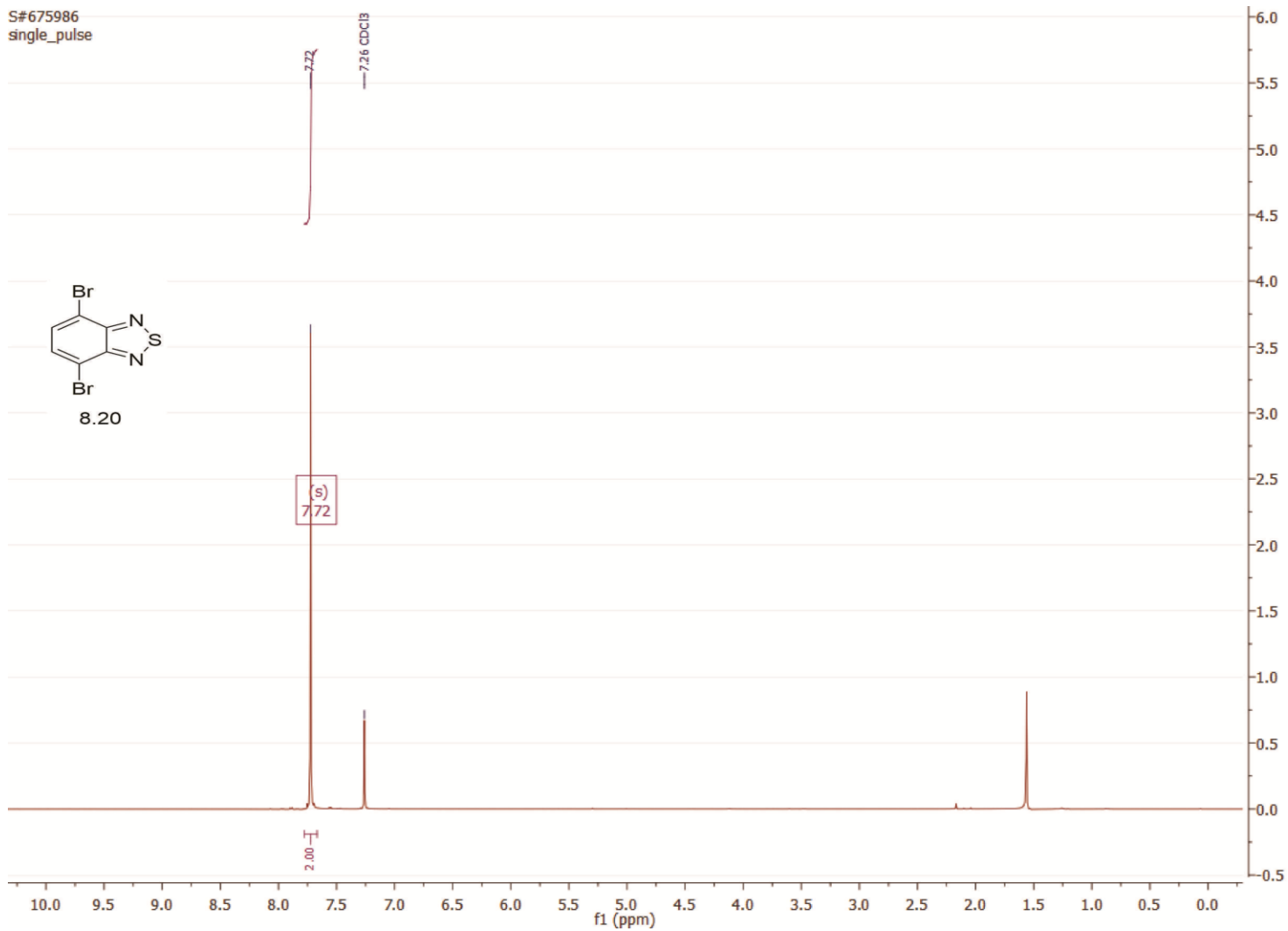


S#434294
single pulse decoupled gated NOE



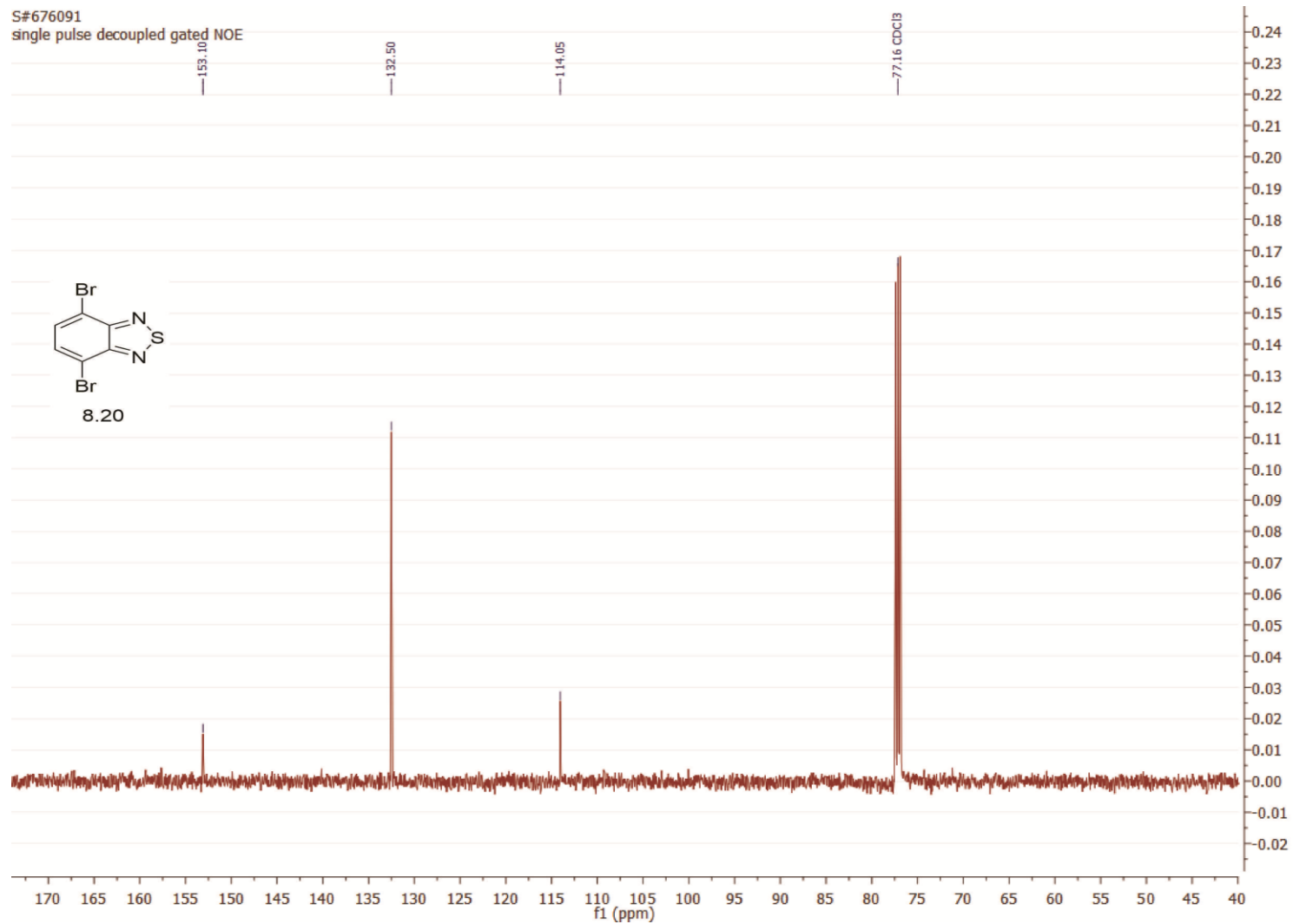
371

S#675986
single_pulse



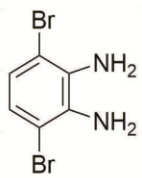
372

S#676091
single pulse decoupled gated NOE

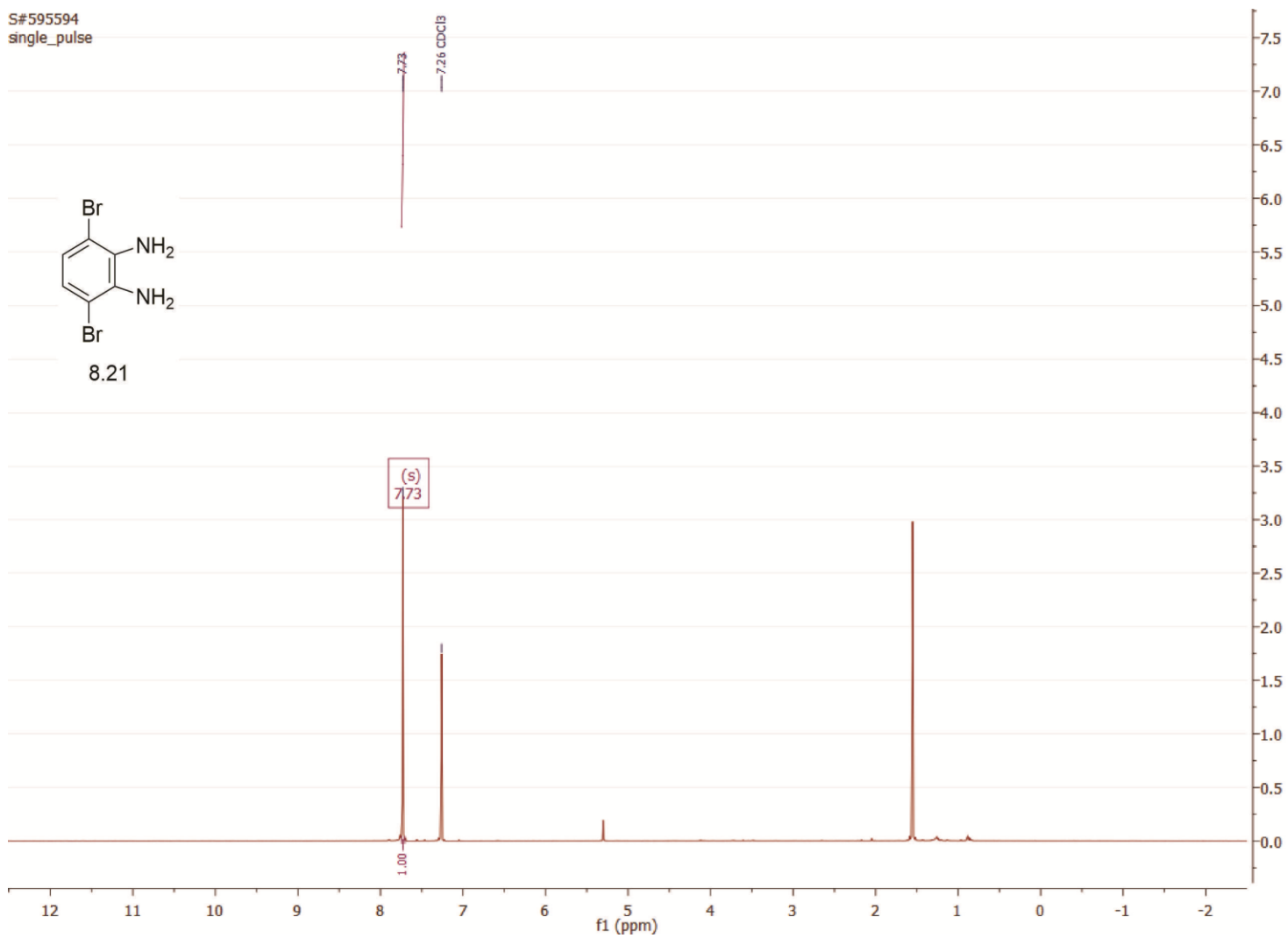


373

S#595594
single_pulse

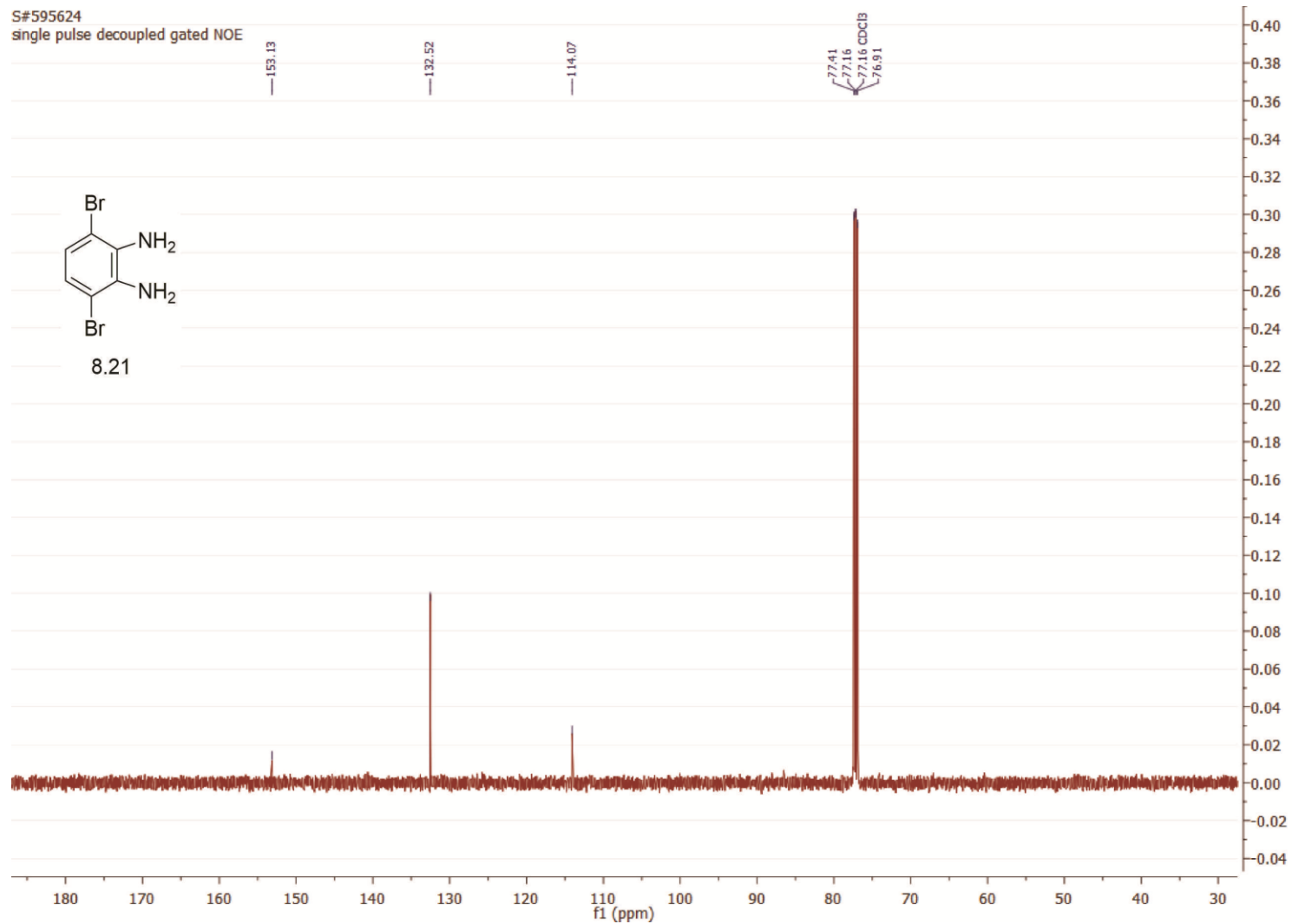


8.21



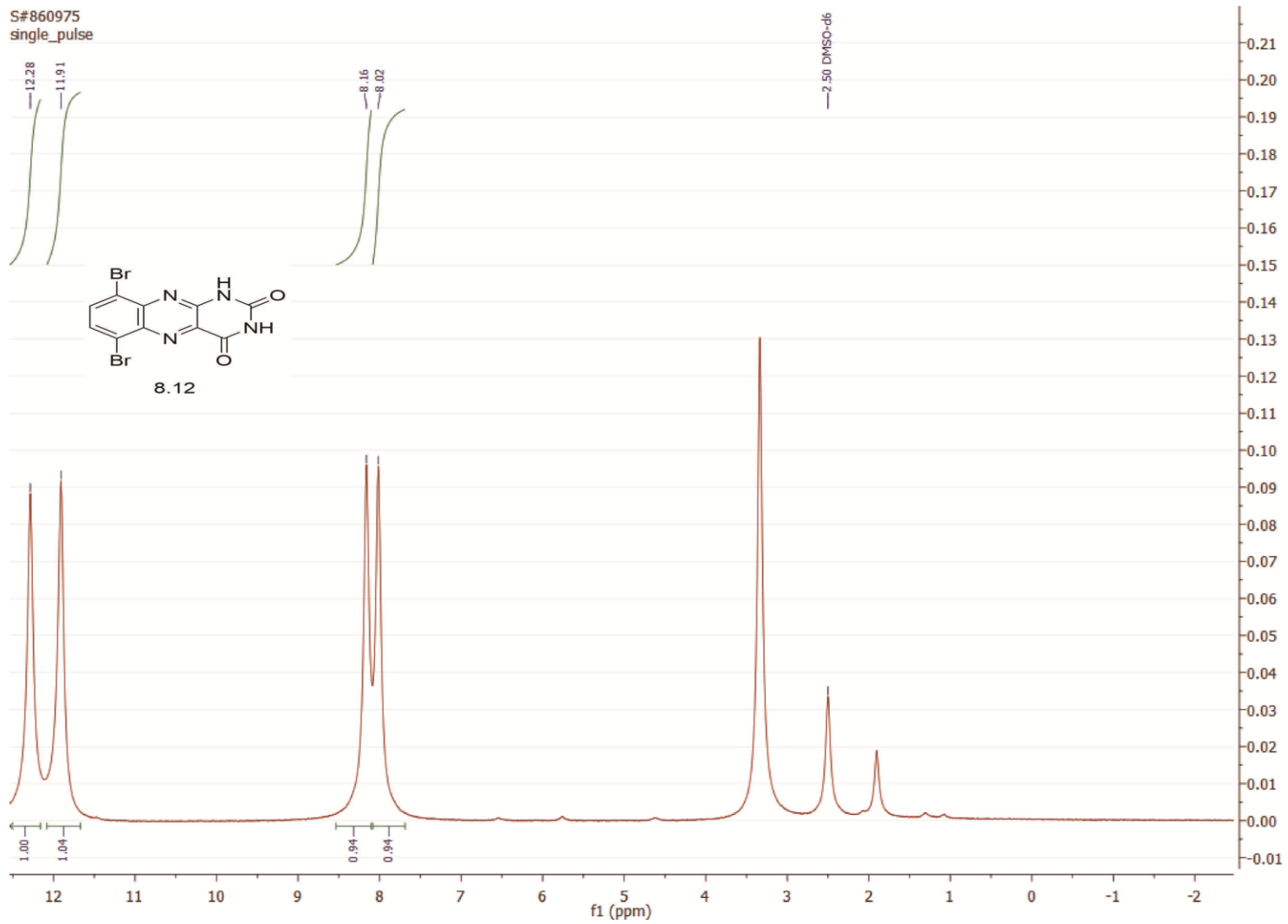
374

S#595624
single pulse decoupled gated NOE

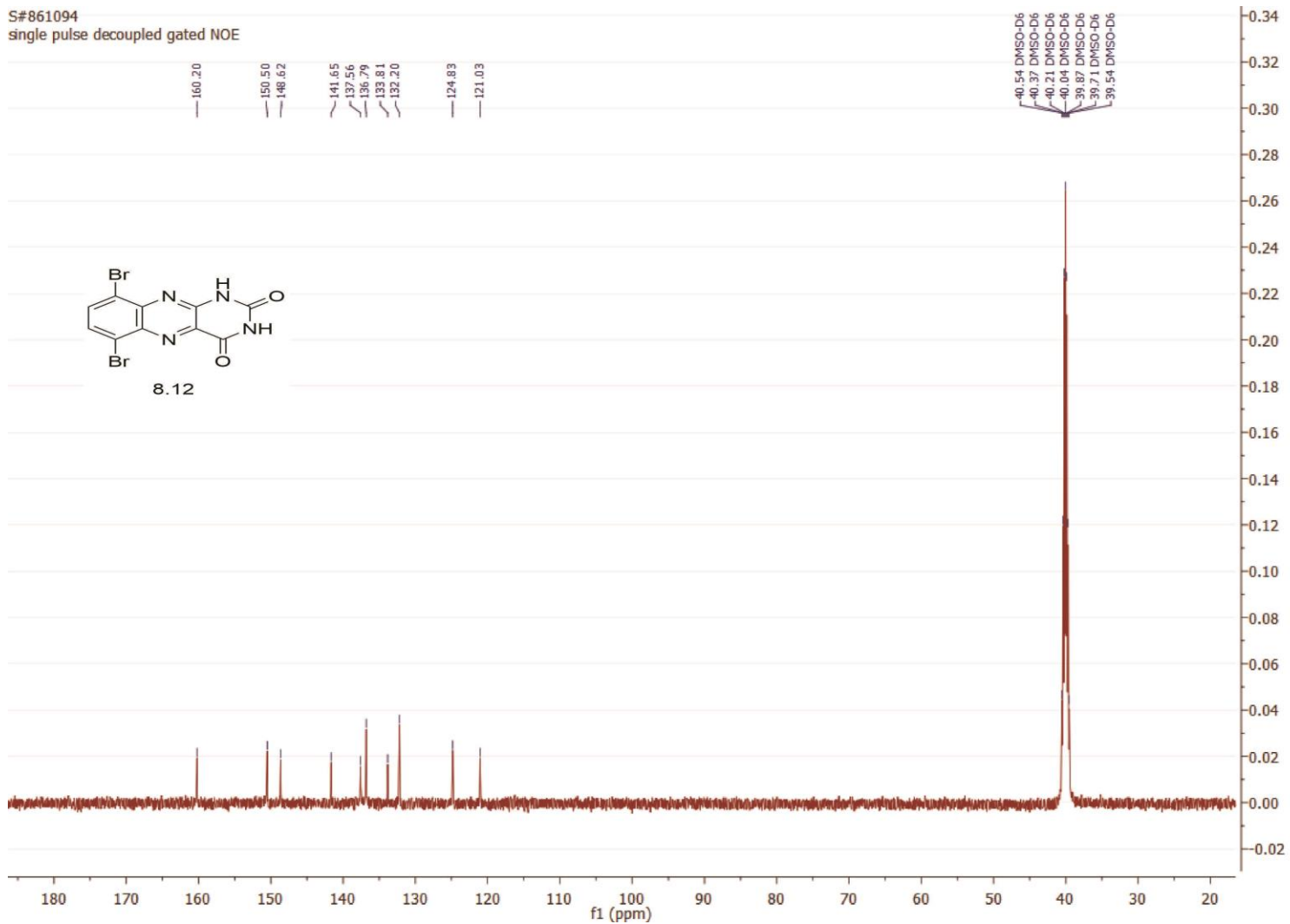


375

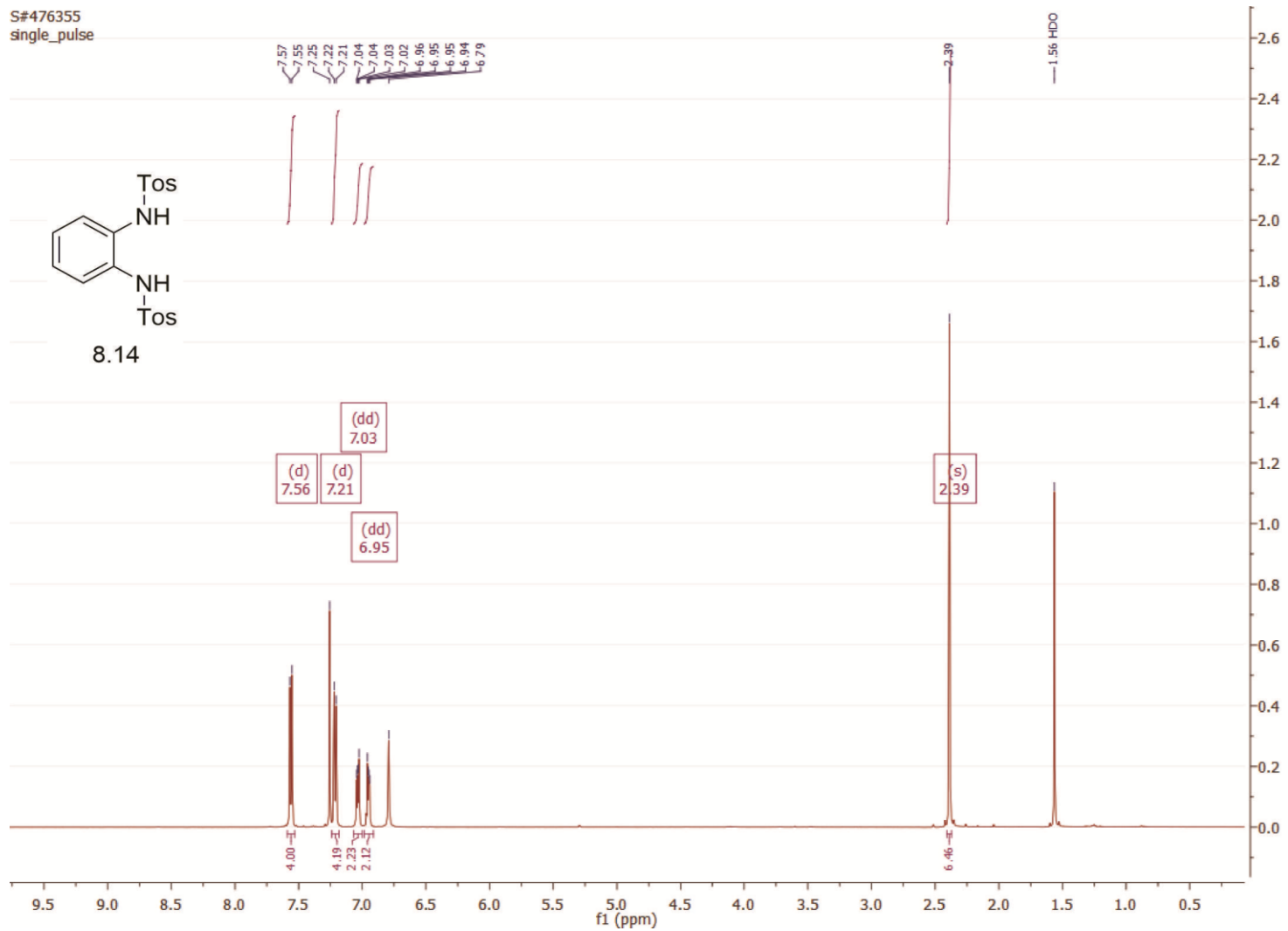
376



S#861094
single pulse decoupled gated NOE

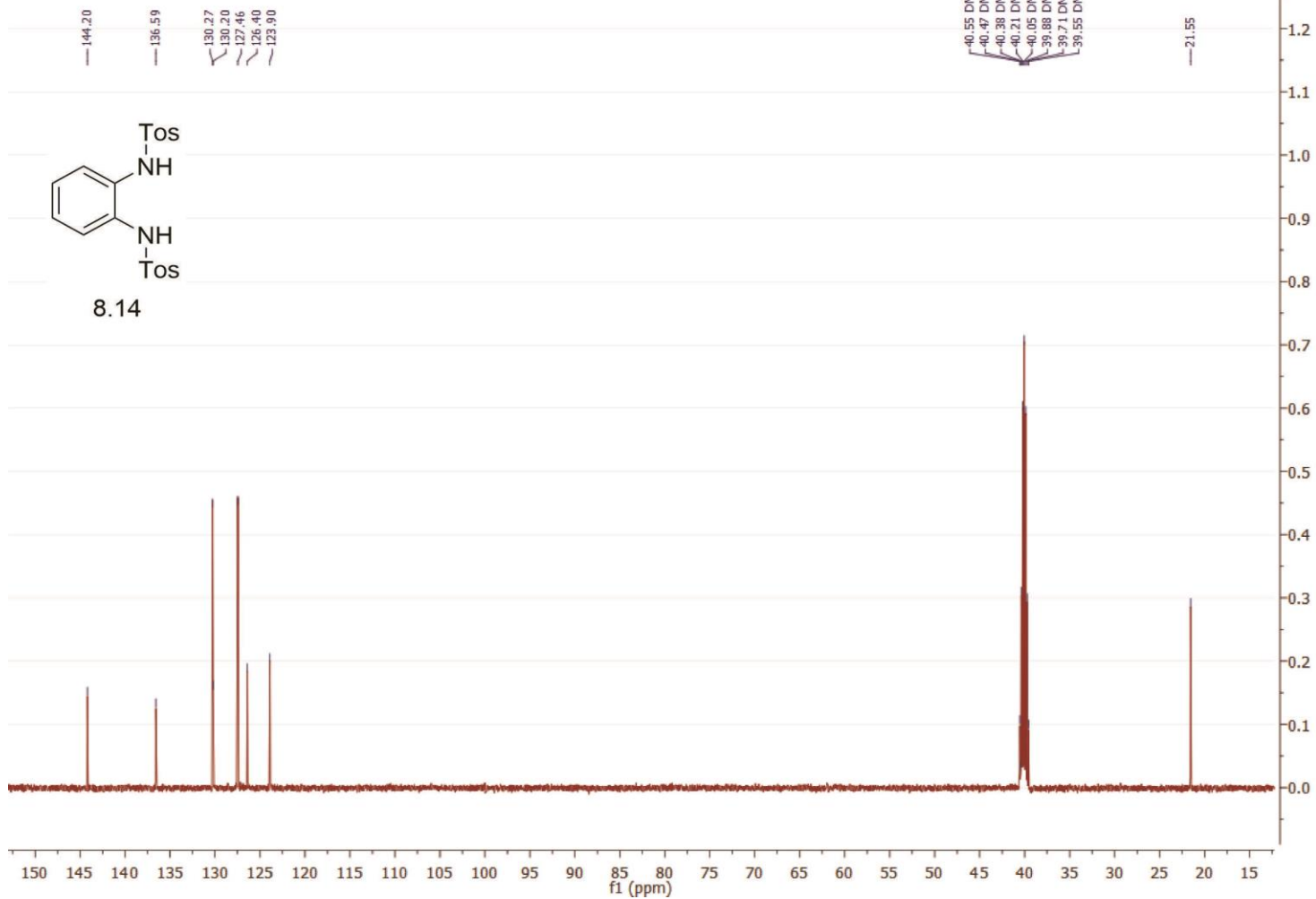


378



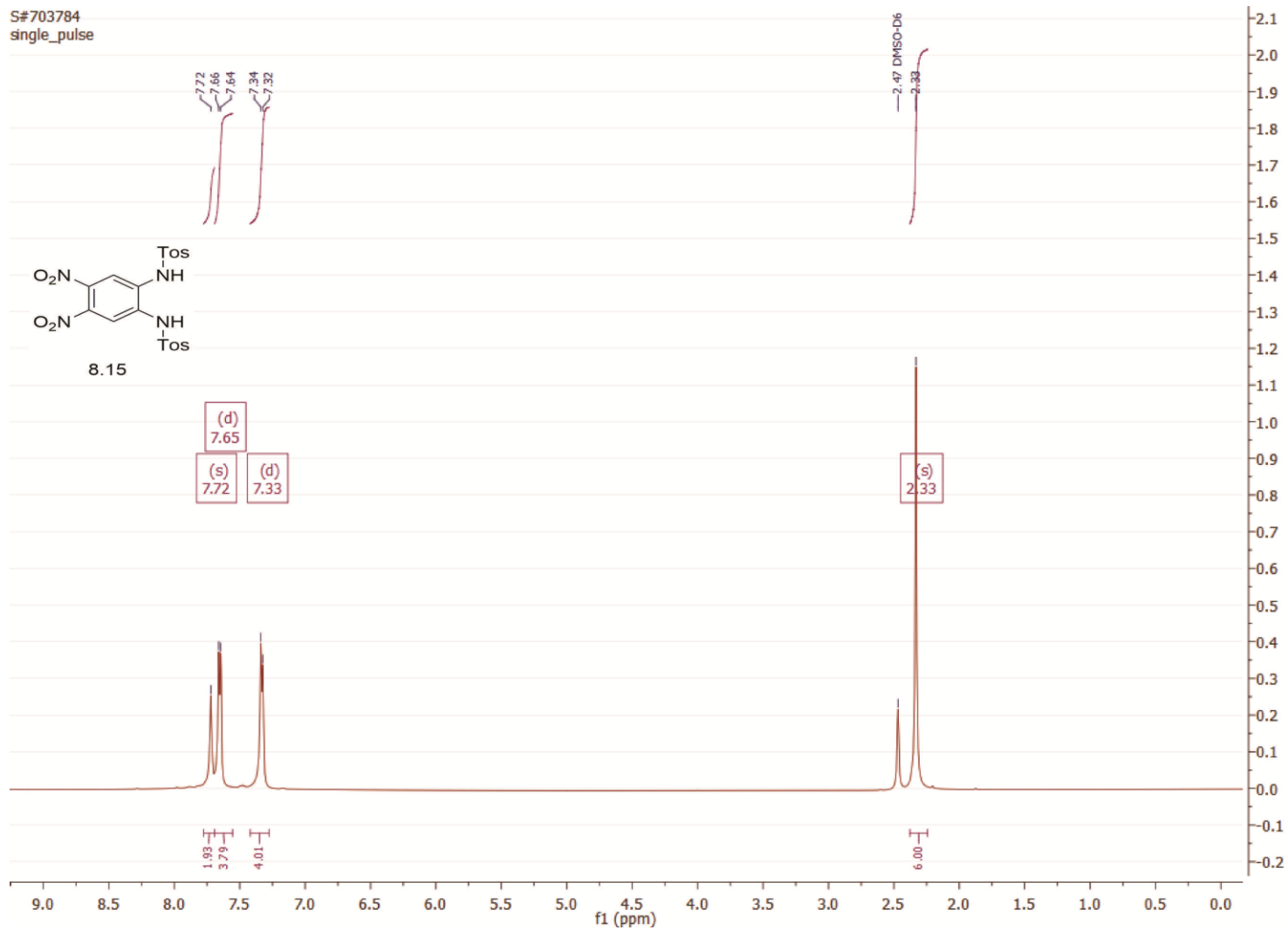
S#511474

single pulse decoupled gated NOE

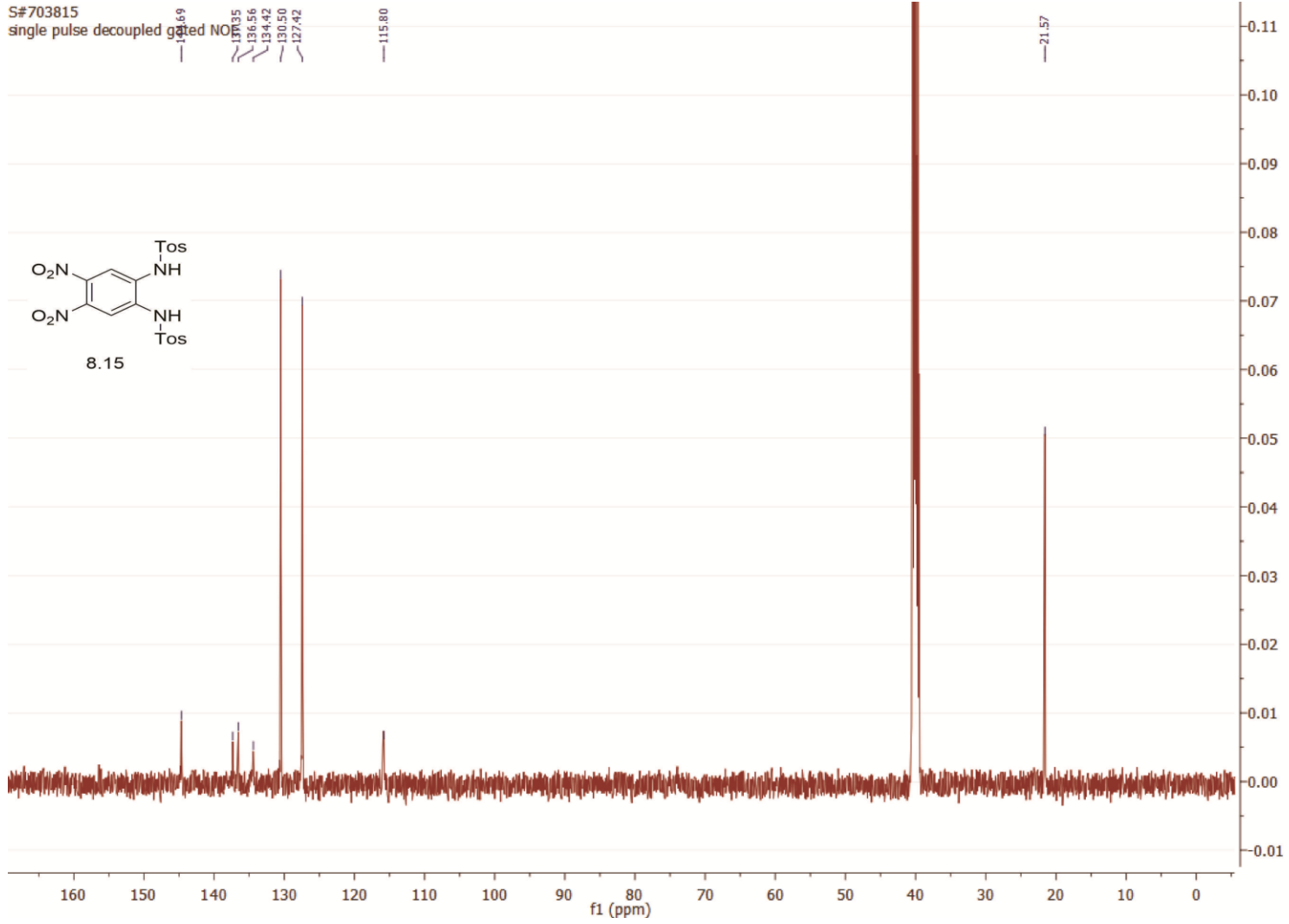


379

380

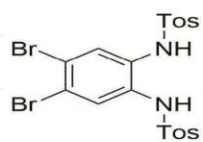


S#703815
single pulse decoupled gated NO

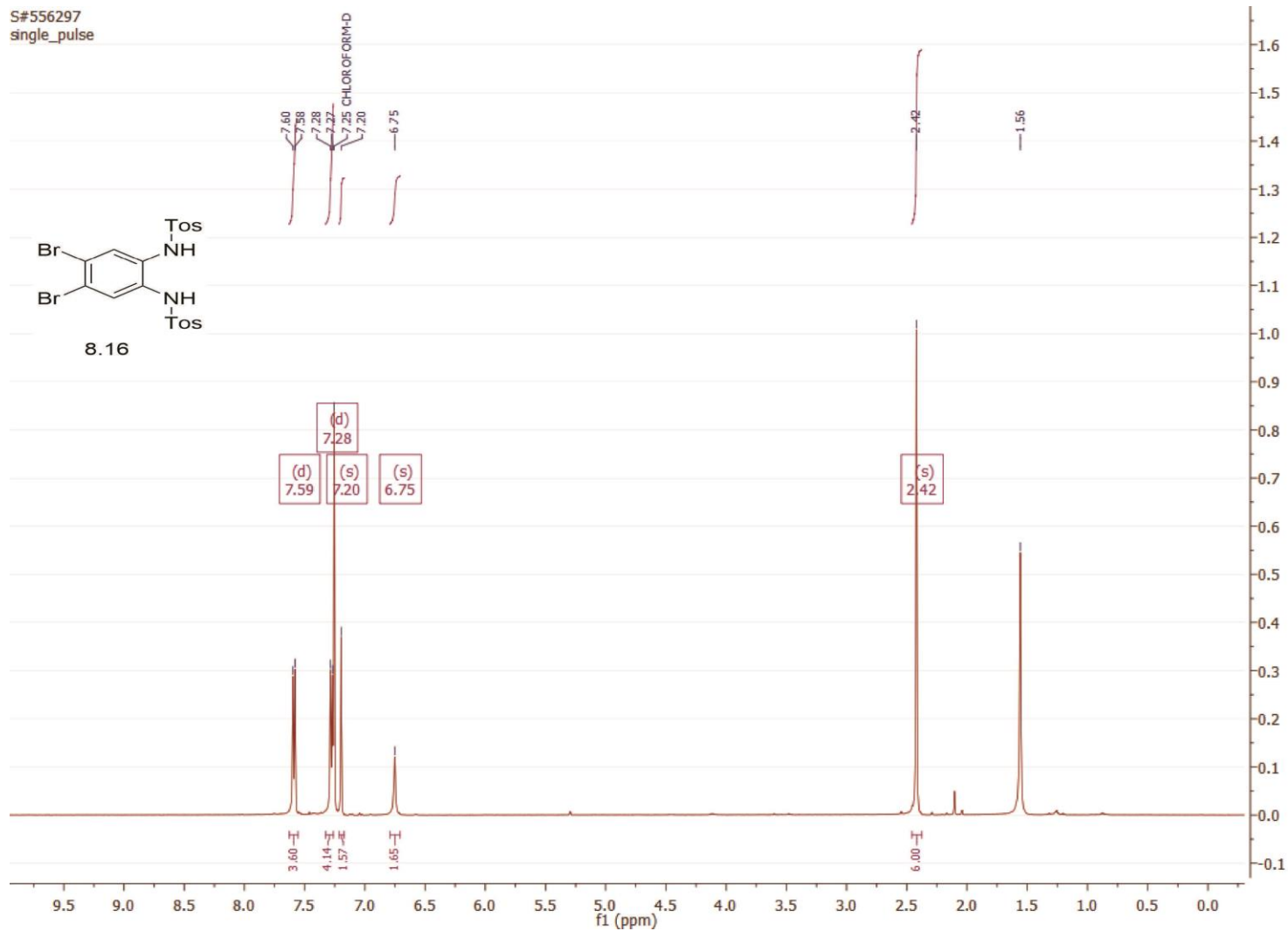


381

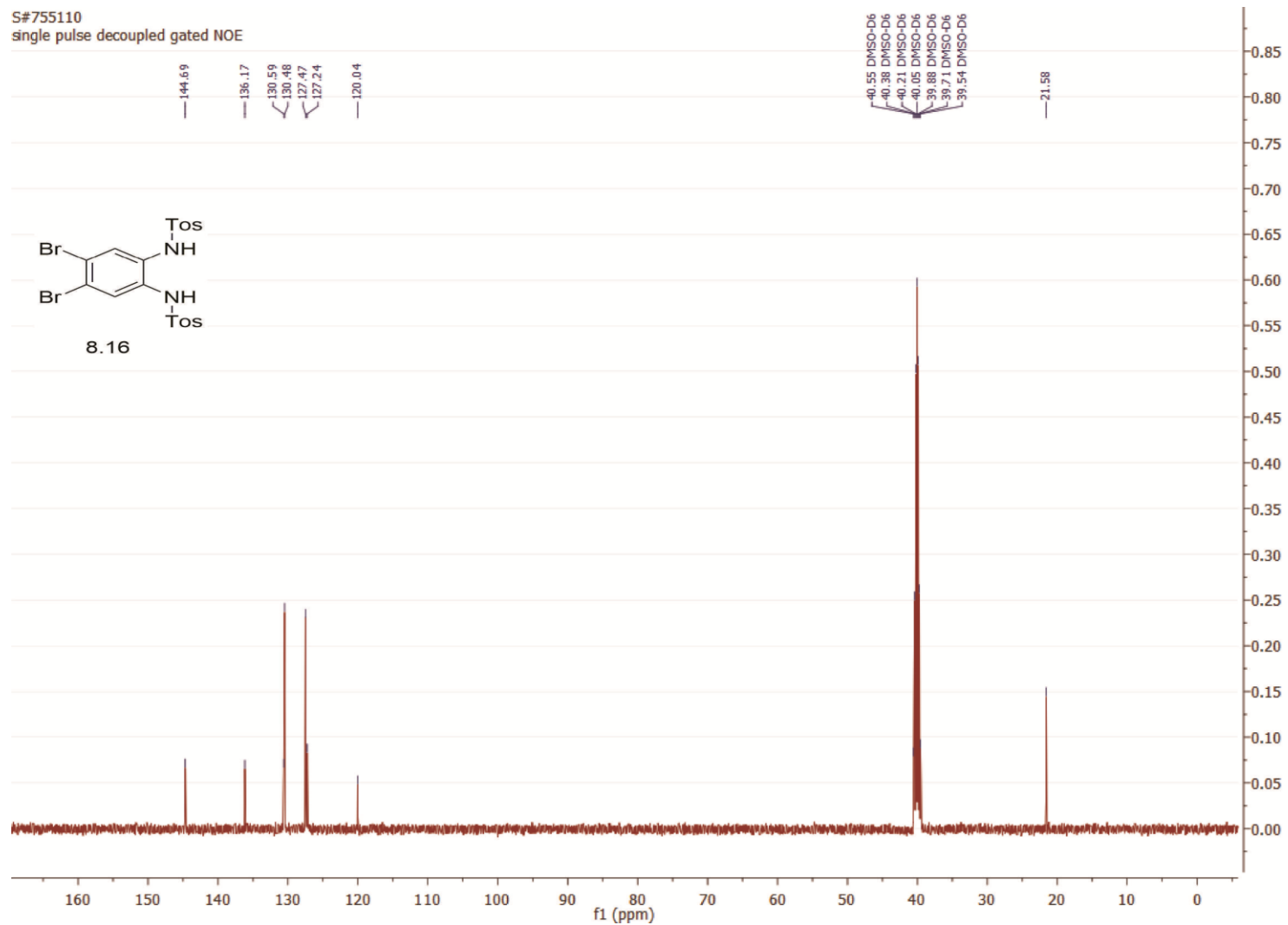
S#556297
single_pulse



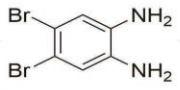
8.16



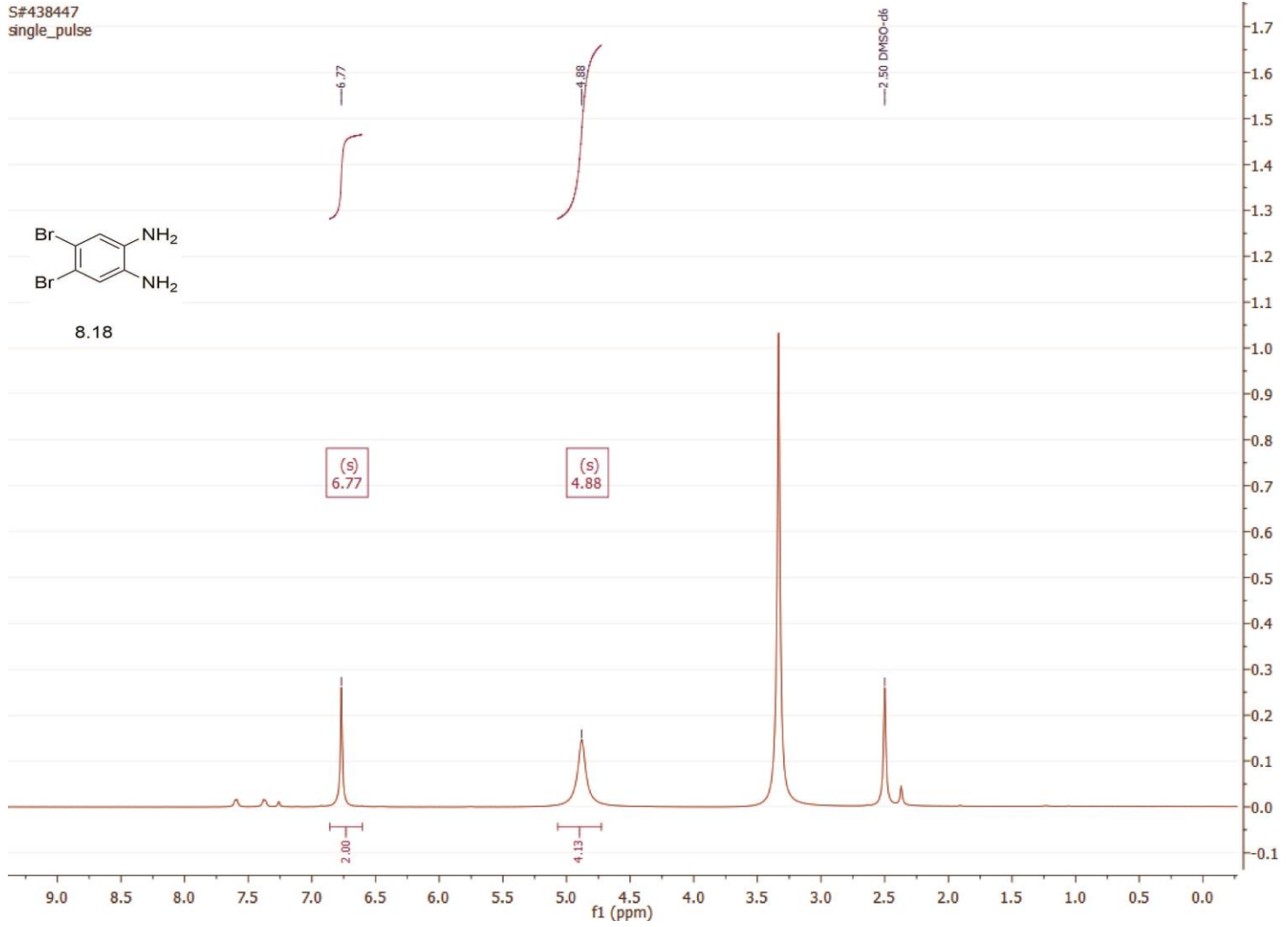
S#755110
single pulse decoupled gated NOE



S#438447
single_pulse

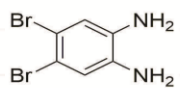


8.18

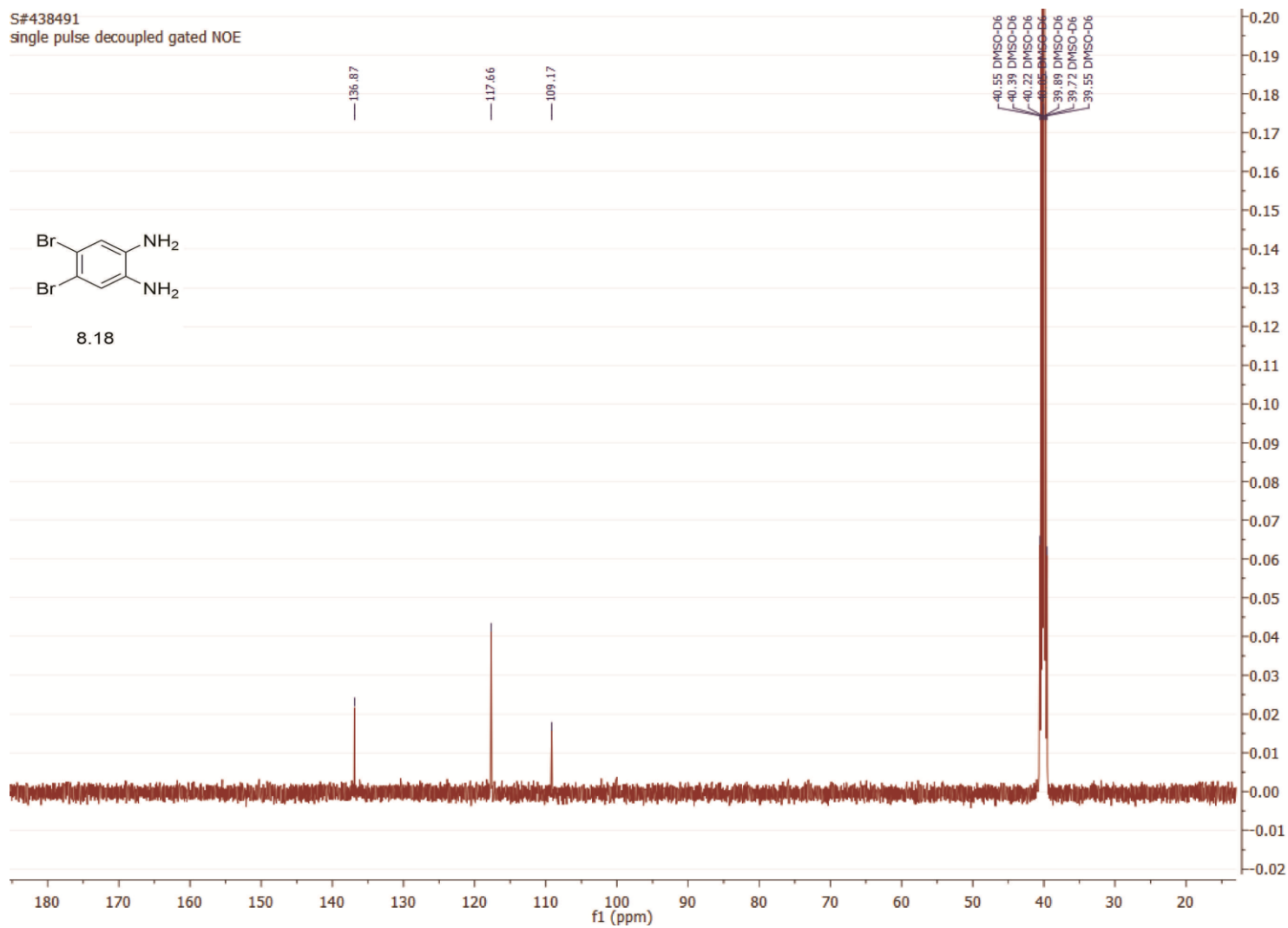


384

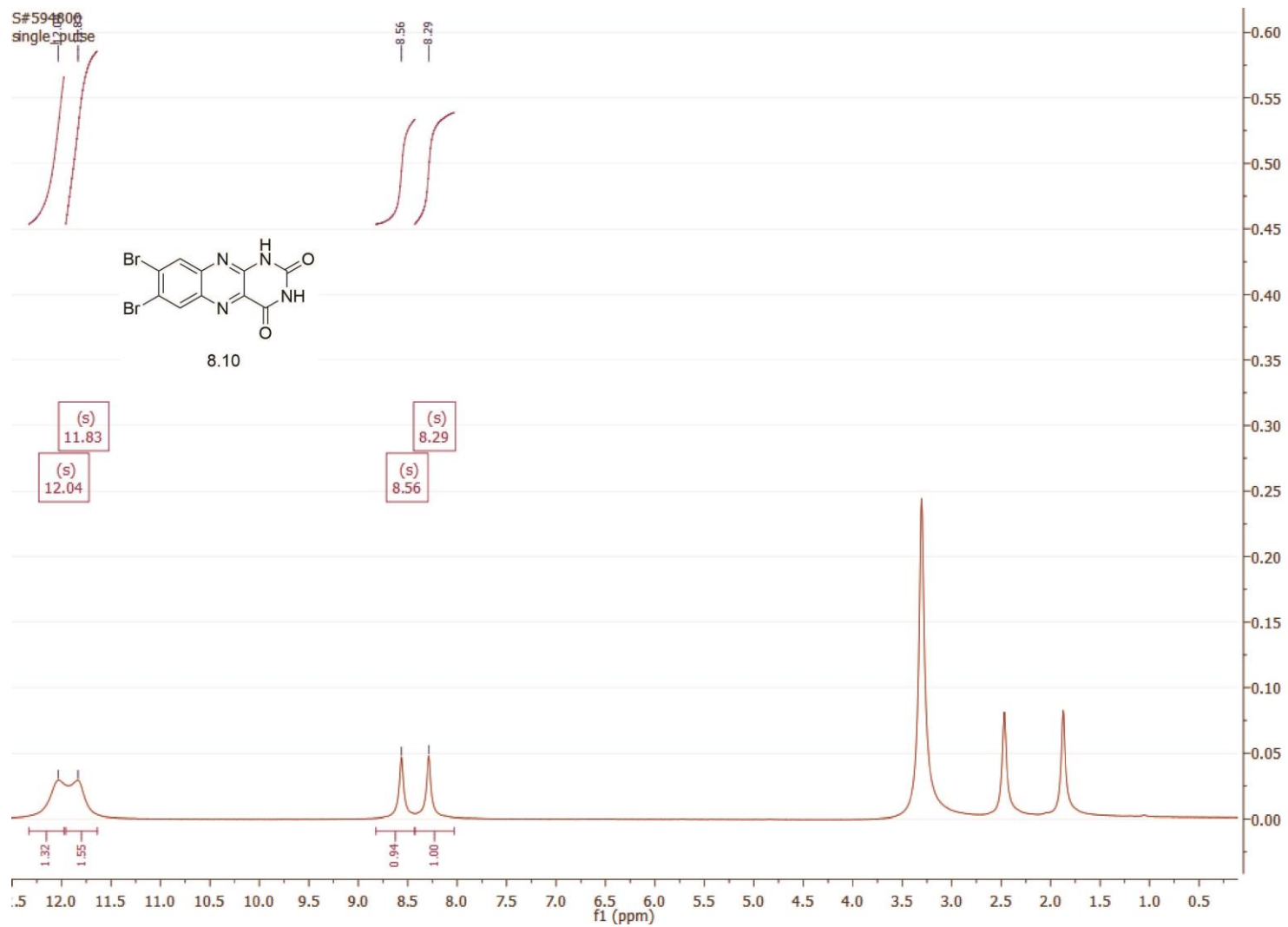
S#438491
single pulse decoupled gated NOE



8.18

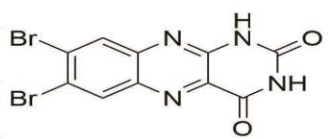


386

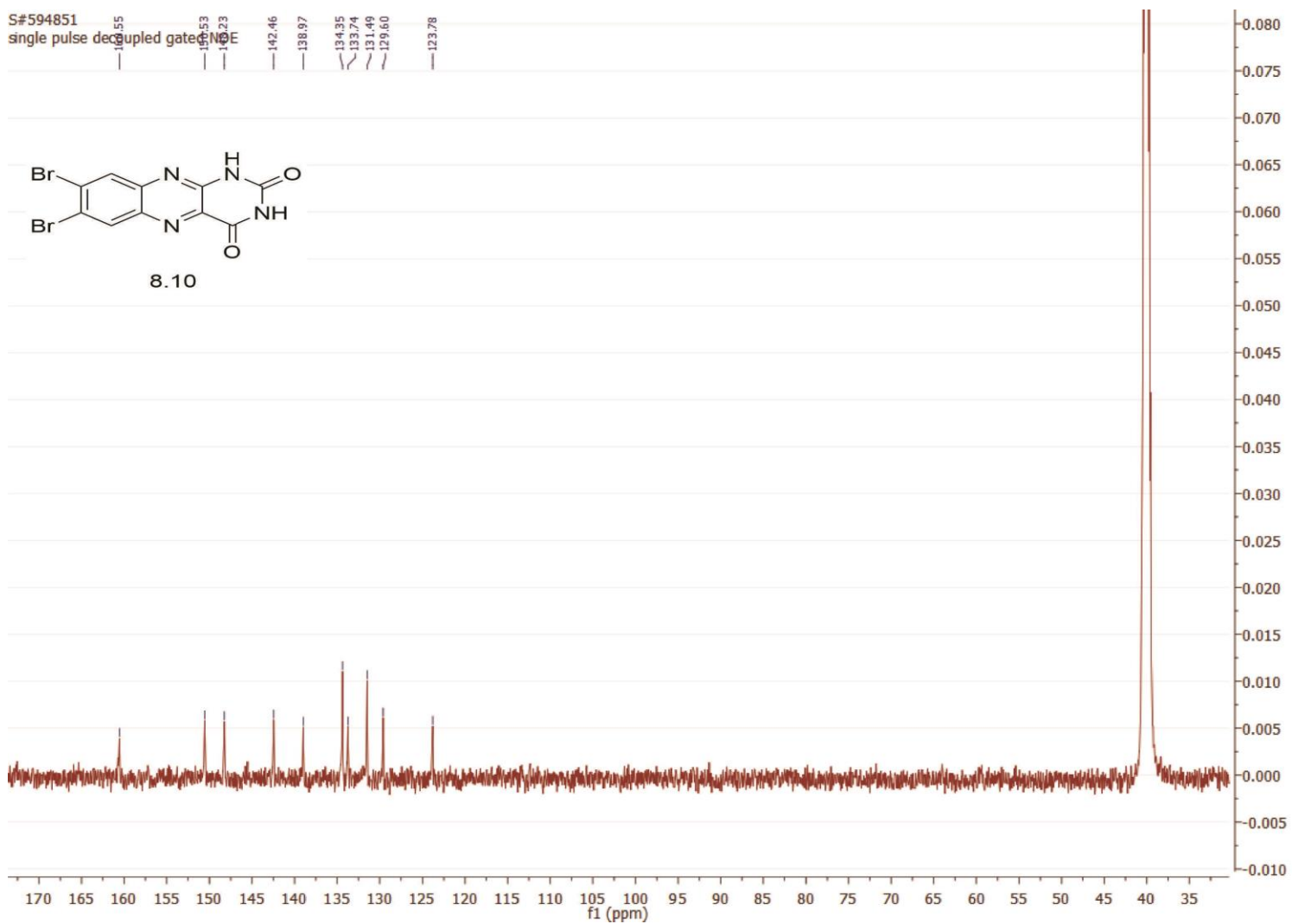


S#594851
single pulse decoupled gated

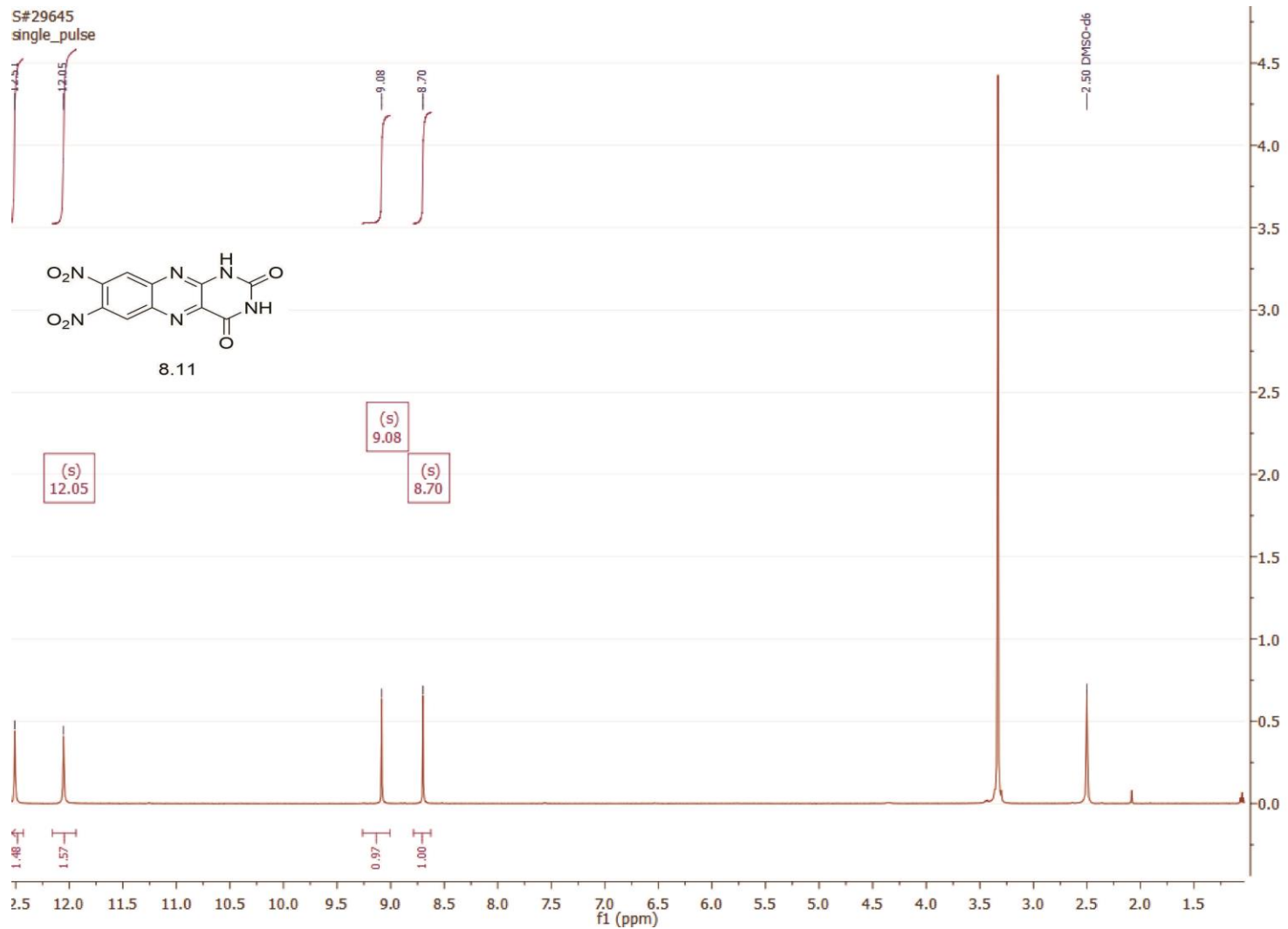
161.55
146.53
142.23
142.46
138.97
134.35
133.74
131.49
129.60
123.78



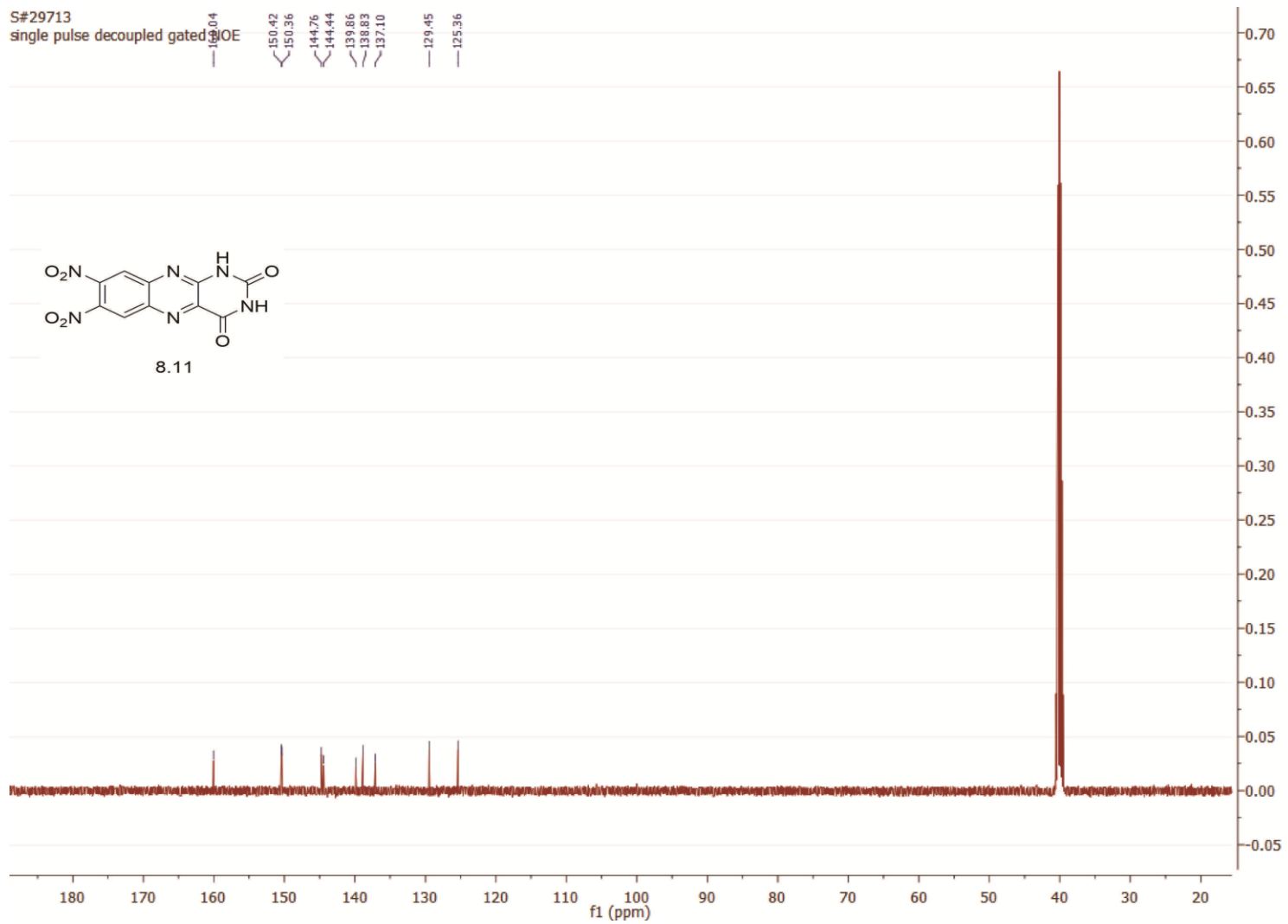
8.10



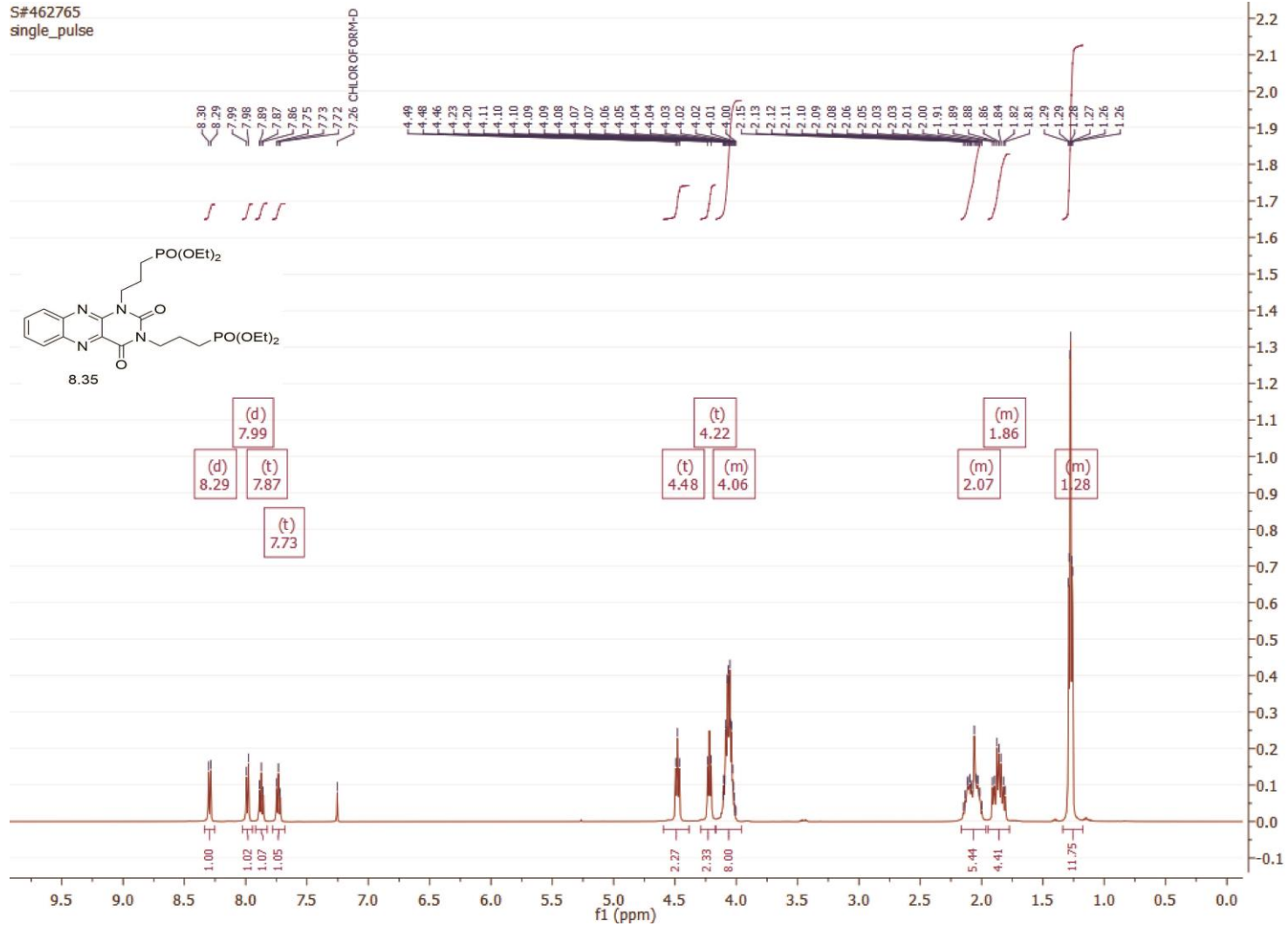
388



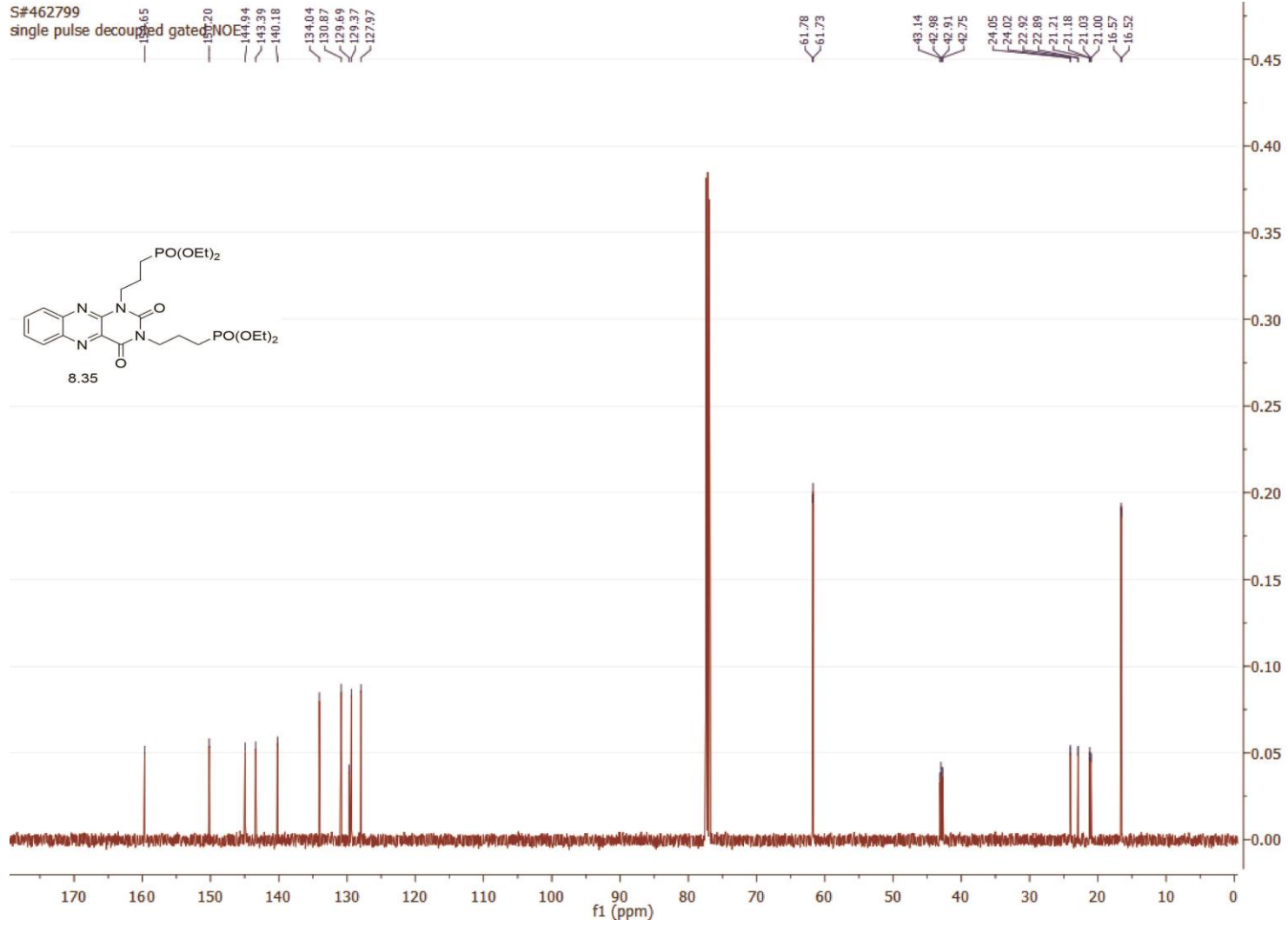
389



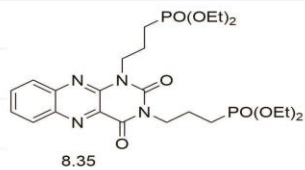
390



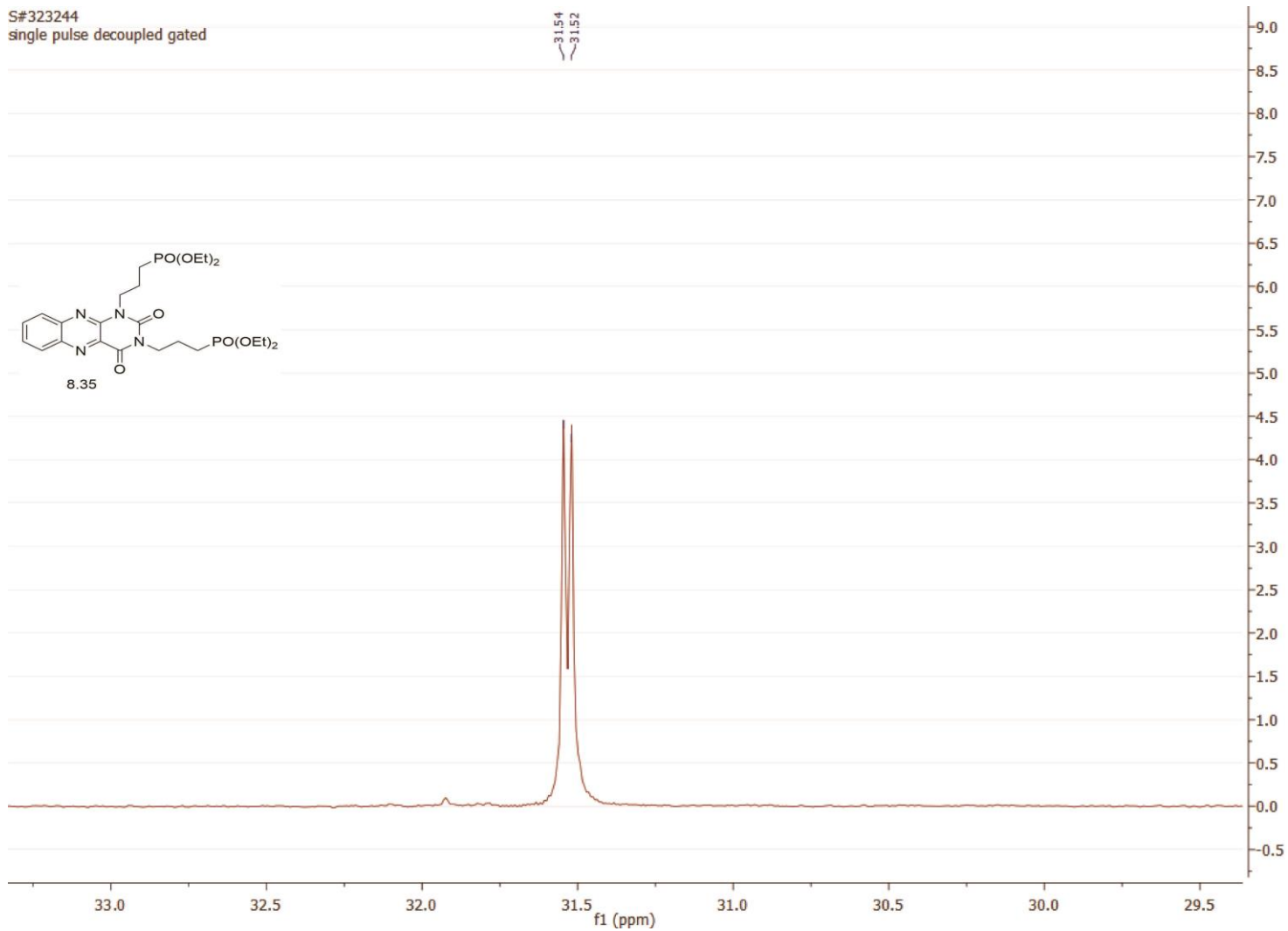
391



S#323244
single pulse decoupled gated

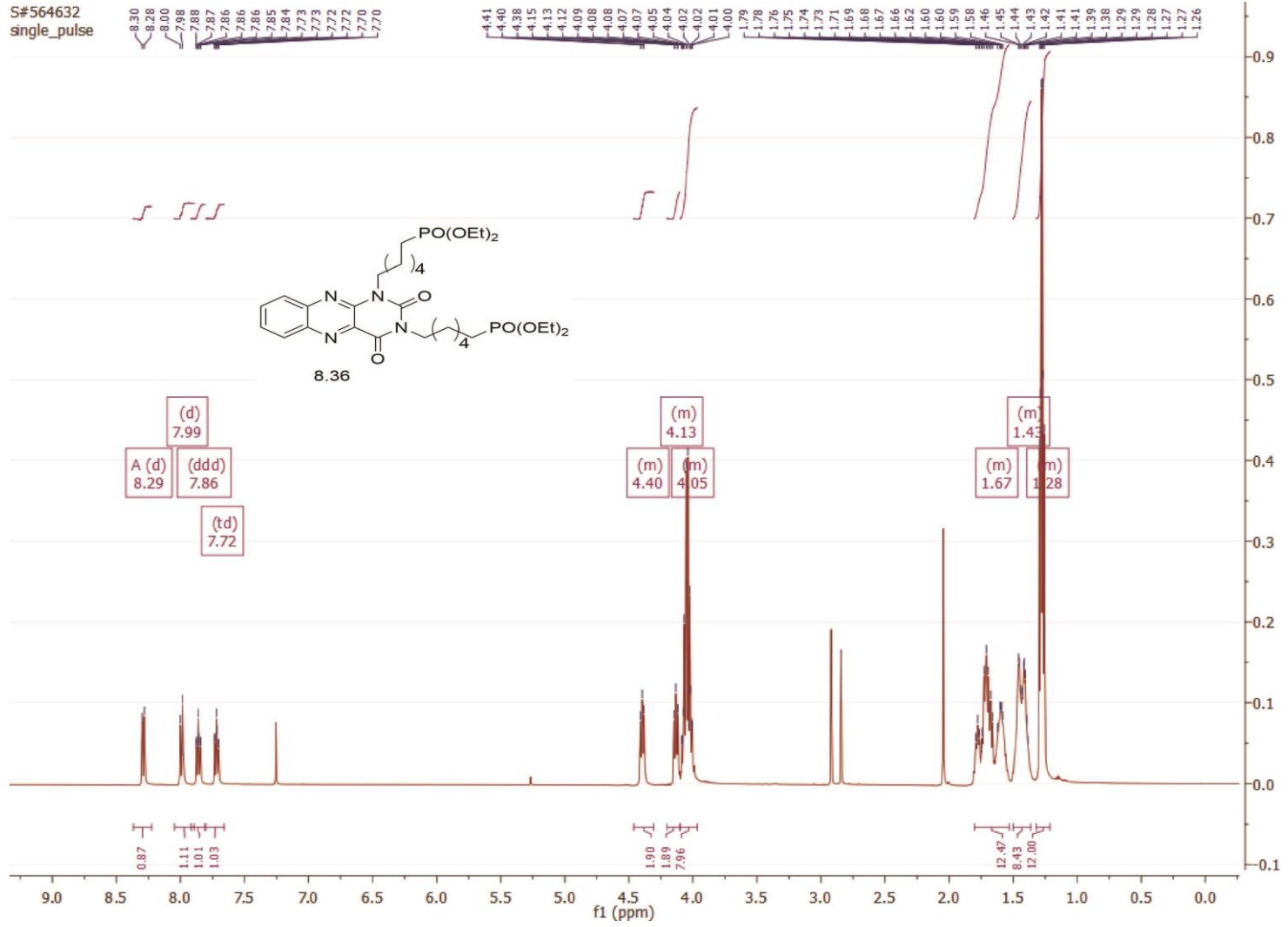


31.54
31.52

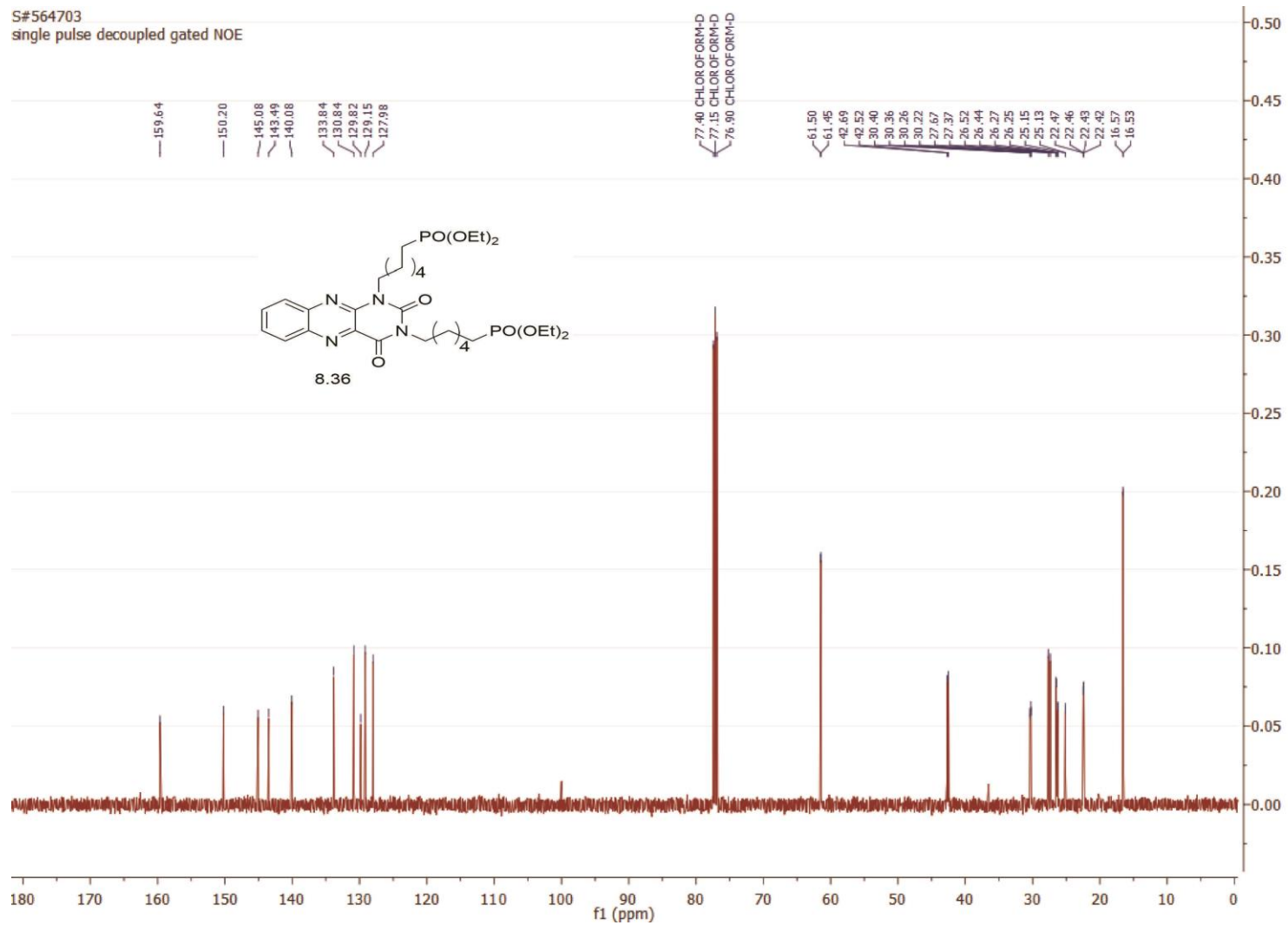


392

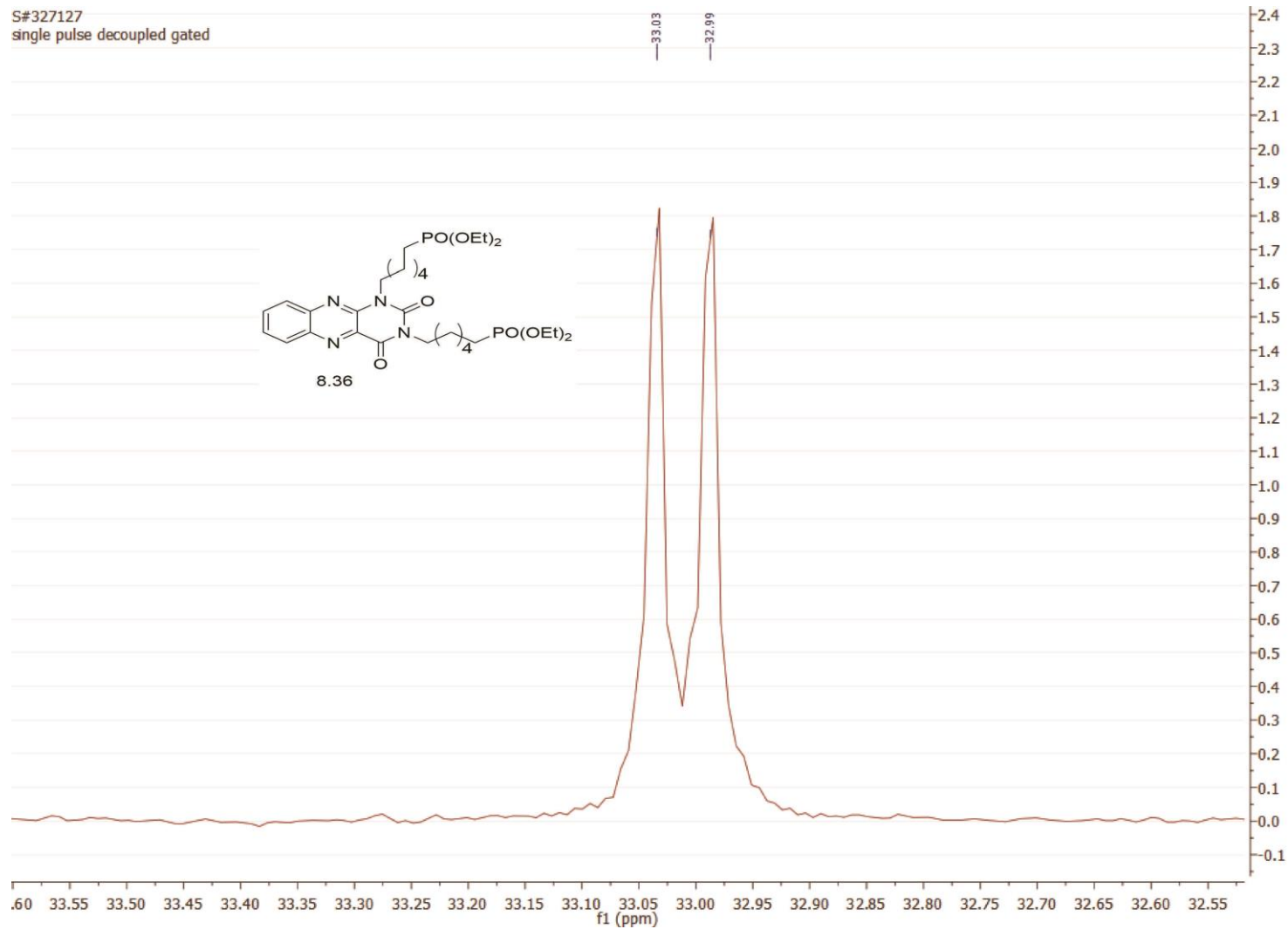
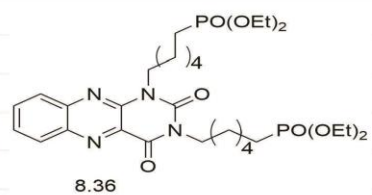
393



S#564703
single pulse decoupled gated NOE

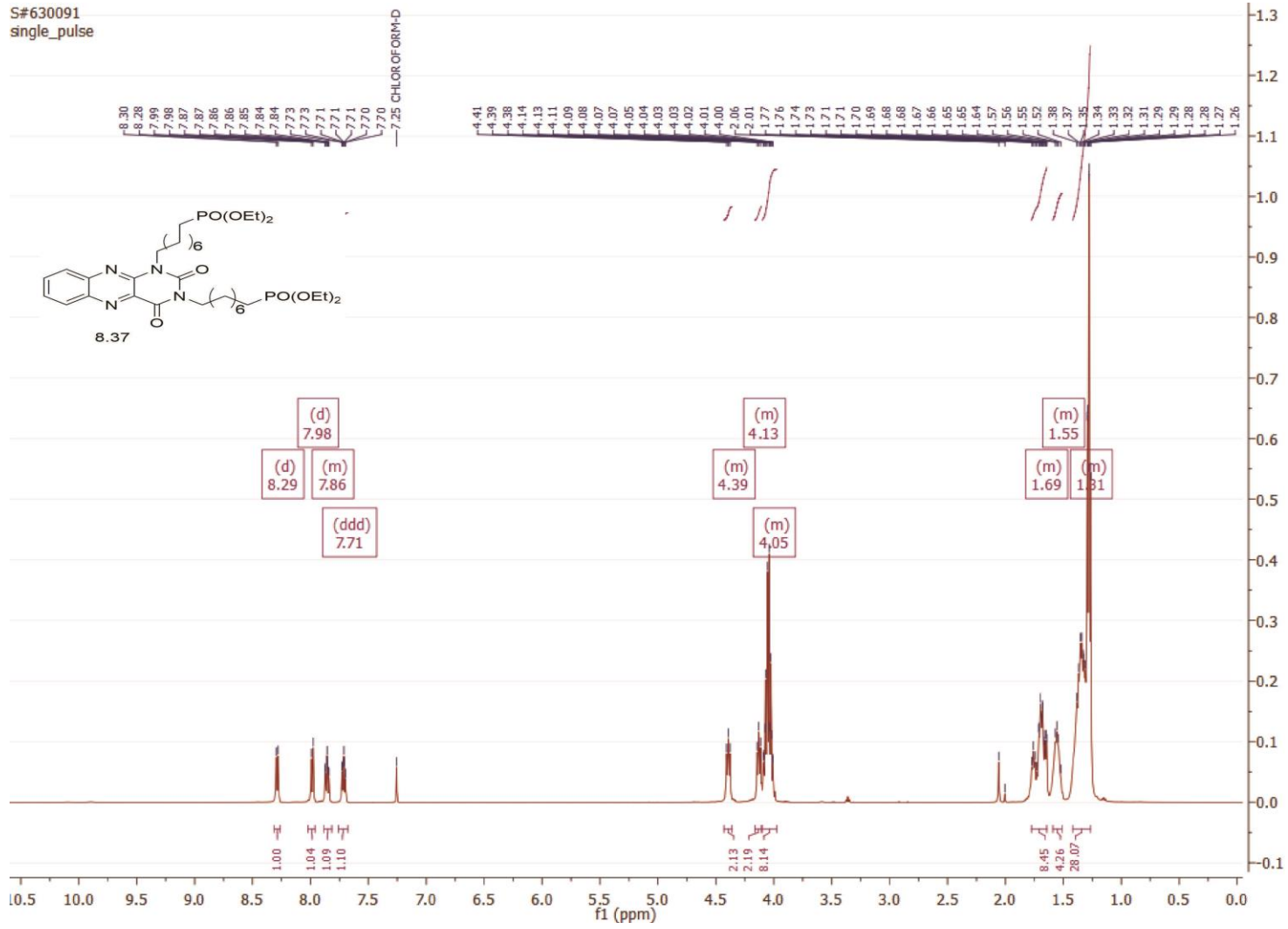


S#327127
single pulse decoupled gated



395

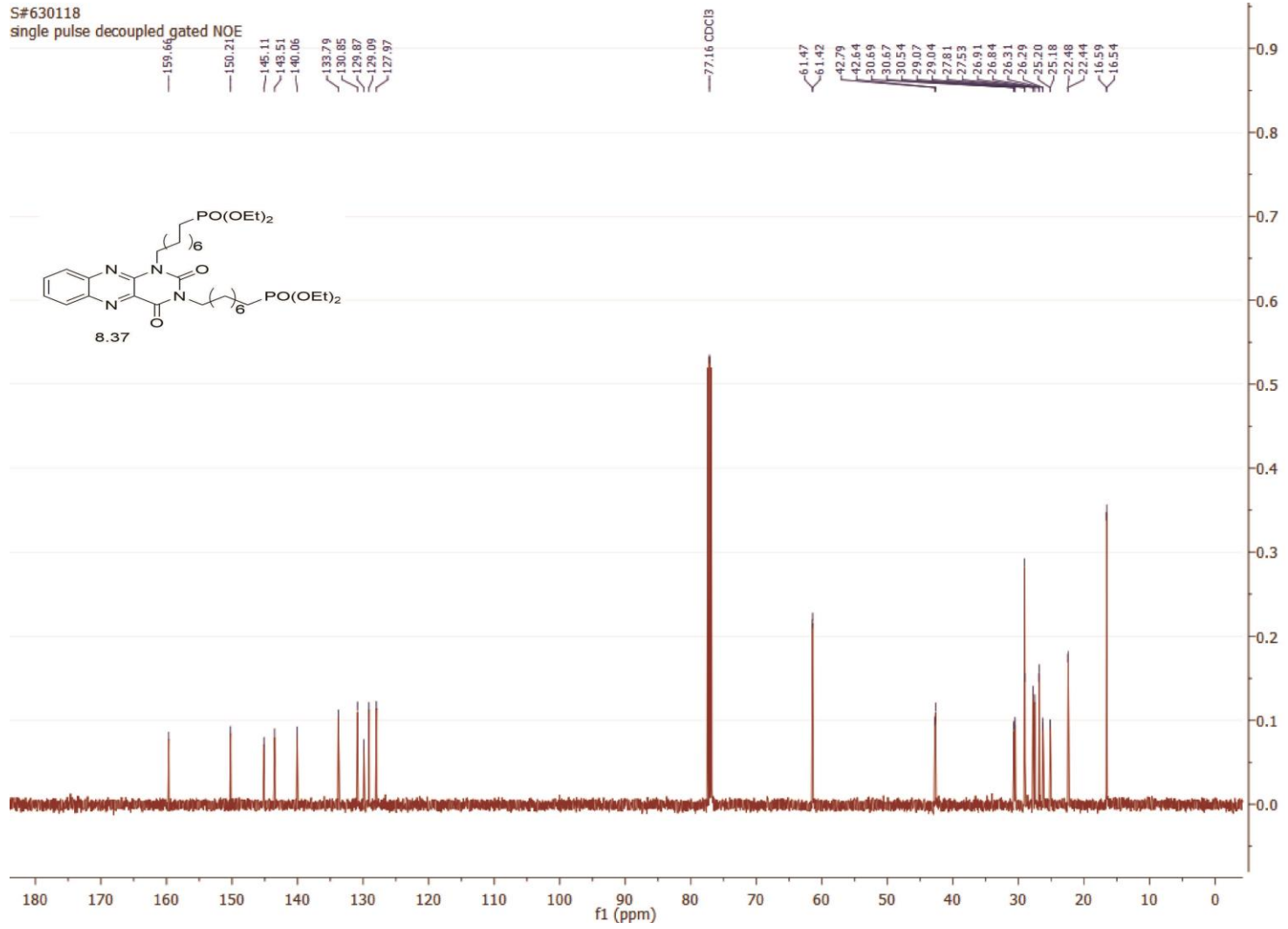
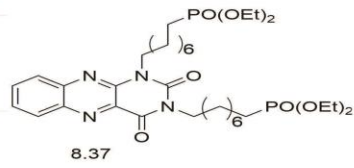
396



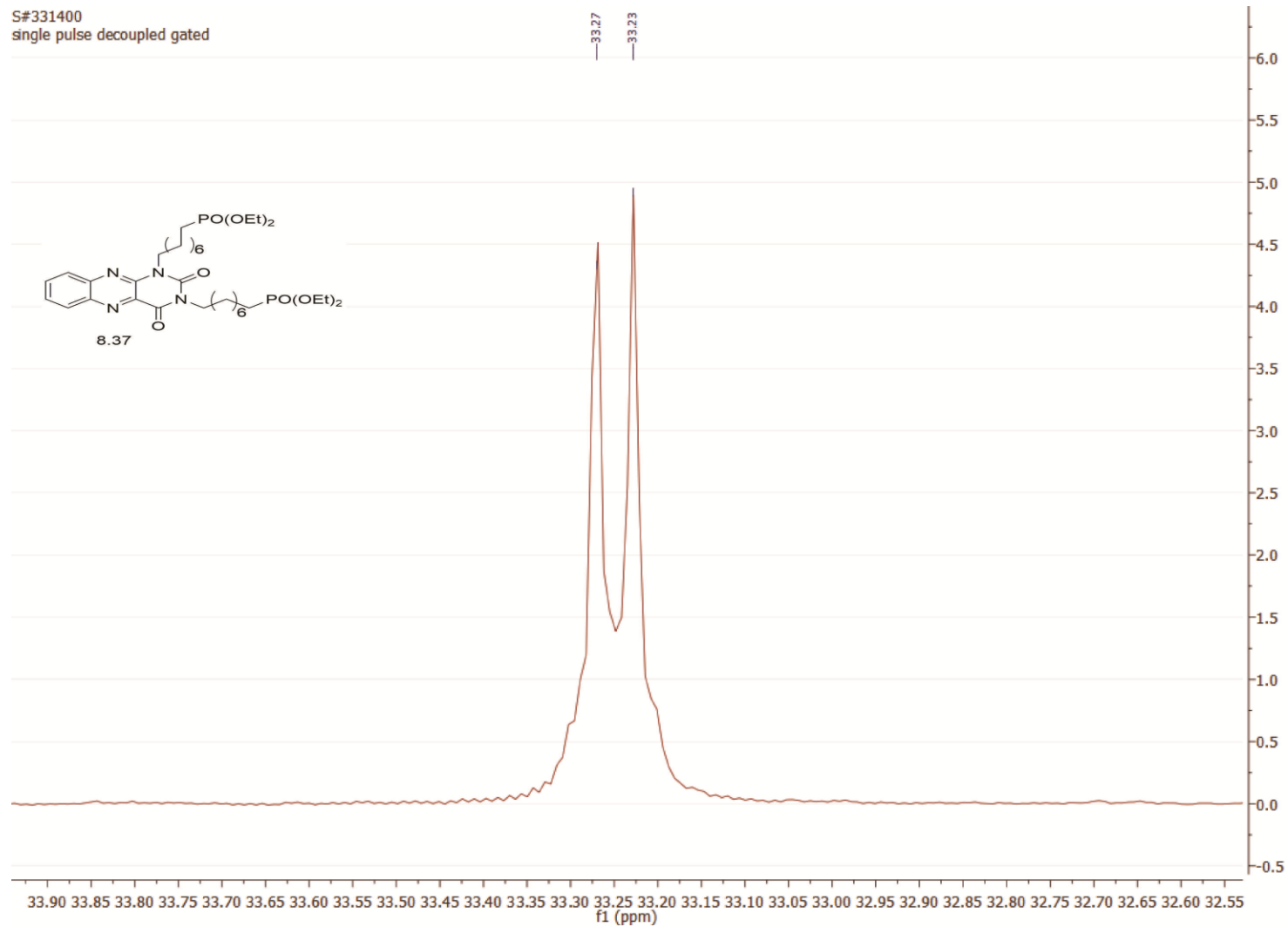
397

S#630118

single pulse decoupled gated NOE



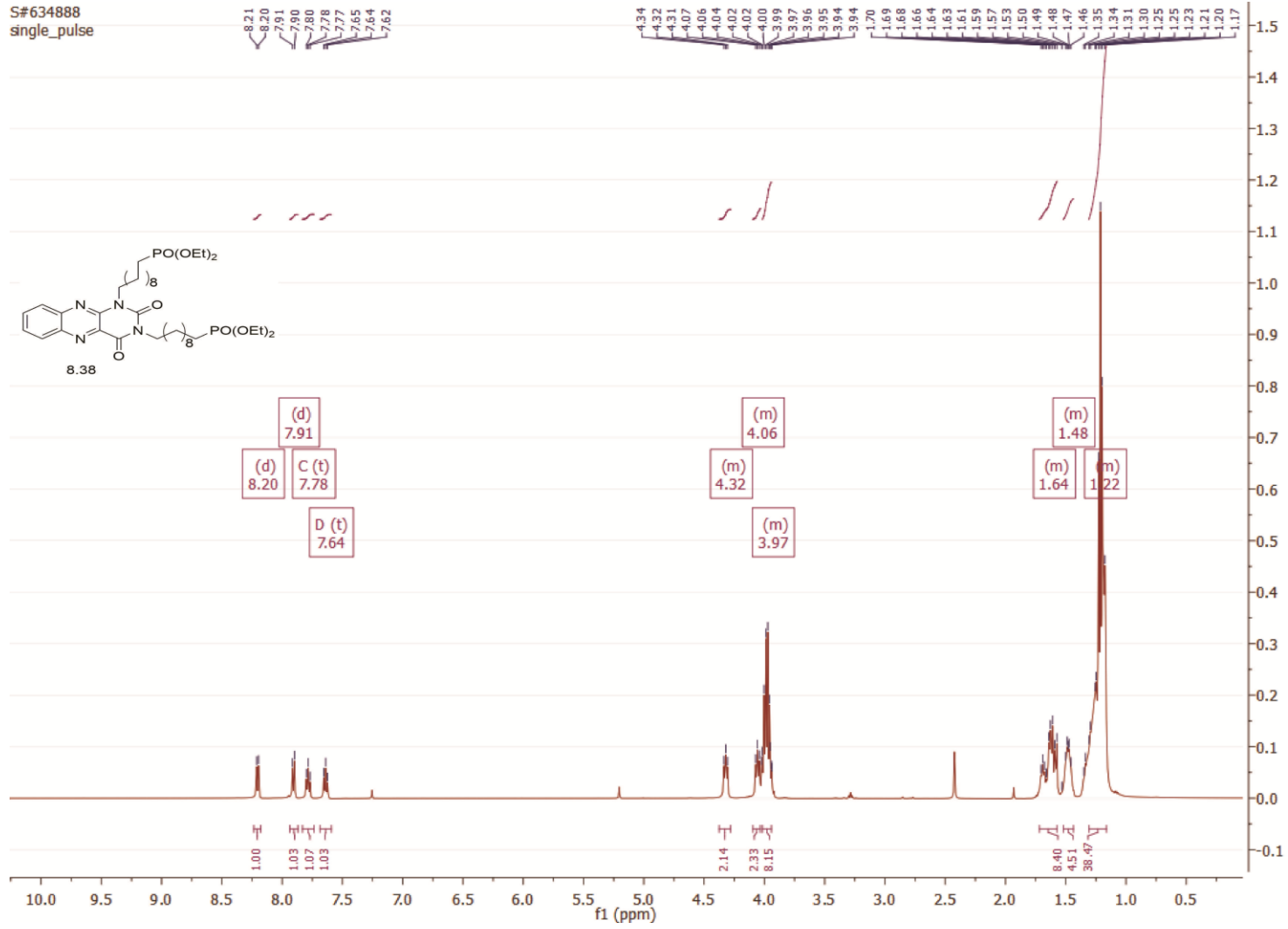
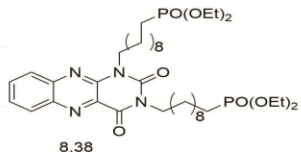
S#331400
single pulse decoupled gated



398

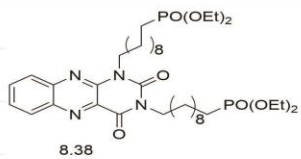
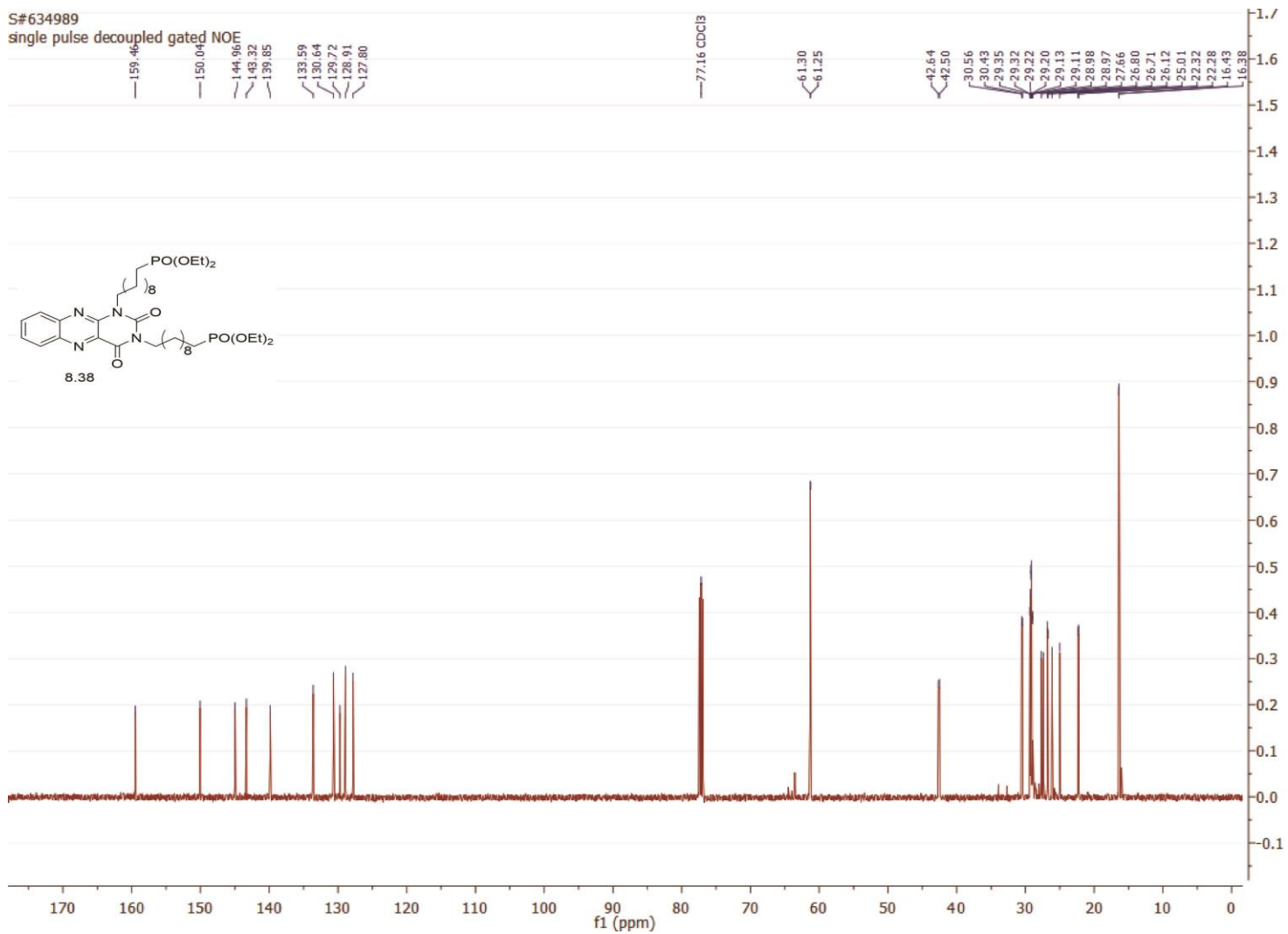
66C

S#634888
single_pulse



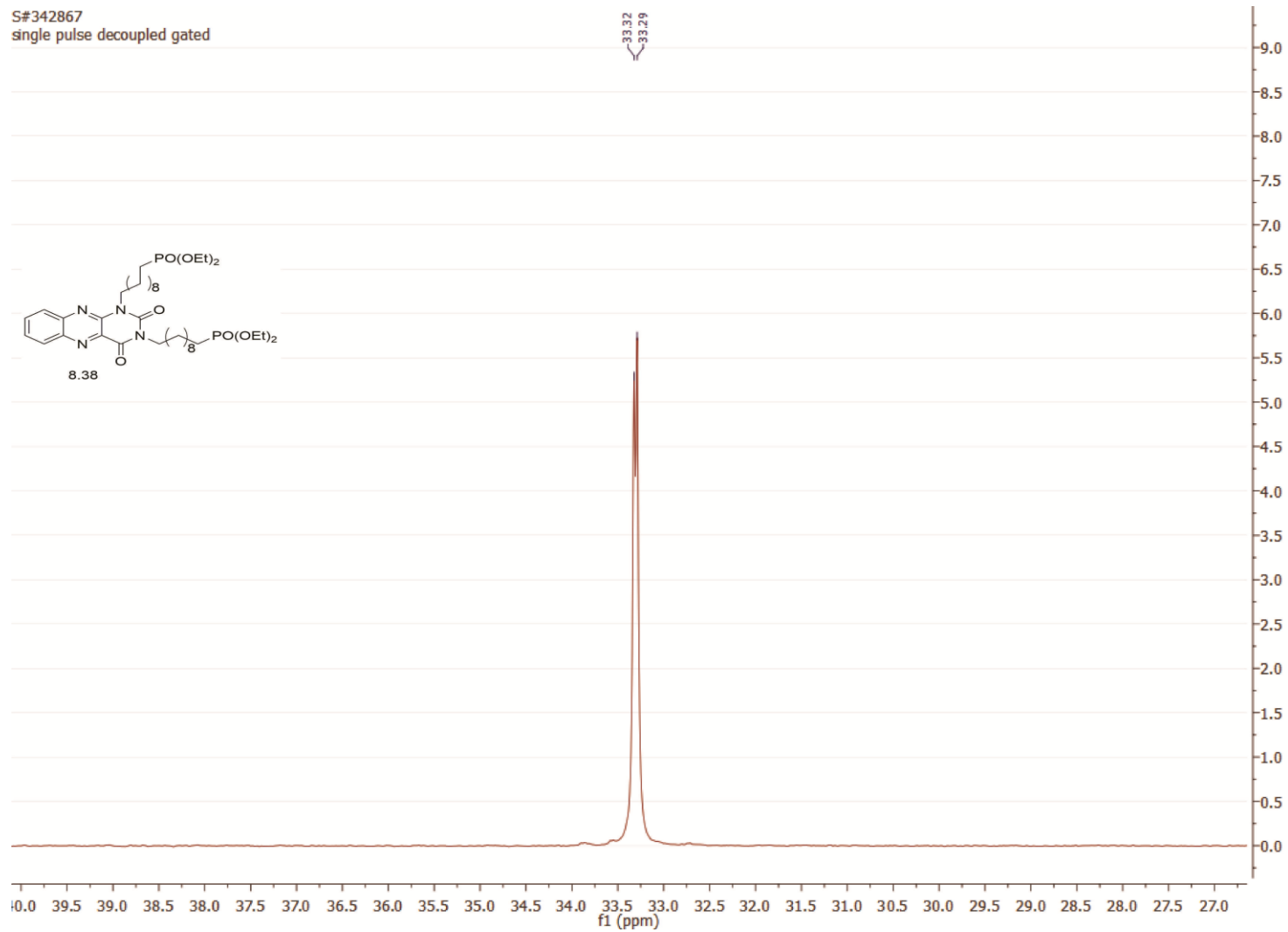
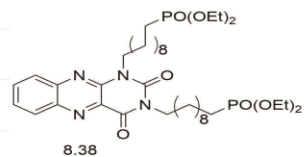
S#634989

single pulse decoupled gated NOE



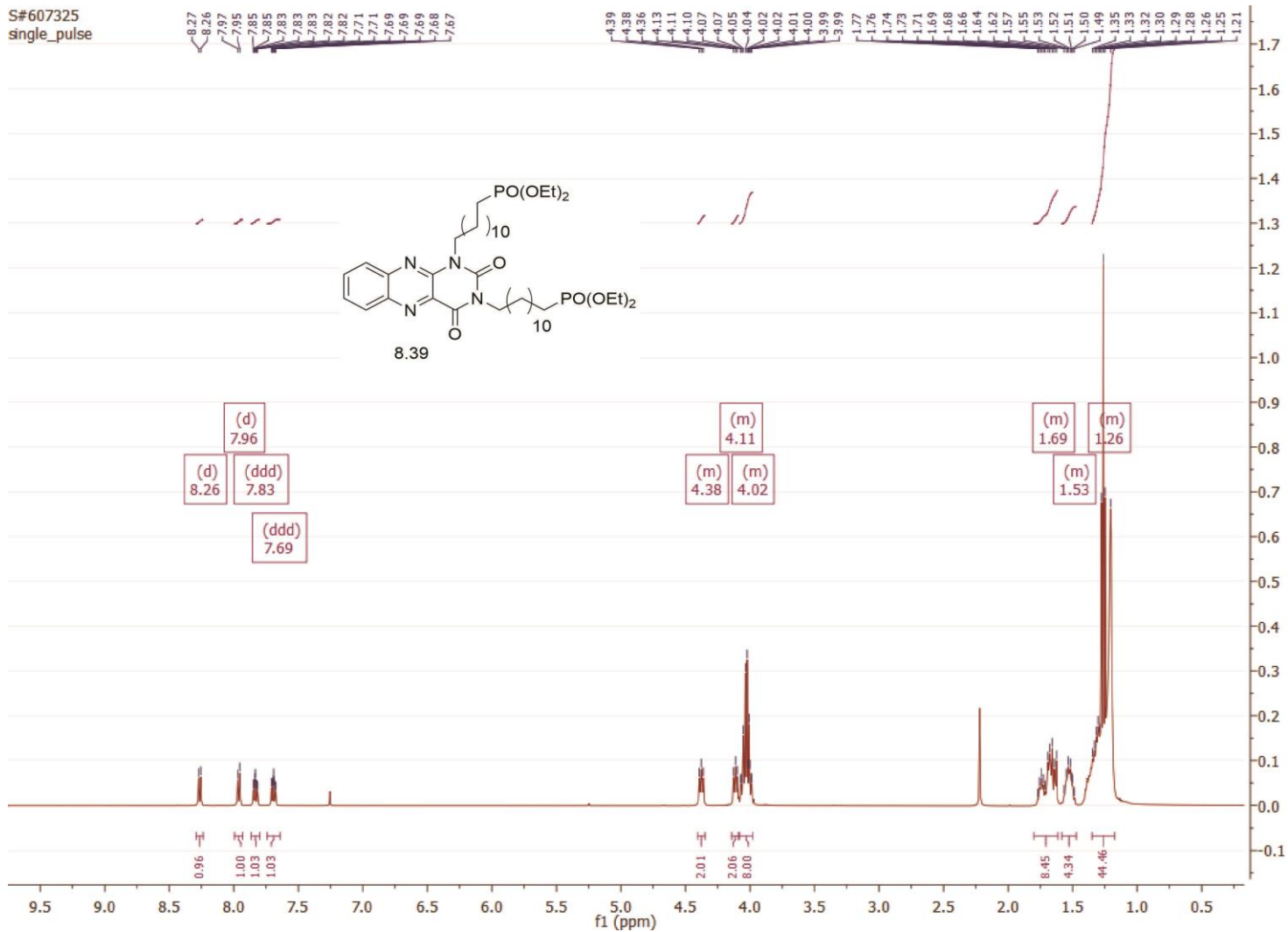
400

S#342867
single pulse decoupled gated



401

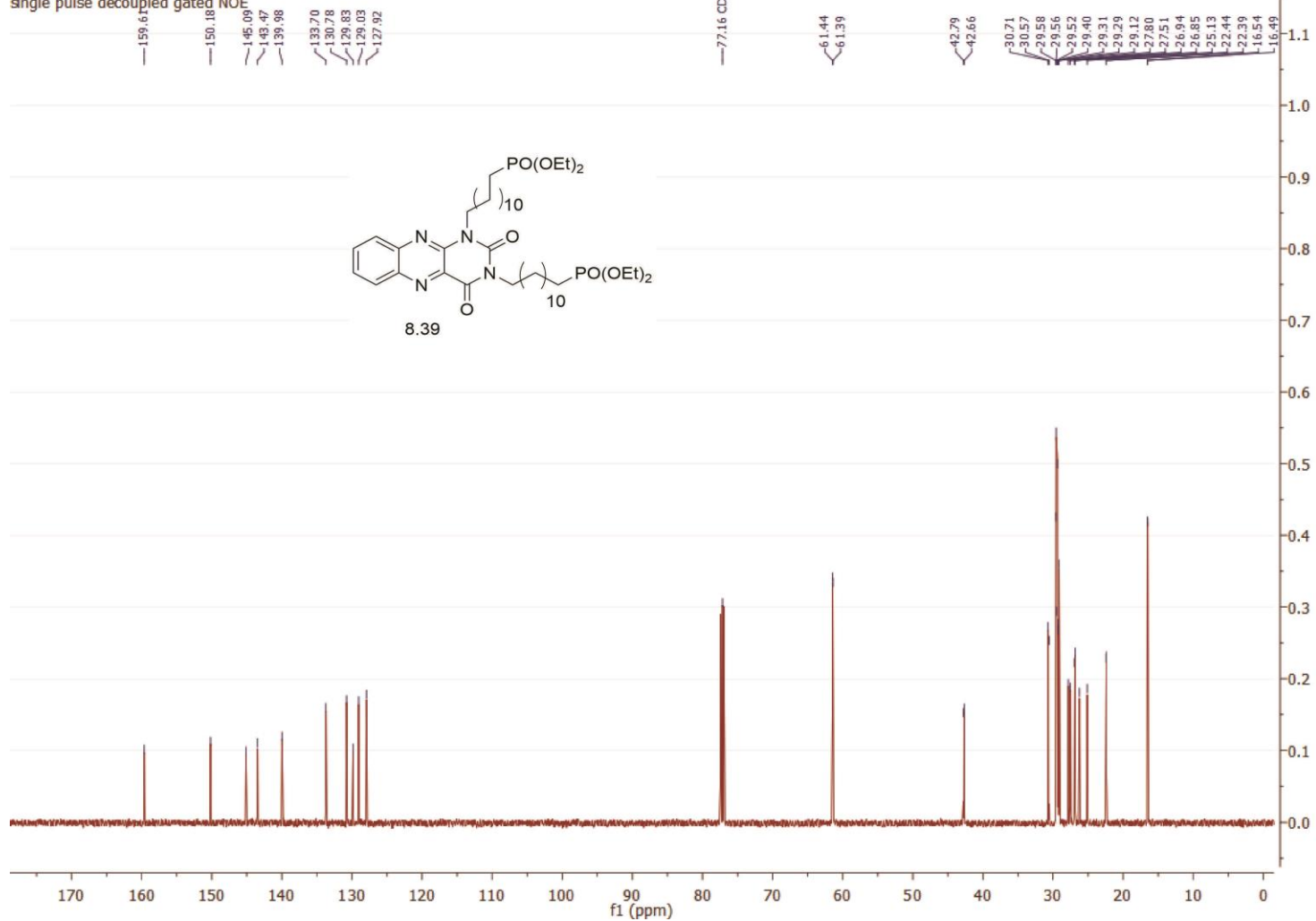
S#607325
single_pulse



402

S#607357

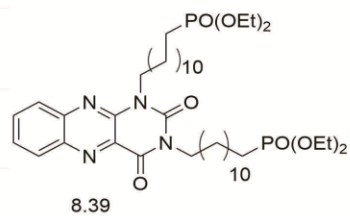
single pulse decoupled gated NOE



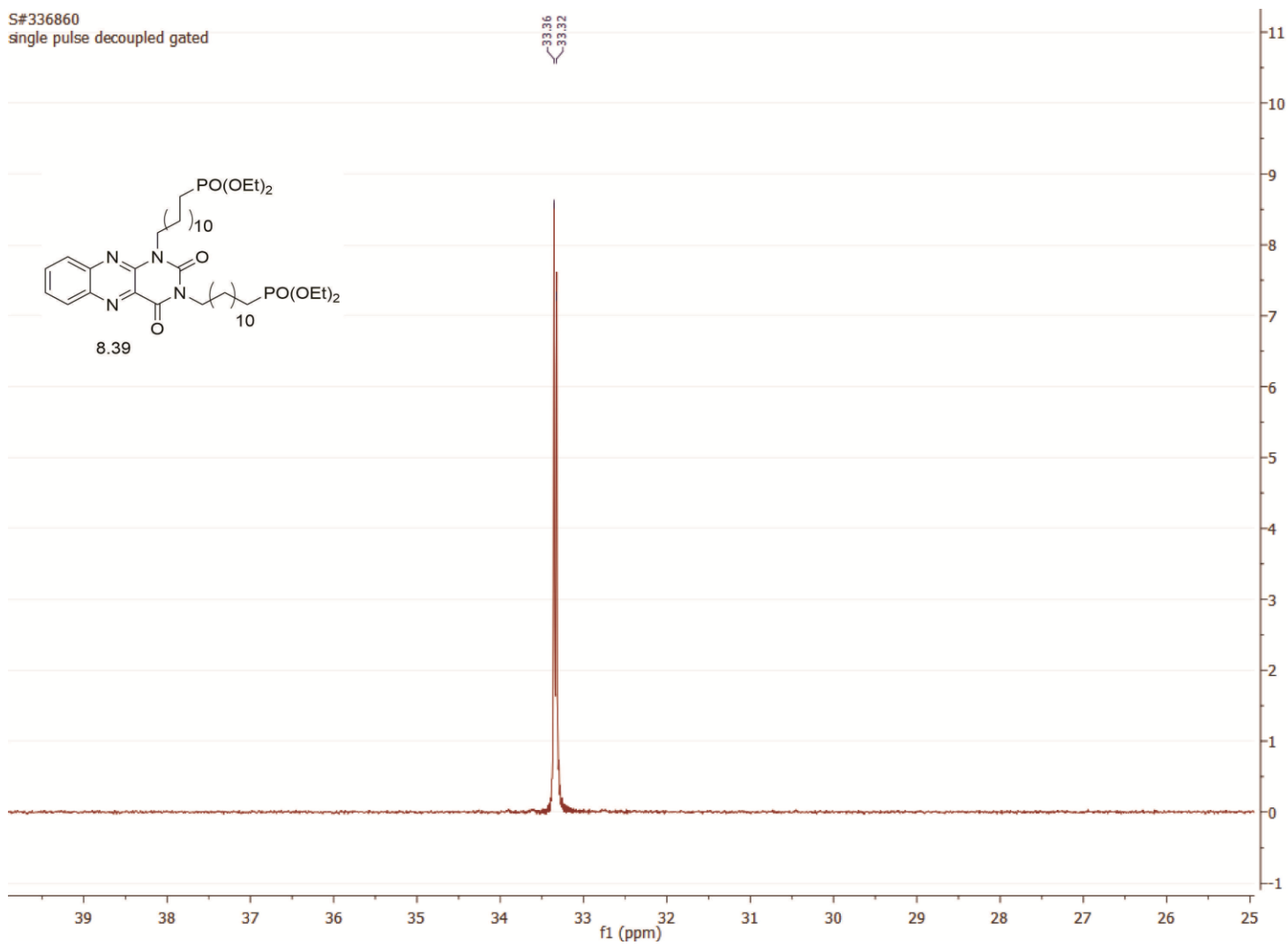
403

S#336860
single pulse decoupled gated

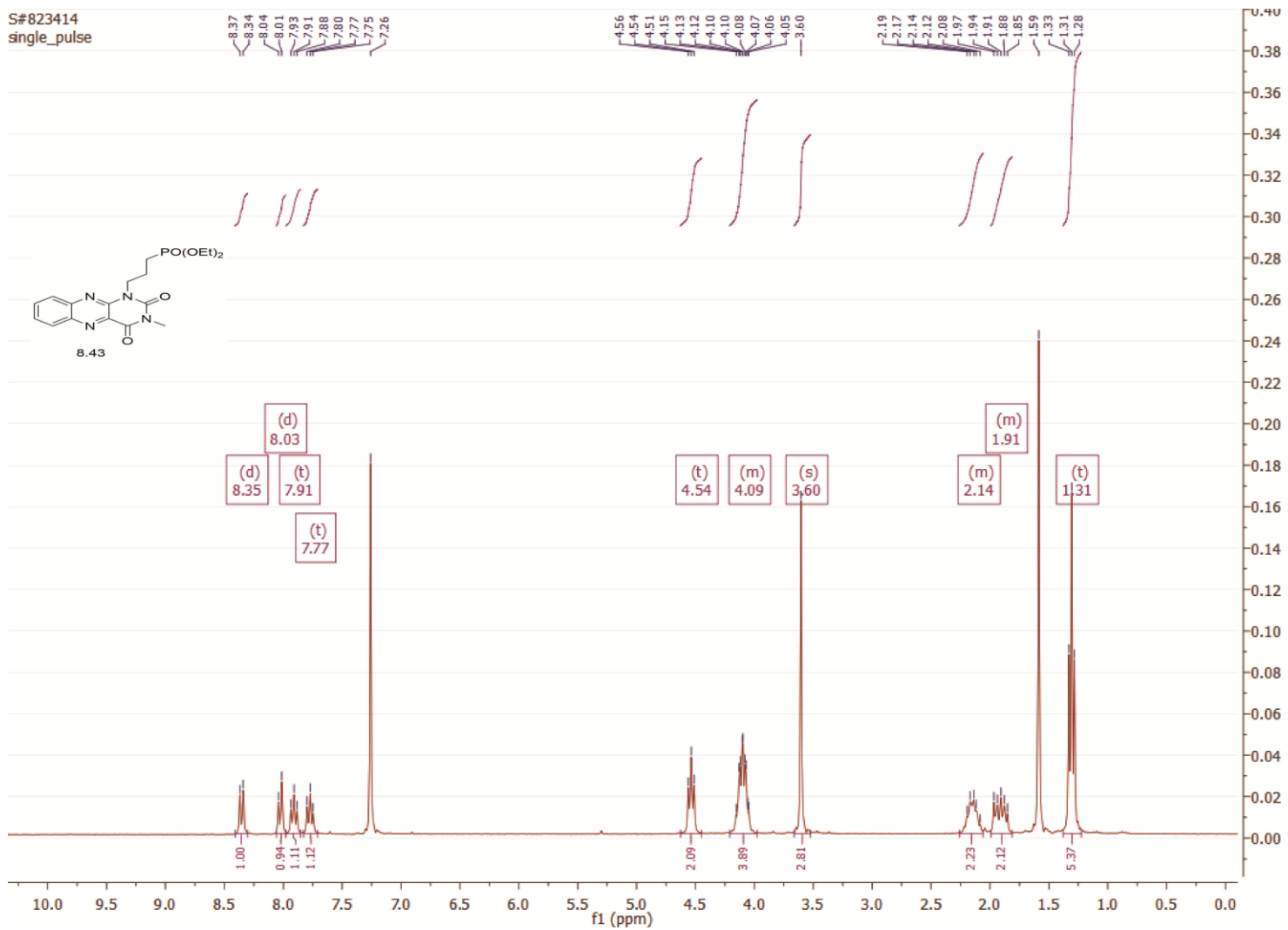
33.316
33.32



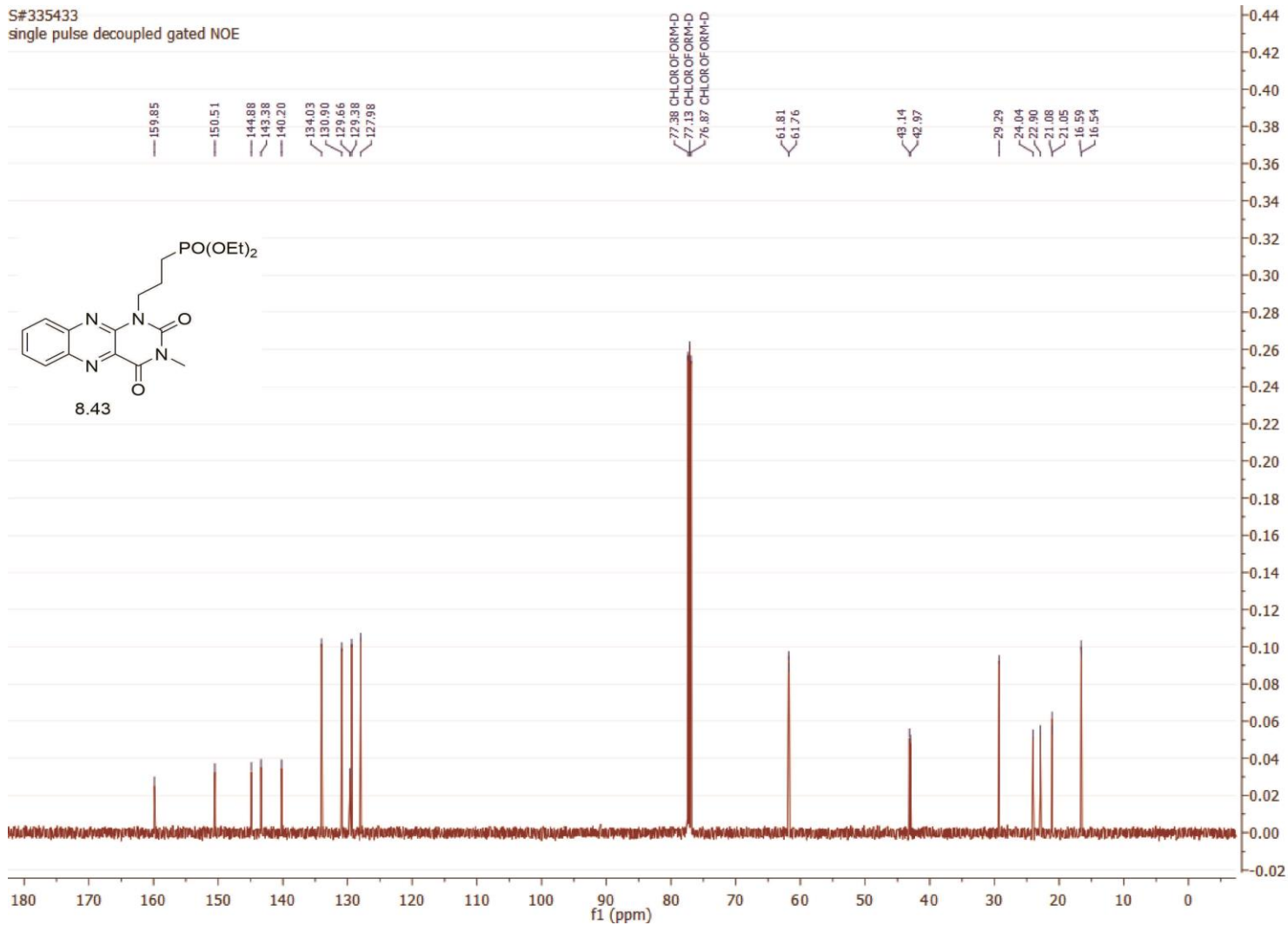
404



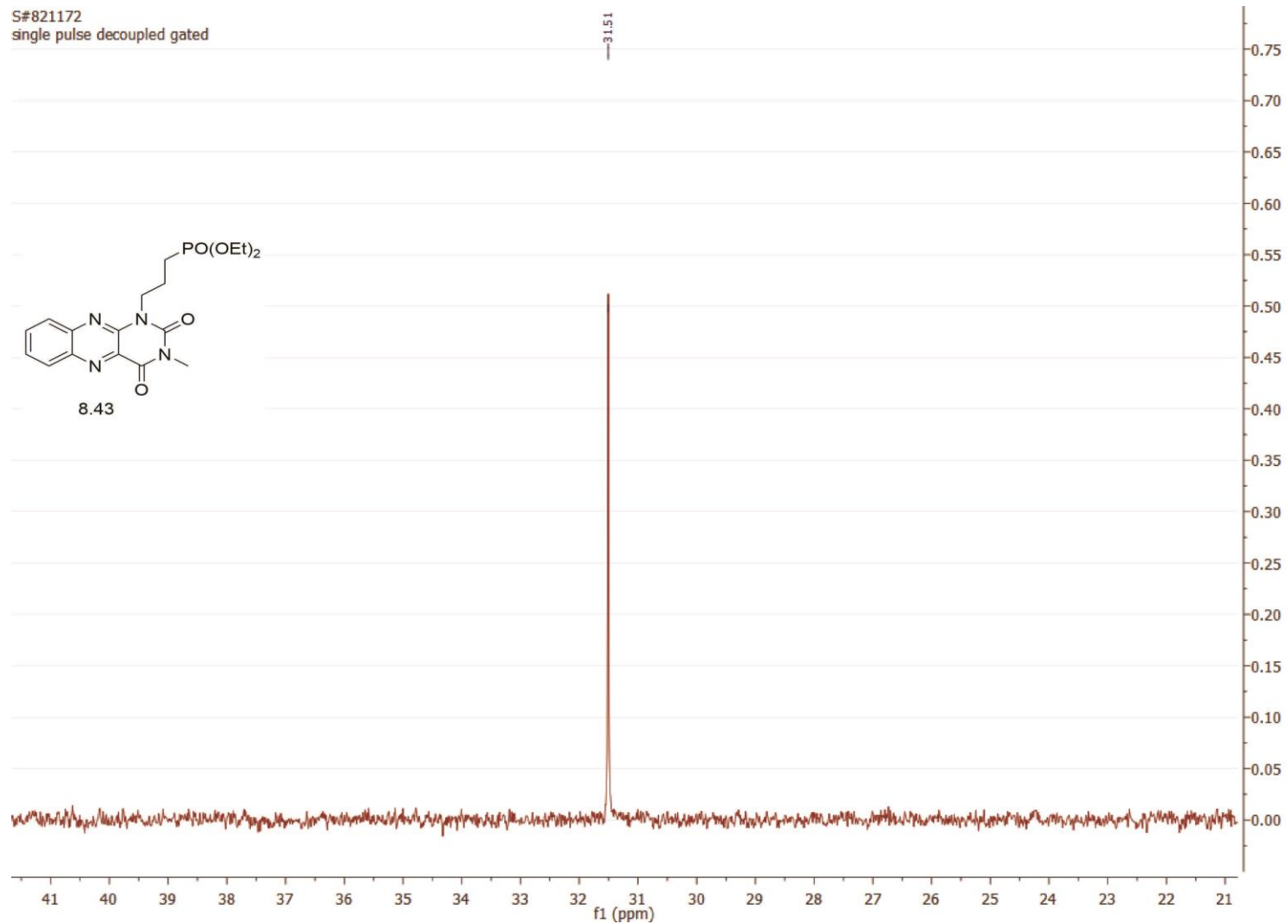
405



S#335433
single pulse decoupled gated NOE

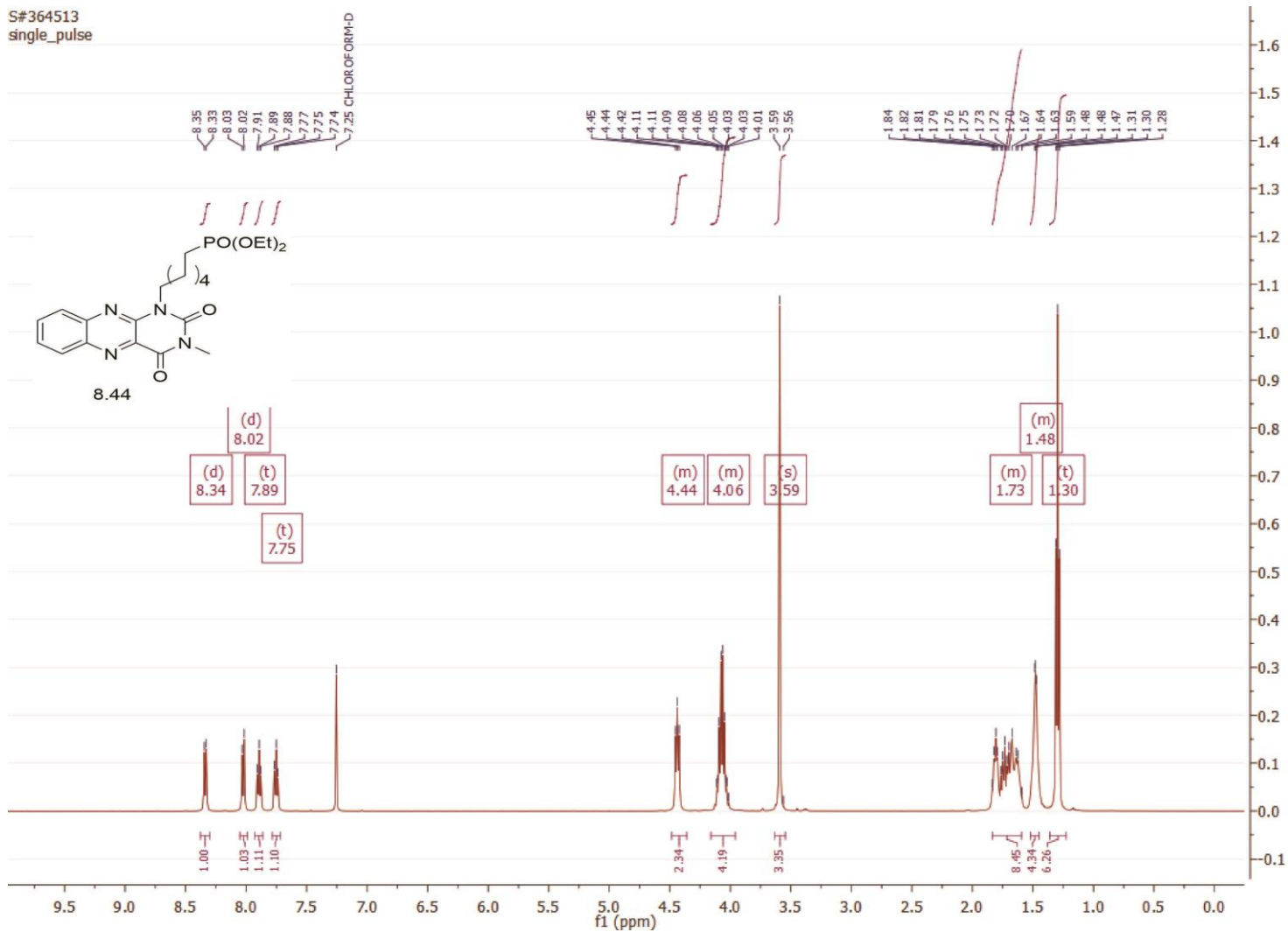


S#821172
single pulse decoupled gated



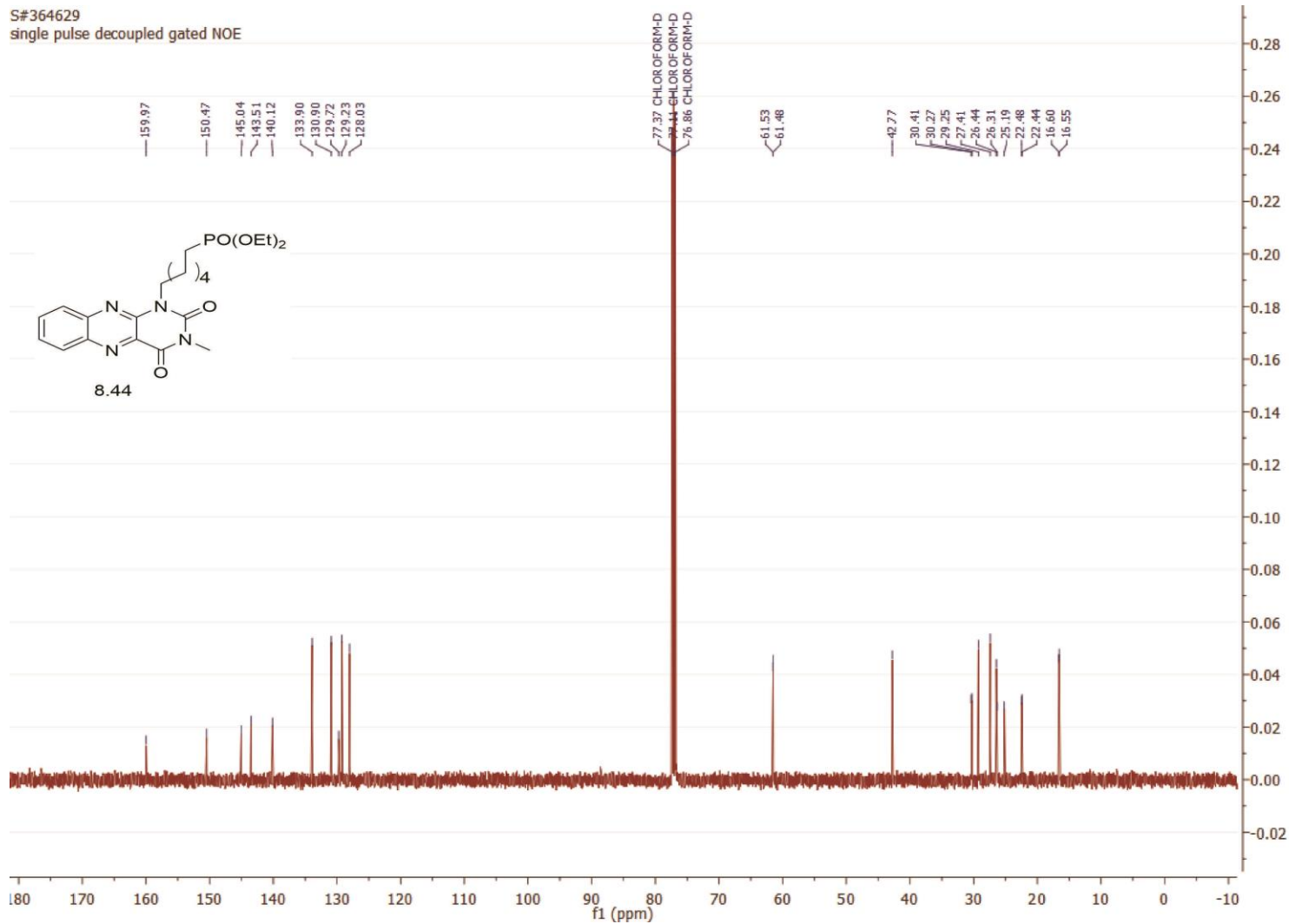
407

S#364513
single_pulse



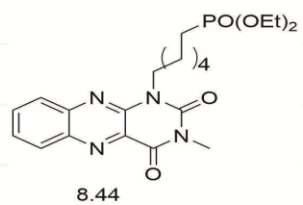
408

S#364629
single pulse decoupled gated NOE



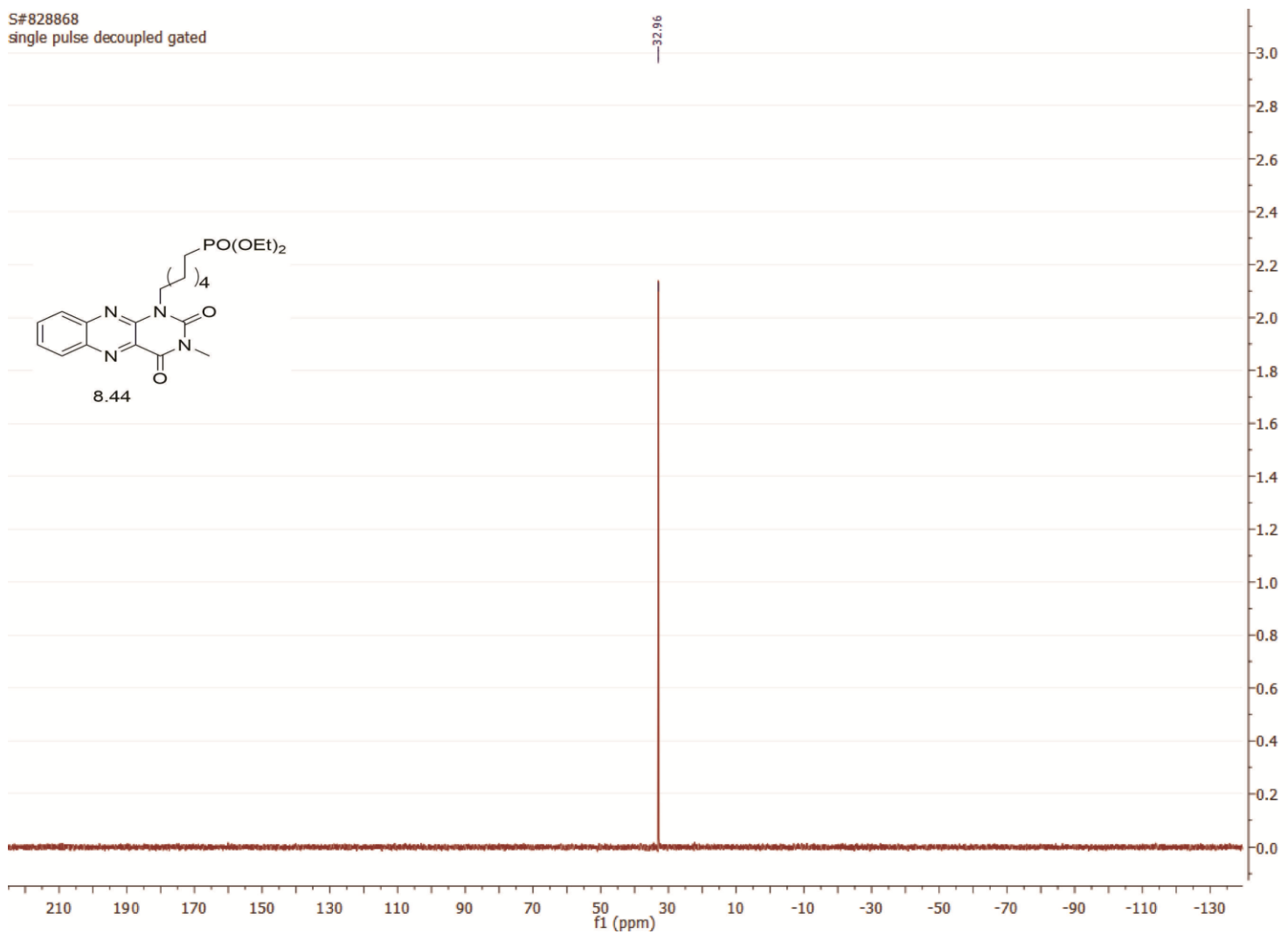
409

S#828868
single pulse decoupled gated

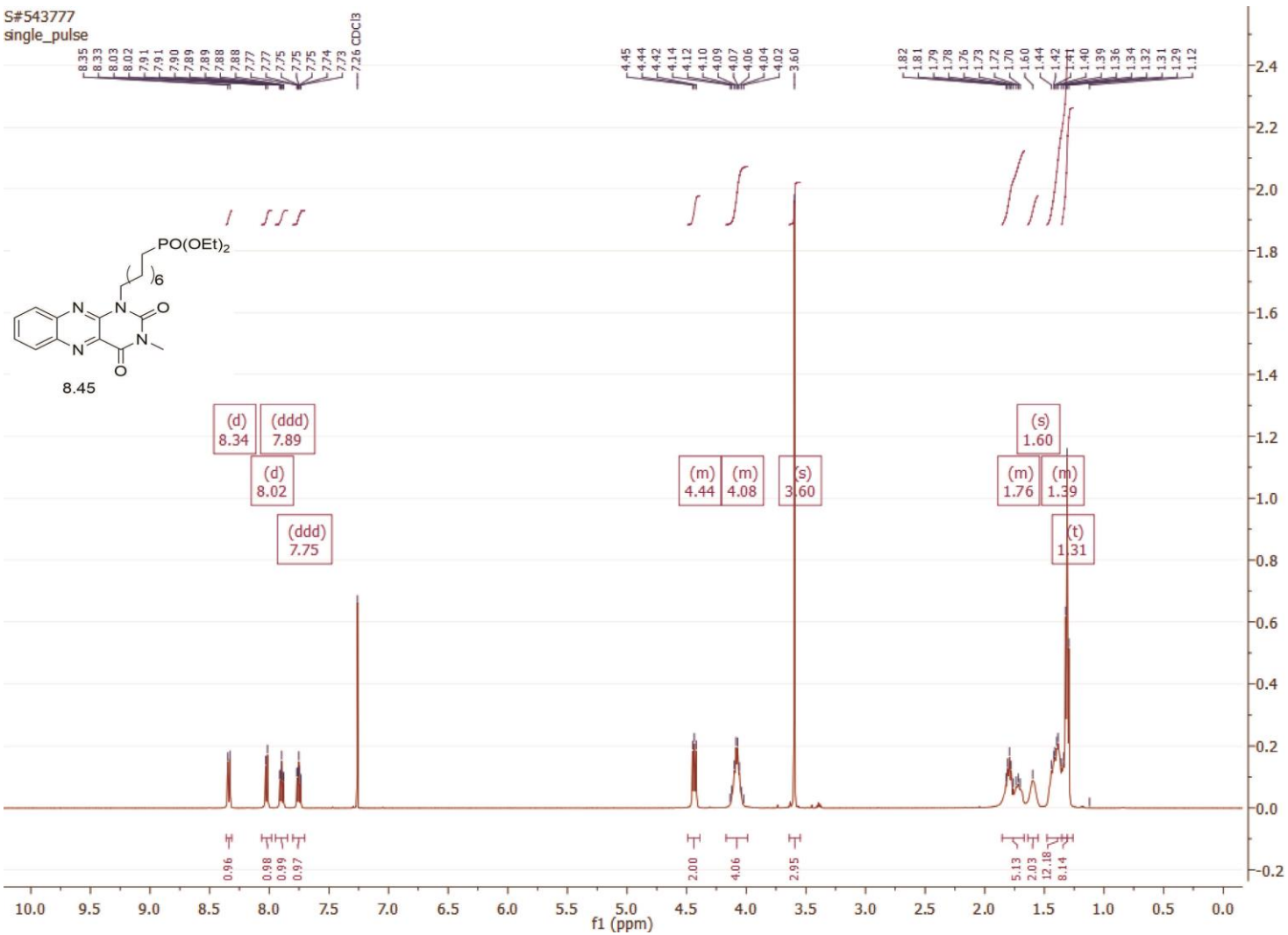


32.96

410

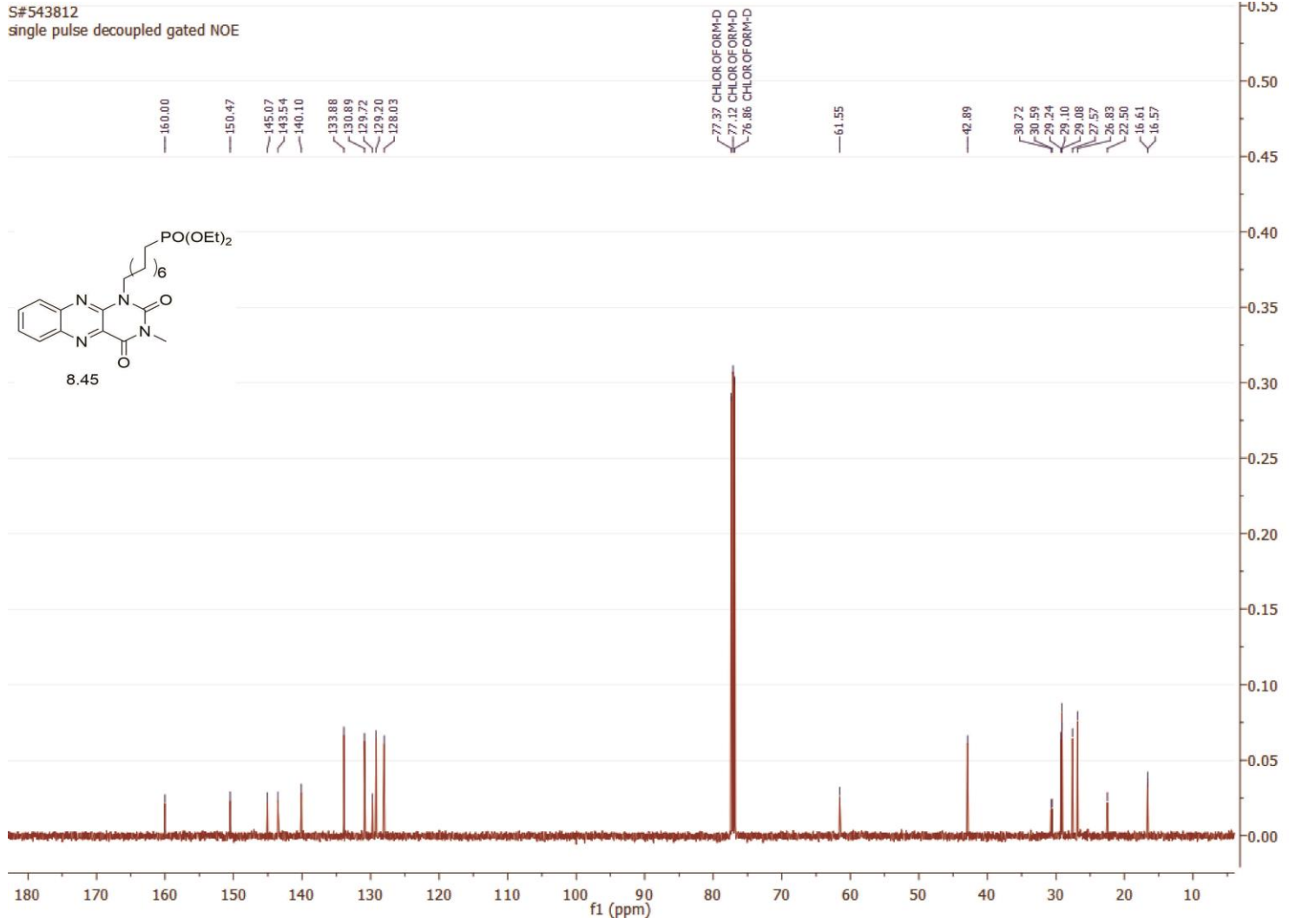


S#543777
single_pulse

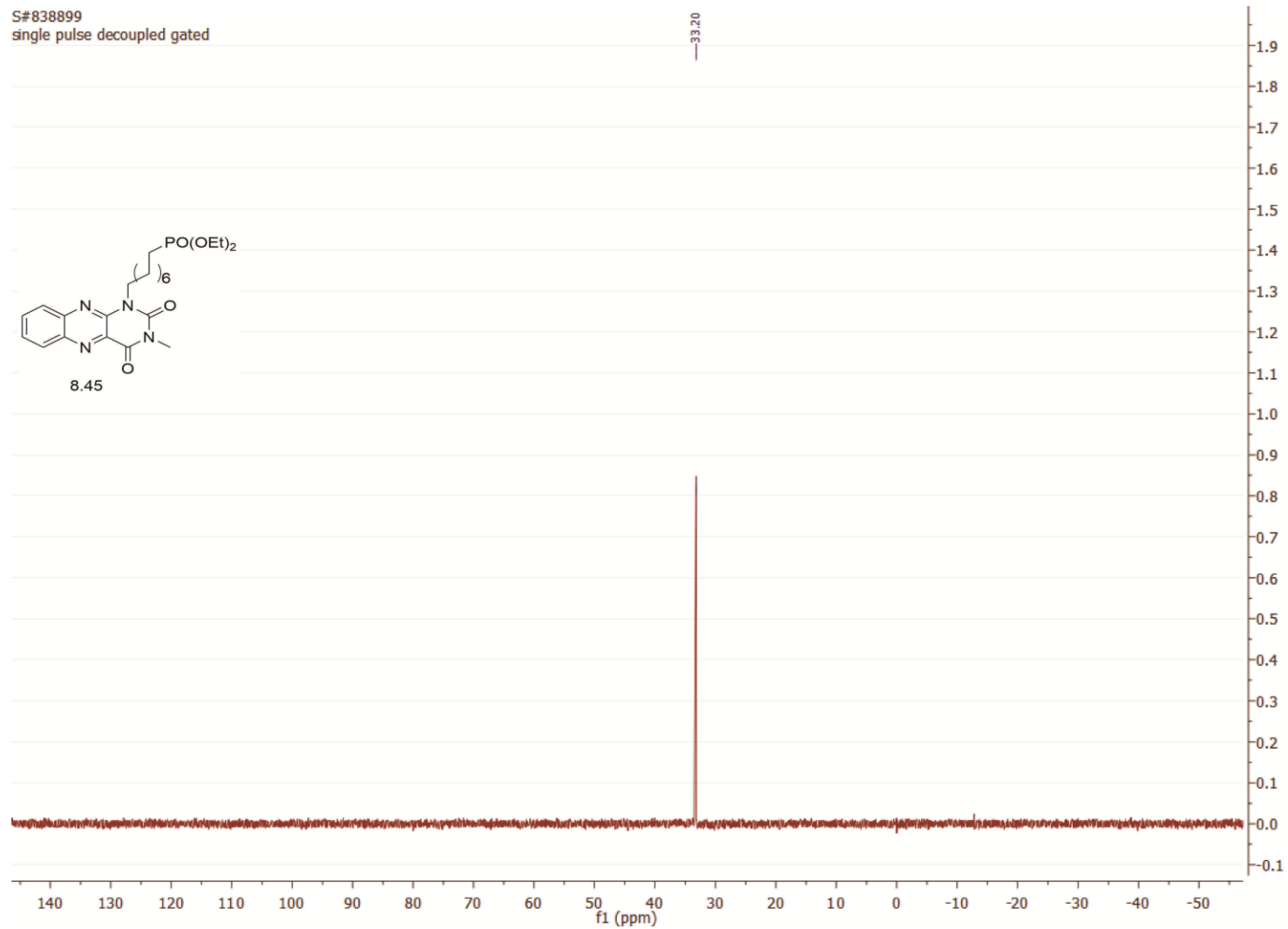
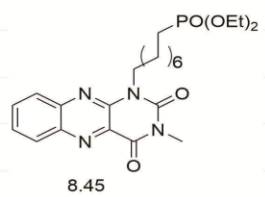


411

S#543812
single pulse decoupled gated NOE

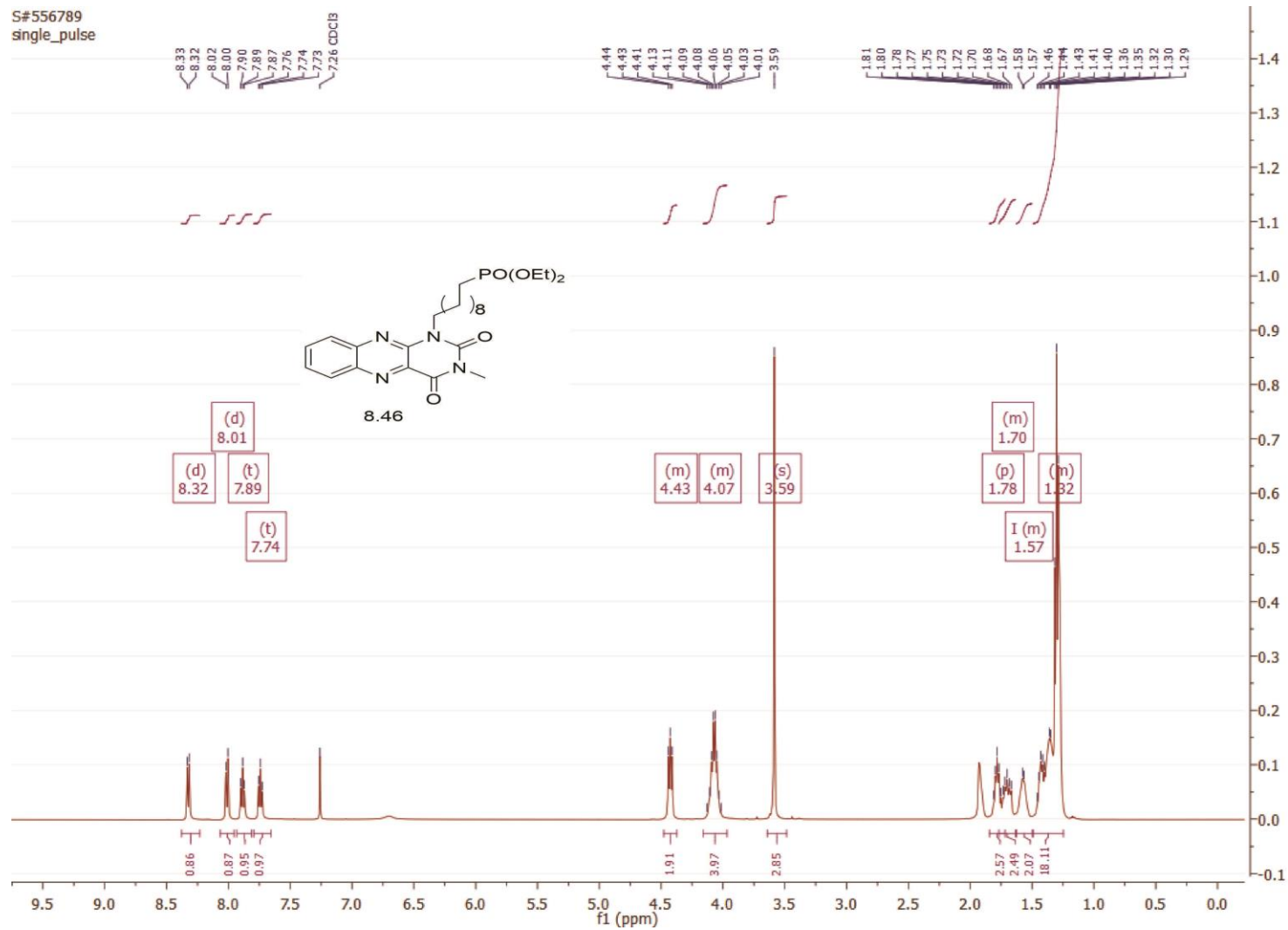


S#838899
single pulse decoupled gated

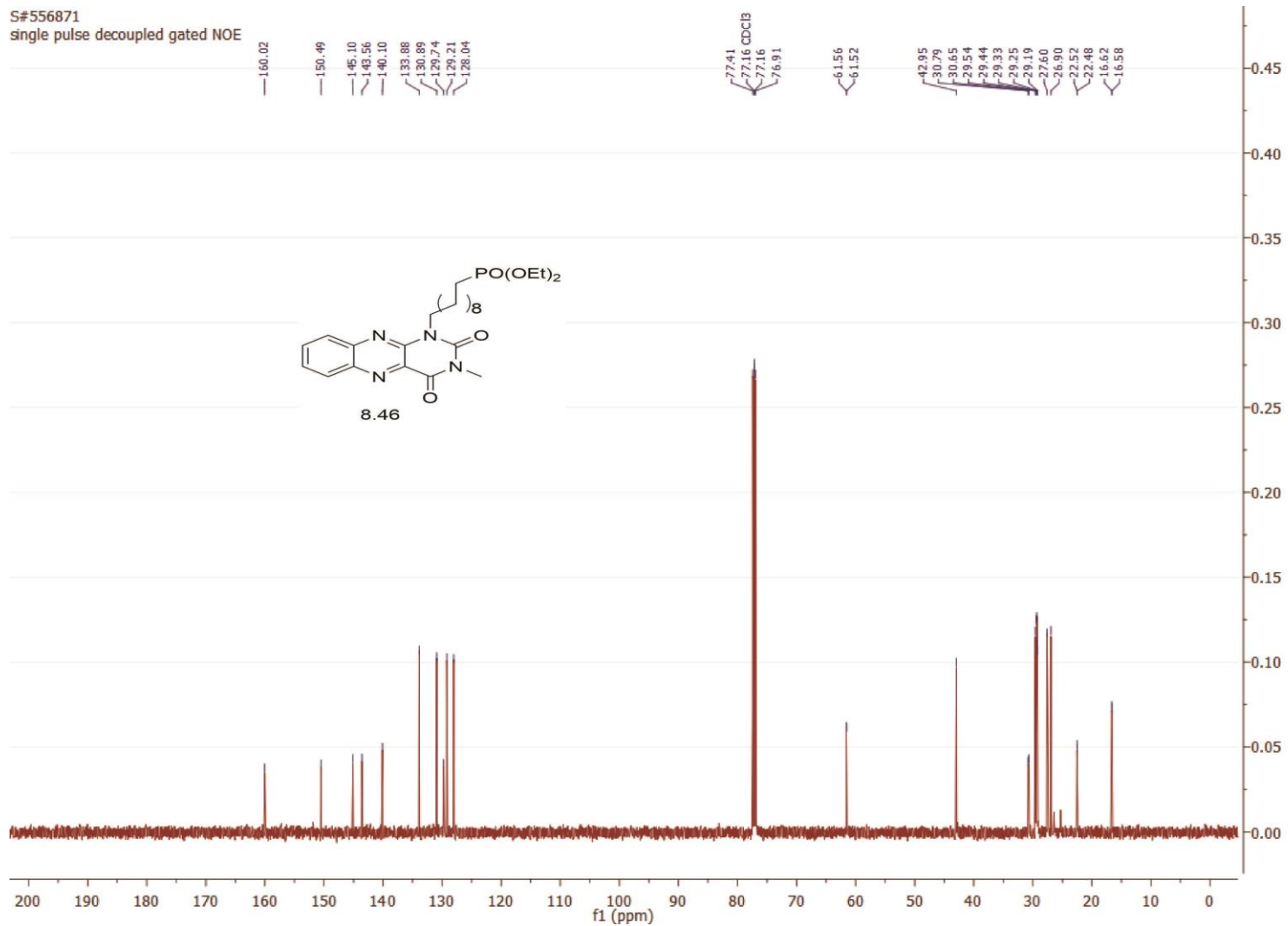


413

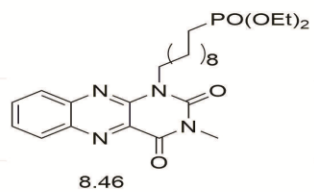
414



S#556871
single pulse decoupled gated NOE



S#845264
single pulse decoupled gated



33.28

11

10

9

8

7

6

5

4

3

2

1

0

70

65

60

55

50

45

40

35

f1 (ppm)

30

25

20

15

10

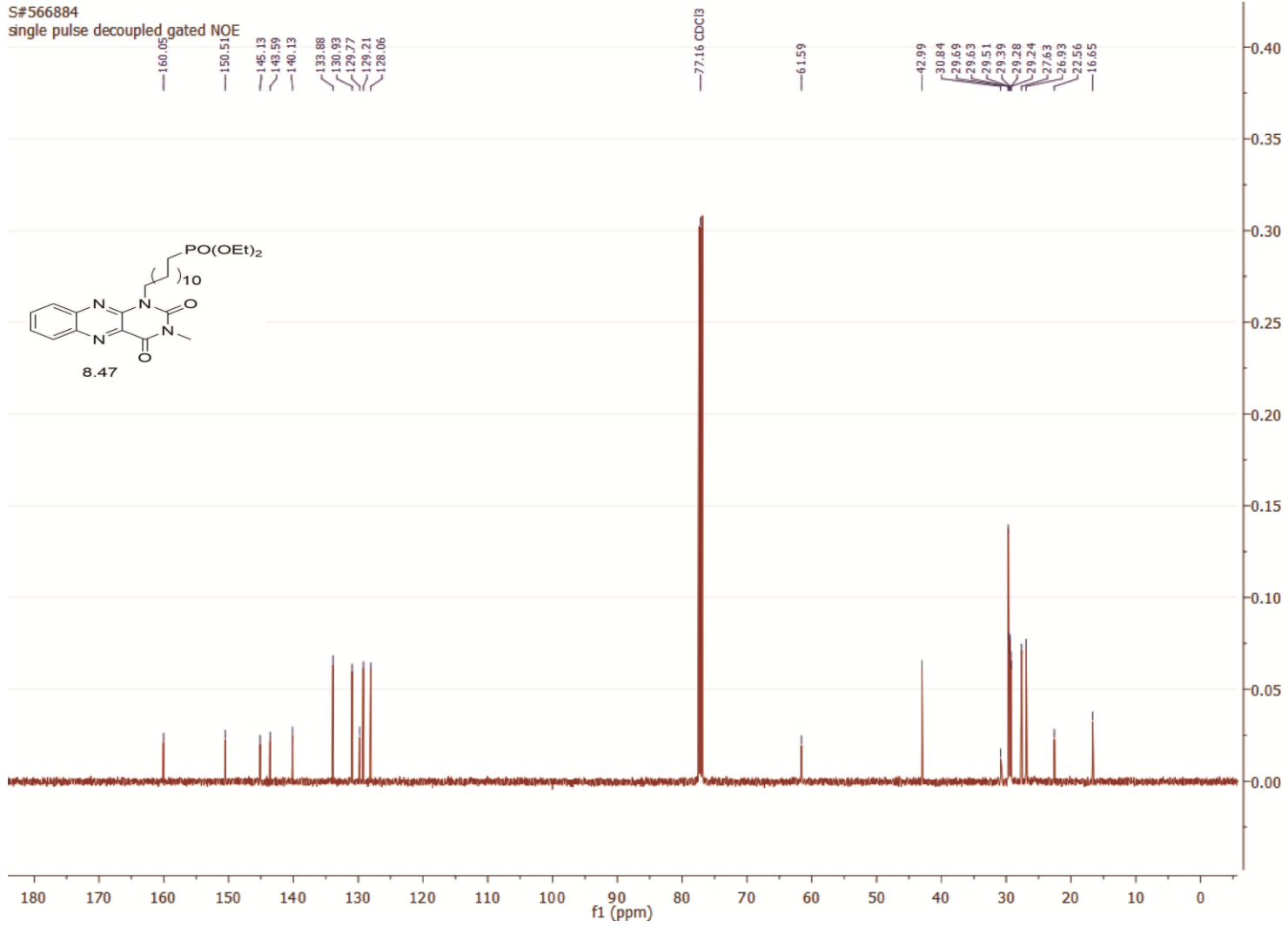
5

0

416

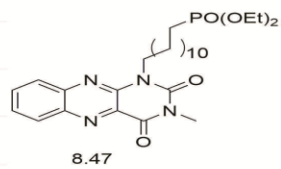
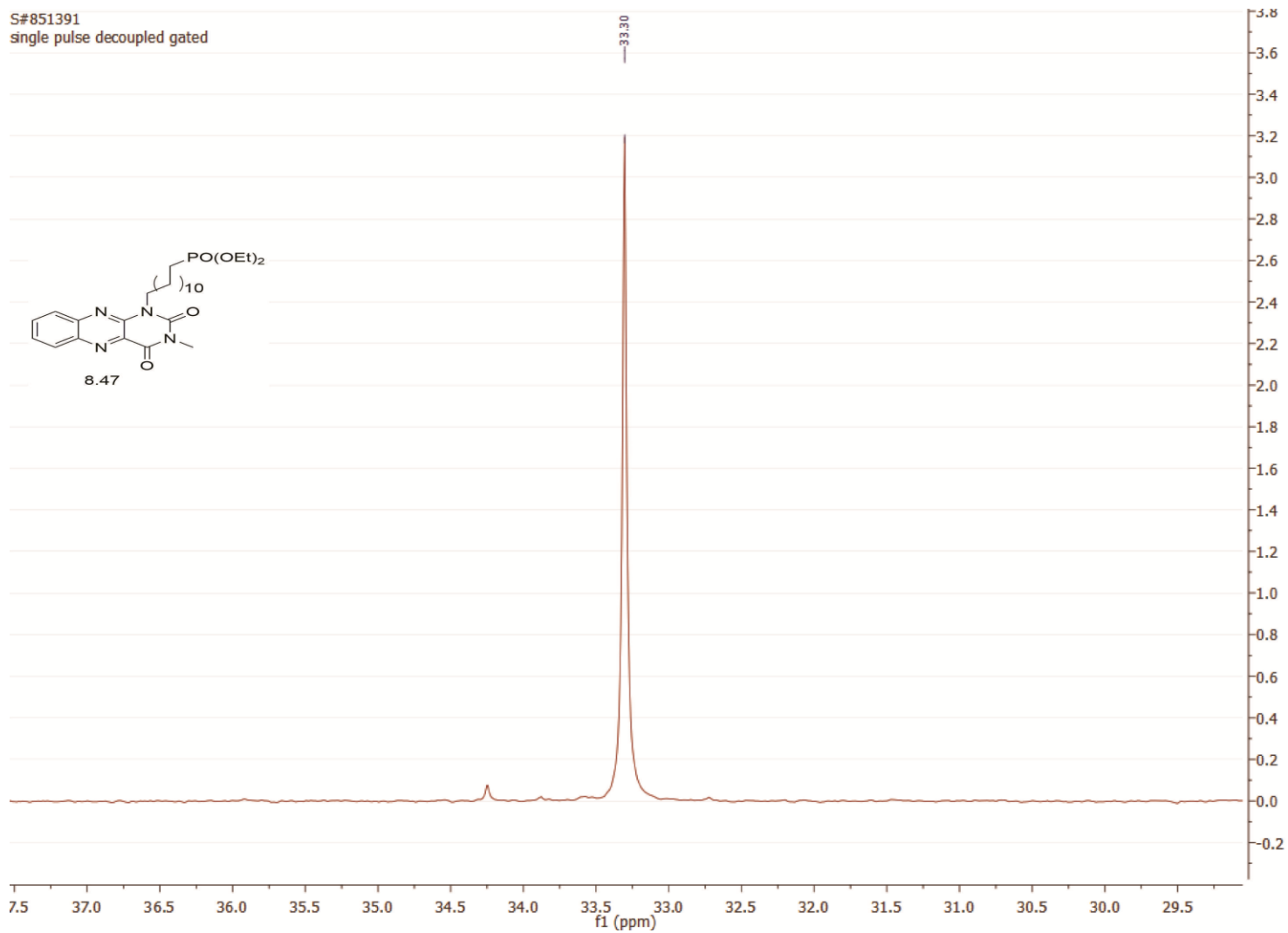
S#566884

single pulse decoupled gated NOE



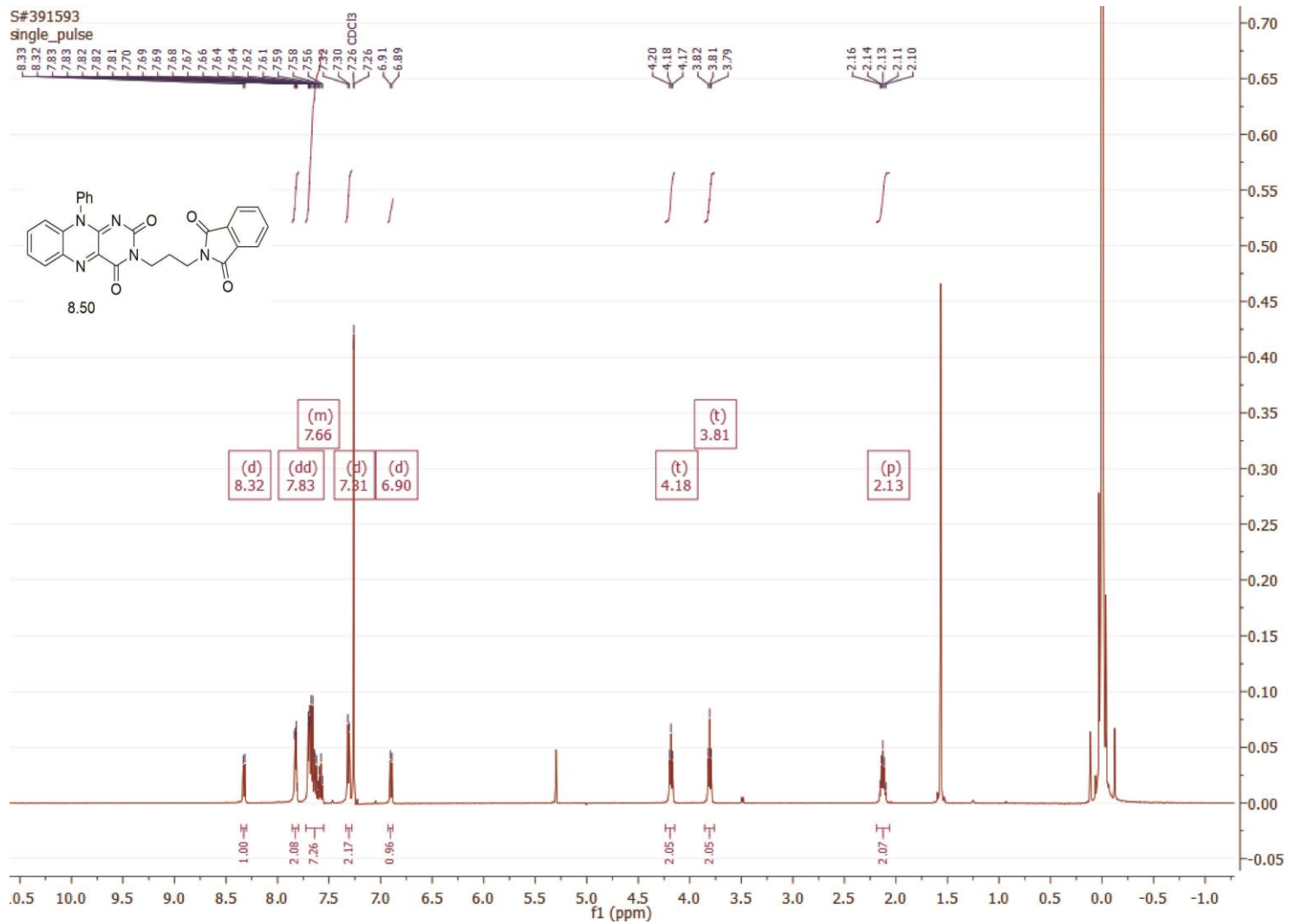
418

S#851391
single pulse decoupled gated

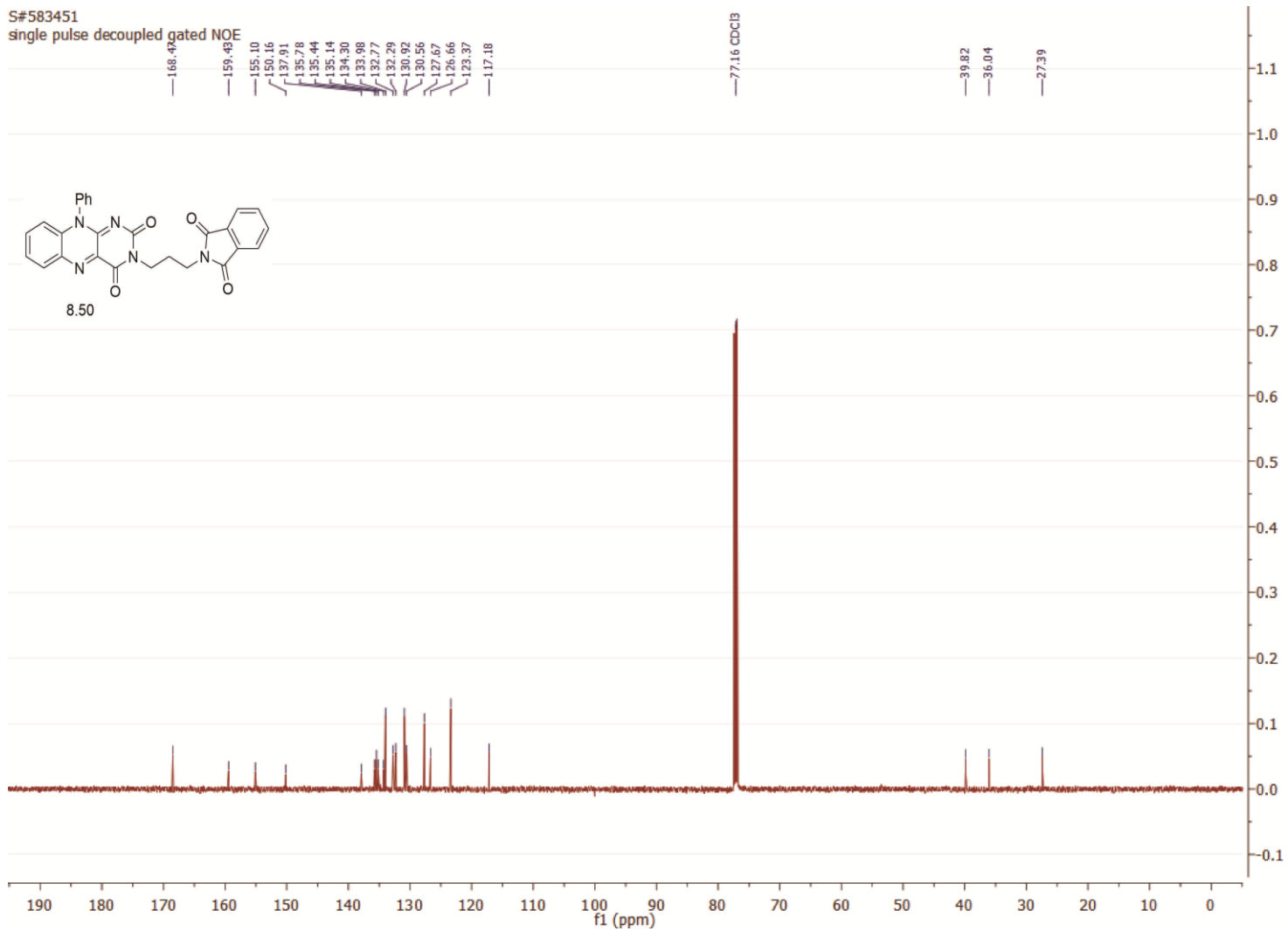


419

420

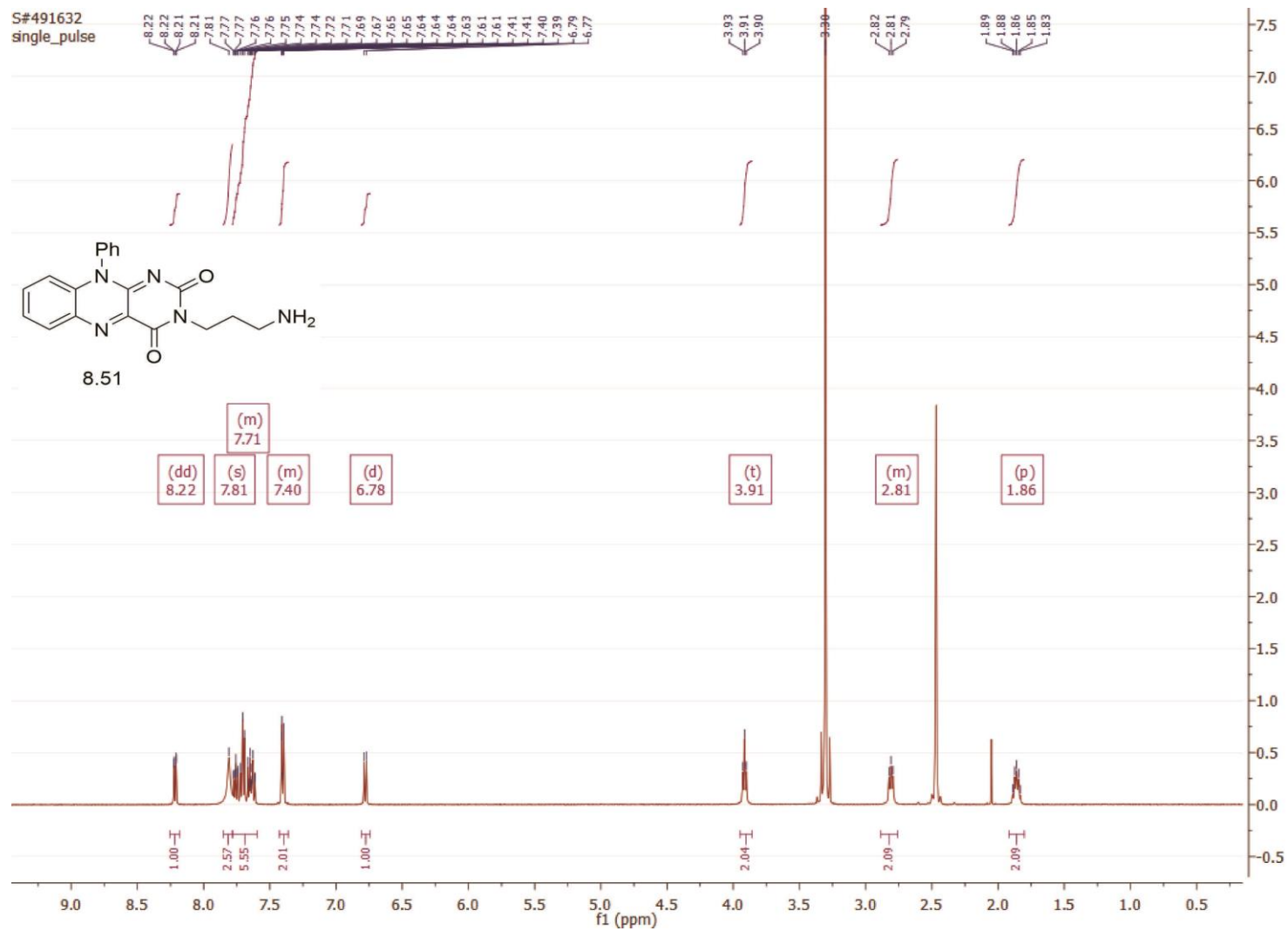


S#583451
single pulse decoupled gated NOE

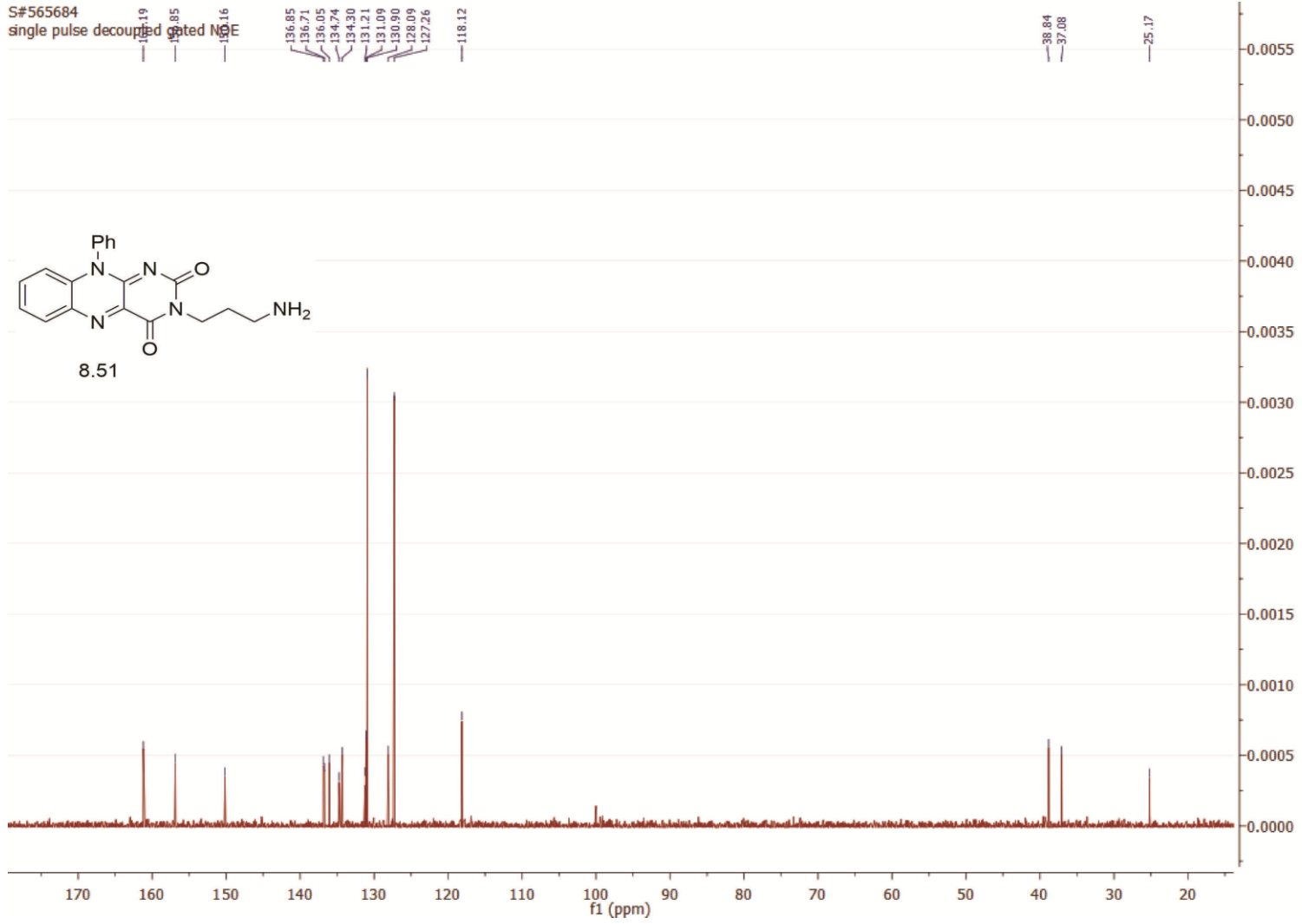


421

422

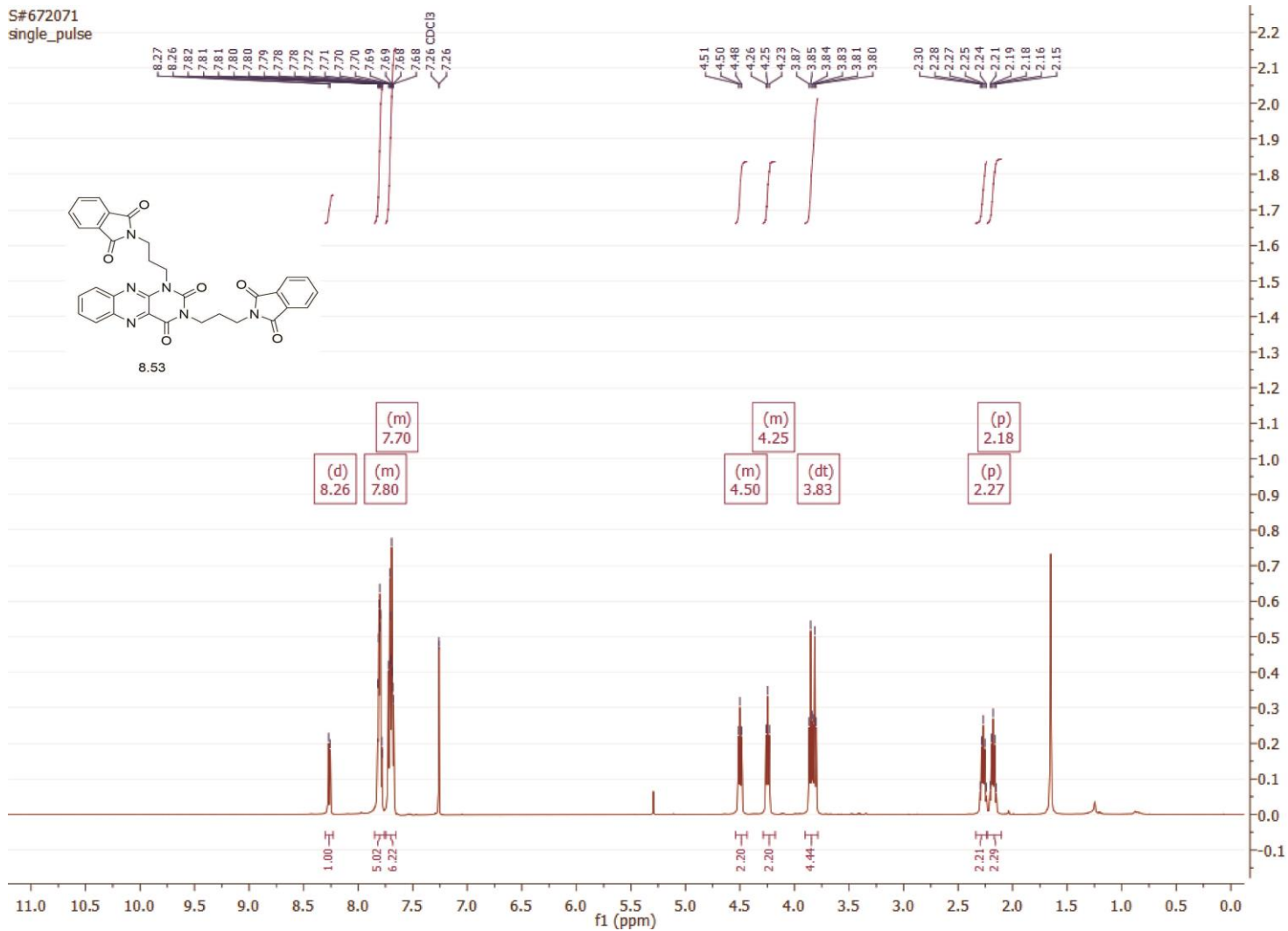


S#565684
single pulse decoupled



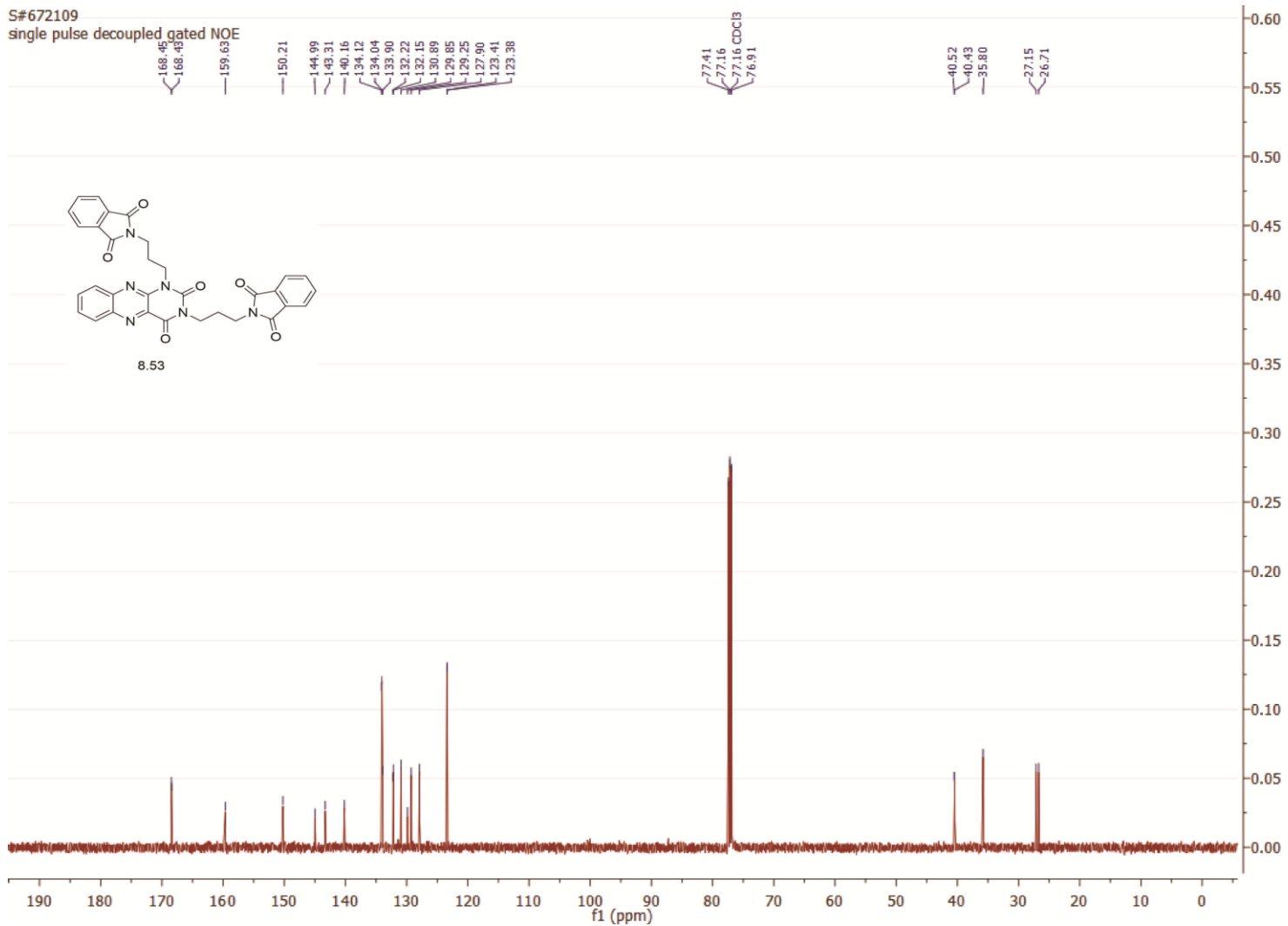
423

S#672071
single_pulse



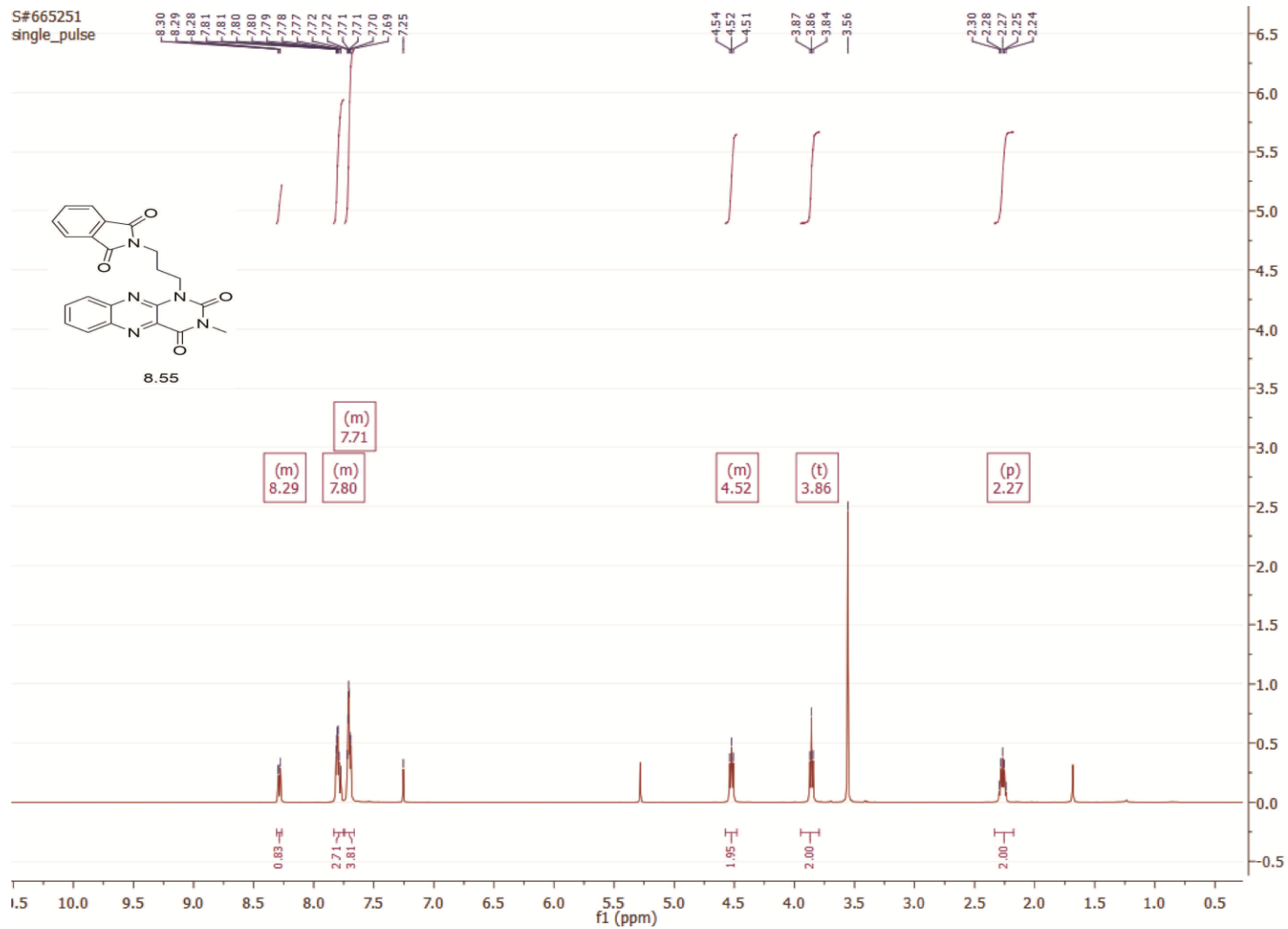
424

S#672109
single pulse decoupled gated NOE

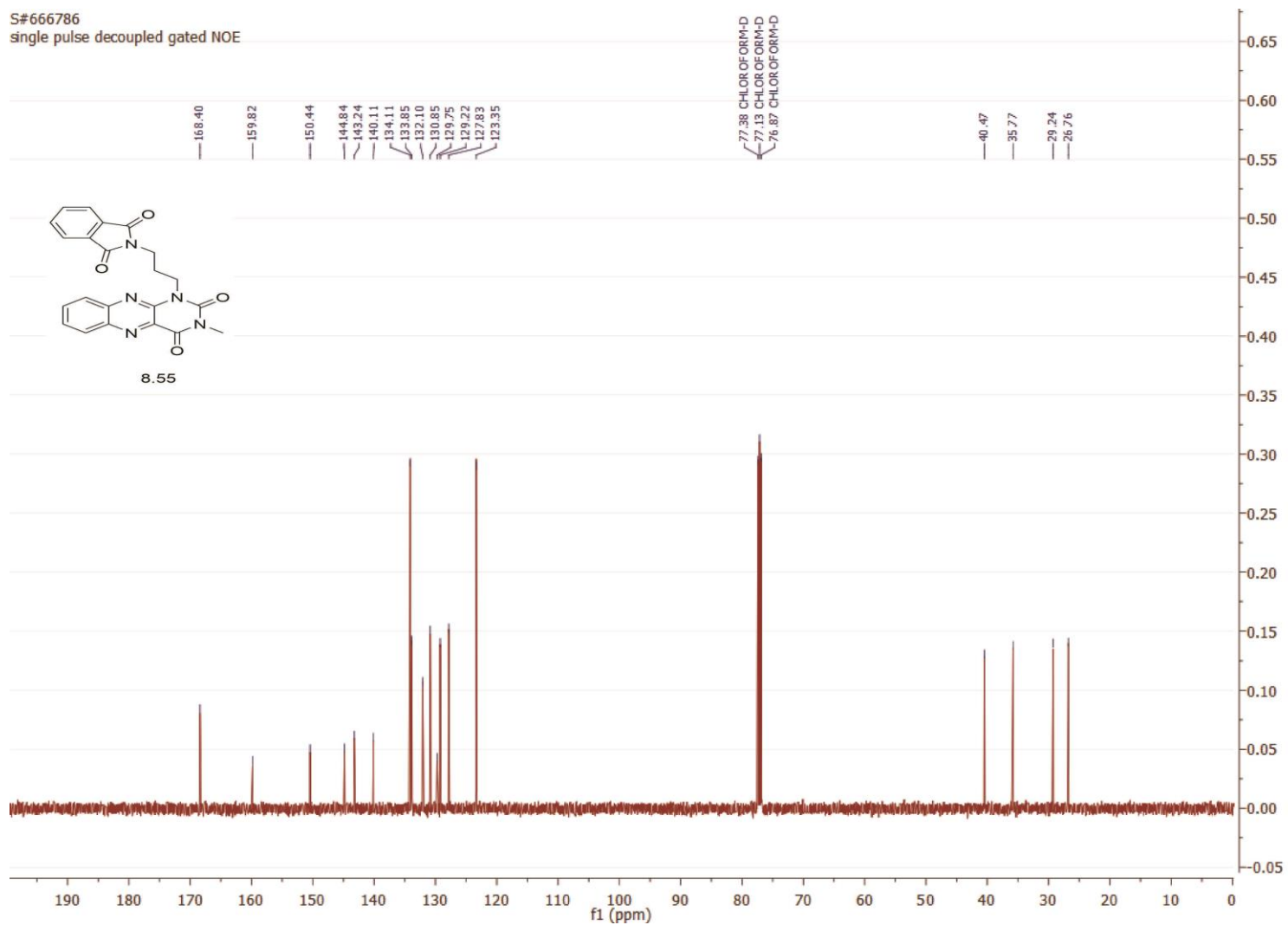


425

426



S#666786
single pulse decoupled gated NOE



427

References

1. Blyth, A. W. *J. Chem. Soc. , Trans.* **1879**, 35, 530-539.
2. Massey, V. *Biochem. Soc. Trans.* **2000**, 28, 283-296.
3. Kuhn, R.; Reinemund, K.; Weygand, F. *Ber. Dtsch. Chem. Ges. B.* **1934**, 67B, 1460-1462.
4. Karrer, P.; Schopp, K.; Benz, F. *Helv. Chim. Acta.* **1935**, 18, 426-429.
5. van Berkel, W. J. H.; Kamerbeek, N. M.; Fraaije, M. W. *J. Biotechnol.* **2006**, 124, 670-689.
6. Kamerbeek, N. M.; Moonen, M. J. H.; Van der Ven, J. G. M.; Van Berkel, W. J. H.; Fraaije, M. W.; Janssen, D. B. *Eur. J. Biochem.* **2001**, 268, 2547-2557.
7. Mihovilovic, M. D.; Muller, B.; Stanetty, P. *Eur. J. Org. Chem.* **2002**, 3711-3730.
8. Kamerbeek, N. M.; Janssen, D. B.; van Berkel, W. J. H.; Fraaije, M. W. *Adv. Synth. Catal.* **2003**, 345, 667-678.
9. Carrea, G.; Redigolo, B.; Riva, S.; Colonna, S.; Gaggero, N.; Battistel, E.; Bianchi, D. *Tetrahedron: Asymmetry* **1992**, 3, 1063-1068.
10. Kelly, D. R.; Knowles, C. J.; Mahdi, J. G.; Taylor, I. N.; Wright, M. A. *Tetrahedron: Asymmetry* **1996**, 7, 365-368.
11. Kamerbeek, N. M.; Olsthoorn, A. J. J.; Fraaije, M. W.; Janssen, D. B. *Appl. Environ. Microbiol.* **2003**, 69, 419-426.
12. Massey, V.; Mueller, F.; Feldberg, R.; Schuman, M.; Sullivan, P. A.; Howell, L. G.; Mayhew, S. G.; Matthews, R. G.; Foust, G. P. *J. Biol. Chem.* **1969**, 244, 3999-4006.
13. Gelalcha, F. G. *Chem. Rev.* **2007**, 107, 3338-3361.
14. Sono, M.; Roach, M. P.; Coulter, E. D.; Dawson, J. H. *Chem. Rev.* **1996**, 96, 2841-2887.
15. Bruice, T. C. *Acc. Chem. Res.* **1980**, 13, 256-262.

16. Donoghue, N. A.; Norris, D. B.; Trudgill, P. W. *Eur. J. Biochem.* **1976**, *63*, 175-192.
17. Torres Pazmino, D. E.; Baas, B.; Janssen, D. B.; Fraaije, M. W. *Biochemistry* **2008**, *47*, 4082-4093.
18. Orru, R.; Dudek, H. M.; Martinoli, C.; Torres Pazmino, D. E.; Royant, A.; Weik, M.; Fraaije, M. W.; Mattevi, A. *J. Biol. Chem.* **2011**, *286*, 29284-29291, S29284/1-S29284/3.
19. Thorpe, C.; Kim, J. P. *Faseb J.* **1995**, *9*, 718-725.
20. List, B. Introduction: Organocatalysis. *Chem. Rev.* **2007**, *107*, 5413-5415.
21. Murahashi, S.; Oda, T.; Masui, Y. *J. Am. Chem. Soc.* **1989**, *111*, 5002-5003.
22. Ball, S.; Bruice, T. C. *J. Am. Chem. Soc.* **1979**, *101*, 4017-4019.
23. Bruice, T. C.; Noar, J. B.; Ball, S. S.; Venkataram, U. V. *J. Am. Chem. Soc.* **1983**, *105*, 2452-2463.
24. Imada, Y.; Iida, H.; Ono, S.; Murahashi, S. *J. Am. Chem. Soc.* **2003**, *125*, 2868-2869.
25. Linden, A. A.; Kruger, L.; Backvall, J. *J. Org. Chem.* **2003**, *68*, 5890-5896.
26. Bergstad, K.; Baeckvall, J. *J. Org. Chem.* **1998**, *63*, 6650-6655.
27. Linden, A. A.; Johansson, M.; Hermanns, N.; Baeckvall, J. *J. Org. Chem.* **2006**, *71*, 3849-3853.
28. Baxova, L.; Cibulka, R.; Hampl, F. *J. Mol. Catal. A: Chem.* **2007**, *277*, 53-60.
29. Cibulka, R.; Baxova, L.; Dvorakova, H.; Hampl, F.; Menova, P.; Mojz, V.; Plancq, B.; Sayin, S. *Collect. Czech. Chem. Commun.* **2009**, *74*, 973-993.
30. Zurek, J.; Cibulka, R.; Dvorakova, H.; Svoboda, J. *Tetrahedron Lett.* **2010**, *51*, 1083-1086.
31. Jurok, R.; Cibulka, R.; Dvorakova, H.; Hampl, F.; Hodacova, J. *Eur. J. Org. Chem.* **2010**, 5217-5224.
32. Mojz, V.; Herzig, V.; Budesinsky, M.; Cibulka, R.; Kraus, T. *Chem. Commun.* **2010**, 46, 7599-7601.

33. Mazzini, C.; Lebreton, J.; Furstoss, R. *J. Org. Chem.* **1996**, *61*, 8-9.
34. Mazzini, C.; Lebreton, J.; Furstoss, R. **1997**, *45*, 1161-1167.
35. Murahashi, S.; Ono, S.; Imada, Y. *Angew. Chem. Int. Ed.* **2002**, *41*, 2366-2368.
36. Imada, Y.; Iida, H.; Murahashi, S.; Naota, T. *Angew. Chem. Int. Ed.* **2005**, *44*, 1704-1706.
37. Murov, S. L., Carmichael, I.; Hug, G. L. *Handbook of Photochemistry* **1993**.
38. Bach, T.; Bergmann, H.; Harms, K. *Org. Lett.* **2001**, *3*, 601-603.
39. Amouyal, E. *Sol. Energy Mater. Sol. Cells* **1995**, *38*, 249-276.
40. Julliard, M.; Chanon, M. *Chem. Rev.* **1983**, *83*, 425-506.
41. Massey, V. *Biochem. Soc. Trans.* **2000**, *28*, 283-296.
42. Fukuzumi, S.; Tanii, K.; Tanaka, T. *J. Chem. Soc. Chem. Commun.* **1989**, 816-818.
43. Svoboda, J.; Schmaderer, H.; Koenig, B. *Chem. - Eur. J.* **2008**, *14*, 1854-1865.
44. Lechner, R.; Koenig, B. *Synthesis* **2010**, 1712-1718.
45. Ishimitsu, S.; Fujimoto, S.; Ohara, A. *Chem. Pharm. Bull.* **1985**, *33*, 1552-1556.
46. Silva, E.; Ugarte, R.; Andrade, A.; Edwards, A. M. *J. Photochem. Photobiol. , B* **1994**, *23*, 43-48.
47. Garcia, J.; Silva, E. *J. Nutr. Biochem.* **1997**, *8*, 341-345.
48. Miskoski, S.; Garcia, N. A. *Toxicol. Environ. Chem.* **1989**, *25*, 33-43.
49. Haggi, E.; Bertolotti, S.; Miskoski, S.; Amat-Guerri, F.; Garcia, N. A. *Can. J. Chem.* **2002**, *80*, 62-67.
50. Escalada, J. P.; Pajares, A.; Gianotti, J.; Massad, W. A.; Bertolotti, S.; Amat-Guerri, F.; Garcia, N. A. *Chemosphere* **2006**, *65*, 237-244.
51. Massad, W.; Criado, S.; Bertolotti, S.; Pajares, A.; Gianotti, J.; Escalada, J. P.; Amat-Guerri, F.; Garcia, N. A. *Chemosphere* **2004**, *57*, 455-461.
52. Chu, W.; Chan, K. H.; Jafvert, C. T.; Chan, Y. S. *Chemosphere* **2007**, *69*, 177-183.

53. Larson, R. A.; Ellis, D. D.; Ju, H. L.; Marley, K. A. *Environ. Toxicol. Chem.* **1989**, *8*, 1165-1170.
54. Tatsumi, K.; Ichikawa, H.; Wada, S. *J. Contam. Hydrol.* **1992**, *9*, 207-219.
55. Silva, E.; Edwards, A. M.; Pacheco, D. *J. Nutr. Biochem.* **1999**, *10*, 181-185.
56. Cui, H.; Hwang, H.; Cook, S.; Zeng, K. *Chemosphere* **2001**, *44*, 621-625.
57. Cui, H.; Hwang, H.; Zeng, K.; Glover, H.; Yu, H.; Liu, Y. *Chemosphere* **2002**, *47*, 991-999.
58. Insinska-Rak, M.; Sikorska, E.; Bourdelande, J. L.; Khmelinskii, I. V.; Prukala, W.; Dobek, K.; Karolczak, J.; Machado, I. F.; Ferreira, L. F. V.; Dulewicz, E.; Komasa, A.; Worrall, D. R.; Kubicki, M.; Sikorski, M. *J. Photochem. Photobiol. , A* **2007**, *186*, 14-23.
59. Remucal, C. K.; McNeill, K. *Environ. Sci. Technol.* **2011**, *45*, 5230-5237.
60. Xu, F.; Song, X.; Sheng, G.; Luo, H.; Li, W.; Yao, R.; Yu, H. *Sep. Purif. Technol.* **2015**, *142*, 18-24.
61. Heelis, P. F. *Chem. Soc. Rev.* **1982**, *11*, 15-39.
62. Chacon, J. N.; McLearn, J.; Sinclair, R. S. *Photochem. Photobiol.* **1988**, *47*, 647-656.
63. Jenuwein, T.; Allis, C. D. *Science* **2001**, *293*, 1074-1080.
64. Lima SCS , Hernandez-Vargas H Herceg Z: *Curr Opin Mol Ther* **2010** *12*.
65. Glozak, M. A.; Seto, E. *Oncogene* **2007**, *26*, 5420-5432.
66. Shi, Y.; Lan, F.; Matson, C.; Mulligan, P.; Whetstine, J. R.; Cole, P. A.; Casero, R. A.; Shi, Y. *Cell* **2004**, *119*, 941-953.
67. Huang, J.; Sengupta, R.; Espejo, A. B.; Lee, M. G.; Dorsey, J. A.; Richter, M.; Opravil, S.; Shiekhattar, R.; Bedford, M. T.; Jenuwein, T.; Berger, S. L. *Nature* **2007**, *449*, 105-108.
68. Dickens, M. P.; Roxburgh, P.; Hock, A.; Mezna, M.; Kellam, B.; Vousden, K. H.; Fischer, P. M. *Bioorg. Med. Chem.* **2013**, *21*, 6868-6877.

69. Sancar, A. *Chem. Rev.* **2003**, *103*, 2203-2237.
70. Epple, R.; Wallenborn, E.; Carell, T. *J. Am. Chem. Soc.* **1997**, *119*, 7440-7451.
71. Song, Q.; Tang, W.; Hei, X.; Wang, H.; Guo, Q.; Yu, S. *Eur. J. Org. Chem.* **2005**, 1097-1106.
72. Mertens, M. E.; Frese, J.; Boelukbas, D. A.; Hrdlicka, L.; Golombek, S.; Koch, S.; Mela, P.; Jockenhoevel, S.; Kiessling, F.; Lammers, T. *Theranostics* **2014**, *4*, 1002-1013, 12.
73. Noell, G.; Trawoeger, S.; von Sanden-Flohe, M.; Dick, B.; Grininger, M. *ChemBioChem* **2009**, *10*, 834-837.
74. Jacobson, F.; Walsh, C. *Biochemistry* **1984**, *23*, 979-988.
75. Ferry, J. G. *Crit. Rev. Biochem. Mol. Biol.* **1992**, *27*, 473-503.
76. Yoneda, F.; Tsukuda, K.; Shinozuka, K.; Hirayama, F.; Uekama, K.; Koshiro, A. *Chem. Pharm. Bull.* **1980**, *28*, 3049-3056.
77. Tanaka, K.; Kimura, T.; Chen, X.; Kawamoto, T.; Yoneda, F. *Chem. Pharm. Bull.* **1990**, *38*, 312-317.
78. Lelais, G.; MacMillan, D. W. C. *Aldrichimica Acta.* **2006**, *39*, 79-87
79. Dakin, H. D. *Amer. Chem. J.* **1909**, *42*, 477-498.
80. Baeyer, A.; Villiger, V. *Ber. Dtsch. Chem. Ges.* **1899**, *32*, 3625-3631
81. Matsumoto, M.; Kobayashi, K.; Hotta, Y. *J. Org. Chem.* **1984**, *49*, 4740-4741.
82. Hansen, B. *Acta Chem. Scand.* **1963**, *17*, 1375-1379.
83. Principles of Organic Synthesis, 3rd edition, Norman, R.O.C page 447.
84. Hocking, M. B. *Can. J. Chem.* **1973**, *51*, 2384-2392.
85. Yamazaki, S. *Chem. Lett.* **1997**, *12*, 127-128
86. Bernini, R.; Coratti, A.; Provenzano, G.; Fabrizib, G.; Tofanic, D. *Tetrahedron*, **2005**, *61*, 1821-1825

87. Silva, E. T. D.; Caamara, C. A.; Antunes, O. A. C.; Barreiro, E. J.; Fraga, C. A. M. *Synth. Commun.* **2008**, *38*, 784–788
88. Kaballm, G. W.; Reddy, N. K.; Narayana, C. *Tetrahedron Lett.* **1992**, *33*, 865-866.
89. Roy, A.; Reddy, K. R.; Mohanta, P. K.; Ila, H.; Junjappat, H. *Synth. Commun.* **1999**, *29*, 3781-3791
90. Varma, R. S.; Naicker, K. P. *Org. Lett.* **1999**, *1*, 189-191
91. Chen, S.; Hossain, M. S.; Foss, F. W. *Org. Lett.* **2012**, *14*, 2806-2809.
92. (a) Bruice, T. C. *J. Chem. Soc. , Chem. Commun.* **1983**, 14-15 (c) Kemal, C.; Chan, T. W.; Bruice, T. C. *Proc. Natl. Acad. Sci. U. S. A.* **1977**, *74*, 405-409. (d) Ball, S.; Bruice, T. C. *J. Am. Chem. Soc.* **1980**, *102*, 6498-6503
93. Hocking, M. B.; Ong, J. H. *Can. J. Chem.* **1977**, *55*, 102-110.
94. Murray, A. T.; Matton, P.; Fairhurst, N. W. G.; John, M. P.; Carbery, D. R. *Org. Lett.* **2012**, *14*, 3656–36.
95. Hantzsch, A. *Justus Liebigs Ann. Chem.* **1882**, *215*, 1-82.
96. Kumar, A.; Maurya, R. A.; Sharm, S. *Bioorg. Med. Chem. Lett.* **2009**, *19*, 4432-4436.
97. Love, B.; Goodman, M.; Snader, K.; Tedeschi, R.; Macko, E. *J. Med. Chem.* **1974**, *17*, 956-965.
98. Bossert, F.; Meyer, H.; Wehinger, E. *Angew. Chem. Int. Ed.Engl.* **1981**, *20*, 762-769.
99. Guengerich, F. P.; Brian, W. R.; Iwasaki, M.; Sari, M. A.; Baarnhielm, C.; Berntsson, P. *J. Med. Chem.* **1991**, *34*, 1838-1844.
100. Bischoff, H.; Angerbauer, R.; Bender, E.; Bischoff, J. A.; Petzinna, D.; Pfitzner, J.; Porter, M. C.; Schmidt, D.; Thomas, G. *Atherosclerosis* **1997**, *135*, 119.
101. Mashraqui, S. H.; Kamik, M. A. *Tetrahedron Lett.* **1998**, *39*, 4895-4898.
102. Heravi, M. M.; Derikvand, F.; Hassan-Pour, S.; Bakhtiari, K.; Bamoharram, F. F.; Oskooie H. A. *Bioorg. Med. Chem. Lett.* **2007**, *17*, 3305-3309.

103. Chai, L.; Zhao, Y.; Sheng, Q.; Liu, Z-Q. *Tetrahedron Lett.* **2006**, *47*, 9283-9285.
104. Nakamichi, N.; Kawashita, Y.; Hayashi, M. *Org. Lett.* **2002**, *4*, 3955-3957.
105. Eynde, J.-J. V.; D'Oraxio, R.; Haverbeke, Y. V. *Tetrahedron* **1994**, *50*, 2419-2484.
106. Wang, D.; Liu, Q; Chen, B.; Zhang, L.; Tung, C.; Wu, L. *Chinese.Sci. Bull.* **2010**, *55*, 2855–2858
107. Le Bozec, L.; Moody, C. J. *Aust. J. Chem.* **2009**, *62*, 639–647.
108. Zhu, C; Falck, J. R. *ChemCatChem.* **2011**, *3*, 1850-1851.
109. Zhu, C.; Akiyama, T. *Org. Lett.* **2009**, *11*, 4180-4183.
110. Yadav, G. S.; Senthilkumar, G. P. *Int. J. Pharm. Drug Dev. Res.***2011**, *3*, 1-7.
111. Bochatay, V. N.; Boissarie, P. J.; Murphy, J. A.; Suckling, C. J.; Lang, S. *J. Org. Chem.* **2013**, *78*, 1471-1477.
112. Zhao, J.; Huang, H.; Wu, W.; Chen, H.; Jiang, H. *Org. Lett.* **2013**, *15*, 2604-2607.
113. Sun, Y.; Jiang, H.; Wu, W.; Zeng, W.; Wu, X. *Org. Lett.*, **2013**, *15*, 1598-1601.
114. Liao, Y.; Qi, H.; Chen, S.; Jiang, P.; Zhou, W.; Deng, G.-J. *Org.Lett.* **2012**, *14*, 6004–6007.
115. Abdel-Mohsen, H. T.; Conrad, J.; Beifuss, U. *Green Chem.* **2012**, *14*, 2686-2690.
116. Chen. S., Design and synthesis of flavin-based organocatalysts for biomimetic aerobic oxidation reactions; Ph.D. Dissertation, The University of Texas at Arlington: Arlington, 2013.
117. Menova, P.; Cibulka, R. *J. Mol. Catal. A: Chem.* **2012**, *363-364*, 362-370.
118. Chen, S.; Foss, F. W. *Org. Lett.* **2012**, *14*, 5150-5153.
119. Sorm, F.; Piskala, A.; Cihak, A.; Vesely, J. *Experientia* **1964**, *20*, 202-203.
120. Yoneda, F. Syntheses of 5-deazaflavins. *Methods Enzymol.* **1980**, *66*, 267-277.
121. Das, J.; Bhan, A.; Mandal, S. S.; Lovely, C. J. *Bioorg. Med. Chem. Lett.* **2013**, *23*, 6183-6187.

122. Ansari, K. I.; Kasiri, S.; Grant, J. D.; Mandal, S. S. *J. Biomol. Screening* **2011**, *16*, 26-35.
123. Ansari, K. I.; Grant, J. D.; Woldemariam, G. A.; Kasiri, S.; Mandal, S. S. *Org. Biomol. Chem.* **2009**, *7*, 926-932.
124. Ansari, K. I.; Kasiri, S.; Grant, J. D.; Mandal, S. S. *Dalton Trans.* **2009**, 8525-8531.
125. Ansari, K. I.; Grant, J. D.; Kasiri, S.; Woldemariam, G.; Shrestha, B.; Mandal, S. S. *J. Inorg. Biochem.* **2009**, *103*, 818-826.
126. Morris, G. M.; Huey, R.; Lindstrom, W.; Sanner, M. F.; Belew, R. K.; Goodsell, D. S.; Olson, A. J. *J. Comput. Chem.* **2009**, *30*, 2785-2791.
127. Iida, H.; Imada, Y.; Murahashi, S. *Org. Biomol. Chem.* **2015**, *13*, 7599-7613.
128. Kubota, Y.; Niwa, C.; Ohnuma, T.; Ohko, Y.; Tatsuma, T.; Mori, T.; Fujishima, A. *J. Photochem. Photobiol. A.* **2001**, *141*, 225-230.
129. Choi, W.; Termin, A.; Hoffmann, M. R. *J. Phys. Chem.* **1994**, *98*, 13669-13679.
130. Yang, J. C.; Kim, Y. C.; Shul, Y. G.; Shin, C. H.; Lee, T. K. *Appl. Surf. Sci.* **1997**, *121/122*, 525-529.
131. Rao, K. V. S.; Lavedrine, B.; Boule, P. *J. Photochem. Photobiol. A.* **2003**, *154*, 189-193.
132. Subramanian, V.; Wolf, E. E.; Kamat, P. V. *Langmuir* **2003**, *19*, 469-474.
133. Halman, M. M. Photodegradation of water pollutants; CRC Press:Boca Raton, **1996**.
134. Paz, Y.; Luo, Z.; Rabenberg, L.; Heller, A. J. *Mater. Res.* **1995**, *10*, 2842-2848.
135. Paramasivam, I.; Jha, H.; Liu, N.; Schmuki, P. *Small* **2012**, *8*, 3073.
136. Brodard-Sevarac, F.; Guerrero, G.; Maquet, J.; Florian, P.; Gervais, C.; Mutin, P. H. *Chem. Mater.* **2008**, *20*, 5191-5196.
137. Cheeseman, P.; Toms-Wood A.; R. S. Wolfe, *J. Bacteriol.* **1972**, *112*, 527-531.
138. Eirich, L. D.; Vogels G. D.; Wolfe, R. S. *Biochemistry* **1978**, *17*, 4583-4593.

139. McCormick, J. R. D.; Morton, G. O. *J. Am. Chem. Soc.* **1982**, *104*, 4014–4015.
140. Isabelle, D.; Simpson D. R.; Daniels, L. *Appl. Environ. Microbiol.* **2002**, *68*, 5750–5755.
141. Howland, J. L. *Biochem. Educ.* **1995**, *23*, 114.
142. DiMarco, A.; Bobik, T. A.; Wolfe, R. S. *Annu. Rev. Biochem.* **1990**, *59*, 355–394.
143. Ferry, J. G. *Methanogenesis*, Springer Science & Business Media, **1993**.
144. Lin, X. L.; White, R. H. *J. Bacteriol.* **1986**, *168*, 444–448.
145. Jacobson, F.; Walsh, C. *Biochemistry* **1984**, *23*, 979–988.
146. Ferry, J. G. *Crit. Rev. Biochem. Mol. Biol.* **1992**, *27*, 473–503.
147. Decamps, L.; Philmus, B.; Benjdia, A.; White, R.; Begley, T. P., Berteau, O. *J. Am. Chem. Soc.* **2012**, *134*, 18173– 18176.
148. Le Van, Q.; Schwarzkopf, B.; Bacher, A.; Keller, P. J., Lee, S.; Floss, H. G. *J. Am. Chem. Soc.* **1985**, *107*, 8300– 8301.
149. Glas, A. F.; Maul, M. J.; Cryle, M.; Barends, T. R. M.; Schneider, S.; Kaya, E.; Schlichting, I.; Carell, T. *Proc. Natl. Acad. Sci. U. S. A.* **2009**, *106*, 11540–11545.
150. O'Brien, D. E.; Weinslock, L. T.; Cheng, C. C. *J. Heterocycl. Chem.* **1970**, *7*, 99–105.
151. Ashton, W. T.; Brown, R. D.; Jacobsen, F. E.; Walsh, C. T. *J. Am. Chem. Soc.* **1979**, *101*, 4419–4420.
152. Ashton, W. T.; Brown, R. D. *J. Heterocycl. Chem.* **1980**, *17*, 1709–1712.
153. Tanaka, K.; Kimachi, T.; Kawase, M.; Yoneda, F. *J. Chem. Soc., Chem. Commun.* **1988**, 524–526.
154. Kimachi, T.; Kawase, M., Matsuki, S., Tanaka, K.; Yoneda, F. *J. Chem. Soc., Perkin Trans. 1*, **1990**, 253–256.
155. Janda, M.; Hemmerich, P. *Angew. Chem., Int. Ed. Engl.* **1976**, *15*, 443–444.

156. Chaudhuri, O S.; Batabyal, S.; Polley, N.; Pal, S. K. *J. Phys. Chem. A* **2014**, *118*, 3934–3943.
157. Carlson, E. E.; Kiessling, L. L. *J. Org. Chem.* **2004**, *69*, 2614–2617.
158. Manstein, D. J.; Pai, E. F.; Schopfer, L. M.; Massey, V. *Biochemistry* **1986**, *25*, 6807–6816.
159. Zhang, Z.; Zhang, L.; Schlueter, J. A.; Redfern, P. C.; Curtiss, L.; Amine, K. *J. Power Sources* **2010**, *195*, 4957–4962.
160. Knaggs, S.; Malkin, H.; Osborn, H. M. I.; Williams, N. A. O.; P. Yaqoob, *Org. Biomol. Chem.* **2005**, *3*, 4002–4010.
161. Artigas, G.; Marchan, V. *J. Org. Chem.* **2013**, *78*, 10666–10677.
162. Yoneda, F.; US Patent 4, 567, 260, Jan. 28th, **1986**.
163. Warkentin, E.; Mamat, B.; Sordel Klippert, M.; Wicke, M.; Thauer, R. K.; Iwata, M.; Iwata, S.; Ermler, U.; Shima, S. A. *EMBO J.* **2001**, *20*, 6561–6569.
164. Kunow, J.; Schwörer, B.; Stetter, K. O.; Thauer, R. K. *Arch. Microbiol.*, **1993**, *160*, 199.
165. Cristau, H.; Pirat, J.; Drag, M. *Tetrahedron Lett.* **2000**, *41*, 9781-9785.
166. Ha, Y.; Facchetti, A.; Marks, T. J. *Chem. Mater.* **2009**, *21*, 1173-1175.
167. Jin, Y.; Kim, Y.; Kim, S. H.; Song, S.; Woo, H. Y.; Lee, K.; Suh, H. *Macromolecules* **2008**, *41*, 5548-5554.
168. Dincalp, H.; Saltan, G. M.; Aykut, D.; Zafer, C. *Spectrochim. Acta, Part A* **2015**, *149*, 157-165.
169. Liu, R.; von Malotki, C.; Arnold, L.; Koshino, N.; Higashimura, H.; Baumgarten, M.; Mullen, K. *J. Am. Chem. Soc.* **2011**, *133*, 10372-10375.

170. Rombouts, J. A.; Ravensbergen, J.; Frese, R. N.; Kennis, J. T. M.; Ehlers, A. W.; Slootweg, J. C.; Ruijter, E.; Lammertsma, K.; Orru, R. V. A. *Chem. - Eur. J.* **2014**, *20*, 10285-10291.
171. Kleineweischede, A.; Mattay, J. *Eur. J. Org. Chem.* **2006**, 947-957.
172. Shao, J.; Chang, J.; Chi, C. *Org. Biomol. Chem.* **2012**, *10*, 7045-7052.
173. Sharma, A.; Kumar, R.; Sharma, N.; Kumar, V., Sinha, A.K. *Adv. Synth. Catal.* **2008**, *350*, 2910-2920.
174. Rosenblatt, D. H. *J. Am. Chem. Soc.* **1953**, *75*, 4607-4608.
175. Carpino, L. A. *J. Org. Chem.* **1989**, *54*, 3303-3310.
176. Hattori, S. *Acta. Phytochimica* **1931**, *5*, 219-237.
177. Uldrikjjs, J. *Khim Geterotsikl+*, **1975**, *9*, 1230-1237.
178. Kikugawa, K. *Chem. Pharm. Bull.* **1987**, *35*, 4656-60.
179. Guangxun, L.; Rong, C.;, Lei, W.; Qingquan, F.; Xiaomei, Z.; Zhuo, T. *Angew. Chem. Int. Edit.* **2013**, *52*, 8432-8436.
180. Bagley, M C. *Synthesis* **2006**, *8*, 1283-1288.
181. Choi, S-J. *Bioorgan. Med. Chem.* **2006**, *14*, 1229-1235.
182. Deligeorgiev, T. C. *Dyes Pigments* 1990, *12*, 243-248.
183. Fomina, M. V. *Russ. Chem. Bull.* **2010**, *59*, 1974-1978.
184. Barra, M. *J Photoch Photobio A.* **2011**, *225*, 113-116.
185. Smith, W T. *J. Org. Chem.* **1962**, *27*, 676-678.
186. Mancilha, F. S. *Eur. J. Org. Chem.* **2006**, *21*, 4924-4933.
187. Elderfield, R. C. *J. Am. Chem. Soc.* **1954**, *76*, 1887-1891.
188. Shang, X-F. *J. Fluorine Chem.* **2007**, *128*, 530-534.
189. Yueksel, F. *New J. Chem.* **2005**, *29*, 726-732.
190. Cheeseman, G. W. H. *J. Chem. Soc.* **1962**, 1170-1176.

Biographical Information

Mohammad Shawkat Hossain was born in Narayanganj, Bangladesh. He secured his BS in Chemistry and MS in Organic Chemistry from the University of Dhaka, Bangladesh. He studied the isolation of secondary metabolites from endophytic fungus from medicinal plants under supervision of Dr. Mosihuzzaman and Dr. Nilufar Nahar. Mohammad joined Ahsanullah University of Science and Technology as a lecturer in Chemistry in 2005. In 2007, he joined Kochi University, Japan as a graduate student. He studied the distribution of type II PKS genes in actinomycetes from metagenomic DNA. After securing his M.Ag. degree in Bioresources Science from Kochi university in 2009, Mohammad worked as a research assistant at Dr. Kouhei Ohnishi's laboratory. He joined the University of Texas at Arlington in 2010 as a Doctoral student and secured his Doctoral degree in 2015 under supervision of Dr. Frank W. Foss Jr. His dissertation was focused on the biomimetic application of artificial flavins in redox chemistry.